Environmental Studies Relative to Potential Sand Mining in the Vicinity of the City of Virginia Beach, Virginia

Final Report

January 1998

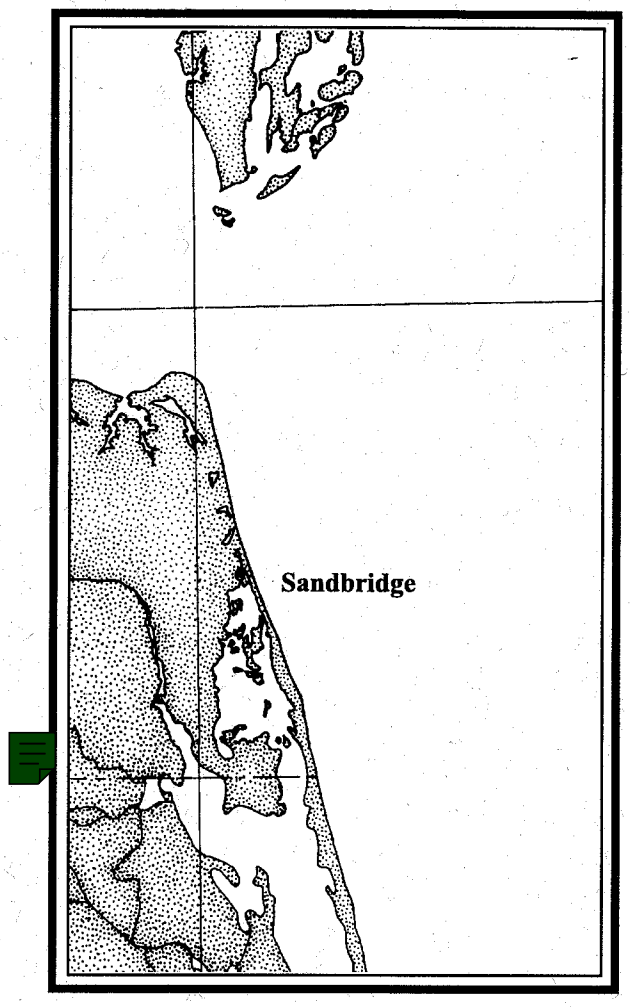

MMS U.S. Department of the Interior
Minerals Management Service

College of William and Mary
VIMS
Virginia Institute of Marine Science
School of Marine Science

DISCLAIMER

This report has been reviewed by the Minerals Management Service and approved for publication. Approval does not signify that the contents necessarily reflect the views and policies of the Service, nor does mention of trade names or commercial products constitute endorsement or recommendation for use.

Environmental Studies Relative to Potential Sand Mining in the Vicinity of the City of Virginia Beach, Virginia

Final Report

January 1998

Part 1: Benthic Habitats and Biological Resources Off the Virginia Coast 1996 and 1997

G. R. Cutter, Jr. and R. J. Diaz

Part 2: Preliminary Shoreline Adjustments to Dam Neck Beach Nourishment Project Southeast Virginia Coast

C. S. Hardaway, Jr., D. A. Milligan, G. R. Thomas, and C. H. Hobbs, III

Part 3: Nearshore Waves and Currents Observations and Modeling

J. D. Boon

Part 4: Coastal Currents

A. Valle-Levinson

Part 5: Benthic Foraminifera and Ostracoda from Virginia Continental Shelf

T. M. Cronin, S. Ishman, R. Wagner, and G. R. Cutter, Jr.

Project Manager:

Carl H. Hobbs, III
Virginia Institute of Marine Science

Prepared under MMS Cooperative
Agreement 14-35-0001-3087 through
Virginia Institute of Marine Science of the
College of William & Mary

MMS U.S. Department of the Interior
Minerals Management Service

College of William and Mary
VIMS
Virginia Institute of Marine Science
School of Marine Science

The Department of the Interior

As the Nations's principal conservation agency, the Department of the Interior has responsibility for most of our nationally owned public lands and natural resources. This includes fostering sound use of our land and water resources, protecting our fish, wildlife, and biological diversity, preserving the environmental and cultural values of our national parks and historic places; and providing for the enjoyment of life through outdoor recreation. The Department assesses our energy and mineral resources and works to ensure that their development is in the best interests of all our people by encouraging stewardship and citizen participation in their care. The Department also has a major responsibility for American Indian reservation communities and for people who live in island territories under U.S. Administration.

The Minerals Management Service Mission

As a bureau of the Department of the Interior, the Minerals Management Service's (MMS) primary responsibilities are to manage the mineral resources located on the Nations's Outer Continental Shelf (OCS), collect revenue from the Federal OCS and onshore federal and Indian lands, and distribute those revenues.

Moreover, in working to meet its responsibilities, the Offshore Minerals Management Program administers the OCS competitive leasing program and oversees the safe and environmentally sound exploration and production of our Nation's offshore natural gas, oil and other mineral resources. The MMS Royalty Management Program meets its responsibilities by entrusting the efficient, timely and accurate collection and distribution of revenue from mineral leasing and production due to Indian tribes andallottees, States and the U. S. Treasury

the MMS strives to fulfill its responsibilities through the general guiding principles of: (1) being responsive to the public's concerns and interests by maintaining a dialog with all potentially affected parties and (2) carrying out its programs with an emphasis on working to enhance the quality of life for all Americans by lending MMS assistance and expertise to economic development and environmental protection.

Environmental Studies Relative to Potential Sand Mining in the Vicinity of the City of Virginia Beach, Virginia

Part 1: Benthic Habitats and Biological Resources Off the Virginia Coast 1996 and 1997

Final Report

January 1998

Authors:

G. R. Cutter, Jr
R. J. Diaz
Virginia Institute of Marine Science

Project Manager:

Carl H. Hobbs,. III
Virginia Institute of Marine Science

Prepared under MMS Cooperative Agreement 14-35-0001-3087 through Virginia Institute of Marine Science of the College of William & Mary

MMS U.S. Department of the Interior
Minerals Management Service

College of William and Mary
VIMS
Virginia Institute of Marine Science
School of Marine Science

DISCLAIMER

This report has been reviewed by the Minerals Management Service and approved for publication. Approval does not signify that the contents necessarily reflect the views and policies of the Service, nor does mention of trade names or commercial products constitute endorsement or recommendation for use.

Benthic habitats and biological resources off the Virginia coast 1996 and 1997

Introduction

The issues of coastline protection have become increasingly critical as erosion and coastal sediment transport have significantly altered or even eliminated ecologically and recreationally important coastal habitats. Increased public use of beaches, development of coastal lands, and preservation of the limited and sensitive coastal ecosystems have all lead to the need for beach nourishment as a means of stabilization and protection. The sand resources suitable for economical beach nourishment are usually located in the near shore coastal zones adjacent to the project areas. However, ongoing and planned beach nourishment activities along the coast of Virginia required sands from federal waters beyond the three mile line. The U. S. Mineral Management Service controls these sand resources and formed Cooperative Agreement (# 14-35-001-30807), "Environmental Studies Relative to Potential Sand Mining in the Vicinity of the City of Virginia Beach, Virginia" with the Virginia Institute of Marine Science and Old Dominion University in order to assess impacts of sandmining. Task 1 of this Cooperative Agreement ("Benthic Habitat Mapping and Evaluation of Existing Benthic Resources") involved benthic surveys of the region conducted by V. I. M. S. using sediment profile imaging and bottom grab samples.

Environmental concerns which arise in connection with proposals to excavate or mine sand from those areas identified as suitable for beach nourishment focus on potential ecological impacts associated either directly or indirectly with:

1. Removal or dredging of the sand from near coastal areas

2. Placement of the sand on the beach.

The configuration and location of the borrow site and the methods of handling the dredged material can be an important determinant in the level of impact. The level of potential impact would vary as a function of the characteristics of the material to be dredged, the exposure to currents and wave action, and the benthic resources (Thompson, 1973; Tuberville and March 1982; Hobbs, et al. 1985; Schaffner and Hobbs, 1992). Of the two geographic areas of concern associated with any beach-nourishment project, the source or borrow area and the beach area being nourished, we are focusing on the offshore source or borrow sites. In particular, the three sites off of Virginia Beach (Fig. 1) that will be used to nourish Virginia coastal beaches will be studied as a model project for evaluating environmental concerns.

Benthic habitats and non-commercial biological communities offshore Virginia were surveyed 1996 and 1997 in the vicinity of potential sandmining activities, where borrow areas had been identified and in regions of possible future interest . Benthic surveys were conducted semi-annually, during which sediment profile imaging (SPI) and standard bottom photographic camera systems and Smith-MacIntyre grabs were deployed.

SPI and standard photographs allow relatively rapid determination and assessment of benthic habitat characteristics and capability for broad areal sampling coverage. Grabs allow detailed determination of benthic biological community characteristics. Together, SPI and grab sampling provide complementary data which are capable of forming the basis for resource maps. Grab data may serve as the basis for confirming inferences made about biological and physical habitat characteristics using SPI data, and SPI data may be used to

produce habitat coverage maps which should represent the potential limits of biological community manifestations.

SPI and grab data allow mapping of substrate types, biological community characteristics and functional aspects of the communities, delineation of habitat spaces, and determination of spatial heterogeneity of habitats and resources (Bonsdorff et al., 1996). Spatial and temporal patterns of habitats and community characteristics and the local and regional water flow patterns determine benthic community response to disturbance events such as sandmining, and therefore are important to the activities proposed off Virginia. This study provides determinations of benthic habitat types, spatial extent of substrate properties and habitats, benthic secondary production and biological community characteristics off the Virginia coast in and around areas where sandmining is proposed.

Study Area

The study area offshore Virginia extended from just inside the three-mile line to approximately 10 miles offshore, and from the latitude of the southern shore of Chesapeake Bay mouth (36.925° N) to a few miles south of Sandbridge, VA (36.675° N) (**Figures** 1 and 2). Within this broad region, smaller regions of interest were sampled at higher spatial densities during spring and fall 1996 and fall 1997 (**Figure** 2). Spring and fall 1996 sampling was done using three sample grids, one off Virginia Beach (northwest grid), one to the northeast of that (northeast grid) off the Chesapeake Bay mouth, and one off Sandbridge (southern or Sandbridge grid) (**Figure** 3: SPI, and **Figures** 4- 5: grab). The entire region was sampled at lower spatial density during the spring 1997 deployment. The 1996 study areas covered approximately 30 NM^2, the spring 1997 study area covered approximately 60 NM^2, and the fall 1997 study area covered approximately 10 NM^2. The fall 1997 deployment involved a very high density sample coverage in the vicinity of Sandbridge shoal and the proposed borrow areas (**Table** 1).

Previous descriptions of the study region include geological and geotechnical descriptions of the Virginia inner continental shelf have been done by Williams (1987) Berquist and Hobbs (1988); Kimball and Dame (1989); and biological descriptions by Ranasinghe, et al. (1985), and Dauer (1981). The study areas generally encompassed various sand substrates typical of the inner continental shelf, and substrates composed of finer grain-size materials delivered to the shelf by the Chesapeake Bay excurrent plume.

Methods

Sediment Profile Imagery (SPI) and Smith-MacIntyre grabs sampling

Spatial mapping of benthic habitats was accomplished using sediment profile imaging and standard bottom photography. Three different spatial supports for the data were utilized. During 1996, three study grids were defined and divided into cells which were approximately 0.2 NM on a side. One grid extended offshore Virginia Beach and Dam Neck and was composed of 200 cells (numbered 1 - 200), one grid composed of 100 cells was located to the northeast of the Virginia Beach grid, and cells were numbered 201 - 300, and one grid was located offshore Sandbridge, in the vicinity of Sandbridge shoal and was composed of 100 cells (numbered 301 - 400) (**Figures** 3 - 4). The prefix 96 was prepended to station numbers from 1996 (96001 - 96400) for presentation of the SPI data to provide consistency with the spring 1997 sample labels (**Figures** 3 - 5, and **Table** 1). Cells called 1 - 400 from spring and fall 1996 are synonymous with cells 96001 - 96400. Although it was unfeasible to revisit the exact point sampled upon subsequent sampling, revisited sample site numbers were maintained and positions recorded. Standard deviations of positions between seasons or years at a given sample site typically were on the order of 0.0005 degree latitude or longitude.

Grids were located in regions where sandmining activities were either planned (Sandbridge shoal area) or likely because of nearby localities (Virginia Beach, VA). Grids were composed of regularly spaced cell rows whose nearshore boundaries paralleled the Virginia Coast. Ten cells were defined for each cell row west to east across each 1996 grid. Because of the shape and arrangement of the grids, 1996 SPI samples were separated

east to west neighbor by approximately 0.4 NM, northwest to southeast neighbor by approximately 0.25 NM, and northeast to southwest neighbor by approximately 0.2 NM.

The spring 1996 sampling cruise began May 14, 1996 upon the R/V Bay Eagle (V.I.M.S) and was halted by weather May 15, 1996. Completion of the spring 1996 sampling effort occurred aboard the R/V Bay Eagle (V.I.M.S), June 4 - 7, 1996. The fall 1996 cruise began October 21-22 aboard the R/V Langley (V.I.M.S) and November 4 - 6, 1996 aboard the R/V Bay Eagle.

A broadly spaced sample coverage was implemented for the spring 1997 deployment. A single staggered grid extending from Cape Henry to south of Sandbridge, Virginia was divided into grid cells measuring 1 NM per side. SPI samples were taken at each grid cell centroid (**Figure** 6), and grab samples were taken at a random subset of the stations, in addition to revisited locations sampled 1996 (**Figure** 7). Several stations from the 1996 survey were revisited during the spring 1997 deployment, and SPI and grab samples were taken. The spring 1997 cruise occurred June 16 - 19, 1997 aboard the R/V Bay Eagle.

Fall 1997 sampling was concentrated on the proposed borrow areas in the vicinity of Sandbridge shoal. Borrow Areas A to the south and B to the north coincided with the crest of Sandbridge shoal (**Figure** 8). SPI samples were taken at six stations from eight north to south transects crossing or nearby Borrow Area A, and from several points along three transects which crossed into Borrow Area B perpendicular to each of the sides defining B (**Figure** 9). Grab samples were taken at a random subset of the stations, in addition to revisited locations sampled 1996 and spring 1997 (**Figure** 10). Fall 1997 sampling occurred October 6 and 7, 1997 aboard the R/V Bay Eagle. **Table** 1 lists all

positions (in decimal degrees latitude and longitude) occupied during sampling and the type of sample acquired during the two year study, and **Table** 2 lists coordinates for the corners of the proposed borrow areas off Sandbridge. All samples taken in the vicinity of the proposed borrow areas 1996 and 1997 are labeled, along with the boundaries of the borrow areas, in **Figure** 11.

SPI samples were taken at points defining by the centroids of grid cells. SPI samples were taken at every other cell centroid point and were staggered from row to row, odd numbered cells visited one row, even numbered cells the next. At each station (grid cell centroid), the SPI camera system was deployed twice. If there was uncertainty about camera function or success, additional drops were made. During the spring 1996 cruise a Benthos model 3731 sediment profiling camera was used until it malfunctioned. From then on and throughout the next three cruises, a Hulcher model Minnie sediment profiling camera was used attached to a Benthos stainless steel frame. After deployment, depth of prism penetration and frame count was recorded. Camera tests were done periodically to ensure proper function. 350 pounds of lead and steel were used to weight the camera prism during May 14 and 15, and 450 pounds of lead and steel were used for all of the subsequent deployments. Color slide film (Fujichrome 100 professional) was used in the cameras.

Smith-MacIntyre grabs were taken from randomly selected cells from each grid, following a stratified random sampling design. 150 pounds of lead were used to weight the grab in order to produce consistently deep bites into the bottom. Grabs were only accepted if over half the volume of the grab was filled with sediment and the sediment surface was preserved intact. Grab success rate was high, confounded only when large

gravel or intact shells wedged the grab jaws open. The sediment surface of these inner shelf sands and muds was preserved very well by the grab.

The top millimeter of sediment in grab samples from spring and fall 1996 were scraped off using a flat blade, and stained and refrigerated for analysis of living foraminifera and ostracoda (Cronin, et al. 1998). Subcores (circular 10 cm diameter and 10 to 15 cm deep) were also taken from 1996 grab samples, and preserved in formalin for later analysis of meiofaunal and macrofaunal communities. The rest of the volume from 1996 grab samples and all the volume from 1997 grab samples were washed upon 500 μm sieves aboard the vessel just after they were collected. Residue upon each sieve was stored in a cloth bag and preserved in 10% formalin solution and contained in 5 gal. buckets for transport to the laboratory.

Laboratory processing and analyses

Sediment profile images were analyzed by visual counts and measures of sedimentary and biogenic features in images projected upon a calibrated grid. Measurements were made of SPI prism penetration depth (PEN), average depth of the apparent color redox potential discontinuity (RPD), sediment surface relief (Sed. Rel.), relief type, sediment type, epifaunal presence and type, presence of tubes at the sediment-water interface, amount of biogenic shell material present; number, type and depth of infauna visible; number, depth and type of water filled infaunal feeding voids present (whether surrounded by anoxic or oxidized sediments); number and depth of gas voids present; and number and type of infaunal burrow structures present (**Tables** 3 - 6). Notes were also made concerning any unusual features encountered during SPI analysis. Details

on analyses and more extensive description of SPI parameters may be found in Rhoads and Germano (1982) and in Diaz and Schaffner (1988).

SPI parameter determination and delineation of habitats have been shown effective and comparable to sediment core sample data habitat delineation (Bonsdorff, et al., 1996) when samples have come from widely varying habitats and distinct geomorphic regions. Mapping the individual SPI parameters as well as biological community characteristics and production for this study was done for the inner shelf, allowing comparisons of SPI - grab delineation capabilities within a relatively uniform geomorphologic region. For habitat mapping, SPI feature types were designated biological or physical if features from either origin composed most of the SPI image. If both feature types were present in approximately equal amounts, feature type was designated combination.

In the laboratory, grab samples were processed to obtain secondary production estimates and organismal densities and biomasses. Organisms were sorted into major taxa and enumerated. Samples which retained a large amount of sand which would not pass through 500 μm sieves were elutriated and the organisms then extracted for sorting. Processing for secondary production calculations involved resieving the sorted taxa through a series of sieve sizes (6.3, 3.35, 2.0, 1.0, and 0.5 mm), then counting and weighing the organisms in each size fraction. Counts and biomass were converted to m^{-2} by multiplying by 11.1.

Production was calculated using the technique described in Brey (1990). Total wet weight per sample taxa per size class was converted to mean individual weight per

size class using the number of individuals counted. Wet weights were converted to ash-free dry weights (AFDW) using the conversion factor of Waters (1977):

AFDW (g) = Wet Weight (g) * 0.152.

Combined weights from all size classes allowed determination of biomass and production for each taxa per sample. Mean individual weight and total biomass per square meter for each major taxa and size fraction allowed estimation of secondary production using the multiple regression models of Brey (1990) including different coefficients for each taxa. When very small biomasses were present, production estimates were unrealistically high due to the limited range for which Brey's (1990) model applies. Therefore if mean annual biomass was estimated to be less than 0.02 g m^2, the value was excluded and production was not calculated for that observation. Production estimates reported are from 1996. Calculation of production for 1997 is in progress.

Maps

Maps representative of SPI parameters, habitat types, and biological densities and secondary production estimates were produced using the SPI and grab data. For each parameter mapped, the legends are consistent between maps from different sample dates, easing comparison. Interpolation and contouring of SPI and grab data was done by an inverse distance weighted (IDW) squared, nearest 12 neighbor method using Arcview for Windows NT. For habitat maps, the IDW squared method was used, but with only one neighbor to prevent generation of apparent intermediate habitat classes by interpolation.

Results

SPI analysis

SPI analyses data for spring and fall 1996 and spring and fall 1997 sampling efforts are presented in **Tables** 3 to 6. Maps constructed using these data are addressed hereon. While most parameters for 1997 were not plotted as maps, the data are available in **Tables** 5 and 6. SPI prism penetration patterns were similar between the seasons and years. Deepest penetration depths occurred in the northwestern part of the study area. Shallowest penetrations occurred in the northeastern part of the study area. Patches of shallow penetration were observed in the vicinity of Sandbridge shoal, and patches of deep penetration were observed just to the east and west of the shoal (**Figure**s 12 - 14). Spring 1996 SPI prism penetration depth ranged from < 5 to > 20 cm. Deepest penetrations (>10 to 20 cm) in the spring of 1996 were in the northwest portion of the study area (**Figure** 12). Fall 1996 penetration was also deepest in the northwest part of the study region, some exceeding 20 cm (**Figure** 13), and also in parts of the study area off Sandbridge. Spring 1997 sampling revealed a similar pattern, with deep penetration in the northwest, shallow penetration in the northeast, and patches of deep and shallow penetration off Sandbridge (**Figure** 14). SPI prism penetration within the proposed borrow areas ranged was generally within the 5 to 10 cm range (**Figure**s 13 and 14).

Sediment-water interface (SWI) relief (surface relief) ranged from < 1 to 10 cm from spring 1996 through spring 1997 (**Figure**s 15 - 17). Lowest relief (smoothest surfaces) was observed in the study area off Sandbridge, just inshore from Sandbridge shoal and the proposed borrow areas, and in the northeastern part of the study area, as well as in patches within the study region off Virginia Beach. Highest sediment-water

interface relief was observed in the northwest portion of the study area and off Sandbridge within borrow area A (**Figure** 16). Most of the images in the study area from spring and fall 1996 and spring 1997 revealed SWI relief of 1 to 2 cm. The area between the northwest and northeast parts of the 1996 study area was interpolated to have relief from 1 to 2 cm using spring 1996 data, and 2 to 4 cm using fall 1996 data (**Figure**s 15 - 16). The points sampled spring 1996 and 1997 within this zone revealed lower relief (< 1 cm) suggesting that the high relief observed from cell 281 fall 1996 was a temporary artifact.

The apparent color redox potential discontinuity (RPD) layer depth ranged from < 1 to > 10 cm during spring and fall 1996 (**Figure**s 18 - 19). RPD depth measurements from 1997 samples has not yet been completed. Spring 1996 sampling revealed a large area off Virginia Beach and a point within borrow area B with RPD depths of 5 to 10 cm. In the northeastern part of the study area, RPD depths were nearly all between 1 to 3 cm. Shallowest RPD depths were observed off Sandbridge, just inshore of Sandbridge shoal and the proposed borrow areas (**Figure** 18). Fall 1996 sampling revealed slightly lower RPD depths in the northwestern part of the study area, off Virginia Beach, and similar RPD depths in the northeast. RPD depths in the study area off Sandbridge were deepest fall 1996, most between 5 to 10 cm and one > 10 cm (**Figure** 19).

Infaunal tubes were present in many of the SPI images during spring 1996, with highest numbers of tubes in the northwestern part of the study area (> 25), and very few in most of the northeastern-most part of the study area (**Figure** 20), except at a few stations where there were high numbers (10 to 25). Spring 1997 SPI images revealed lower numbers of tubes over most of the study area. Most of the images had no tubes visible at the sediment-water interface (**Figure** 21). There were some tubes visible in images from

the northwestern part of the 1997 study area, as seen also in spring 1996. However, the high numbers observed in the northwestern part of the 1996 study area were not apparent in spring 1997 images. The absence of tubes in numbers > 25 per SPI image from spring 1997 may indicate changes in community composition or limited spatial patches dominated by tube-dwelling infauna, perhaps not as extensive in coverage as suggested by the interpolation displayed in **Figure** 20. Most of the tube building infauna were polychaetes, from the families Maldanidae (*Clymenella, Asychis, Euclymene, Maldanopsis*), Ampharetidae (*Asabellides oculata*), or Onuphidae (*Diopatra cuprea*). Species were confirmed by grab samples, but tube structures were usually distinct enough to discern tube types in SPI images. Grab samples produced many other species as well which were not detected in SPI images (See section on grab sample analysis below).

Sediment types in the study region were primarily sands from -1 to 4 phi, but some muds (4 to 8 phi) were also present. Muds were prevalent in the northwestern part of the study area and in patches across the region (**Figure** 22). The muds were typically silt to clayey silt, and sands ranged from very fine sands to coarse sands and granule (**Figure** 23). Fine sands (2 to 3 phi) were most common throughout the study area. The spring 1997 sampling grid did not encounter as many silty sediment patches as the 1996 sampling. Sediment grain size and alkalinity determined from spring 1997 grab samples are listed in **Table** 7.

Habitats classifications from SPI images

The variety of sediment types and habitat types were apparent in images from spring and fall 1996 when more dense sampling grids were employed. Nine gross habitat

classes were identified from a set of sixteen habitats initially identified using 1996 SPI images. Habitat classes were labeled A - I, and are summarized in **Table** 8. SPI images representative of the nine habitat types are displayed in **Figure**s 24 - 32. Habitat determinations from 1997 data are not yet complete. Habitat maps made using the nine habitat type classes reveal the diversity of bottom types across the study area encountered spring 1996 (**Figure** 33) and fall 1996 (**Figure** 34).

Seven of the habitat types were identified in SPI images from spring 1996. The most common and extensive habitat types spring and fall 1996 were (class C) silty-sand to very fine sand sediments with both biological and physical characteristics, and (class D) fine sand sediments with primarily physical features (**Figure** 26). Overall, across the entire study region, 73 of the 157 cells from which determinations were made using SPI images from spring 1996 were habitat class C, and 31 were class D. Eight of the nine habitat types were identified from fall 1996 SPI images. For the entire study region, 100 of 191 cells revealed habitat class C, 39 were class D, and 28 were class F (**Table** 9). The entire grid block in the northeastern part of the study area (cells 96201 - 96300) was found to have only habitat class C (combined biological and physical fine sands) spring and fall 1996 (**Figures** 33 - 34).

Biologically dominated silts (class A) and fine sands (class E) were also present across much of the study area, though slightly fewer during fall 1996 sampling than spring 1996. Physically dominated silt sediment habitats (class B) were present only during fall 1996 at three stations off Virginia Beach. Physically dominated medium sand and shell sediments (class F) were present most in the study area off Sandbridge, and were more extensive fall 1996. Biologically dominated medium sand and shell sediment habitats

(class G) were apparent at some of the sample stations off Sandbridge, just outside the proposed borrow areas, and also at several stations in the study area off Virginia Beach. Physically dominated coarse sands to gravel sediments (class H) were encountered only off Sandbridge, just inshore of the proposed borrow areas spring and fall 1996, and at one station off Virginia Beach spring 1996. Apparently transitional substrates, composed of coarser grain-size sediments layered over finer grain-size sediments (class I) were encountered fall 1997 at three stations off Virginia Beach, and at one station off Sandbridge (**Figure**s 33 - 34).

Grouping the habitats in terms of dominance by biological or physical features, or combined interaction of biological and physical features, without respect to sediment type reveals broad and apparently continuous regions of either physically or biologically dominated substrates spring 1996 (**Figure** 35). During spring 1996, biologically dominated habitats were prevalent in the northwestern part of the study area off Virginia Beach, physically dominated habitats are prevalent in the vicinity of the proposed borrow areas off Sandbridge, and combination habitats were interspersed in those two regions and ubiquitous in the northeastern part of the study area (**Figure** 35). Similarly, fall 1996 SPI images revealed biologically dominated habitats in the northwest part of the study area and in the study area off Sandbridge, however in apparently non-continuous, smaller patches than during spring 1996 (**Figure** 36). Habitats with combined biological and physical interaction were present in the study areas off Virginia Beach and Sandbridge and pervasive across the northeastern grid. **Table** 10 lists positions, cell numbers and habitat classifications.

Of the seven habitat types identified using SPI images in the northwest sample grid off Virginia Beach spring and fall 1996, four were biologically dominated or combination biological/physical substrates, and three were biologically dominated or combination during fall 1996. In the northeastern sample grid 1996, only one habitat type was identified during spring or fall, and that had combination biological and physical features. In the sample grid off Sandbridge, five habitats were identified spring 1996, and of those two were biologically dominated or combination. Similarly, in fall 1996, in the sample grid off Sandbridge, two of seven habitats identified were biologically dominated or combination.

Secondary production

Total benthic secondary production calculated using the technique of Brey (1990) ranged from < 1 g m^{-2} yr^{-1} to > 50 g m^{-2} yr^{-1} (**Figure** 37). Low (< 5 g m^{-2} yr^{-1}) to high (> 25 g m^{-2} yr^{-1}) production was observed in the northwestern part of the 1996 study area off Virginia Beach. Low to moderate (5 to 25 g m^{-2} yr^{-1}) production was found in the northeastern sample grid and in the study area off Sandbridge in the vicinity of the proposed borrow areas. The high total production values correspond to high combined production by molluscs (**Figure** 38), and annelids (**Figure** 39), and to a lesser degree by crustaceans (**Figure** 40). Mollusc production was high at one site in the northwestern sample grid off Virginia Beach, and low to moderate throughout the rest of the study area (**Figure** 38). Annelid production was high at a site just west of where mollusc production was highest, in the central part of the northwestern sample grid off Virginia Beach, and was low to moderate elsewhere (**Figure** 39). Crustacean production was low throughout

the study area , but relatively higher in the northwest sample grid and at one site in the study area off Sandbridge, within proposed borrow area B (**Figure** 40). Miscellaneous taxa, composed primarily of echinoderms and cnidarians, had very low production across the area. However, some patches of relatively higher production by miscellaneous taxa corresponded with higher production by molluscs, annelids and crustaceans (**Figure** 41).

Sandbridge study area analysis, including proposed borrow areas

Habitat types in the study area off Sandbridge were mostly physically dominated fine to medium sands along Sandbridge shoal crest in spring 1996 (**Figure** 42) and combination biological-physical silty sands or biologically dominated silts around the shoal. Habitats were similarly distributed fall 1996 (**Figure** 43) but slightly fewer biologically dominated muds were encountered, one sample revealed silt in part of borrow area A. Another site had sediments which had apparently undergone recent transition, with a coarser grain-size sediment layer overlain upon clayey silt (**Figure** 43). Both spring and fall 1996 SPI images reveal primarily physically dominated habitats throughout most of borrow area B, and approximately half of borrow area A (**Figures** 44 - 45). Biologically moderated habitats were found to the west (inshore), east, and south of the proposed borrow area (**Figures** 44 - 45).

Total community secondary production from 1996 within the study area off Sandbridge was low to moderate, and relatively highest in at one site near the southern boundary of borrow area A and to the west of borrow area A (**Figure** 46 with cell numbers labelled, and **Figure** 47). Production by molluscs was very low to low throughout the study area off Sandbridge, except at a station to the west where

production was moderate (**Figure** 48). Polychaete production in the study area off Sandbridge was very low to low. Lowest polychaete production was found in borrow area B (**Figure** 49). Crustacean production was very low (< 1 g m^{-2} yr^{-1}) at all except three stations where production was low (1 - 5 g m^{-2} yr^{-1}) in the study area off Sandbridge, 1996 (**Figure** 50).

Total infaunal densities ranged from < 100 to > 2000 m^{-2} in the study area off Sandbridge. Highest overall densities (> 2000 m^{-2}) were found to the west and in the center of borrow area B (**Figure** 51). Lowest overall densities were observed in samples taken just to the south and west of the sample with high density in the center of borrow area B. Molluscs were found in highest densities at one cell to the west of the proposed borrow areas,. and were found in higher densities inshore of the borrow areas within the study area off Sandbridge (**Figure** 52). Polychaete densities were high inshore of the proposed borrow areas and at one cell in the center of borrow area B and one cell to the east of borrow area A (**Figure** 53). Crustacean densities in the study area off Sandbridge, 1996 were relatively high (> 1000 m^{-2}) in borrow area B, and low to moderate elsewhere (**Figure** 54). Comparisons of apparent general habitat type determined using SPI to benthic secondary production (**Figure** 55) and faunal densities (**Figure** 56) reveal that total community production and densities for all taxa agree fairly well with the habitat delineations made using SPI.

Grab sample analysis

Benthic Community Species Composition

At total of 119 taxa were identified from 13 of the Smith-MacIntrye grabs collected in 1996 (**Tables** 11 - 12). Half of the top 14 taxa in terms of occurance and abundance were polychaetes. The other half were one representitive each from the amphiods, decapods, bivalves, nemerteans, tanaids, echniderms, and chordates (**Table** 13). The distribution of species among the taxa was similar to other benthic studies from the region. **Table** 14 compares our study to that of Dauer (1981). While Dauer's data are for about 3.5 times as much bottom area as ours, the total numbers of species from both studies are close. Dauer's (1981) survey of the benthos at the proposed Norfolk District COE open water disposal site, about 15 miles East of the entrance to Chesapeake Bay is the closest historical data set to our study area. The Dauer study was at the same latitude as the northernmost extent of our study area, and about 8 miles to the east, but was at similar sediment types and depths.

Overall, the community composition within our study area was typical for sandy shallow continental shelf habitats. Detailed studies by Boesch (1979) off the coasts of New Jersey and Maryland, Maurer et al. (1976) off Delaware, and Day et al. (1971) off North Carolina reported simialar species composition for similiar depths and sediment types. While there were many differences in the species composition, several species and taxa were consistently reported by these studies, such as, *Spiophanes bombyx*, various *Nephtys* species, *Tellina agilis*, *Magelona rosea*, *Aricidea* spp., *Spio setosa*, *Nassarius trivittatus*, *Ampelicsa verrilli*, *Unciola irrorata*, and *Mellita quinquiesperforata*. All of these are know to be high salinity sand species.

Benthic Community Size Spectra

The size distribution of the benthos, both biomass and number of individuals, is an important factor in determining the potential food resources available to bottom feeding fish and crabs (Diaz and Schaffner 1990, Edgar 1990) and was the data used in calculation of secondary production. Size spectra of the benthos (Class intervals of 0.5 to 0.9, 1.0 to 1.9, 2.0 to 3.3, >6.3 mm) were determined from the grab samples and followed a pattern typical for marine communities, where the highest biomass was in the larger size classes and highest number of individuals was in the smaller size classses (**Figures** 57 - 58). Overall for June and November 1996 data, 15 % of all individuals and 81 % of the wet weight biomass were in the larger biomass size fractions, 3.35 and 6.3 mm size classes. The taxonomic composition of the larger biomass size fractions spanned a broad range with only the total biomass of anemones and amphipods being less than 50 % in the larger size fractions (**Table** 15). In terms of numbers, only echinoderms, bivalves, and chordates had 50 % or greater of their total abundance in the larger size fractions (**Table** 15).

Overall, total biomass about doubled between June to November, going from 4.1 to 7.7 g wet wt m^2 (**Table** 16). Annelids, the dominant taxonomic group in biomass, numbers and trophically, are typical of this trend and averaged about 13 g wet wt m^2 in June and 28 in November. The modal biomass size fraction for annelids in both June and November was 3.35 mm. Maldanid and Nephtid polychaetes were the predominant families that accounted for most of the 3.35 mm size fraction biomass.

Total abundance declined from June to November being 2350 and 1850 ind. m2, respectively. Again, annelids were typical of this trend declining from 960 to 910 ind. m2 with the modal size fraction being 1.0 mm (**Table** 16). This increase in biomass and

decline in abundance are likely due to post settlement seasonal growth and mortality of macrofauna.

Discussion

Deep SPI prism penetrations in the northwestern portion of the study area coincided with the Chesapeake Bay plume deposits, composed of finer grain-size sediments. Deep prism penetration in other parts of the study area appeared to coincide with the depositional environments induced by large-scale bottom features such as Sandbridge shoal. The shoal consisted of coarsest sediments along the crest and was surrounded by a rim or at least patches of finer sediments, silts to clayey silts. Biological activity and numbers of macro-infaunal organisms and structures were high in these finer sediments, as apparent in the sediment profile images (**Figure** 45) and in the grab samples (**Figure** 51).

Relief was generally caused by sediment bedforms, primarily smooth-crested wave-orbital ripples. Bedform heights were observed to be 1 to 2 cm and as demonstrated by the surface relief, or SWI relief, measurements. Larger bedforms were observed in the study area off Sandbridge, within borrow area A, and in the northern part of the study region off Virginia Beach.

Habitat mapping using SPI and sediment grab sampling was very effective for covering large regions such as the study areas off Virginia Beach. Relative resource evaluations would then be made using parameters measured from SPI and grab samples. This is in contrast to indices, such as the organism-sediment index (OSI) (Rhoads and Germano 1982) which includes only certain SPI data, and benthic index of biotic integrity (B-IBI) (Weisberg, et al. 1997) derived only from grab data. Such indices are of questionable value for assessing resources over broad areas. The OSI, for instance, relies upon the RPD depth without considering the sediment type or grain size. RPD depth,

however, may be influenced significantly by grain size. Thus OSI may be useful for comparing habitat properties within a relatively uniform sedimentary environment, but for comparison across sediment type regions, it is confounded by not accounting for collinearities in habitat parameters. Thus, interpretation of the SPI and grab data is necessary to provide a habitat resource value assessment, unless a new index is developed, or one is modified, which accounts for inter-regional parameter behavior.

Using only two parameters determined from SPI analysis, a rapid assessment of gross habitat type can be made. Using just an assessment of sediment grain size class (coarse to very fine sand, coarse to fine silt, and clay, and mixtures) and determination of prevalence of biological features or physical structures provides a simple method for initial delineation of benthic habitats. These may be further refined by determination of dominant fauna or surficial geological characteristics, both available using SPI data or inferences about features present in SPI images confirmed by grab data.

Benthic secondary production for 1996 was high (> 25 g m^{-2} yr^{-1}) in the northern portion of the northwest sample grid off Virginia Beach and low (< 5 g m^{-2} yr^{-1}) to moderate (5 - 25 g m^{-2} yr^{-1}) throughout the rest of the study area (**Figure** 37). In the northwest sample grid, off Virginia Beach, the high production calculated using grab sample data corresponded to regions which were identified using SPI images as biologically dominated fine sand during spring 1996 (**Figure** 33), but as physically dominated fine sand fall 1996 (**Figure** 34). Habitats were identified as physically dominated at some locations using SPI images, but relatively high production was found using grab data. In some sediments, especially non-cohesive sands, biological features may not persist, and fauna may be inconspicuous.

Therefore, dependent upon substrate characteristics, more or less effort with the different sampling techniques may be necessary. Accurate habitat mapping then may require initial reconaissance and subsequent allocation of sampling effort. Some habitat determinations using SPI may not have agreed with observed high or low production or biological densities because of small spatial-scale variabilities since grabs were not necessarily acquired on the exact spot where images were taken. General agreement is good between the two sampling techniques for gross characterizations of habitat and for biological resource assessment. The agreement between the interpolations made using SPI and grab sampling is encouraging, especially considering that each was done upon a different support, the sample spatial structure.

Discriminant analysis using SPI and grab data should reveal whether the habitat determinations convey objective discretions. Evaluation of the pertinence of the 1996 determinations will be used to delineate habitats using 1997 data. In general, if SPI can be used to reliably relate habitat characteristics which allow prediction of benthic community attributes, then statistical spatial models may be constructed for habitats and resources with efficiency. Refined SPI and grab sampling strategies may accomplish regional benthic resource assessment and mapping with a reasonable effort.

Where persistence of SPI features would be confounded by lack of sediment cohesivity, we expect that habitat delineations will underestimate community attribute variability. However, SPI and grab data and maps for the region off the Virginia coast elucidate an overall more complex benthic system than was expected based upon the generalized descriptions of previous studies for the inner continental shelf off Virginia.

References

Berquist, C. R. Jr., and C. H. Hobbs. 1988. Study of economic heavy minerals of the Virginia inner continental shelf. Virginia Division of Mineral Resources Open File Report 88-4, 149 pp.

Boesch, D.F. 1979. Benthic ecological studies: macrobenthos. Special Rpt. Appl. Mar. Sci. Ocean Engin. No. 194, Virginia Institute of Marine Science. 301 pp.

Bonsdorff, E., R. J. Diaz, R. Rosenberg, A. Norkko, and G. R. Cutter Jr. 1996. Characterization of soft-bottom benthic habitats of the Aland Islands, northern Baltic Sea. Mar. Ecol. Prog. Ser., 142, 235-245.

Brey, T. 1990. Estimating productivity of macrobenthic invertebrates from biomass and mean individual weight. Meeresforsch. 32: 329-343.

Cronin, T. M., S. Ishman, R. Wagner, and G. R. Cutter, Jr. 1998. Benthic foraminifera and osctracoda from Virginia Continental Shelf. Final Report to the Minerals Management Service, Office of International Activities and Marine Minerals Agreement No. 14-35-0001-30807.

Day, J.H., J.G. Field and M.P. Mongomery. 1971. The use of numerical methods to determine the distribution of the benthic fuana across the continental shelf of North Carolina. J. Anim. Ecol. 40:93-125.

Diaz, R. J., and L. C. Schaffner. 1988. Comparison of sediment landscapes in Chesapeake Bay as seen by surface and profile imaging; in: Understanding the estuary: Advances in Chesapeake Bay research. Proceedings of a conference. 29-31 March 1988. Baltimore Maryland. Chesapeake Research Consortium Publication 129. CBP/TRS 24/88.

Diaz, R.J. and L.C. Schaffner. 1990. The functional role of estuarine benthos. p. 25-56. In: M. Haire and E.C. Krome (eds.). Perspectives on the Chesapeake Bay, 1990. Advances in estuarine sciences. Chesapeake Research Consortium, Gloucester Pt., Virginia. Rpt. No. CBP/TRS41/90.

Dauer, D.M. 1981. Benthic monitoring of the Norfolk disoposal site. Appendix A, Chapter III, An assessment of the ecological impact of open ocean disposal of materials dredged from a highly industrialized estuary. Old Dominion University, Final EIS Norfolk Disposal Site, to the Norfolk District COE. pp. A21-A147.

Edgar, G. J. 1990. The use of the size structure of benthic macrofaunal communities to estimate faunal biomass and secondary production. J. Exp. Mar. Biol. Ecol. 137: 195-214.

Kimball, S, and J. K. Dame. 1989. Geotechnical evaluation of sand resources on the inner shelf of southern Virginia. Final report to the City of Virginia Beach. Two volumes. Virginia Institute of Marine Science, Gloucester Point, Virginia.

Maurer, D., P. Kinner, W. Leatham, and L. Watling. 1976. Benthic faunal assemblages off the Delaware peninsula. Est. Coast. Mar. Sci. 4:163-177.

Ranasinghe, J. A, W. T. Harlan, and D. M. Dauer. 1985. Macrobenthic communities of the Dam Neck disposal site. Old Dominion University Final Report for the Department of the Army, Norfolk district, Corps of Engineers, Norfolk, Virginia.

Rhoads, D.C., and J. D. Germano. 1982. Characterization of organism-sediment relations using sediment profile imaging: an efficient method of remote ecological monitoring of the seafloor (Remots(Trademark) system). Mar. Ecol. Prog. Ser., 8, 115-128.

Waters, T.F. 1977. Secondary production in inland waters. Adv. Ecol. Res. 14:91-164.

Weisberg, S.B., J.A. Ranasinghe, D.M. Dauer, L.C. Schaffner, R.J. Diaz and J.B. Frithsen. 1997. An estuarine benthic index of biotic integrity (B-IBI) for Chesapeake Bay. Estuaries 20:149-158.

Williams, S. J. 1987. Geologic framework and sand resources of the Quaternary deposits offshore Virginia, Cape Henry to Virginia Beach. U.S.G.S. Open File Report 87-667, 60 pp.

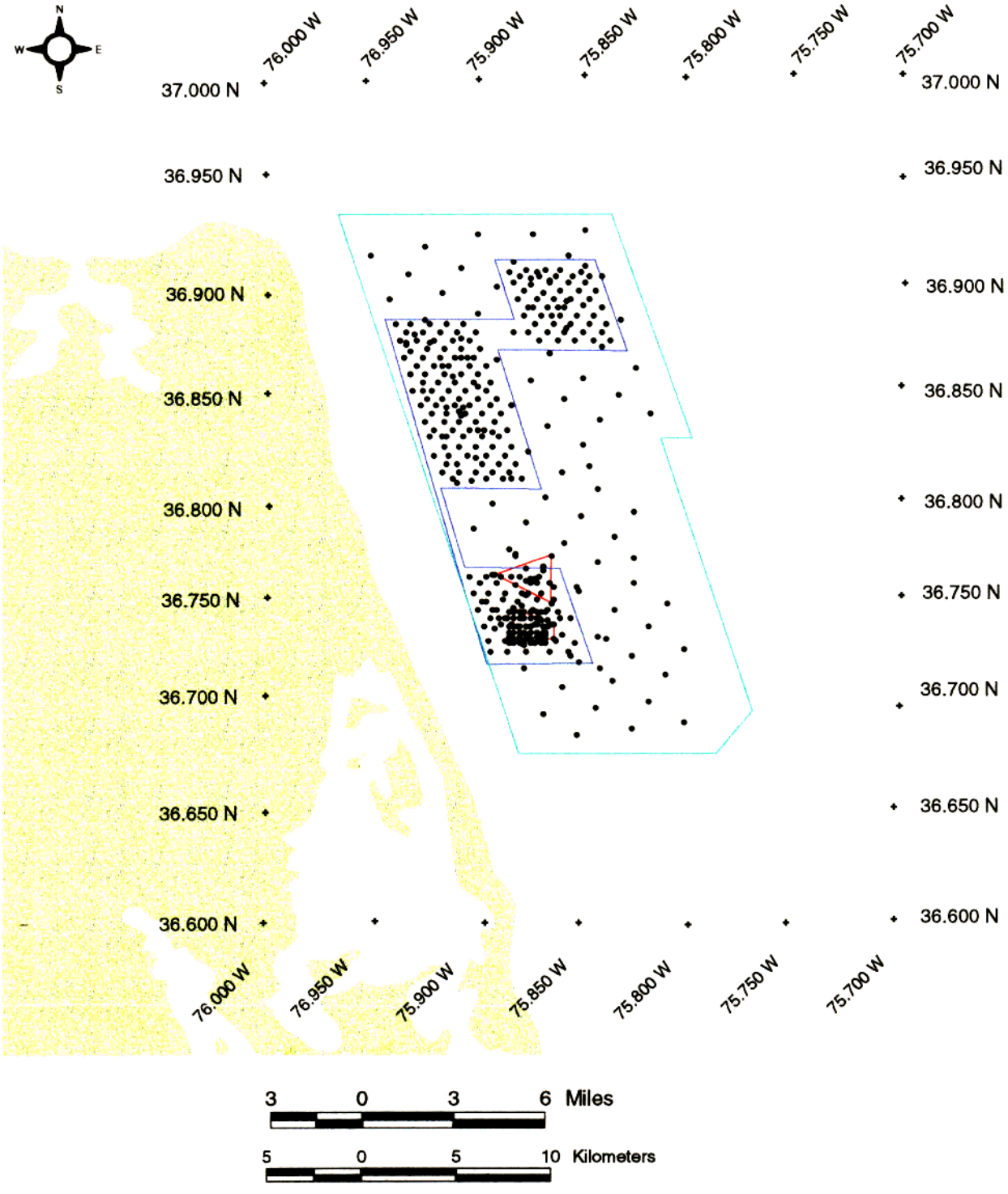

Figure 1. Benthic survey study areas off Virginia Beach 1996 and 1997 with reference grid listing latitude and longitude in decimal degrees.

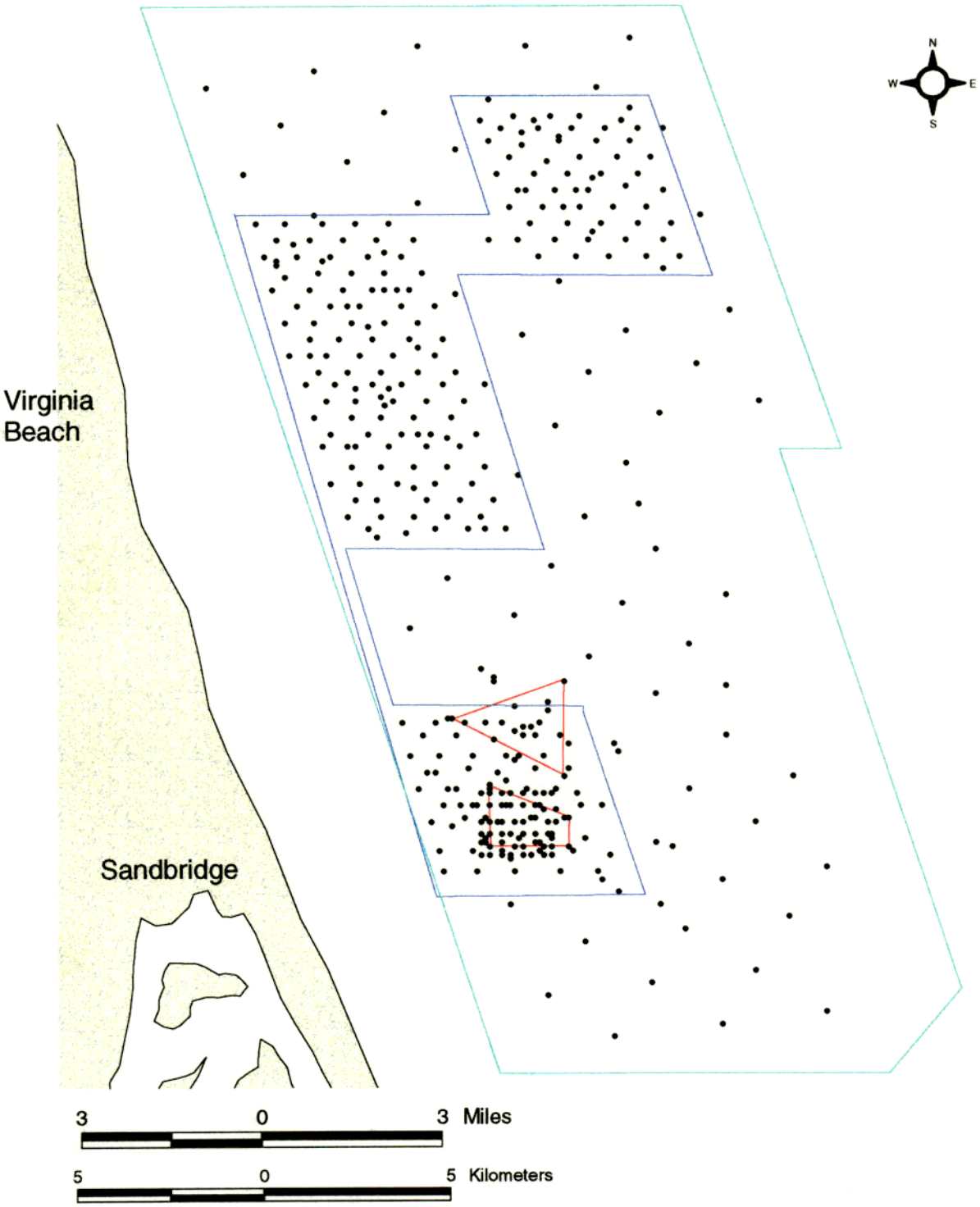

Figure 2. SPI and Smith-MacIntyre grab site locations off the Virginia coast, spring and fall 1996 and 1997. Red lines indicate proposed borrow areas A (southern) and B (northern) for sandmining, blue lines indicate limits of 1996 study region, and green lines indicate limits of 1997 study region.

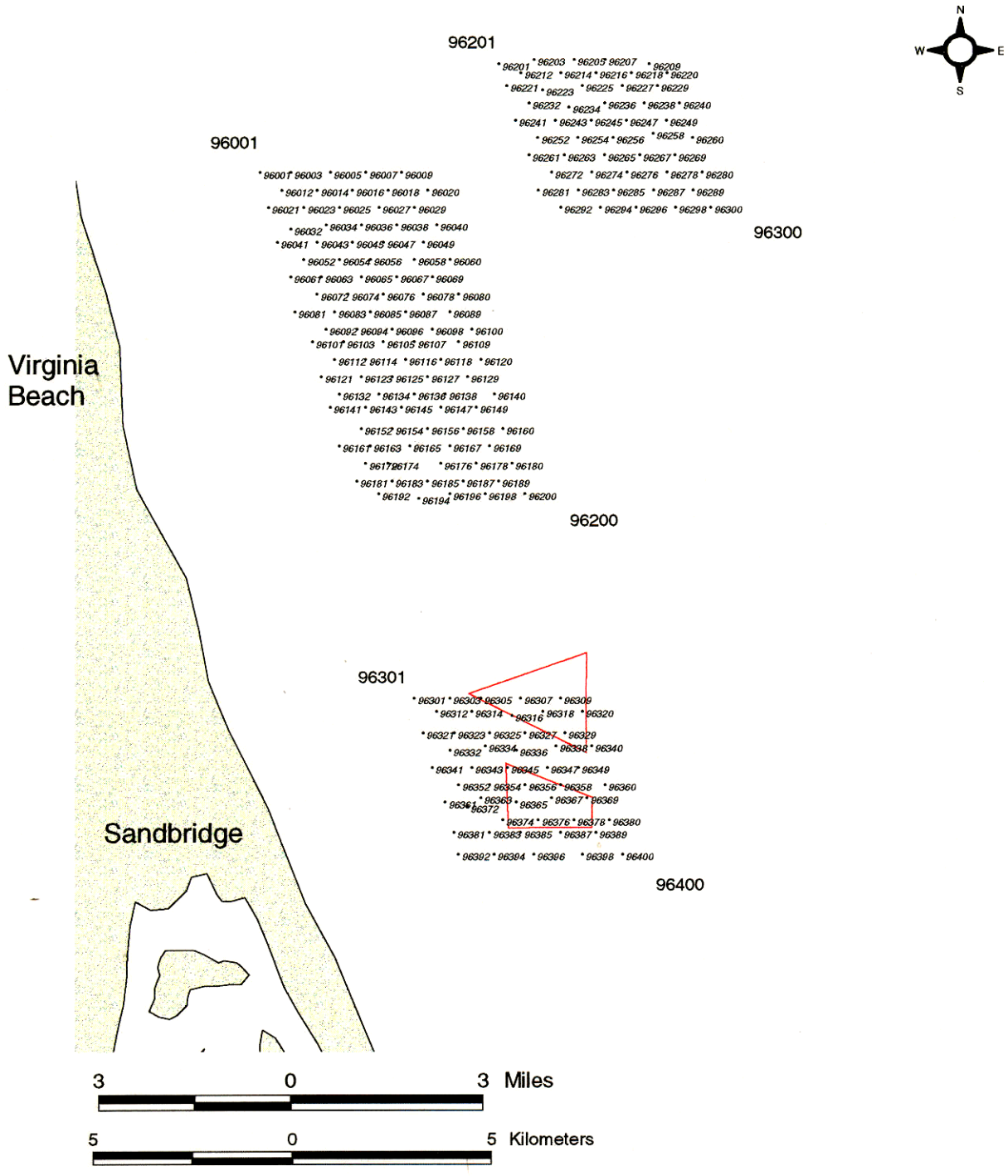

Figure 3. SPI sample site locations off the Virginia coast, spring and fall 1996.

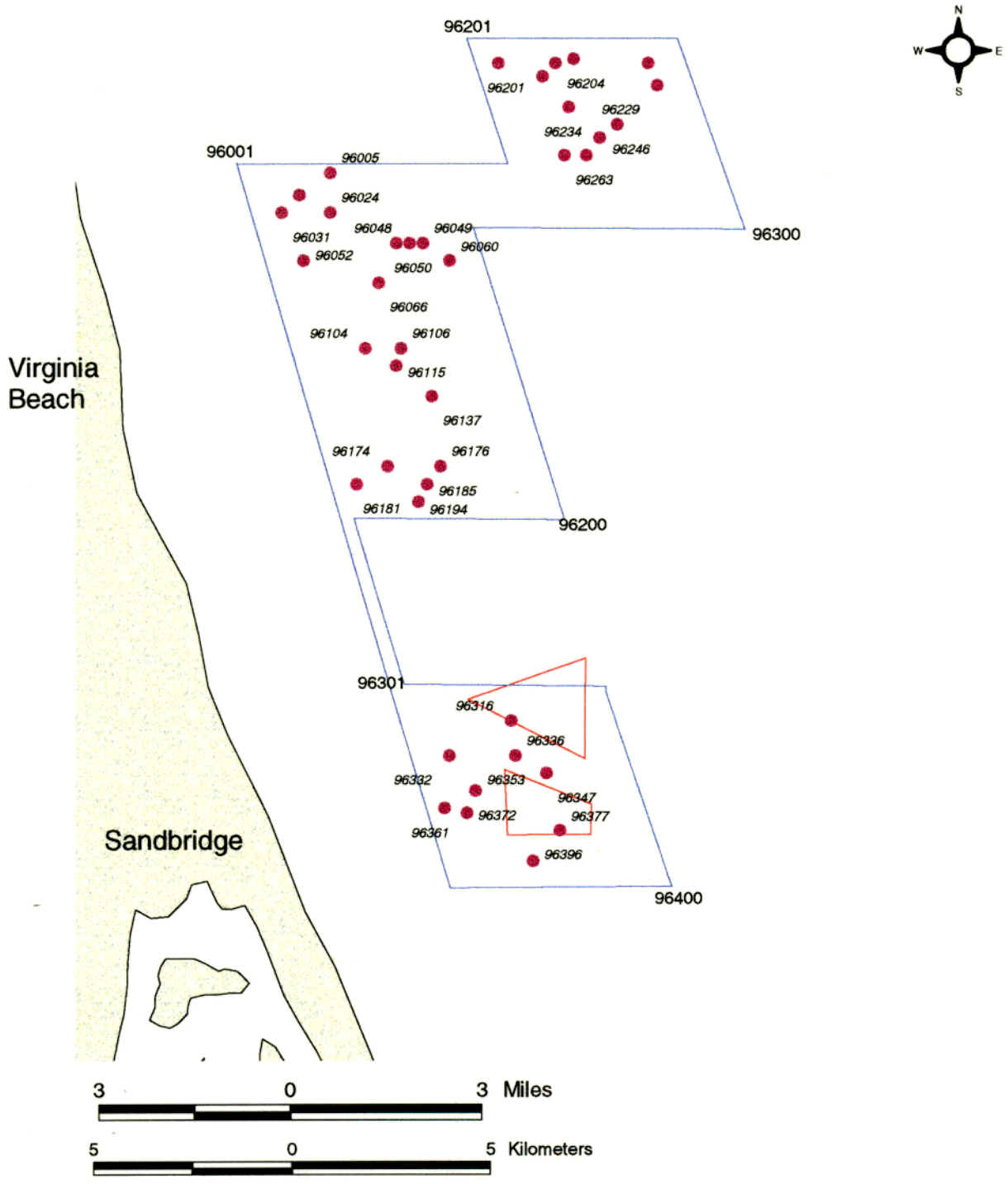

Figure 4. Smith-MacIntyre grab site locations off the Virginia coast, spring 1996.

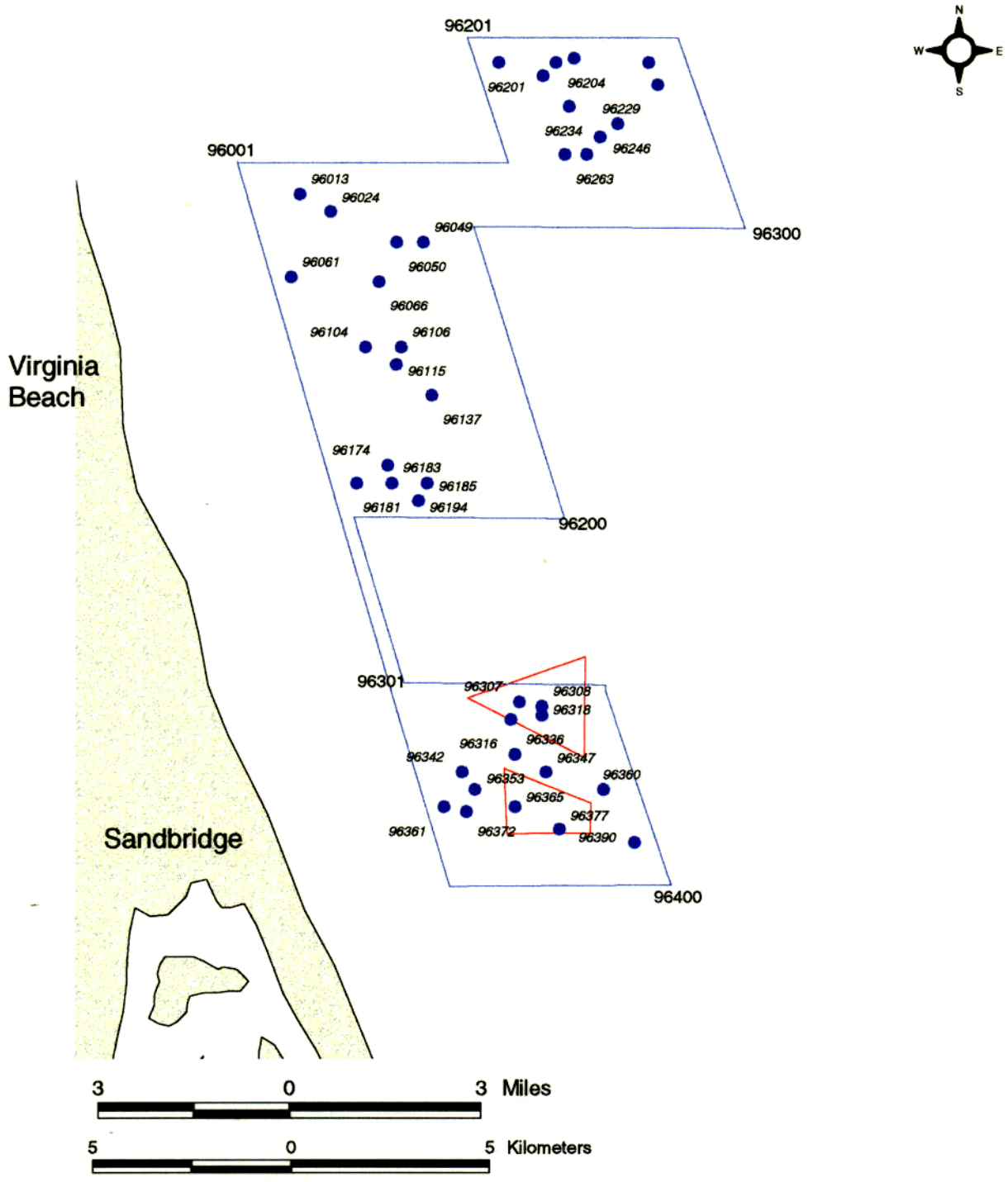

Figure 5. Smith-MacIntyre grab site locations off the Virginia coast, fall 1996.

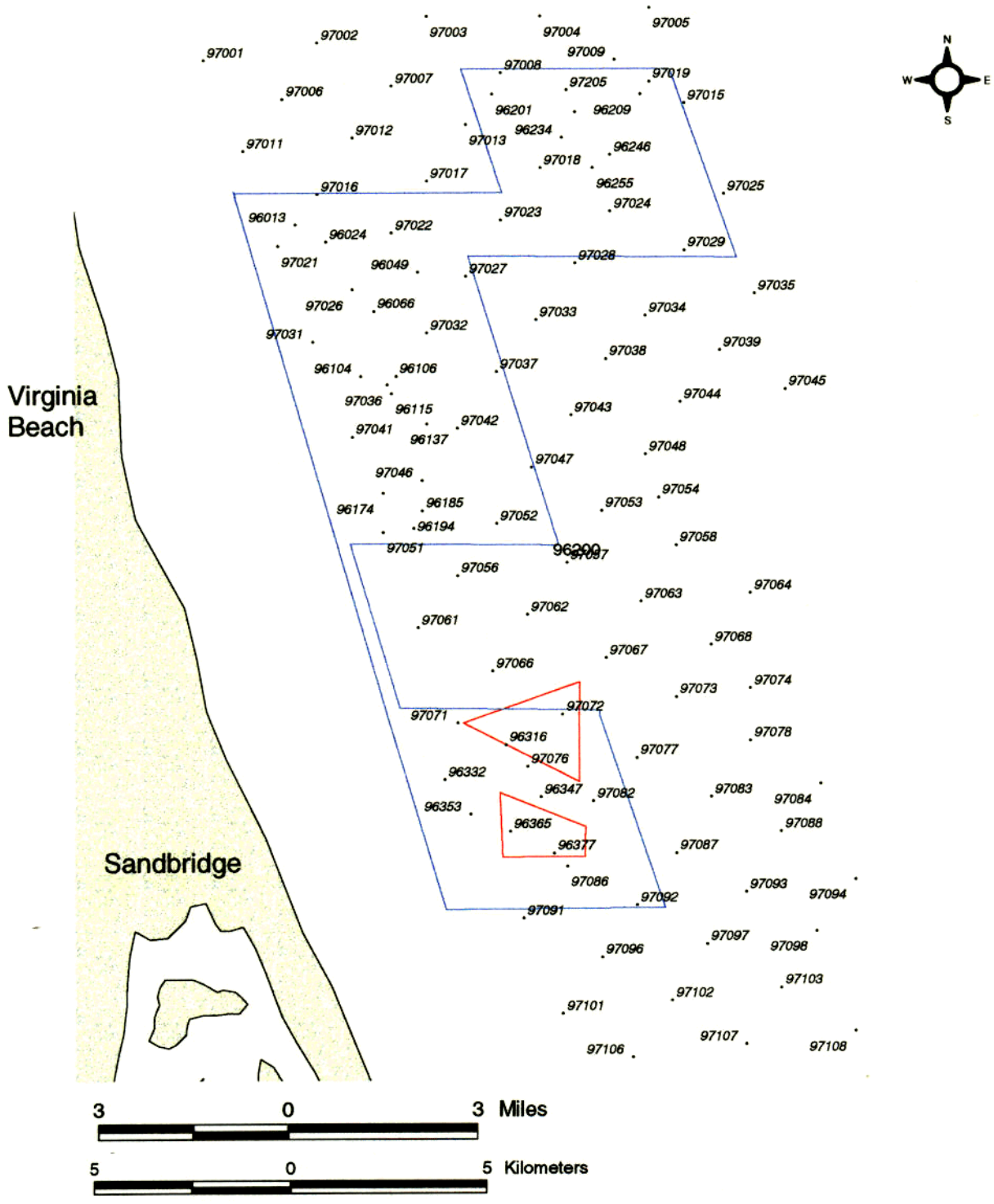

Figure 6. SPI sample site locations off the Virginia coast, spring 1997.

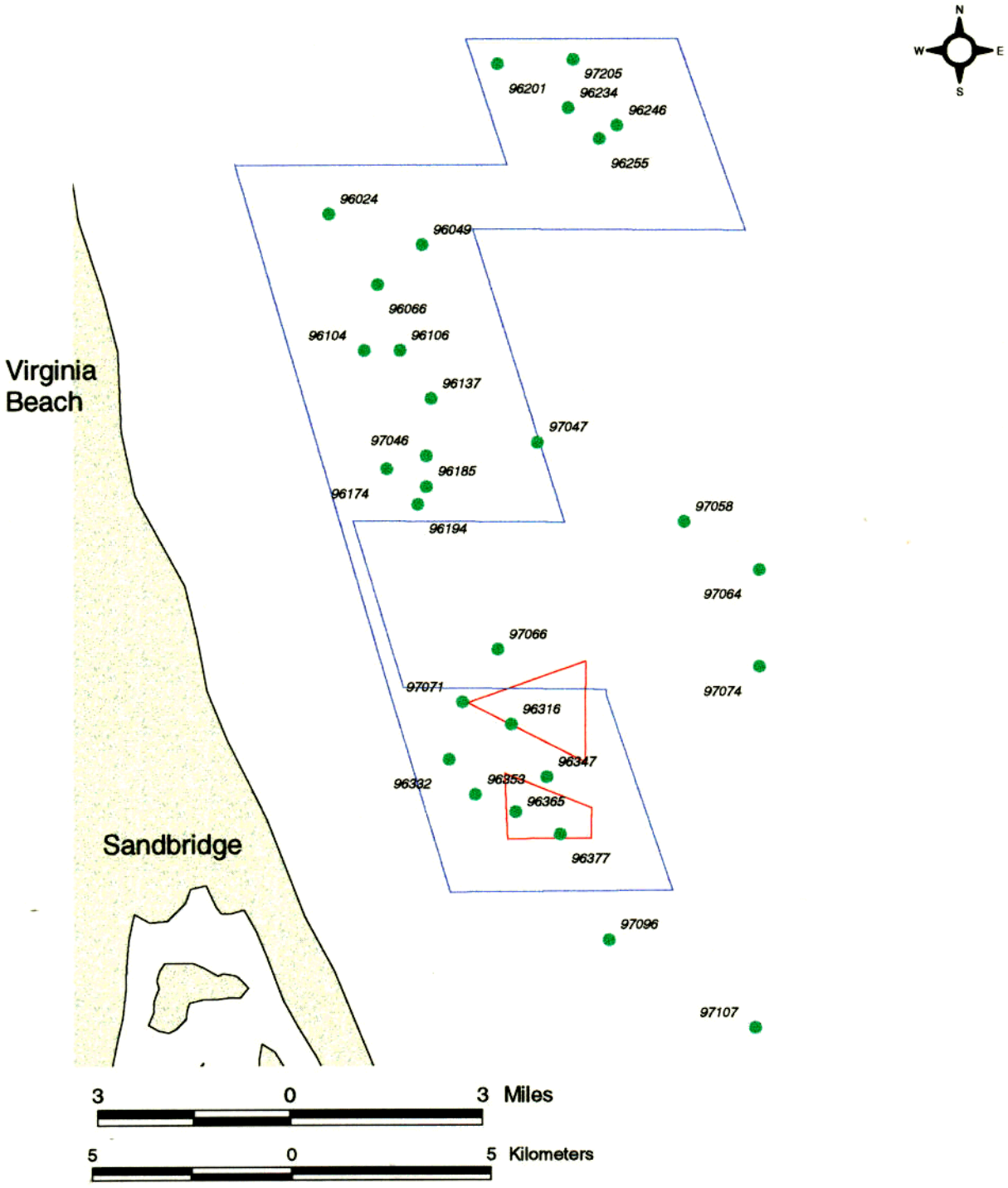

Figure 7. Smith-MacIntyre grab sample site locations off the Virginia coast, spring 1997.

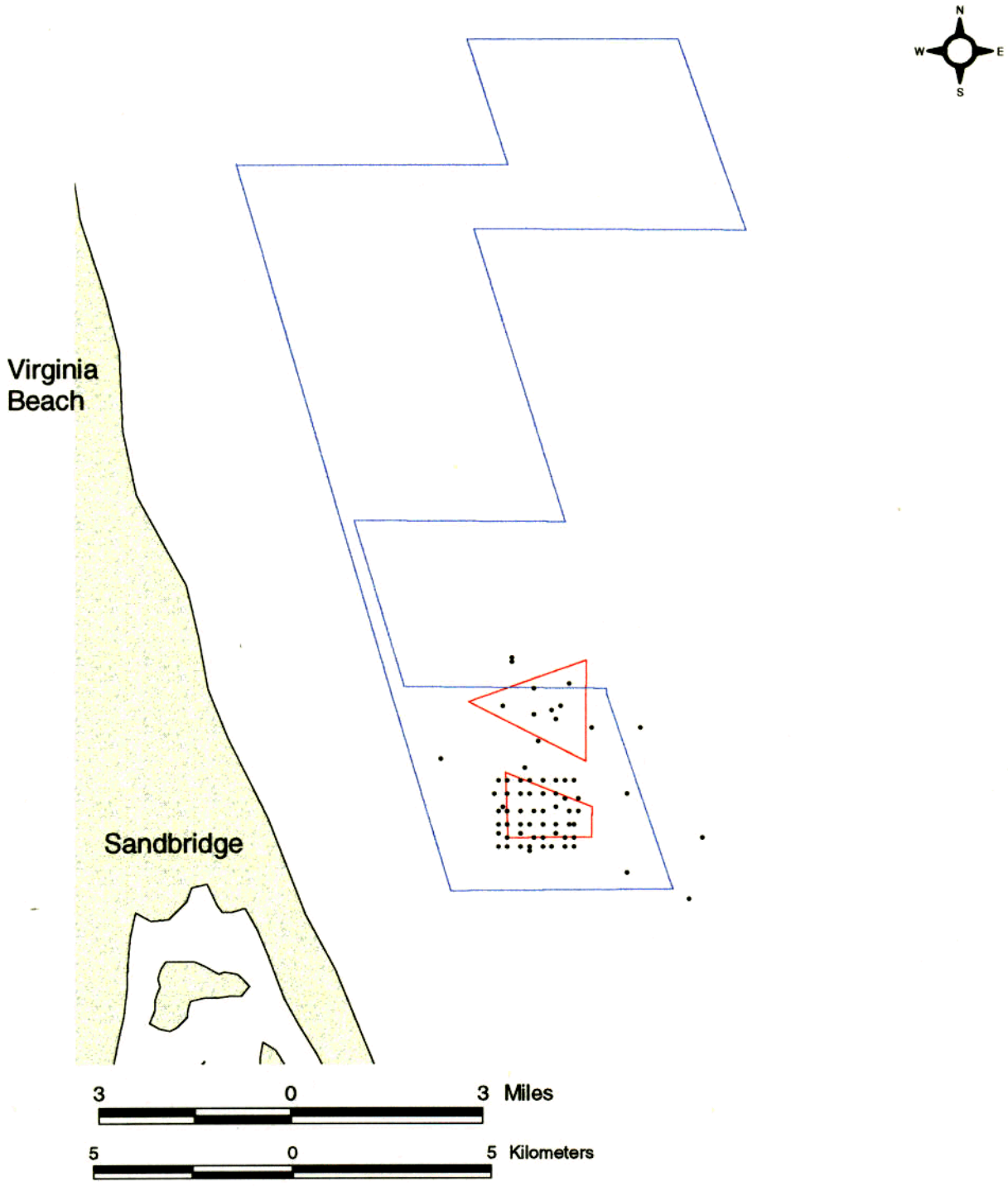

Figure 8. SPI and Smith-MacIntyre grab site locations off the Virginia coast, fall 1997 in the vicinity of Sandbridge shoal and the proposed borrow areas (red lines) for sandmining.

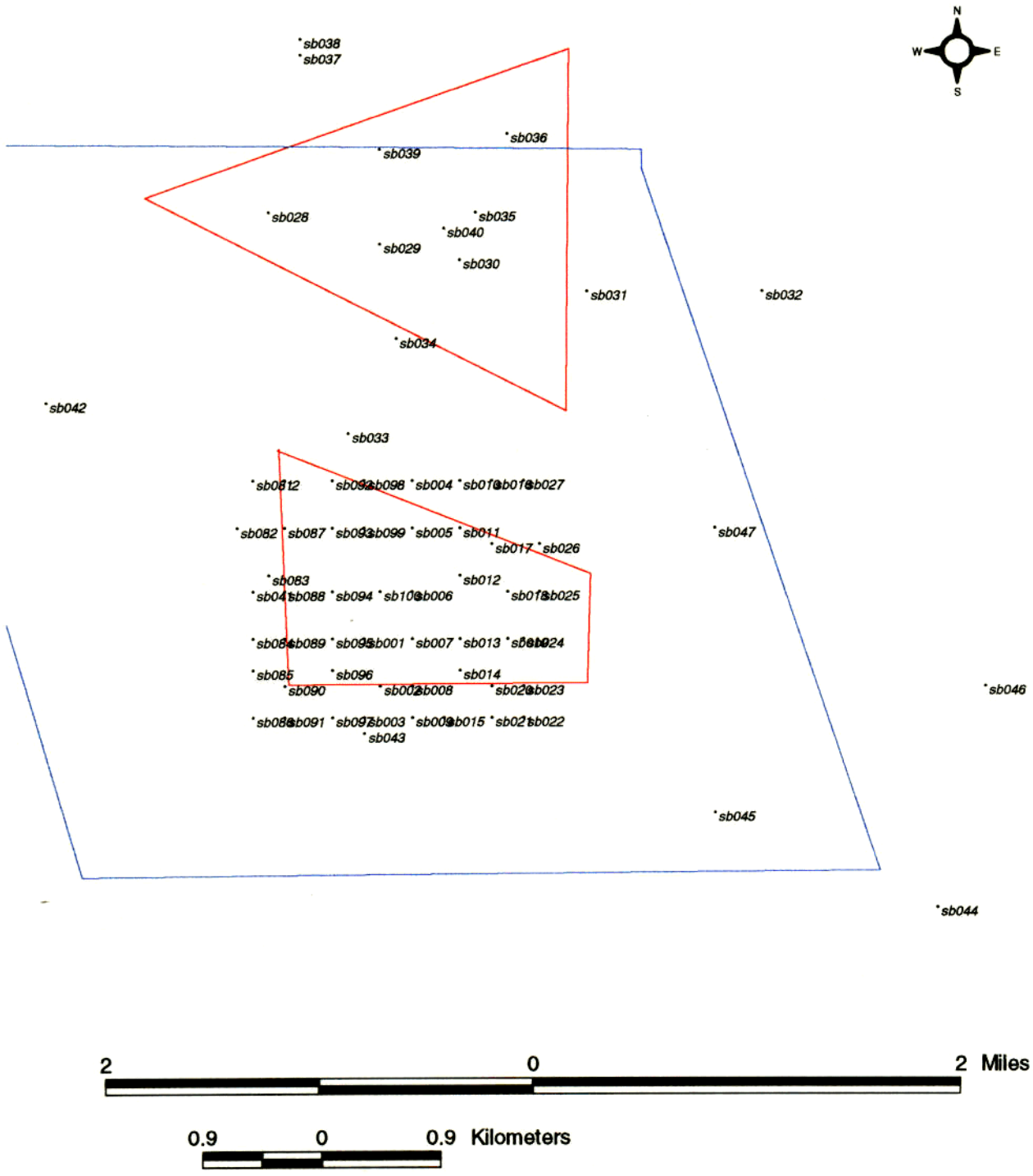

Figure 9. SPI sample site locations, fall 1997.

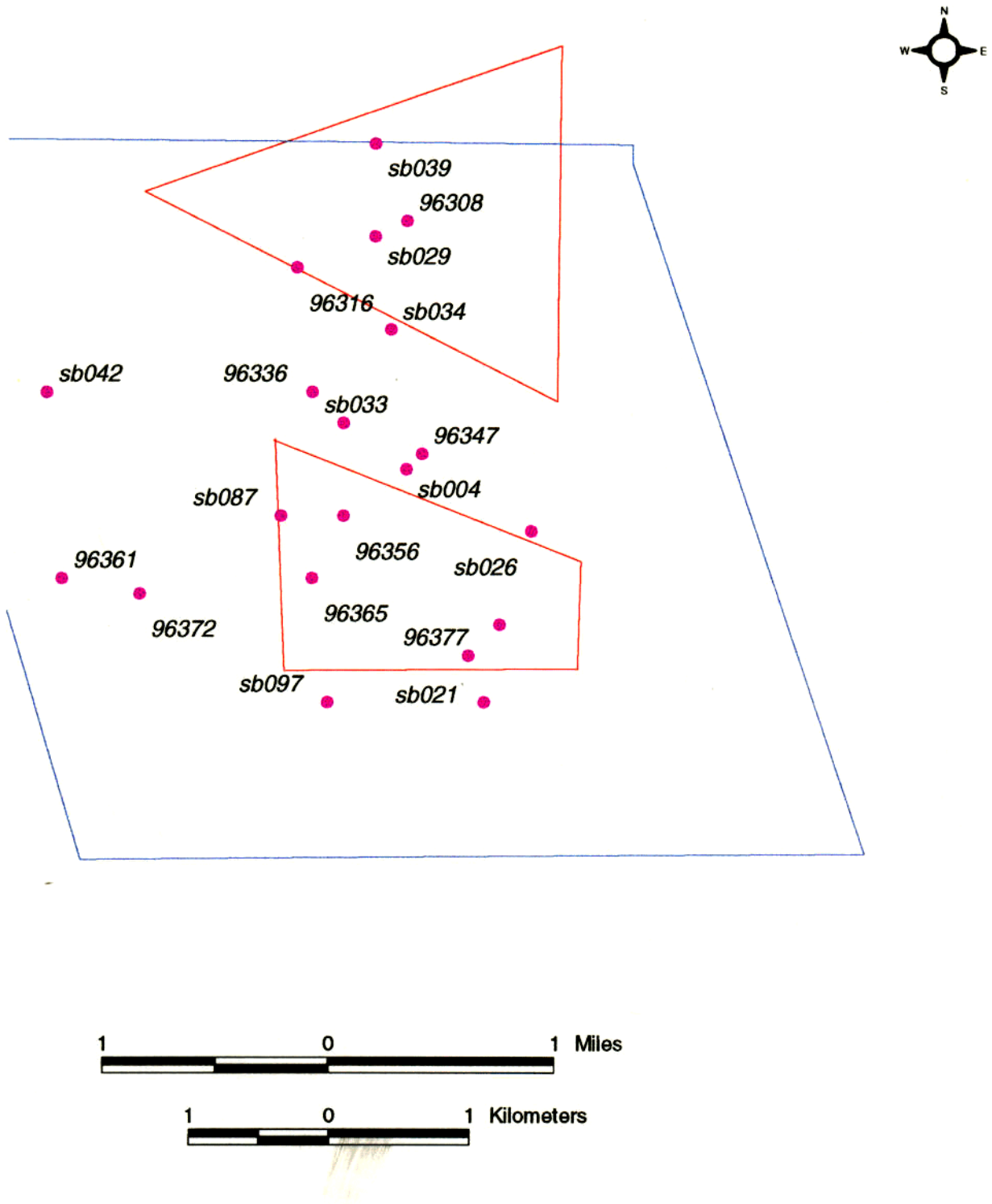

Figure 10. Smith-MacIntyre grab sample site locations, fall 1997.

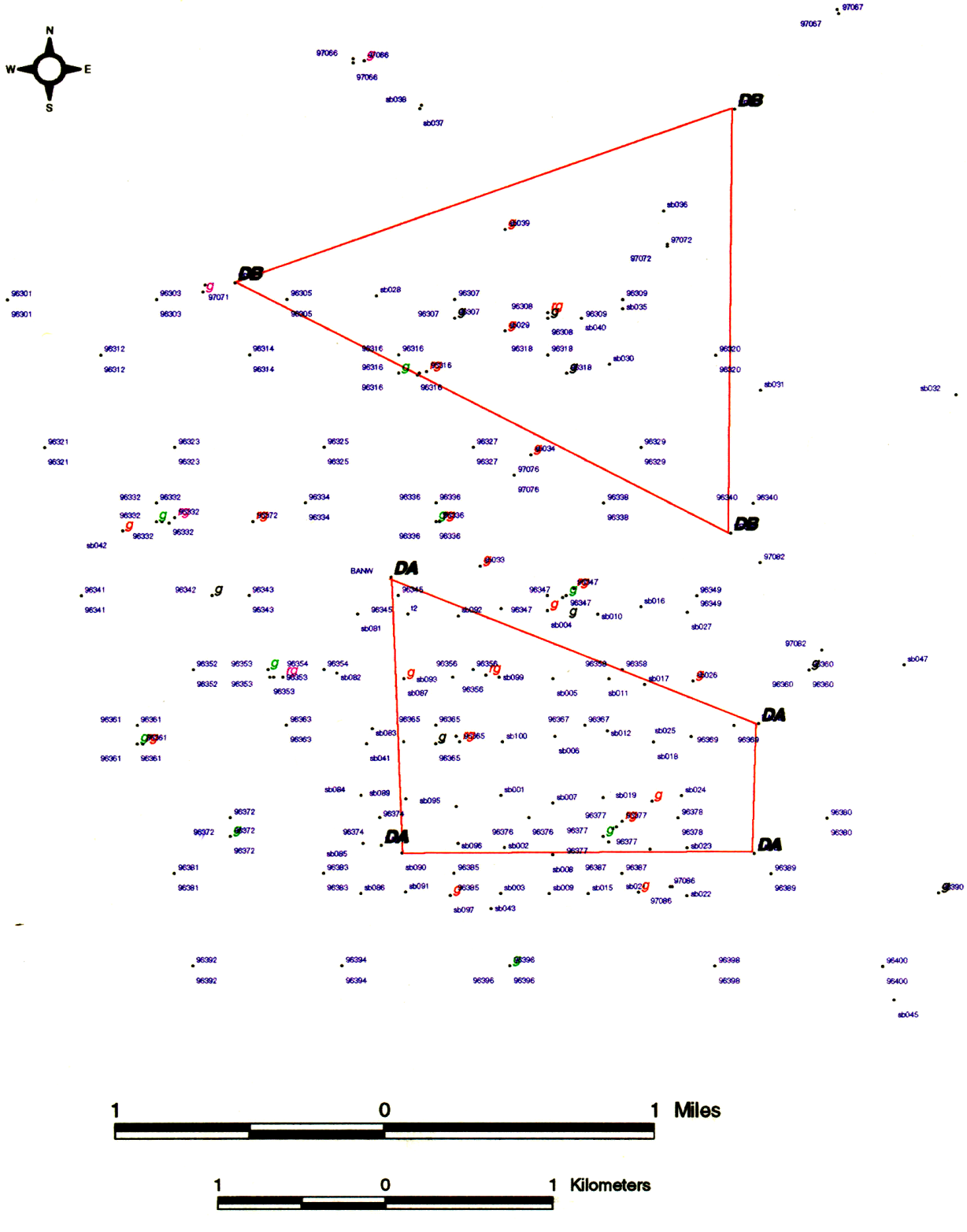

Figure 11. Sandbridge shoal region sample sites and Dredge Areas A and B (with corners marked).

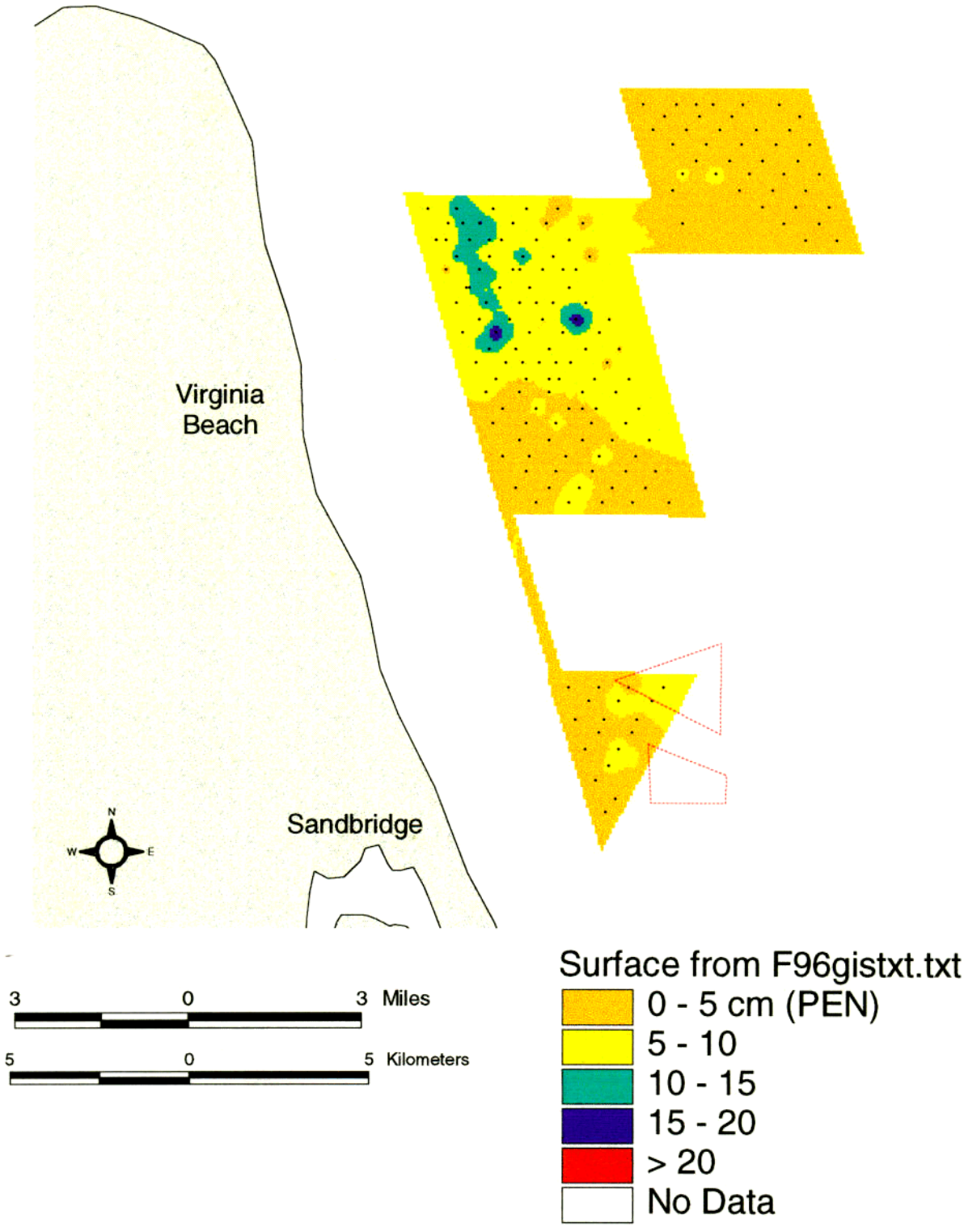

Figure 12. Spring 1996 SPI prism penetrationdepth (cm). Potential borrow areas A (southern) and B (northern) are delineated by red lines.

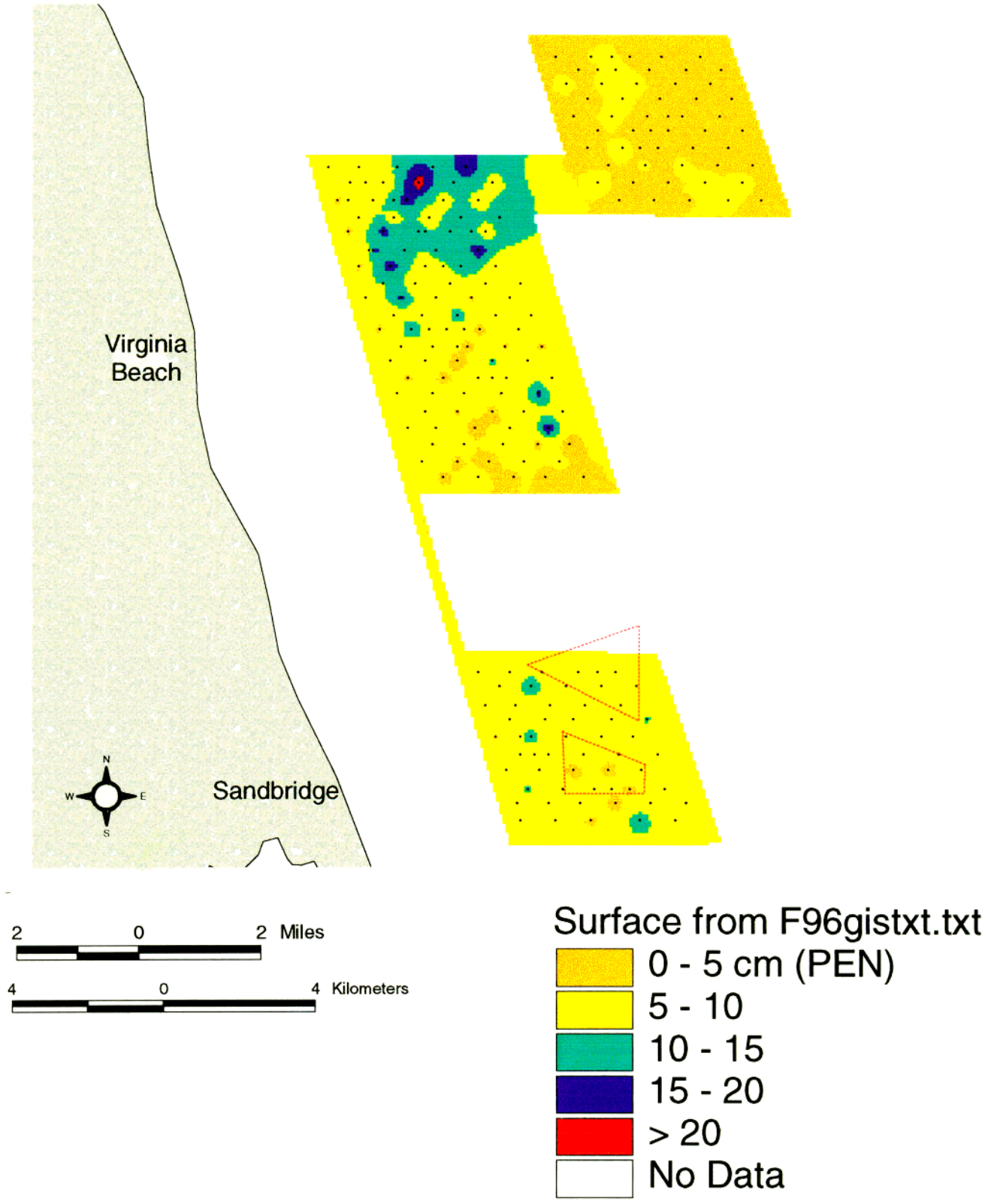

Figure 13. Fall 1996 SPI prism penetrationdepth (cm).

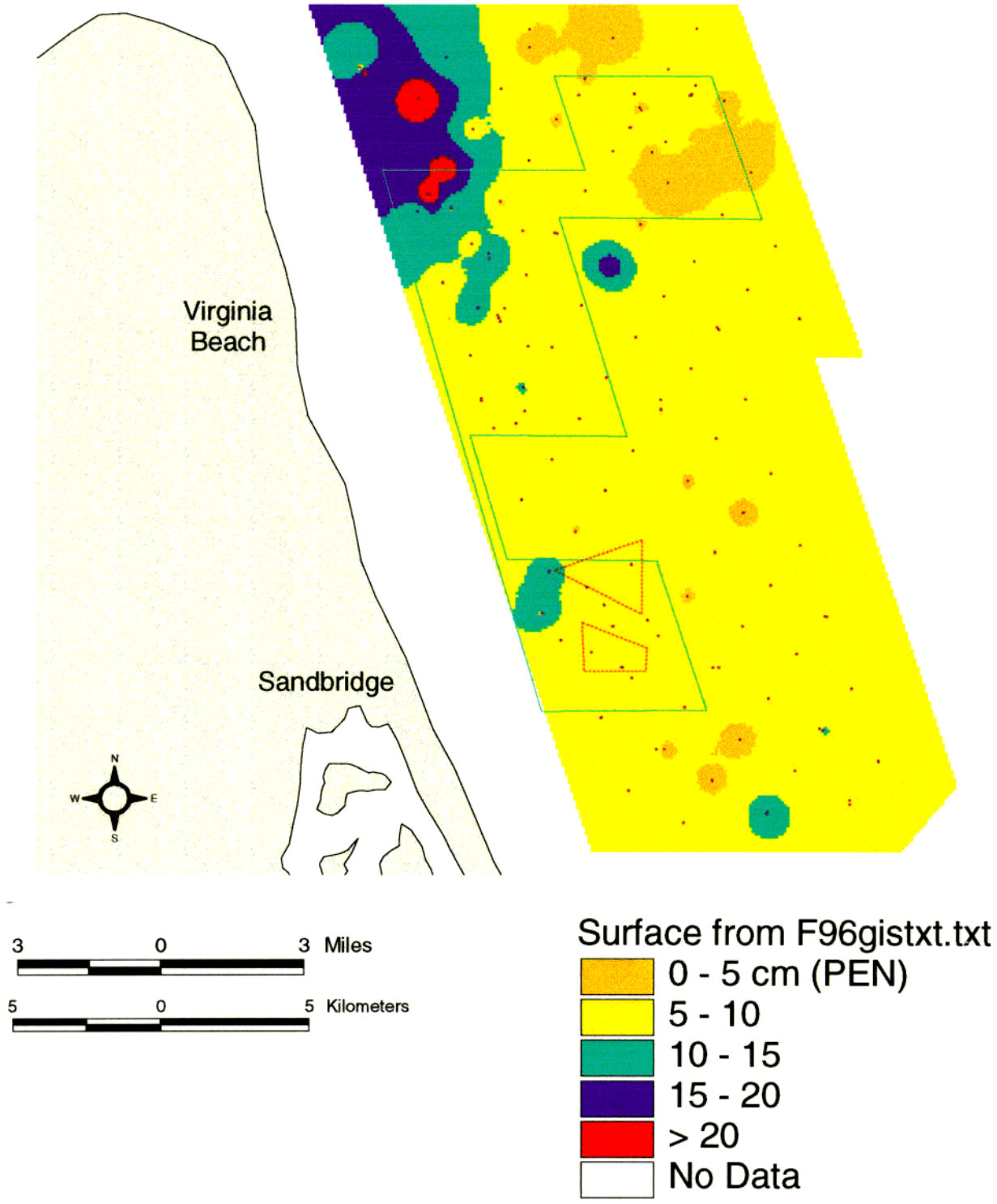

Figure 14. Spring 1997 SPI prism penetration depth (cm). 1996 study region is delineated by green line and borrow areas are delineated by red line.

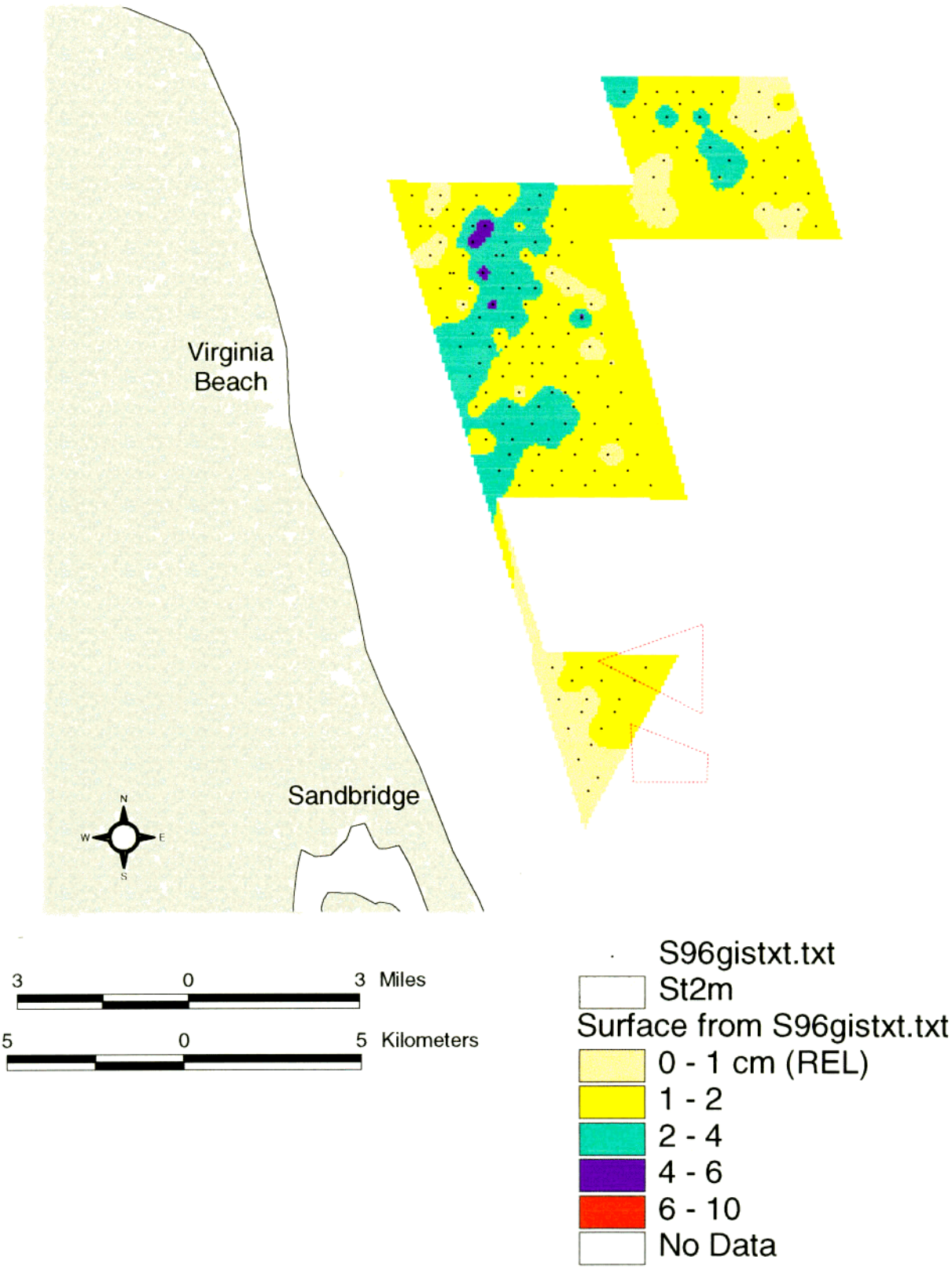

Figure 15. Spring 1996 sediment surface relief (cm) from SPI.

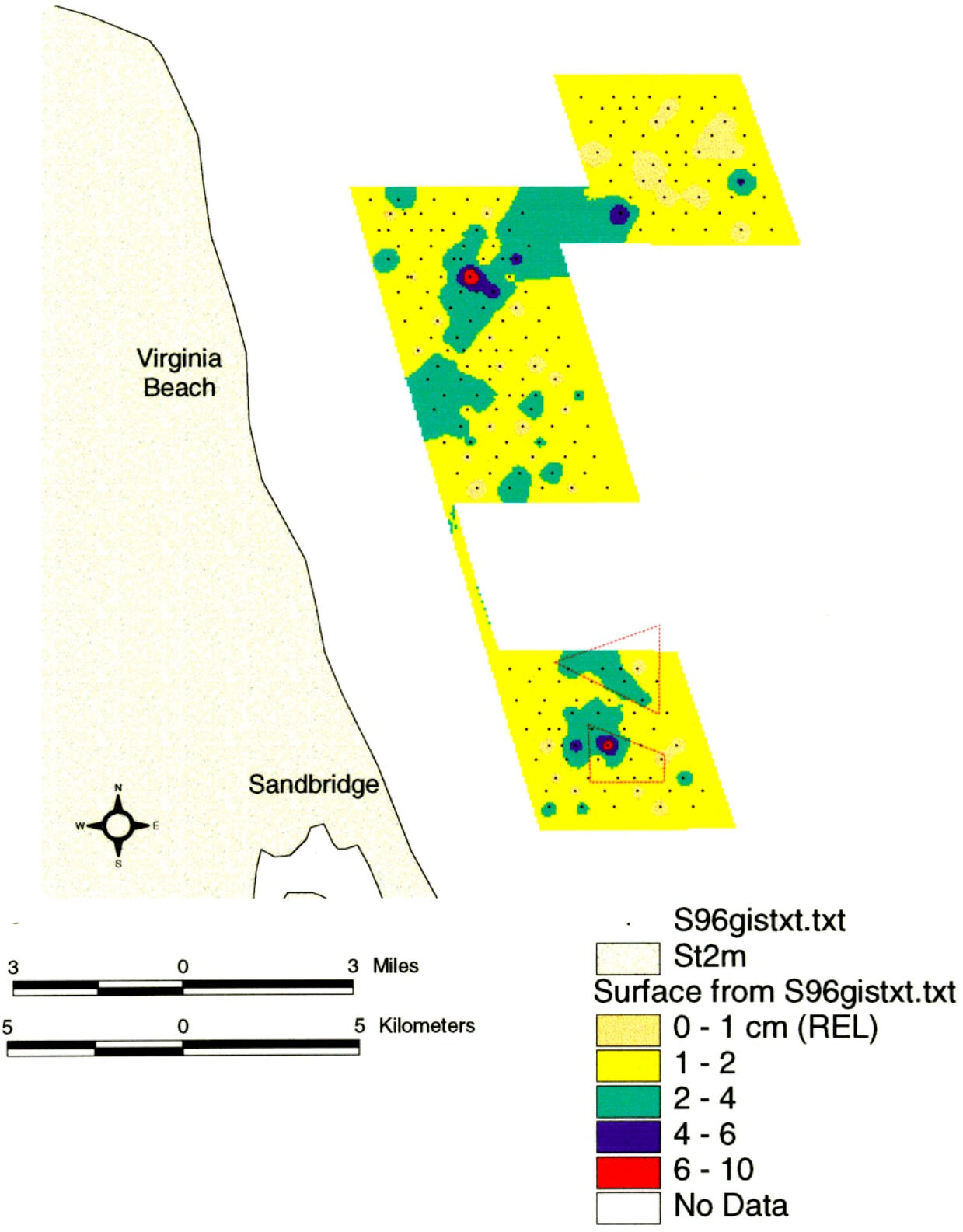

Figure 16. Fall 1996 sediment surface relief (cm) from SPI.

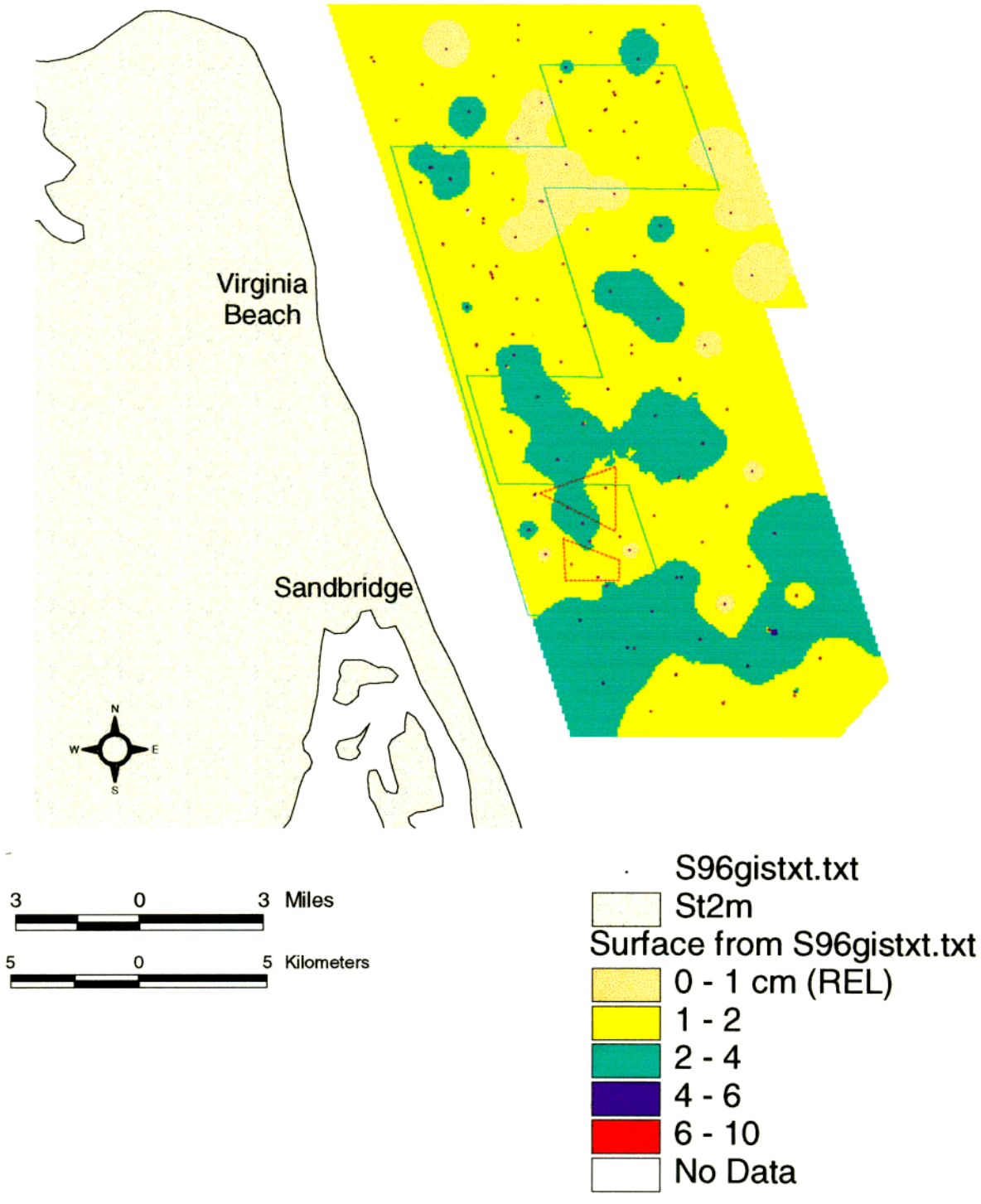

Figure 17. Spring 1997 sediment surface relief (cm) from SPI.

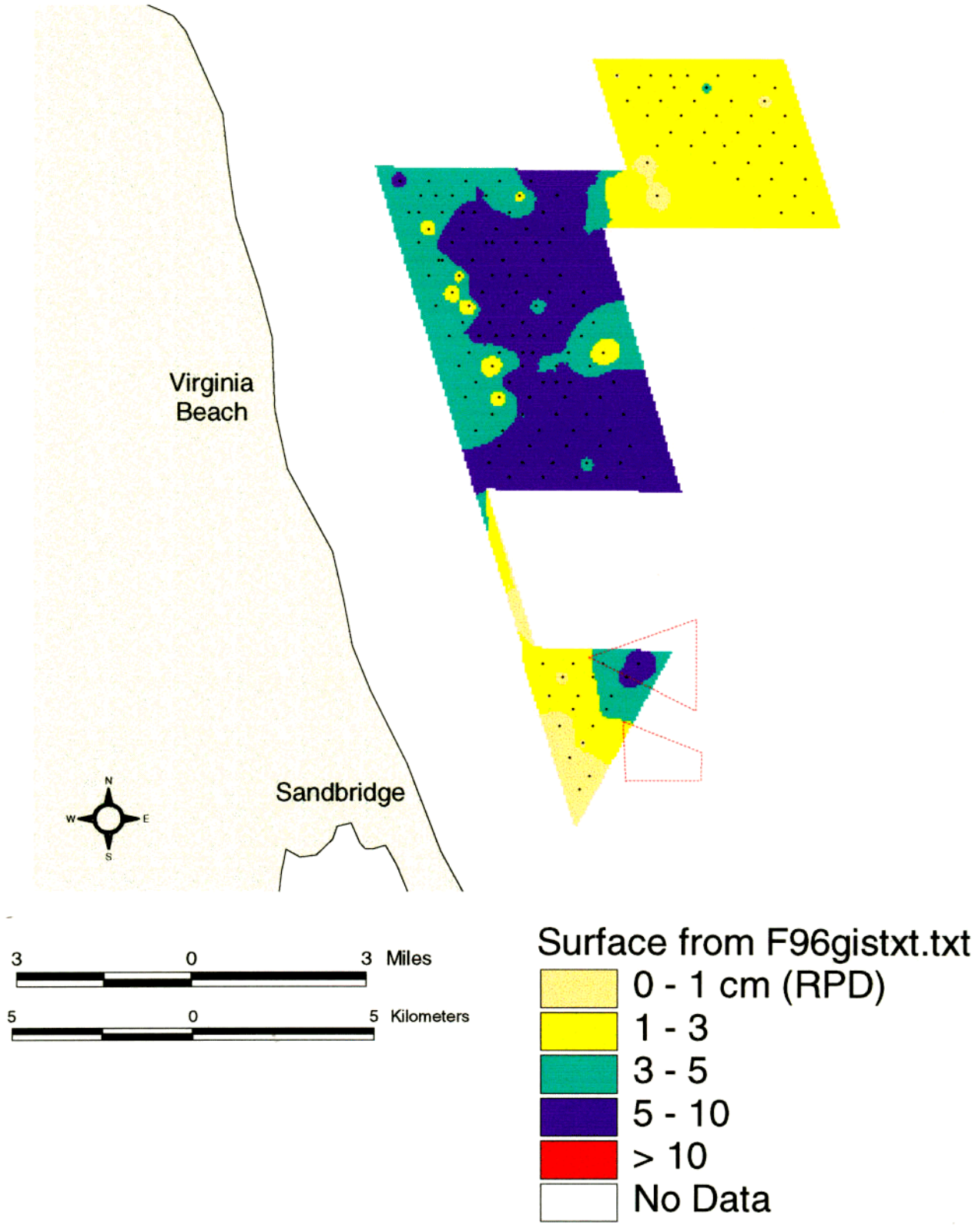

Figure 18. Spring 1996 redox potential discontinuity (RPD) layer depth (cm).

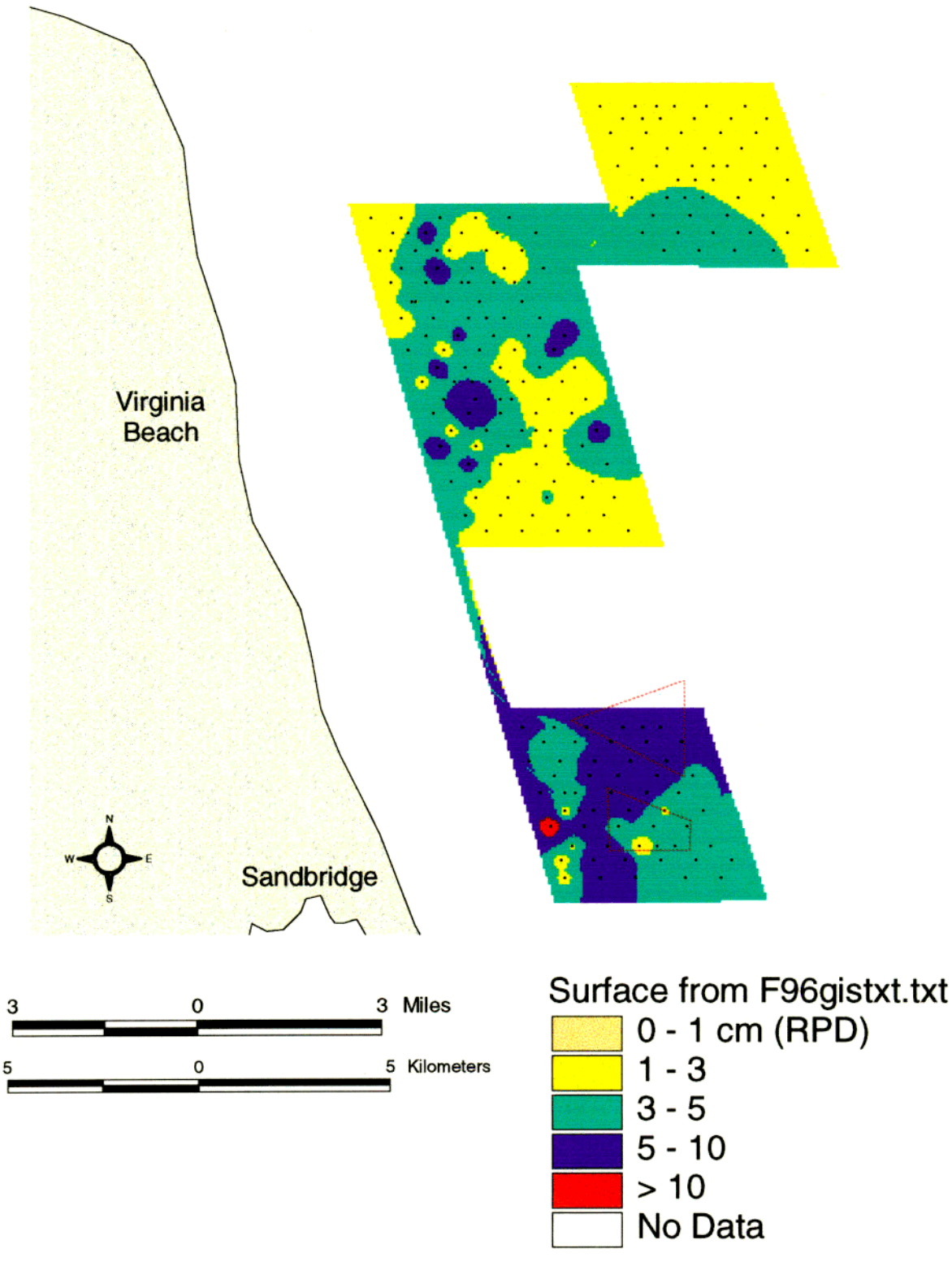

Figure 19. Fall 1996 redox potential discontinuity (RPD) layer depth (cm) from SPI.

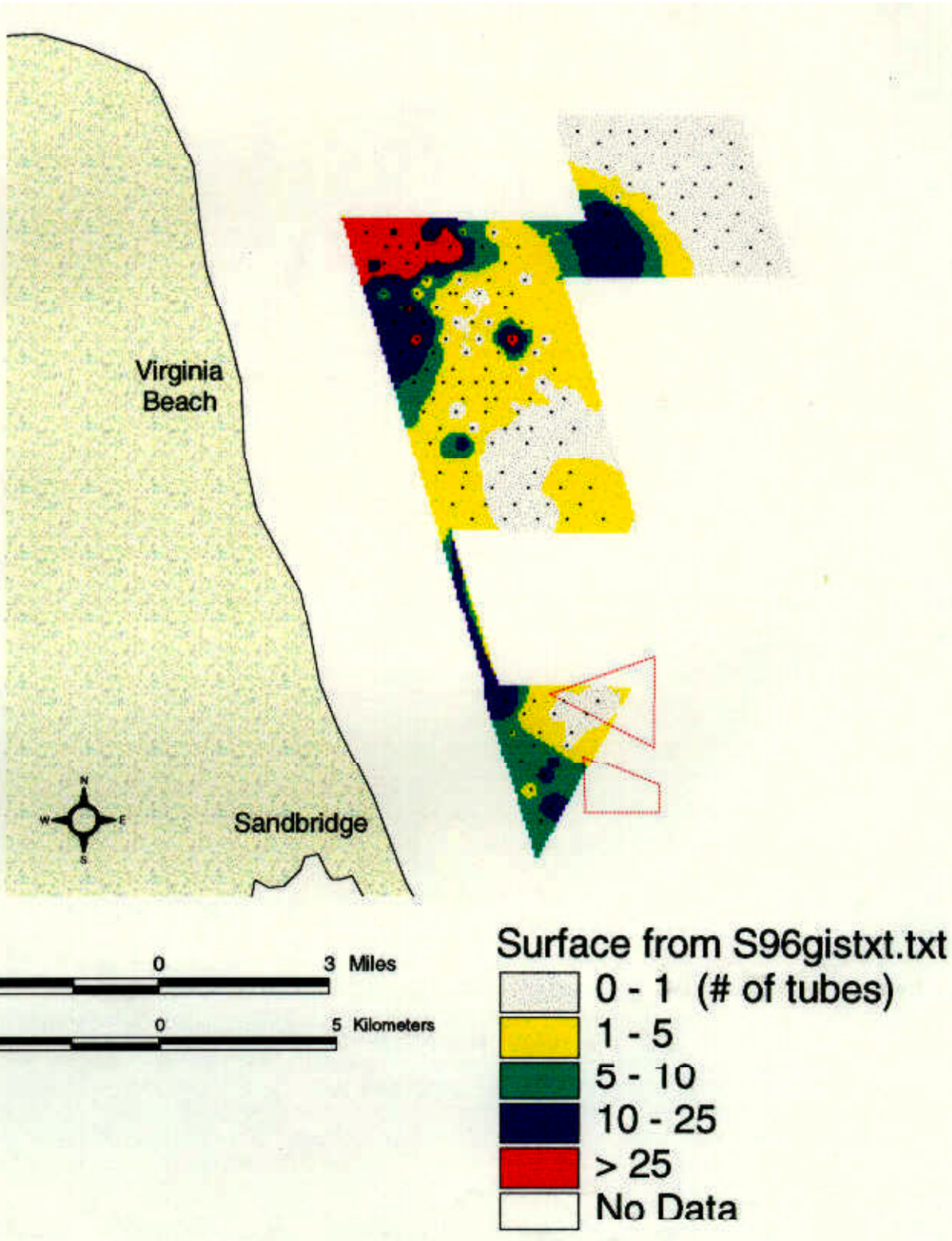

Figure 20. Spring 1996, number of infaunal tubes visible at the sediment-water interface.

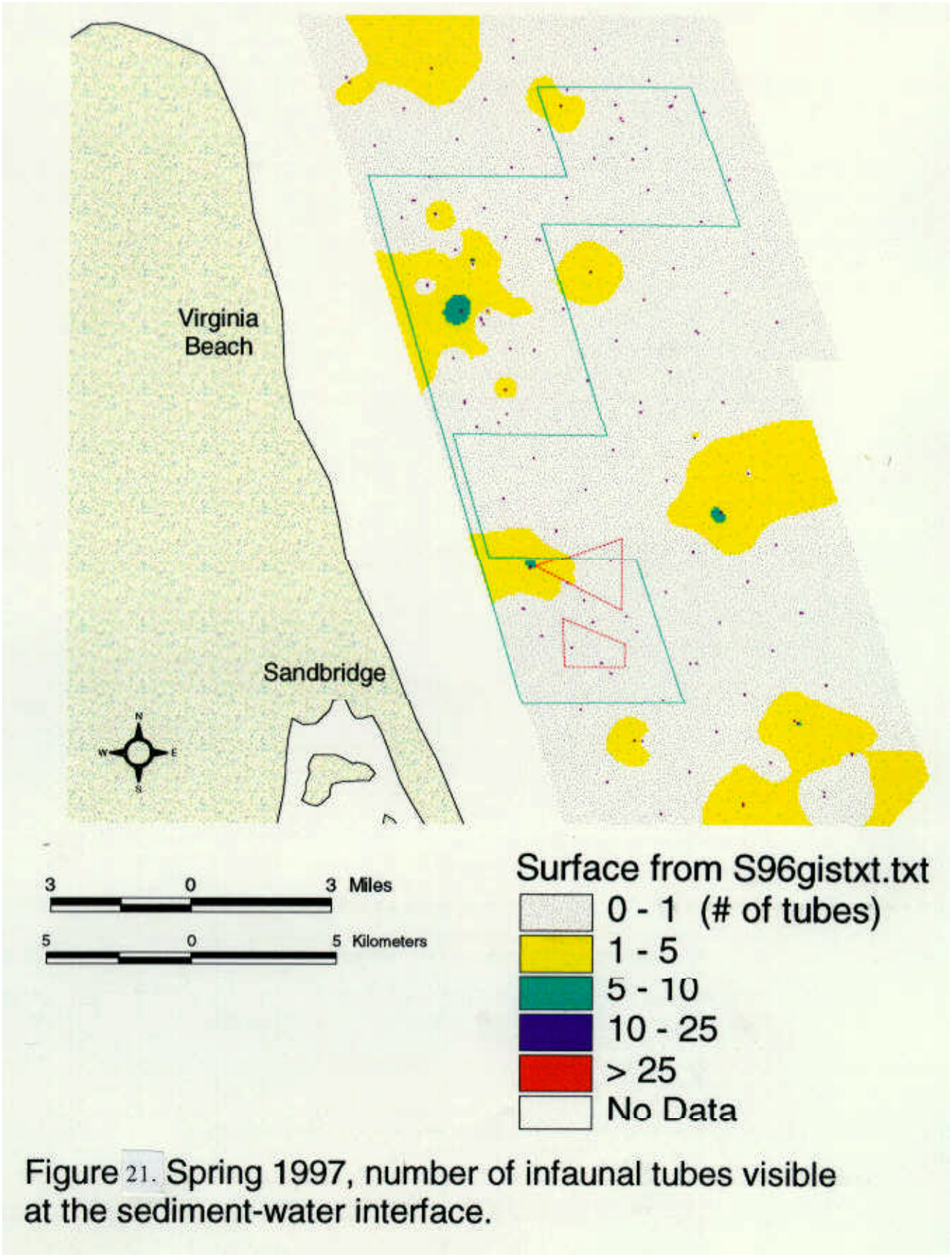

Figure 21. Spring 1997, number of infaunal tubes visible at the sediment-water interface.

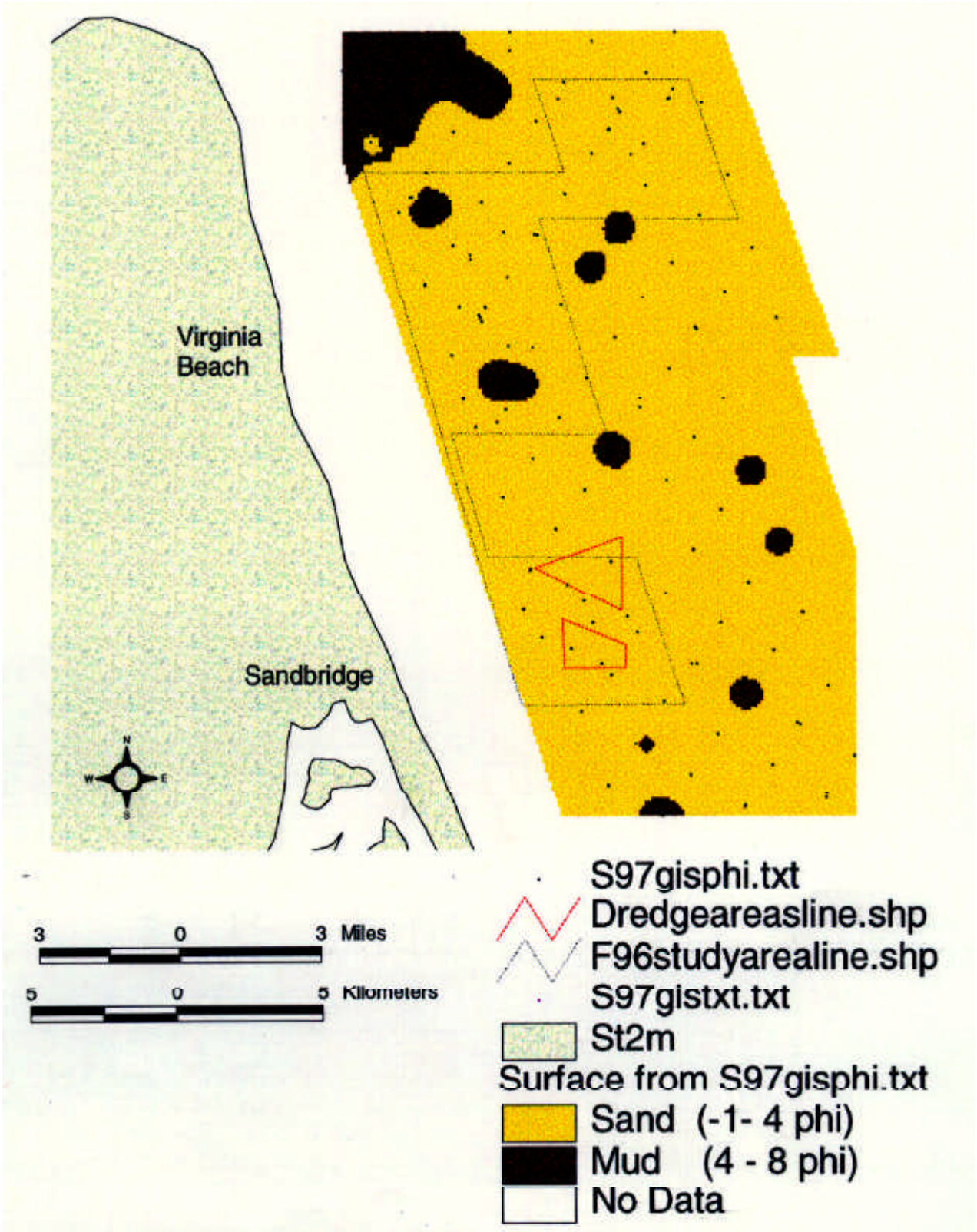

Figure 22. Spring 1997 sediment type offshore Virginia.

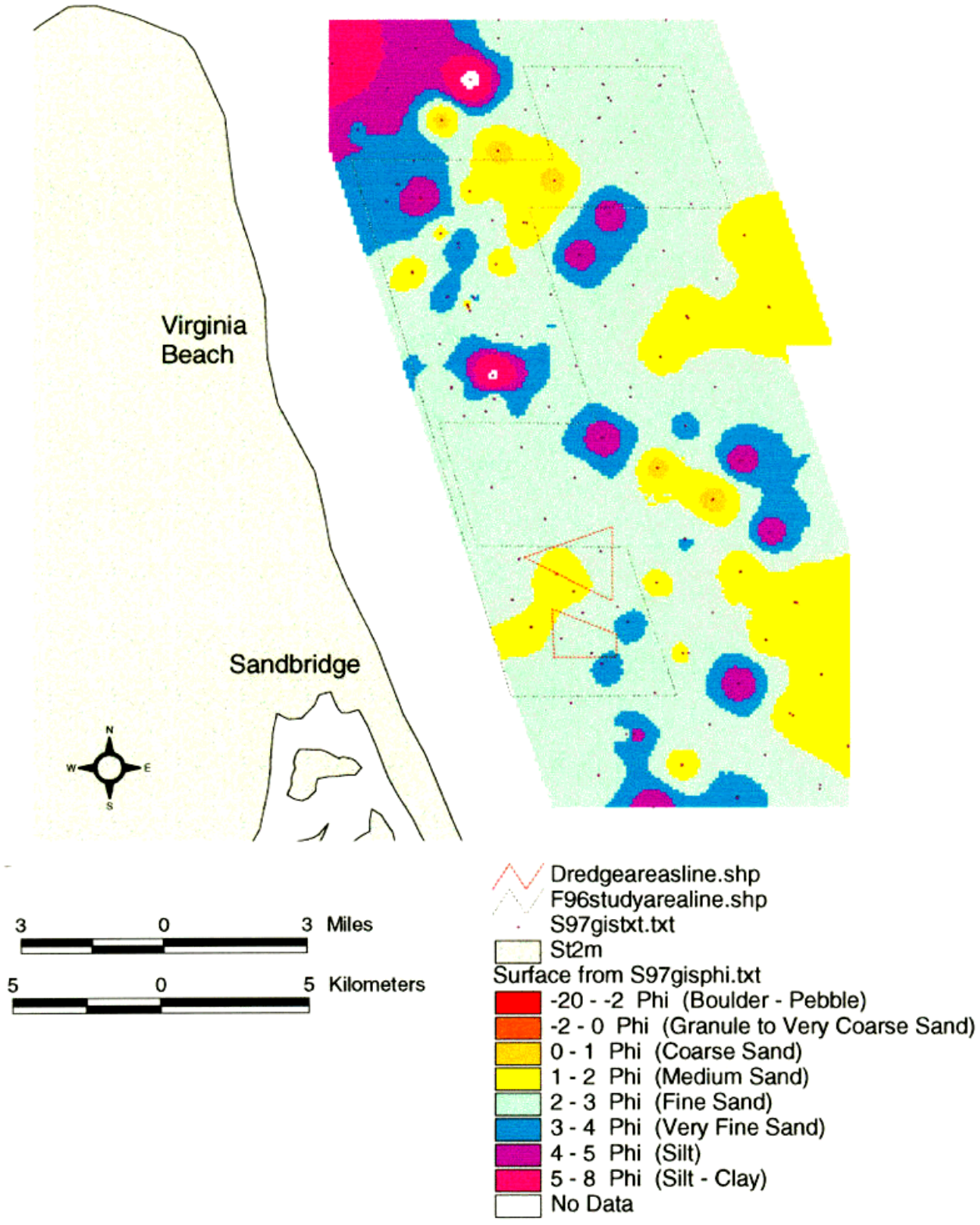

Figure 23. Spring 1997 sediment phi offshore Virginia.

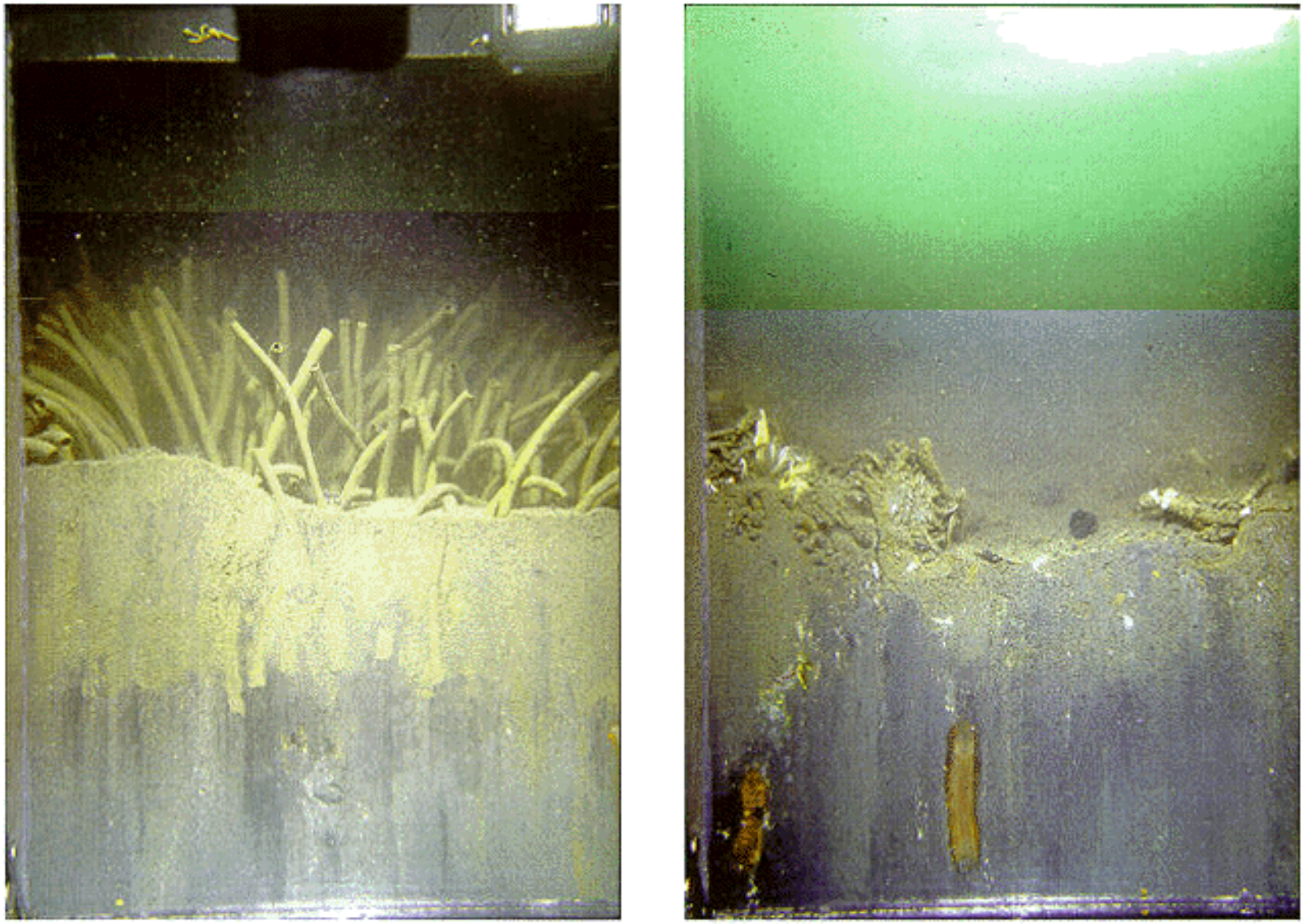

Figure 24. Habitat class A, biologically dominated silty sediments

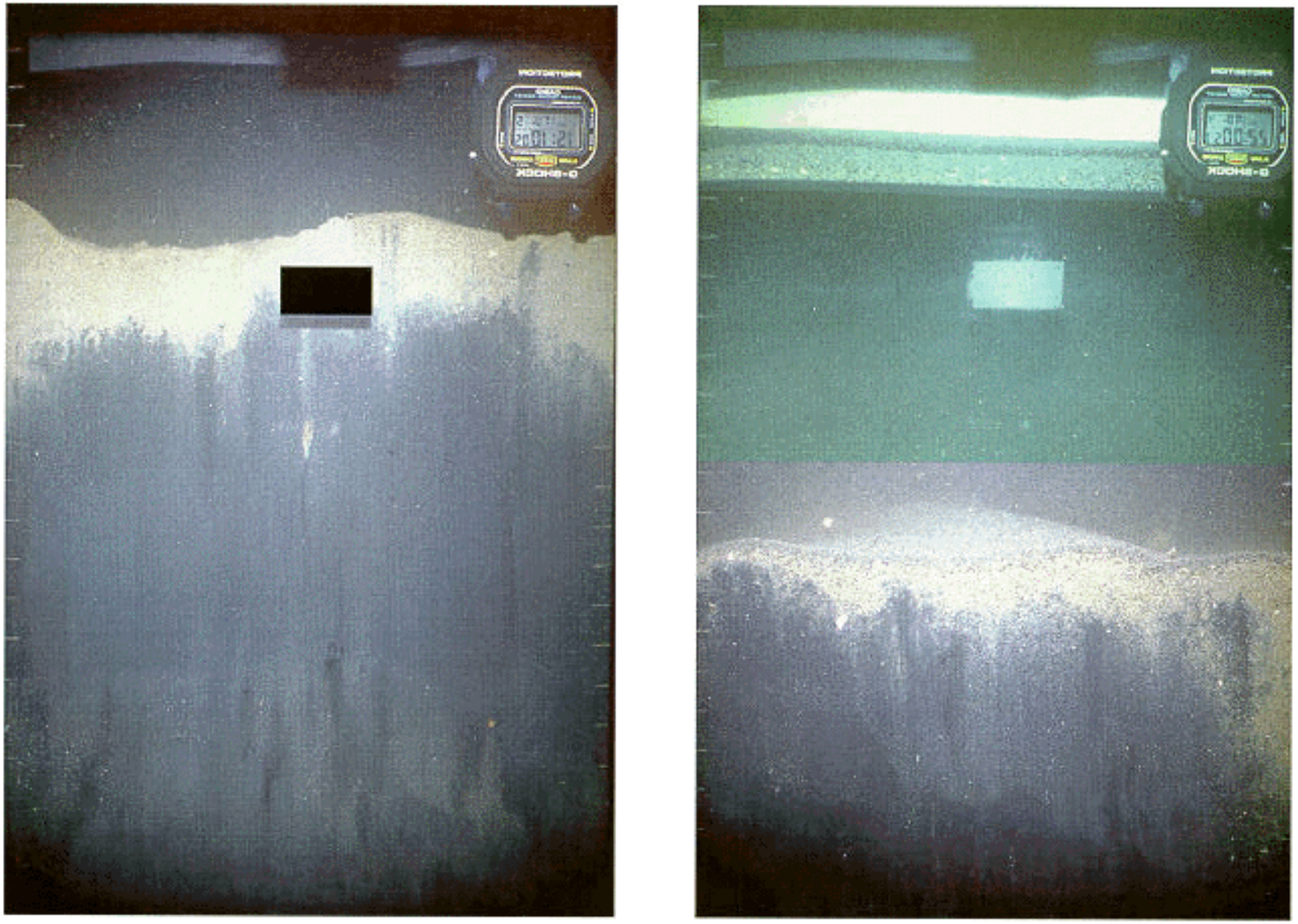

Figure 25. Habitat class B, physically dominated silty sediments.

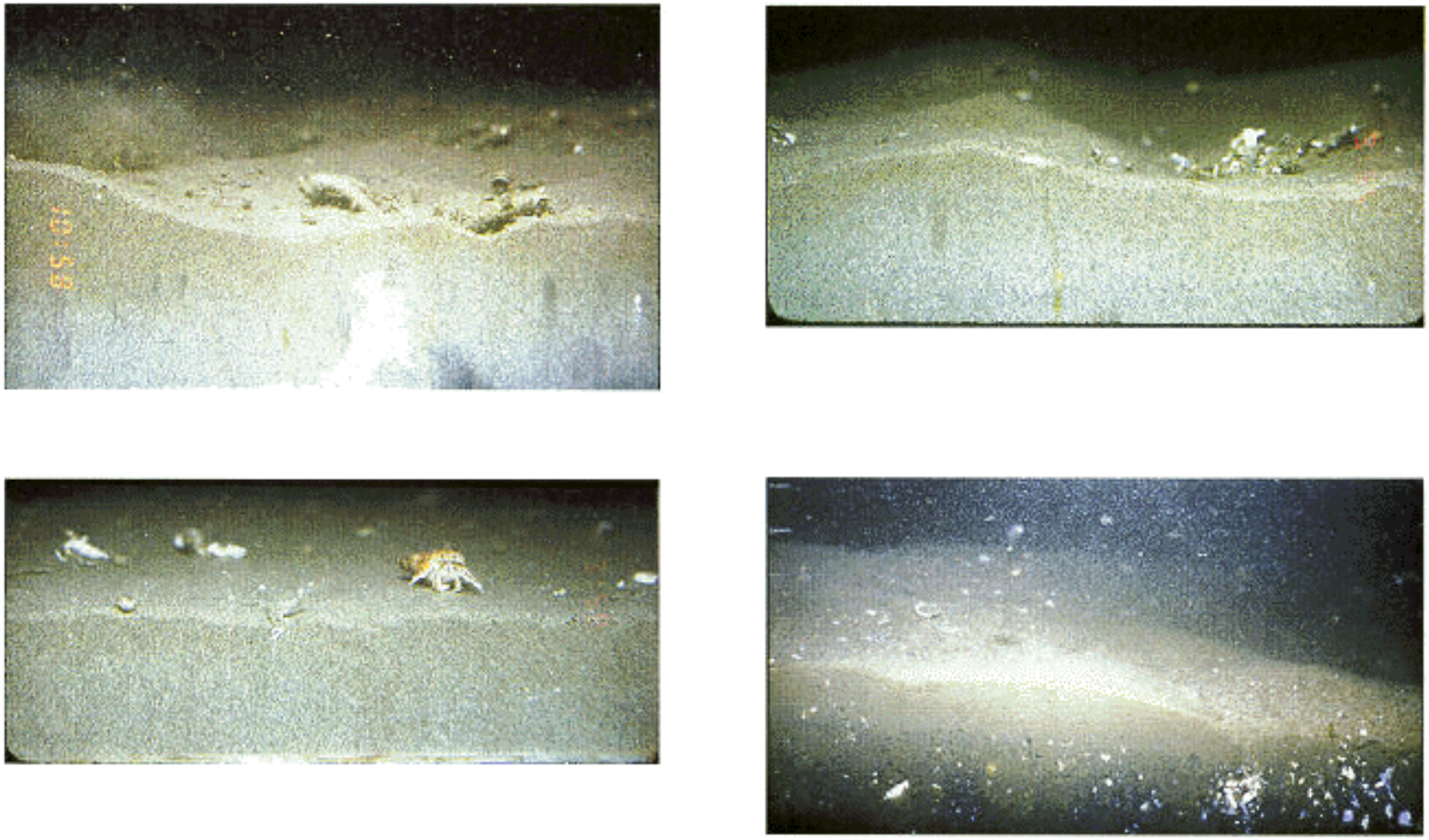

Figure 26. Habitat class C, combined biological and physical feature presence, silty fine sand to very fine sand sediments.

Figure 27. Habitat class D. physically dominated fine sand sediments.

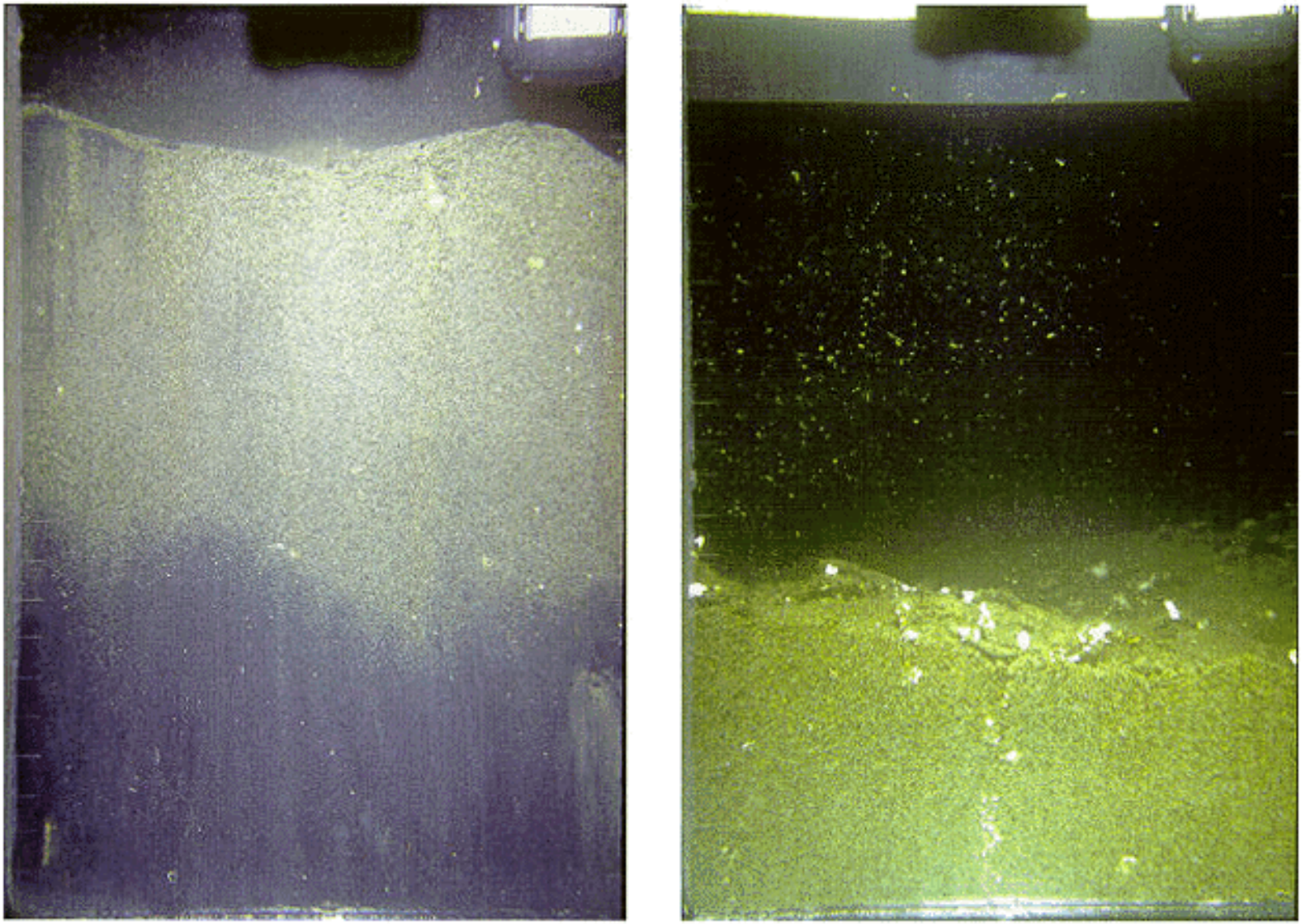

Figure 28. Habitat class E, biologically dominated fine sand sediments

Figure 29. Habitat class F, physically dominated medium sand sediments with shell fragments.

Figure 30. Habitat class G, biologically dominated medium sand sediments with shell fragments.

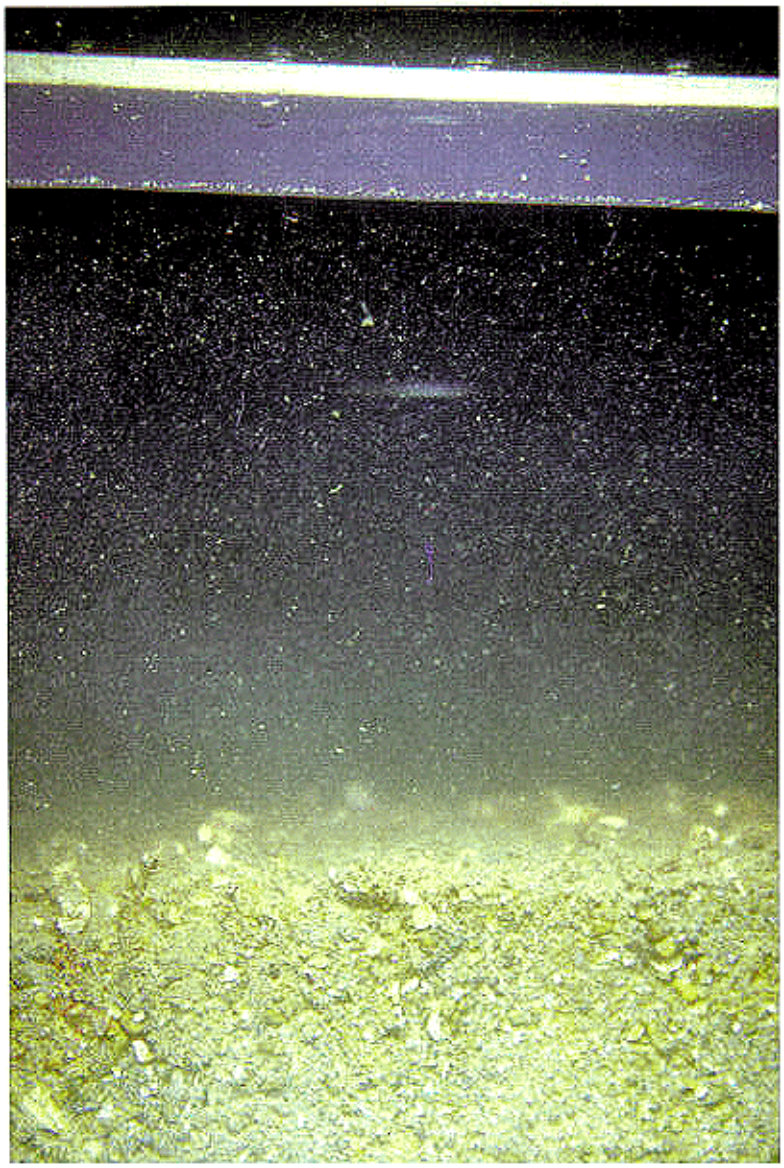

Figure 31. Habitat class H, physically dominated coarse sand to gravel sediments.

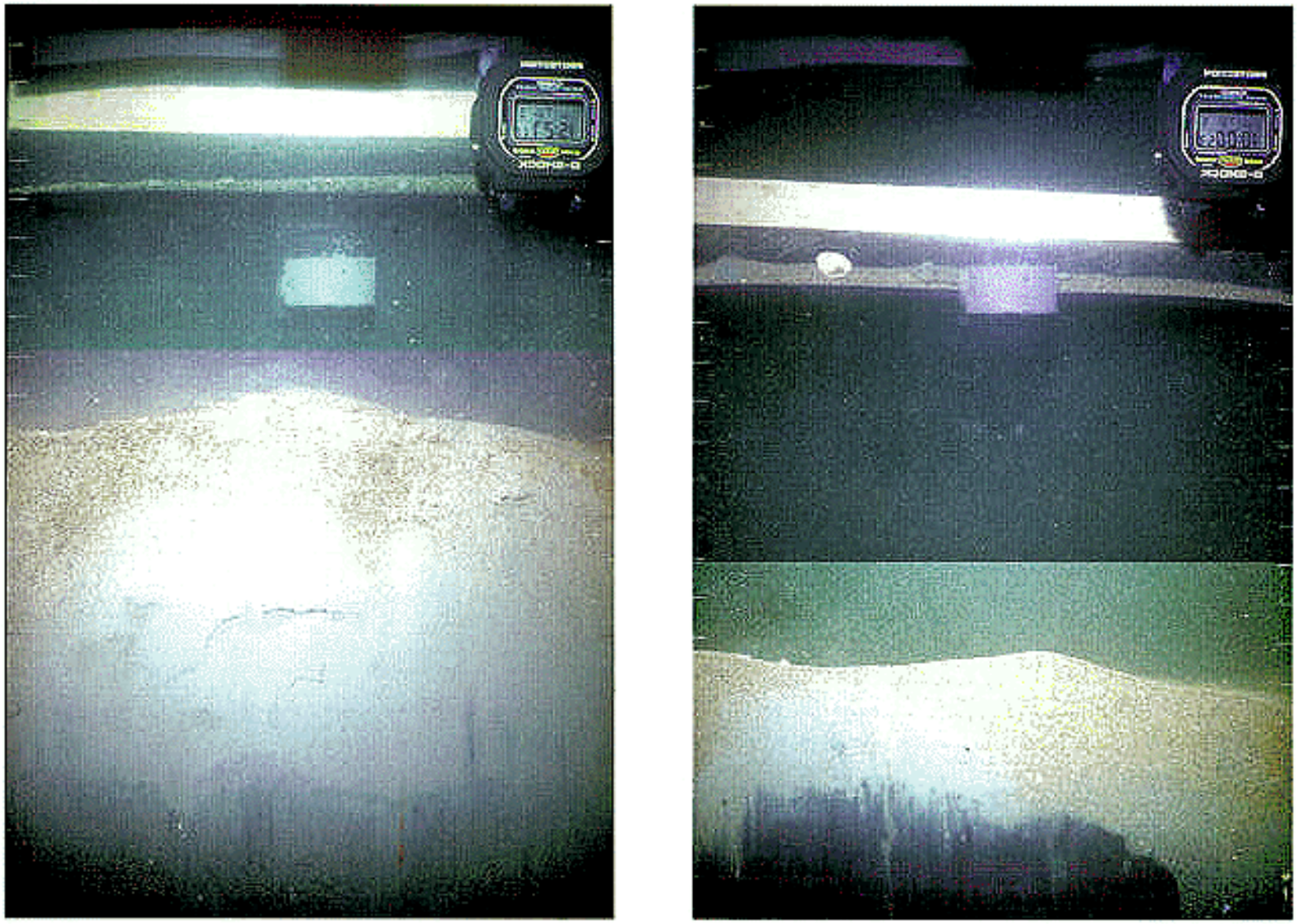

Figure32. Habitat class I. physically dominated transitional sediments: coarser grain-size material layered over finer material

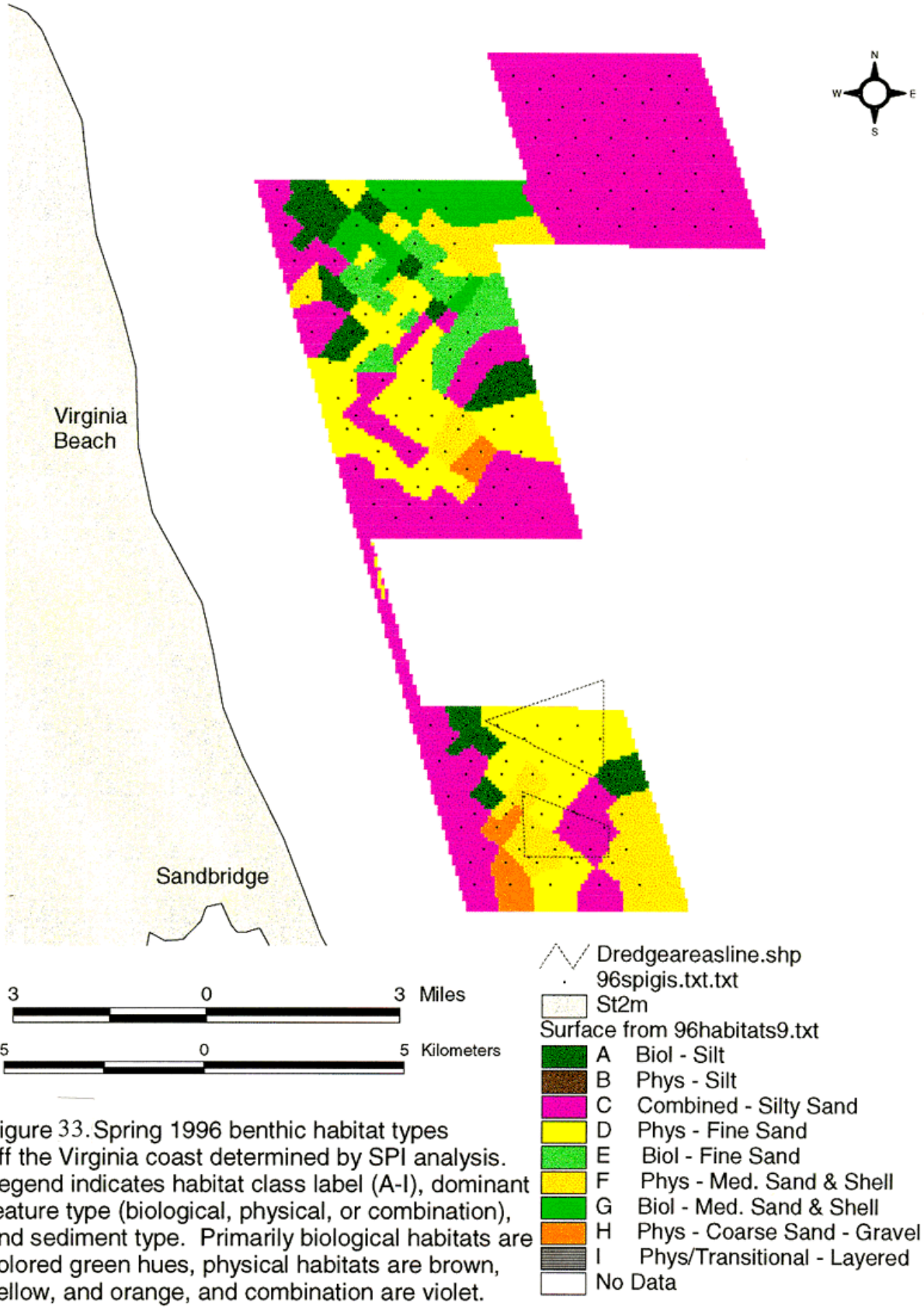

Figure 33. Spring 1996 benthic habitat types off the Virginia coast determined by SPI analysis. Legend indicates habitat class label (A-I), dominant feature type (biological, physical, or combination), and sediment type. Primarily biological habitats are colored green hues, physical habitats are brown, yellow, and orange, and combination are violet.

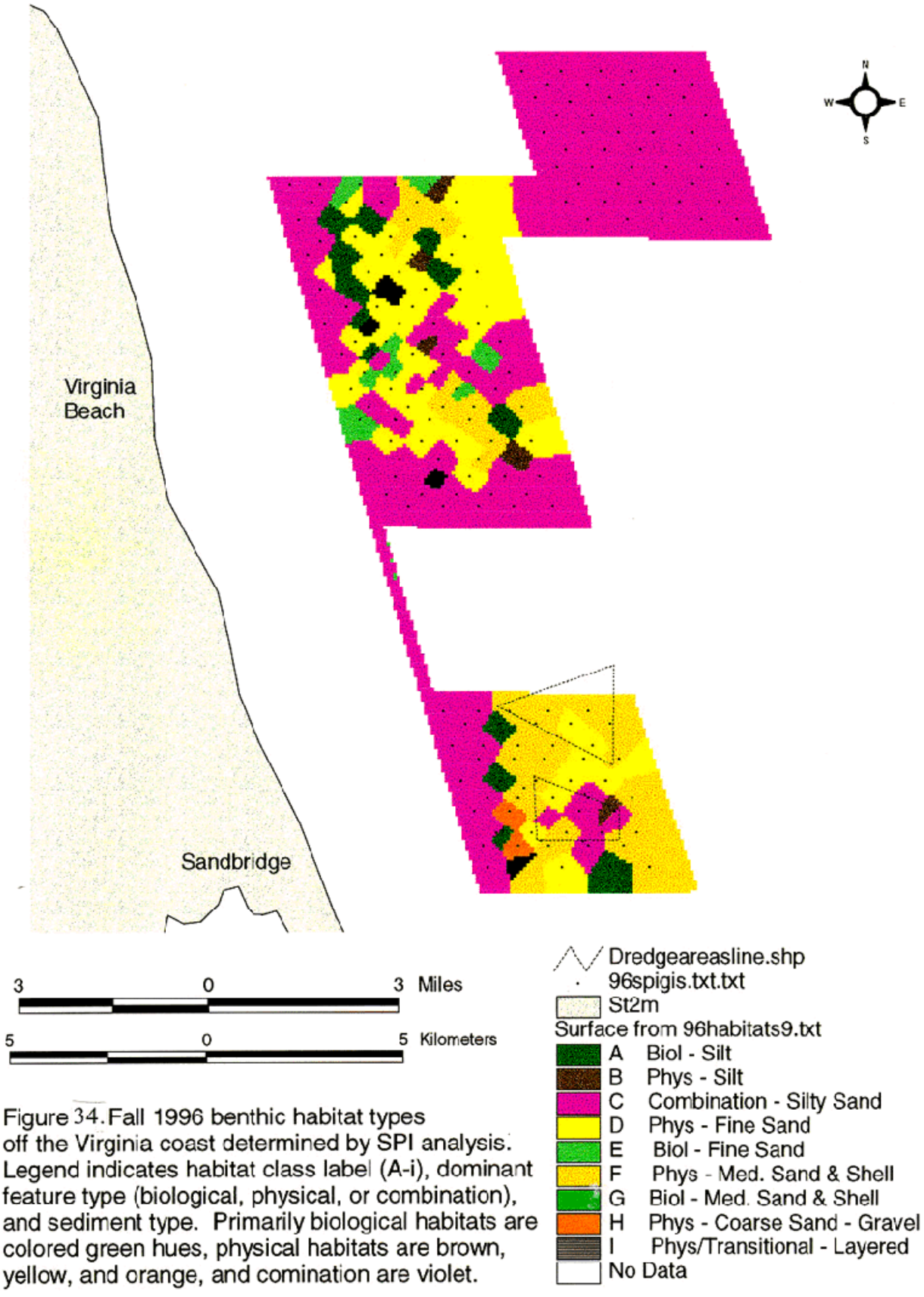

Figure 34. Fall 1996 benthic habitat types off the Virginia coast determined by SPI analysis. Legend indicates habitat class label (A-i), dominant feature type (biological, physical, or combination), and sediment type. Primarily biological habitats are colored green hues, physical habitats are brown, yellow, and orange, and comination are violet.

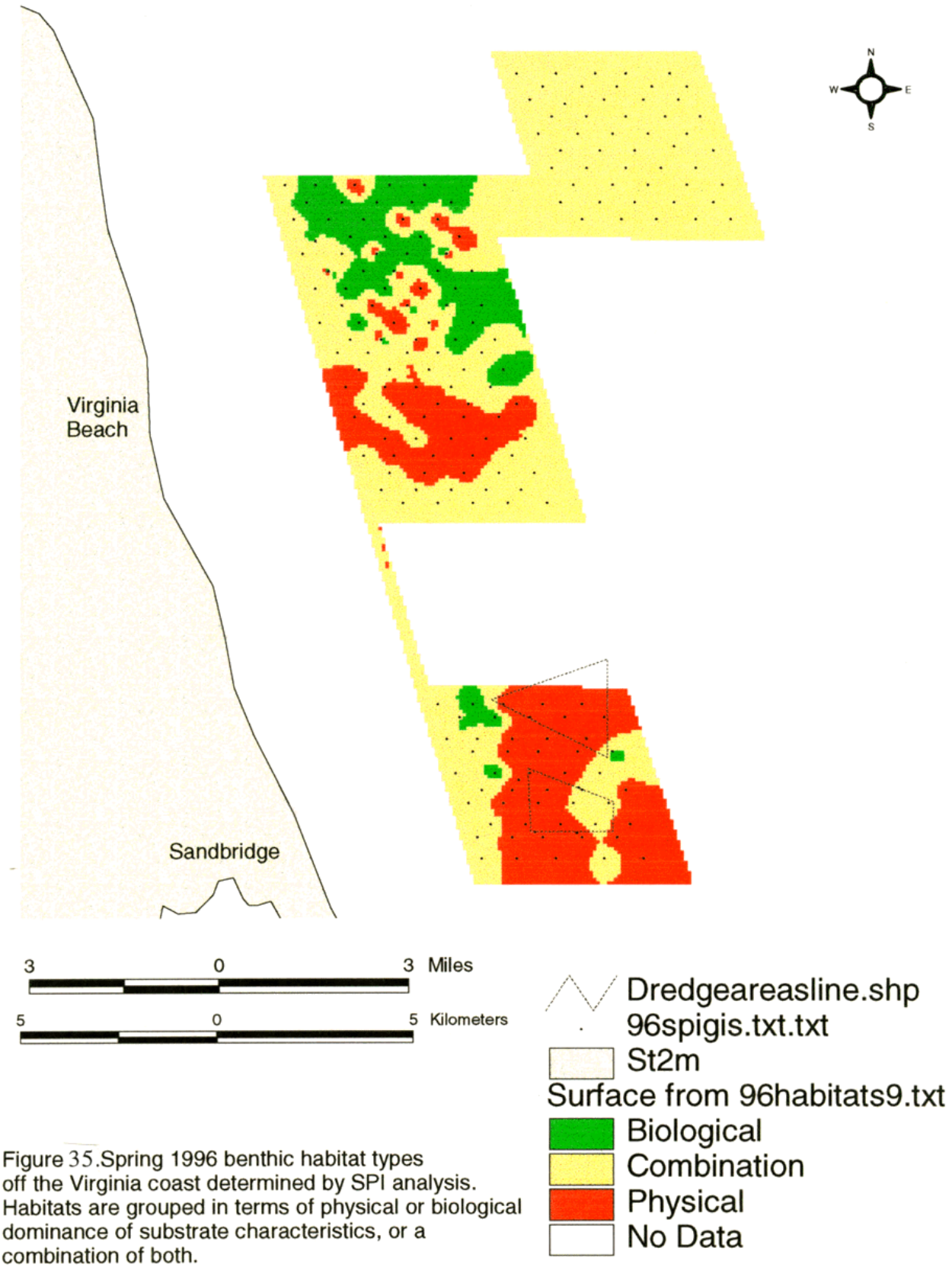

Figure 35.Spring 1996 benthic habitat types off the Virginia coast determined by SPI analysis. Habitats are grouped in terms of physical or biological dominance of substrate characteristics, or a combination of both.

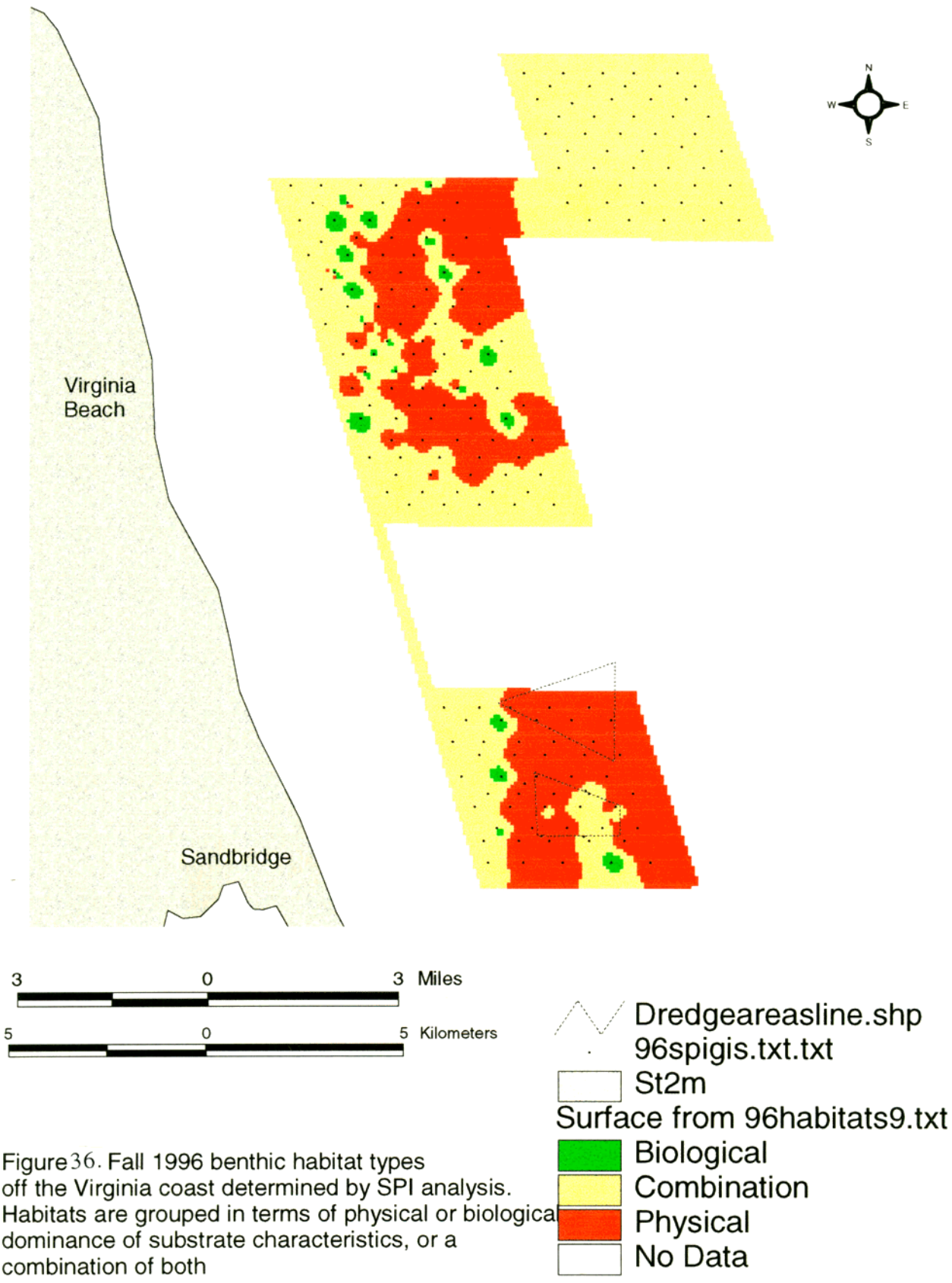

Figure 36. Fall 1996 benthic habitat types off the Virginia coast determined by SPI analysis. Habitats are grouped in terms of physical or biological dominance of substrate characteristics, or a combination of both

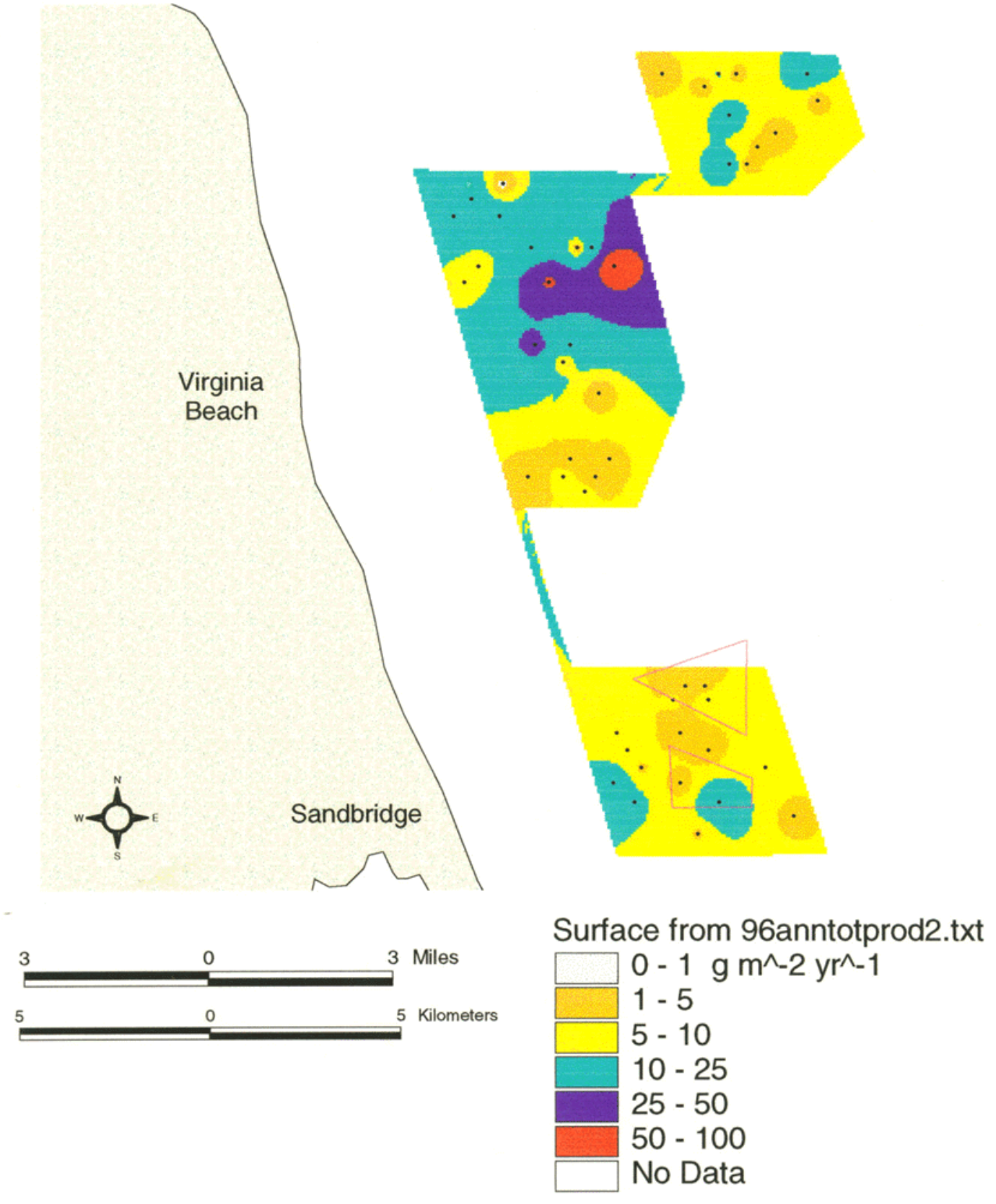

Figure 37. 1996 total annual community secondary production (g m^-2 yr^-1).

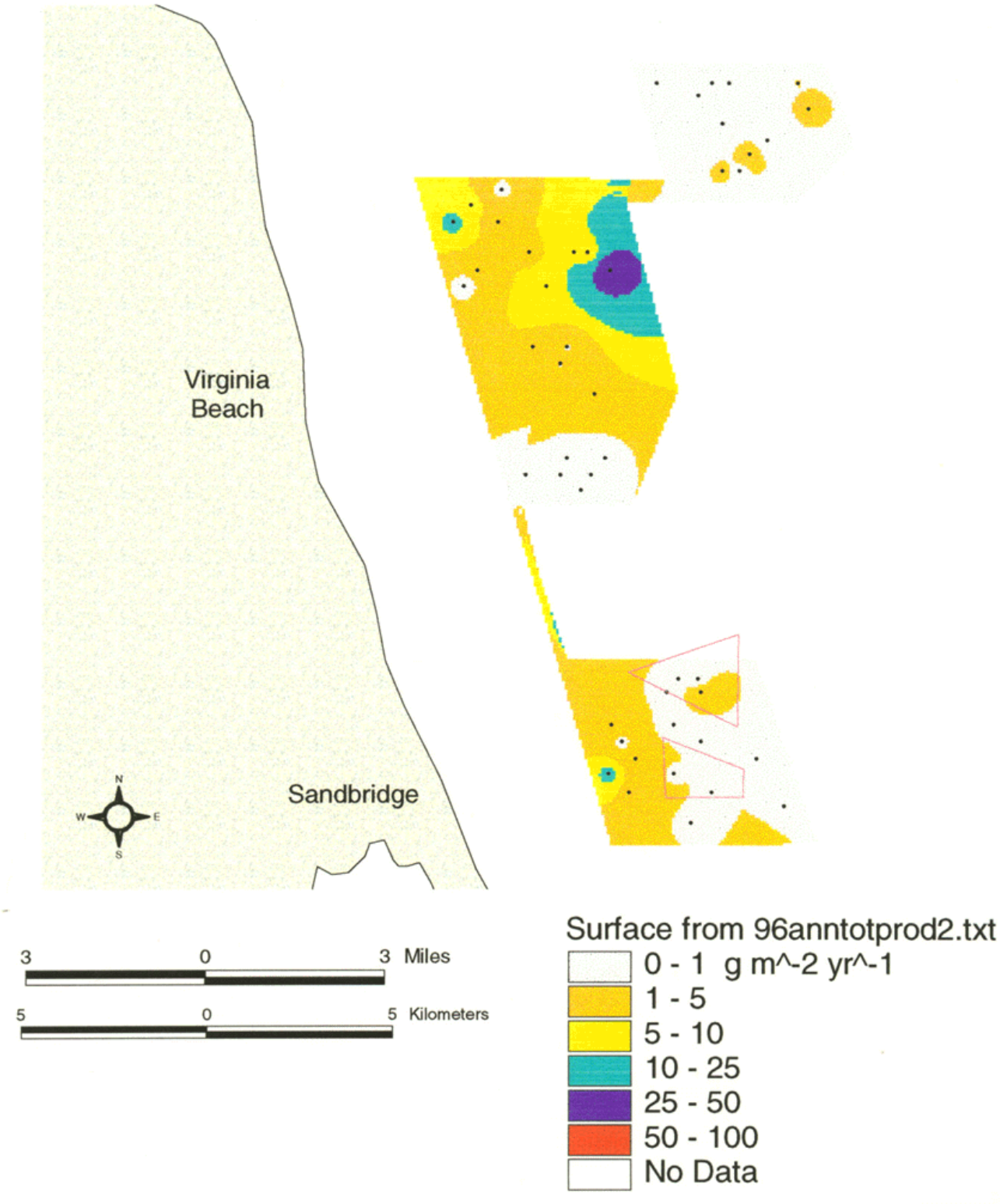

Figure 38. 1996 total annual molluscan secondary production (g m^-2 yr^-1).

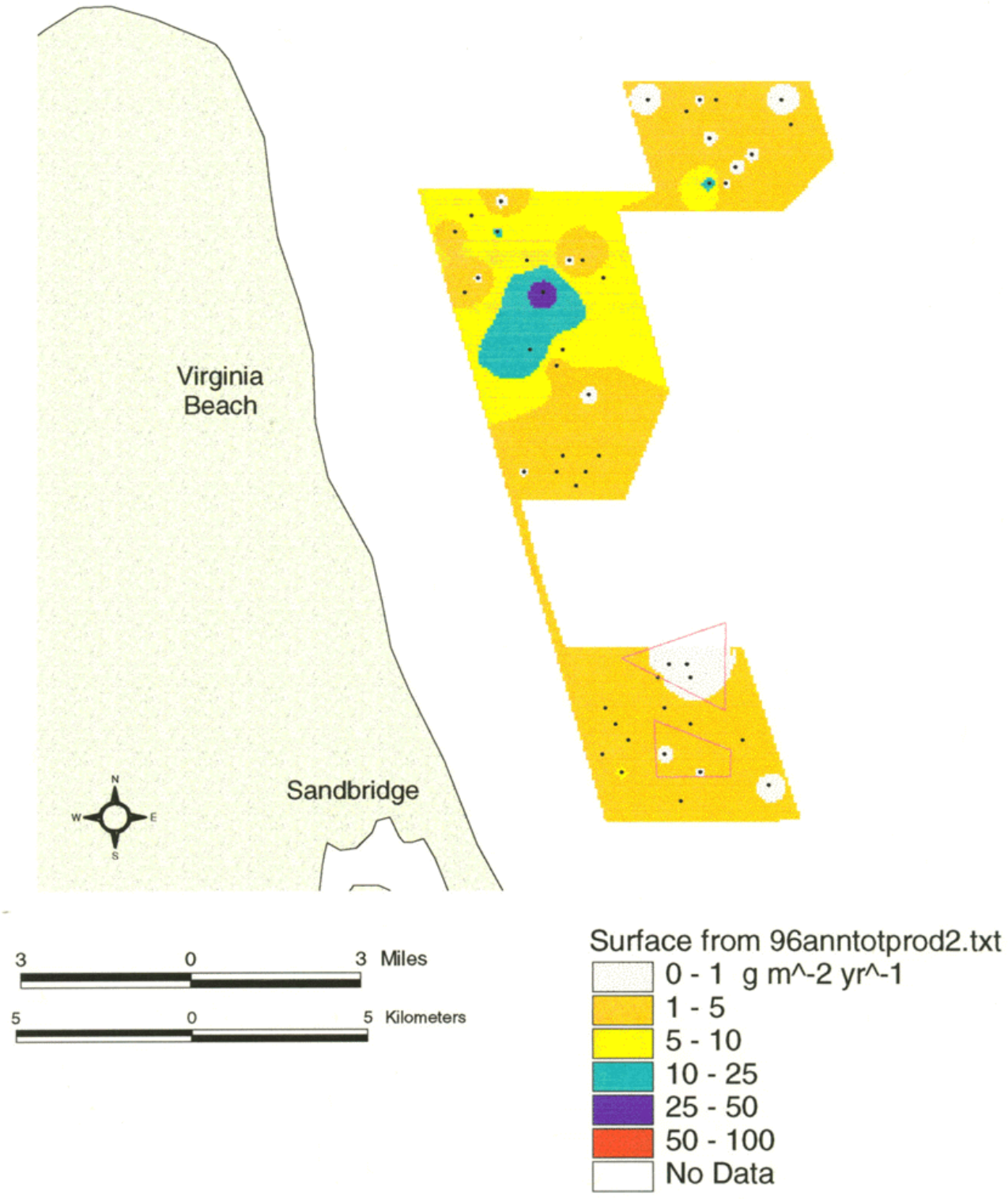

Figure 39. 1996 total annual annelid secondary production (g m^-2 yr^-1).

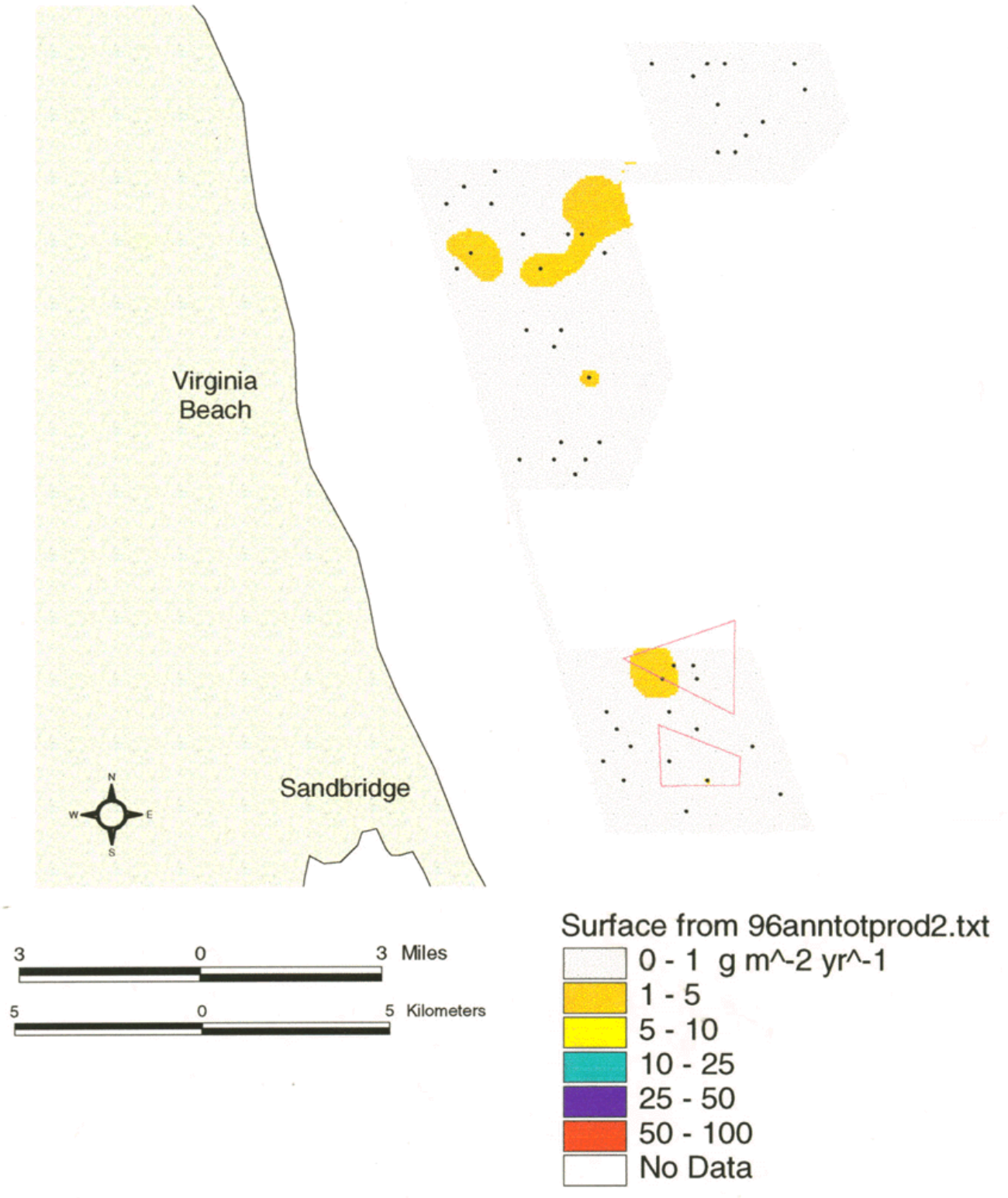

Figure 40. 1996 total annual crustacean secondary production (g m^-2 yr^-1).

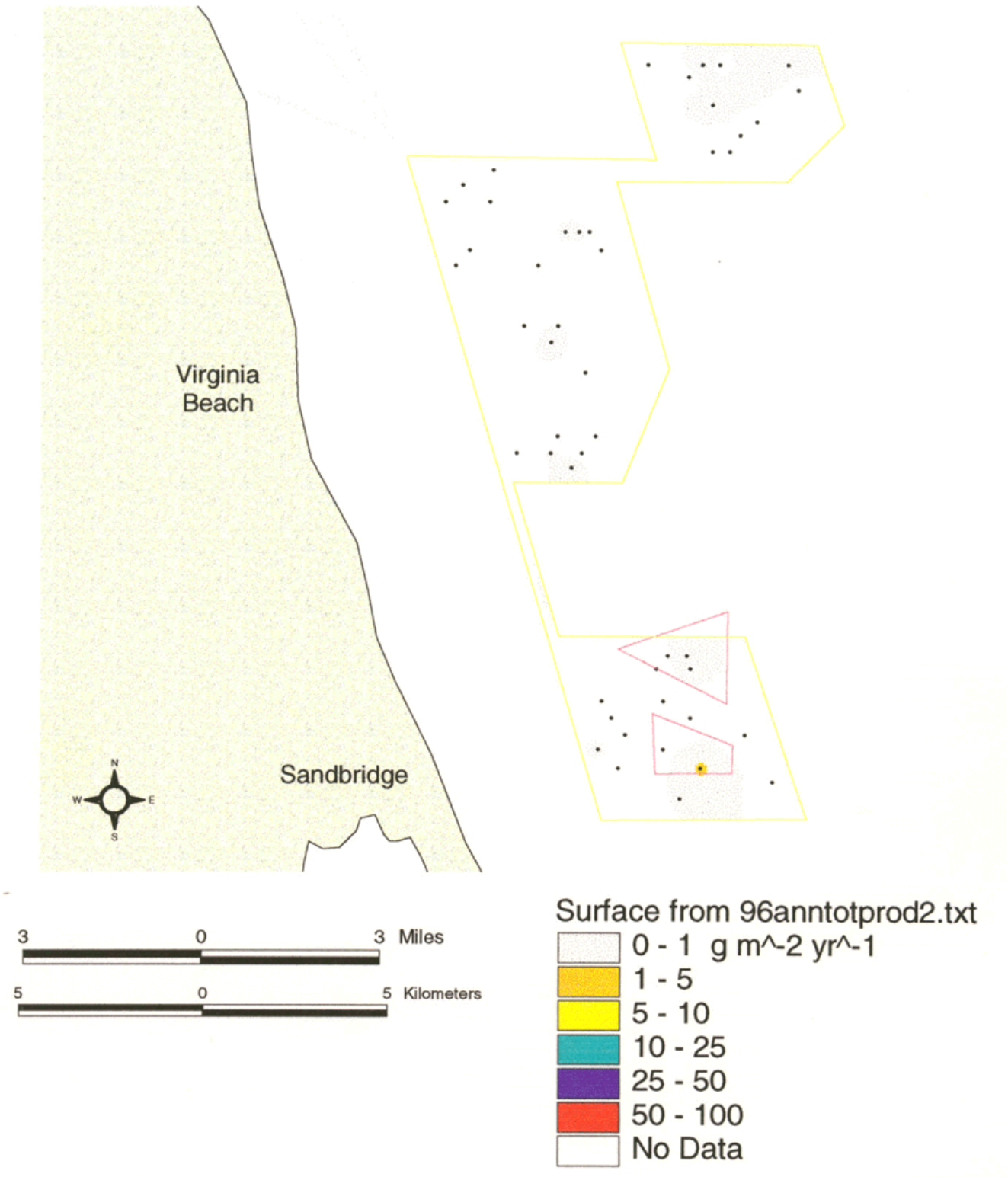

Figure 41. 1996 total annual secondary production (g m^-2 yr^-1) for miscellaneous taxa.

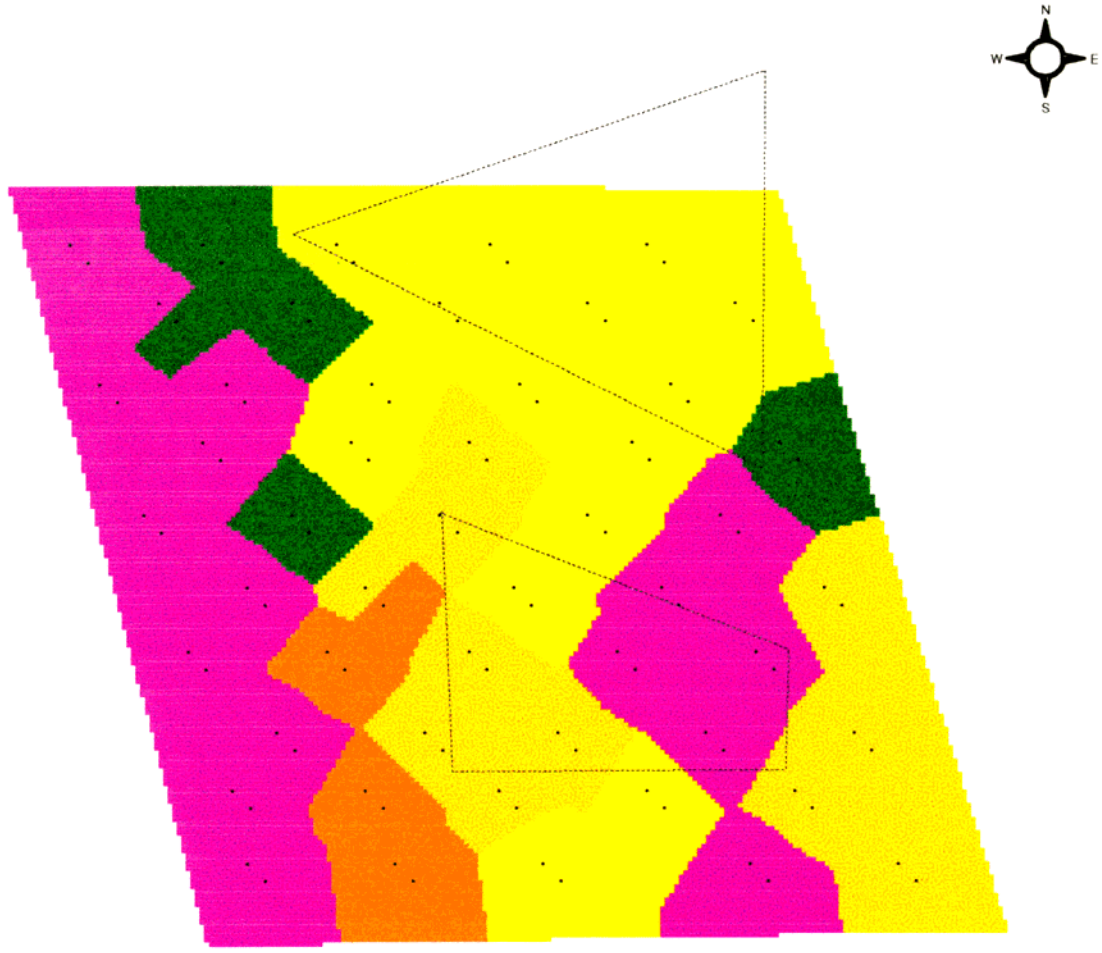

1 0 1 Miles

1 0 1 Kilometers

Dredgeareasline.shp
96habitats9.txt
Surface from 96habitats9.txt
A Biol - Silt
B Phys - Silt
C Combined - Silty Sand
D Phys - Fine Sand
E Biol - Fine Sand
F Phys - Med. Sand & Shell
G Biol - Med. Sand & Shell
H Phys - Coarse Sand - Gravel
I Phys/Transitional - Layered
No Data

Figure 42. Spring 1996 benthic habitat types in the vicinity of Sandbridge shoal determined by SPI analysis.
Legend indicates habitat class label (A-I), dominant feature type (biological, physical, or combination), and sediment type. Primarily biological habitats are colored green hues, physical habitats are brown, yellow, and orange, and combination are violet.

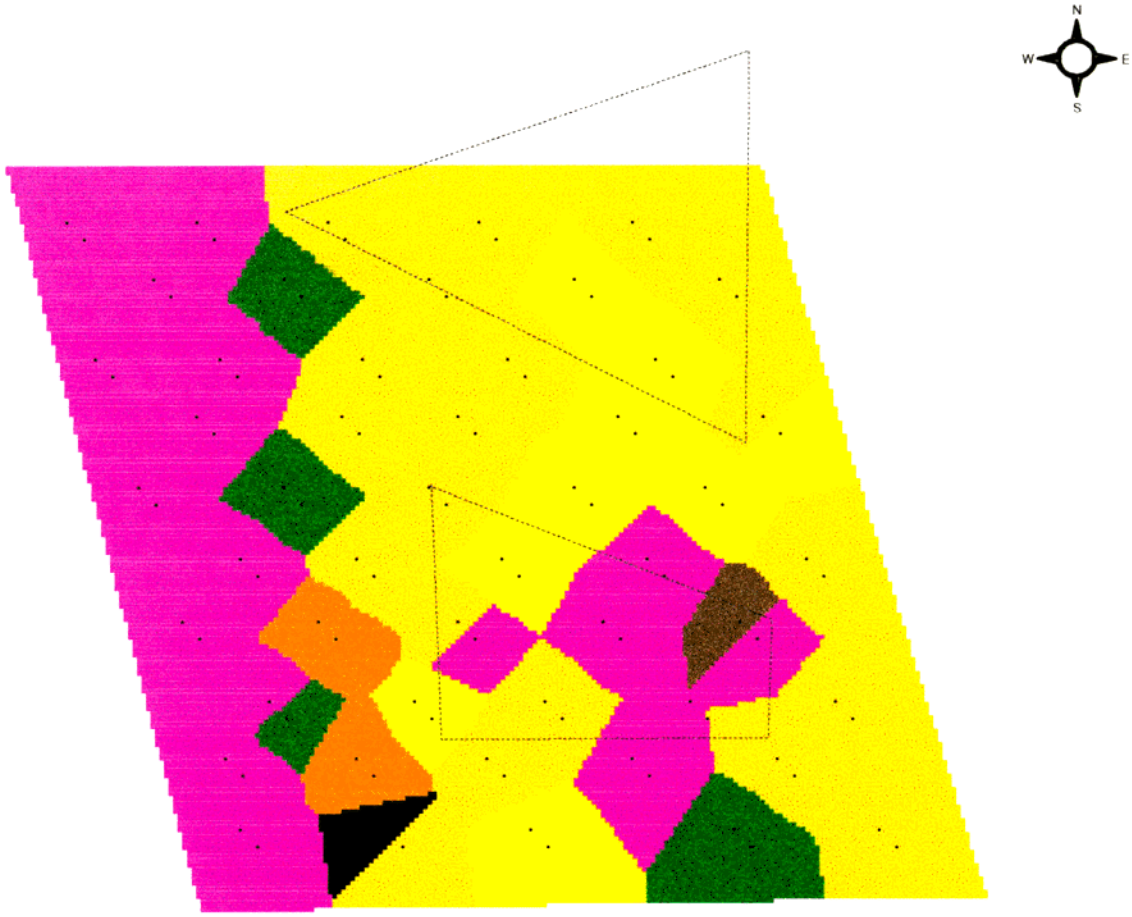

1 0 1 Miles

1 0 1 Kilometers

96habitats9.txt
Dredgeareasline.shp
St2m
Surface from 96habitats9.txt
A Biol - Silt
B Phys - Silt
C Combined - Silty Sand
D Phys - Fine Sand
E Biol - Fine Sand
F Phys - Med. Sand & Shell
G Biol - Med. Sand & Shell
H Phys - Coarse Sand - Gravel
I Phys/Transitional - Layered
No Data

Figure 43. Fall 1996 benthic habitat types in the vicinity of Sandbridge shoal determined by SPI analysis.
Legend indicates habitat class label (A-I), dominant feature type (biological, physical, or combination), and sediment type. Primarily biological habitats are colored green hues, physical habitats are brown, yellow, and orange, and combination are violet.

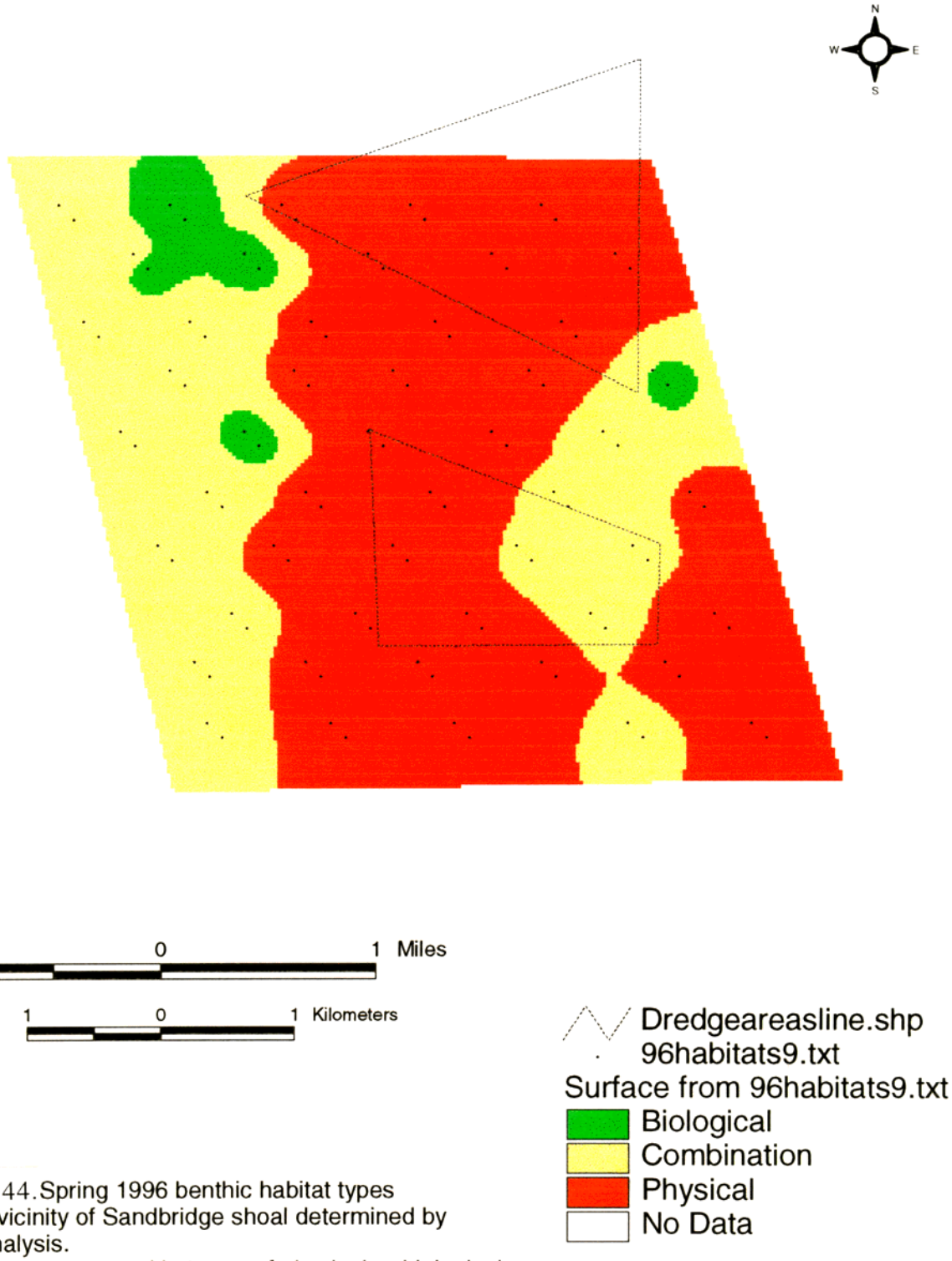

Figure 44. Spring 1996 benthic habitat types in the vicinity of Sandbridge shoal determined by SPI analysis.
Habitats are grouped in terms of physical or biological dominance of substrate characteristics, or a combination of both

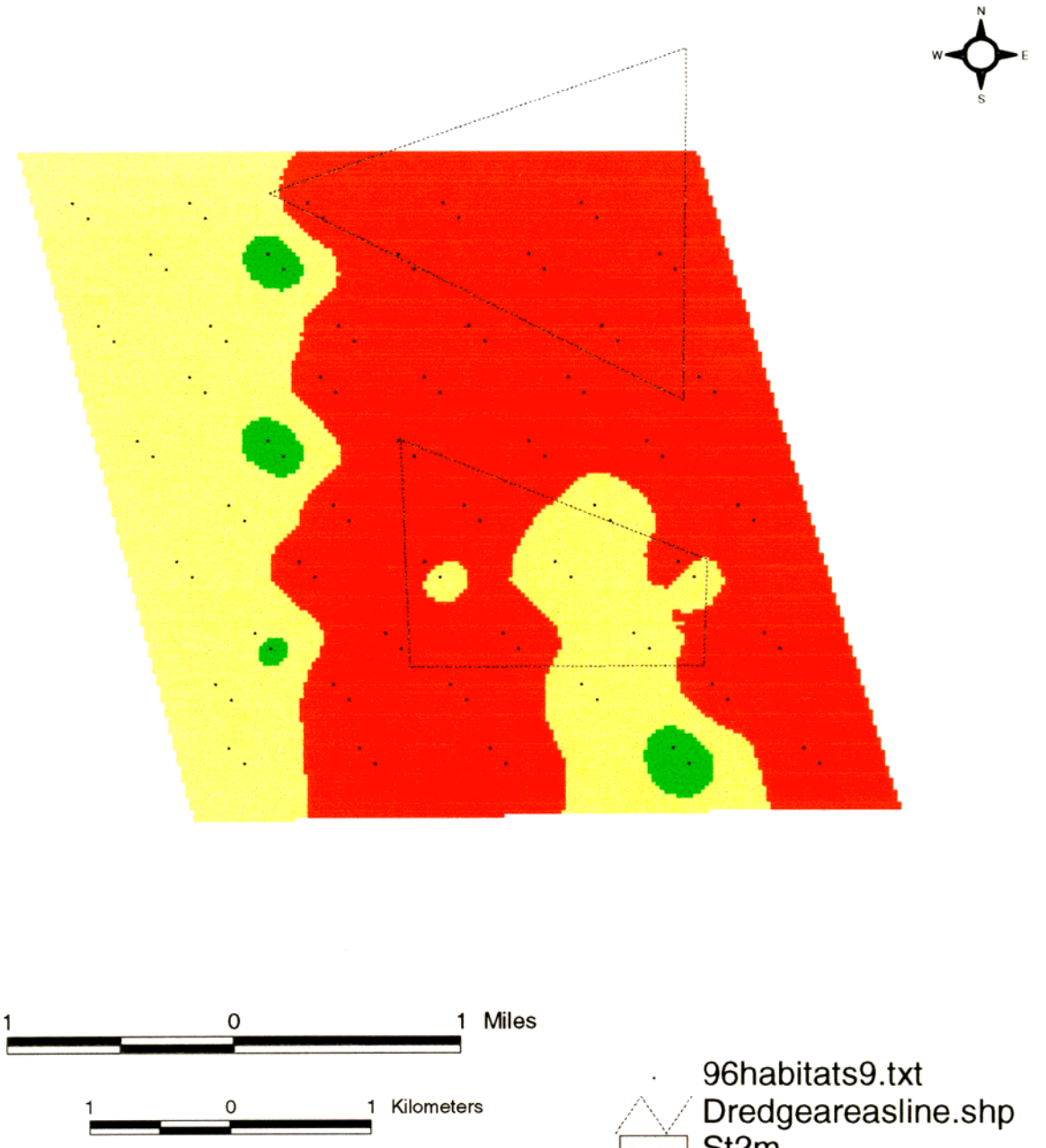

Figure 45. Fall 1996 benthic habitat types in the vicinity of Sandbridge shoal determined by SPI analysis.
Habitats are grouped in terms of physical or biological dominance of substrate characteristics, or a combination of both

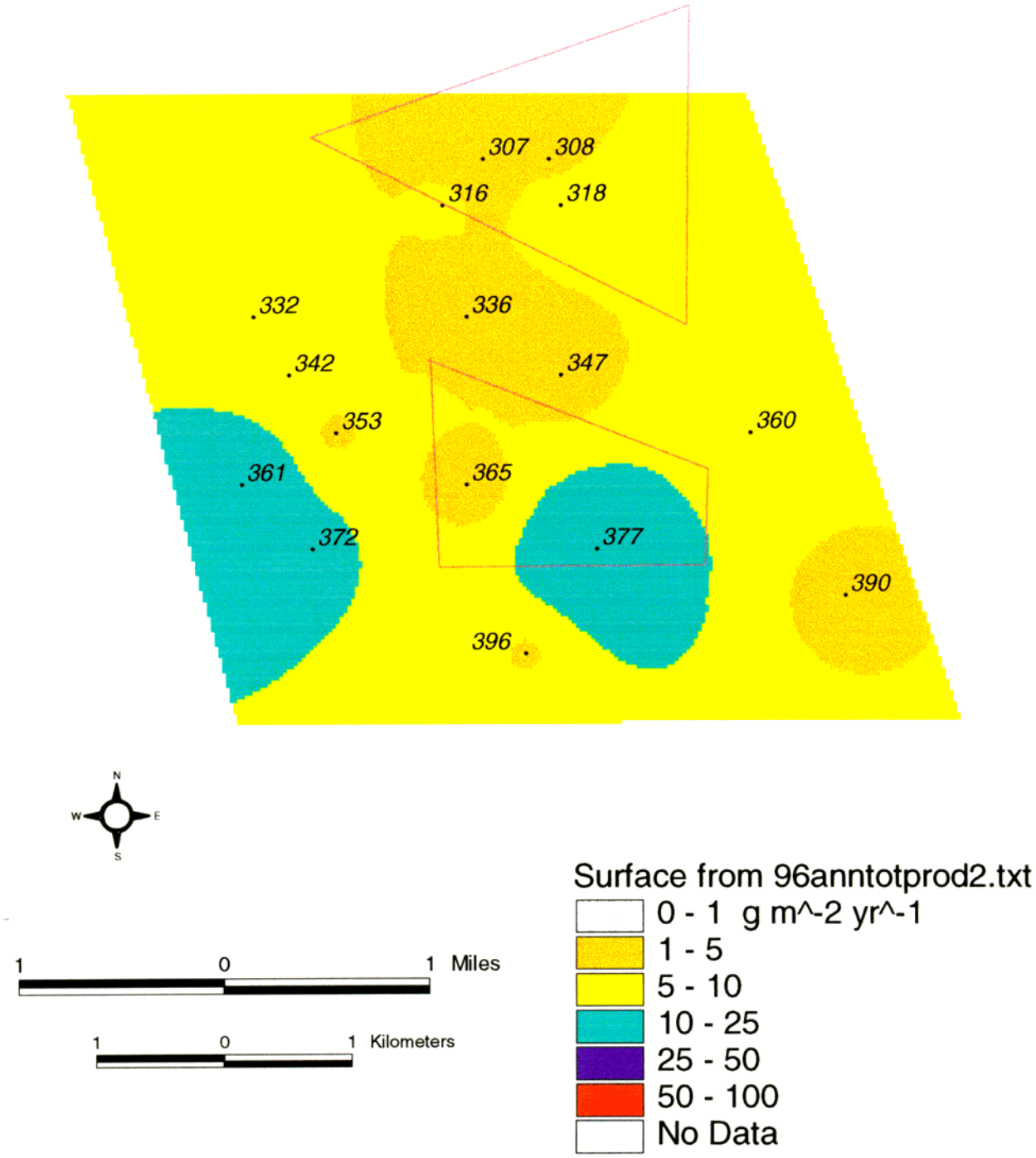

Figure 46. 1996 total annual community secondary production (g m^-2 yr^-1) in the vicinity of Sandbridge shoal and the proposed borrow areas. 1996 Cell numbers are labelled.

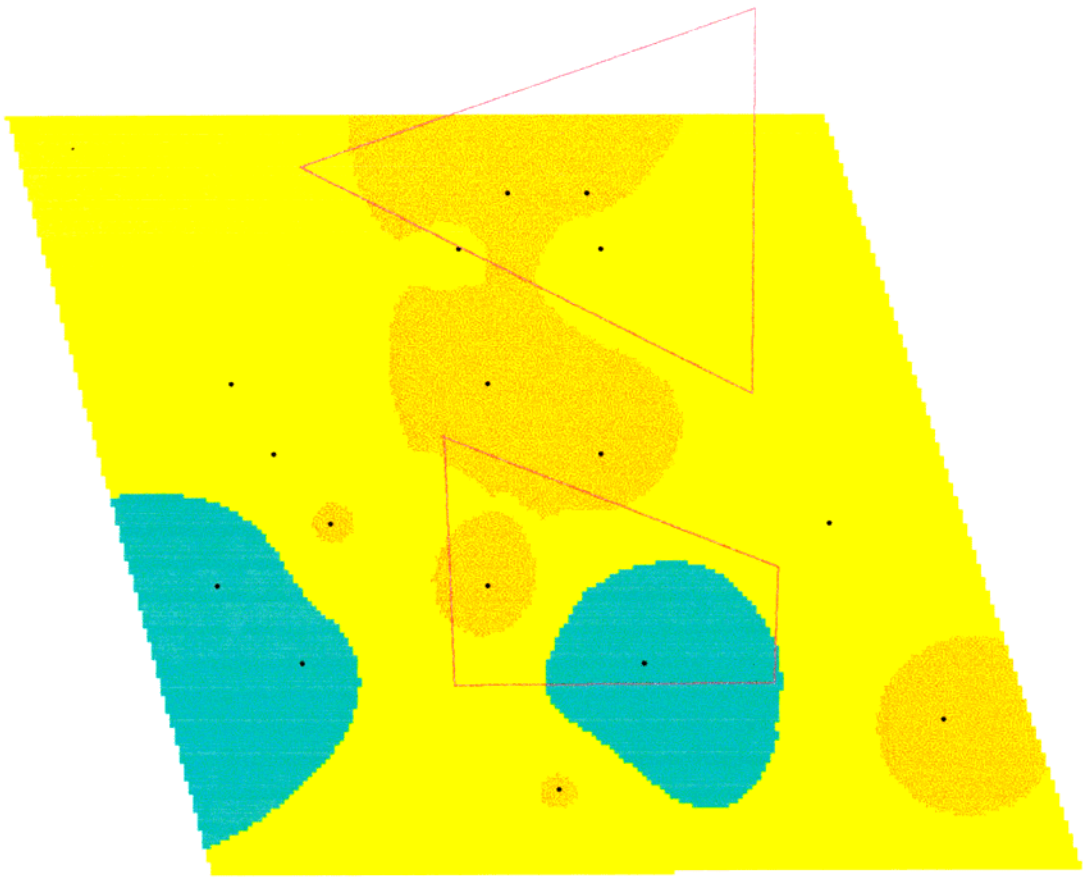

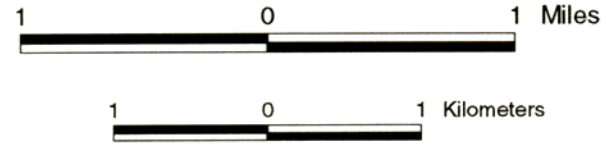

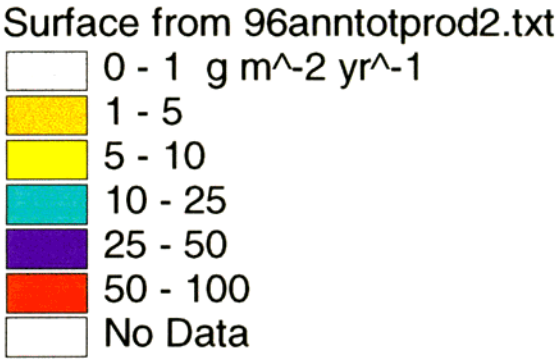

Figure 47 1996 total annual community secondary production (g m^-2 yr^-1) in the vicinity of Sandbridge shoal and the proposed borrow areas.

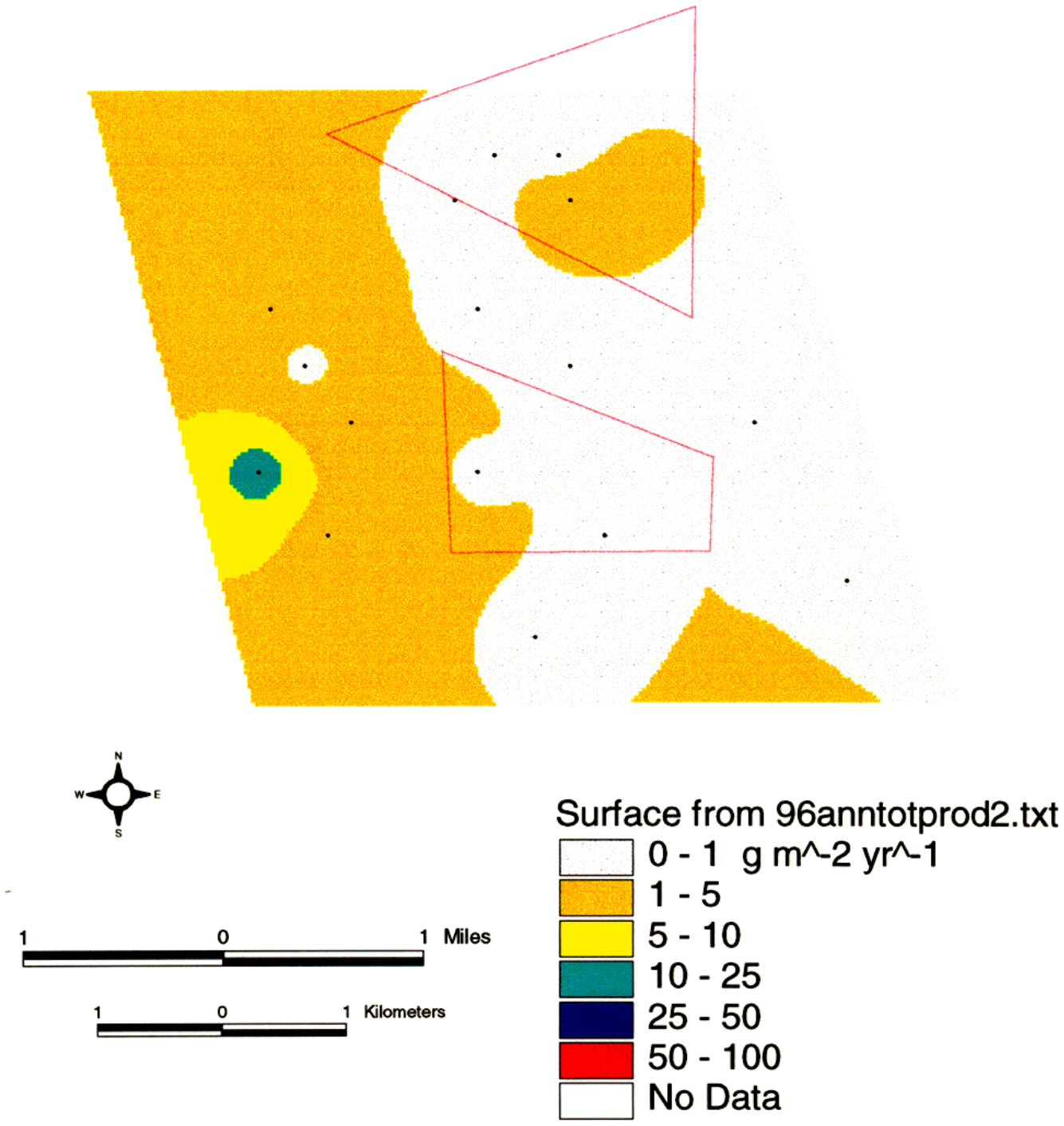

Figure 48. 1996 total annual molluscan secondary production (g m^-2 yr^-1) in the vicinity of Sandbridge shoal and the proposed borrow areas.

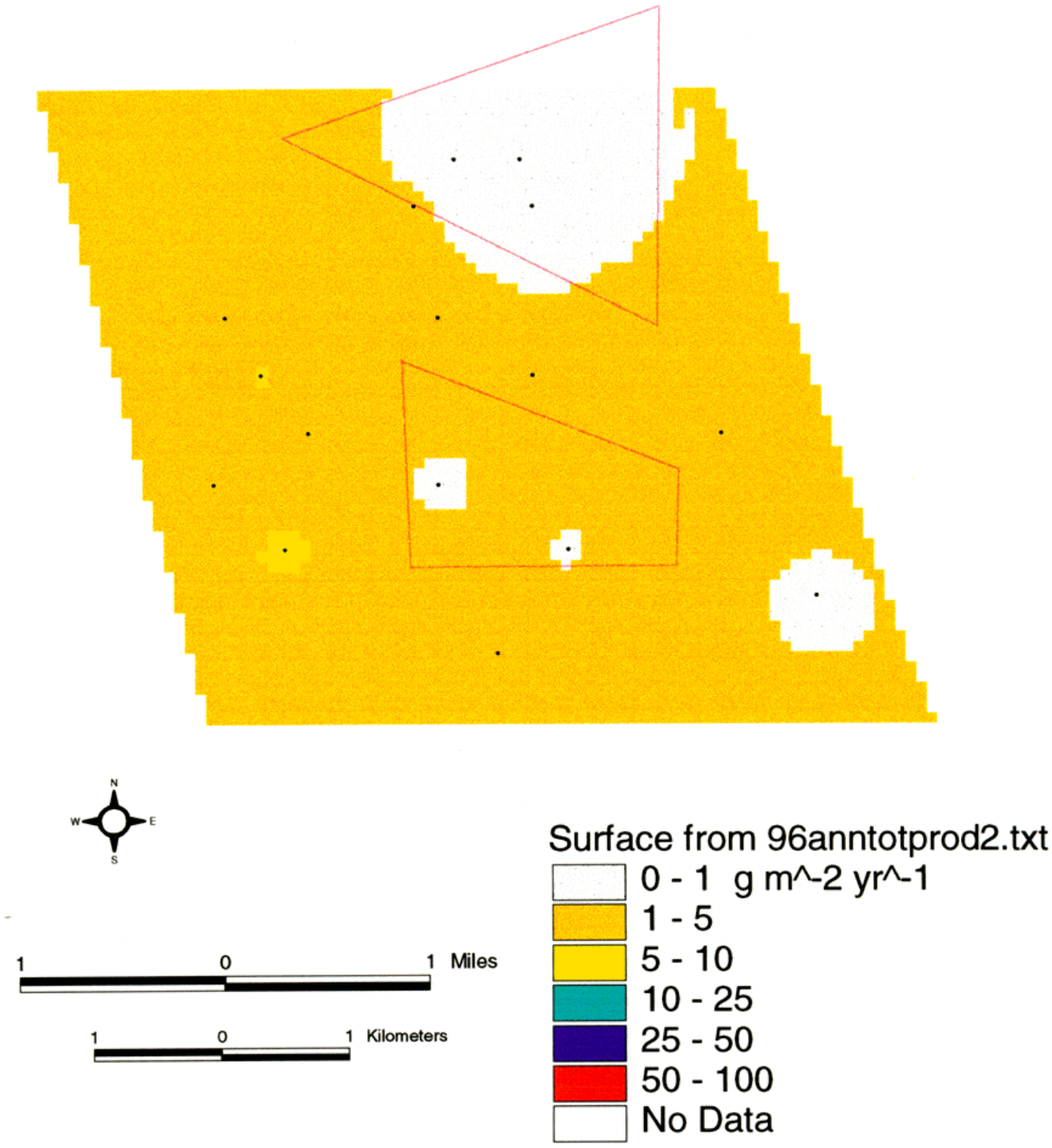

Figure 49. 1996 total annual polychaete secondary production (g m^-2 yr^-1) in the vicinity of Sandbridge shoal and the proposed borrow areas.

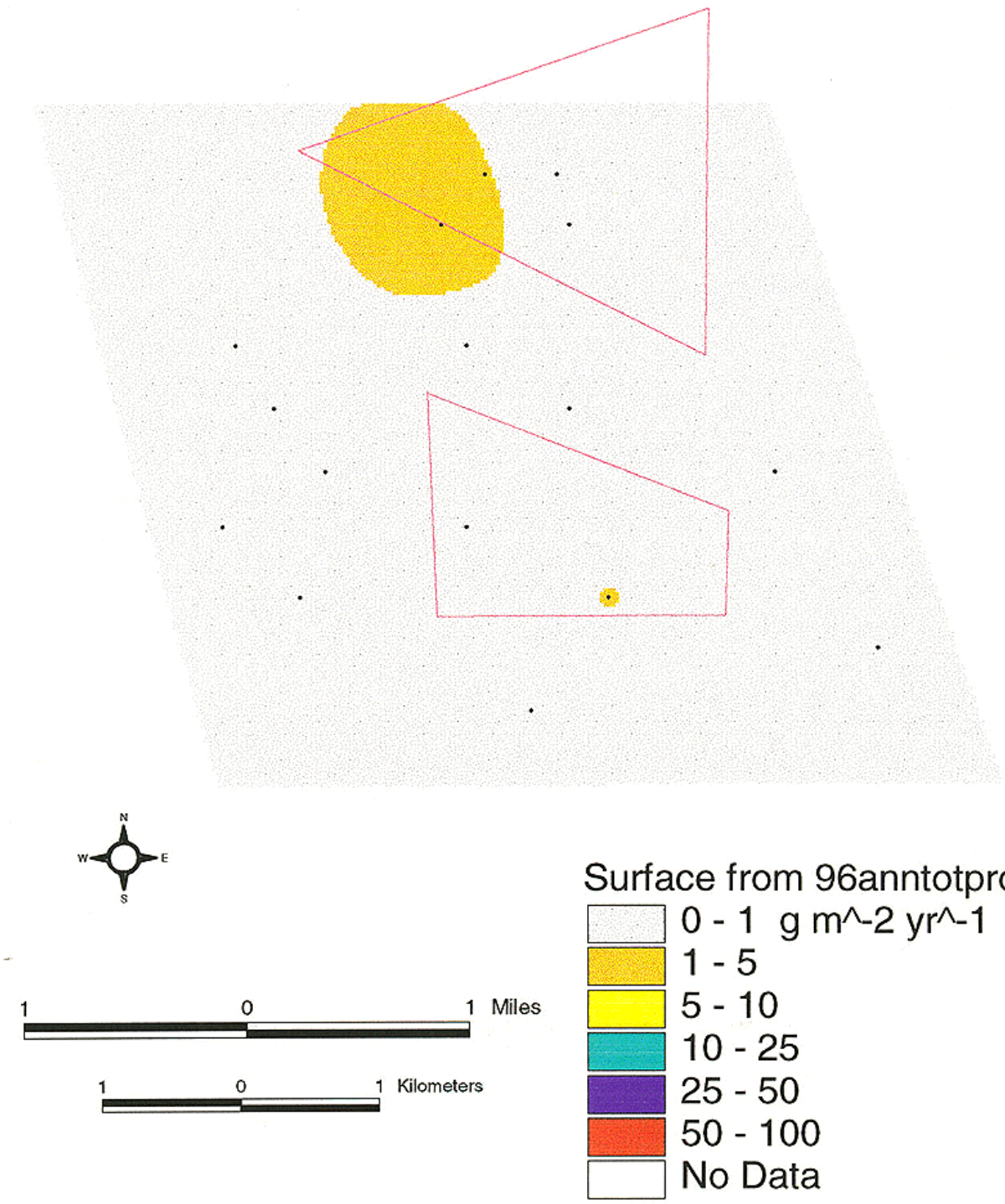

Figure 50. 1996 total annual crustacean secondary production (g m^-2 yr^-1) in the vicinity of Sandbridge shoal and the proposed borrow areas.

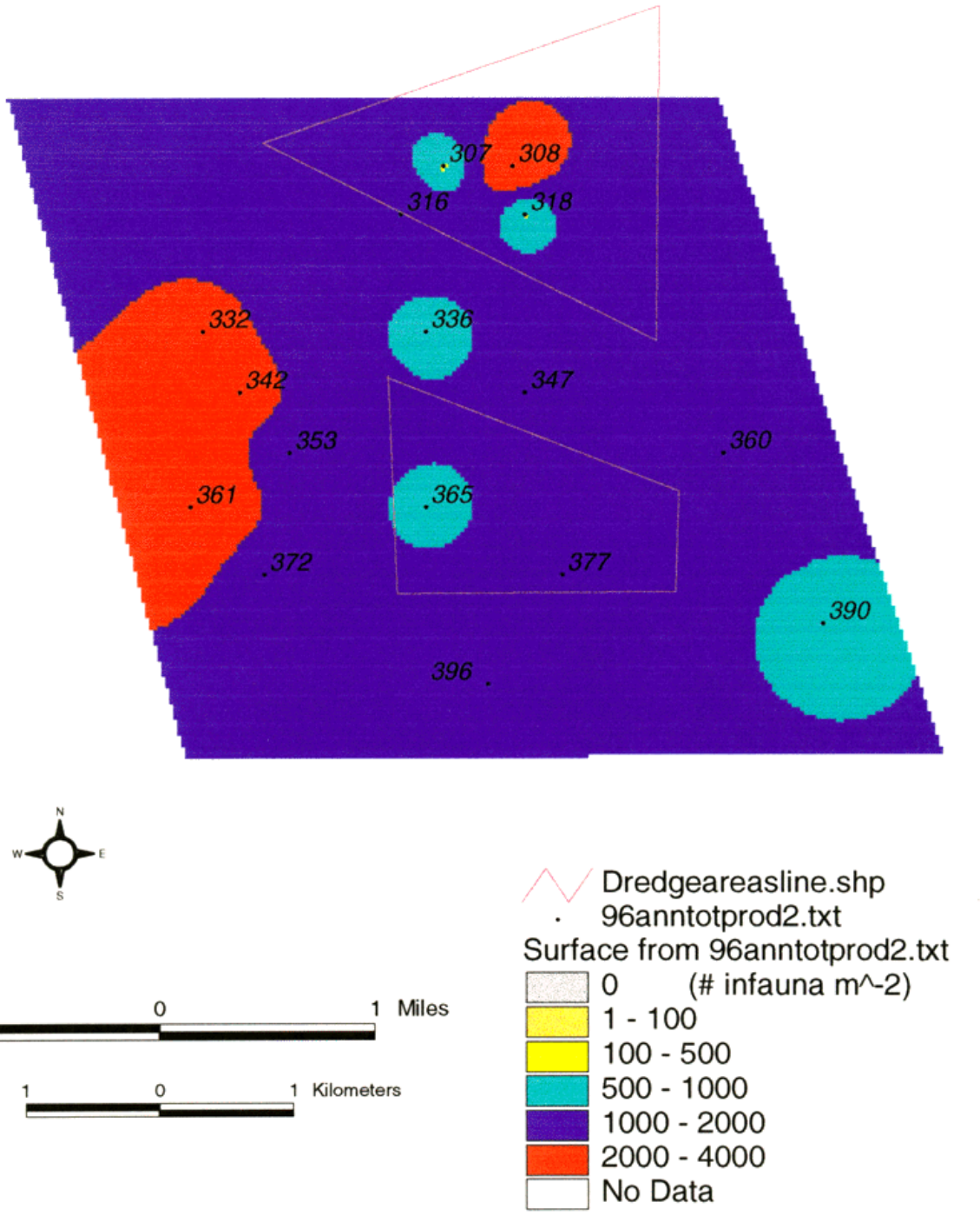

Figure 51. 1996 mean annual densities of all infauna (# m^-2) in the vicinity of Sandbridge shoal and the proposed borrow areas. Grab sample cell numbers are labelled.

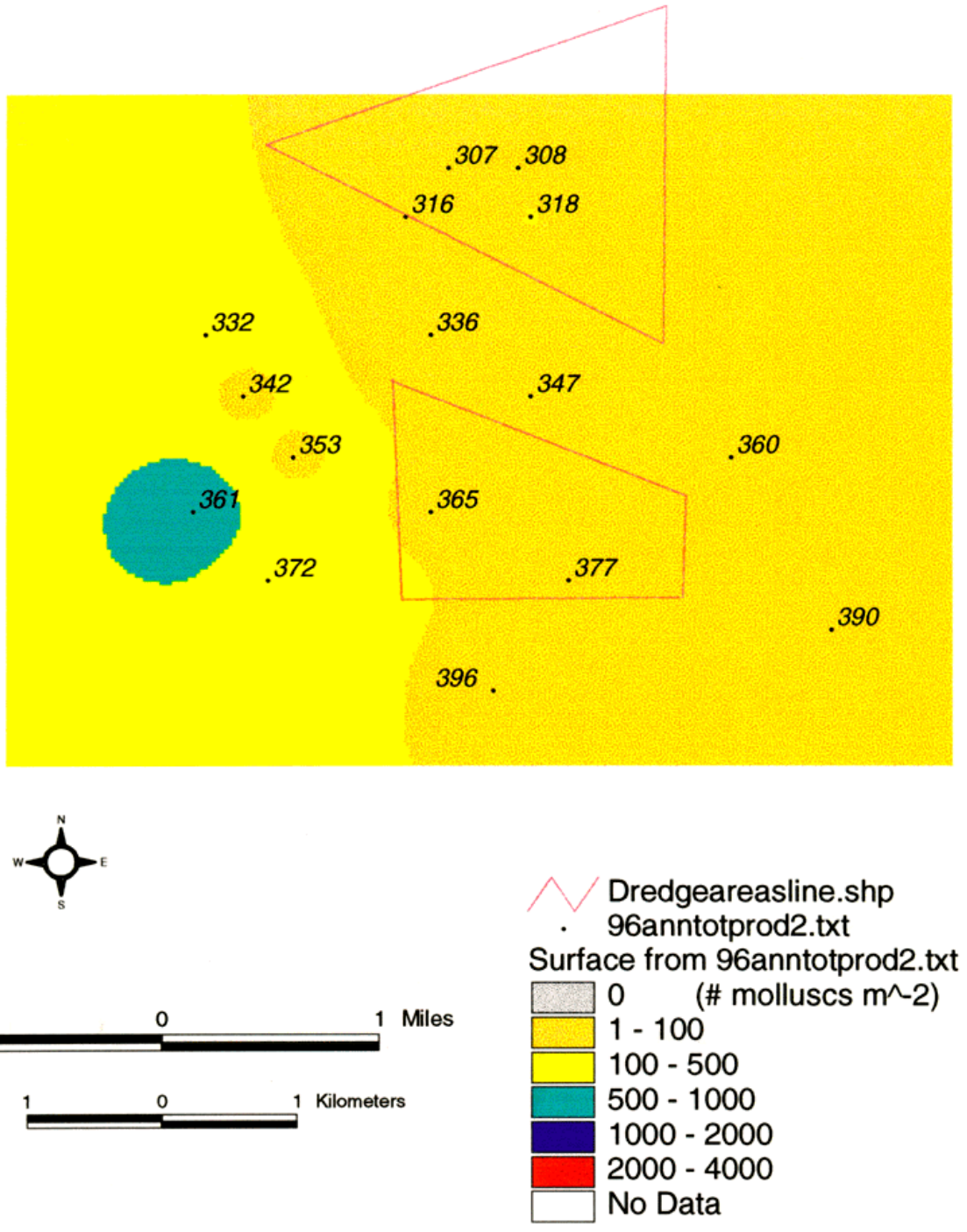

Figure 52. 1996 mean annual densities of molluscs (# m^-2) in the vicinity of Sandbridge shoal and the proposed borrow areas. Grab sample cell numbers are labelled.

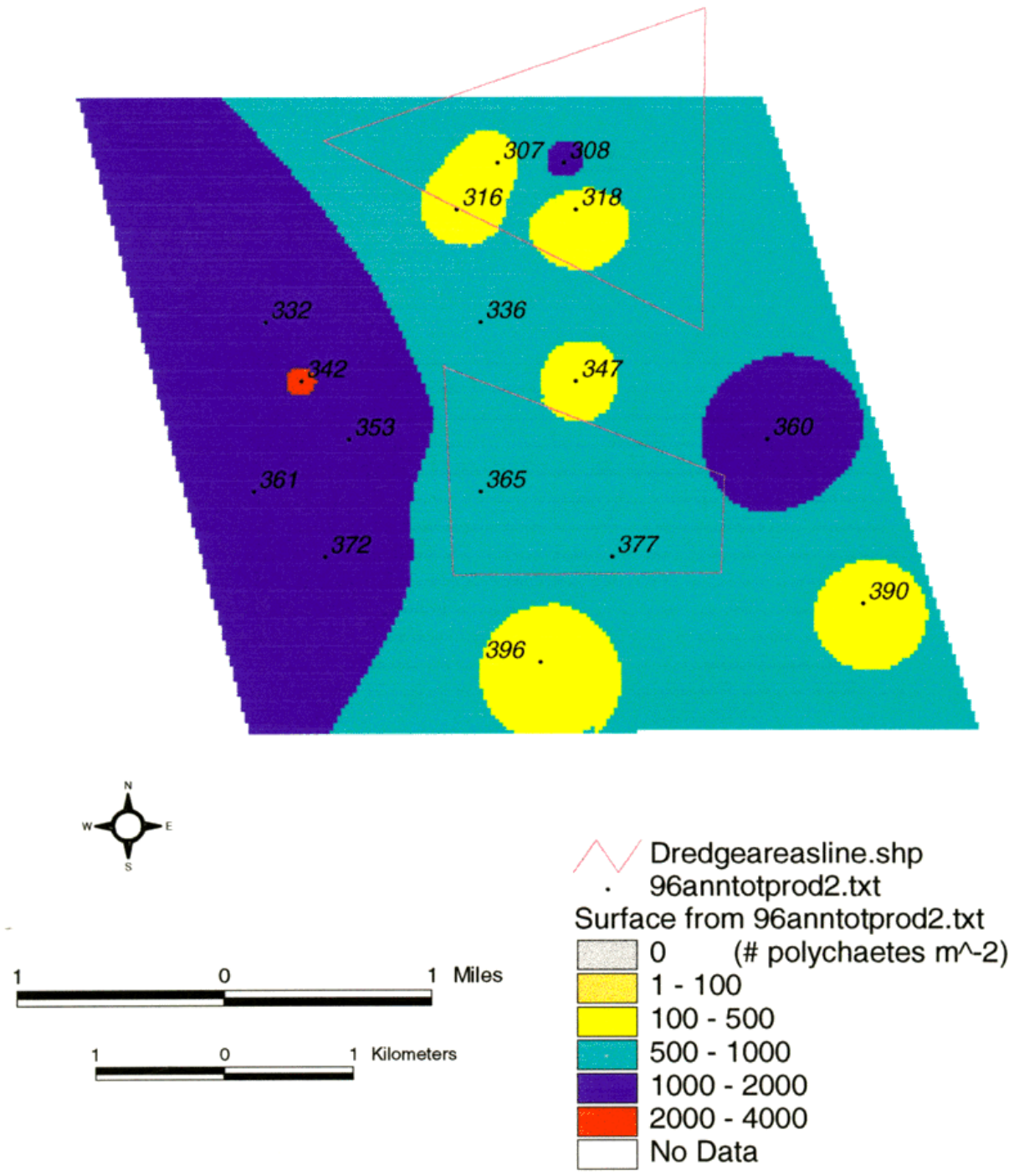

Figure 53. 1996 mean annual densities of polychaetes (# m^-2) in the vicinity of Sandbridge shoal and the proposed borrow areas. Grab sample cell numbers are labelled.

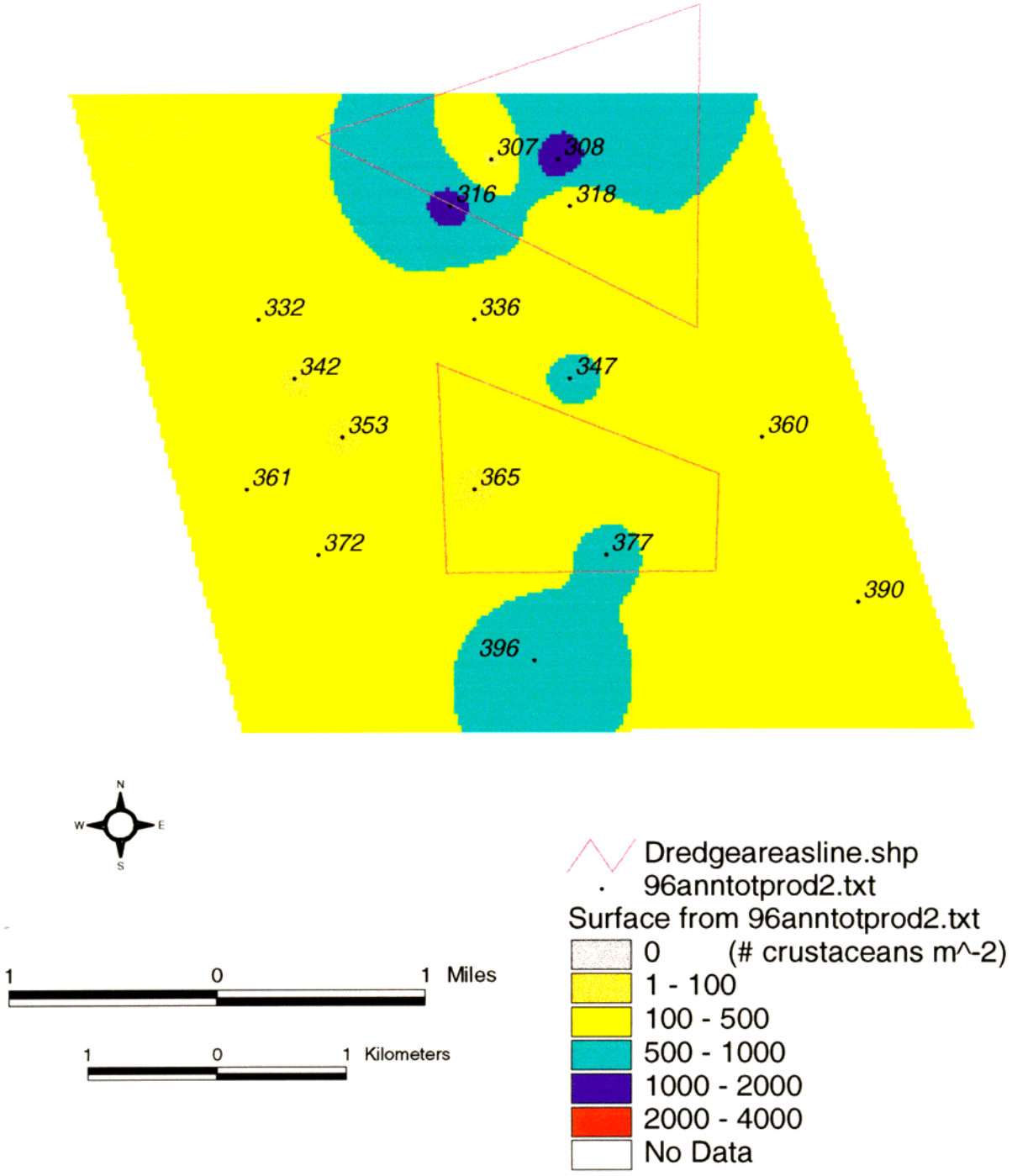

Figure 54. 1996 mean annual densities of crustaceans (# m^-2) in the vicinity of Sandbridge shoal and the proposed borrow areas. Grab sample cell numbers are labelled.

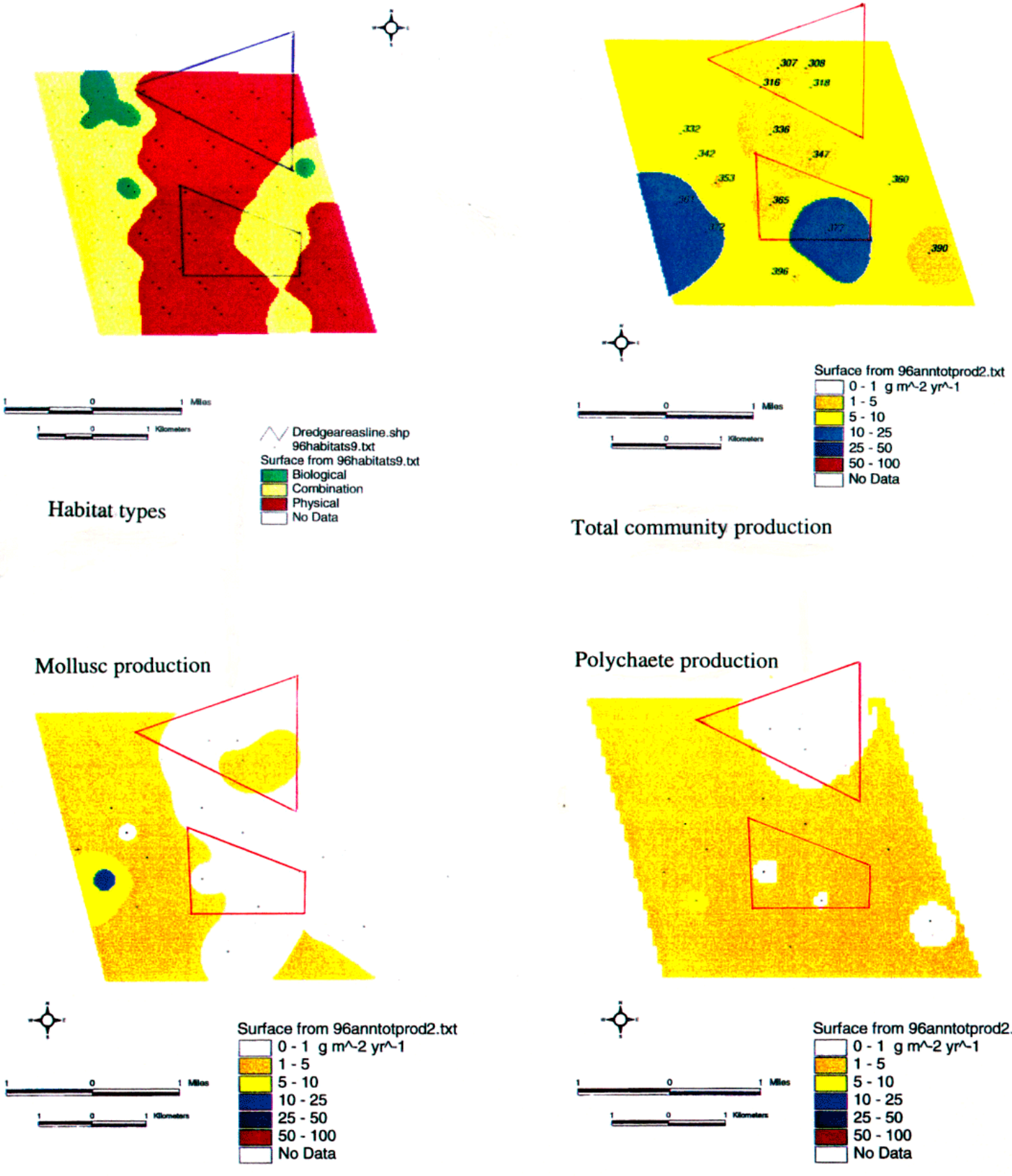

Figure 55. Comparison of gross habitat type determinations from SPI to secondary production calculated using grab data for the study area off Sandbridge, in the vicinity of the proposed borrow areas.

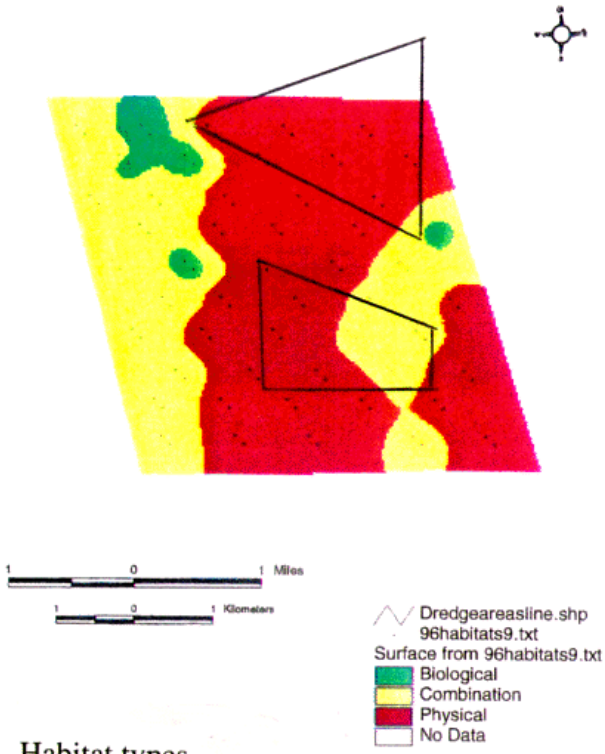

Habitat types

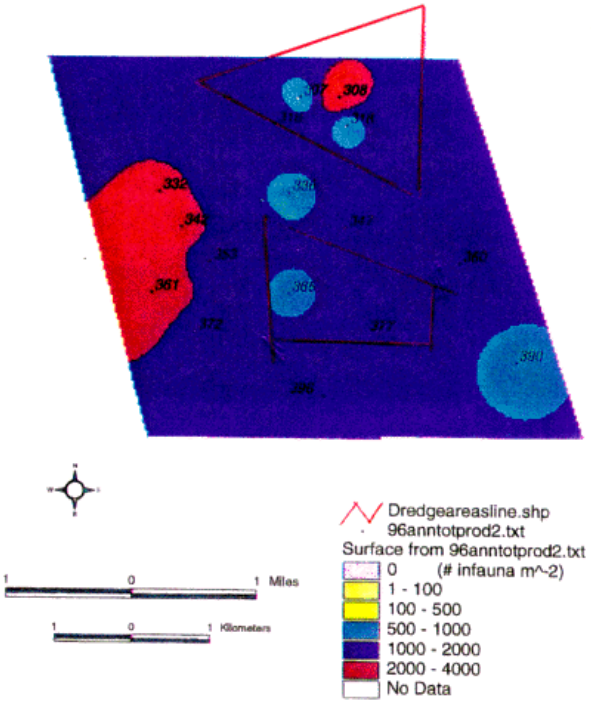

Total infaunal densities

Polychaete densities

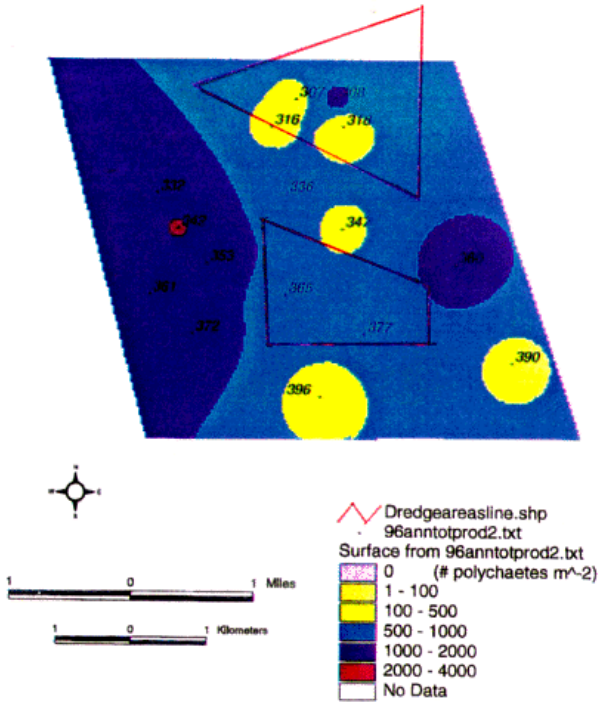

Mollusc densities

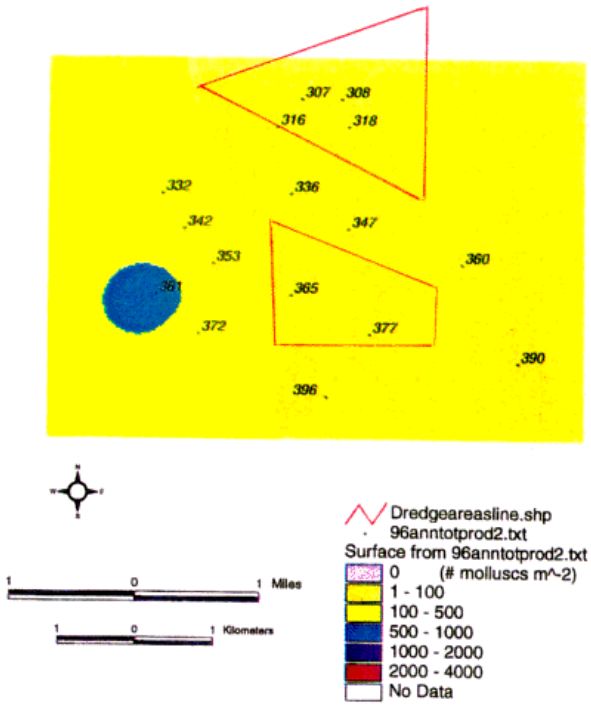

Figure 56. Comparison of gross habitat type determinations from SPI to infaunal densities from grab data for the study area off Sandbridge, in the vicinity of the proposed borrow areas.

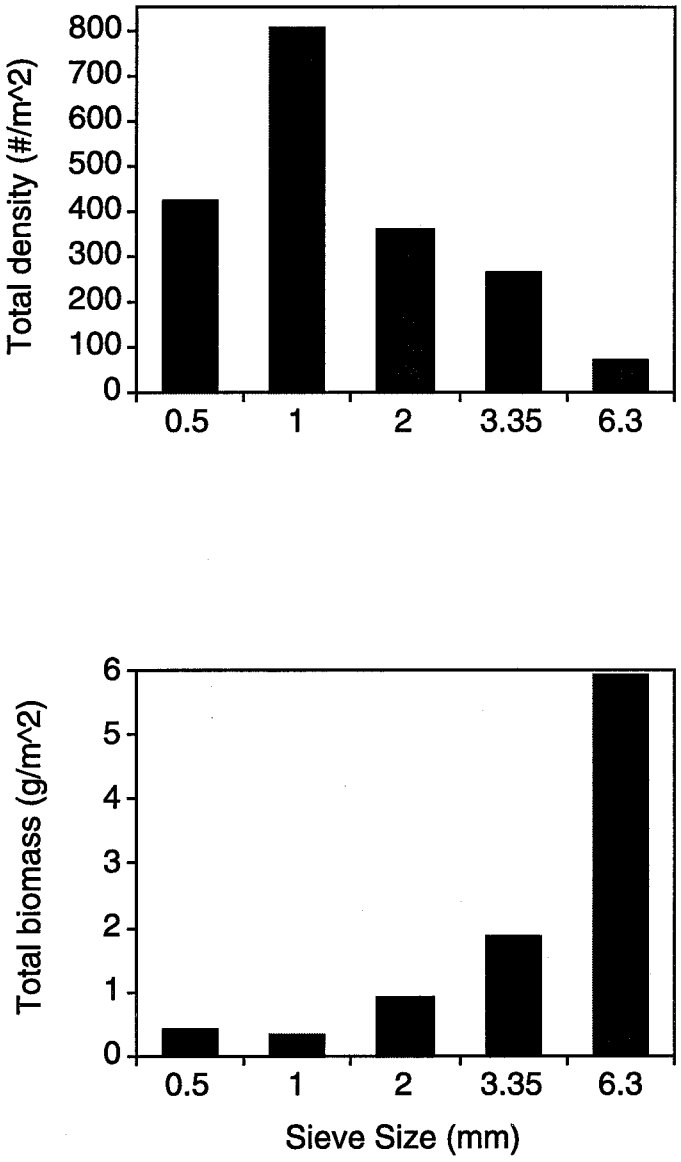

Figure 57. Size class distributions of total biomass and number of individuals per m^2 for all 1996 grab data.

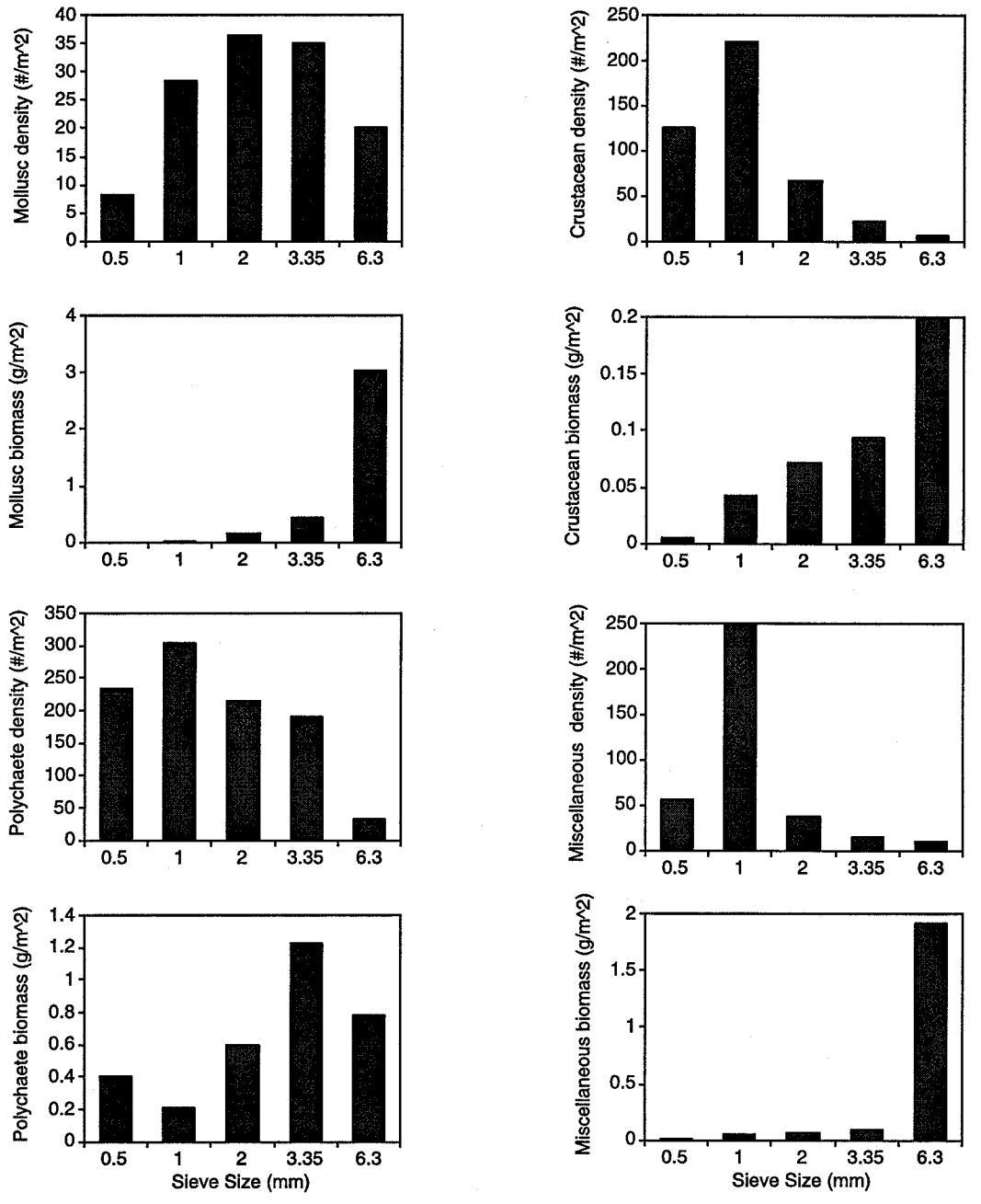

Figure 58. Size class distributions of mollusc, polychaet, crustacean, and other (miscellaneous) taxa biomass and number of individuals per m^2 for all 1996 grab data.

Table 1. Spring and fall 1996 and 1997 positions.

CELL	N	LAT	-LON	SPR96spi	SPR96gr	FAL96spi	FAL96gr	SPR97spi	SPR97gr	FAL97spi	FAL97gr
96001	2	36.883	-75.939	+		+					
96003	2	36.883	-75.932	+		+					
96005	3	36.883	-75.923	+		+	+				
96007	2	36.883	-75.915	+		+					
96009	2	36.883	-75.907	+		+					
96012	2	36.879	-75.934	+		+					
96013	4	36.878	-75.930		+		+	+			
96014	2	36.879	-75.926	+		+					
96016	2	36.879	-75.918	+		+					
96018	2	36.879	-75.910	+		+					
96020	2	36.879	-75.901	+		+					
96021	2	36.875	-75.937	+		+					
96023	2	36.875	-75.929	+		+					
96024	5	36.874	-75.923		+		+	+	+		
96025	2	36.875	-75.921			+					
96027	2	36.875	-75.912	+		+					
96029	2	36.875	-75.904	+		+					
96031	1	36.874	-75.934				+				
96032	2	36.870	-75.932	+		+					
96034	2	36.871	-75.924	+		+					
96036	2	36.871	-75.916	+		+					
96038	2	36.871	-75.908	+		+					
96040	2	36.871	-75.899	+		+					
96041	2	36.867	-75.935	+		+					
96043	2	36.867	-75.926	+		+					
96045	2	36.867	-75.918	+		+					
96047	2	36.867	-75.911	+		+					
96048	1	36.867	-75.905				+				
96049	7	36.867	-75.902	+	+	+	+	+	+		
96050	2	36.867	-75.908		+		+				
96052	3	36.863	-75.929	+		+	+				
96054	2	36.863	-75.921	+		+					
96056	2	36.863	-75.914	+		+					
96058	2	36.863	-75.904	+		+					
96060	3	36.863	-75.896	+		+	+				
96061	3	36.859	-75.932	+	+	+					
96063	2	36.859	-75.925	+		+					
96065	2	36.859	-75.916	+		+					

Table 1. Spring and fall 1996 and 1997 positions.

CELL	N	LAT	-LON	SPR96spi	SPR96gr	FAL96spi	FAL96gr	SPR97spi	SPR97gr	FAL97spi	FAL97gr
96066	5	36.858	-75.912		+		+	+	+		
96067	2	36.859	-75.908	+		+					
96069	2	36.859	-75.900	+		+					
96072	2	36.855	-75.926	+		+					
96074	2	36.855	-75.919	+		+					
96076	2	36.855	-75.911	+		+					
96078	2	36.855	-75.902	+		+					
96080	2	36.855	-75.894	+		+					
96081	2	36.851	-75.931			+					
96083	2	36.851	-75.922	+		+					
96085	2	36.851	-75.914	+		+					
96087	2	36.851	-75.906	+		+					
96089	2	36.851	-75.896	+		+					
96092	2	36.847	-75.924			+					
96094	2	36.847	-75.917	+		+					
96096	2	36.847	-75.909	+		+					
96098	2	36.847	-75.900	+		+					
96100	2	36.847	-75.891	+		+					
96101	2	36.844	-75.927			+					
96103	2	36.844	-75.920			+					
96104	5	36.843	-75.915		+		+	+	+		
96105	2	36.844	-75.911			+					
96106	5	36.843	-75.907		+		+	+	+		
96107	2	36.844	-75.904			+					
96109	2	36.844	-75.894	+		+					
96112	2	36.840	-75.922			+					
96114	2	36.840	-75.915			+					
96115	5	36.839	-75.908		+		+	+			
96116	2	36.840	-75.906			+					
96118	2	36.840	-75.898			+					
96120	2	36.840	-75.889	+		+					
96121	2	36.836	-75.925	+		+					
96123	2	36.836	-75.916	+		+					
96125	2	36.836	-75.909			+					
96127	2	36.836	-75.901			+					
96129	2	36.836	-75.892	+		+					
96132	2	36.832	-75.921	+		+					
96134	2	36.832	-75.912	+		+					
96136	2	36.832	-75.904			+					

Table 1. Spring and fall 1996 and 1997 positions.

CELL	N	LAT	-LON	SPR96spi	SPR96gr	FAL96spi	FAL96gr	SPR97spi	SPR97gr	FAL97spi	FAL97gr
96137	5	36.832	-75.900		+		+	+	+		
96138	2	36.832	-75.897			+					
96140	2	36.832	-75.886	+		+					
96141	2	36.829	-75.923	+		+					
96143	2	36.829	-75.915	+		+					
96145	2	36.829	-75.907	+		+					
96147	2	36.829	-75.898			+					
96149	2	36.829	-75.890			+					
96152	2	36.824	-75.916	+		+					
96154	2	36.824	-75.909	+		+					
96156	2	36.824	-75.901	+		+					
96158	2	36.824	-75.893			+					
96160	2	36.824	-75.884			+					
96161	2	36.820	-75.921	+		+					
96163	2	36.820	-75.914	+		+					
96165	2	36.820	-75.905	+		+					
96167	2	36.820	-75.896	+		+					
96169	2	36.820	-75.887			+					
96172	2	36.816	-75.915	+		+					
96174	7	36.816	-75.910	+	+	+	+	+	+		
96176	3	36.816	-75.898	+		+	+				
96178	2	36.816	-75.890	+		+					
96180	2	36.816	-75.882			+					
96181	4	36.812	-75.917	+	+	+	+				
96183	3	36.812	-75.909	+	+	+					
96185	7	36.812	-75.901	+	+	+	+	+	+		
96187	2	36.812	-75.893	+		+					
96189	2	36.812	-75.885			+					
96192	2	36.809	-75.912	+		+					
96194	7	36.808	-75.903	+	+	+	+	+	+		
96196	2	36.809	-75.896	+		+					
96198	2	36.809	-75.888			+					
96200	2	36.809	-75.879	+		+					
96201	7	36.908	-75.885	+	+	+	+	+	+		
96203	2	36.909	-75.877	+		+					
96204	2	36.908	-75.872		+		+				
96205	4	36.909	-75.868	+	+	+	+				
96207	2	36.909	-75.861	+		+					
96209	9	36.908	-75.851	+	+	+	+	+			

Table 1. Spring and fall 1996 and 1997 positions.

CELL	N	LAT	-LON	SPR96spi	SPR96gr	FAL96spi	FAL96gr	SPR97spi	SPR97gr	FAL97spi	FAL97gr
96212	2	36.906	-75.880	+		+					
96213	2	36.905	-75.875		+		+				
96214	2	36.906	-75.871	+		+					
96216	2	36.906	-75.863	+		+					
96218	2	36.906	-75.855	+		+					
96220	2	36.906	-75.847	+		+					
96221	2	36.903	-75.883	+		+					
96223	2	36.902	-75.875	+		+					
96225	2	36.903	-75.866	+		+					
96227	2	36.903	-75.857	+		+					
96229	4	36.903	-75.849	+	+	+	+				
96232	2	36.899	-75.878	+		+					
96234	7	36.898	-75.869	+	+	+	+	+	+		
96236	2	36.899	-75.861	+		+					
96238	2	36.899	-75.852	+		+					
96240	2	36.899	-75.844	+		+					
96241	2	36.895	-75.881	+		+					
96243	2	36.895	-75.872	+		+					
96245	2	36.895	-75.864	+		+					
96246	5	36.894	-75.858		+		+	+	+		
96247	2	36.895	-75.856	+		+					
96249	2	36.895	-75.847	+		+					
96252	2	36.891	-75.876	+		+					
96254	2	36.891	-75.867	+		+					
96255	5	36.891	-75.862		+		+	+	+		
96256	2	36.891	-75.859	+		+					
96258	2	36.892	-75.850	+		+					
96260	2	36.891	-75.841	+		+					
96261	2	36.887	-75.878	+		+					
96263	4	36.887	-75.870	+	+	+	+				
96264	2	36.887	-75.865		+		+				
96265	2	36.887	-75.861	+		+					
96267	2	36.887	-75.853	+		+					
96269	2	36.887	-75.845	+		+					
96272	2	36.883	-75.873	+		+					
96274	2	36.883	-75.864	+		+					
96276	2	36.883	-75.856	+		+					
96278	2	36.883	-75.847	+		+					
96280	2	36.883	-75.839	+		+					

Table 1. Spring and fall 1996 and 1997 positions.

CELL	N	LAT	-LON	SPR96spi	SPR96gr	FAL96spi	FAL96gr	SPR97spi	SPR97gr	FAL97spi	FAL97gr
96281	2	36.879	-75.876	+		+					
96283	2	36.879	-75.867	+		+					
96285	2	36.879	-75.859	+		+					
96287	2	36.879	-75.850	+		+					
96289	2	36.879	-75.841	+		+					
96292	2	36.875	-75.871	+		+					
96294	2	36.875	-75.862	+		+					
96296	2	36.875	-75.854	+		+					
96298	2	36.875	-75.845	+		+					
96300	2	36.875	-75.837	+		+					
96301	2	36.762	-75.904	+		+					
96303	2	36.762	-75.896	+		+					
96305	2	36.762	-75.889	+		+					
96307	3	36.762	-75.880	+	+	+					
96308	2	36.761	-75.875		+						+
96309	2	36.762	-75.871	+		+					
96312	2	36.759	-75.899	+		+					
96314	2	36.759	-75.891	+		+					
96316	8	36.758	-75.882	+	+	+	+	+	+		+
96318	3	36.759	-75.875	+	+	+					
96320	2	36.759	-75.866	+		+					
96321	2	36.754	-75.902	+		+					
96323	2	36.754	-75.895	+		+					
96325	2	36.754	-75.887	+		+					
96327	2	36.754	-75.879	+		+					
96329	2	36.754	-75.870	+		+					
96332	6	36.750	-75.896	+		+	+	+	+		
96334	2	36.751	-75.888	+		+					
96336	5	36.750	-75.881	+	+	+	+				+
96338	2	36.751	-75.872	+		+					
96340	2	36.751	-75.864	+		+					
96341	2	36.746	-75.900	+		+					
96342	1	36.746	-75.893		+						
96343	2	36.746	-75.891	+		+					
96345	2	36.746	-75.883	+		+					
96347	9	36.746	-75.874	+	+	+	+	+	+		+
96349	2	36.746	-75.867	+		+					
96352	2	36.742	-75.894	+		+					
96353	5	36.742	-75.890		+		+	+	+		

Table 1. Spring and fall 1996 and 1997 positions.

CELL	N	LAT	-LON	SPR96spi	SPR96gr	FAL96spi	FAL96gr	SPR97spi	SPR97gr	FAL97spi	FAL97gr
96354	2	36.742	-75.887	+		+					
96356	3	36.742	-75.879	+		+					+
96358	2	36.742	-75.871	+		+					
96360	3	36.742	-75.861	+	+	+					
96361	5	36.738	-75.897	+	+	+	+				+
96363	2	36.739	-75.889	+		+					
96365	7	36.738	-75.881	+	+	+		+	+		+
96367	2	36.739	-75.873	+		+					
96369	2	36.739	-75.865	+		+					
96372	5	36.737	-75.892	+	+	+	+				+
96374	2	36.734	-75.884	+		+					
96376	2	36.734	-75.876	+		+					
96377	6	36.733	-75.871		+		+	+	+		+
96378	2	36.734	-75.868	+		+					
96380	2	36.734	-75.860	+		+					
96381	2	36.731	-75.895	+		+					
96383	2	36.731	-75.887	+		+					
96385	2	36.731	-75.880	+		+					
96387	2	36.731	-75.871	+		+					
96389	2	36.731	-75.863	+		+					
96390	1	36.730	-75.854		+						
96392	2	36.726	-75.894	+		+					
96394	2	36.726	-75.886	+		+					
96396	3	36.726	-75.877	+		+	+				
96398	2	36.726	-75.866	+		+					
96400	2	36.726	-75.857	+		+					
97001	2	36.916	-75.951					+			
97002	2	36.920	-75.925					+			
97003	2	36.926	-75.900					+			
97004	2	36.926	-75.874					+			
97005	2	36.928	-75.849					+			
97006	2	36.907	-75.933					+			
97007	2	36.910	-75.908					+			
97008	2	36.913	-75.883					+			
97009	2	36.916	-75.857					+			
97011	2	36.895	-75.942					+			
97012	2	36.898	-75.917					+			
97013	2	36.901	-75.891					+			
97014	2	36.904	-75.866					+			

Table 1. Spring and fall 1996 and 1997 positions.

CELL	N	LAT	-LON	SPR96spi	SPR96gr	FAL96spi	FAL96gr	SPR97spi	SPR97gr	FAL97spi	FAL97gr
97015	2	36.906	-75.841					+			
97016	2	36.885	-75.925					+			
97017	2	36.888	-75.900					+			
97018	2	36.891	-75.874					+			
97019	2	36.911	-75.849					+			
97021	2	36.873	-75.934					+			
97022	2	36.876	-75.908					+			
97023	2	36.879	-75.883					+			
97024	2	36.881	-75.858					+			
97025	2	36.885	-75.832					+			
97026	2	36.863	-75.917					+			
97027	2	36.866	-75.891					+			
97028	2	36.869	-75.866					+			
97029	2	36.872	-75.841					+			
97031	2	36.851	-75.926					+			
97032	2	36.853	-75.900					+			
97033	2	36.856	-75.875					+			
97034	2	36.857	-75.850					+			
97035	2	36.862	-75.825					+			
97036	2	36.841	-75.909					+			
97037	2	36.844	-75.884					+			
97038	2	36.847	-75.859					+			
97039	2	36.849	-75.833					+			
97041	2	36.829	-75.917					+			
97042	2	36.831	-75.893					+			
97043	2	36.834	-75.867					+			
97044	2	36.837	-75.842					+			
97045	2	36.840	-75.818					+			
97046	3	36.819	-75.901					+	+		
97047	3	36.822	-75.876					+	+		
97048	2	36.825	-75.850					+			
97051	2	36.807	-75.910					+			
97052	2	36.809	-75.884					+			
97053	2	36.812	-75.860					+			
97054	2	36.815	-75.847					+			
97056	2	36.797	-75.893					+			
97057	2	36.800	-75.868					+			
97058	3	36.804	-75.843					+	+		
97061	2	36.785	-75.902					+			

Table 1. Spring and fall 1996 and 1997 positions.

CELL	N	LAT	-LON	SPR96spi	SPR96gr	FAL96spi	FAL96gr	SPR97spi	SPR97gr	FAL97spi	FAL97gr
97062	2	36.788	-75.877					+			
97063	2	36.791	-75.851					+			
97064	3	36.793	-75.826					+	+		
97066	3	36.775	-75.885					+	+		
97067	2	36.778	-75.859					+			
97068	2	36.781	-75.835					+			
97071	3	36.763	-75.893					+	+		
97072	2	36.765	-75.869					+			
97073	3	36.769	-75.843					+			
97074	3	36.771	-75.826					+	+		
97076	2	36.753	-75.877					+			
97077	2	36.755	-75.852					+			
97078	2	36.759	-75.826					+			
97082	2	36.745	-75.862					+			
97083	2	36.746	-75.835					+			
97084	2	36.749	-75.810					+			
97086	2	36.730	-75.868					+			
97087	2	36.733	-75.843					+			
97088	2	36.738	-75.819					+			
97091	2	36.718	-75.878					+			
97092	2	36.721	-75.852					+			
97093	2	36.724	-75.827					+			
97094	2	36.727	-75.802					+			
97096	3	36.709	-75.860					+	+		
97097	2	36.712	-75.836					+			
97098	2	36.715	-75.811					+			
97101	2	36.696	-75.869					+			
97102	2	36.699	-75.844					+			
97103	2	36.702	-75.819					+			
97104	3	36.705	-78.166					+	+		
97106	2	36.686	-75.853					+			
97107	3	36.689	-75.827					+	+		
97108	2	36.692	-75.802					+			
97205	3	36.909	-75.868					+	+		
sb001	1	36.735	-75.878							+	
sb002	1	36.732	-75.877							+	
sb003	1	36.730	-75.878							+	
sb004	1	36.745	-75.875							+	+
sb005	1	36.742	-75.875							+	

Table 1. Spring and fall 1996 and 1997 positions.

CELL	N	LAT	-LON	SPR96spi	SPR96gr	FAL96spi	FAL96gr	SPR97spi	SPR97gr	FAL97spi	FAL97gr
sb006	1	36.738	-75.875							+	
sb007	1	36.735	-75.875							+	
sb008	1	36.732	-75.875							+	
sb009	1	36.730	-75.875							+	
sb010	1	36.745	-75.872							+	
sb011	1	36.742	-75.872							+	
sb012	1	36.739	-75.872							+	
sb013	1	36.735	-75.872							+	
sb014	1	36.733	-75.872							+	
sb015	1	36.730	-75.873							+	
sb016	1	36.745	-75.870							+	
sb017	1	36.741	-75.870							+	
sb018	1	36.738	-75.869							+	
sb019	1	36.735	-75.869							+	+
sb020	1	36.732	-75.870							+	
sb021	1	36.730	-75.870							+	+
sb022	1	36.730	-75.868							+	
sb023	1	36.732	-75.868							+	
sb024	1	36.735	-75.868							+	
sb025	1	36.738	-75.867							+	
sb026	1	36.741	-75.867							+	+
sb027	1	36.745	-75.868							+	
sb028	1	36.762	-75.884							+	
sb029	1	36.760	-75.877							+	+
sb030	1	36.759	-75.872							+	
sb031	1	36.757	-75.864							+	
sb032	1	36.757	-75.853							+	
sb033	1	36.748	-75.879							+	+
sb034	1	36.754	-75.876							+	+
sb035	1	36.762	-75.871							+	
sb036	1	36.767	-75.869							+	
sb037	1	36.772	-75.882							+	
sb038	1	36.773	-75.882							+	
sb039	1	36.766	-75.877							+	+
sb040	1	36.761	-75.873							+	
sb041	1	36.738	-75.885							+	
sb042	1	36.750	-75.898							+	+
sb043	1	36.729	-75.878							+	
sb044	1	36.718	-75.842							+	

Table 1. Spring and fall 1996 and 1997 positions.

CELL	N	LAT	-LON	SPR96spi	SPR96gr	FAL96spi	FAL96gr	SPR97spi	SPR97gr	FAL97spi	FAL97gr	
sb045	1	36.724	-75.856							+		
sb046	1	36.732	-75.839							+		
sb047	1	36.742	-75.856							+		
sb081	1	36.745	-75.885							+		
sb082	1	36.742	-75.886							+		
sb083	1	36.739	-75.884							+		
sb084	1	36.735	-75.885							+		
sb085	1	36.733	-75.885							+		
sb086	1	36.730	-75.885							+		
sb087	1	36.742	-75.883							+	+	
sb088	1	36.738	-75.883							+		
sb089	1	36.735	-75.883							+		
sb090	1	36.732	-75.883							+		
sb091	1	36.730	-75.883							+		
sb092	1	36.745	-75.880							+		
sb093	1	36.742	-75.880							+		
sb094	1	36.738	-75.880							+		
sb095	1	36.735	-75.880							+		
sb096	1	36.733	-75.880							+		
sb097	1	36.730	-75.880							+	+	
sb098	1	36.745	-75.878							+		
sb099	1	36.742	-75.878							+		
sb100	1	36.738	-75.877							+		
t2	1	36.745	-75.883							+		
BANE	1	36.739	-75.864									BANE
BANW	1	36.747	-75.883									BANW
BASE	1	36.732	-75.864									BASE
BASW	1	36.733	-75.884									BASW
BBNE	1	36.772	-75.865									BBNE
BBSE	1	36.749	-75.865									BBSE
BBW	1	36.763	-75.892									BBW

Table 2. Coordinates for proposed borrow areas off Sandbridge, Virginia.

All are NAD 1983

Borrow Area A

NE Corner	State Plane, ft.		N 3439350	E 12255330
	Lat Long	d m s	36 44 20.71403	075 51 49.29479
		d m	36 44.345	075 51.822
NW Corner	State Plane, ft.		N 3442070	E 12249483
	Lat Long	d m s	36 44 49.20672	075 53 00.17432
		d m	36 44.820	075 53.003
SE Corner	State Plane, ft		N 3436800	E 12255330
	Lat Long	d m s	36 43 55.50997	075 51 50.16946
		d m	36 43.925	075 51.836
SW Corner	State Plane, ft		N 3436802	E 12249483
	Lat Long	d m s	36 43 57.13779	075 53 01.96781
		d m	36 43.952	075 53.033

Borrow Area B

NE Corner	State Plane, ft		N 3452440	E 12254600
	Lat Long	d m s	36 46 20.41249	075 51 54.11446
		d m	36 46.340	075 51.902
Western End	State Plane, ft		N 3447250	E 12249080
	Lat Long	d m s	36 45 46.51629	075 53 03.36072
		d m	36 45.775	075 53.506
SE Corner	State Plane, ft		N 3443100	E 12254800
	Lat Long	d m s	36 44 57.92513	075 51 54.51787
		d m	36 44.965	075 51.909

Table 3. Spring 1996 SPI analysis.

		Virginia Beach Sandmining Project SPI visual analysis: Spring,											Surface struct.											
								Sed.	Sed.	Relief			--Tubes--		Subsur	---Infauna----			Voids					
					Date	PEN	RPD	Type	Rel.	Type	Epifauna		+/-	Pellets	Shell	#	Type	Depth	#	Type	Depth	Gas	Depth	Burrow	Type
LON	LAT	cell	rep		96	(cm)	(cm)		(cm)		(+/-)													
-75.94	36.882	1	A	2	spr	5.2	5.2	VFS-SI	1.6	BD, TUBES	+	CLAM	75	+	TRACE	0			0			0		0	
-75.93	36.882	3	B	2	spr	11			0.25		-		22	+	TRACE	4	WORM	5,7.5	0			0		0	
-75.92	36.882	5			spr	6.5			1.5		-		15		TRACE	1	WORM	1.5	0			0		0	
-75.91	36.882	7	A	2	spr	5.4			1.4																
-75.91	36.882	7	B	2	spr	7.2	5	CS	0.8	BD	-		3	-	NONE	0			0			0		0	
-75.91	36.882	9			spr	3.9			2.3		-														
-75.91	36.882	9	B	1	spr	5.8	5.8	CS	2	BD	-		0	+	NONE	0			0			0		1	OX
-75.93	36.878	12	B	2	spr	10	3	VFS-SI	0.5	BD, TUBES	-		113	+	NONE	6	WORM	1.5,4	0			0		1	OX
-75.93	36.878	14	B	2	spr	15.25			1.75		-		24	+		3	WORM	3	0			0		0	
-75.92	36.878	16	A	2	spr	9.5			1		-		67	+		6	WORM	3	0			0		0	
-75.91	36.878	18	A	2	spr	4.2			4																
-75.91	36.878	18	B	1	spr	6.3	2.6	VFS-SI	3	BD, TUBES	-		8	+	TRACE	2	WORM	2,4	0			0		0	
-75.9	36.878	20	A	2	spr	4.7			1																
-75.9	36.878	20	B	2	spr	7.2	7.2		0.7		-		3	+	TRACE	0			0			0		0	
-75.94	36.874	21	B	2	spr	7			2		-		17	-	TRACE	0			0			0		0	
-75.93	36.874	23	B	2	spr	11			1.25		-		76	IND		2	WORM	3,8.5	0			0		0	
-75.92	36.874	25	B	2	spr	10			6		-			IND	TRACE	0			0			0		0	
-75.91	36.874	27	B	2	spr	8			1.75		-			IND	TRACE	0			0			0		0	
-75.9	36.874	29			spr	6.5			1.7					IND	TRACE	0			0			0		0	
-75.93	36.87	32	B	2	spr	11	2	VFS-SI	0.3	BD, TUBES	-		18	+	TRACE	5	WORM	2.5,3	0			0		0	
-75.92	36.87	34	B	2	spr	7			5.25		-		1	IND					0			0		0	

Table 3. Spring 1996 SPI analysis.

		Virginia Beach Sandmining Project SPI visual analysis: Spring, 1											Surface struct.											
								Sed.	Sed.	Relief			--Tubes--		Subsuri	---Infauna----			Voids					
					Date	PEN	RPD	Type	Rel.	Type	Epifauna		+/-	Pellets	Shell	#	Type	Depth	#	Type	Depth	Gas	Depth	Burrow	Type
LON	LAT	cell	rep		96	(cm)	(cm)		(cm)		(+/-)													
-75.92	36.87	36	B	2	spr	11.75			2.75		-		0	+					0			0		0	
-75.91	36.87	38	A	2	spr	7			3		-		2	+	TRACE	1	WORM	6.75	0			0		0	
-75.9	36.87	40	B	2	spr	4			1.8		-		0	+	TRACE	1	WORM	4	0			0		0	
-75.93	36.867	41	B	2	spr	4	4	VFS-FS	0.3	BD, TUBES	-		4	-	TRACE	0			0			0		0	
-75.93	36.867	43	B	2	spr	13.5	9	FS	1.2	BD, TUBES	+	GAST	1	-	NONE	0			0			0		1	OX
-75.92	36.867	45			spr	9.5			2.5		-		1	IND	TRACE	0			0			0		0	
-75.91	36.867	47			spr	6.75			1.5		-		0	+	1	1	UNID	1	0			0		0	
-75.9	36.867	49	B	2	spr	9.25			1.5		-		4	+	TRACE	0			0			0		0	
-75.93	36.862	52	B	2	spr	13	4	SI-VFS	1	BD, TUBES	-		37	+	TRACE	4	WORM	3,5,9	0			0		0	
-75.92	36.862	54	B	2	spr	10	10	MS	5	BD	-		0	-	NONE	0			0			0		0	
-75.91	36.862	56	B	2	spr	7			4		+		2	+	TRACE	0			0			0		0	
-75.9	36.862	58	B	2	spr	5.75			0.25		+		1	+	TRACE	0			0			0		0	
-75.93	36.862	60	B	2	spr	5.7			1.7		-		0	+	TRACE	0			0			0		0	
-75.92	36.858	63	B	2	spr	11	2.1	FS	0.8	BD, TUBES	-		18	+	TRACE	1	WORM	5	0			0		1	OX
-75.92	36.858	65	B	2	spr	8	8	FS-MS	2	BD, DEBRIS	-		0	-	TRACE	0						0		0	
-75.91	36.858	67	B	2	spr	10			2.5		-		0	IND	0	0			0			0		0	
-75.9	36.858	69	B	2	spr	9.5			0.5		-		2	+	TRACE	0			0			0		0	
-75.93	36.854	72	B	2	spr	5	2	FS	0.5	BD, TUBES	-		30	+	TRACE	0			0			0		0	
-75.92	36.854	74	B	2	spr	10	10	MS	4.6	BD	-		0	-	TRACE	1	WORM	0.8	0			0		0	
-75.91	36.854	76	B	2	spr	6.5	6.5	FS	1.9	BD	-		0	-	TRACE	0			0			0		0	
-75.9	36.854	78	B	2	spr	19			1		-		38	+		3	WORM	3,6,1	0			0		0	

Table 3. Spring 1996 SPI analysis.

		Virginia Beach Sandmining Project SPI visual analysis: Spring, 1										Surface struct.											
							Sed.	Sed.	Relief			--Tubes--		Subsur	---Infauna----			Voids					
					Date	PEN	RPD	Type	Rel.	Type	Epifauna	+/-	Pellets	Shell	#	Type	Depth	#	Type	Depth	Gas	Depth	Burrow	Type
LON	LAT	cell	rep		96	(cm)	(cm)		(cm)		(+/-)													
-75.89	36.854	80	B	2	spr	7			0.25		+	0	IND	TRACE	0			0			0		0	
-75.92	36.851	83	B	2	spr	18	0.7	SI	3.5	BD, TUBES	-	8	-	NONE	5	WORM	5,9,1	0			0		1	OX
-75.91	36.851	85	B	2	spr	10	10	MS	2.8	BD	-	0	-	NONE	0			0			0		0	
-75.91	36.851	87	B	2	spr	8.8	4.3	FS	1	BD	-	1	-	NONE	0			0			0		0	
-75.9	36.851	89	B	2	spr	8			4.25		-	0	-	TRACE	2	WORM	3,3	0			0		0	
-75.92	36.847	94	B	2	spr	7	7	FS-MS	1.7	BD	-	2	-	TRACE	0			0			0		0	
-75.91	36.847	96	B	2	spr	6	6	FS	1.5	BD, TUBES	-	4	+	1	0			0			0		0	
-75.9	36.847	98	B	2	spr	6.5	6.5	FS	1.3	BD, SHELL	+	0	-	TRACE	0			0			0		0	
-75.89	36.847	100	B	2	spr	5			1		-	2		TRACE	0			0			0		0	
-75.89	36.843	109	B	1	spr	4.3	4.3	FS	0.5	BD	-	0	-	NONE	0			0			0		0	
-75.89	36.839	120	B	2	spr	10	1		1		-	0	-	NONE	0			7	6OX,1AN	2.2,4.5	0		0	
-75.92	36.836	121			spr	5.8			4															
-75.92	36.836	123	A	2	spr	4			1.1															
-75.92	36.836	123	B	2	spr	5.1	1.6	FS	0.9	BD, SHELL	-	0	-	TRACE	0			0			0		0	
-75.92	36.832	132			spr	3			1.5															
-75.91	36.832	134	A	2	spr	6.2	6.2	FS	0.3	BD	-	0	-	NONE	0			0			0		0	
-75.91	36.832	134	B	2	spr	7.3			0.6															
-75.89	36.832	140	A	2	spr	6.2	6.2		1.1		-	0	-	TRACE	0			0			0		0	
-75.92	36.828	141			spr	4			1.9															
-75.91	36.828	143	A	2	spr	1.5			2.8															
-75.91	36.828	143	B	2	spr	6	2	SI-FS	2.3	BD, TUBES	-	13	-	1	2	WORM	2,2	0			0		0	

Table 3. Spring 1996 SPI analysis.

		Virginia Beach Sandmining Project SPI visual analysis: Spring, 1										Surface struct.											
								Sed.	Sed.	Relief			--Tubes--		Subsurf	---Infauna----			Voids				
					Date	PEN	RPD	Type	Rel.	Type	Epifauna		+/-	Pellets	Shell	#	Type	Depth	#	Type	Depth	Gas	Depth	Burrow	Type
LON	LAT	cell	rep		96	(cm)	(cm)		(cm)		(+/-)													
-75.91	36.828	145	A	2	spr	6	6	FS-MS	3	BD	-		0	-	NONE	0			0			0		0	
-75.92	36.824	152	A	2	spr	2.9			2.9																
-75.91	36.824	154	A	2	spr	4.3			3																
-75.91	36.824	154	B	2	spr	5	5		2.2		-		0	-	TRACE	0			0			0		0	
-75.9	36.824	156	A	2	spr	2.8			2.5																
-75.9	36.824	156	B	2	spr	6.7	6.7		1.3		-		0	-	TRACE	0			0			0		0	
-75.92	36.82	161	A	2	spr	3.5			1.6																
-75.91	36.82	163	A	2	spr	1.5			2																
-75.9	36.82	165	A	2	spr	0.9			2.4																
-75.9	36.82	165	B	2	spr	5.2	5.2	FS	2.1	BD	-		0	-	TRACE	0			0			0		0	
-75.9	36.82	167	A	2	spr	6.2			1.4																
-75.9	36.82	167	B	2	spr	8.4	8.4	MS-CS	1.4	BD	-		0	-	TRACE	0			0			0		0	
-75.91	36.816	172	A	2	spr	4.7			2.2																
-75.91	36.816	174	A	2	spr	3			1.4																
-75.9	36.816	176	A	2	spr	4.3			1.3																
-75.9	36.816	176	B	2	spr	6.9	6.9	FS	1.9	BD	+	GAST	0	-	NONE	0						0		0	
-75.89	36.816	178	A	2	spr	4.8			0.6																
-75.89	36.816	178	B	2	spr	7.3	7.3	FS	0.6	BD, TUBES	-		5	-	NONE	1	WORM	1	1	OX	2.5	0		0	
-75.92	36.812	181	A	2	spr	3.3			2.4																
-75.91	36.812	183	A	2	spr	4.5			1.5																
-75.9	36.812	185	A	2	spr	8.6			1.8																

Table 3. Spring 1996 SPI analysis.

		Virginia Beach Sandmining Project SPI visual analysis: Spring,											Surface struct.												
								Sed.	Sed.	Relief			--Tubes--		Subsuri	---Infauna----			Voids						
					Date	PEN	RPD	Type	Rel.	Type	Epifauna		+/-	Pellets	Shell	#	Type	Depth	#	Type	Depth	Gas	Depth	Burrow	Type
LON	LAT	cell	rep		96	(cm)	(cm)		(cm)		(+/-)													
-75.89	36.812	187	A	2	spr	3.7			1.3															
-75.89	36.812	187	B	2	spr	6.2	4.5	FS	1.1	BD	+	GAST	0	-	NONE	0			0			0		0	
-75.9	36.808	194	A	2	spr	6.2			1																
-75.9	36.808	196	A	2	spr	2.3			1.5																
-75.89	36.908	201	1		spr	3.5	1	F-MS	2.5	BD	N		Y	N	1	0			0			0		0	
-75.89	36.908	201	2		spr	4.5	1.5	F-MS	2	BD	N		N	N	1	0			0			0		0	
-75.88	36.908	203	1		spr	3.5	1.5	F-MS	2	BD	N		N	N	1	0			0			0		0	
-75.88	36.908	203	2		spr	7	1.5	F-MS	1	BD	Y?		Y	N	1	1?	?	3	0			0		IND	
-75.87	36.908	204	1		spr	2.5	ALL	F-MS	1.5	BD	N		N	N	0.5	0			0			0		0	
-75.87	36.908	205	1		spr	3	1	F-MS	1.25	BD	N		N	N	0.25	0			0			0		1?	OX
-75.87	36.908	205	2		spr	2.5	1	F-MS	1.25	BD,SH,TUBE	1,HC		Y,1	N	0.5	0			0			0		0	
-75.86	36.908	207	1		spr	3.75	1	F-MS	1	BD	N		Y	N	1	1?	WORM?		3.5			0		0	
-75.86	36.908	207	2		spr	5.5	1	F-MS	1.5	BD	N		N	N	1	0			0			0		1	OX
-75.85	36.908	209	1		spr	1.5	ALL	F-MS	0.5	BD,BIO	KU		N	N	0.5	0			0			0		0	
-75.85	36.908	209	2		spr	2.75	0.5	FS	1.5	BD	N		N	N	0.25	0			0			0		IND	
-75.85	36.908	209	3		spr	4.5	0.5	FS	0.5		N		Y	N	1	0			0			0		IND	
-75.88	36.905	212	1		spr	4	1.5	F-MS	1.5	BD	N		N	N	0.5	0			0			0		0	
-75.88	36.905	212	2		spr	4	1.5	F-MS	2	BD	?		N	N	0.5	0			0			0		0	
-75.87	36.905	214	1		spr	5	1	F-MS	1.5	BD	N		N	N	1	0			0			0		0	
-75.87	36.905	214	2		spr	4	1	F-MS	2	BD	N		Y*	N	1	0			0			0		0	
-75.86	36.905	216	1		spr	3.5	ALL	F-MS	2	BD	N		N	N	0.5	0			0			0		0	

Table 3. Spring 1996 SPI analysis.

		Virginia Beach Sandmining Project SPI visual analysis: Spring,									Surface struct.											
							Sed.	Sed.	Relief		--Tubes--		Subsur	---Infauna----			Voids					
				Date	PEN	RPD	Type	Rel.	Type	Epifauna	+/-	Pellets	Shell	#	Type	Depth	#	Type	Depth	Gas	Depth	Burrow	Type
LON	LAT	cell	rep	96	(cm)	(cm)		(cm)		(+/-)												
-75.86	36.905	**216**	1	spr	2.5	1	F-MS	1	BD,PT?	N	N	Y?	0.5	0			0			0		0
-75.86	36.905	**216**	2	spr	2.25	0.5	F-MS	0.5		N	Y,1	N	0.5	0			0			0		0
-75.85	36.905	**220**	1	spr	3.5	2	F-MS	1.25	BD,SH,CL	N	N?	N	0.25	0			0			0		0
-75.85	36.905	**220**	2	spr	3.5	2	F-MS	1.25	BD	N	N	N	0.5	1?	WORM?	2	0			0		0
-75.88	36.902	**221**	3	spr	<1	NA	F-MS	NA	BD,SH	N	N	N	NA	NA			NA			0		0A
-75.87	36.902	**223**	1	spr	4	1.5-2	F-MS	3	BD	N	Y*	N	0.5	0			0			0		0
-75.87	36.902	**223**	2	spr	6	1.5-2	F-MS	2	BD	N	N	N	0.25	0			0			0		0
-75.87	36.902	**223**	3	spr	4	2	F-MS	2.5	BD	N	N	N	0.25	0			0			0		0
-75.87	36.902	**225**	1	spr	4.5	1.5-2	F-MS	2.5	BD	N	N	N	0.5	0			0			0		0
-75.87	36.902	**225**	2	spr	3.5	1-1.5	F-MS	1.5	BD	N	Y*	N	1	0			0			0		0
-75.86	36.902	**227**	1	spr	3	2-ALL	F-MS	0.25		N	N	N	0.5	0			0			0		0
-75.86	36.902	**227**	2	spr	3.5	1.5	F-MS	0.5		N	Y	N	1	0			0			0		0
-75.85	36.902	**229**	1	spr	3.25	0.5	F-MS	<.5	SH,CL	N	N	N	1	0			0			0		0
-75.85	36.902	**229**	2	spr	3	0.5	F-MS	0.5	BD,SH	N	N	N	0.5	0			0			0		2
-75.88	36.898	**232**	1	spr	3.5	1-1.5	F-MS	1.5	BD	N	N	N	0.5	0			0			0		0
-75.88	36.898	**232**	2	spr	6	1-1.5	F-MS	1	BD	N	N	N	1	0			0			0		0
-75.88	36.898	**232**	3	spr	4	1.5	F-MS	2	BD	N	N	N	0.25	0			0			0		0
-75.87	36.898	**234**	1	spr	4	1-1.5	F-MS	1	BD	N	N	N	0.25	0			0			0		0
-75.87	36.898	**234**	2	spr	3.5	1-1.5	F-MS	2	BD	N	N	N	0.25	0			0			0		0
-75.86	36.898	**236**	1	spr	4	1.5	F-MS	2	BD	N	N	N	0.25	0			0			0		0
-75.86	36.898	**236**	2	spr	3.5	2	F-MS	1.5	BD	N	N	N	0.5	0			0			0		0

Table 3. Spring 1996 SPI analysis.

		Virginia Beach Sandmining Project SPI visual analysis: Spring, 1									Surface struct.											
							Sed.	Sed.	Relief		--Tubes--		Subsuri	---Infauna----			Voids					
				Date	PEN	RPD	Type	Rel.	Type	Epifauna	+/-	Pellets	Shell	#	Type	Depth	#	Type	Depth	Gas	Depth	Burrow	Type
LON	LAT	cell	rep	96	(cm)	(cm)		(cm)		(+/-)													
-75.86	36.898	**236**	3	spr	3	1.5	F-MS	1	BD	N	N	N	0.25	0			0			0		0	
-75.85	36.898	**238**	1	spr	5	1.25	F-MS	0.25		N	Y	N	0.5	2	WORM		0			0		1	OX
-75.85	36.898	**238**	2	spr	3.75	1	F-MS	0.3		N	Y,1	N	0.5	0			0			0		0	
-75.84	36.898	**240**	1	spr	3.5	2-ALL	F-MS	1	BD,SH,CL	N	N	N	1	0			0			0		0	
-75.84	36.898	**240**	2	spr	4	2-ALL	F-MS	2	BD	N	Y	N	0.5	0			0			0		0	
-75.87	36.894	**243**	1	spr	4	1.5-2	F-MS	1.75	BD	N	N	N	0.5	0			0			0		0	
-75.87	36.894	**243**	2	spr	5.5	1.5	F-MS	1.5	BD	N	1	N	0.5	0			0			0		0	
-75.86	36.894	**245**	2	spr	4	1.5-2	F-MS	3	BD	N	N	N	0.5	0			0			0		0	
-75.86	36.894	**247**	1	spr	3.5	2.5	F-MS	2	BD	N	N	N	0.5	0			0			0		0	
-75.86	36.894	**247**	2	spr	3.5	2	F-MS	2.5	BD	?,UNID	N	N	0.5	0			0			0		0	
-75.85	36.894	**249**	1	spr	3.5	1.5	F-MS	1.5	BD	N	Y?	N	1	0			0			0		0	
-75.85	36.894	**249**	2	spr	3.5	2	F-MS	1.5	BD	N	Y?	N	1	0			0			0		0	
-75.88	36.891	**252**	1	spr	5.5	2-2.5?	F-MS	0.5		N	N	N	1	0			3	SMALL,OX,AN		0		1	ACTIVE
-75.88	36.891	**252**	2	spr	3	1-1.5?	F-MS	0.5		N	Y?,1	N	0.5	0			0			0		0	
-75.87	36.891	**254**	1	spr	6	1.5-2	F-MS	1.5	BD	N	1	N	0.5	0			0			0		0	
-75.87	36.891	**254**	2	spr	6	1.5-2	F-MS	1	BD	N	N	N	0.5	0			0			0		0	
-75.86	36.891	**256**	1	spr	4	2	F-MS	3	BD	N?	N	N	0.5	0			0			0		0	
-75.86	36.891	**256**	2	spr	3.5	1.5-2	F-MS	2	BD	Y?	N	N	0.25	0			0			0		0	
-75.85	36.891	**258**	1	spr	3.5	1.5	F-MS	1.8	BD	N	N	N	0.5	0			0			0		0	
-75.85	36.891	**258**	2	spr	3.5	2	F-MS	0.8		N	?	N	0.5	0			0			0		0	
-75.85	36.891	**258**	3	spr	3	1.5	F-MS	2	BD	N	N	N	1	0			0			0		0	

Table 3. Spring 1996 SPI analysis.

		Virginia Beach Sandmining Project SPI visual analysis: Spring,									Surface struct.											
							Sed.	Sed.	Relief		--Tubes--		Subsur	---Infauna----			Voids					
				Date	PEN	RPD	Type	Rel.	Type	Epifauna	+/-	Pellets	Shell	#	Type	Depth	#	Type	Depth	Gas	Depth	Burrow	Type
LON	LAT	cell	rep	96	(cm)	(cm)		(cm)		(+/-)													
-75.84	36.891	260	1	spr	4	2	F-MS	1.5	BD	N?	N	N	1	0			0			0		0	
-75.84	36.891	260	2	spr	3.5	1.5	F-MS	1.5	BD	N?	N	N	0.5	1?	WORM		1			0		0	
-75.88	36.887	261?	1	spr	3.75	0.5	F-MS	0.5		N	Y,MANY	N	.1-.25	1	WORM?	2	0			0		1	OX SUBTUBE
-75.88	36.887	261?	2	spr	3	0.5	F-MS	0.5	BIO MOUND?	N	Y, MAN	N	0.1	0			0			0		1	OX
-75.86	36.887	265	1	spr	3.5	2-2.5	F-MS	2	BD	N	N	N	0.5	0			0			0		0	
-75.86	36.887	265	2	spr	5	2	F-MS	2	BD	N	N	N	0.5	0			0			0		0	
-75.85	36.887	267	1	spr	5	1.5-2	F-MS	2	BD	N	N	N	1	0			0			0		1	
-75.84	36.887	269	1	spr	3.5	2.5	F-MS	1	BD	N	N	N	0.5	0			0			0		0	
-75.84	36.887	269	2	spr	3	2	F-MS	1	BD	,UNID	N	N	0.5	0			0			0		0	
-75.86	36.883	276	1	spr	4	1-2	F-MS	2	BD	N	Y	N	0.25	0			0			0		0	
-75.86	36.883	276	2	spr	3.5	1-2	F-MS	0.5	BD	N	N	N	0.25	0			0			0		0	
-75.85	36.883	278	1	spr	3.5	2	F-MS	1.5	BD	N	N	N	0.5	0			0			0		0	
-75.85	36.883	278	2	spr	3.5	2	F-MS	0.5		N	N	N	0.5	0			0			0		0	
-75.84	36.883	280	1	spr	3	2	F-MS	2	BD	N	N	N	1	0			0			0		0	
-75.84	36.883	280	2	spr	3.5	2	F-MS	1		N	N	N	1	0			0			0		0	
-75.88	36.878	281?	1	spr	5	.5-.75	F-MS	0.75	SLOPE	N	Y,MANY	Y?	0.25	1	WORM	1.5	0			0		2	OX,ACT
-75.88	36.878	281?	2	spr	6	1.5	F-MS	0.5	BIO MOUND	Y?	Y,MANY	N?	0.1	0			0			0		2	OX
-75.85	36.878	287	1	spr	4.5	1.5	F-MS	0.5		N	N	N	0.1	0			0			0		0	
-75.85	36.878	287	2	spr	5	1.5	F-MS	0.5-1		N?	Y	N	0.25	0			0			0		1	
-75.84	36.878	289	2	spr	3	1-1.5	F-MS	0.5		N	N	N	0.1	0			0			0		1	
-75.84	36.878	289	3	spr	3.5	1-1.5	F-MS	0.5		HC	1	N	0.1	0			0			0		0	

Table 3. Spring 1996 SPI analysis.

		Virginia Beach Sandmining Project SPI visual analysis: Spring, 1									Surface struct.												
							Sed.	Sed.	Relief		--Tubes--		Subsurf	---Infauna----			Voids						
				Date	PEN	RPD	Type	Rel.	Type	Epifauna	+/-	Pellets	Shell	#	Type	Depth	#	Type	Depth	Gas	Depth	Burrow	Type
LON	LAT	cell	rep	96	(cm)	(cm)		(cm)		(+/-)													
-75.84	36.874	298	1	spr	3	1.5	F-MS	0.5		N	N	N	0.1	0			0			0		0	
-75.84	36.874	298	2	spr	3	1.5-2	F-MS	0.5		N	Y	N	0.1	0			0			0		0	
-75.84	36.874	300	1	spr	4	1.5-2	F-MS	2	BD	N	Y	N	0.1	0			0			0		0	
-75.84	36.874	300	2	spr	3.5	1.5	F-MS	1.5	BD	?	Y	N	0.1	0			0			0		1	
-75.9	36.761	301	1	spr	5	ABNORMA	SI-VFS	0.75	BIO?	N	Y,MANY	Y	0.1	0			0			0		0	
-75.9	36.761	301	2	spr	2.5	NA	SI-VFS	3	BIO PIT?	N?	Y,MANY	Y	0.1	0			0			0		1	OX
-75.9	36.761	303	1	spr	3.5	1.5	VFS-FS	1	BEDF/RIP	N?	Y,FEW	Y	0.1	1?			0			0		0	
-75.9	36.761	303	2	spr	3	1	VFS-FS	0.75	MND,TUBE	N	Y,SOME	Y	0.1	0			0			0		1	OX SUBTUBE
-75.89	36.761	305	1	spr	4	ALL	MS*	2	BEDF	N	N	N	0.25	0			0			0		0	
-75.89	36.761	305	2	spr	9	8.5	MS-CS	8	BEDF*	N	N	N	1	0			0			0		0	
-75.88	36.761	307	1	spr	6	ALL	MS-CS	1	BEDF	N	N	N	0.5	0			0			0		0	
-75.88	36.761	307	2	spr	8	ALL	MS-CS	3	BEDF	N	N	N	0.1	0			0			0		0	
-75.9	36.758	312	1	spr	2.5	0.75	VFS-FS	1.5	SLOPE,TUBE	N?	Y,FEW	Y	0.05	0			0			0		0	
-75.9	36.758	312	2	spr	2.5	0.5	FS	2.5	BEDF,TUBES	N	Y,MANY	N	0.05	2*	WORMS	TUBE	0			0		0	
-75.89	36.758	314	1	spr	NA	NA	SI	NA	NA	NA	NA	NA	0.1	3-4	WORM	NA	1	AN		0		2	OX,ACT
-75.89	36.758	314	2	spr	10?	IND	SI	NA	TUBES	N	Y,>50	Y	0.01	10	WORMS IN	1-3	0			0		19	OX SUBTUBE
-75.88	36.758	316	1	spr	6	ALL	MS-CS	1.75	BEDF	N	N	N	0.5	0			0			0		0	
-75.88	36.758	316	2	spr	7	ALL	MS-CS	3	BEDF,CLAST	N	N	N	1	0			0			0		0	
-75.9	36.753	321	1	spr	1	NA	FS?	0.75	BIO,TUBES	N	Y,SOME	N	IND	IND			IND			0		0	
-75.9	36.753	321	2	spr	2.25	1	FS	0.5	BIO,TUBES	N	Y,MANY	N?	0.05	11	WORM	1.5	0			0		0	
-75.89	36.753	323	1	spr	3.5	1	FS	0.5	BIO,TUBE	N	Y,4	Y	0.05	1	WORM/TUI	1.5	0			0		2	OX

Table 3. Spring 1996 SPI analysis.

		Virginia Beach Sandmining Project SPI visual analysis: Spring,									Surface struct.												
							Sed.	Sed.	Relief		--Tubes--		Subsur	---Infauna----			Voids						
				Date	PEN	RPD	Type	Rel.	Type	Epifauna	+/-	Pellets	Shell	#	Type	Depth	#	Type	Depth	Gas	Depth	Burrow	Type
LON	LAT	cell	rep	96	(cm)	(cm)		(cm)		(+/-)													
-75.89	36.753	323	2	spr	4.5	1.5	FS	1	BEDF,TUBE	N	Y,FEW	Y	0.05	0			0			0		2	OX
-75.89	36.753	325	1	spr	4.5	4.4	MS-CS	1.75	BEDF	N	N	N	0.25	0			0			0		0	
-75.89	36.753	325	2	spr	7.5	ALL	MS-VCS	3.5	BEDF	N	N	N	0.25	0			0			0		0	
-75.9	36.75	332	1	spr	3.5	1	FS	0.75	BIO,TUBES	N	Y,7	Y	0.05	0			0			0		1	OX
-75.9	36.75	332	2	spr	2.5	0.3	FS	1	BIO,TUBES	N?	Y,8-10	Y	0.05	2	WORMS/T	0.5,2	0			0		4	1ACT,3OX
-75.89	36.75	334	1	spr	3.5	ALL	MS-GRV	1	BEDF,SHELL	Y,HC	N	N	0.25	0			0			0		0	
-75.89	36.75	334	2	spr	3.5	ALL	MS-GRV	0.75	BEDFSLOPE	N	N	N	0.25	0			0			0		0	
-75.9	36.746	341	1	spr	2.5	0.3	SI-VFS	0.5	BIO,TUBES	,GAST	Y,6	Y	0.05	1-2	WORMS/T	0.5	0			0		IND	
-75.9	36.746	341	2	spr	3.5	0.5?	SI-VFS	1.25	BIO,TUBES	N	Y,10	Y	0.05	2	WORMS	2	0			0		5	3ACT,2OX
-75.89	36.746	343	1	spr	7	1.25	SI-VFS	1.5	BIO,TUBE	N	Y,10-1	IND	0.1	1	WORM	3	0			0		5	OX,ACT
-75.89	36.746	343	2	spr	8	1.25	SI-VFS	0.75	SLOPE,TUBE	N	Y,10-1	Y	0.1	0			0			0		8	OX
-75.89	36.742	352	1	spr	5.5	1	VFS-FS	1	BEDF?,TUBES	N	Y,10-1	Y?	0.05	0			0			0		3	OX
-75.89	36.742	352	2	spr	3.5	0.5	VFS-FS	1	MD,TUBES	,UNID?	Y,10-1	Y	0.01	0			0			0		3	OX
-75.9	36.738	361	1	spr	3.75	1	VFS-FS	0.75	BEDF,TUBES	N?	Y,3	IND	0.01	1	WORM	2.5	0			0		1	ACT
-75.89	36.733	372	1	spr	3.75	0.25	VFS-FS	0.5	MD,TUBES	N	Y,10-2	Y?	0.1	1	WORM	2	0			0		3	OX,SUBTUBE
-75.89	36.733	372	2	spr	6.5	1.5	SI-FS	1	MD,TUBES	N	Y,>15	IND	0.01	1	WORM	3	0			0		2	OX,SUBTUBE
-75.89	36.73	381	2	spr	4	0.5	VFS-FS	0.5	MD,TUBES	N	Y,6	IND	0.01	0			0			0		3	OX
-75.89	36.73	381	1	spr	4	0.75	VFS-FS	1	MD,TUBES	N	Y,3	Y	0.1	0			0			0		1	OX

Table 4. Fall 1996 SPI analysis.

		Virginia Beach Sandmining Project SPI visual analysis: Fal									Surface struct.											
							Sed.	Sed.	Relief		--Tubes--		Subsurf	---Infauna----			Voids					
				Date	PEN	RPD	Type	Rel.	Type	Epifau	+/-	ellet	Shell	#	Type	Depth	#	Type	Depth	Gas	Depth	Burrow	Type
LON	LAT	cell	rep	96	(cm)	(cm)		(cm)		(+/-)													
-75.939	36.882	1		fall	5.5	2		1.75		-	0	Pos.	None	0			0			0		
-75.932	36.882	3		fall	7.25	1.75		3.25		-	0	Pos.	2	2	Worm	4.75	0			0		
-75.906	36.882	9		fall	19			1		+	0	None	Trace	2	Worm	16.5	0			0		
-75.934	36.8783	12		fall	7	2		0.5		-	0	Pos.	None	0			0			0		
-75.926	36.8783	14		fall	6.75	6.75		2		+	0	None	Trace	0			0			0		
-75.918	36.8783	16	1b	fall	22	2.25		2		-	1	None	None	2	Worm	10	0			0		
-75.909	36.8783	18	1b	fall	11			0.5		-	0	None	Trace	0			0			0		
-75.9	36.8783	20		fall	9			3.25		+	0	None	Trace	0			0			0		
-75.937	36.8742	21		fall	4.75	1.25		1		-	8	Pos.	1	0			0			0		
-75.928	36.8742	23		fall	9.5	4.5		1.25		-	2	None	None	0			0			0		
-75.92	36.8742	25		fall	17.25	1.75		1		+	8	None	None	1	Worm	13	0			0		
-75.912	36.8742	27		fall	7.5			2.5		-	0	None	Trace	0			0			0		
-75.903	36.8742	29		fall	8			3		-	0	None	Trace	0			0			0		
-75.932	36.87	32		fall	8	3.5		2		+	8	None	None	0			0			0		
-75.923	36.87	34		fall	7.5	7.5		1		-	0	None	Trace	0			0			0		
-75.915	36.87	36		fall	6			2		-	0	None	None	0			0			0		
-75.908	36.87	38		fall	14	1.25		1.25		-	0	Pos.	4	0			0			0		
-75.898	36.87	40		fall	12.25			2		-	0	None	Trace	0			0			0		
-75.934	36.8667	41		fall	4.5	2		3		-	1	Pos.	1	0			0			0		
-75.926	36.8667	43		fall	16.25			1		-	6	None	None	1	Worm	14	0			0		
-75.918	36.8667	45		fall	11			2.5		-	0	None	None	0			0			0		

Table 4. Fall 1996 SPI analysis.

		Virginia Beach Sandmining Project SPI visual analysis: Fal									Surface struct.												
							Sed.	Sed.	Relief		--Tubes--		Subsurf	---Infauna----			Voids						
				Date	PEN	RPD	Type	Rel.	Type	Epifau	+/-	Pellet	Shell	#	Type	Depth	#	Type	Depth	Gas	Depth	Burrow	Type
LON	LAT	cell	rep	96	(cm)	(cm)		(cm)		(+/-)													
-75.91	36.8667	47		fall	12.75	4		1		-	0	None	Trace	0			0			0			
-75.902	36.8667	49		fall	8			4.75		-	0	None	None	0			0			0			
-75.928	36.8622	52		fall	19.25	2.75		0.5		-	0	None	None	4	Worm	10 &18	0			0			
-75.921	36.8622	54		fall	11			1.25		-	0	None	None	0			0			0			
-75.913	36.8622	56		fall	11.5			9		-	0	None	None	0			0			0			
-75.903	36.8622	58		fall	18			1.75		-	8	None	Trace	4	Worm	10.5	0			0			
-75.929	36.8622	60		fall	4.25	4.25		1.5		-	0	None	Trace	0			0			0			
-75.932	36.8583	61		fall	4.5	2		2		-	4	Pos.	Trace	0			0			0			
-75.924	36.8583	63		fall	17.25			2		-	3	None	None	6	Worm	14	0			0			
-75.916	36.8583	65	1b	fall	6.25			3		-	0	None	None	0			0			0			
-75.908	36.8583	67		fall	12			5		-	0	None	Trace	0			0			0			
-75.899	36.8583	69		fall	6.5	5		1.5		-	0	None	Trace	0			0			0			
-75.926	36.8542	72		fall	10			1		-	2	None	None	1	Worm	5	0			0			
-75.918	36.8542	74		fall	5.5	5.5		2		-	0	None	None	0			0			0			
-75.91	36.8542	76		fall	7			2.25		-	0	None	None	0			0			0			
-75.902	36.8542	78		fall	10	4.25		0.25		-	0	Pos.	1	2	Worm	8	0			0			
-75.893	36.8542	80		fall	6.25	6.25		1.25		-	0	None	None	0			0			0			
-75.93	36.8508	81	1b	fall	6			1		-	0	None	None	0			0			0			
-75.922	36.8508	83		fall	16	1.75		0.5		-	7	Pos.	None	1	Worm	9.5	0			0			
-75.913	36.8508	85		fall	8			4		+	0	None	Trace	0			0			0			
-75.905	36.8508	87		fall	4.5	1.75		1.25		-	0	None	Trace	0			0			0			

Table 4. Fall 1996 SPI analysis.

		Virginia Beach Sandmining Project SPI visual analysis: Fal									Surface struct.												
							Sed.	Sed.	Relief		--Tubes--		Subsurf	---Infauna----			Voids						
				Date	PEN	RPD	Type	Rel.	Type	Epifau	+/-	?ellet	Shell	#	Type	Depth	#	Type	Depth	Gas	Depth	Burrow	Type
LON	LAT	cell	rep	96	(cm)	(cm)		(cm)		(+/-)													
-75.896	36.8508	89		fall	6.25	6.25		2		-	0	None	Trace	0			0			0			
-75.923	36.8467	92		fall	6.5	6.5		2		-	0	None	Trace	0			0			0			
-75.917	36.8467	94		fall	6			4		-	0	None	Trace	0			0			0			
-75.908	36.8467	96		fall	13	2.5		0.75		-	8	Pos.	Trace	0			0			0			
-75.899	36.8467	98		fall	9.5	3.75		1		-	0	Pos.	Trace	0			0			0			
-75.891	36.8467	100		fall	5.75	2		1.5		-	1	None	10	0			0			0			
-75.927	36.8433	101		fall	4.5	2.5		0.75		-	0	Pos.	None	0			0			0			
-75.919	36.8433	103		fall	14			1.25		+	0	Pos.	None	0			0			0			
-75.911	36.8433	105		fall	5			1.25		-	0	None	None	0			0			0			
-75.903	36.8433	107		fall	4	2		2		-	0	None	None	0			0			0			
-75.894	36.8433	109		fall	6.25	2		1		-	0	None	7	0			0			0			
-75.922	36.8392	112		fall	7			3.5		-	0	None	Trace	0			0			0			
-75.914	36.8392	114		fall	7.25	7.25		1		-	0	None	Trace	0			0			0			
-75.906	36.8392	116		fall	4.5			0.75		-	0	None	None	0			0			0			
-75.897	36.8392	118		fall	4.75	1.75		0.5		-	0	None	Trace	0			0			0			
-75.888	36.8392	120		fall	4.75	2		1		-	0	None	11	0			0			0			
-75.924	36.8358	121		fall	7.5			2		-	0	None	Trace	0			0			0			
-75.916	36.8358	123		fall	8	8		3		-	0	None	Trace	0			0			0			
-75.908	36.8358	125		fall	4			2		-	0	Pos.	None	0			0			0			
-75.9	36.8358	127		fall	10.75			1.75		-	0	None	Trace	0			0			0			
-75.892	36.8358	129		fall	8.25	2.75		0.75		-	1	None	None	0			0			0			

Table 4. Fall 1996 SPI analysis.

		Virginia Beach Sandmining Project SPI visual analysis: Fal									Surface struct.												
							Sed.	Sed.	Relief		--Tubes--		Subsurf	---Infauna----			Voids						
				Date	PEN	RPD	Type	Rel.	Type	Epifau	+/-	ellet	Shell	#	Type	Depth	#	Type	Depth	Gas	Depth	Burrow	Type
LON	LAT	cell	rep	96	(cm)	(cm)		(cm)		(+/-)													
-75.92	36.8317	132		fall	4.75	2		2.75		-	8	None	Trace	0			0			0			
-75.912	36.8317	134		fall	4.5			3		-	0	None	Trace	0			0			0			
-75.903	36.8317	136		fall	6			2		-	0	None	Trace	0			0			0			
-75.897	36.8317	138		fall	6			2.25		-	0	None	Trace	0			0			0			
-75.886	36.8317	140		fall	6.5	6		2.25		-	0	None	Trace	0			0			0			
-75.923	36.828	141		fall	6.25	6.25		2.25		-	0	None	Trace	0			0			0			
-75.914	36.828	143		fall	6	2.5		1.75		-	1	None	Trace	0			0			0			
-75.907	36.828	145		fall	6.5			2		-	0	None	None	0			0			0			
-75.898	36.828	147		fall	5			3		-	0	None	2	0			0			0			
-75.889	36.828	149		fall	15.5			0.75		-	0	None	None	1	Worm	4	0			0			
-75.916	36.8237	152		fall	6.5	6.5		2.25		-	0	None	None	0			0			0			
-75.908	36.8237	154		fall	5	2.5		0.75		-	0	Pos.	None	0			0			0			
-75.9	36.8237	156		fall	4.75			0.25		-	0	None	Trace	0			0			0			
-75.893	36.8237	158	1b	fall	5			1.5		-	0	None	7	0			0			0			
-75.883	36.8237	160		fall	5.5			1.5		-	0	None	2	0			0			0			
-75.92	36.8197	161		fall	5.25	3.25		2		-	0	None	1	0			0			0			
-75.913	36.8197	163		fall	6.25	3		2.25		-	1	None	Trace	0			0			0			
-75.904	36.8197	165		fall	4.75	2		1.25		+	0	None	Trace	0			0			0			
-75.896	36.8197	167		fall	5			2.25		-	0	None	Trace	0			0			0			
-75.887	36.8197	169		fall	17.75			1.75		-	0	None	None	0			0			0			
-75.914	36.8158	172		fall	5	2.5		0.75		-	0	Pos.	2	1	Worm	0.25	0			0			

Table 4. Fall 1996 SPI analysis.

		Virginia Beach Sandmining Project SPI visual analysis: Fal									Surface struct.											
							Sed.	Sed.	Relief		--Tubes--		Subsurf	---Infauna----			Voids					
				Date	PEN	RPD	Type	Rel.	Type	Epifau	+/-	ellet	Shell	#	Type	Depth	#	Type	Depth	Gas	Depth	Burrow	Type
LON	LAT	cell	rep	96	(cm)	(cm)		(cm)		(+/-)													
-75.907	36.8158	174		fall	5.25	2.5		1.25		-	0	None	Trace	0			0			0		
-75.898	36.8158	176		fall	6	3.25		0.75		-	0	None	None	0			0			0		
-75.889	36.8158	178		fall	4.25			2		-	0	None	None	0			0			0		
-75.882	36.8158	180		fall	2.75			1.25		-	0	None	Trace	0			0			0		
-75.917	36.8117	181		fall	5.5	3.25		1.75		-	0	None	1	0			0			0		
-75.908	36.8117	183		fall	5	2		1		-	0	Pos.	1	0			0			0		
-75.901	36.8117	185		fall	4.5	2.25		2.5		-	0	Pos.	Trace	0			0			0		
-75.893	36.8117	187		fall	7.5	1.5		2.75		+	0	Pos.	None	0			0			0		
-75.884	36.8117	189		fall	5.25			2		-	0	Pos.	None	0			0			0		
-75.912	36.808	192		fall	5			0.5		-	0	Pos.	None	3	Worm	2.75	0			0		
-75.903	36.808	194		fall	5.25	2		3		-	0	None	Trace	0			0			0		
-75.895	36.808	196		fall	4.5	2.75		1.75		-	0	Pos.	1	0			0			0		
-75.888	36.808	198		fall	3.5			0.75		-	0	Pos.	3	0			0			0		
-75.878	36.808	200		fall	4			1.25		-	0	None	1	0			0			0		
-75.885	36.9083	201		fall	5			2		+	0	None	Trace	0			0			0		
-75.877	36.9083	203		fall	5.25	1.75		1.75		-	0	None	1	0			0			0		
-75.868	36.9083	205		fall	4.25	1.5		1.5		-	0	None	None	0			0			0		
-75.88	36.9053	212		fall	2.5			1.25		+	0	None	Trace	0			0			0		
-75.871	36.9053	214		fall	6.5	1.5		2		-	0	None	None	0			0			0		
-75.863	36.9053	216		fall	4.5			0.5		-	1	None	None	0			0			0		
-75.854	36.9053	218		fall	3	1.25		1.75		-	0	Pos.	1	0			0			0		

Table 4. Fall 1996 SPI analysis.

		Virginia Beach Sandmining Project SPI visual analysis: Fal									Surface struct.												
							Sed.	Sed.	Relief		--Tubes--		Subsurf	---Infauna----			Voids						
				Date	PEN	RPD	Type	Rel.	Type	Epifau	+/-	ellet	Shell	#	Type	Depth	#	Type	Depth	Gas	Depth	Burrow	Type
LON	LAT	cell	rep	96	(cm)	(cm)		(cm)		(+/-)													
-75.846	36.9053	220		fall	3.75	1.5		1.75		-	0	None	4	0			0			0			
-75.883	36.902	221		fall	6			1.5		+	0	None	None	0			0			0			
-75.874	36.902	223		fall	5.75			1		-	0	None	None	0			0			0			
-75.866	36.902	225		fall	5.5			0.75		-	0	None	None	0			0			0			
-75.857	36.902	227		fall	4.5	1.25		2		-	0	None	None	0			0			0			
-75.848	36.902	229		fall	3.25	1.5		0.25		-	0	None	Trace	0			0			0			
-75.878	36.8983	232	1b	fall	3			1.75		-	0	None	None	0			0			0			
-75.869	36.8983	234		fall	6			1		-	0	None	None	0			0			0			
-75.86	36.8983	236		fall	5	1.5		1.5		-	0	None	None	0			0			0			
-75.852	36.8983	238		fall	4	1.5		0.25		-	0	None	Trace	0			0			0			
-75.843	36.8983	240		fall	3	1.5		1.25		+	0	None	Trace	0			0			0			
-75.881	36.8942	241		fall	3.25			0.25		+	0	None	2	0			0			0			
-75.872	36.8942	243		fall	6.5			1		-	0	None	None	0			0			0			
-75.863	36.8942	245		fall	3			1.5		-	0	None	Trace	0			0			0			
-75.855	36.8942	247		fall	2.25			0.75		+	0	None	None	0			0			0			
-75.846	36.8942	249		fall	2.75	1		0.5		+	0	None	Trace	1	Worm	0.75	0			0			
-75.875	36.8908	252		fall	5			1.25		-	0	None	None	0			0			0			
-75.867	36.8908	254		fall	3			0.5		+	0	None	2	0			0			0			
-75.858	36.8908	256		fall	3			1.5		-	0	None	Trace	0			0			0			
-75.85	36.8908	258		fall	2.5			1		+	0	None	None	0			0			0			
-75.841	36.8908	260		fall	3.5			1		+	0	None	None	0			0			0			

Table 4. Fall 1996 SPI analysis.

		Virginia Beach Sandmining Project SPI visual analysis: Fal									Surface struct.											
							Sed.	Sed.	Relief		--Tubes--		Subsurf	---Infauna----			Voids					
				Date	PEN	RPD	Type	Rel.	Type	Epifau	+/-	ellet	Shell	#	Type	Depth	#	Type	Depth	Gas	Depth	Burrow	Type
LON	LAT	cell	rep	96	(cm)	(cm)		(cm)		(+/-)													
-75.878	36.8867	261		fall	4.5			1.25		-	0	None	None	0			0			0		
-75.869	36.8867	263		fall	6			0.5		-	0	None	None	0			0			0		
-75.861	36.8867	265		fall	3.75			1.25		-	0	None	1	0			0			0		
-75.853	36.8867	267		fall	2.75			1.25		-	0	None	Trace	0			0			0		
-75.844	36.8867	269		fall	3.5			4.5		-	0	None	Trace	0			0			0		
-75.873	36.8825	272		fall	5			1.5		-	0	None	Trace	0			0			0		
-75.864	36.8825	274		fall	5.25	4.5		0.5		-	0	None	None	0			0			0		
-75.855	36.8825	276		fall	6			0.25		-	0	None	Trace	0			0			0		
-75.847	36.8825	278	1b	fall				1.75		+	0	None	None	0			0			0		
-75.838	36.8825	280		fall	3			1.25		+	0	None	None	0			0			0		
-75.875	36.8783	281		fall	5.5			6.15		-	0	None	None	0			0			0		
-75.867	36.8783	283		fall	4.5	3.75		1.5		-	0	None	Trace	0			0			0		
-75.858	36.8783	285		fall	4.75	3.75		1.5		-	1	None	None	0			0			0		
-75.85	36.8783	287		fall	6			1.25		+	0	None	Trace	0			0			0		
-75.841	36.8783	289		fall	7			1.75		-	0	None	Trace	0			0			0		
-75.87	36.8742	292		fall	4.75			1		-	0	None	None	0			0			0		
-75.862	36.8742	294		fall	4.75	3.5		1.75		-	0	None	None	0			0			0		
-75.853	36.8742	296		fall	5	4		1		-	0	None	Trace	0			0			0		
-75.844	36.8742	298		fall	5.25			0.5		-	0	None	Trace	1	Worm	1.25	0			0		
-75.836	36.8742	300		fall	3.25			1.5		-	0	None	None	0			0			0		
-75.896	36.7613	303		fall	5.5			1.5		-	0	None	None	1	Worm	2.5	0			0		

Table 4. Fall 1996 SPI analysis.

		Virginia Beach Sandmining Project SPI visual analysis: Fal									Surface struct.												
							Sed.	Sed.	Relief		--Tubes--		Subsurf	---Infauna----			Voids						
				Date	PEN	RPD	Type	Rel.	Type	Epifau	+/-	ellet	Shell	#	Type	Depth	#	Type	Depth	Gas	Depth	Burrow	Type
LON	LAT	cell	rep	96	(cm)	(cm)		(cm)		(+/-)													
-75.888	36.7613	305		fall	6.5	6.5		2.75		-	0	None	Trace	0			0			0			
-75.88	36.7613	307		fall	7			3		-	0	None	Trace	0			0			0			
-75.871	36.7613	309		fall	8.5	8.5		0.25		-	0	None	Trace	0			0			0			
-75.898	36.758	312		fall	5			1.5		-	0	Pos.	None	0			0			0			
-75.891	36.758	314		fall	15	3.5		1.25		-	4	Pos.	None	2	Worm	11.5	0			0			
-75.883	36.758	316		fall	7.5			1.25		-	0	None	Trace	0			0			0			
-75.874	36.758	318		fall	6.5	6.5		3.5		-	0	None	Trace	0			0			0			
-75.866	36.758	320		fall	7	7		1.75		-	0	None	None	0			0			0			
-75.902	36.7533	321		fall	5			1.5		-	0	None	Trace	0			0			0			
-75.895	36.7533	323		fall	6	3		1.75		-	0	None	None	1	Worm	3.5	0			0			
-75.886	36.7533	325		fall	6.5	6.5		1.25		-	0	None	Trace	0			0			0			
-75.878	36.7533	327		fall	6.5	6.5		1.5		-	0	None	None	0			0			0			
-75.87	36.7533	329		fall	7	7		2.25		-	0	None	Trace	0			0			0			
-75.896	36.75	332		fall	6			1		-	0	None	Trace	1	Worm	5	0			0			
-75.888	36.75	334	1b	fall	5.5	5.5		2.5		+	0	None	Trace	0			0			0			
-75.881	36.75	336		fall	7.5	7.5		2.75		-	0	None	Trace	0			0			0			
-75.872	36.75	338		fall	6.75	6.75		1.25		-	0	None	None	0			0			0			
-75.863	36.75	340		fall	10.25	4		1.75		-	0	None	Trace	0			0			0			
-75.899	36.7458	341		fall	5			1		-	0	None	None	0			0			0			
-75.891	36.7458	343		fall	12	3.5		1		-	7	Pos.	None	1	Worm	2.5	0			0			
-75.883	36.7458	345		fall	8	8		4		-	0	None	Trace	0			0			0			

Table 4. Fall 1996 SPI analysis.

		Virginia Beach Sandmining Project SPI visual analysis: Fal									Surface struct.												
							Sed.	Sed.	Relief		--Tubes--		Subsurf	---Infauna----			Voids						
				Date	PEN	RPD	Type	Rel.	Type	Epifau	+/-	ellet:	Shell	#	Type	Depth	#	Type	Depth	Gas	Depth	Burrow	Type
LON	LAT	cell	rep	96	(cm)	(cm)		(cm)		(+/-)													
-75.874	36.7458	347		fall	5.5	5.5		1.5		+	0	None	None	0			0			0			
-75.867	36.7458	349		fall	6	4		2		+	0	None	Trace	0			0			0			
-75.893	36.7417	352		fall	6.5	2		0.5		-	1	Pos.	None	0			0			0			
-75.887	36.7417	354		fall	8	8		5		-	0	None	None	0			0			0			
-75.878	36.7417	356		fall	7	7		7.25		-	0	None	None	0			0			0			
-75.87	36.7417	358		fall	5	2.75		1.25		+	0	None	Trace	0			0			0			
-75.861	36.7417	360		fall	5.5			0.75		-	0	None	1	0			0			0			
-75.897	36.738	361		fall	6.25	14		1		-	0	None	None	0			0			0			
-75.889	36.738	363		fall	6	6		2		-	0	None	None	0			0			0			
-75.881	36.738	365		fall	3.75	3		0.75		+	0	None	Trace	0			0			0			
-75.873	36.738	367		fall	4.5	3		1.5		+	0	None	2	1	Worm	3	0			0			
-75.865	36.738	369		fall	9.75			0.5		-	1	None	Trace	0			0			0			
-75.892	36.7333	372		fall	10.5	2.75		0.75		-	0	None	None	0			0			0			
-75.883	36.7333	374	1b	fall	6	6		1.5		-	0	None	Trace	0			0			0			
-75.876	36.7333	376		fall	6.5	1		1.75		-	0	None	Trace	0			0			0			
-75.868	36.7333	378		fall	4.5			2		+	0	Pos.	None	0			0			0			
-75.859	36.7333	380		fall	6.5			2.5		-	0	None	Trace	0			0			0			
-75.894	36.73	381		fall	6.5	2		1.5		+	0	None	Trace	0			0			0			
-75.887	36.73	383		fall	6.75	6.75		0.75		+	0	None	Trace	0			0			0			
-75.879	36.73	385		fall	6.25	6.25		1.5		+	0	None	Trace	0			0			0			
-75.871	36.73	387	1b	fall	4.25			0.75		+	0	None	Trace	0			0			0			

Table 4. Fall 1996 SPI analysis.

		Virginia Beach Sandmining Project SPI visual analysis: Fal									Surface struct.											
							Sed.	Sed.	Relief		--Tubes--		Subsurf	---Infauna----			Voids					
				Date	PEN	RPD	Type	Rel.	Type	Epifau	+/-	ellet	Shell	#	Type	Depth	#	Type	Depth	Gas	Depth	Burrow	Type
LON	LAT	cell	rep	96	(cm)	(cm)		(cm)		(+/-)													
-75.863	36.73	389		fall	5.25			1		-	0	None	Trace	0			0			0			
-75.893	36.7258	392		fall	5.5	2.5		2.25		+	0	Pos.	None	0			0			0			
-75.885	36.7258	394	1b	fall	8.5	7.5		2.25		+	0	None	Trace	0			0			0			
-75.877	36.7258	396		fall	4.75			1.75		-	0	None	Trace	0			0			0			
-75.865	36.7258	398		fall	14			0.75		-	6	None	None	1	Worm	8	0			0			
-75.857	36.7258	400		fall	5.5			2		-	0	None	Trace	0			0			0			

Table 5. Spring 1997 SPI analysis.

		Virginia Beach Sandmining Project SPI visual analysis: Spring, 19									Surface struct.												
								Sed.	Sed.	Relief		--Tubes--		Subsuri	---Infauna----			Voids					
					Date	PEN	RPD	Type	Rel.	Type	Epifauna	+/-	Pellet:	Shell	#	Type	Depth	#	Type	Depth	Gas	Depth	Burrow	Type
LON	LAT	cell	rep		97	(cm)	(cm)		(cm)		(+/-)													
-75.9511	36.9166	97VB001	1	b	spr	8.0	2.1	SI	1	PIT,SHELL	NONE	NONE	NONE	NONE	0			0			0		0	
-75.9501	36.9151	97VB001	2	b	spr	21.3	1.5	SI-CL	1.3	PIT,MOUND	NONE	2	NONE	15	0			0			0		3	AN
-75.9248	36.9196	97VB002	1	b	spr	12	3	SI	0.5	SHELL	NONE	5	NONE	10	0			0			0		5	AN
-75.9248	36.9196	97VB002	2	b	spr	14.2	6	SI-CL	1.2	PIT,MOUND	NONE	1	NONE	10	1	WORM	10.3	0			0		0	
-75.8996	36.9227	97VB003	1	b	spr	4.3	4.3	FS	1	BEDFORM,SI	NONE	1	NONE	5	0			0			0		0	
-75.8996	36.9283	97VB003	2	a	spr			FS	1.8	BEDFORM,SI	NONE	NONE	NONE	TRACE	0			0			0		0	
-75.8742	36.9256	97VB004	1	b	spr	3.3	3.3	FS	1.7	BEDFORM,SI	NONE	NONE	NONE	NONE	0			0			0		0	
-75.8742	36.9256	97VB004	2	b	spr	4.5	2.5	FS	2.1	SHELL	7 SAND D(	NONE	NONE	5	0			0			0		0	
-75.8488	36.9284	97VB005	1	b	spr	8.3		FS	1.9	BEDFORM,SI	2 SAND D(	NONE	NONE	TRACE	0			0			0		0	
-75.8488	36.9284	97VB005	2	b	spr	7.1	2.2	FS	1.4	BEDFORM	3 SAND D(	NONE	NONE	TRACE	0			0			0		0	
-75.8574	36.9160	97VB009	1	b	spr	6.4	0.3	FS	3.4	PIT,SHELL	CRUSTACE/	NONE	NONE	5	0			0			0		0	
-75.8574	36.9160	97VB009	2	b	spr	4.7	0.7	FS	1.7	BEDFORM,SI	NONE	NONE	NONE	TRACE	0			0			0		0	
-75.8828	36.9131	97VB008	1	b	spr	4.2	3	FS	2.3	SHELL,PIT	NONE	NONE	NONE	5	0			0			0		0	
-75.8828	36.9131	97VB008	2	b	spr	6.8	2	FS	2	SHELL,PIT	NONE	NONE	NONE	TRACE	0			0			0		0	
-75.9081	36.9101	97VB007	1	b	spr																			
-75.9081	36.9101	97VB007	2	a	spr			CL		ROCKY	HERMIT C(	NONE	NONE	50	0			0			0		0	
-75.9332	36.9071	97VB006	1	b	spr	>24		SI	IND	IND	IND	IND	IND	5	3	WORMS	IND	0			0		1	AN
-75.9332	36.9071	97VB006	2	b	spr	18.6	2.8	SI	1.3	MOUND	NONE	NONE	NONE	TRACE	0			0			0		0	
-75.9423	36.8946	97VB011	1	b	spr	19.4	2.9	FS-SI	1.5	BEDFORM	NONE	NONE	NONE	NONE	0			0			0		0	
-75.9423	36.8946	97VB011	2	b	spr	20.4	4.2	SI	1	SHELL	NONE	NONE	NONE	NONE	0			0			0		0	
-75.9168	36.8976	97VB012	1	b	spr	8.3	8.3	CS	2.5	BEDFORM	NONE	NONE	NONE	5	0			0			0		0	

Table 5. Spring 1997 SPI analysis.

		Virginia Beach Sandmining Project SPI visual analysis: Spring, 19										Surface struct.												
								Sed.	Sed.	Relief		--Tubes--		Subsur	---Infauna----			Voids						
					Date	PEN	RPD	Type	Rel.	Type	Epifauna	+/-	Pellet	Shell	#	Type	Depth	#	Type	Depth	Gas	Depth	Burrow	Type
LON	LAT	cell	rep		97	(cm)	(cm)		(cm)		(+/-)													
-75.9168	36.8976	97VB012	2	b	spr	11.5	11.5	CS	1.2	BEDFORM	NONE	NONE	NONE	5	0			0			0		0	
-75.8913	36.9007	97VB013	1	b	spr	4.8	3	FS	0.3	EVEN	NONE	NONE	NONE	NONE	0			0			0		0	
-75.8913	36.9007	97VB013	2	b	spr	5.2	1.7	FS	0.7	SHELL	NONE	NONE	NONE	TRACE	0			0			0		0	
-75.8656	36.9035	97VB014	1	b	spr	5.2	2.6	FS	2	BEDFORM	NONE	NONE	NONE	TRACE	0			0			0		0	
-75.8661	36.9044	97VB014	2	b	spr	4.4	3.2	FS	1.3	BEDFORM,SI	NONE	NONE	NONE	5	0			0			0		0	
-75.8405	36.9064	97VB015	1	b	spr	4.8	3	FS	1.4	BEDFORM,SI	SAND DOLI	NONE	NONE	TRACE	0			0			0		0	
-75.8405	36.9064	97VB015	2	b	spr	5.2	1.7	FS	1.5	BEDFORM,SI	SAND DOLI	NONE	NONE	TRACE	0			0			0		0	
-75.8492	36.9111	97VB019	1	b	spr	5.1	2.7	FS	1.6	BEDFORM,SI	NONE	NONE	NONE	TRACE	0			0			0		0	
-75.8492	36.9111	97VB019	2	b	spr	5.1	4	FS	1	BEDFORM	NONE	NONE	NONE	TRACE	0			0			0		0	
-75.8743	36.8910	97VB018	1	b	spr	5.6	4.4	FS	1.7	BEDFORM	NONE	NONE	NONE	TRACE	0			0			0		0	
-75.8743	36.8910	97VB018	2	b	spr	4.3	4.3	FS	1.9	BEDFORM,SI	NONE	NONE	NONE	TRACE	0			0			0		0	
-75.8998	36.8881	97VB017	1	b	spr	8.3	3.2	CS	0.7	SHELL	NONE	NONE	NONE	5	0			0			0		0	
-75.8998	36.8881	97VB017	2	b	spr	8.3	3.9	CS	0.3	BEDFORM,SI	NONE	NONE	NONE	5	0			0			0		0	
-75.9253	36.8852	97VB016	1	b	spr	23.5	4.2	FS-SI	1.8	PIT,MOUND	NONE	NONE	NONE	TRACE	1	WORM	8.2	1	AN	17.5	0		2	OX
-75.9253	36.8852	97VB016	2	b	spr	10.2	7	CS	0.3	BEDFORM,SI	NONE	1	NONE	5	0			0			0		0	
-75.9336	36.8726	97VB021	1	b	spr	10.5	6.2	FS-SI	1.5	BEDFORM	NONE	NONE	NONE	NONE	1	CRUSTACI	6.3	0			0		1	AN
-75.9336	36.8726	97VB021	2	b	spr	12	6	FS	1.5	BEDFORM	NONE	2	NONE	TRACE	0			0			0		2	OX
-75.9083	36.8757	97VB022	1	b	spr	4.8	4.8	MS	1.4	MOUND	NONE	NONE	NONE	TRACE	0			0			0		0	
-75.9083	36.8757	97VB022	2	b	spr	9.1	6	MS	0.7	BEDFORM,SI	NONE	NONE	NONE	TRACE	1	WORM	2.3	0			0		0	
-75.8827	36.8789	97VB023	1	b	spr	6.5	1.8	CS	0.7	ROCK,SHELI	NONE	NONE	NONE	5	0			0			0		0	
-75.8576	36.8814	97VB024	1	b	spr	1.8	1.8	FS	1.1	BEDFORM	NONE	NONE	NONE	NONE	0			0			0		0	

Table 5. Spring 1997 SPI analysis.

		Virginia Beach Sandmining Project SPI visual analysis: Spring, 19										Surface struct.												
								Sed.	Sed.	Relief		--Tubes--		Subsur	---Infauna----			Voids						
					Date	PEN	RPD	Type	Rel.	Type	Epifauna	+/-	Pellet	Shell	#	Type	Depth	#	Type	Depth	Gas	Depth	Burrow	Type
LON	LAT	cell	rep		97	(cm)	(cm)		(cm)		(+/-)													
-75.8576	36.8814	**97VB024**	2	b	spr	5.5	3.7	FS	1.5	BEDFORM	NONE	NONE	NONE	NONE	0			0			0		0	
-75.8324	36.8845	**97VB025**	1	b	spr	4.9	4.9	FS	0.4	SHELL,BED	NONE	NONE	NONE	NONE	0			0			0		0	
-75.8324	36.8845	**97VB025**	2	b	spr	6.1		FS	3	BEDFORM,SI	NONE	NONE	NONE	NONE	0			0			0		0	
-75.8411	36.8717	**97VB029**	1	b	spr	5.3	3.7	FS	1.5	BEDFORM,SI	NONE	NONE	NONE	NONE	0			0			0		0	
-75.8411	36.8717	**97VB029**	2	b	spr	5.3	5.3	FS	1.9	BEDFORM,SI	NONE	NONE	NONE	NONE	0			0			0		0	
-75.8659	36.8687	**97VB028**	1	b	spr	4.9	2.2	SI	0.7	SHELL,MOU	NONE	NONE	NONE	TRACE	0			0			0		0	
-75.8659	36.8687	**97VB028**	2	b	spr	5.8	3	SI	0.6	SHELL	NONE	2	NONE	5	0			0			0		0	
-75.8910	36.8659	**97VB027**	1	b	spr	10	10	MS	0.9	SHELL	NONE	NONE	NONE	TRACE	0			0			0		0	
-75.8919	36.8661	**97VB027**	2	b	spr	6.4	6.4	MS	0.6	EVEN	NONE	NONE	NONE	TRACE	0			0			0		0	
-75.9171	36.8628	**97VB026**	1	b	spr	7.8	4.2	MS	0.9	BEDFORM	NONE	NONE	NONE	5	0			0			0		0	
-75.9171	36.8628	**97VB026**	2	b	spr	13.9	6.3	MS-CL	1.1	BEDFORM	NONE	NONE	NONE	5	0			0			0		0	
-75.9257	36.8507	**97VB031**	1	b	spr	7.9	6	MS	2	BEDFORM	NONE	NONE	NONE	10	0			0			0		0	
-75.9257	36.8511	**97VB031**	2	b	spr	8.5	8.5	MS	0.7	EVEN	NONE	1	NONE	TRACE	0			0			0		0	
-75.9004	36.8533	**97VB032**	1	b	spr	5.9	5.5	CS-FS	0.3	EVEN	NONE	NONE	NONE	TRACE	0			0			0		0	
-75.9004	36.8533	**97VB032**	2	b	spr	6.7	6.7	MS	0.6	BEDFORM	NONE	3	NONE	TRACE	0			0			0		0	
-75.8752	36.8562	**97VB033**	1	b	spr	17.5	6.8	SI	1	PLANT DET	NONE	4	NONE	5	0			0			0		0	
-75.8752	36.8562	**97VB033**	2	b	spr	7.5	5.9	FS-SI	1.2	PLANT DET	NONE	NONE	NONE	TRACE	0			0			0		0	
-75.8495	36.8574	**97VB034**	1	b	spr	6	5.5	FS	2.3	BEDFORM	NONE	NONE	NONE	TRACE	0			0			0		0	
-75.8495	36.8574	**97VB034**	2	b	spr	6	4.8	FS	1.2	BEDFORM	NONE	NONE	NONE	TRACE	0			0			0		0	
-75.8250	36.8621	**97VB035**	1	b	spr	7.7	6.7	MS	0.7	BEDFORM	NONE	NONE	NONE	TRACE	0			0			0		0	
-75.8250	36.8621	**97VB035**	2	b	spr	6.3	6.3	MS	0.7	BEDFORM,SI	NONE	NONE	NONE	NONE	0			0			0		0	

Table 5. Spring 1997 SPI analysis.

		Virginia Beach Sandmining Project SPI visual analysis: Spring, 19						Surface struct.															
								Sed.	Sed.	Relief		--Tubes--		Subsur	---Infauna----			Voids					
					Date	PEN	RPD	Type	Rel.	Type	Epifauna	+/-	Pellet	Shell	#	Type	Depth	#	Type	Depth	Gas	Depth	Burrow	Type
LON	LAT	cell	rep		97	(cm)	(cm)		(cm)		(+/-)													
-75.8333	36.8489	**97VB039**	1	b	spr	5.3	5.3	FS	1.3	BEDFORM, SI	NONE	NONE	NONE	TRACE	0			0			0		0	
-75.8333	36.8489	**97VB039**	2	b	spr	7	7	MS	1.4	BEDFORM, SI	NONE	NONE	NONE	10	0			0			0		0	
-75.8587	36.8468	**97VB038**	1	b	spr	6.1		FS	2	BEDFORM, SI	NONE	NONE	NONE	5	0			0			0		0	
-75.8587	36.8468	**97VB038**	2	b	spr	5.7		FS	0.9	BEDFORM, SI	NONE	NONE	NONE	TRACE	0			0			0		1	AN
-75.8837	36.8439	**97VB037**	1	b	spr	5.5	5	FS	1.4	BEDFORM, PI	NONE	1	NONE	TRACE	0			0			0		0	
-75.8837	36.8439	**97VB037**	2	b	spr	6	3.5	FS	0.8	BEDFORM, SI	NONE	NONE	NONE	TRACE	0			0			0		0	
-75.9091	36.8409	**97VB036**	1	b	spr	9.7		MS	1.8	SLOPE	NONE	NONE	NONE	TRACE	0			0			0		0	
-75.9088	36.8402	**97VB036**	2	b	spr	6.2	6.2	MS-FS	0.4	SHELL	NONE	NONE	NONE	TRACE	0			0			0		0	
-75.9174	36.8287	**97VB041**	1	b	spr	6	0.7	FS	2.1	SHELL, BEDI	NONE	NONE	NONE	TRACE	0			0			0		0	
-75.9174	36.8287	**97VB041**	2	b	spr	6.3	6.3	FS	1.8	SHELL, BEDI	NONE	NONE	NONE	TRACE	0			0			0		0	
-75.8926	36.8312	**97VB042**	1	b	spr	7.3	3.8	FS	1.3	BEDFORM, SI	NONE	NONE	NONE	5	0			0			0		0	
-75.8926	36.8312	**97VB042**	2	b	spr	6.4	2	FS-SI	2	BEDFORM	NONE	NONE	NONE	TRACE	0			0			0		0	
-75.8672	36.8342	**97VB043**	1	b	spr	6.1	4.2	FS	2.4	SHELL, BEDI	NONE	NONE	NONE	TRACE	0			0			0		0	
-75.8672	36.8342	**97VB043**	2	b	spr	5.9	2.7	FS	2.2	SHELL, BEDI	NONE	NONE	NONE	NONE	0			0			0		0	
-75.8425	36.8373	**97VB044**	1	b	spr	8.9	8.9	MS	2.1	BEDFORM	NONE	NONE	NONE	TRACE	0			0			0		0	
-75.8420	36.8367	**97VB044**	2	b	spr	6.9	6.9	MS-FS	1.3	SHELL, BEDI	HERMIT CI	NONE	NONE	5	0			0			0		0	
-75.8175	36.8400	**97VB045**	1	b	spr	7.5	7.5	MS	0.6	BEDFORM	NONE	NONE	NONE	NONE	0			0			0		0	
-75.8176	36.8401	**97VB045**	2	b	spr	6.2	6.2	MS	0.9	SHELL, BEDI	NONE	NONE	NONE	NONE	0			0			0		0	
-75.8504	36.8247	**97VB048**	1	b	spr	5.7	5.7	MS	3.7	SHELL, BEDI	SAND DOLI	NONE	NONE	TRACE	0			0			0		0	
-75.8761	36.8219	**97VB047**	1	b	spr	5.4	5.4	FS	1.6	SHELL, BEDI	NONE	NONE	NONE	TRACE	0			0			0		0	
-75.8761	36.8220	**97VB047**	2	a	spr		5.7	FS	1.9	DISTURBED	NONE	NONE	NONE	NONE	0			0			0		0	

Table 5. Spring 1997 SPI analysis.

		Virginia Beach Sandmining Project SPI visual analysis: Spring, 19										Surface struct.											
								Sed.	Sed.	Relief		--Tubes--		Subsur	---Infauna----			Voids					
					Date	PEN	RPD	Type	Rel.	Type	Epifauna	+/-	Pellet	Shell	#	Type	Depth	#	Type	Depth	Gas	Depth	Burrow	Type
LON	LAT	cell	rep		97	(cm)	(cm)		(cm)		(+/-)													
-75.9014	36.8190	**97VB046**	1	b	spr	15.5	15.5	CL	0.7	MOUND	NONE	3	NONE	NONE	0			6	1 OX,5	AN	0	1	AN
-75.9013	36.8191	**97VB046**	2	b	spr	5.7	1.4	CL-SI	1.9	SHELL,BEDI	NONE	NONE	NONE	NONE	0			0			0	0	
-75.9102	36.8065	**97VB051**	1	b	spr	5.8	4	FS	1.4	SHELL,BEDI	NONE	NONE	NONE	NONE	0			0			0	0	
-75.9102	36.8065	**97VB051**	2	b	spr	6.2	4.8	FS	1	BEDFORM	NONE	NONE	NONE	TRACE	0			0			0	0	
-75.8843	36.8093	**97VB052**	1	b	spr	7.3	6	FS	1.6	BEDFORM	NONE	NONE	NONE	NONE	0			0			0	0	
-75.8844	36.8093	**97VB052**	2	b	spr	5.9	5.9	FS	1.9	BEDFORM	NONE	NONE	NONE	NONE	0			0			0	0	
-75.8596	36.8123	**97VB053**	1	b	spr	4.8	4.8	FS	1.6	SHELL,BEDI	NONE	NONE	NONE	TRACE	0			0			0	0	
-75.8596	36.8124	**97VB053**	2	b	spr	5.3	5.3	FS	1.8	MOUND	NONE	NONE	NONE	TRACE	0			0			0	0	
-75.8596	36.8153	**97VB054**	1	b	spr	5.3	4	FS	1.1	BEDFORM	NONE	NONE	NONE	NONE	0			0			0	0	
-75.8340	36.8154	**97VB054**	2	b	spr	5.8	5.8	FS	0.5	SHELL	NONE	NONE	NONE	NONE	0			0			0	0	
-75.8428	36.8034	**97VB058**	1	b	spr	8	8	SI	2.7	SHELL,ROCI	NONE	NONE	NONE	50	0			0			0	1	AN
-75.8428	36.8035	**97VB058**	2	b	spr	7.2	7.2	MS	1.2	SHELL,MOUI	NONE	2	NONE	25	0			0			0	0	
-75.8681	36.7997	**97VB057**	1	b	spr	6.4	6.4	SI	0.3	SHELL,BEDI	NONE	NONE	NONE	5	0			0			0	0	
-75.8680	36.7997	**97VB057**	2	b	spr	5	5	SI	1.8	SHELL,BEDI	NONE	NONE	NONE	5	0			0			0	0	
-75.8926	36.7970	**97VB056**	1	b	spr	8.5	8.5	FS	2.7	MOUND,BEDI	NONE	NONE	NONE	NONE	0			0			0	0	
-75.8926	36.7970	**97VB056**	2	b	spr	6.8	6.8	FS	1.5	BEDFORM	NONE	NONE	NONE	NONE	0			0			0	0	
-75.9018	36.7848	**97VB061**	1	b	spr	5	2	FS	2	SHELL,BEDI	NONE	NONE	NONE	NONE	0			0			0	0	
-75.9018	36.7846	**97VB061**	2	b	spr	7.8	7.8	FS	1.5	BEDFORM	NONE	NONE	NONE	TRACE	0			0			0	0	
-75.8765	36.7875	**97VB062**	1	b	spr	8	8	FS	3.4	SLOPE	NONE	NONE	NONE	20	0			0			0	0	
-75.8765	36.7876	**97VB062**	2	b	spr	11	4.6	FS	0.9	BEDFORM	NONE	NONE	NONE	20	0			0			0	0	
-75.8514	36.7905	**97VB063**	1	b	spr	4.9	4.9	CS	3.2	SHELL,SLOI	NONE	NONE	NONE	50	0			0			0	0	

Table 5. Spring 1997 SPI analysis.

		Virginia Beach Sandmining Project SPI visual analysis: Spring, 19						Surface struct.															
								Sed.	Sed.	Relief		--Tubes--		Subsuri	---Infauna----			Voids					
					Date	PEN	RPD	Type	Rel.	Type	Epifauna	+/-	Pellets	Shell	#	Type	Depth	#	Type	Depth	Gas	Depth	Burrow	Type
LON	LAT	cell	rep		97	(cm)	(cm)		(cm)		(+/-)													
-75.8514	36.7905	**97VB063**	2	b	spr	5.3	5.3	CS	2.1	SHELL,ROC	NONE	NONE	NONE	50	0			0			0		0	
-75.8262	36.7927	**97VB064**	1	b	spr	6.2	4	SI	1.5	ROCK,SHELI	NONE	1	NONE	5	0			0			0		0	
-75.8347	36.7807	**97VB068**	1	b	spr	4.2	4.2	CS	3.3	MOUND	NONE	11	NONE	TRACE	0			0			0		0	
-75.8345	36.7809	**97VB068**	2	a	spr			CS	1.6	SHELL,SLO	NONE	NONE	NONE	5	0			0			0		0	
-75.8934	36.7628	**97VB071**	1	b	spr	12.5	12.5	FS	1.2	BEDFORM	NONE	10	NONE	NONE	0			0			0	4	1 OX,3 A	
-75.8935	36.7624	**97VB071**	2	b	spr	9.9	7	FS	0.8	BEDFORM	NONE	NONE	NONE	TRACE	0			0			0		0	
-75.8855	36.7748	**97VB066**	1	b	spr	7.8	7.8	FS	1.1	SHELL	NONE	NONE	NONE	5	0			0			0		0	
-75.8855	36.7750	**97VB066**	2	b	spr	2.5	2.5	FS	4.5	MOUND,SHE	NONE	NONE	NONE	5	0			0			0		0	
-75.8686	36.7649	**97VB072**	1	b	spr	5.5	5.5	FS	1.4	SHELL,MOU	NONE	NONE	NONE	5	0			0			0		0	
-75.8686	36.7650	**97VB072**	2	b	spr	6.5	6.5	FS	1.5	SHELL,BED	NONE	NONE	NONE	5	0			0			0		0	
-75.8431	36.7685	**97VB073**	1	b	spr	6.4	6.4	FS	1.3	SHELL	NONE	NONE	NONE	50	0			0			0		0	
-75.8431	36.7687	**97VB073**	2	a	spr		8.8	FS	1.3	SHELL	NONE	NONE	NONE	50	0			0			0		0	
-75.8431	36.7688	**97VB073**	3	b	spr	4	4	FS	4.8	SHELL	NONE	NONE	NONE	25	0			0			0		0	
-75.8431	36.7685	**97VB074**	1	b	spr	8.8	8.8	SI	0.8	ROCK,SHEL	NONE	NONE	NONE	30	0			0			0		0	
-75.8174	36.7709	**97VB074**	2	b	spr	8	8	SI	0.7	ROCK,SHELI	NONE	NONE	NONE	10	0			0			0		0	
-75.9297	36.8778	**96VB013**	1	b	spr	22	10	FS-SI	2.9	MOUND,PIT	NONE	NONE	NONE	NONE	0			1	AN	11.3	0		0	
-75.9304	36.8778	**96VB013**	2	b	spr	23.1	16.2	FS-SI	1.8	MOUND	IND	IND	IND	IND	5	WORMS	12,16	0			0	2	I OX,1 A	
-75.9233	36.8739	**96VB024**	1	b	spr	16	4.3	FS-SI	1.4	BEDFORM	NONE	3	NONE	NONE	1	WORM	17	0			0		0	
-75.9232	36.8736	**96VB024**	2	b	spr	7.7	7.7	FS-CL	4	MOUND	NONE	NONE	NONE	NONE	1	WORM	8.7	0			0		0	
-75.9015	36.8667	**96VB049**	1	b	spr	8.7	8.7	FS	1.3	SHELL,BED	NONE	NONE	NONE	TRACE	0			0			0		0	
-75.9015	36.8667	**96VB049**	2	b	spr	8	8	FS	0.5	BEDFORM	NONE	NONE	NONE	NONE	0			0			0		0	

Table 5. Spring 1997 SPI analysis.

		Virginia Beach Sandmining Project SPI visual analysis: Spring, 19										Surface struct.												
								Sed.	Sed.	Relief		--Tubes--		Subsur	---Infauna----			Voids						
					Date	PEN	RPD	Type	Rel.	Type	Epifauna	+/-	Pellet	Shell	#	Type	Depth	#	Type	Depth	Gas	Depth	Burrow	Type
LON	LAT	cell	rep		97	(cm)	(cm)		(cm)		(+/-)													
-75.9117	36.8584	96VB066	1	b	spr	13.5	13.5	FS-SI	1.1	BEDFORM	NONE	NONE	NONE	TRACE	0			0			0		0	
-75.9118	36.8598	96VB066	2	b	spr	13	3.7	FS-SI	1.3	BEDFORM	NONE	6	NONE	TRACE	0			0			0		0	
-75.9150	36.8433	96VB104	1	b	spr	11.8	6	FS-SI	1.4	BEDFORM	NONE	7	FEW	NONE	0			0			0		0	
-75.9151	36.8432	96VB104	2	b	spr	14.9	7.2	FS-SI	2	MOUND,PIT	NONE	13	NONE	NONE	0			0			0		0	
-75.9071	36.8432	96VB106	1	b	spr	8.5	8.5	FS	1.1	SHELL	NONE	NONE	NONE	TRACE	0			0			0		0	
-75.9071	36.8431	96VB106	2	b	spr	7.8	2.4	FS-SI	1.4	SHELL,DIS	NONE	2	NONE	TRACE	0			0			0		0	
-75.9083	36.8390	96VB115	1	b	spr	5.5	5.5	FS	2.6	SHELL,BED	NONE	NONE	NONE	TRACE	0			0			0		0	
-75.9083	36.8391	96VB115	2	b	spr	9.3	9.3	FS	0.7	BEDFORM	NONE	NONE	FEW	NONE	0			0			0		0	
-75.9000	36.8316	96VB137	1	b	spr	7.5	7.5	FS	1.7	ROCK,SHEL	NONE	NONE	NONE	25	0			0			0		0	
-75.9000	36.8316	96VB137	2	b	spr	5.5	5.5	FS	3	ROCK,SHEL	NONE	NONE	NONE	25	0			0			0		0	
-75.9140	36.8149	96VB174	1	b	spr	5.7	5.7	FS	2.1	SHELL,BED	NONE	NONE	NONE	TRACE	0			0			0		0	
-75.9140	36.8155	96VB174	2	b	spr	6.5	6.5	FS	1	SHELL,BED	NONE	NONE	NONE	TRACE	0			0			0		0	
-75.9009	36.8117	96VB185	1	b	spr	6.3	6.3	FS	1.9	SHELL,BED	NONE	NONE	NONE	TRACE	0			0			0		1	OX
-75.9008	36.8117	96VB185	2	b	spr	4.8	4.8	FS	3.5	BEDFORM	NONE	NONE	NONE	5	0			0			0		0	
-75.9035	36.8079	96VB194	1	b	spr	5.3	5.3	FS	3.3	BEDFORM	NONE	NONE	NONE	TRACE	0			0			0		0	
-75.9034	36.8079	96VB194	2	b	spr	6.7	6.7	FS	1	SHELL,BED	NONE	NONE	NONE	NONE	0			0			0		0	
-75.8820	36.7579	96VB316	1	b	spr	6	6	MS	1.5	PIT,MOUND	NONE	NONE	NONE	5	0			0			0		0	
-75.8819	36.7580	96VB316	2	b	spr	11.5	11.5	MS	3.7	SHELL,BED	NONE	2	NONE	TRACE	0			0			0		0	
-75.8957	36.7500	96VB332	1	b	spr	8.8	6.8	FS	2.3	MOUND,PIT	NONE	NONE	NONE	NONE	0			0			0		0	
-75.8953	36.7499	96VB332	2	b	spr	12.8	4.6	FS	2	BEDFORM	NONE	NONE	NONE	NONE	2	WORM	3.4,11	0			0		1	OX
-75.8742	36.7459	96VB347	1	b	spr	9.5	9.5	FS	3.1	SHELL,BED	NONE	NONE	NONE	TRACE	0			0			0		0	

Table 5. Spring 1997 SPI analysis.

		Virginia Beach Sandmining Project SPI visual analysis: Spring, 19										Surface struct.											
								Sed.	Sed.	Relief		--Tubes--		Subsur	---Infauna----			Voids					
					Date	PEN	RPD	Type	Rel.	Type	Epifauna	+/-	Pellet	Shell	#	Type	Depth	#	Type	Depth	Gas	Depth	Burrow	Type
LON	LAT	cell	rep		97	(cm)	(cm)		(cm)		(+/-)													
-75.8740	36.7460	**96VB347**	2	b	spr	8.2	8.2	FS	1.1	BEDFORM	NONE	NONE	NONE	NONE	0			0			0		0	
-75.8899	36.7416	**96VB353**	1	b	spr	10.5	10.5	MS	0.5	ROCK,SHELI	NONE	1	NONE	50	0			0			0		0	
-75.8897	36.7416	**96VB353**	2	b	spr	7.5	7.5	MS	1.2	ROCK,SHELI	NONE	NONE	NONE	50	0			0			0		0	
-75.8806	36.7381	**96VB365**	1	b	spr	7.2	7.2	FS	1.8	SHELL,MOUI	NONE	NONE	NONE	TRACE	0			0			0		0	
-75.8806	36.7381	**96VB365**	2	b	spr	8	8	FS	0.8	SHELL,BEDI	NONE	NONE	NONE	5	0			0			0		0	
-75.8715	36.7334	**97VB377**	1	b	spr	8.5	8.5	FS	1.3	BEDFORM.D	NONE	NONE	NONE	NONE	0			0			0		0	
-75.8713	36.7335	**96VB377**	2	b	spr	4.7	3.9	FS	0.7	BEDFORM	NONE	NONE	NONE	NONE	0			0			0		0	
-75.8684	36.7303	**97VB086**	1	b	spr																			
-75.8683	36.7303	**97VB086**	2	b	spr	7.5	3.5	FS-SI	2.4	BEDFORM	NONE	NONE	NONE	TRACE	0			0			0		0	
-75.8438	36.7334	**97VB087**	1	b	spr	9.1	9.1	MS	2	SHELL,BEDI	NONE	NONE	NONE	25	0			0			0		0	
-75.8420	36.7335	**97VB087**	2	b	spr	5	5	FS	2.5	BEDFORM,SI	NONE	NONE	NONE	TRACE	0			0			0		0	
-75.8185	36.7375	**97VB088**	1	b	spr	5.9	5.9	MS	1.9	BEDFORM,SI	NONE	NONE	NONE	5	0			0			0		0	
-75.8185	36.7375	**97VB088**	2	b	spr	10.7	10.7	MS	2	BEDFORM	NONE	NONE	NONE	TRACE	0			0			0		0	
-75.8093	36.7490	**97VB084**	1	b	spr	6	6	CS	4	SHELL,SLOI	NONE	NONE	NONE	25	0			0			0		0	
-75.8098	36.7491	**97VB084**	2	b	spr	8.5	8.5	FS	1.9	SHELL	NONE	NONE	NONE	30	0			0			0		0	
-75.8348	36.7459	**97VB083**	1	b	spr	6.7	6.7	FS	1.2	SHELL,BEDI	NONE	NONE	NONE	15	0			0			0		0	
-75.8348	36.7459	**97VB083**	2	b	spr	4.8	4.8	FS	1.3	BEDFORM,SI	NONE	NONE	NONE	TRACE	0			0			0		0	
-75.8603	36.7431	**97VB082**	1	b	spr	7	1.3	FS-SI	0.6	BEDFORM,SI	NONE	NONE	NONE	TRACE	0			0			0		0	
-75.8636	36.7478	**97VB082**	2	b	spr	6.8	6.8	FS	1.5	BEDFORM,SI	NONE	NONE	FEW	NONE	0			0			0		0	
-75.8768	36.7525	**97VB076**	1	b	spr	10	10	MS	2.5	SHELL,BEDI	NONE	NONE	NONE	TRACE	0			0			0		0	
-75.8768	36.7525	**97VB076**	2	b	spr	7.1	7.1	FS	1.3	BEDFORM	NONE	NONE	NONE	TRACE	0			0			0		0	

Table 5. Spring 1997 SPI analysis.

		Virginia Beach Sandmining Project SPI visual analysis: Spring, 19									Surface struct.													
								Sed.	Sed.	Relief		--Tubes--		Subsur	---Infauna----			Voids						
					Date	PEN	RPD	Type	Rel.	Type	Epifauna	+/-	Pellet	Shell	#	Type	Depth	#	Type	Depth	Gas	Depth	Burrow	Type
LON	LAT	cell	rep		97	(cm)	(cm)		(cm)		(+/-)													
-75.8516	36.7552	97VB077	1	b	spr	4.8	4.8	MS	1.7	SLOPE	NONE	NONE	NONE	5	0			0			0		0	
-75.8516	36.7552	97VB077	2	b	spr	7.3	7.3	MS	0.8	BEDFORM, SI	NONE	NONE	NONE	5	0			0			0		0	
-75.8263	36.7585	97VB078	1	b	spr	5.5	5.5	MS	1.3	SHELL, BEDI	NONE	NONE	NONE	TRACE	0			0			0		0	
-75.8262	36.7587	97VB078	2	b	spr	7	7	MS	0.8	BEDFORM, SI	NONE	NONE	NONE	TRACE	0			0			0		0	
-75.8018	36.7269	97VB094	1	b	spr	8.3	8.3	MS	1.7	BEDFORM	NONE	NONE	NONE	TRACE	0			0			0		0	
-75.8018	36.7271	97VB094	2	b	spr	6.5	6.5	MS	2.1	BEDFORM	NONE	NONE	NONE	TRACE	0			0			0		0	
-75.8270	36.7239	97VB093	1	b	spr	6	4.7	SI	0.7	SHELL, BEDI	NONE	NONE	NONE	5	0			0			0		0	
-75.8270	36.7241	97VB093	2	b	spr	8.1	2.3	SI	0.8	SHELL	NONE	NONE	NONE	10	0			0			0		0	
-75.8523	36.7213	97VB092	1	b	spr	9	9	FS	2.8	MOUND, SHEI	NONE	NONE	NONE	5	1	CRUSTACI	0.7	0			0	1	AN	
-75.8523	36.7214	97VB092	2	b	spr	5.8	5.8	FS	4.5	SHELL, BEDI	NONE	NONE	NONE	TRACE	0			0			0		0	
-75.8777	36.7181	97VB091	1	b	spr	7	7	FS	2	SHELL, BEDI	NONE	NONE	NONE	10	0			0			0		0	
-75.8776	36.7182	97VB091	2	b	spr	5.3	5.3	FS	3.5	BEDFORM	NONE	NONE	NONE	TRACE	0			0			0		0	
-75.8586	36.7085	97VB096	1	b	spr	3.3	3.3	SI	2.3	SHELL, SLOI	NONE	NONE	NONE	TRACE	0			0			0	1	AN	
-75.8610	36.7086	97VB096	2	b	spr	8.1	8.1	FS	2.3	SLOPE	NONE	4	NONE	5	0			1	OX	7.5	0		0	
-75.8356	36.7114	97VB097	1	b	spr	3.3	3.3	FS	3	SHELL, BEDI	NONE	NONE	NONE	TRACE	0			0			0		0	
-75.8356	36.7116	97VB097	2	b	spr	5.2	4.7	FS	2.3	SHELL, BEDI	NONE	NONE	NONE	TRACE	0			0			0		0	
-75.8104	36.7144	97VB098	1	b	spr	11.8	11.8	MS	5	BEDFORM	NONE	6	NONE	TRACE	0			0			0		0	
-75.8114	36.7149	97VB098	2	b	spr	5.8	5.8	MS	1.3	BEDFORM	NONE	1	NONE	TRACE	0			0			0		0	
-75.7936	36.7048	97VB104	1	b	spr	10.3	10.3	MS	2	BEDFORM	NONE	NONE	NONE	TRACE	0			0			0		0	
-75.7936	36.7050	97VB104	2	b	spr	5.5	5.5	MS	1.8	SHELL, BEDI	NONE	2	NONE	TRACE	0			0			0		0	
-75.8189	36.7020	97VB103	1	b	spr	8.5	8.5	FS	2.2	BEDFORM	NONE	NONE	NONE	TRACE	0			0			0		0	

Table 5. Spring 1997 SPI analysis.

		Virginia Beach Sandmining Project SPI visual analysis: Spring, 19						Surface struct.															
								Sed.	Sed.	Relief		--Tubes--		Subsur	---Infauna----			Voids					
					Date	PEN	RPD	Type	Rel.	Type	Epifauna	+/-	Pellet	Shell	#	Type	Depth	#	Type	Depth	Gas	Depth	Burrow	Type
LON	LAT	cell	rep		97	(cm)	(cm)		(cm)		(+/-)													
-75.8189	36.7021	**97VB103**	2	b	spr	5.4	5.4	FS	2	SHELL,BED	NONE	1	NONE	TRACE	0			0			0		0	
-75.8440	36.6989	**97VB102**	1	b	spr	4	4	MS	2.4	BEDFORM	NONE	NONE	NONE	TRACE	0			0			0		0	
-75.8440	36.6992	**97VB102**	2	b	spr	5	5	MS	0.5	SHELL,BED	NONE	NONE	NONE	TRACE	0			0			0		0	
-75.8694	36.6958	**97VB101**	1	b	spr	9.5	9.5	FS	2.7	SHELL,BED	NONE	1	NONE	5	0			0			0		0	
-75.8694	36.6960	**97VB101**	2	b	spr	9.3	9.3	FS	3.7	SHELL,BED	NONE	NONE	NONE	5	0			0			0		0	
-75.8527	36.6861	**97VB106**	1	b	spr	6.7	6.7	SI	1.2	SHELL	NONE	1	NONE	10	0			0			0	1	AN
-75.8527	36.6862	**97VB106**	2	b	spr	6.1	3	SI	1.5	SHELL	NONE	NONE	NONE	TRACE	0			0			0		0	
-75.8274	36.6889	**97VB107**	1	b	spr	10	3.2	FS-SI	1.5	SHELL,MOU	HERMIT CI	1	NONE	NONE	1	WORM	9	0			0	4	OX
-75.8273	36.6894	**97VB107**	2	b	spr	14.5	6.4	FS-SI	1.1	MOUND,SHE	NONE	5	NONE	NONE	1	WORM	5.6	0			0		0	
-75.8023	36.6917	**97VB108**	1	b	spr	5.2	5.2	FS	0.9	BEDFORM	NONE	1	NONE	TRACE	0			0			0		0	
-75.8022	36.6930	**97VB108**	2	b	spr	6.3	6.3	FS	2.3	BEDFORM	NONE	NONE	NONE	TRACE	0			0			0		0	
-75.8847	36.9081	**96VB201**	1	b	spr	7.1	7.1	FS	1.7	BEDFORM	NONE	4	NONE	TRACE	0			0			0		0	
-75.8846	36.9082	**96VB201**	2	b	spr	7.1	7.1	FS	1.3	BEDFORM	NONE	2	NONE	TRACE	0			0			0		0	
-75.8677	36.9084	**96VB205**	1	b	spr	6.3	6.3	FS	1.4	BEDFORM	NONE	NONE	NONE	TRACE	0			0			0		0	
-75.8678	36.9086	**96VB205**	2	b	spr	5.3	5.3	FS	0.7	NONE	NONE	NONE	NONE	TRACE	0			0			0		0	
-75.8506	36.9082	**96VB209**	1	b	spr	5.8	5.8	FS	1.4	SHELL,BED	NONE	NONE	NONE	TRACE	0			0			0		0	
-75.8505	36.9082	**96VB209**	2	b	spr	5.4	5.4	FS	0.3	SHELL,BED	HERMIT CI	NONE	NONE	TRACE	0			0			0		0	
-75.8503	36.9084	**96VB209**	3	b	spr	5	5	FS	2.8	SHELL,BED	NONE	NONE	NONE	TRACE	0			0			0		0	
-75.8509	36.9080	**96VB209**	4	b	spr	4.7	4.7	FS	2.6	BEDFORM	NONE	NONE	NONE	TRACE	0			0			0		0	
-75.8692	36.8981	**96VB234**	1	b	spr	5	5	FS	1.4	SHELL,BED	NONE	NONE	NONE	TRACE	0			0			0		0	
-75.8688	36.8983	**96VB234**	2	b	spr	6.8	6.8	FS	2.3	SHELL,BED	NONE	NONE	NONE	NONE	0			0			0		0	

Table 5. Spring 1997 SPI analysis.

		Virginia Beach Sandmining Project SPI visual analysis: Spring, 19										Surface struct.												
								Sed.	Sed.	Relief		--Tubes--		Subsuri	---Infauna----			Voids						
					Date	PEN	RPD	Type	Rel.	Type	Epifauna	+/-	Pellets	Shell	#	Type	Depth	#	Type	Depth	Gas	Depth	Burrow	Type
LON	LAT	cell	rep		97	(cm)	(cm)		(cm)		(+/-)													
-75.8583	36.8939	**96VB246**	1	b	spr	5.6	5.6	FS	1.1	SHELL,BEDI	NONE	NONE	NONE	TRACE	0			0			0		0	
-75.8582	36.8939	**96VB246**	2	b	spr	5.3	5.3	FS	1.5	BEDFORM	NONE	NONE	NONE	NONE	0			0			0		0	
-75.8624	36.8907	**96VB255**	1	b	spr	4.7	4.7	FS	1.1	BEDFORM,SI	NONE	NONE	NONE	NONE	0			0			0		0	
-75.8624	36.8907	**96VB255**	2	b	spr	6.2	6.2	FS	1.5	SHELL,BEDI	NONE	NONE	NONE	NONE	0			0			0		0	

Table 6. Fall 1997 SPI analysis (Sandbridge area).

Virginia Beach Sandmining Project SPI visual analysis										Surface struct.													
						Sed.	Sed.	Relief		--Tubes--			Subsurf	---Infauna----			Voids						
			Date	PEN	RPD	Type	Rel.	Type	Epifauna	+/-	Pellet	Shell	#	Type	Depth	#	Type	Depth	Gas	Depth	Burrow	Type
cell	rep		97	(cm)	(cm)		(cm)		(+/-)													
SO-001	1	B	FAL	5	ALL	FS	1	BEDFORM	0	0	0	TRACE	0			0			0		0	
SO-001	2	B	FAL	6	1.4	FS	1.2	BEDFORM	0	0	3	TRACE	0			0			0		0	
SO-002	1	B	FAL	7	ALL	MS	1	BEDFORM	0	0	1	TRACE	0			0			0		0	
SO-002	2	B	FAL	6	ALL	MS	0.8	SLOPE	0	0	0	1, TRA	0			0			0		0	
SO-003	1	B	FAL	6	4.2	FS	1.1	BEDFORM	0	0	2	TRACE	0			0			0		0	
SO-003	2	B	FAL	6.4	2.7	FS	0.4	BEDFORM	0	0	0	TRACE	0			0			0		0	
SO-004	1	B	FAL	6	ALL	MS	0.5	BEDFORM	1	0	0	TRACE	0			0			0		0	
SO-004	2	B	FAL	6	1.7	FS	0.2	EVEN	0	0	0	TRACE	0			0			0		0	
SO-005	1	B	FAL	7	ALL	FS	0.8	BEDFORM	1, SANDI	0	0	3	0			0			0		0	
SO-005	2	B	FAL	5	ALL	FS	2.1	SLOPE	1, SANDD	0	0	TRACE	0			0			0		0	
SO-006	1	B	FAL	7.8	ALL	MS	2	BEDFORM	0	0	1	TRACE	0			0			0		0	
SO-006	2	B	FAL	4	ALL	MS	0.4	EVEN	0	0	0	1, TRA	0			0			0		0	
SO-007	1	B	FAL	4.5	1.6	FS	0.9	BEDFORM	0	0	0	TRACE	0			0			0		0	
SO-007	2	B	FAL	4.5	0.8	FS-SI	1.5	BEDFORM	0	0	0	TRACE	0			0			0		0	
SO-008	1	B	FAL	6	ALL	MS	1.8	BEDFORM	0	0	0	TRACE	0			0			0		0	
SO-008	2	B	FAL	7	ALL	MS	3.2	SLOPE	0	0	0	TRACE	0			0			0		0	
SO-009	1	B	FAL	8	ALL	MS	2.8	SLOPE	0	0	0	1, TRA	0			0			0		0	
SO-009	2	B	FAL	5	ALL	MS	0.3	EVEN	0	0	0	TRACE	0			0			0		0	
SO-010	1	B	FAL	5	ALL	MS	4	MOUND	0	0	0	TRACE	0			0			0		0	
SO-010	2	B	FAL	6	ALL	MS	4.7	SLOPE	0	0	0	0	0			0			0		0	
SO-011	1	B	FAL	4	0.4	FS-SI	0.2	EVEN	0	0	0	TRACE	0			0			0		0	

Table 6. Fall 1997 SPI analysis (Sandbridge area).

Virginia Beach Sandmining Project SPI visual analysis										Surface struct.													
						Sed.	Sed.	Relief		--Tubes--			Subsurf	---Infauna----			Voids						
			Date	PEN	RPD	Type	Rel.	Type	Epifauna	+/-	Pellet	Shell	#	Type	Depth	#	Type	Depth	Gas	Depth	Burrow	Type
cell	rep		97	(cm)	(cm)		(cm)		(+/-)													
SO-011	2	B	FAL	4.7	0.3	FS-SI	0.3	EVEN	0	0	0	TRACE	0			0			0		0	
SO-012	1	B	FAL	4.3	0.2	FS-SI	0.2	EVEN	0	0	0	TRACE	0			0			0		1	AN
SO-012	2	B	FAL	5.6	0.4	FS-SI	0.3	BEDFORM	0	0	0	TRACE	0			0			0		0	
SO-013	1	B	FAL	7.5	1.5	FS	3	BEDFORM	0	0	11	0	0			0			0		0	
SO-013	2	B	FAL	1.8	ALL	FS	0.7	BEDFORM	0	0	15	0	0			0			0		0	
SO-014	1	B	FAL	4	1.2	FS	1.2	BEDFORM	0	0	3	0	0			0			0		0	
SO-014	2	B	FAL	4.5	1.4	FS-SI	0.8	BEDFORM	0	0	0	TRACE	0			0			0		0	
SO-015	1	B	FAL	5.2	1.2	FS	1.2	BEDFORM	0	0	0	TRACE	0			0			0		0	
SO-015	2	B	FAL	6	ALL	MS	2.1	SLOPE	0	0	0	TRACE	0			0			0		0	
SO-016	1	B	FAL	8	0.6	FS-SI	0.2	EVEN	0	1	16	TRACE	0			0			0		0	
SO-016	2	B	FAL	11	0.4	FS-SI	0.3	EVEN	0	0	3	1, TRA	0			0			0		1	OX
SO-017	1	B	FAL	5	0.4	FS-SI	1	BEDFORM	0	4	0	TRACE	0			0			0		2	AN
SO-017	2	B	FAL	4	0.7	FS-SI	0.6	BEDFORM	0	0	2	2, TRA	0			0			0		2	OX
SO-018	1	B	FAL	3.7	0.4	FS-SI	0.7	BEDFORM	0	0	0	TRACE	0			0			0		0	
SO-018	2	B	FAL	4	0.3	FS-SI	0.4	BEDFORM	0	0	2	2, TRA	0			0			0		0	
SO-019	1	B	FAL	4	0.2	FS-SI	0.6	BEDFORM	0	0	0	TRACE	0			0			0		0	
SO-019	2	B	FAL	3.7	0.4	FS-SI	0.7	BEDFORM	1, HERM	0	0	trace	0			0			0		0	
SO-020	1	B	FAL	1.5	0.2	FS-SI	0.6	BEDFORM	0	0	0	TRACE	0			0			0		0	
SO-020	2	B	FAL	4	0.2	FS-SI	1	BEDFORM	0	0	0	TRACE	0			0			0		0	
SO-021	1	B	FAL	14.2	1	FS-SI	0.3	BEDFORM	0	0	2	TRACE	0			0			0		3	1, 0X 2, AN
SO-021	2	B	FAL	12	0.3	FS-SI	1.2	MOUND	0	0	1	TRACE	2	WORM	5, 3	0			0		0	

Table 6. Fall 1997 SPI analysis (Sandbridge area).

Virginia Beach Sandmining Project SPI visual analysis										Surface struct.													
						Sed.	Sed.	Relief		--Tubes--			Subsurf	---Infauna----			Voids						
			Date	PEN	RPD	Type	Rel.	Type	Epifauna	+/-	Pellets	Shell	#	Type	Depth	#	Type	Depth	Gas	Depth	Burrow	Type
cell	rep		97	(cm)	(cm)		(cm)		(+/-)													
SO-022	1	B	FAL	4.5	0.5	FS-SI	0.7	BEDFORM	0	0	0	1, TRAC	0			0			0		0	
SO-022	2	B	FAL	6	0.3	FS-SI	0.2	EVEN	0	0	0	TRACE	0			0			0		0	
SO-023	1	B	FAL	3.7	0.4	FS-SI	0.5	BEDFORM	0	1	0	TRACE	0			0			0		0	
SO-023	2	B	FAL	8	2.4	FS-SI	0.3	EVEN	1, HERMIT	0	0	TRACE	0			0			0		0	
SO-024	1	B	FAL	3.5	0.3	FS-SI	0.9	BEDFORM	0	0	0	TRACE	0			0			0		0	
SO-024	2	B	FAL	5	0.6	FS-SI	0.7	BEDFORM	0	0	0	TRACE	0			0			0		0	
SO-025	1	B	FAL	6.7	2.9	FS-SI	0.3	EVEN	0	0	0	TRACE	0			0			0		0	
SO-025	2	B	FAL	6.5	2.7	FS-SI	0.1	EVEN	0	0	0	2, TRAC	0			0			0		0	
SO-026	1	B	FAL	6.3	1.7	FS-SI	0.5	BEDFORM	0	1	2	TRACE	0			0			0		0	
SO-027	1	B	FAL	4.7	1.3	FS	0.3	EVEN	0	0	0	TRACE	0			0			0		0	
SO-027	2	B	FAL	6	0.5	MS	0.5	BEDFORM	0	0	0	TRACE	0			0			0		0	
SO-028	1	B	FAL	7	ALL	MS	4	SLOPE	0	0	0	TRACE	0			0			0		0	
SO-028	2	B	FAL	6	ALL	MS	0.4	EVEN	0	0	0	TRACE	0			0			0		0	
SO-029	1	B	FAL	6	ALL	MS	1.2	BEDFORM	0	0	0	TRACE	0			0			0		0	
SO-029	2	B	FAL	6	ALL	MS	3.2	SLOPE	0	0	0	TRACE	0			0			0		0	
SO-030	1	B	FAL	6	ALL	MS	2	BEDFORM	0	0	0	TRACE	0			0			0		0	
SO-030	2	B	FAL	7	ALL	MS	4.2	SLOPE	0	0	2	TRACE	0			0			0		0	
SO-031	1	B	FAL	7	4.2	FS	0	EVEN	0	0	0	TRACE	0			0			0		0	
SO-031	2	B	FAL	6	ALL	MS	2.1	BEDFORM	0	0	0	TRACE	0			0			0		0	
SO-032	1	B	FAL	7	ALL	MS	1.2	BEDFORM	0	0	0	TRACE	0			0			0		0	
SO-032	2	B	FAL	7	ALL	MS	2	MOUND	0	0	0	TRACE	0			0			0		0	

Table 6. Fall 1997 SPI analysis (Sandbridge area).

Virginia Beach Sandmining Project SPI visual analysis										Surface struct.												
						Sed.	Sed.	Relief		--Tubes--		Subsur	---Infauna----			Voids						
			Date	PEN	RPD	Type	Rel.	Type	Epifauna	+/-	Pellet	Shell	#	Type	Depth	#	Type	Depth	Gas	Depth	Burrow	Type
cell	rep		97	(cm)	(cm)		(cm)		(+/-)													
SO-033	1	B	FAL	10	ALL	MS	5	SLOPE	0	0	0	TRACE	0			0			0		0	
SO-033	2	B	FAL	9	ALL	MS	4.3	SLOPE	0	0	0	TRACE	0			0			0		0	
SO-034	1	B	FAL	8	ALL	MS	4	MOUND	0	0	0	TRACE	0			0			0		0	
SO-034	2	B	FAL	9	ALL	MS	3.6	MOUND	0	0	0	TRACE	0			0			0		0	
SO-035	1	B	FAL	7	ALL	MS	0.2	EVEN	0	0	0	TRACE	0			0			0		0	
SO-035	2	B	FAL	5	ALL	FS	2.5	BEDFORM	0	0	0	TRACE	0			0			0		0	
SO-036	1	B	FAL	6	ALL	MS	0.5	BEDFORM	0	0	3	TRACE	0			0			0		0	
SO-036	2	B	FAL	7.5	3.2	FS-SI	0.2	EVEN	0	0	0	TRACE	0			0			0		0	
SO-036	2	B	FAL	6	2.5	MS	0.4	BEDFORM	0	0	0	TRACE	0			0			0		0	
SO-037	1	B	FAL	7	1.3	MS-SI	0.2	EVEN	0	0	0	TRACE	0			0			0		0	
SO-037	2	B	FAL	9	3.4	MS	2.3	SLOPE	0	0	2	TRACE	0			0			0		0	
SO-038	1	B	FAL	9	2.3	MS	2.4	MOUND	0	0	0	TRACE	0			0			0		0	
SO-038	2	B	FAL	5	ALL	MS	0.2	EVEN	0	0	0	TRACE	0			0			0		0	
SO-039	1	B	FAL	5.7	ALL	MS	0	EVEN	0	0	0	TRACE	0			0			0		0	
SO-039	2	B	FAL	8	ALL	FS	2.5	MOUND	0	0	1	TRACE	0			0			0		0	
SO-040	1	B	FAL	6	ALL	FS	3.8	MOUND	0	0	0	TRACE	0			0			0		0	
SO-040	2	B	FAL	5	ALL	FS	0	EVEN	0	0	0	TRACE	0			0			0		0	
SO-041	1	B	FAL	5	ALL	FS	0	EVEN	0	0	0	TRACE	0			0			0		0	
SO-041	2	B	FAL	6	0.3	FS	0.2	EVEN	0	0	3	TRACE	0			0			0		0	
SO-042	1	B	FAL	7	0.2	SI	1	BEDFORM	0	0	0	TRACE	0			0			0		0	
SO-042	2	B	FAL	7	1.3	FS-SI	0.3	BEDFORM	0	0	0	TRACE	0			0			0		0	

Table 6. Fall 1997 SPI analysis (Sandbridge area).

Virginia Beach Sandmining Project SPI visual analysis										Surface struct.												
						Sed.	Sed.	Relief		--Tubes--			Subsurf	---Infauna----			Voids					
			Date	PEN	RPD	Type	Rel.	Type	Epifauna	+/-	Pellets	Shell	#	Type	Depth	#	Type	Depth	Gas	Depth	Burrow	Type
cell	rep		97	(cm)	(cm)		(cm)		(+/-)													
SO-044	1	B	FAL	4.3	ALL	FS	3	EVEN	0	0	2	TRACE	0			0			0		0	
SO-044	2	B	FAL	3.7	2.5	FS	0.3	EVEN	0	0	0	TRACE	0			0			0		0	
SO-045	1	B	FAL	6	2.3	MS	0.2	EVEN	0	0	4	TRACE	0			0			0		0	
SO-045	2	B	FAL	5.7	ALL	MS	0.2	EVEN	0	1	1	TRACE	0			0			0		0	
SO-046	1	B	FAL	7.2	ALL	FS	0.3	BEDFORM	0	0	0	TRACE	0			0			0		0	
SO-046	2	B	FAL	6	2.1	FS	0.4	BEDFORM	0	0	0	TRACE	0			0			0		0	
SO-047	1	B	FAL	6	4.2	FS-SI	0.1	EVEN	3, HERMI	0	0	TRACE	0			0			0		0	
SO-047	2	B	FAL	4	3.1	FS-SI	0.2	EVEN	0	1	0	TRACE	0			0			0		0	
SO-081	2	B	FALL	6.9	ALL	MS	1.6	BD, SHELL	0	0	0	TRACE	0			0			0		0	
SO-081	1	B	FALL	6.9	ALL	MS	0.9	BD, SHELL	0	0	0	TRACE	0			0			0		0	
SO-082	1	B	FAL	6	ALL	MS	0.2	EVEN, SHEI	0	0	0	TRACE	0			1	OX	3	0		0	
SO-082	2	B	FAL	6.3	ALL	MS	2.5	SLOPE	0	0	0	TRACE	0			0			0		0	
SO-083	1	B	FAL	7	ALL	MS	0.3	EVEN	0	0	0	TRACE	0			0			0		0	
SO-083	2	B	FAL	5	ALL	FS	0.2	EVEN	0	0	0	TRACE	0			0			0		0	
SO-084	1	B	FAL	7	2.3	FS	0.5	MOUND	0	0	4	TRACE	0			0			0		0	
SO-084	2	B	FAL	7.4	2.7	FS	1.2	BEDFORM	0	0	0	TRACE	0			0			0		0	
SO-084	3	B	FAL	6	ALL	FS	1.1	BEDFORM	0	0	0	TRACE	0			0			0		0	
SO-085	1	B	FAL	7	ALL	FS	1.2	SLOPE	0	0	0	TRACE	0			0			0		0	
SO-085	2	B	FAL	6	2.7	FS	1.3	BEDFORM	1 SANDDOI	0	3	TRACE	0			0			0		0	
SO-086	1	B	FAL	6	2	MS	0.8	BD, SHELL	0	0	0	5	0			0			0		0	
SO-086	2	B	FAL	6	0.2	MS	0.3	EVEN	0	0	1	1, TRA(	0			0			0		0	

Table 6. Fall 1997 SPI analysis (Sandbridge area).

Virginia Beach Sandmining Project SPI visual analysis										Surface struct.													
						Sed.	Sed.	Relief		--Tubes--			Subsur	---Infauna----			Voids						
			Date	PEN	RPD	Type	Rel.	Type	Epifauna	+/-	Pellet	Shell	#	Type	Depth	#	Type	Depth	Gas	Depth	Burrow	Type
cell	rep		97	(cm)	(cm)		(cm)		(+/-)													
SO-087	1	B	FAL	6.2	2.9	MS	0.4	BEDFORM	0	0	0	TRACE	0			0			0		0	
SO-087	2	B	FAL	6	ALL	FS	0.1	EVEN	0	0	0	TRACE	0			0			0		0	
SO-088	1	B	FAL	7	ALL	FS	1.4	MOUND	0	0	1	TRACE	0			0			0		0	
SO-088	2	B	FAL	8	3.2	FS	0.2	EVEN	0	0	2	TRACE	0			0			0		0	
SO-089	1	B	FAL	7	ALL	MS	1	BEDFORM	0	0	1	TRACE	0			0			0		0	
SO-089	2	B	FAL	5	ALL	FS	3.8	SLOPE	0	0	0	TRACE	0			0			0		0	
SO-090	1	B	FAL	7	ALL	FS	2	SLOPE	0	0	1	TRACE	0			0			0		0	
SO-090	2	B	FAL	6	ALL	MS	2	BEDFORM	0	0	0	TRACE	0			0			0		0	
SO-091	1	B	FAL	6	2.3	MS	0.3	EVEN	0	0	0	TRACE	0			0			0		0	
SO-091	2	B	FAL	6	2.6	MS	0.2	EVEN	0	0	0	TRACE	0			0			0		0	
SO-092	1	B	FAL	6.3	ALL	FS	2	BD, SLOPE	1, SANDD	0	0	TRACE	0			0			0		0	
SO-092	2	B	FAL	7	ALL	FS	0.2	EVEN	0	0	0	TRACE	0			0			0		0	
SO-093	1	B	FAL	6.5	ALL	FS	0.5	BEDFORM	0	0	0	TRACE	0			0			0		0	
SO-093	2	B	FAL	6	ALL	FS	0.6	BEDFORM	0	0	0	TRACE	0			0			0		0	
SO-094	1	B	FAL	5.6	ALL	FS	1.2	BEDFORM	0	0	0	TRACE	0			0			0		0	
SO-094	2	B	FAL	7	2.7	FS	0.3	EVEN	0	0	0	TRACE	0			0			0		0	
SO-095	1	B	FAL	8	1.9	MS	0.8	BEDFORM	0	0	0	0	0			0			0		0	
SO-095	2	B	FAL	6	ALL	MS	0.9	BEDFORM	0	0	0	TRACE	0			0			0		0	
SO-096	1	B	FAL	6	ALL	MS	1.3	BEDFORM	0	0	0	TRACE	0			0			0		0	
SO-096	2	B	FAL	7	2.3	MS	1.2	BEDFORM	0	0	0	TRACE	0			0			0		0	
SO-097	1	B	FAL	6	1.6	MS	1	MOUND	0	0	1	TRACE	0			0			0		0	

Table 6. Fall 1997 SPI analysis (Sandbridge area).

Virginia Beach Sandmining Project SPI visual analysis										Surface struct.													
						Sed.	Sed.	Relief		--Tubes--			Subsur	---Infauna----			Voids						
			Date	PEN	RPD	Type	Rel.	Type	Epifauna	+/-	Pellet	Shell	#	Type	Depth	#	Type	Depth	Gas	Depth	Burrow	Type
cell	rep		97	(cm)	(cm)		(cm)		(+/-)													
SO-097	2	B	FAL	7	4.2	MS	0.3	EVEN	0	0	0	TRACE	0			0			0		0	
SO-098	1	B	FAL	6	ALL	FS	1.3	MOUND	0	0	2	7	0			0			0		0	
SO-098	2	B	FAL	6	ALL	FS	0.3	EVEN	0	0	0	0	0			0			0		0	
SO-099	1	B	FAL	6	3.7	FS	0.4	BEDFORM	0	0	1	5	0			0			0		0	
SO-099	2	B	FAL	5	ALL	FS	0.8	BEDFORM	0	0	0	0	0			0			0		0	
SO-100	1	B	FAL	6	ALL	MS	1.4	BEDFORM	0	0	0	TRACE	0			0			0		0	
SO-100	2	B	FAL	5	ALL	FS	0.3	EVEN	0	0	0	TRACE	0			0			0		0	
T2	1	B	FAL	6	ALL	FS	0.4	BEDFORM	0	0	0	TRACE	0			0			0		0	
T2	2	B	FAL	6.3	ALL	MS	0.2	EVEN	0	0	0	TRACE	0			0			0		0	

Legend for SPI analysis tables 3 - 6.

Heading	Subheading	Meaning
LON		-Longitude W in decimal degrees
LAT		Latitude N in decimal degrees
cell		Sample cell (station) number ("1 - 400" are identical to "96001 - 96400" labeled on maps)
rep		Deployment number at a station
Date		Season, spr (spring) or fall (fall)
PEN		Average SPI prism window penetration depth (cm) into the sediments
RPD		Average depth (cm) of the apparent color redox potential discontinuity (RPD)
Sed. Type		Sediment type class CL = clay SI = silt SA = sand VFS = very fine sand FS = fine sand MS = medium sand CS = coarse sand GRV = gravel (granule to pebbles)
Sed. Rel.		Vertical linear extrema of the sediment-water interface (SWI) contour, difference (cm) between highest and lowest points on the surface
Relief Type		Structure origin primarily responsible for roughness (surface relief)
Epifauna	(+/-)	Presence (+) or absence (-) of epifaunal organisms at the SWI, and
		type of epifauna; GAST (gastropod), SAND DOLLAR, CRUSTACEAN
Tubes		Presence or number of tubes protruding above the sediment surface
Pellets		Presence (+ or Y or Pos.) or Absence (- or N or Neg.) of biological fecal pellets at the SWI
Subsurf. Shell		Amount of shell material mixed in with the sediments, approximate
		percentages or trace presence or absence listed
Infauna	#	Number of infaunal organisms visible in the sediments
	Type	Type of infauna visible; WORM, CRUSTACEAN
	Depth	Depth (cm) of the infauna visible below the SWI
Voids	#	Number of water filled voids
	Type	Type of void
	Depth	Depth (cm) of water filled void below SWI
Gas		Number of gas filled voids
	Depth	Depth (cm) of gas void below SWI
Burrow		Infaunal burrow structures evident in the image
	Type	Oxidized (OX) or anoxic (AN) sediments in and around burrow

Table 7. Sediment grain size analysis for samples from Spring, 1997.

Sample	Date	TS	Alkalinity	Total Weight	Clay	Silt	Sand	Gravel
	MMDDYY	(%)	(meq/g)	(g)	(%)	(%)	(%)	(%)
96013	61897	80.5	2.0	8.01	0	0	100	0
96024	61897	76.8	3.2	13.295	0	9.5149	90.4851	0
96049	61897	86.5	1.8	15.32	0	0	10	0
96066	61897	75.5	3.2	6.505	10.146	21.1376	68.7164	0
96104	61897	70.8	4.8	10.475	1.1933	11.9332	86.8735	0
96106	61897	49.6	11.4	6.05	11.4876	16.4463	72.0661	0
96115	61897	84.1	1.8	13.39	0	0	100	0
96137	61897	91.1	1.8	12.03	0	0	72.818	27.18
96174	61897	76.8	4.0	12.36	0	2.9126	97.0874	0
96185	61897	79.9	2.0	11.2	0	0	100	0
96194	61897	81.8	1.8	11.55	0	0	100	0
96201	61897	82.9	1.4	11.4	0	0	100	0
96205	61897	80.2	1.6	16.53	0	0	100	0
96209	61897	83.2	1.8	13.3	0	0	100	0
96234	61997	84.0	1.2	10.98	0	0	100	0
96246	61997	75.7	1.0	12.27	0	0	100	0
96255	61997	76.6	1.8	11.82	0	0	96.0237	3.98
96316	61897	86.4	1.8	13.55	0	0	99.0406	0.96
96332	61897	76.6	2.6	8.89	0	8.2115	91.7885	0
96347	61897	87.7	1.2	15.97	0	0	100	0
96353	61897	92.1	1.2	12.51	0	0	58.753	41.25
96365	61897	85.6	1.6	14.15	0	0	83.7456	16.25
97076	61897	85.7	1.0	11.11	0	0	100	0
97088	61897	89.6	3.4	12.34	0	0	98.1361	1.86
97096	61897	84.6	1.8	16.47	0	0	45.7802	54.22
97104	61897	84.9	4.8	14.48	0	0	93.232	6.77
97107	61897	75.3	1.6	13.685	0	3.9094	87.9795	8.11

Table 8. Habitat class determinations identified using SPI images spring and fall 1996.

Class	Origin of primary characteristics	Modal sediment type	General description
A	Biological	Silt to silty-clay	Silty mud with high abundance of large infauna and infaunal living structrures, and sediment fabric generally dilated and bioturbated, apparent as color discontinuities or water filled void regions in sediment profile images (SPI)
B	Physical	Silt to sandy-clayey-silt	Silt to sandy-clayey-silt with little or no faunal presence or activity, sediment fabric not bioturbated
C	Combination biological and physical	Silty fine-sand to very fine sand	Silty fine sand to fine sand with variable faunal presence or activity; evidence of some biological activities, but biological features compose less than half of apparent features in the image
D	Physical	Fine to medium sand	Fine to medium sand with little or no faunal or biological feature presence
E	Biological	Fine to medium sand	Fine to medium sand with most apparent features biologically constructed
F	Physical	Medium to coarse sand and shell	Medium to coarse sand mixed with biogenic calcareous shell material, but little or no active faunal presence
G	Biological	Medium to coarse sand and shell	Medium to coarse sand mixed with shell material, and active faunal structures or presence of fauna
H	Physical	Coarse sand to gravel	Coarse sand to gravel with little or no apparent biological activity or recent structures
I	Physical/Transitional	Coarse sediments layered over fine	Layered sediments, where coarse grain-size material has been deposited over fine material, and active biological features are absent; observed: fine sand over clay, very fine sand over clay, and medium sand over clay

Table 9. Counts (number of cells in which the habitat class was present) and percentages of habitat class determinations identified using SPI images spring and fall 1996.

Spring 1996			Fall 1996		
Class	Cell Count	Percentage	Class	Cell Count	Percentage
A	15	9.6	A	12	6.3
B	0	0.0	B	3	1.6
C	73	46.6	C	100	52.1
D	31	19.8	D	39	20.4
E	10	6.1	E	5	2.6
F	15	9.6	F	28	14.7
G	9	5.4	G	0	0.0
H	5	2.9	H	2	1.0
I	0	0.0	I	3	1.3
Total	157	100.0	Total	191	100.0

Table 10. Habitat classifications and types for 1996 SPI images.

-LON	LAT	CELL	Spr. 96	Fall 96	Spr. 96	Fall 96
-75.9388333	36.882	1	C	C	COMBI	COMBI
-75.9398333	36.883	1	C	C	COMBI	COMBI
-75.9316667	36.882	3	A	C	BIO	COMBI
-75.9326667	36.883	3	A	C	BIO	COMBI
-75.9225	36.882	5	D		PHYS	
-75.9235	36.883	5	D		PHYS	
-75.9141667	36.882	7	G		BIO	
-75.9151667	36.883	7	G		BIO	
-75.9073333	36.883	9	G	E	BIO	BIO
-75.9063333	36.882	9	G	B	BIO	PHYS
-75.9336667	36.8783333	12	A	C	BIO	COMBI
-75.9346667	36.8793333	12	A	C	BIO	COMBI
-75.9268333	36.8793333	14	A	E	BIO	BIO
-75.9258333	36.8783333	14	A	D	BIO	PHYS
-75.9175	36.8783333	16	A	C	BIO	COMBI
-75.9185	36.8793333	16	A	C	BIO	COMBI
-75.9091667	36.8783333	18	G	F	BIO	PHYS
-75.9101667	36.8793333	18	G	F	BIO	PHYS
-75.9	36.8783333	20	G	D	BIO	PHYS
-75.901	36.8793333	20	G	D	BIO	PHYS
-75.9366667	36.8741667	21	C	C	COMBI	COMBI
-75.9376667	36.8751667	21	C	C	COMBI	COMBI
-75.9283333	36.8741667	23	A	A	BIO	BIO
-75.9293333	36.8751667	23	A	A	BIO	BIO
-75.9203333	36.8741667	25	G	A	BIO	BIO
-75.9213333	36.8751667	25	G	A	BIO	BIO
-75.9116667	36.8741667	27	D	F	PHYS	PHYS
-75.9126667	36.8751667	27	F	F	PHYS	PHYS
-75.9033333	36.8741667	29	F	F	PHYS	PHYS
-75.9043333	36.8751667	29	F	F	PHYS	PHYS
-75.9326667	36.871	32	A	C	BIO	COMBI
-75.9316667	36.87	32	C	C	COMBI	COMBI
-75.9316667	36.87	32	A		BIO	
-75.9243333	36.871	34	G	D	BIO	PHYS
-75.9233333	36.87	34	G	D	BIO	PHYS
-75.916	36.871	36	G	D	BIO	PHYS
-75.915	36.87	36	G	F	BIO	PHYS
-75.9075	36.87	38	E	A	BIO	BIO
-75.9085	36.871	38	E		BIO	
-75.8993333	36.871	40	F	D	PHYS	PHYS
-75.8983333	36.87	40	F	D	PHYS	PHYS
-75.9351667	36.8676667	41	C	C	COMBI	COMBI
-75.9341667	36.8666667	41	C	C	COMBI	COMBI
-75.9268333	36.8676667	43	C	A	COMBI	BIO
-75.9258333	36.8666667	43	C	A	COMBI	BIO
-75.9185	36.8676667	45	D	D	PHYS	PHYS
-75.9185	36.8676667	45		D		PHYS
-75.9175	36.8666667	45	E		BIO	
-75.91	36.8666667	47	A	B	BIO	PHYS
-75.911	36.8676667	47	G	D	BIO	PHYS
-75.9026667	36.8676667	49	E	D	BIO	PHYS

Table 10. Habitat classifications and types for 1996 SPI images.

-LON	LAT	CELL	Spr. 96	Fall 96	Spr. 96	Fall 96
-75.9016667	36.8666667	49	D	D	PHYS	PHYS
-75.9283333	36.8621667	52	A	A	BIO	BIO
-75.9293333	36.8631667	52	A	A	BIO	BIO
-75.9208333	36.8621667	54	E	D	BIO	PHYS
-75.9218333	36.8631667	54	E	D	BIO	PHYS
-75.9143333	36.8631667	56	G	D	BIO	PHYS
-75.9133333	36.8621667	56	F	D	PHYS	PHYS
-75.9033333	36.8621667	58	E	A	BIO	BIO
-75.9043333	36.8631667	58	E	A	BIO	BIO
-75.9291667	36.8621667	60	F	D	PHYS	PHYS
-75.9301667	36.8631667	60	F	D	PHYS	PHYS
-75.9316667	36.8583333	61		C		COMBI
-75.9326667	36.8593333	61		C		COMBI
-75.9241667	36.8583333	63	A	A	BIO	BIO
-75.9251667	36.8593333	63	A	A	BIO	BIO
-75.9158333	36.8583333	65	E	I	BIO	PHYS
-75.9168333	36.8593333	65	E	I	BIO	PHYS
-75.9075	36.8583333	67	D	D	PHYS	PHYS
-75.9085	36.8593333	67	D	D	PHYS	PHYS
-75.9001667	36.8593333	69	E	D	BIO	PHYS
-75.8991667	36.8583333	69	G	D	BIO	PHYS
-75.9258333	36.8541667	72	C	C	COMBI	COMBI
-75.9268333	36.8551667	72	C	C	COMBI	COMBI
-75.9183333	36.8541667	74	D	D	PHYS	PHYS
-75.9193333	36.8551667	74	D		PHYS	
-75.91	36.8541667	76	E	D	BIO	PHYS
-75.911	36.8551667	76	D	D	PHYS	PHYS
-75.9026667	36.8551667	78	A	C	BIO	COMBI
-75.9016667	36.8541667	78	C	D	COMBI	PHYS
-75.8933333	36.8541667	80	E	D	BIO	PHYS
-75.8943333	36.8551667	80	E	D	BIO	PHYS
-75.93	36.8508333	81		C		COMBI
-75.931	36.8518333	81		C		COMBI
-75.9226667	36.8518333	83	A	A	BIO	BIO
-75.9216667	36.8508333	83	A	I	BIO	PHYS
-75.9133333	36.8508333	85	D	D	PHYS	PHYS
-75.9143333	36.8518333	85	D	D	PHYS	PHYS
-75.906	36.8518333	87	C	C	COMBI	COMBI
-75.905	36.8508333	87	D	C	PHYS	COMBI
-75.8958333	36.8508333	89	E	D	BIO	PHYS
-75.8968333	36.8518333	89	E	D	BIO	PHYS
-75.9233333	36.8466667	92		D		PHYS
-75.9243333	36.8476667	92		D		PHYS
-75.9166667	36.8466667	94	E	E	BIO	BIO
-75.9176667	36.8476667	94	D	D	PHYS	PHYS
-75.9093333	36.8476667	96	C	C	COMBI	COMBI
-75.9083333	36.8466667	96	D	B	PHYS	PHYS
-75.9001667	36.8476667	98	E	C	BIO	COMBI
-75.8991667	36.8466667	98	E	D	BIO	PHYS
-75.8908333	36.8466667	100	C	C	COMBI	COMBI
-75.8918333	36.8476667	100	C	C	COMBI	COMBI
-75.9266667	36.8433333	101		C		COMBI

Table 10. Habitat classifications and types for 1996 SPI images.

-LON	LAT	CELL	Spr. 96	Fall 96	Spr. 96	Fall 96
-75.9276667	36.8443333	101		C		COMBI
-75.9201667	36.8443333	103		A		BIO
-75.9191667	36.8433333	103		C		COMBI
-75.9108333	36.8433333	105		D		PHYS
-75.9118333	36.8443333	105		D		PHYS
-75.903	36.8433333	107		C		COMBI
-75.904	36.8443333	107		C		COMBI
-75.8938333	36.8433333	109	C	E	COMBI	BIO
-75.8948333	36.8443333	109	C	E	COMBI	BIO
-75.9216667	36.8391667	112		E		BIO
-75.9226667	36.8401667	112		D		PHYS
-75.9151667	36.8401667	114		E		BIO
-75.9141667	36.8391667	114		D		PHYS
-75.9058333	36.8391667	116		C		COMBI
-75.9068333	36.8401667	116		D		PHYS
-75.897	36.8391667	118		C		COMBI
-75.898	36.8401667	118		C		COMBI
-75.8883333	36.8391667	120	A	C	BIO	COMBI
-75.8893333	36.8401667	120	A	C	BIO	COMBI
-75.9241667	36.8358333	121	D	D	PHYS	PHYS
-75.9251667	36.8368333	121	D	D	PHYS	PHYS
-75.9168333	36.8368333	123	C	D	COMBI	PHYS
-75.9158333	36.8358333	123	D	D	PHYS	PHYS
-75.9093333	36.8368333	125		C		COMBI
-75.9083333	36.8358333	125		D		PHYS
-75.9	36.8358333	127		E		BIO
-75.901	36.8368333	127		F		PHYS
-75.8916667	36.8358333	129		C		COMBI
-75.8926667	36.8368333	129		C		COMBI
-75.92	36.8316667	132	C	C	COMBI	COMBI
-75.921	36.8326667	132	C	C	COMBI	COMBI
-75.9116667	36.8316667	134	D	D	PHYS	PHYS
-75.9126667	36.8326667	134		D		PHYS
-75.9033333	36.8316667	136		F		PHYS
-75.9043333	36.8326667	136		F		PHYS
-75.8966667	36.8316667	138		F		PHYS
-75.8976667	36.8326667	138		F		PHYS
-75.8858333	36.8316667	140	D	F	PHYS	PHYS
-75.8868333	36.8326667	140		F		PHYS
-75.9225	36.828	141	D	E	PHYS	BIO
-75.9235	36.829	141	D	E	PHYS	BIO
-75.9141667	36.828	143	C	C	COMBI	COMBI
-75.9151667	36.829	143	C	C	COMBI	COMBI
-75.9066667	36.828	145	D	D	PHYS	PHYS
-75.9076667	36.829	145	D	D	PHYS	PHYS
-75.8978333	36.828	147		F		PHYS
-75.8988333	36.829	147		F		PHYS
-75.8891667	36.828	149		A		BIO
-75.8901667	36.829	149		A		BIO
-75.9158333	36.8236667	152	D	D	PHYS	PHYS
-75.9168333	36.8246667	152	D	D	PHYS	PHYS
-75.9083333	36.8236667	154	C	D	COMBI	PHYS

Table 10. Habitat classifications and types for 1996 SPI images.

-LON	LAT	CELL	Spr. 96	Fall 96	Spr. 96	Fall 96
-75.9093333	36.8246667	154	C	D	COMBI	PHYS
-75.9	36.8236667	156	F	D	PHYS	PHYS
-75.901	36.8246667	156	F	D	PHYS	PHYS
-75.8925	36.8236667	158		F		PHYS
-75.8935	36.8246667	158		F		PHYS
-75.8833333	36.8236667	160		D		PHYS
-75.8843333	36.8246667	160		D		PHYS
-75.92	36.8196667	161	C	C	COMBI	COMBI
-75.921	36.8206667	161		C		COMBI
-75.9133333	36.8196667	163	D	C	PHYS	COMBI
-75.9143333	36.8206667	163	D	C	PHYS	COMBI
-75.9041667	36.8196667	165	D	C	PHYS	COMBI
-75.9051667	36.8206667	165	D	C	PHYS	COMBI
-75.8968333	36.8206667	167	H	D	PHYS	PHYS
-75.8958333	36.8196667	167	H	F	PHYS	PHYS
-75.8866667	36.8196667	169		B		PHYS
-75.8876667	36.8206667	169		B		PHYS
-75.9141667	36.8158333	172	C	C	COMBI	COMBI
-75.9151667	36.8168333	172		C		COMBI
-75.9076667	36.8168333	174	D	C	PHYS	COMBI
-75.9066667	36.8158333	174	D	I	PHYS	PHYS
-75.8985	36.8168333	176	D	D	PHYS	PHYS
-75.8975	36.8158333	176	F	D	PHYS	PHYS
-75.8891667	36.8158333	178	C	C	COMBI	COMBI
-75.8901667	36.8168333	178	C	C	COMBI	COMBI
-75.8816667	36.8158333	180		C		COMBI
-75.8826667	36.8168333	180		C		COMBI
-75.9166667	36.8116667	181	C	C	COMBI	COMBI
-75.9176667	36.8126667	181	C	C	COMBI	COMBI
-75.9083333	36.8116667	183	C	C	COMBI	COMBI
-75.9093333	36.8126667	183		C		COMBI
-75.9008333	36.8116667	185	C	C	COMBI	COMBI
-75.9018333	36.8126667	185	C	C	COMBI	COMBI
-75.8925	36.8116667	187	C	C	COMBI	COMBI
-75.8935	36.8126667	187	C		COMBI	
-75.8925	36.8116667	187	C		COMBI	
-75.8851667	36.8126667	189		C		COMBI
-75.8841667	36.8116667	189		C		COMBI
-75.9126667	36.809	192		C		COMBI
-75.9116667	36.808	192		C		COMBI
-75.9043333	36.809	194	C	C	COMBI	COMBI
-75.9033333	36.808	194		C		COMBI
-75.896	36.809	196	C	C	COMBI	COMBI
-75.895	36.808	196	C	C	COMBI	COMBI
-75.8885	36.809	198		C		COMBI
-75.8875	36.808	198		C		COMBI
-75.8793333	36.809	200		C		COMBI
-75.8783333	36.808	200		C		COMBI
-75.886	36.9093333	201	C	C	COMBI	COMBI
-75.885	36.9083333	201	C	C	COMBI	COMBI
-75.8776667	36.9093333	203	C	C	COMBI	COMBI
-75.8766667	36.9083333	203	C	C	COMBI	COMBI

Table 10. Habitat classifications and types for 1996 SPI images.

-LON	LAT	CELL	Spr. 96	Fall 96	Spr. 96	Fall 96
-75.8685	36.9093333	**205**	C	C	COMBI	COMBI
-75.8675	36.9083333	**205**	C	C	COMBI	COMBI
-75.8685	36.9093333	**205**	C		COMBI	
-75.86	36.9083333	**207**	C		COMBI	
-75.861	36.9093333	**207**	C		COMBI	
-75.8508333	36.9083333	**209**	C		COMBI	
-75.8518333	36.9093333	**209**	C		COMBI	
-75.8508333	36.9083333	**209**	C		COMBI	
-75.8806667	36.9063333	**212**	C	C	COMBI	COMBI
-75.8796667	36.9053333	**212**	C	C	COMBI	COMBI
-75.8718333	36.9063333	**214**	C	C	COMBI	COMBI
-75.8708333	36.9053333	**214**	C	C	COMBI	COMBI
-75.8638333	36.9063333	**216**	C	C	COMBI	COMBI
-75.8628333	36.9053333	**216**	C	C	COMBI	COMBI
-75.8551667	36.9063333	**218**		C		COMBI
-75.8541667	36.9053333	**218**		C		COMBI
-75.8468333	36.9063333	**220**	C	C	COMBI	COMBI
-75.8458333	36.9053333	**220**	C	C	COMBI	COMBI
-75.8468333	36.9063333	**220**	C		COMBI	
-75.8825	36.902	**221**		C		COMBI
-75.8835	36.903	**221**		C		COMBI
-75.8741667	36.902	**223**	C	C	COMBI	COMBI
-75.8751667	36.903	**223**	C	C	COMBI	COMBI
-75.8741667	36.902	**223**	C		COMBI	
-75.8668333	36.903	**225**	C	C	COMBI	COMBI
-75.8658333	36.902	**225**	C	C	COMBI	COMBI
-75.8576667	36.903	**227**	C	C	COMBI	COMBI
-75.8566667	36.902	**227**	C	C	COMBI	COMBI
-75.8493333	36.903	**229**	C	C	COMBI	COMBI
-75.8483333	36.902	**229**	C	C	COMBI	COMBI
-75.8785	36.8993333	**232**	C	C	COMBI	COMBI
-75.8775	36.8983333	**232**	C		COMBI	
-75.8785	36.8993333	**232**	C		COMBI	
-75.8691667	36.8983333	**234**	C	C	COMBI	COMBI
-75.8701667	36.8993333	**234**	C	C	COMBI	COMBI
-75.8603333	36.8983333	**236**	C	C	COMBI	COMBI
-75.8613333	36.8993333	**236**	C	C	COMBI	COMBI
-75.8603333	36.8983333	**236**	C		COMBI	
-75.8526667	36.8993333	**238**	C	C	COMBI	COMBI
-75.8516667	36.8983333	**238**	C	C	COMBI	COMBI
-75.8443333	36.8993333	**240**	C	C	COMBI	COMBI
-75.8433333	36.8983333	**240**	C	C	COMBI	COMBI
-75.8818333	36.8951667	**241**		C		COMBI
-75.8808333	36.8941667	**241**		C		COMBI
-75.8726667	36.8951667	**243**	C	C	COMBI	COMBI
-75.8716667	36.8941667	**243**	C	C	COMBI	COMBI
-75.8633333	36.8941667	**245**	C	C	COMBI	COMBI
-75.8643333	36.8951667	**245**		C		COMBI
-75.856	36.8951667	**247**	C	C	COMBI	COMBI
-75.855	36.8941667	**247**	C	C	COMBI	COMBI
-75.8471667	36.8951667	**249**	C	C	COMBI	COMBI
-75.8461667	36.8941667	**249**	C	C	COMBI	COMBI

Table 10. Habitat classifications and types for 1996 SPI images.

-LON	LAT	CELL	Spr. 96	Fall 96	Spr. 96	Fall 96
-75.876	36.8918333	252		C		COMBI
-75.875	36.8908333	252		C		COMBI
-75.8676667	36.8918333	254	C	C	COMBI	COMBI
-75.8666667	36.8908333	254	C	C	COMBI	COMBI
-75.8593333	36.8918333	256	C	C	COMBI	COMBI
-75.8583333	36.8908333	256	C	C	COMBI	COMBI
-75.8506667	36.8918333	258	C	C	COMBI	COMBI
-75.8496667	36.8908333	258	C	C	COMBI	COMBI
-75.8506667	36.8918333	258	C		COMBI	
-75.8408333	36.8908333	260	C	C	COMBI	COMBI
-75.8418333	36.8918333	260	C	C	COMBI	COMBI
-75.8775	36.8866667	261		C		COMBI
-75.8785	36.8876667	261		C		COMBI
-75.8691667	36.8866667	263		C		COMBI
-75.8701667	36.8876667	263		C		COMBI
-75.8608333	36.8866667	265	C	C	COMBI	COMBI
-75.8618333	36.8876667	265	C	C	COMBI	COMBI
-75.8525	36.8866667	267	C	C	COMBI	COMBI
-75.8535	36.8876667	267		C		COMBI
-75.8441667	36.8866667	269	C	C	COMBI	COMBI
-75.8451667	36.8876667	269	C	C	COMBI	COMBI
-75.8725	36.8825	272		C		COMBI
-75.8735	36.8835	272		C		COMBI
-75.8638333	36.8825	274		C		COMBI
-75.8648333	36.8835	274		C		COMBI
-75.855	36.8825	276	C	C	COMBI	COMBI
-75.856	36.8835	276	C	C	COMBI	COMBI
-75.8466667	36.8825	278	C	C	COMBI	COMBI
-75.8476667	36.8835	278	C		COMBI	
-75.8383333	36.8825	280	C	C	COMBI	COMBI
-75.8393333	36.8835	280	C	C	COMBI	COMBI
-75.875	36.8783333	281		C		COMBI
-75.876	36.8793333	281		C		COMBI
-75.8666667	36.8783333	283		C		COMBI
-75.8676667	36.8793333	283		C		COMBI
-75.8583333	36.8783333	285		C		COMBI
-75.8593333	36.8793333	285		C		COMBI
-75.8496667	36.8783333	287	C	C	COMBI	COMBI
-75.8506667	36.8793333	287	C	C	COMBI	COMBI
-75.8408333	36.8783333	289	C	C	COMBI	COMBI
-75.8418333	36.8793333	289	C	C	COMBI	COMBI
-75.87	36.8741667	292		C		COMBI
-75.871	36.8751667	292		C		COMBI
-75.8616667	36.8741667	294		C		COMBI
-75.8626667	36.8751667	294		C		COMBI
-75.8533333	36.8741667	296		C		COMBI
-75.8543333	36.8751667	296		C		COMBI
-75.8441667	36.8741667	298	C	C	COMBI	COMBI
-75.8451667	36.8751667	298	C	C	COMBI	COMBI
-75.8363333	36.8741667	300	C	C	COMBI	COMBI
-75.8373333	36.8751667	300	C	C	COMBI	COMBI
-75.9033333	36.7613333	301	C		COMBI	

Table 10. Habitat classifications and types for 1996 SPI images.

-LON	LAT	CELL	Spr. 96	Fall 96	Spr. 96	Fall 96
-75.9043333	36.7623333	301	C		COMBI	
-75.8958333	36.7613333	303	A	C	BIO	COMBI
-75.8968333	36.7623333	303	A	C	BIO	COMBI
-75.8883333	36.7613333	305	D	F	PHYS	PHYS
-75.8893333	36.7623333	305	D	F	PHYS	PHYS
-75.8796667	36.7613333	307	D	F	PHYS	PHYS
-75.8806667	36.7623333	307	D	F	PHYS	PHYS
-75.8708333	36.7613333	309	D	F	PHYS	PHYS
-75.8718333	36.7623333	309	D	F	PHYS	PHYS
-75.8983333	36.758	312	A	C	BIO	COMBI
-75.8993333	36.759	312	C	C	COMBI	COMBI
-75.8908333	36.758	314	A	A	BIO	BIO
-75.8918333	36.759	314	A	A	BIO	BIO
-75.8825	36.758	316	D	F	PHYS	PHYS
-75.8835	36.759	316	D	F	PHYS	PHYS
-75.8741667	36.758	318	D	D	PHYS	PHYS
-75.8751667	36.759	318	D	D	PHYS	PHYS
-75.8658333	36.758	320	D	F	PHYS	PHYS
-75.8668333	36.759	320	D	F	PHYS	PHYS
-75.9016667	36.7533333	321	C	C	COMBI	COMBI
-75.9026667	36.7543333	321	C	C	COMBI	COMBI
-75.8945	36.7533333	323	C	C	COMBI	COMBI
-75.8955	36.7543333	323	C	C	COMBI	COMBI
-75.8863333	36.7533333	325	D	F	PHYS	PHYS
-75.8873333	36.7543333	325	D	F	PHYS	PHYS
-75.878	36.7533333	327	D	F	PHYS	PHYS
-75.879	36.7543333	327	D	F	PHYS	PHYS
-75.8695	36.7533333	329	D	D	PHYS	PHYS
-75.8705	36.7543333	329		D		PHYS
-75.8958333	36.75	332	C	C	COMBI	COMBI
-75.8968333	36.751	332	C	C	COMBI	COMBI
-75.8875	36.75	334	D	F	PHYS	PHYS
-75.8885	36.751	334	D	F	PHYS	PHYS
-75.8808333	36.75	336	F	F	PHYS	PHYS
-75.8818333	36.751	336	F	F	PHYS	PHYS
-75.8716667	36.75	338	D	D	PHYS	PHYS
-75.8726667	36.751	338	D	D	PHYS	PHYS
-75.8633333	36.75	340	A	D	BIO	PHYS
-75.8643333	36.751	340		F		PHYS
-75.8991667	36.7458333	341	C	C	COMBI	COMBI
-75.9001667	36.7468333	341	C	C	COMBI	COMBI
-75.8908333	36.7458333	343	A	A	BIO	BIO
-75.8918333	36.7468333	343	A	A	BIO	BIO
-75.8825	36.7458333	345	F	F	PHYS	PHYS
-75.8835	36.7468333	345	F	F	PHYS	PHYS
-75.8741667	36.7458333	347	D	D	PHYS	PHYS
-75.8751667	36.7468333	347	D	D	PHYS	PHYS
-75.8666667	36.7458333	349	C	D	COMBI	PHYS
-75.8676667	36.7468333	349	C	D	COMBI	PHYS
-75.8933333	36.7416667	352	C	C	COMBI	COMBI
-75.8943333	36.7426667	352	C	C	COMBI	COMBI
-75.8876667	36.7426667	354	F	F	PHYS	PHYS

Table 10. Habitat classifications and types for 1996 SPI images.

-LON	LAT	CELL	Spr. 96	Fall 96	Spr. 96	Fall 96
-75.8866667	36.7416667	354	H	F	PHYS	PHYS
-75.8783333	36.7416667	356	D	D	PHYS	PHYS
-75.8793333	36.7426667	356	D	D	PHYS	PHYS
-75.871	36.7426667	358	C	C	COMBI	COMBI
-75.87	36.7416667	358		C		COMBI
-75.8608333	36.7416667	360	F	F	PHYS	PHYS
-75.8618333	36.7426667	360		F		PHYS
-75.8966667	36.738	361	C	C	COMBI	COMBI
-75.8976667	36.739	361		C		COMBI
-75.8888333	36.738	363	H	H	PHYS	PHYS
-75.8898333	36.739	363	H	H	PHYS	PHYS
-75.8808333	36.738	365	F	C	PHYS	COMBI
-75.8818333	36.739	365	F	F	PHYS	PHYS
-75.8725	36.738	367	C	C	COMBI	COMBI
-75.8735	36.739	367		C		COMBI
-75.8646667	36.738	369		C		COMBI
-75.8656667	36.739	369	C	B	COMBI	PHYS
-75.8916667	36.7333333	372	C	A	COMBI	BIO
-75.8926667	36.7343333	372	C	C	COMBI	COMBI
-75.8833333	36.7333333	374	F	D	PHYS	PHYS
-75.8843333	36.7343333	374	F		PHYS	
-75.8758333	36.7333333	376	F	F	PHYS	PHYS
-75.8768333	36.7343333	376	F	F	PHYS	PHYS
-75.8675	36.7333333	378	C		COMBI	
-75.8685	36.7343333	378	C		COMBI	
-75.8591667	36.7333333	380	F	F	PHYS	PHYS
-75.8601667	36.7343333	380	F	F	PHYS	PHYS
-75.8941667	36.73	381	C	C	COMBI	COMBI
-75.8951667	36.731	381	C	C	COMBI	COMBI
-75.8866667	36.73	383	H	H	PHYS	PHYS
-75.8876667	36.731	383	H	H	PHYS	PHYS
-75.8801667	36.731	385	F	F	PHYS	PHYS
-75.8791667	36.73	385		F		PHYS
-75.8708333	36.73	387	D	C	PHYS	COMBI
-75.8718333	36.731	387	D	C	PHYS	COMBI
-75.8625	36.73	389	F	F	PHYS	PHYS
-75.8635	36.731	389	F	F	PHYS	PHYS
-75.8933333	36.7258333	392	C	C	COMBI	COMBI
-75.8943333	36.7268333	392	C	C	COMBI	COMBI
-75.885	36.7258333	394	H	F	PHYS	PHYS
-75.886	36.7268333	394	H	I	PHYS	PHYS
-75.8766667	36.7258333	396	D	D	PHYS	PHYS
-75.8776667	36.7268333	396	D	D	PHYS	PHYS
-75.865	36.7258333	398	C	A	COMBI	BIO
-75.866	36.7268333	398	C	A	COMBI	BIO
-75.8566667	36.7258333	400	F	F	PHYS	PHYS
-75.8576667	36.7268333	400	F	F	PHYS	PHYS

Table 11. Complete taxonomic list from 13 processed Smith-MacIntyre grab samples from June and November 1996 collections.

Nemerteans
- Nemertean

Anemones
- Anemones, Burrowing

Platyhelmenths
- Flat worm
- *Stylochus* sp.

Molluscs
- Gastropods
  - Gastropod
  - *Acteocina canaliculata*
  - *Epitonium multistriatum*
  - *Haminoea solitaria*
  - *Mangelia cerina*
  - *Nassarius trivitattus*
  - *Polinices duplicatus*
  - *Pyramidella candida*
  - *Tectonatica pusilla*
  - *Turbonilla interupta*
- Bivalves
  - Bivalva
  - *Brania clavata*
  - *Brania wellfleetensis*
  - *Brania* sp.
  - *Ensis directus*
  - *Lyonsia hyalina*
  - *Macoma tenta*
  - *Macoma* sp.
  - *Pandora trilineata*
  - *Spisula solidissima*
  - *Tellina agilis*

Arthropods
- Tanaids
  - *Heterotanais* sp.
- Isopods
  - Isopod
  - *Chiridotea tuftsi*
  - *Cirolana concharum*
  - *Ptilanthura tenuis*
- Cumaceans
  - *Campylaspis* sp.
  - *Leucon americanus*
  - *Oxyurostylis smithi*

Table . Continued.

- Amphipods
  - Amphipod
  - *Acanthohaustorius millsi*
  - *Ampelisca abdita*
  - *Ampelisca verrilli*
  - *Batea catharinensis*
  - *Bathyporeia porteri*
  - *Corophium tuberculatum*
  - *Lepidactylus dytiscus*
  - *Paraphoxus spinosus*
  - *Pontocrates* sp.
  - *Protohaustorius wigleyi*
  - *Synchelidium americanum*
  - *Trichophoxus epistomus*
  - *Unciola irrorata*
- Decapods
  - Decapod
  - *Crangon septemspinosus*
  - *Pagurus longicarpus*
  - *Panopeus herbstii*
  - *Pinixia retinens*

- Annelids
  - Oligochaetes
    - Tubificidae
  - Polychaetes
    - *Aglaophamus verrilli*
    - *Amastigos caperatus*
    - *Ampharete acutifrons*
    - *Ancistrosyllis hartmanae*
    - *Aphrodita hastata*
    - *Aricidea jeffreysii*
    - *Aricidea wassi*
    - *Asabellides oculata*
    - *Asychis elongata*
    - *Bhwania goodei*
    - *Capitomastus aciculatus*
    - *Clymenella mucosa*
    - *Clymenella torquata*
    - *Clymenella* sp.
    - *Drilonereis magna*
    - *Euclymene zonalis*
    - *Exogone dispar*
    - *Glycera americana*
    - *Glycera dibranchiata*
    - *Glycera robustus*
    - *Harmathoe nodosa*
    - *Harmathoe* sp.

Table . Completed.

Polychaetes (continued)
Lumbrinereis acuta
Lumbrinereis tenuis
Magelona rosea
Maldanopsis elongata
Mangelia cerira
Mediomastus ambiseta
Mediomastus sp.
Nephtys bucera
Nephtys cryptomma
Nephtys incisa
Nephtys picta
Notomastus hemipodus
Notomastus sp.
Notomustus latericeus
Orbinia ornata
Owenia fusiformis
Paleanotus heteroseta
Paraonis fulgeus
Parapionosyllis manca
Phyllodoce arenae
Phyllodoce mucosa
Pista palmata
Podarke obseura
Polydora ligni
Prionospio malmgreni
Protodorvillea egena
Pseudeurythoe paucibranchiata
Scolelepis squamata
Sigalion arenicolae
Sigambra tentaculata
Spio setosa
Spiochaetopterus oculatus
Spiophanes bombyx
Stauronereis rudolphi
Sthenelais limicola
Tharyx setigera

Phoronids
Phoronis spp.

Echinoderms
Arbacia punctulata
Cucumaria pulcherrima
Mellita quinquiesperforata

Hemichordates
Hemichordate

Cordates
Branchiostoma caribaeum

Table 12. Species data from 13 of the Smith-MacIntyre grabs collected in 1996.

Taxa	Station	336	336	342	347	347	353	353	361	361	372	372	377	396	
	Date	Jun	Nov	Jun	Jun	Nov	Jun	Nov	Jun	Nov	Jun	Nov	Jun	Nov	Total
Acanthohaustorius millsi		2	3	0	2	0	0	0	0	0	0	0	0	2	9
Acteocina canaliculata		0	0	0	0	0	0	0	0	0	0	1	0	0	1
Aglaophamus verrilli		0	1	18	0	0	0	0	21	42	21	34	2	0	139
Amastigos caperatus		0	0	0	0	0	0	1	7	0	1	0	0	0	9
Ampelisca abdita		0	0	1	0	0	0	0	0	3	0	24	0	0	28
Ampelisca verrilli		0	0	0	0	0	0	0	4	26	0	0	0	0	30
Ampharete acutifrons		0	0	0	0	0	2	0	0	0	0	0	0	0	2
Amphipod		0	0	0	0	0	0	0	0	0	0	0	1	0	1
Ancistrosyllis hartmanae		0	0	0	0	0	3	0	0	0	0	0	1	0	4
Anemones, Burrowing		0	0	0	0	0	0	0	5	0	0	0	0	0	5
Aphrodita hastata		0	1	0	1	0	0	0	0	0	0	0	0	0	2
Arbacia punctulata		0	0	0	1	0	0	0	0	0	0	0	0	0	1
Aricidea jeffreysii		1	0	0	5	1	4	0	0	0	0	0	1	0	12
Aricidea wassi		0	0	0	1	0	0	0	0	0	0	0	4	0	5
Asabellides oculata		0	0	64	0	0	4	0	43	0	11	0	1	0	123
Asychis elongata		0	0	0	0	0	0	0	0	0	0	7	1	0	8
Batea catharinensis		0	0	1	0	0	0	0	0	0	0	0	0	0	1
Bathyporeia porteri		0	0	0	0	0	0	0	0	0	0	0	0	1	1
Bhwania goodei		0	0	0	0	0	0	0	1	0	0	0	0	0	1
Bivalva		1	0	0	4	0	1	2	0	0	0	0	0	0	8
Branchiostoma caribaeum		0	1	0	4	2	0	12	0	0	0	1	3	6	29
Brania clavata		0	0	0	2	0	36	0	0	0	0	0	0	0	38
Brania sp.		1	0	0	0	0	0	0	0	0	0	0	0	0	1
Brania wellfleetensis		0	0	0	0	0	3	0	0	0	0	0	1	0	4
Campylaspis sp.		0	0	0	0	0	0	0	2	0	0	0	0	0	2
Capitomastus aciculatus		0	0	0	0	0	0	1	0	0	0	0	0	0	1
Chiridotea tuftsi		0	0	0	2	0	0	0	0	0	0	0	0	0	2
Cirolana concharum		4	0	0	0	0	0	0	0	0	0	0	0	0	4
Clymenella mucosa		0	0	0	0	0	4	0	0	0	0	0	0	0	4
Clymenella sp.		0	0	1	0	0	0	0	0	0	0	0	0	0	1
Clymenella torquata		0	0	5	0	0	1	0	0	1	5	10	0	0	22
Corophium tuberculatum		0	0	0	0	0	0	0	0	0	7	0	0	0	7
Crangon septemspinosus		0	0	0	0	0	0	0	0	2	0	0	1	0	3
Cucumaria pulcherrima		0	0	0	0	0	1	0	0	0	0	0	0	0	1
Decapod		0	0	0	0	0	0	0	0	0	0	7	0	3	10
Drilonereis magna		0	0	0	0	0	0	0	1	1	0	0	0	0	2
Ensis directus		0	0	0	0	0	0	0	138	5	0	6	0	0	149
Epitonium multistriatum		0	0	0	0	0	0	1	0	0	0	1	0	0	2
Euclymene zonalis		0	0	0	0	0	0	0	0	1	0	0	0	0	1
Exogone dispar		0	0	0	13	0	1	0	0	0	0	0	0	0	14
Flat worm		0	0	0	0	0	0	0	2	0	0	0	0	0	2
Gastropod		0	0	0	0	0	0	1	0	0	0	0	0	0	1
Glycera americana		0	0	1	1	0	5	0	0	0	1	1	0	0	9
Glycera dibranchiata		1	0	0	0	0	0	3	0	0	0	0	1	0	5
Glycera robustus		0	0	0	0	0	1	0	0	0	0	0	0	0	1
Haminoea solitaria		0	0	0	0	1	0	0	0	0	0	1	1	0	3

Table . Continued.

Taxa	Station / Date	336 Jun	336 Nov	342 Jun	347 Jun	347 Nov	353 Jun	353 Nov	361 Jun	361 Nov	372 Jun	372 Nov	377 Jun	396 Nov	Total
Harmathoe nodosa		0	0	0	0	0	0	0	0	0	1	0	0	0	1
Harmathoe sp.		0	0	0	0	0	1	0	1	0	0	0	0	0	2
Hemichordate		0	0	0	0	0	1	0	0	0	0	0	0	0	1
Heterotanais sp.		1	0	0	43	0	0	0	0	0	0	0	0	0	44
Isopod		0	0	0	0	0	0	0	0	0	0	0	0	3	3
Lepidactylus dytiscus		0	0	0	0	2	0	2	0	0	0	0	0	0	4
Leucon americanus		0	0	0	1	0	0	0	0	0	0	0	0	0	1
Lumbrinereis acuta		1	0	1	0	0	0	0	0	0	2	0	1	0	5
Lumbrinereis tenuis		0	0	0	0	0	2	9	0	1	0	0	0	0	12
Lyonsia hyalina		0	0	0	0	0	1	0	0	0	0	0	0	0	1
Macoma sp.		0	0	0	1	0	0	0	0	0	0	0	0	0	1
Macoma tenta		0	0	0	0	0	0	2	0	0	0	0	0	0	2
Magelona rosea		0	65	0	4	28	0	0	1	1	0	14	14	14	141
Maldanopsis elongata		0	0	6	0	0	0	0	0	0	7	0	0	0	13
Mangelia cerira		0	0	0	0	3	0	0	0	0	0	6	0	0	9
Mediomastus ambiseta		0	0	2	0	0	0	0	3	0	0	0	0	0	5
Mediomastus sp.		0	0	0	0	0	0	0	0	0	0	1	0	0	1
Mellita quinquiesperforata		0	1	0	15	1	24	0	0	0	3	0	102	1	147
Nassarius trivitattus		0	0	4	0	5	0	0	0	5	0	11	0	1	26
Nemertean		0	2	0	2	1	5	5	0	0	3	1	0	0	19
Nephtys bucera		2	0	0	0	2	0	1	0	0	0	0	0	1	6
Nephtys cryptomma		0	1	7	2	0	1	0	31	0	5	0	8	1	56
Nephtys incisa		0	0	0	0	0	0	0	0	1	0	0	0	0	1
Nephtys picta		0	0	2	1	0	0	0	1	9	5	1	15	2	36
Notomastus hemipodus		0	0	1	0	0	0	0	0	0	1	0	0	0	2
Notomastus latericeus		0	0	0	0	0	3	0	0	0	0	0	0	0	3
Notomastus sp.		0	0	0	0	0	0	0	0	0	0	0	1	0	1
Orbinia ornata		0	0	0	0	0	0	0	0	0	0	0	1	0	1
Owenia fusiformis		0	0	0	0	0	0	0	0	1	0	0	0	0	1
Oxyurostylis smithi		0	0	0	3	0	8	0	1	0	0	0	0	0	12
Pagurus longicarpus		0	0	0	2	1	2	1	0	3	0	9	3	0	21
Paleanotus heteroseta		0	0	0	0	0	2	11	0	0	0	2	0	0	15
Pandora trilineata		0	0	0	2	0	0	0	0	0	0	5	0	1	8
Panopeus herbstii		0	0	0	0	0	0	2	0	0	0	0	0	0	2
Paraonis fulgeus		0	0	0	0	0	0	0	0	0	0	0	2	0	2
Paraphoxus spinosus		0	0	0	0	0	0	0	0	0	0	0	2	0	2
Parapionosyllis manca		0	0	0	0	0	1	0	0	0	0	0	0	0	1
Phoronis spp.		0	0	1	0	0	0	0	9	0	0	7	0	0	17
Phyllodoce arenae		0	0	0	0	0	0	0	2	0	0	0	0	0	2
Phyllodoce mucosa		0	0	0	0	0	0	0	1	0	0	0	0	0	1
Pinixia cylindrica		0	0	0	0	0	3	0	0	0	0	0	0	0	3
Pinixia retinens		0	0	1	0	0	0	0	0	0	0	0	0	0	1
Pista palmata		0	0	0	0	0	1	0	0	0	0	2	0	0	3
Podarke obseura		0	0	0	0	0	0	1	0	0	0	0	0	0	1
Polinices duplicatus		0	0	0	1	0	0	0	0	0	0	0	0	0	1
Polydora ligni		0	0	12	0	0	3	0	7	0	3	0	0	0	25
Pontocrates sp.		0	0	0	2	0	0	0	0	0	0	0	0	0	2

Table . Continued.

Taxa	Station	336	336	342	347	347	353	353	361	361	372	372	377	396	
	Date	Jun	Nov	Jun	Jun	Nov	Jun	Nov	Jun	Nov	Jun	Nov	Jun	Nov	Total
Prionospio malmgreni		0	0	45	0	0	0	0	50	3	50	9	0	1	158
Protodorvillea egena		0	0	0	0	0	3	11	0	0	0	0	0	0	14
Protohaustorius wigleyi		0	0	0	19	0	0	0	0	0	0	0	11	7	37
Pseudeurythoe paucibranchiata		0	0	0	0	0	1	0	0	0	0	0	0	0	1
Ptilanthura tenuis		0	0	0	0	0	0	0	0	1	0	0	0	0	1
Pyramidella candida		0	0	0	0	0	0	0	0	0	0	1	0	0	1
Scolelepis squamata		0	11	0	0	0	0	0	0	0	0	0	0	0	11
Sigalion arenicolae		0	0	0	0	0	0	0	0	0	0	0	0	1	1
Sigambra tentaculata		0	0	0	0	0	0	0	1	0	0	0	0	0	1
Spio setosa		0	0	1	0	0	6	0	3	0	0	0	0	0	10
Spiochaetopterus oculatus		0	0	1	1	0	0	0	0	0	0	3	0	0	5
Spiophanes bombyx		0	0	17	1	1	1	3	5	8	9	36	1	4	86
Spisula solidissima		1	0	0	0	0	0	0	0	0	0	0	0	0	1
Stauronereis rudolphi		0	0	0	0	0	1	0	0	0	0	0	0	0	1
Sthenelais limicola		0	0	0	0	0	0	0	0	1	0	0	0	0	1
Stylochus sp.		0	0	0	0	0	0	0	3	0	0	0	0	0	3
Synchelidium americanum		0	0	0	4	0	1	0	0	0	0	0	3	0	8
Tectonatica pusilla		0	0	0	0	0	0	0	0	0	0	1	0	0	1
Tellina agilis		1	0	0	0	0	0	0	0	0	0	7	5	0	13
Tharyx setigera		0	0	0	5	0	0	0	0	0	0	0	4	0	9
Trichophoxus epistomus		0	0	0	0	0	0	0	0	0	0	0	0	1	1
Tubificidae		0	0	0	0	0	33	0	0	0	0	0	4	0	37
Turbonilla interupta		0	0	0	0	5	0	0	0	7	0	6	0	0	18
Unciola irrorata		3	0	4	24	0	0	1	3	1	0	3	0	23	62
Grand Total		19	86	196	169	53	170	70	346	123	135	218	195	73	

Table 13. Top ranked taxa, in terms of both occurrence and abundance from 13 of the Smith-MacIntyre grabs processed from 1996. Occur. is total occurrences out of 13 grabs and Abund. is summed abundance from the 13 grabs.

Taxa	Major Taxon	Occur.	Abund.
Spiophanes bombyx	Pl*	11	86
Magelona rosea	Pl	8	141
Unciola irrorata	Am	8	62
Nephtys cryptomma	Pl	8	56
Nephtys picta	Pl	8	36
Mellita quinquiesperforata	Ec	7	147
Aglaophamus verrilli	Pl	7	139
Branchiostoma caribaeum	Ch	7	29
Pagurus longicarpus	De	7	21
Nemertean	Ne	7	19
Prionospio malmgreni	Pl	6	158
Asabellides oculata	Pl	5	123
Ensis directus	Bv	3	149
Heterotanais sp.	Ta	2	44

* Pl Polychaete
Am Amphipod
Ec Echnioderm
Ch Chordate
De Decapod
Ne Nemertean
Bv Bivalve
Ta Tanaid

Table 14. Summary of the number of species per major taxon. Data from the Norfolk Disposal Site, NDS, are from Dauer (1981) and represent total number of species from approximately 4.8 m^2 of bottom. The VA-B data are from the 13 grabs processed for species and represent totals for 1.3 m^2 of bottom.

Taxonomic Group	Number of Species VA-B	NDS
Polychaetes	55	81
Amphipods	13	24
Bivalves	8	14
Gastropods	9	14
Cumaceans	3	5
Decapods	4	4
Isopods	3	3
Oligochaetes	3	2
Echinoderms	1	2
Other	8	6

Table 15. Percent of small and large wet weight biomass (Wt Wt %) and total individuals (No. %) summarized by major taxonomic group, from June and November 1996 Smith-MacIntyre grab data. The small category is the sum of 0.5, 1.0 and 2.0 mm sieve fractions. The large category is the sum of 3.35 and 6.3 mm sieve fractions.

Major Taxa	Date	Wt Wt % Small	Wt Wt % Large	No. % Small	No. % Large
Echnioderms	June	0.02	0.98	0.40	0.60
Sand Dollars	June	0.04	0.96	0.99	0.01
Crustaceans	June	0.04	0.96	0.63	0.37
Bivalves	June	0.09	0.91	0.50	0.50
Gastropods	June	0.10	0.90	0.69	0.31
Chordates	June	0.18	0.82	0.46	0.54
Annelids	June	0.30	0.70	0.76	0.24
Misc.	June	0.32	0.68	0.57	0.43
Anemones	June	0.66	0.34	0.80	0.20
Amphiods	June	0.81	0.19	0.97	0.03
All Taxa	June	0.17	0.83	0.86	0.14
Echnioderms	November	0.00	1.00	0.00	1.00
Sand Dollars	November	0.01	0.99	0.71	0.29
Bivalves	November	0.03	0.97	0.38	0.63
Gastropods	November	0.04	0.96	0.70	0.30
Crustaceans	November	0.09	0.91	0.85	0.15
Chordates	November	0.27	0.73	0.46	0.54
Misc.	November	0.28	0.72	0.81	0.19
Annelids	November	0.42	0.58	0.79	0.21
Anemones	November	0.72	0.28	0.83	0.17
Amphiods	November	0.87	0.13	0.97	0.03
All Taxa	November	0.20	0.80	0.84	0.16
Totals	June+Nov	0.19	0.81	0.85	0.15

Table 16. Size class distribution of biomass (g wet wt) and individuals by major taxonomic groupings for June and November 1996 grab data.

	Seive Size (mm)	June Sum of 42 grabs No.	Wet Wt	% No	% wt	November Sum of 39 grabs No.	Wet Wet	% No	% Wt	June Average per garb (0.1 m^2) No.	Wet Wt	November No.	Wet Wt
Amphiods	0.5	413	0.092	0.30	0.03	393	0.143	0.28	0.05	9.83	0.00	10.08	0.00
	1	819	0.917	0.59	0.31	685	0.976	0.48	0.31	19.50	0.02	17.56	0.03
	2	111	1.394	0.08	0.47	299	1.589	0.21	0.51	2.64	0.03	7.67	0.04
	3.35	42	0.520	0.03	0.18	41	0.411	0.03	0.13	1.00	0.01	1.05	0.01
	6.3	2	0.033	0.00	0.01	0	0.000	0.00	0.00	0.05	0.00	0.00	0.00
	Totals	1387	2.956			1418	3.119			33.02	0.07	36.36	0.08
Annelids	0.5	997	0.716	0.25	0.01	826	20.157	0.23	0.18	23.74	0.02	21.18	0.52
	1	1134	2.843	0.28	0.05	1241	7.910	0.35	0.07	27.00	0.07	31.82	0.20
	2	924	12.970	0.23	0.23	740	17.404	0.21	0.16	22.00	0.31	18.97	0.45
	3.35	916	29.641	0.23	0.53	559	33.032	0.16	0.30	21.81	0.71	14.33	0.85
	6.3	66	9.276	0.02	0.17	196	30.774	0.06	0.28	1.57	0.22	5.03	0.79
	Totals	4037	55.446			3562	109.277			96.12	1.32	91.33	2.80
Anemones	0.5	0	0.000	0.00	0.00	0	0.000	0.00	0.00	0.00	0.00	0.00	0.00
	1	0	0.000	0.00	0.00	2	0.011	0.17	0.09	0.00	0.00	0.05	0.00
	2	12	0.129	0.80	0.66	8	0.081	0.67	0.64	0.29	0.00	0.21	0.00
	3.35	3	0.066	0.20	0.34	2	0.035	0.17	0.28	0.07	0.00	0.05	0.00
	6.3	0	0.000	0.00	0.00	0	0.000	0.00	0.00	0.00	0.00	0.00	0.00
	Totals	15	0.195			12	0.127			0.36	0.00	0.31	0.00
Bivalves	0.5	32	0.022	0.09	0.00	4	0.004	0.02	0.00	0.76	0.00	0.10	0.00
	1	44	0.166	0.13	0.01	26	0.067	0.14	0.00	1.05	0.00	0.67	0.00
	2	93	2.701	0.27	0.08	39	1.864	0.21	0.03	2.21	0.06	1.00	0.05
	3.35	150	8.832	0.44	0.27	24	2.426	0.13	0.04	3.57	0.21	0.62	0.06
	6.3	22	20.853	0.06	0.64	91	56.762	0.49	0.93	0.52	0.50	2.33	1.46
	Totals	341	32.574			184	61.123			8.12	0.78	4.72	1.57

Table 16. Continued.

	Seive Size (mm)	June Sum of 42 grabs No.	Wet Wt	% No	% wt	November Sum of 39 grabs No.	Wet Wet	% No	% Wt	June Average per garb (0.1 m^2) No.	Wet Wt	November No.	Wet Wt
Chordates	0.5	0	0.000	0.00	0.00	0	0.000	0.00	0.00	0.00	0.00	0.00	0.00
	1	4	0.035	0.05	0.01	6	0.090	0.05	0.02	0.10	0.00	0.15	0.00
	2	35	0.387	0.41	0.16	51	1.324	0.41	0.26	0.83	0.01	1.31	0.03
	3.35	33	0.691	0.39	0.29	43	2.302	0.35	0.44	0.79	0.02	1.10	0.06
	6.3	13	1.250	0.15	0.53	24	1.459	0.19	0.28	0.31	0.03	0.62	0.04
	Totals	85	2.363			124	5.175			2.02	0.06	3.18	0.13
Crustaceans	0.5	35	0.015	0.19	0.00	131	0.031	0.29	0.00	0.83	0.00	3.36	0.00
	1	45	0.063	0.25	0.01	173	0.238	0.39	0.03	1.07	0.00	4.44	0.01
	2	34	0.183	0.19	0.03	76	0.498	0.17	0.06	0.81	0.00	1.95	0.01
	3.35	44	1.706	0.24	0.26	46	2.154	0.10	0.26	1.05	0.04	1.18	0.06
	6.3	22	4.708	0.12	0.71	22	5.423	0.05	0.65	0.52	0.11	0.56	0.14
	Totals	180	6.675			448	8.344			4.29	0.16	11.49	0.21
Echnioderms	0.5	1	0.001	0.20	0.00	0	0.000	0.00	0.00	0.02	0.00	0.00	0.00
	1	1	0.006	0.20	0.02	0	0.000	0.00	0.00	0.02	0.00	0.00	0.00
	2	0	0.000	0.00	0.00	0	0.000	0.00	0.00	0.00	0.00	0.00	0.00
	3.35	2	0.051	0.40	0.16	3	0.227	0.60	0.26	0.05	0.00	0.08	0.01
	6.3	1	0.256	0.20	0.82	2	0.645	0.40	0.74	0.02	0.01	0.05	0.02
	Totals	5	0.314			5	0.872			0.12	0.01	0.13	0.02
Gastropods	0.5	11	0.018	0.06	0.00	18	0.071	0.06	0.00	0.26	0.00	0.46	0.00
	1	76	0.305	0.44	0.03	76	0.743	0.25	0.01	1.81	0.01	1.95	0.02
	2	32	0.635	0.19	0.06	120	2.924	0.39	0.03	0.76	0.02	3.08	0.07
	3.35	47	6.513	0.27	0.66	52	4.712	0.17	0.06	1.12	0.16	1.33	0.12
	6.3	6	2.450	0.03	0.25	38	75.698	0.13	0.90	0.14	0.06	0.97	1.94
	Totals	172	9.921			304	84.148			4.10	0.24	7.79	2.16

Table 16. Continued.

	Seive Size (mm)	June Sum of 42 grabs No.	Wet Wt	% No	% wt	November Sum of 39 grabs No.	Wet Wet	% No	% Wt	June Average per garb (0.1 m^2) No.	Wet Wt	November No.	Wet Wt
Misc.	0.5	1	0.001	0.14	0.01	26	0.060	0.28	0.03	0.02	0.00	0.67	0.00
	1	1	0.018	0.14	0.17	14	0.110	0.15	0.06	0.02	0.00	0.36	0.00
	2	2	0.016	0.29	0.15	35	0.359	0.38	0.19	0.05	0.00	0.90	0.01
	3.35	3	0.074	0.43	0.68	12	0.953	0.13	0.51	0.07	0.00	0.31	0.02
	6.3	0	0.000	0.00	0.00	6	0.405	0.06	0.21	0.00	0.00	0.15	0.01
	Totals	7	0.109			93	1.887			0.17	0.00	2.38	0.05
Sand Doll.	0.5	406	0.135	0.17	0.00	0	0.000	0.00	0.00	9.67	0.00	0.00	0.00
	1	1905	2.250	0.79	0.03	10	0.019	0.10	0.00	45.36	0.05	0.26	0.00
	2	94	0.307	0.04	0.00	58	0.458	0.60	0.01	2.24	0.01	1.49	0.01
	3.35	10	0.187	0.00	0.00	10	0.280	0.10	0.01	0.24	0.00	0.26	0.01
	6.3	9	61.570	0.00	0.96	18	32.245	0.19	0.98	0.21	1.47	0.46	0.83
	Totals	2424	64.449			96	33.002			57.71	1.53	2.46	0.85
Totals	0.5	2274	1.077	0.23	0.01	1660	20.578	0.23	0.07	54.14	0.03	42.56	0.53
	1	4803	7.457	0.49	0.04	2745	10.902	0.38	0.04	114.36	0.18	70.38	0.28
	2	1414	19.933	0.14	0.12	1649	27.592	0.23	0.09	33.67	0.47	42.28	0.71
	3.35	1248	47.095	0.13	0.27	787	44.789	0.11	0.15	29.71	1.12	20.18	1.15
	6.3	121	95.721	0.01	0.56	375	197.988	0.05	0.66	2.88	2.28	9.62	5.08
	Totals	9860	171.283			7216	301.849			234.76	4.08	185.03	7.74
June+Nov	0.5	3934	21.655	0.23	0.05	48.57	0.27						
	1	7548	18.359	0.44	0.04	93.19	0.23						
	2	3063	47.525	0.18	0.10	37.81	0.59						
	3.35	2035	91.884	0.12	0.19	25.12	1.13						
	6.3	496	293.709	0.03	0.62	6.12	3.63						
	TOTAL	17076	473.132			210.81	5.84						

The Department of the Interior

As the Nations's principal conservation agency, the Department of the Interior has responsibility for most of our nationally owned public lands and natural resources. This includes fostering sound use of our land and water resources, protecting our fish, wildlife, and biological diversity, preserving the environmental and cultural values of our national parks and historic places; and providing for the enjoyment of life through outdoor recreation. The Department assesses our energy and mineral resources and works to ensure that their development is in the best interests of all our people by encouraging stewardship and citizen participation in their care. The Department also has a major responsibility for American Indian reservation communities and for people who live in island territories under U.S. Administration.

The Minerals Management Service Mission

As a bureau of the Department of the Interior, the Minerals Management Service's (MMS) primary responsibilities are to manage the mineral resources located on the Nations's Outer Continental Shelf (OCS), collect revenue from the Federal OCS and onshore federal and Indian lands, and distribute those revenues.

Moreover, in working to meet its responsibilities, the Offshore Minerals Management Program administers the OCS competitive leasing program and oversees the safe and environmentally sound exploration and production of our Nation's offshore natural gas, oil and other mineral resources. The MMS Royalty Management Program meets its responsibilities by entrusting the efficient, timely and accurate collection and distribution of revenue from mineral leasing and production due to Indian tribes andallottees, States and the U. S. Treasury

the MMS strives to fulfill its responsibilities through the general guiding principles of: (1) being responsive to the public's concerns and interests by maintaining a dialog with all potentially affected parties and (2) carrying out its programs with an emphasis on working to enhance the quality of life for all Americans by lending MMS assistance and expertise to economic development and environmental protection.

Final Report

January 1998

Environmental Studies Relative to Potential Sand Mining in the Vicinity of the City of Virginia Beach, Virginia

Part 2: Preliminary Shoreline Adjustments to Dam Neck Beach Nourishment Project Southeast Virginia Coast

Authors:

C. Scott Hardaway, Jr.
Donna A. Milligan
George R. Thomas
Carl H. Hobbs, III
Virginia Institute of Marine Science

Project Manager:

Carl H. Hobbs, III
Virginia Institute of Marine Science

Prepared under MMS Cooperative Agreement 14-35-0001-3087 through Virginia Institute of Marine Science of the College of William & Mary

MMS U.S. Department of the Interior
Minerals Management Service

College of William and Mary
Virginia Institute of Marine Science
School of Marine Science

DISCLAIMER

This report has been reviewed by the Minerals Management Service and approved for publication. Approval does not signify that the contents necessarily reflect the views and policies of the Service, nor does mention of trade names or commercial products constitute endorsement or recommendation for use.

The Department of the Interior

As the Nations's principal conservation agency, the Department of the Interior has responsibility for most of our nationally owned public lands and natural resources. This includes fostering sound use of our land and water resources, protecting our fish, wildlife, and biological diversity, preserving the environmental and cultural values of our national parks and historic places; and providing for the enjoyment of life through outdoor recreation. The Department assesses our energy and mineral resources and works to ensure that their development is in the best interests of all our people by encouraging stewardship and citizen participation in their care. The Department also has a major responsibility for American Indian reservation communities and for people who live in island territories under U.S. Administration.

The Minerals Management Service Mission

As a bureau of the Department of the Interior, the Minerals Management Service's (MMS) primary responsibilities are to manage the mineral resources located on the Nations's Outer Continental Shelf (OCS), collect revenue from the Federal OCS and onshore federal and Indian lands, and distribute those revenues.

Moreover, in working to meet its responsibilities, the Offshore Minerals Management Program administers the OCS competitive leasing program and oversees the safe and environmentally sound exploration and production of our Nation's offshore natural gas, oil and other mineral resources. The MMS Royalty Management Program meets its responsibilities by entrusting the efficient, timely and accurate collection and distribution of revenue from mineral leasing and production due to Indian tribes andallottees, States and the U. S. Treasury

the MMS strives to fulfill its responsibilities through the general guiding principles of: (1) being responsive to the public's concerns and interests by maintaining a dialog with all potentially affected parties and (2) carrying out its programs with an emphasis on working to enhance the quality of life for all Americans by lending MMS assistance and expertise to economic development and environmental protection.

Introduction

The purpose of this report is to 1) describe the shoreline morphology and historical movement of the Virginia's southeast ocean coast from Rudee Inlet to north Sandbridge and 2) document the sediment movement of the recent Dam Neck Beach Nourishment Project (DNBNP) after one year. This study was modified to accommodate the Dam Neck project which came online after the original scope of work for the Minerals Management Service (MMS) was developed. The DNBNP involved placement of over 1,000,000 cubic yards (cy) of sand fill that was dredged from Sandbridge Shoal in Federal waters and placed along about 9,000 ft. of shoreline. Monitoring of the project by VIMS includes before and after aerial imagery, beach profiles and collecting sediment samples. A detailed three year monitoring project is being conducted by the Navy.

Monitoring objectives for the DNBNP included: 1) acquiring low-level aerial photos in order to track the beach planform movement of the beach fill mass; 2) performing beach profiles to document the alongshore changes of beach fill onto adjacent shores; 3) acquiring beach and nearshore sediments to characterize grain size trends as the beach fill disperses; and 4) determining gross bathymetric changes of the nearshore region. Three monitoring periods were determined to be sufficient to accomplish objectives. Detailed monitoring was done for the pre-fill condition (August 1996), post-fill six-months (May 1997) and post-fill one year (Oct 1997).

The DNBNP was completed in November1996. Monitoring of the project for this study extended alongshore from north Sandbridge to Rudee Inlet, a distance of approximately 29,000 ft. The landward extent of the monitoring extended into the dune field roughly 400 to 500 ft.from mean sea level (MSL). Offshore sampling and bathymetry extended to at least the -24 ft. contour, approximately 2,000 ft. from MSL.

In general, Virginia’s southeast ocean coast is receding. This ongoing process prompted the Navy to proceed with a large beach nourishment project. With a large sand source just over 3 miles offshore (i.e. Sandbridge Shoal), the DNBNP became a cost effective shore protection option. MMS serves as the government steward of that sand resource and, therefore, is responsible for its wise use. The two-year, five-task monitoring project by the Virginia Institute of Marine Science (VIMS) and Old Dominion University (ODU) will evaluate several facets of offshore sand mining for the purpose of beach nourishment and attempt to determine initial and potential impacts of the DNBNP to benthic resources, modification to the wave climate, tidal current influence and modification the shore zone.

Physical Setting

Geography and Background

The southeast Virginia coast extends from Cape Henry at the mouth of the Chesapeake Bay to False Cape and the North Carolina state line. The False Cape offshore shoal complex and Cape Henry with its associated offshore shoals essentially act as large headland features that

bound a long, curvilinear shoreline embayment (Figure 1). This embayed shore includes the coast from Rudee Inlet south to False Cape. The primary study area of Dam Neck lies within this larger shore cell or reach.

The shoreline between Cape Henry and False Cape is a barrier beach and dune system typical of the mid-Atlantic coast. The north half of the reach generally lacks a backbarrier lagoon. The southern half of the reach is backed by North Bay and Back Bay down to False Cape. The only break in this shore reach is Rudee Inlet which has been in existence since at least 1585 (Everts *et al.*, 1983).

Until 1988, the most significant anthropogenic impact in the Cape Henry to False Cape reach was the annual beach nourishment at the Resort Strip that extends from Rudee Inlet northward about 3 miles. The Resort Strip is the commercial, recreational district in the City of Virginia Beach which has been maintained as a recreational, tourist beach through beach nourishment. Sand has been used to recreate the beach yearly since the mid-1950s primarily by truck haul from upland borrow areas and sediment bypassing at Rudee Inlet by cutter head dredge. Approximately 150,000 cy of sand is bypassed annually at Rudee Inlet onto the Resort Strip and another 100,000 to 150,000 cy is trucked in.

In 1988, a second anthropogenic impact to the reach began in earnest. Many residents of the 4.5 mile subreach known as Sandbridge began an extensive bulkheading program to prevent dune erosion. These bulkheads were made primarily of steel, and between 1988 and 1990, about 12,850 ft. of shore was bulkheaded (Basco *et al.*, 1997). By 1995, almost15,545 ft. of shoreline at Sandbridge had bulkheads. Since then, many have failed, have been rebuilt or have been removed.

The most recent anthropogenic impact to Virginia's southeast coast has been the large beach nourishment project at Dam Neck (Fleet Combat Training Center, Atlantic). This project is part of a larger shoreline protection project installed by the Navy at Dam Neck. Before the beach material was placed, a large dune was built using sand from upland sources. This dune, which was constructed with a rock core, is the last line of defense for land based infrastructure the Navy values at about $95 million. Over 1,000,000 cy of borrowed sand from Sandbridge Shoal was pumped onto Dam Neck in November 1996.

Previous Studies of Shore Change

Numerous studies have been performed along the southeast ocean coast of Virginia that pertain to shoreline change. Studies by Everts *et al.* (1983), Dolan (1985), Wright *et al.* (1987), and Basco (1991) document the patterns and rates of shoreline change. Goldsmith (1977), Hardaway and Thomas (1990) and Basco (1997) have performed and analyzed beach surveys along various portions of the reach.

Figure 2 is a composite figure found in Basco (1991) showing shoreline change as determined by Everts *et al.* (1983) and Dolan (1985) as well as shore cells and wave height variation as determined by Wright *et al.* (1987). The general, long-term shore change pattern shows significant shore recession between latitude 36° 40' and 36° 45', just south of Sandbridge,

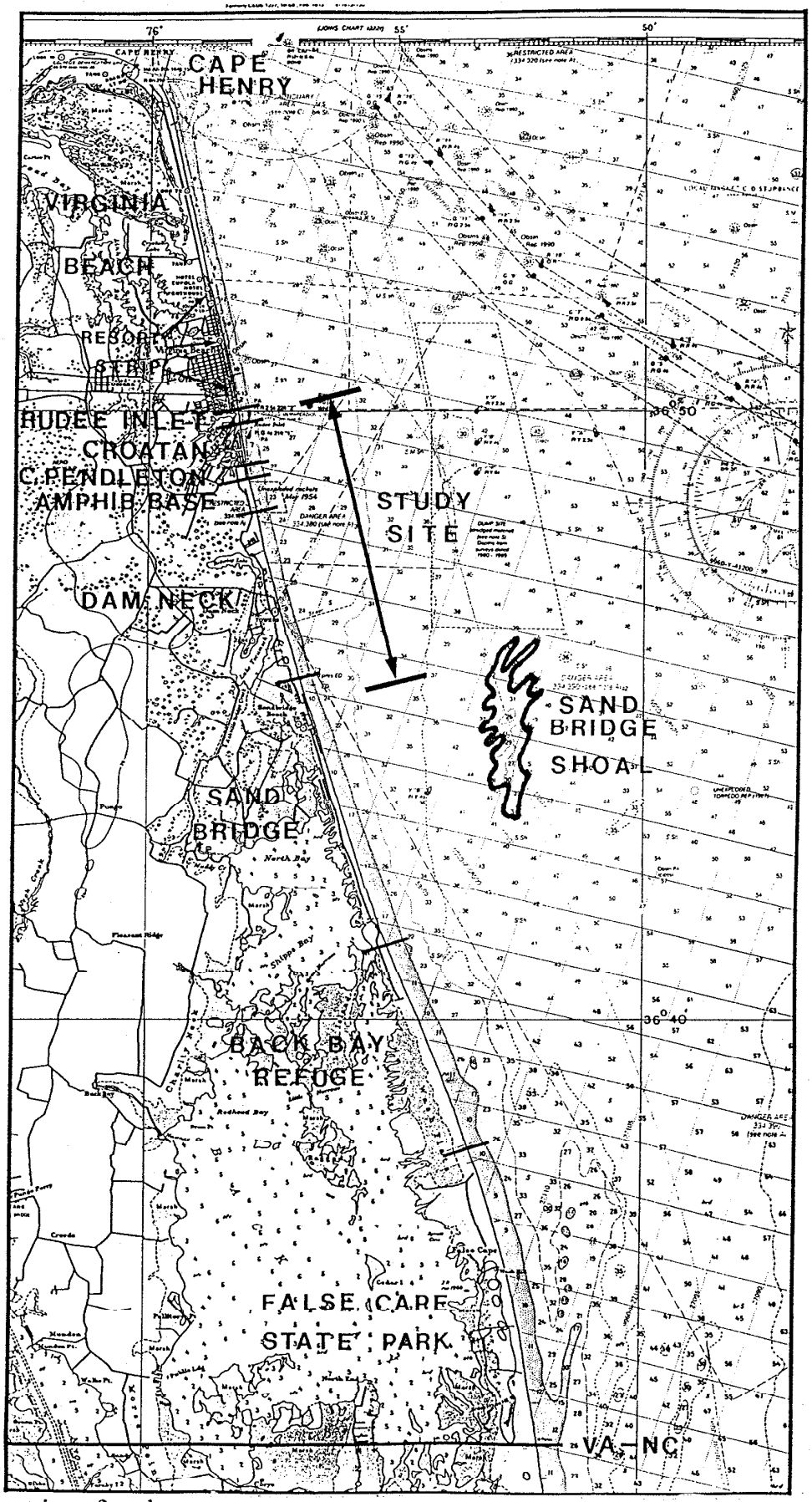

Figure 1. Location of study area.

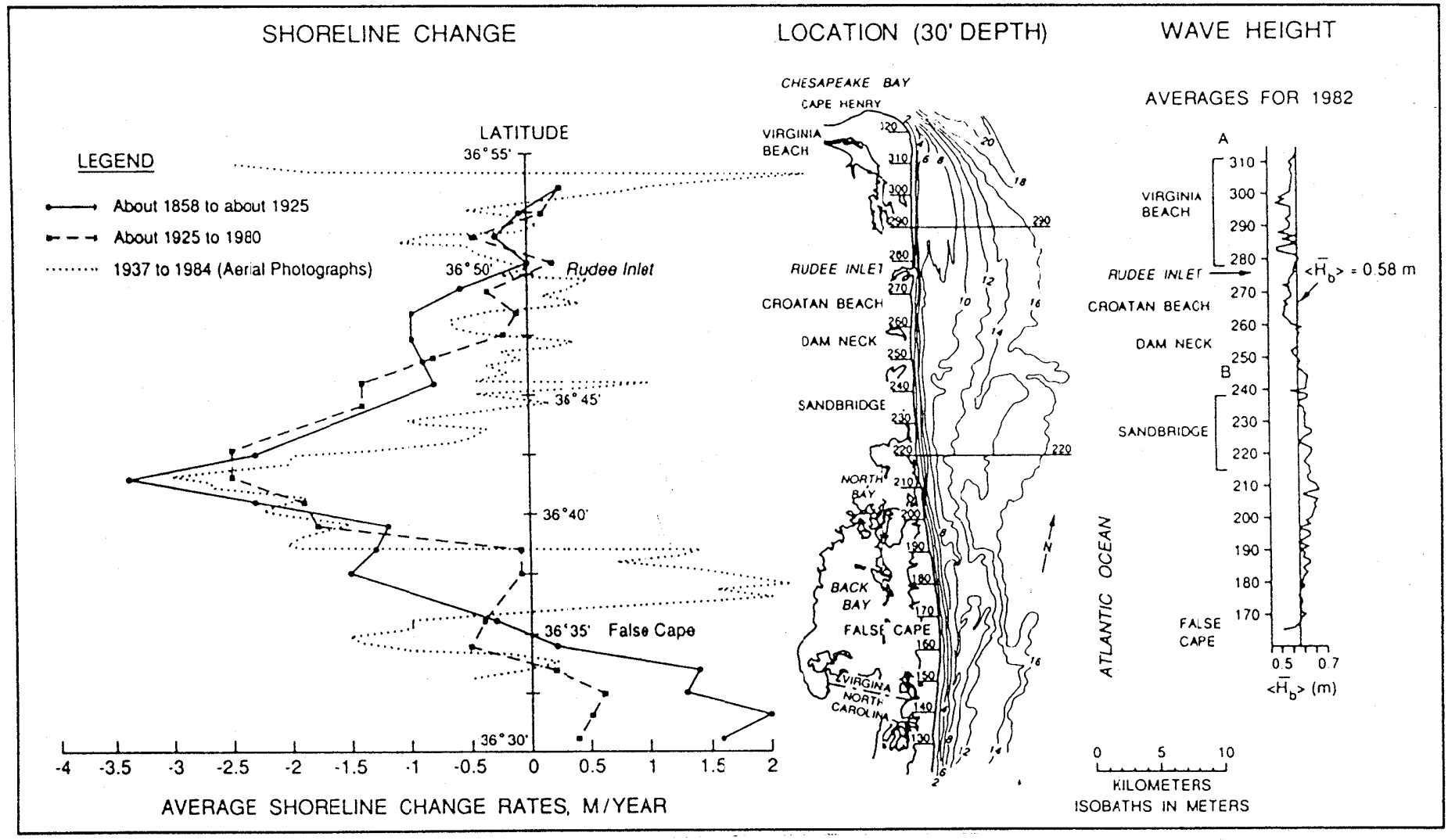

Figure 2. Composite of shoreline change rates (modified from Basco, 1991).

with a maximum erosion rate of 11.5 ft/yr at 36° 41.5' according to Everts *et al.* (1983) and Dolan (1985). This area of high shoreline recession also corresponds to high average breaker wave height (H_b) according to Wright *et al.* (1987). Accretionary trends are evident in several areas of the reach: around False Cape; just south of Rudee Inlet; and at Cape Henry. For the study area between Rudee Inlet and north Sandbridge, the erosion is more variable with some accretionary trends determined by Dolan (1985). These areas have a lower range of average breaker wave heights.

The analysis by Everts *et al.* (1983) is based, in part, on cartographic data using Federal government surveys from 1858 to 1925 and 1925 to 1980 (Figure 2). According to Everts *et al.* (1983), the topographic supplement to the hydrographic surveys were done mostly by plane table. After 1927, aerial photography and photogrammetric methods were used to provide coastal topography (Shalowitz, 1964). The main coastal feature that depicts the shoreline is mean high water (MHW). However, both in the field and from aerial imagery, the determination of this line or datum is somewhat interpretive and can contain a certain degree of error.

The analysis by Dolan (1985) depicted on Figure 2 utilized 47 years of aerial imagery from 1937 to 1984. More recent efforts have attempted to improve shoreline change analysis; several methods and their limitations are presented in Crowell *et al*. (1997), Crowell *et al.* (1991), and Dolan *et al.* (1991). Foster and Savage (1989) determined that the amount of error associated with shore change analysis varies with method. For map data, the error can be +/- 9.1 m, for aerial photos +/- 6.1 m and +/- 3.1 m for surveyed points. One factor is evident, the more closely spaced data points, the better the analysis.

Previous Sediment Studies

The sedimentology of the study area is based on both active processes as well as the underlying geology of the region. Sorting and winnowing of the sediments by the littoral currents and waves occurs continuously in the nearshore region and erosion can expose outcrops of material deposited long ago. Numerous studies have looked at the southeast ocean coast of Virginia in terms of its surficial sediment characteristics, mainly to identify and characterize possible sites for dredging of sand for beach nourishment projects. Williams (1987) studied the area between Cape Henry and Sandbridge. He compiled data from U.S. Army Corps of Engineers core log descriptions to create map of generalized distribution of surficial sediments (Figure 3). Most of the region has muddy fine to medium sand on the bottom. Clean sand is located in a narrow band on the shoreface landward of the 25 ft. contour with a few other isolated areas associated with shoals or relict paleochannels. The areas of mud are located in the thalweg on the western flank of the Chesapeake Bay entrance channel and could be old estuarine outcrops.

Hobbs' (1997) findings essentially agreed with Williams (1987) since his analysis revealed that inner continental shelf (depths less than 100 ft.) is dominated by coarser sediments, most of which contained in excess of 90% to 95% sand. Most sands are medium to coarse sand (>2 phi). Small pockets of fine grained sediments were related to Chesapeake Bay mouth and the others to outcrops of muddy sediments. Berquist and Hobbs (1988) found the inner shelf and shoreface region within 3 miles of the Sandbridge shoreline, depths generally less than 50 ft., have surface sediments of uniform gray to olive gray, fine to very fine sand with a consistent mean grain size of

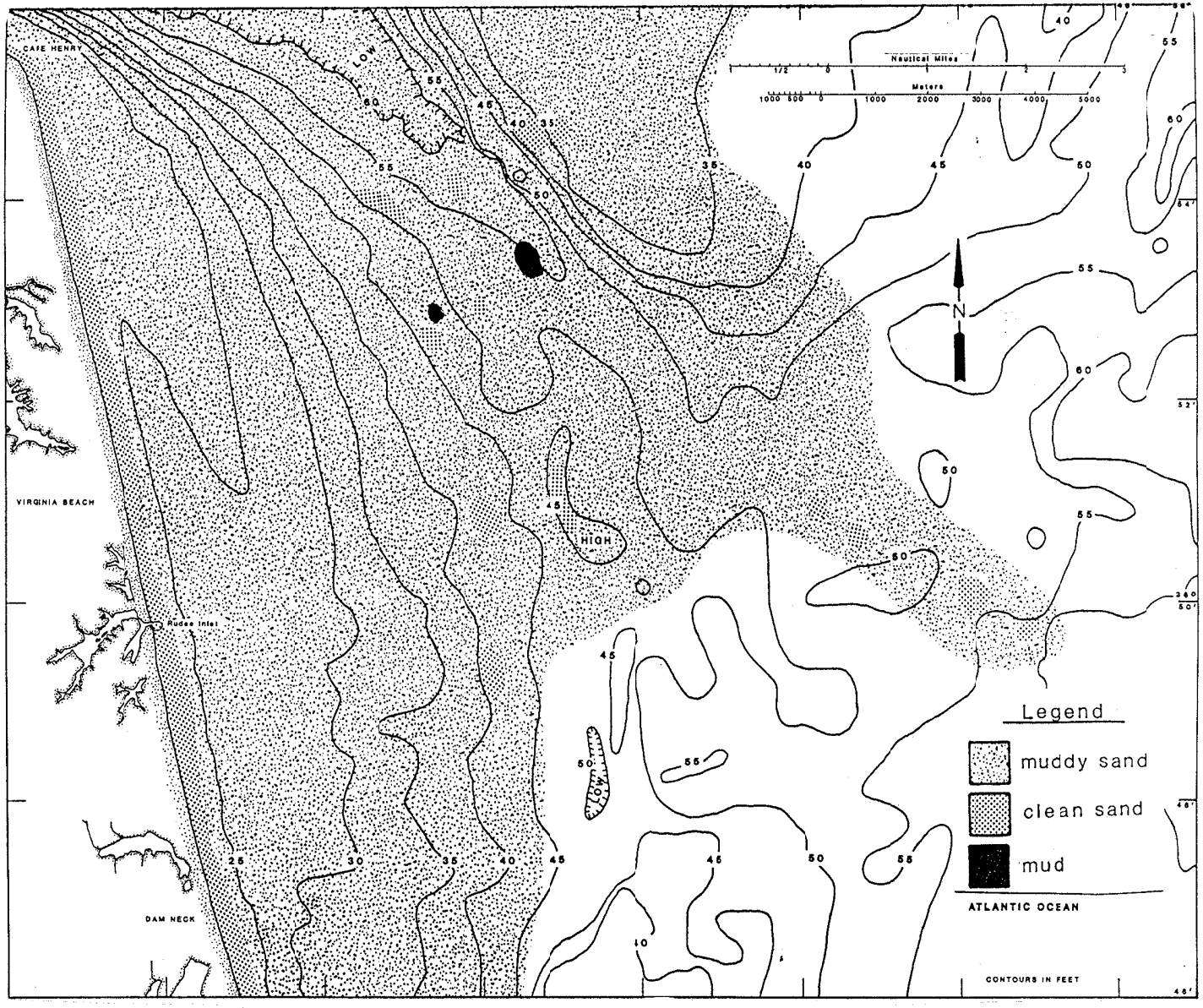

Figure 3. Surficial sediment distribution offshore Virginia Beach (from Williams, 1987).

0.125 mm (3.0 phi). The percentage of mud is high ranging from 16% to greater than 20%. Hobbs (1997) concluded that the sediments of southeastern Virginia ocean coast is more varied than previously thought. Even though most are sands, the density of the sampling grid allows identification of a greater spatial variability in grain-size characteristics.

Kimball and Dame (1989) used vibracores to confirm the characterization of sediments within Sandbridge Shoal as "medium grained sands" with mean grain size of 0.3 mm (1.5 phi); many samples had over 10% by weight pebbles. Their study of the bottom near Rudee Inlet indicated the region had a surface mean 3.05 phi (0.12 mm) and a standard deviation 0.5 phi, (0.71 mm). Off of Sandbridge the mean was 1.5 phi (0.35 mm) and the standard deviation was 0 .5 phi (0.71 mm).

Wright *et al*. (1987) summarized beach sediment data from various sources. There is considerable variability both cross-shore and alongshore, but in general, the average foreshore (beach between the berm and the beach TOE) mean along the Resort Strip in Virginia Beach was 2.0 phi (0.25 mm) and had a standard deviation or sorting value of 0.8 phi (0.57 mm). At the -10 ft.contour the $D_{50,}$ or median, varies between 2.3 phi and 2.5 phi (0.18 mm and 0.20 mm). Between Rudee Inlet and Fort Story, the D_{50} increased threefold (0.25 mm to 0.75 mm) from south to north. Between Rudee Inlet and Back Bay, the D_{50} of the oreshore is larger than other subaerial samples, and the D_{50} at -10 ft.contour is 2.1 phi (0.23 mm). On a winter beach, the minimum D_{50} seaward of the foreshore is 1.9 phi (0.26 mm) and varies to a maximum of 1.6 phi (0.32 mm). Sandbridge has a foreshore mean 1.75 phi (0.3 mm). Wright *et al.* (1987) suggest that a beach nourishment program along the Dam Neck/Sandbridge reach would best be served with sand larger than 2.0 phi (0.25 mm). The average grain size of the DNBNP is 0.4mm (1.2 phi).

Waterway Surveys and Engineering (1986) conducted an analysis of the beach at Sandbridge. Their study found that the D_{50} of the dune face or the base of the bulkhead ranges from 2 to 1.2 phi (0.25 to 4.0 mm) which is medium sand. This range also occurred in the midberm region. The D_{50} of the foreshore portion of the beach ranged from 2.3 to 1.0 phi (0.2 to 0.5 mm) and is classified as fine and medium sand. The low tide terrace had a D_{50} range of 2.3 to 2 phi (0.2 to 0.25 mm) which is fine sand. In general, the foreshore sands are coarsest with the backshore and dune slightly less coarse than foreshore. The outer part of low tide terrace has the finest sand, even finer than the samples from the 10 ft. depths. Sorting is best at outer edge of low tide terrace and on the dunes and in the backshore.

Hydrodynamic Setting

Wave Climate

For this study, the main hydrodynamic forces operating along the project area are the waves and wave-induced currents and tidal currents. The wave climate operating along the southeast Virginia coast is controlled, in part, by the nearshore bathymetric configuration and tidal currents (Ludwick, 1978; Wright *et al.*, 1987). Influence by tidal inlets is negligible, except locally at Rudee Inlet. Wave measurements at several locations including NOAA buoy 44014

(Figure 4) from Maa (1995) and WIS phase III stations 77 and 78 (Figure 5) from Jensen (1983) indicate a dominant southeasterly component to the wave field. However, the predominant storm direction is from the northeast and tends to counter the southeasterly-driven, longshore movement of beach material.

The distribution of the longshore component of wave energy along the southeast Virginia coast is controlled by the nearshore bathymetry. Wright *et al.* (1987) performed a wave climate analysis using a linear wave propagation model, RCPWAVE, developed by the U.S. Army Corps of Engineers (Ebersole *et al.*, 1986) that computes changes in wave characteristics that result naturally from refraction, shoaling, and diffraction over complex shoreface topography. The results of the analysis in Wright *et al.* (1987) indicate a concentration of wave energy in the area just south of Sandbridge. This corresponds to a nearshore increase in water depth where higher potential wave energies may reach the coast (Figure 2). This region also has the highest rate of shoreline recession on the southeast Virginia ocean coast and is considered an area of divergence, or a "nodal" zone, where shore zone sediments are transported northward and southward toward Cape Henry and False Cape (Everts *et al.*, 1983).

Further complications in nearshore bathymetry exist due to the occurence of Sandbridge Shoal (Figure 1). Maa (1995) indicates that the existence of Sandbridge Shoal may tend of concentrate wave energy into the area of high shoreline recession. Boon (1997) found a similar tendency. The inference here is that removal of Sandbridge Shoal due to mining for beach nourishment may decrease the wave concentration in the area of highest shoreline recession.

The onshore-offshore component of sediment transport at Sandbridge was described by Wright *et al.* (1991). Wave gauge deployment during November 1988 on the shoreface of Sandbridge embraced some contrasting moderate wave energy events and provided insight into the processes that operate during non-storm autumn and winter periods. The results for Sandbridge indicate that incident waves are the principal agent of sediment flux and suggest that wave-driven transport in the seaward direction may be nearly as important as in the shoreward direction (Wright *et al.*, 1991).

On a regional scale, the nearshore zone along the southeast coast of Virginia influences the wave climate because the False Cape and Cape Henry shoal complexes tend to act as headlands. The southeasterly wave field is impacted first by the False Cape headland which refracts and diffracts the wave field. Northeasterly waves are refracted and diffracted by the Cape Henry shoals. Sediments of the shore and shoreface are driven both north and south from the nodal divergence zone by the impinging wave climate to help "feed" the adjacent headland shoal areas. The headland shoals display a much gentler offshore bathymetric gradient than the nodal divergence area. A steeper shoreface bathymetric gradient near the nodal point allows significant "planing" by wave processes and sea-level rise that cut into the underlying coastal strata which serves as a sediment source (Swift *et al.*, 1985).

Sediment Transport

Everts *et al.* (1983) described the divergence or nodal zone just south of Sandbridge where transport processes cause alongshore sediment movement north and south. This was

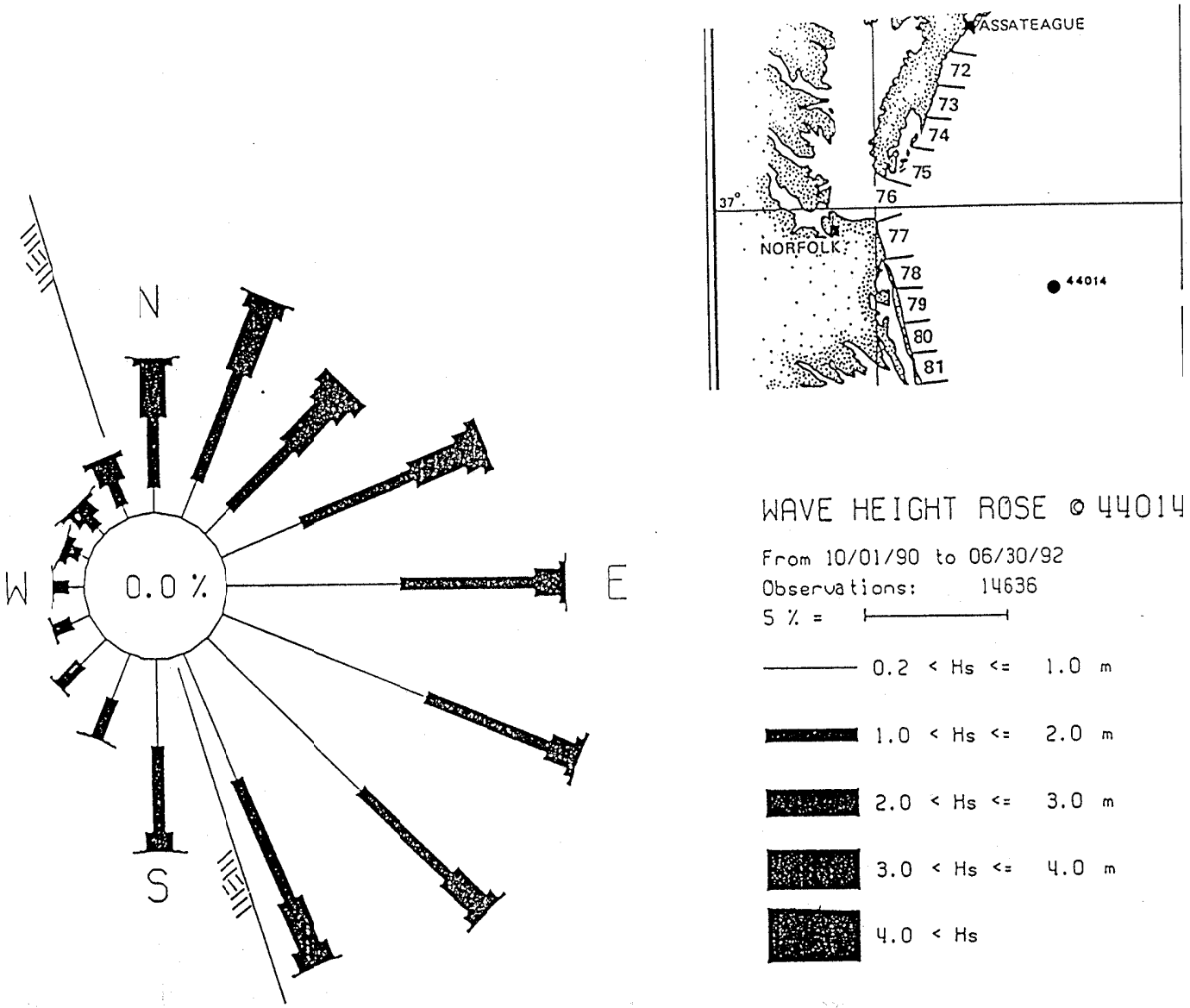

Figure 4. Wave rose diagram from NOAA Buoy 44014 (from Maa, 1995) and locations of Buoy and Wis Stations.

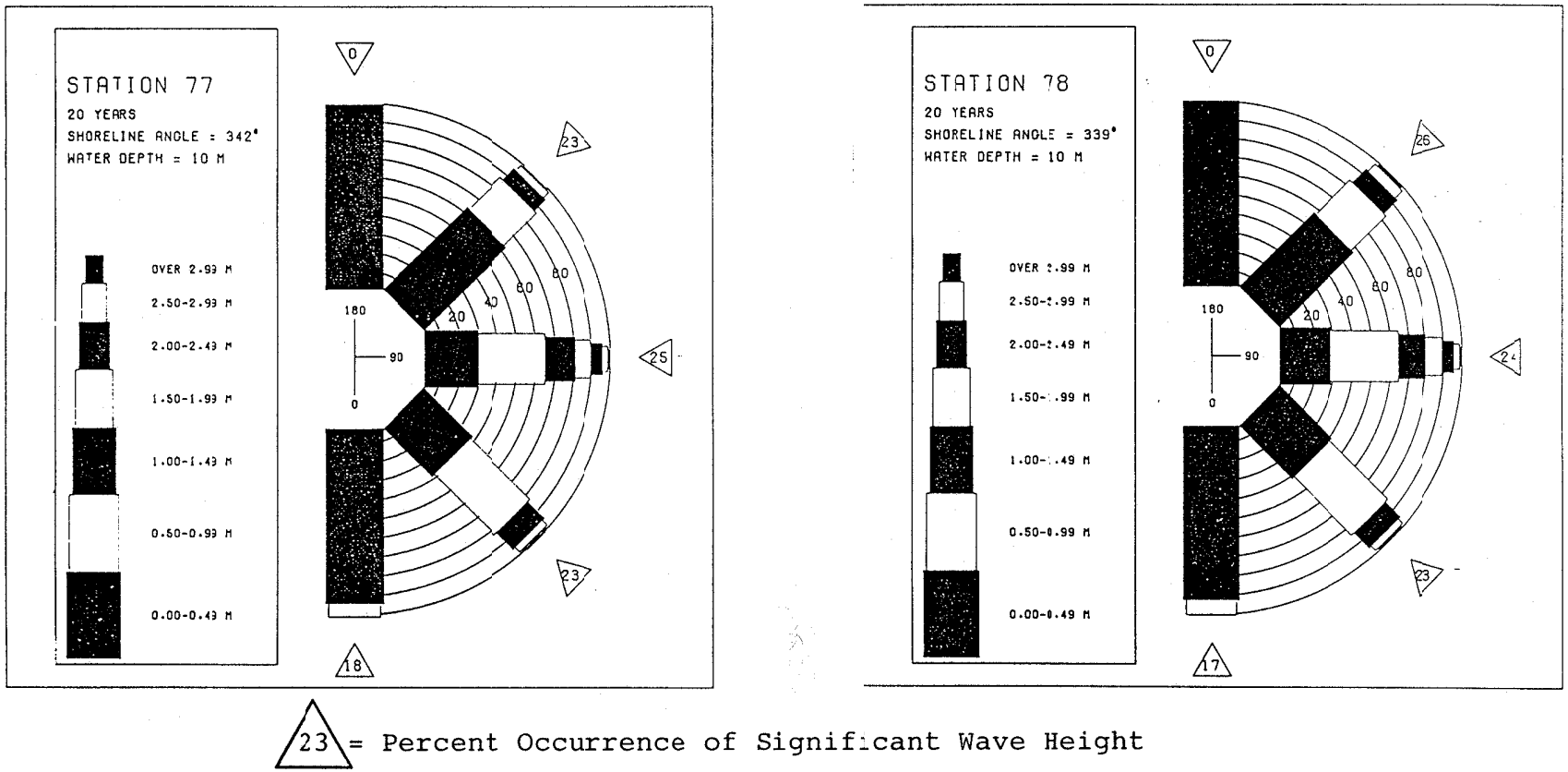

Figure 5. Wave rose diagram from WIS Phase III stations 77 and 78.

substantiated by Waterways Surveys and Engineering (1986) and Wright *et al.* (1987). Waterways Surveys and Engineering (1986) determined sediment transport rates from sedimentation and dredging of Rudee Inlet. They estimated a gross transport rate (Q) to the north of 488,000 cy per year and a Q to the south of 288,000 cy per year. This results in a net northerly alongshore rate of 200,000 cy of sand per year. The implication at Dam Neck would be a similar net rate of alongshore sediment transport to the north. Onshore-offshore transport is not included in this estimate but may be a significant factor related to the DNBNP.

Methods

Shore Profiles

A long-term beach and nearshore profile survey data set was obtained from the City of Virginia Beach's survey department. This data set was created between 1980 and 1996 and includes dune and beach surveys to MLW. Early surveys were taken each quarter (i.e. spring, summer, fall and winter). Two times per year, select profiles (numbered 43, 45, 48) are run offshore to approximately 25 ft. below mean sea level (MSL). The survey methods include transit and stadia for the beach and dune portions of the profile and fathometer and sled for the offshore section. For this project, eight of the City's profiles, numbered 43 to 50, from Rudee Inlet to the north end of Sandbridge were analyzed (Figure 6 and Table 1). Profiles 43 and 44 define the boundaries of Croatan Beach. Profile 45 is on the Naval Amphibious Base property. Profiles 46, 47 and 48 are on Dam Neck property, and profiles 49 and 50 occupy the north end of Sandbridge.

The location of VIMS's survey at profile 43 was slightly south and about 25 ft. in front of the City's profile since the City's profile crosses the beach near the groin, and sediment samples could not be taken directly offshore. The City stopped survey profile 45 in 1984 and profile 46 in 1990 (Table 1). Access to profile 45 was difficult since it is a military training area; the City's benchmark was not recovered. VIMS personnel set a wood stake at the approximate location of profile 45 and used the Global Positioning System (GPS) to locate the stake and get an elevation. The City benchmark at Profile 46 still exists, but surveying is difficult since it is a military rifle range. The benchmarks at profiles 47 and 49 were reset in 1996. Profile 49 was reset in about the same location, but profile 47 was moved about eight ft. north and 25 ft. east.

The City's raw data from field books were databased with the Interactive Survey Reduction Program (ISRP) (U.S. Army Corps of Engineers, 1994). The data was plotted and checked for errors and bad points. Profile analysis followed procedures outlined by Larson and Kraus (1994). This includes an analysis of individual profile parameters including change in the position of MHW, the average shoreline change through time, seasonal plots, and the maximum and minimum, the mean profile and standard deviation.

The profiles were surveyed by the City in August 1996 before the DNBNP. The same profile lines were surveyed by the VIMS six months (May 1997) after installation and one year later (October/November 1997). The subaerial beach, out to 2 ft. below MLW, was surveyed in detail with transit and stadia. Due to lack of high resolution offshore survey gear, only depth change at the position of sediment sampling was measured (see section C, below). Sediment

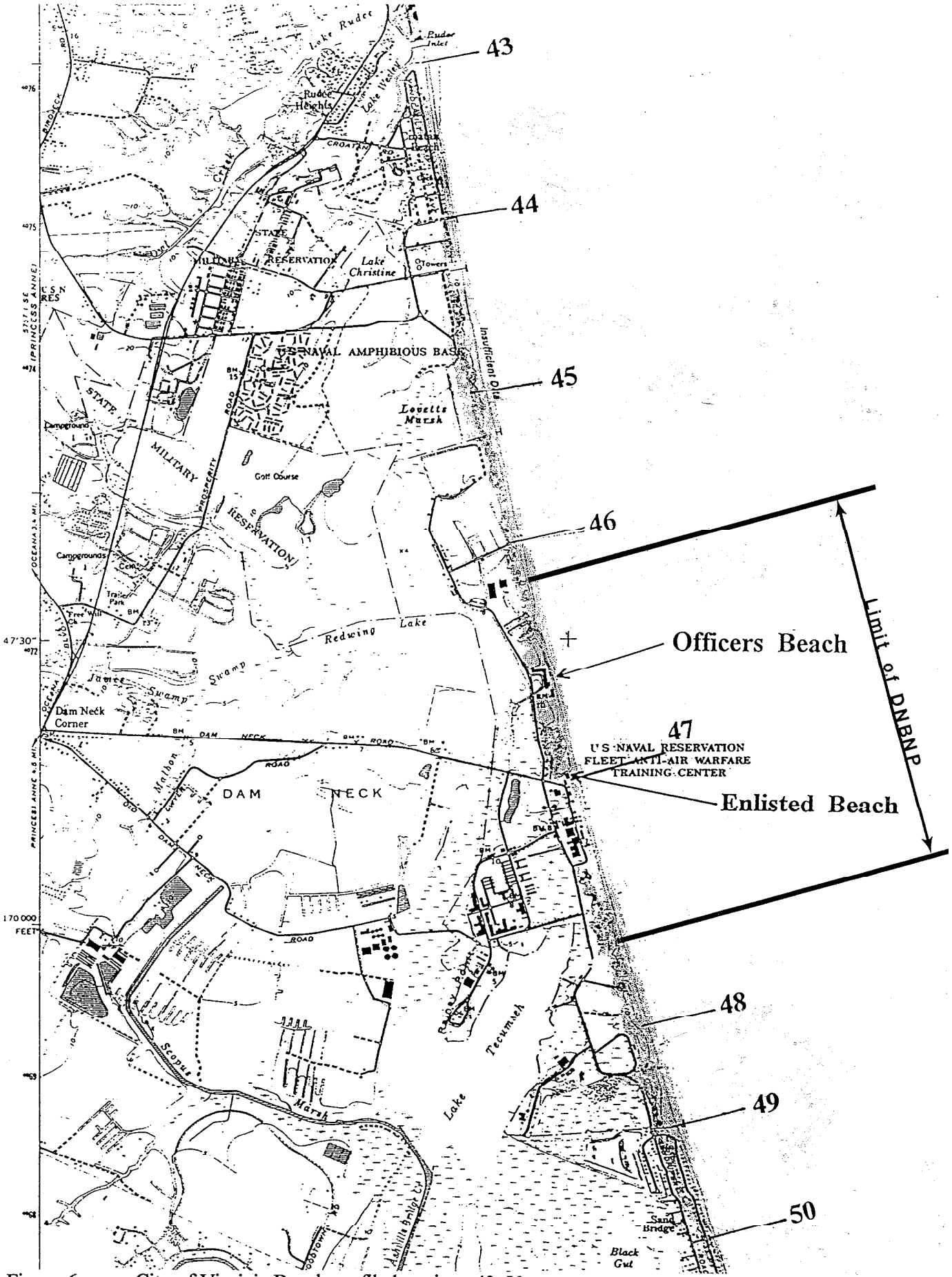

Figure 6. City of Virginia Beach profile locations 43-50.

samples also were acquired at each date for the beach and offshore regions, to a depth of 24 ft. below MSL.

Aerial Imagery

VIMS operates a U-6A DeHavilland Beaver to further its research and educational mandates. The very low minimum controlled flight speed is an asset both to aerial observation and photography and to operations in and out of short, unimproved landing areas. VIMS can obtain vertical photography in 70-mm format on a variety of film types. Two Hasselblad 500ELM cameras can be used together allowing the acquisition of identical images on two different film types. The cameras are equipped with motor driven film advances, simultaneously controlled, electronic shutter releases, and an intervalometer.

The study site was flown by VIMS's plane and personnel before the fill project (August 1996), just after the project (November 1996), in April 1997, and September 1997 to obtain low-level vertical imagery. Eight inch square, non-rectified photos with 60% overlap at a scale of 1"=200' were obtained. A mosaic was created with the photos and used to plot the position of MHW through time.

Sediments

Sediment sampling locations followed the general plan outlined in Figure 7. Sediment grab samples were taken along profiles 43 to 50 prior to the DNBNP (August 1996), after six-months (May 1997) and after one year (October/November 1997). Dune, beach and nearshore samples to -2 ft. MLW were taken by hand from shore. Offshore sediments at -6, -12, -18 and -24 were acquired with a grab sampler from a boat. Three grab samples were taken for each offshore location to create a composite sample.

Offshore sampling for the three sampling periods was based on returning to the same location (i.e. latitude/longitude) each time by using a differential GPS. Depths for the second and third sampling period may have changed, but the sample names remained the same. Dune, beach and nearshore samples were taken at the designated morphologic feature (i.e. dune, berm, mid-beach, etc.). Sediments were analyzed for percent gravel, sand, silt and clay. The VIMS Rapid Sand Analyzer (RSA) was used to determine the grain size distribution of the sand fraction. Sediment sample information is in Appendix A including the latitude and longitude position of the offshore samples and the distance from the benchmark of the beach samples.

The grain size distribution of beach sand generally varies across the shore and to a lesser degree, alongshore as a function of the mode of deposition. The coarsest sand particles usually are found where the backwash meets the incoming swash in a zone of maximum turbulence at the base of the subaerial beach; here the sand is abruptly deposited creating a step or TOE. Just offshore, the sand becomes finer. Another area of coarse particle accumulation is the berm crest, which is sometimes coincident with the last high tide line (LHT), where runup deposits all grain sizes as the swash momentarily stops before the backwash starts. The dune or backshore generally contains the finest particles because deposition here is limited by the wind's ability to entrain and move sand (Bascom, 1959; Stauble *et al.*, 1993).

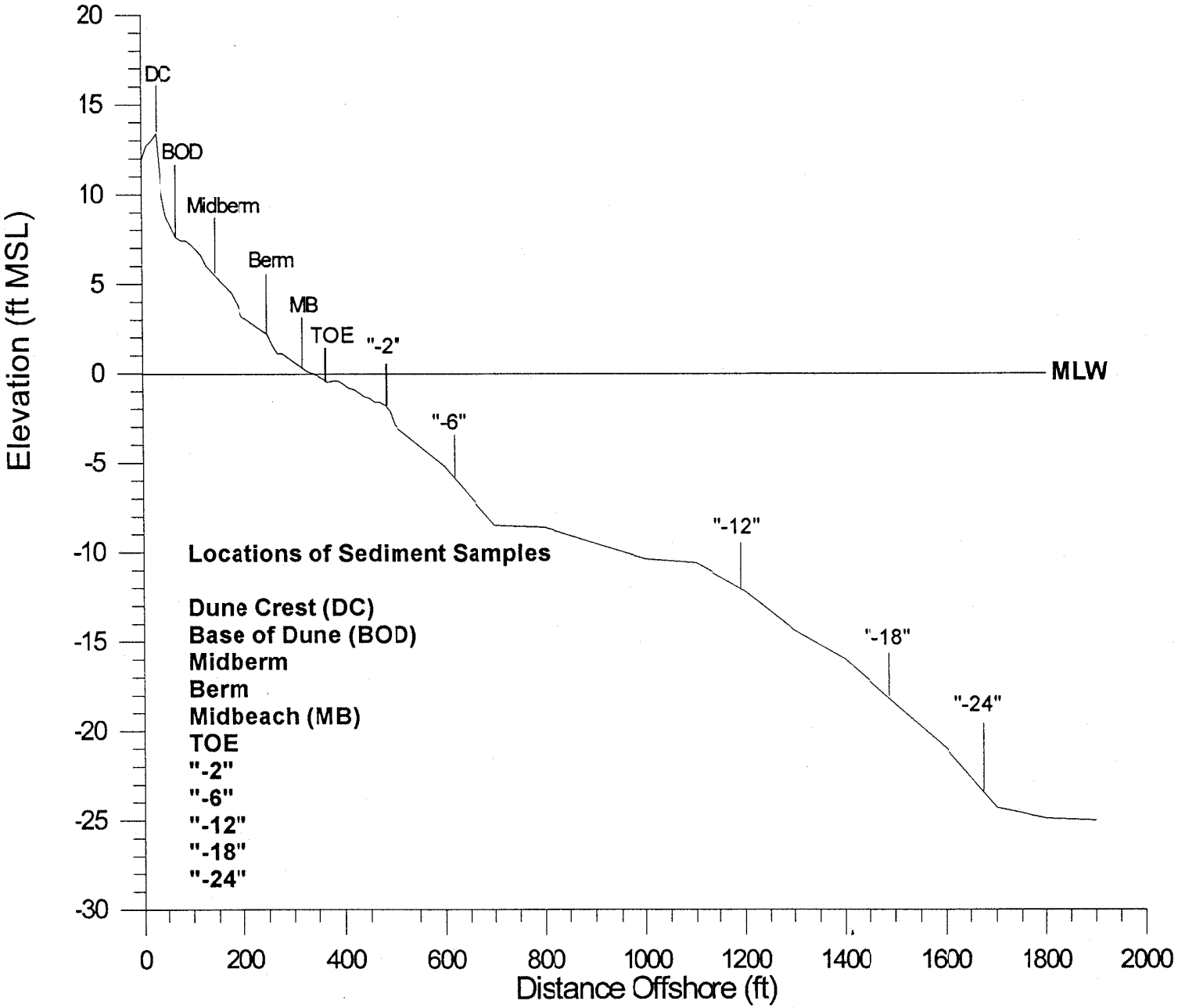

Figure 7. Typical profile and morphologic features with sediment sample locations.

Sediment statistics were developed for median grain size and sorting. Both statistics are common parameters in discussing sediment characteristics and are used frequently in beach assessments (Stauble *et al.* 1993; Larson and Kraus, 1994). The median is defined by one half the particles are coarser and one half are finer, but it is not particularly useful for bimodal sediments. The mean is a better parameter but the median is most commonly used (Folk, 1980). Sorting is a measure of sediment uniformity and can be obtained by several methods of determining standard deviation. The spread of the grain size distribution about the mean defines the concept of sorting. Well-sorted sands have only a few size classes present in the sample. Poorly-sorted sands are represented by most size classes (Friedman and Sanders, 1978). For this study, the Inclusive Graphic Standard Deviation (Folk, 1980) is used. The method of moments was used on the sediment data (Appendix A), but even though it is generally a more accurate method of describing a sample, it is not discussed since previous studies of the sediment characteristics of Virginia's southeast coast utilize the graphic method of statistic determination.

Table 1

Station VIMS	Designation Virginia Beach	Mark Type	NAD 1983 (ft) 198 Northing	NAD 1983 (ft) Easting	NGVD 1929 Elevation	Date Established	Total Surveys	Inclusive Dates	Long Short
43	M-07 (Reset)	Disk	3,471,104.9210	12,223,512.1990	11.28	August 1982	33	1980-1996	L
44	PRO 5-2	Disk	3,467,422.8220	12,224,120.0630	18.79	July 1980	33	1980-1996	S
45	M-08	Disk	3,464,472.3276	12,224,827.4200	15.22 (1929)	July 1980			
	DN3 (VIMS)	Stake	3,463,509.2776	12,225,077.4048	21.65 (1983)	August 1996	17	1980-1984	L
46	PRO 6-2	Disk	3,459,920.4941	12,225,924.9005	22.691	June 1980	22	1980-1990	S
47	N-010	Disk	3,454,568.3790	12,227,383.0190	22.98	July 1980			
	N-010A	Disk	3,454,576.4990	12,227,407.8060	22.81	1996	32	1980-1996	S
48	PRO 7-2 (Reset)	Disk	3,448,874.9164	12,229,068.5090	13.071	June 1980	32	1980-1996	L
49	PRO 8-2	Disk			15.55	June 1980			
	PRO 8-2A	Disk	3,446,301.3690	12,229,839.4310	14.22	1996	34	1980-1996	S
50	N-012	Disk	3,443,888.5360	12,230,750.8950	8.57	June 1980	29	1980-1996	S

Information on the City of Virginia Beach's profile data.

Results

Long-Term Historical Trends

The long-term rate of shore change at the location of the eight study profiles was determined by Everts *et al.* (1983) (Figure 8) and is summarized in Table 2. The MHW position was determined for each date at each profile location. From 1859 to 1925, there is a similar rate of shoreline erosion for all profiles that ranges from -4.5 ft. per year (ft/yr) at profile 46 to -2.9 ft/yr at profile 49. The trends from 1925 to 1980 show similar magnitude of recession between profiles 47 to 50. However, a significant accretionary trend becomes evident in profiles 43 and 44, a reduced erosion rate at profile 45 and slight accretion at profile 46. This may be attributable to the stabilization of Rudee Inlet by jetties and the subsequent bypass system. The jetties would act as littoral barriers that stack sand to the south. The jetties and inlet dredging significantly modify the net long-term trend from 1859 to 1980 for profiles 43 and 44.

Table 2

	Historic Shore (ft/yr)		Change*	Virginia Beach *Net Shore* (ft/yr)		Profiles *Change*	Average Change (ft/yr)
Date	1859-1925	1925-1980	1859-1980	1980-1996	1980-1984	1980-1990	
Span (yrs)	66	55	121	16	4	10	
Profile #							
43	-3.0	5.1	0.66	2.9			19.4
44	-3.0	0.5	-1.7	1.2			12.9
45	-3.6	-0.91	-2.4		-3.8		1.8
46	-4.5	1.4	-2.1			-2	1.4
47	-3.0	-2.0	-2.5	-5.4			-1.9
48	-3.3	-2.55	-3.1	-0.6			-0.4
49	-2.9	-4.4	-3.4	-0.6			4.7
50	-3.2	-3.82	-3.5	-3.4			-4.9

* Data from Everts *et al.* (1983)

Shoreline change rates from historical data and the City of Virginia Beach's data set.

City Monitoring, 1980-1997

Analysis of the City's beach survey data shows the variability of shoreline and shoreface change along this subreach over the past 16 years. One portrayal of shore change is the movement of a tidal contour through time. Following historical methods, the position of MHW for each study profile was plotted through time (Figures 9A-9H). Except for the very high

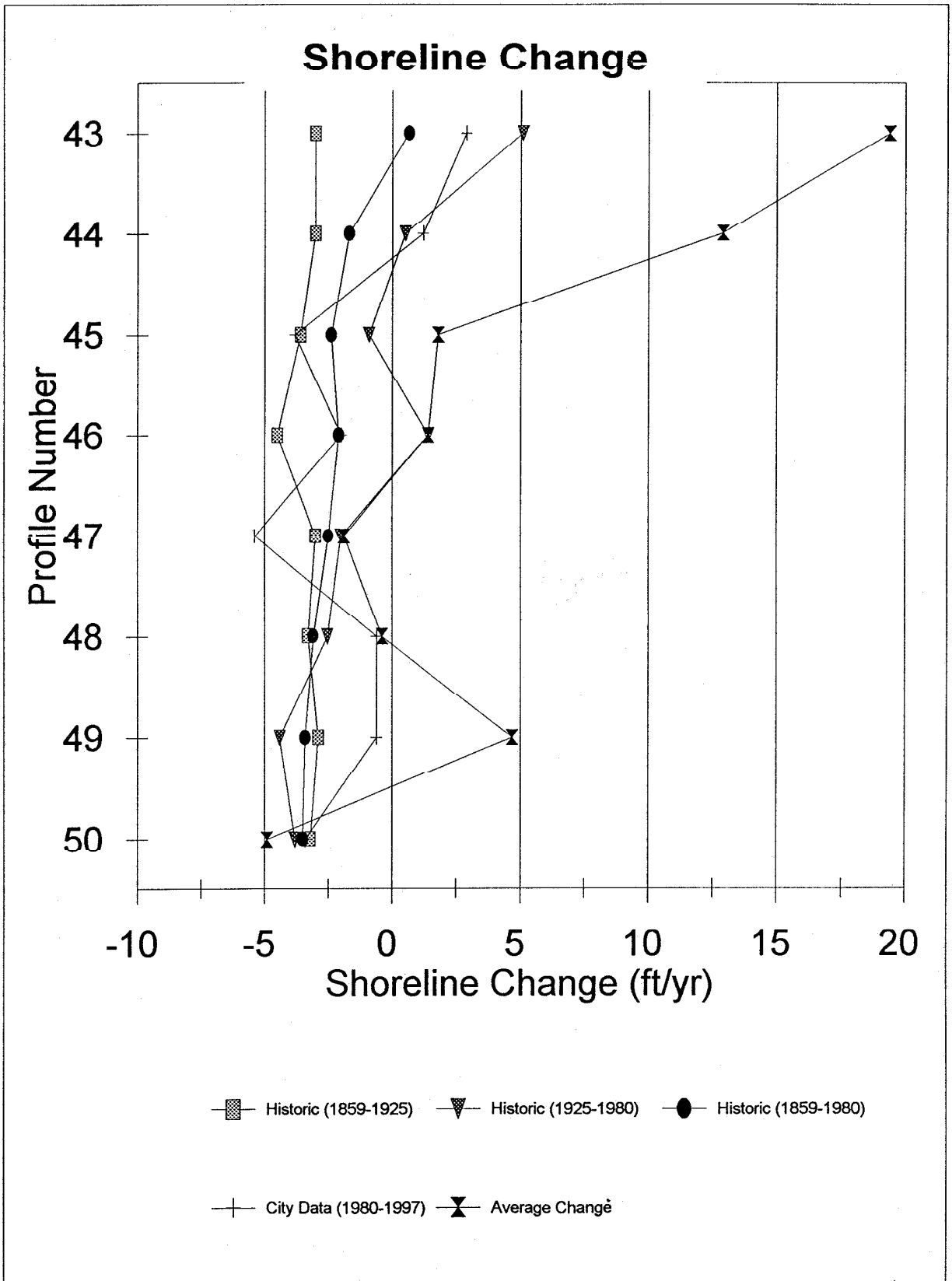

Figure 8. Historical shore change for the eight study profiles (long-term data from Everts *et al.*, 1983 and City data).

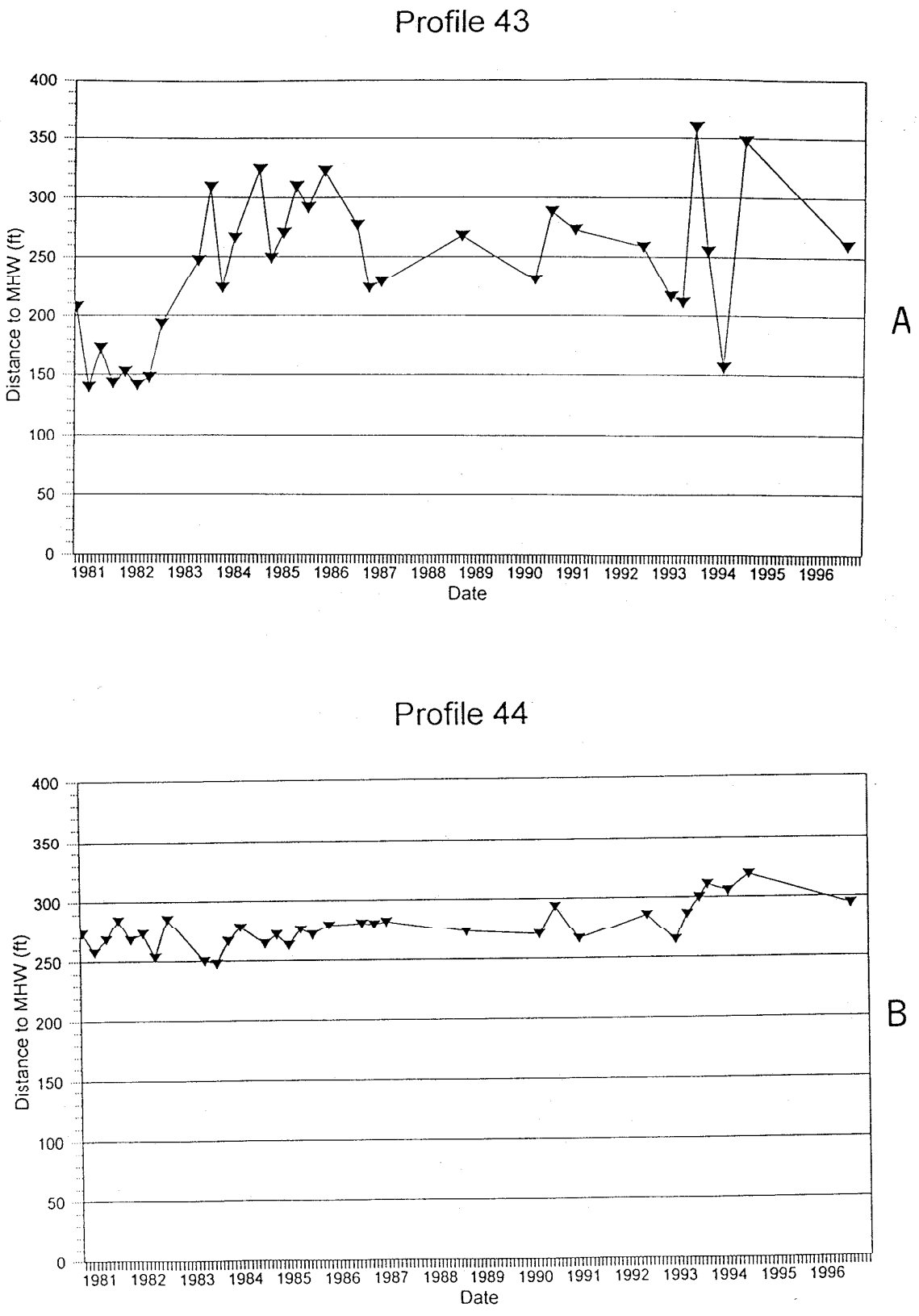

Figure 9. Change in position of MHW for A) profile 43 and B) profile 44.

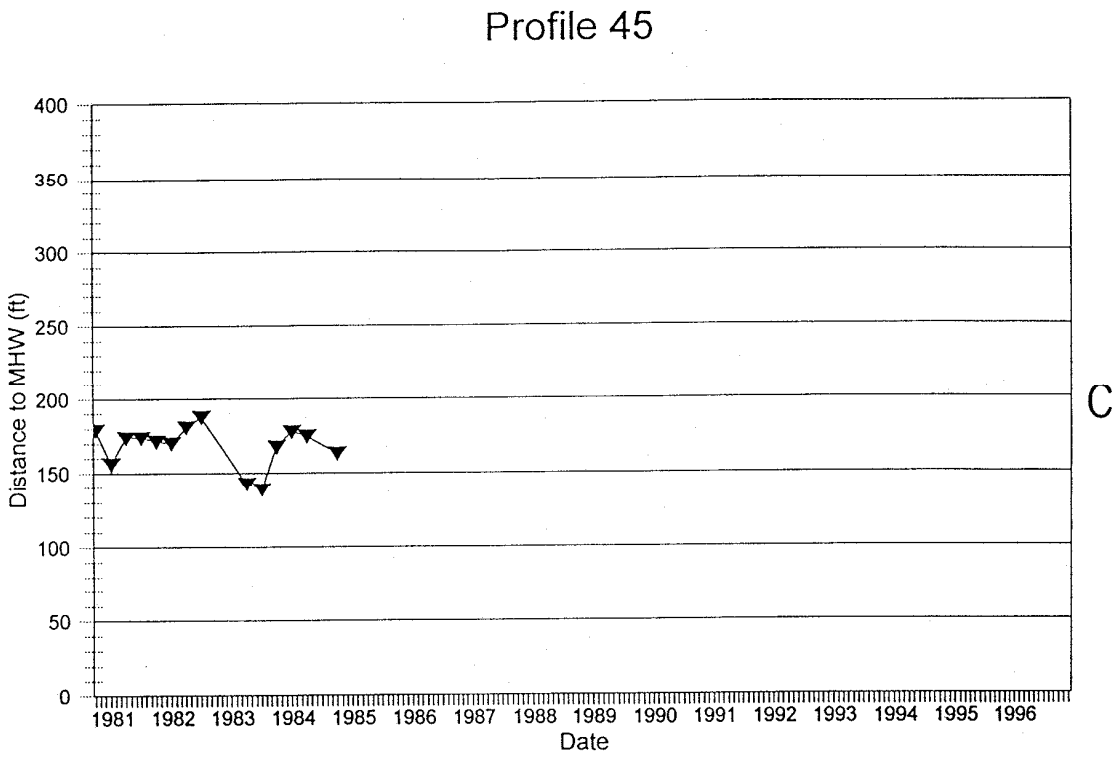

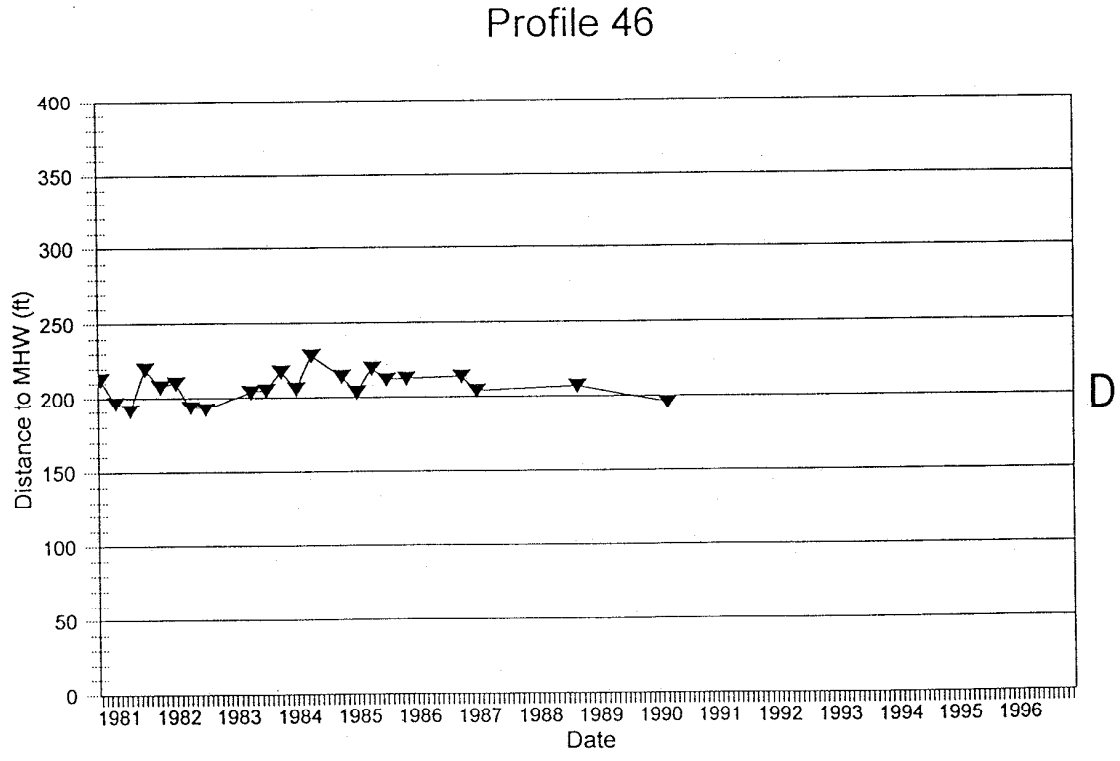

Figure 9. Change in position of MHW for C) profile 45 and D) profile 46.

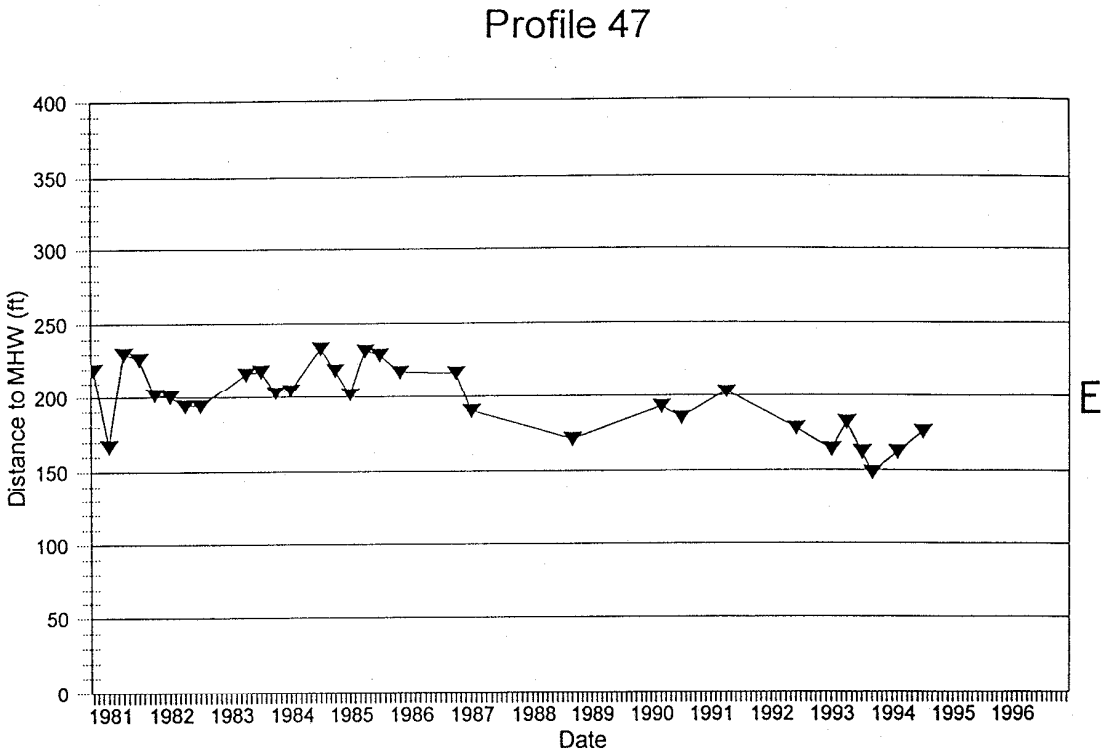

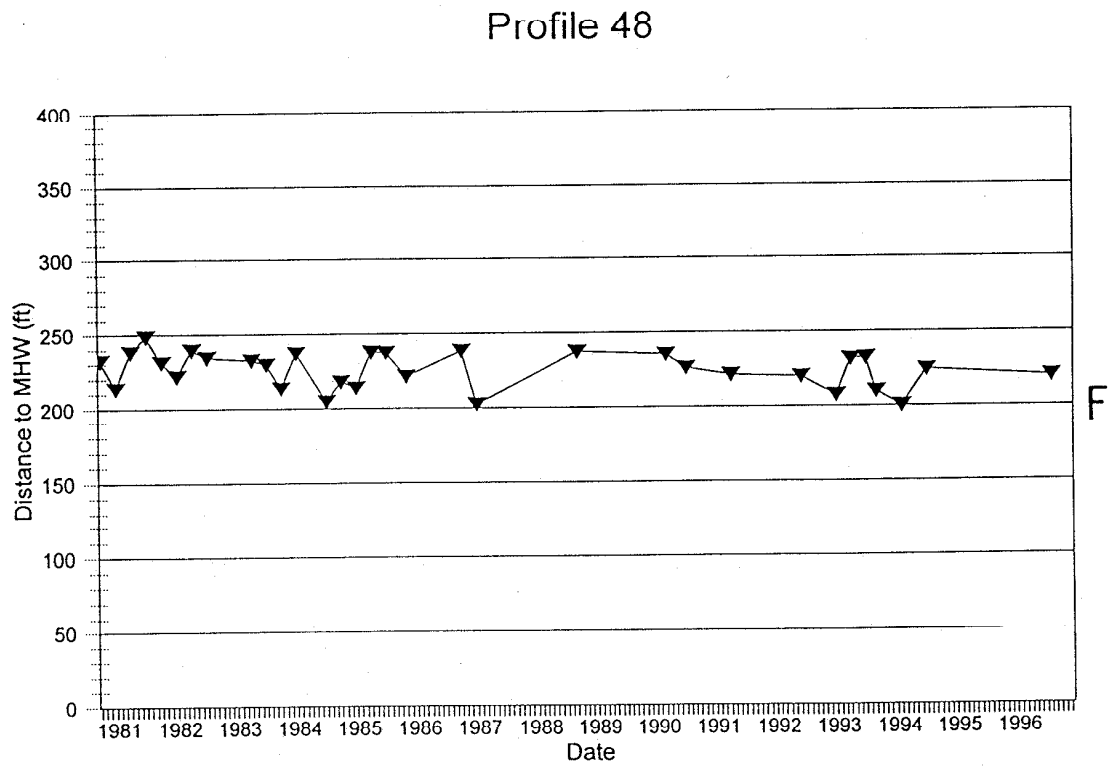

Figure 9. Change in position of MHW for E) profile 47 and F) profile 48.

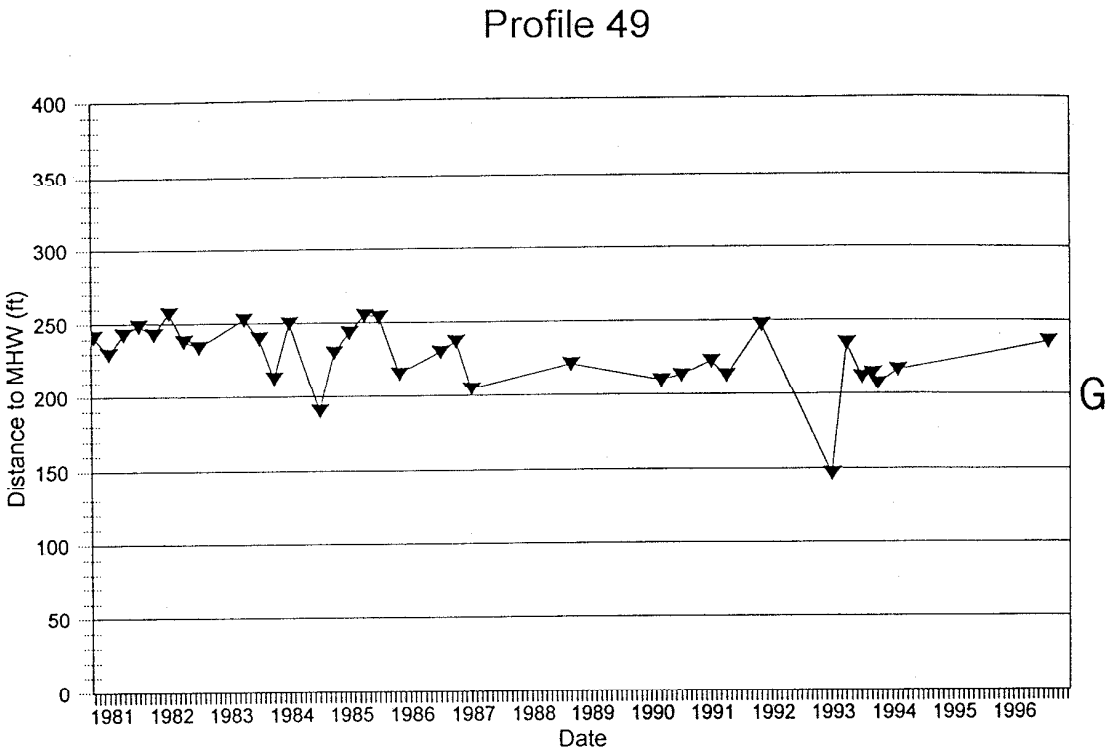

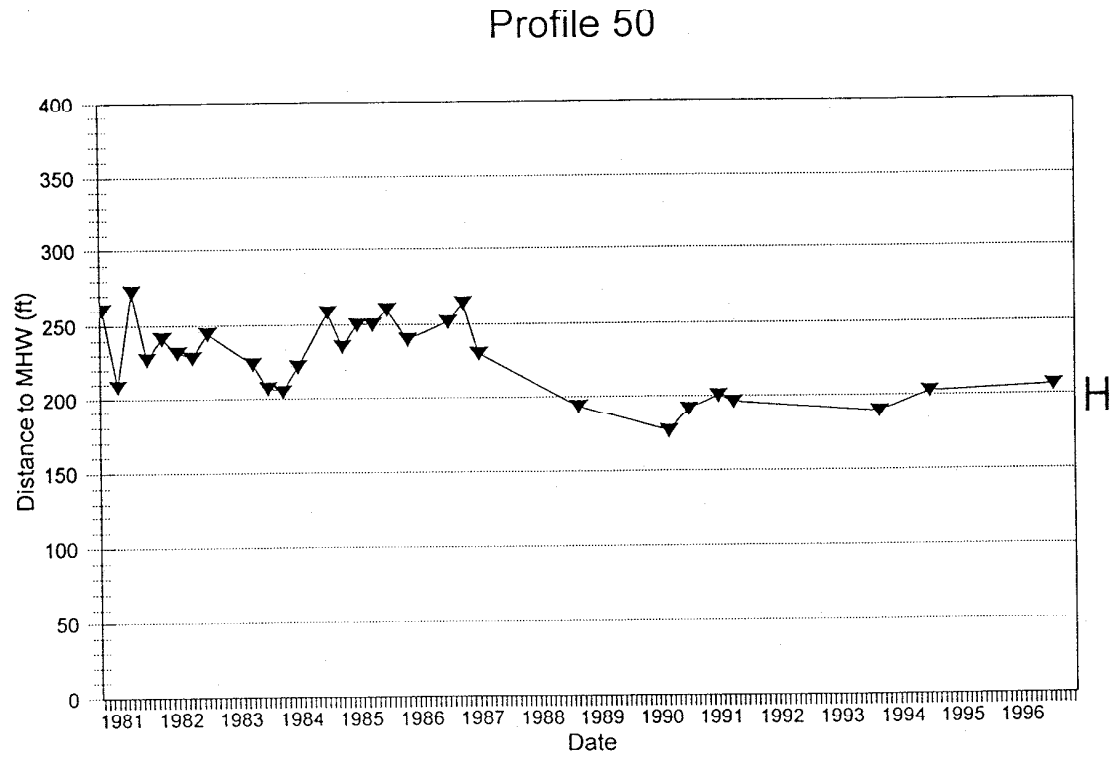

Figure 9. Change in position of MHW for G) profile 49 and H) profile 50.

variability in profile 43 (Figures 9A), the other profiles indicate large seasonal fluctuations where data was taken quarterly and possibly a subtle trend toward erosion, accretion or relative stability depending on the individual profile. The rate at which these trends occur along this subreach has broader regional implications as modifications to the shoreline continue to have an impact (i.e. Sandbridge bulkheads, DNBNP, and a proposed beach nourishment at Sandbridge).

A simple method to determine rate of change is the **End Point Rate** method (EPR), described by Fenster *et al.* (1993), which is similar to picking a tidal datum off aerial imagery in its relative randomness. For example, for this study, the difference between the positions of MHW at two dates were multiplied by the number of years between the dates to get a rate of change in ft/yr for each profile. These rates are shown in Figure 8 and compared against rates from Everts *et al.* (1983). Since this method is similar, these data could be the position of MHW from two aerial photos flown at those times. However, all in all, the trends using the **EPR** are similar to the historical plots.

In order to ascertain an overall trend for each profile, the average shoreline change at MSL in ft/yr was determined (Figures 10A-10H). This average of the rates through time for each profile also is plotted against the historical trends and the values obtained by the EPR method (Figure 8). The plot describes the accretionary trend that is being enhanced by Rudee Inlet. Although more detailed analysis is necessary, the present study shows an increased rate of accretion south of Rudee Inlet according to City data. This trend appears significant down to profile 46 with profile 43, which is adjacent to Rudee Inlet, having the highest average rate of shoreline change at +19.4 ft/yr. Shoreline recession continues at profiles 47 and 48 but at less than historical rates. Finally, the north end of Sandbridge has an increased accretion rate at profile 49 and a corresponding loss at profile 50. This plot includes data prior to and after bulkheading began in 1988 which, no doubt, modifies the natural trend.

Seasonal fluctuations across the study profiles, shown in Figures 11A-11H, are plotted along with the average profile for all surveys. Table 3 lists the survey dates that were assigned to each grouping used to determine the seasonal mean profile. The mean seasonal profiles are represented for winter, spring, summer and fall by January, April, July and October, respectively. Generally, subaerial beach accretion occurs in the summer or fall; beach erosion occurs in the winter or spring. The plots show that the July or summer profile has the highest berm. Most of the profiles are lowest in January except profiles 43, 44 and 45 which have their lowest profiles in April. Both the January and April mean profiles can be indicative of a winter profile. The maximum vertical change occurs across the beach berm feature between +4 and +6 ft. MSL and the backshore region. This is the active subaerial beach and swash zone that is subject to frequent wave runup and overtopping. Profile 50 shows the development of a nearshore bar on the January mean profile indicating that sand is stored in a bar system during the winter.

Since the long profiles (43, 45 and 48) generally are surveyed only in the spring and fall, mean profiles plotted for winter and summer do not extend beyond about MLW. The offshore trend shows that there is a "crossing point" on the long profiles where the inshore portion of the profile to MLW show accretion in the fall and erosion in the spring. Seaward of the crossing, the trend is less clear, but, generally, the opposite is occurring with profile accretion in the spring and erosion in the fall. After a summer of milder waves, sand has moved closer to the shoreline since

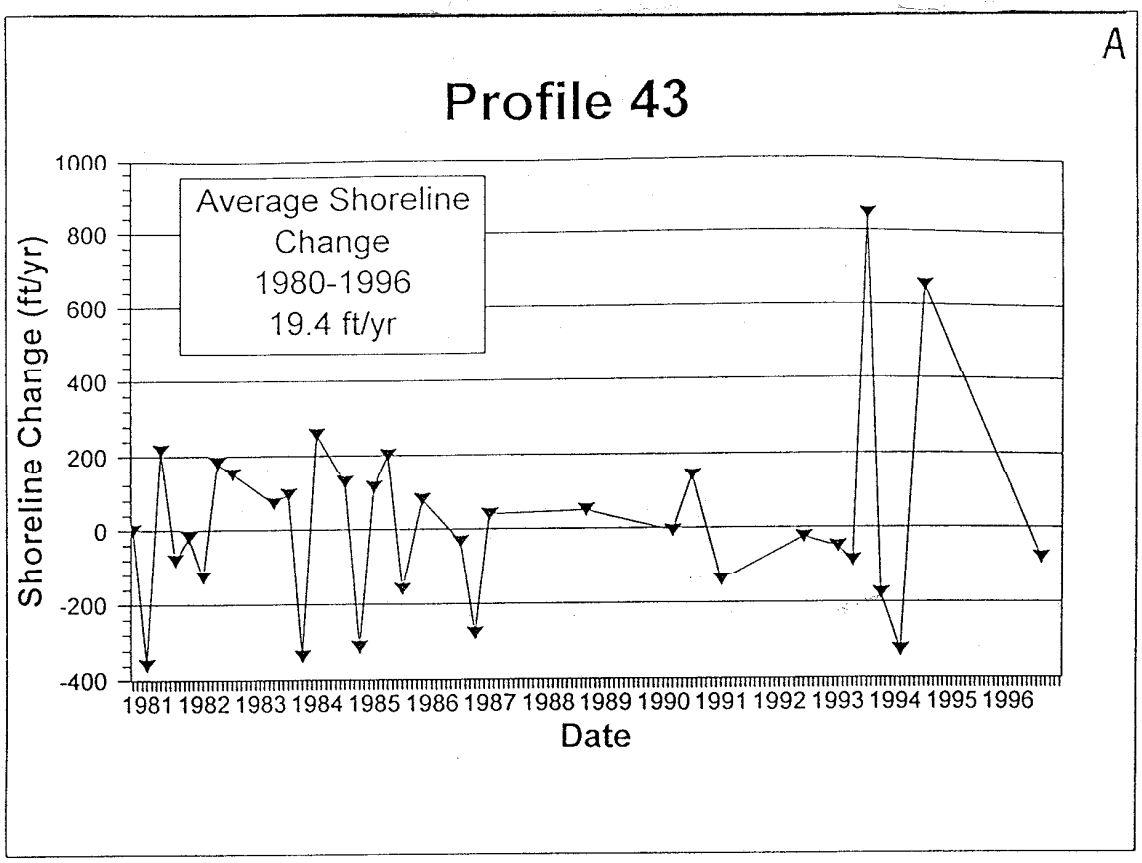

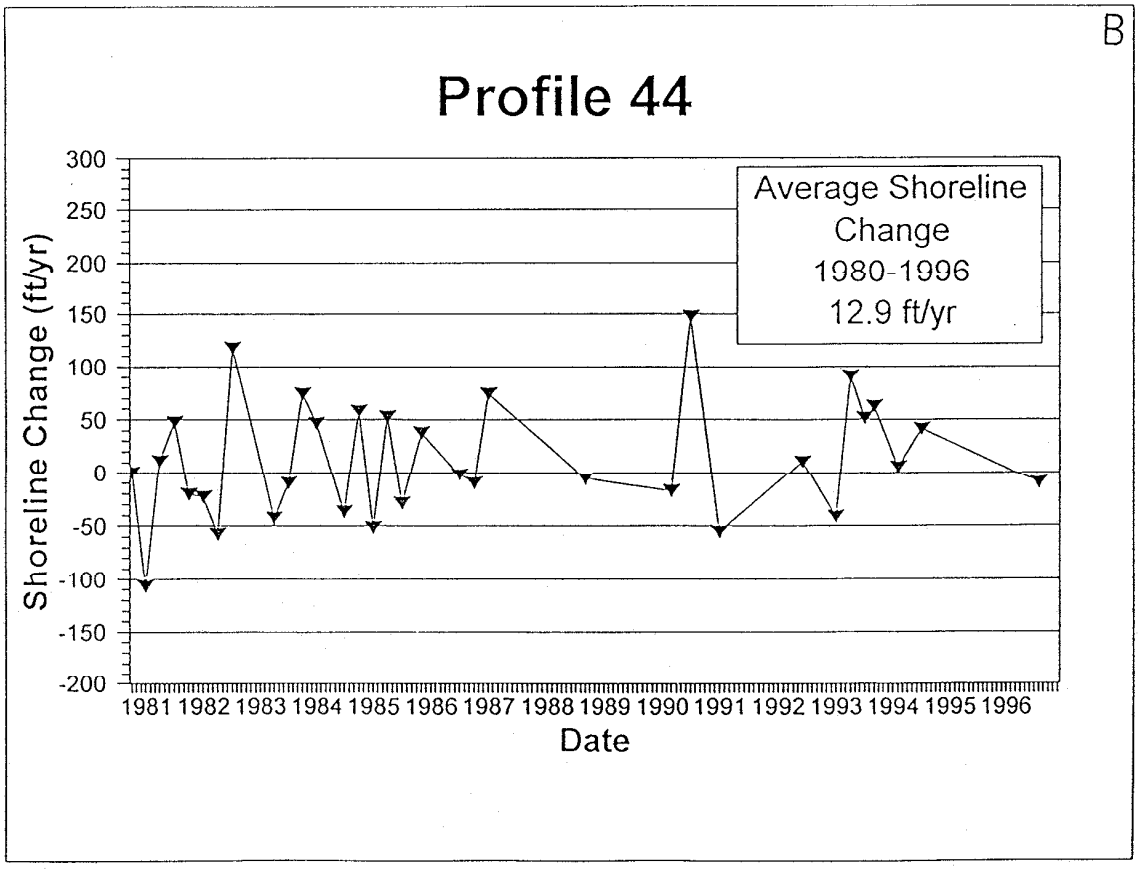

Figure 10. Rate of shoreline change for A) profile 43 and B) profile 44.

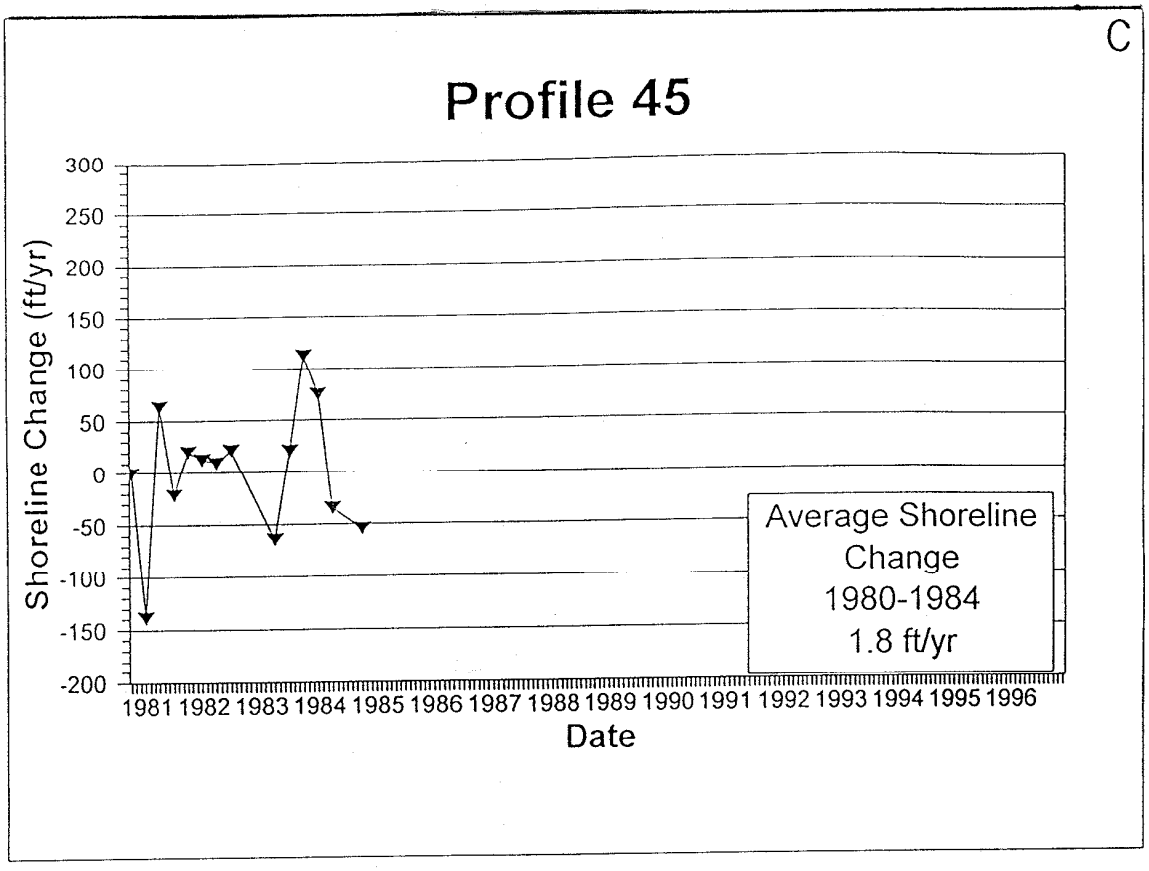

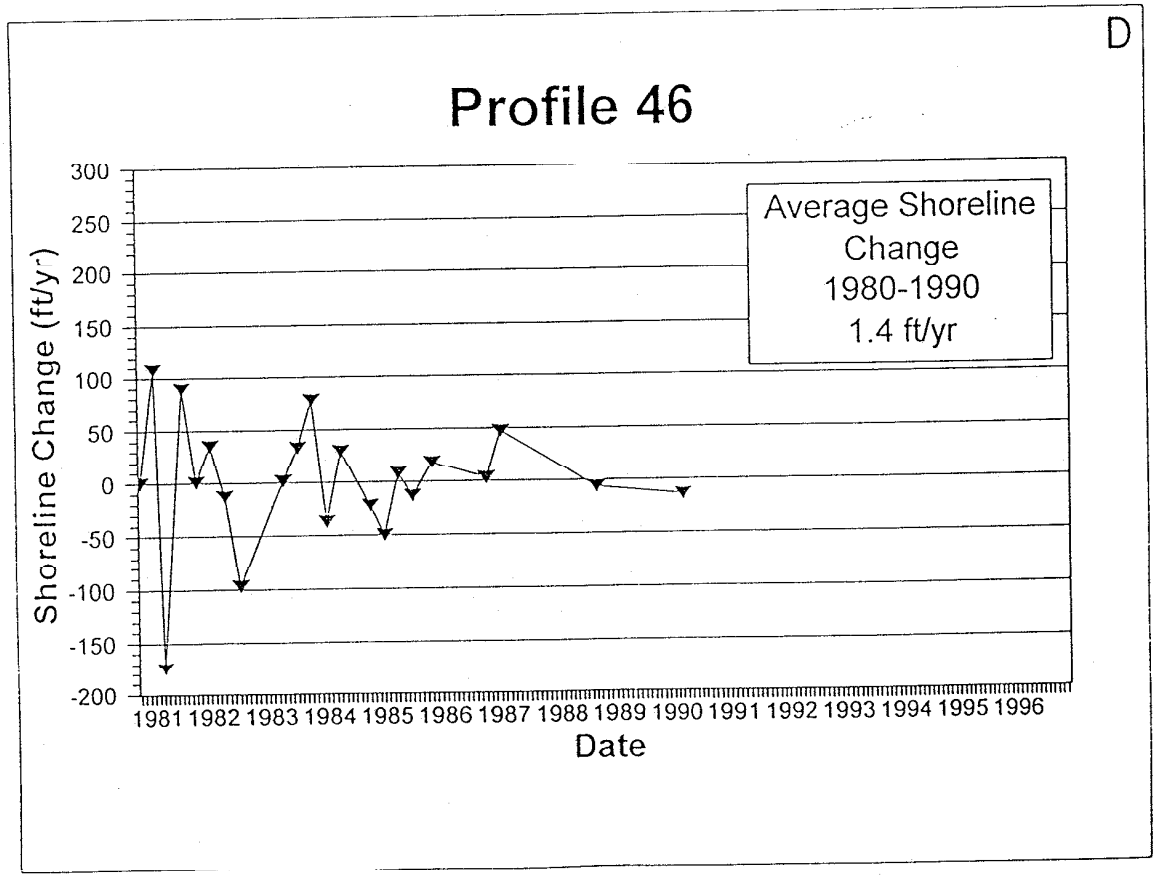

Figure 10. Rate of shoreline change for C) profile 45 and D) profile 46.

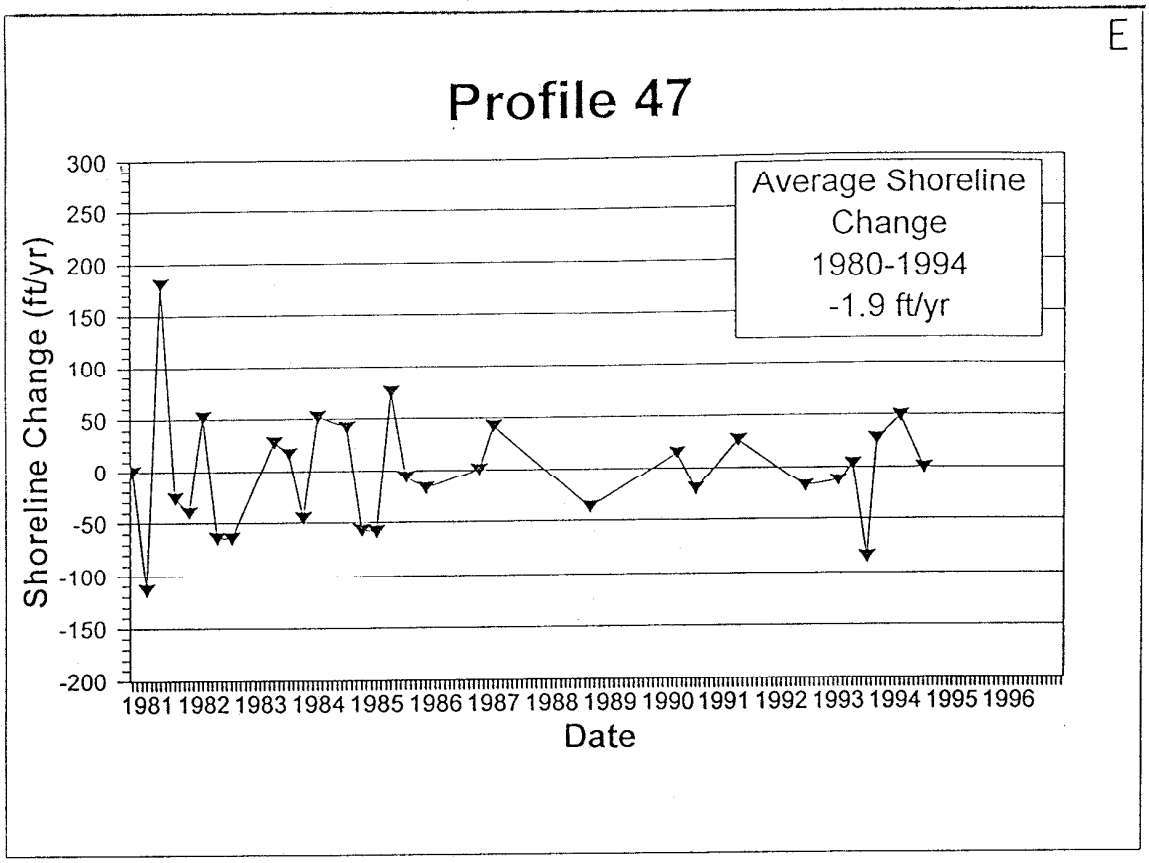

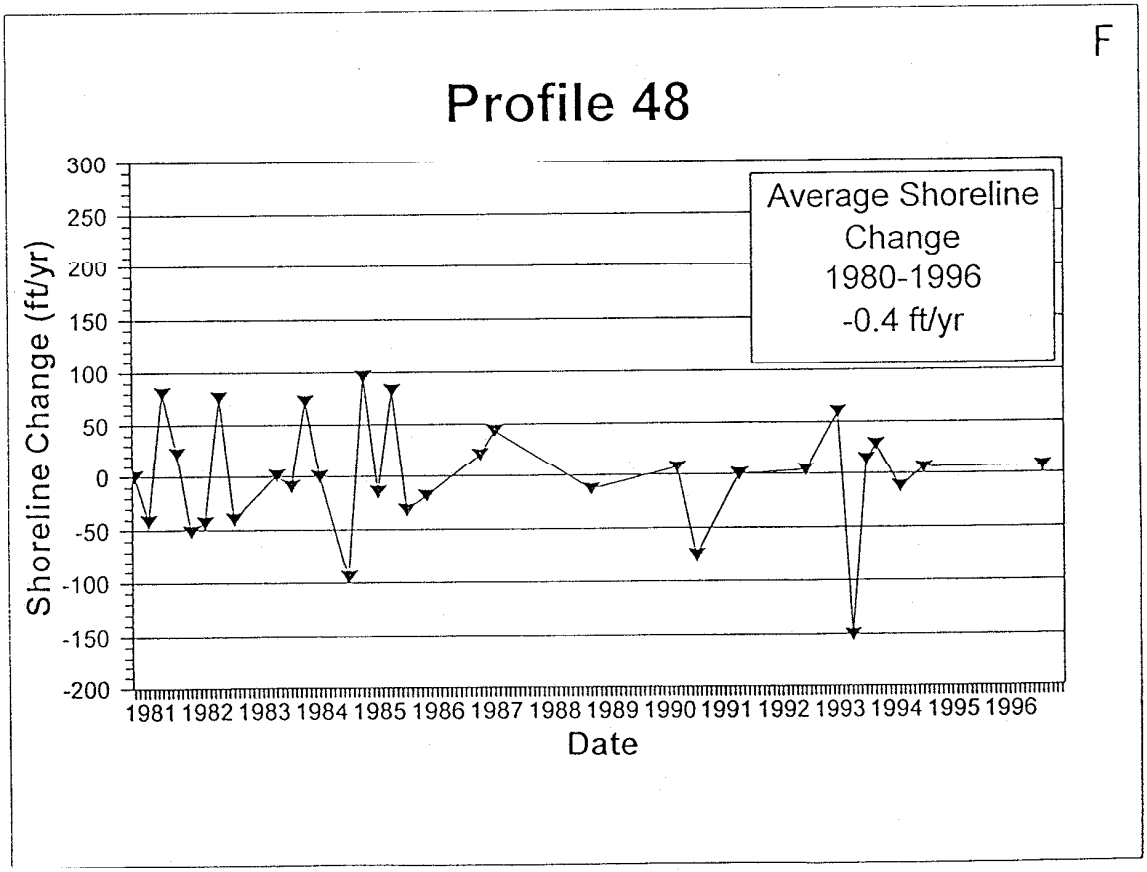

Figure 10. Rate of shoreline change for E) profile 47 and F) profile 48.

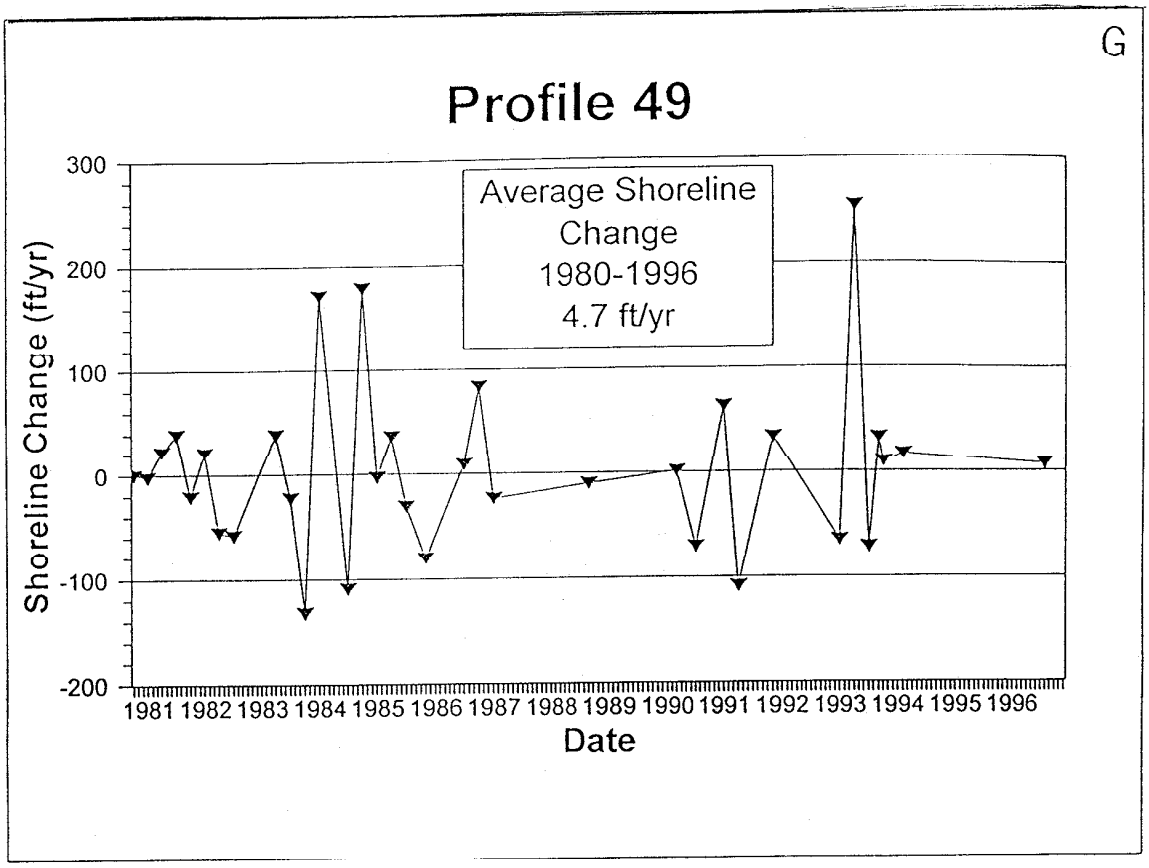

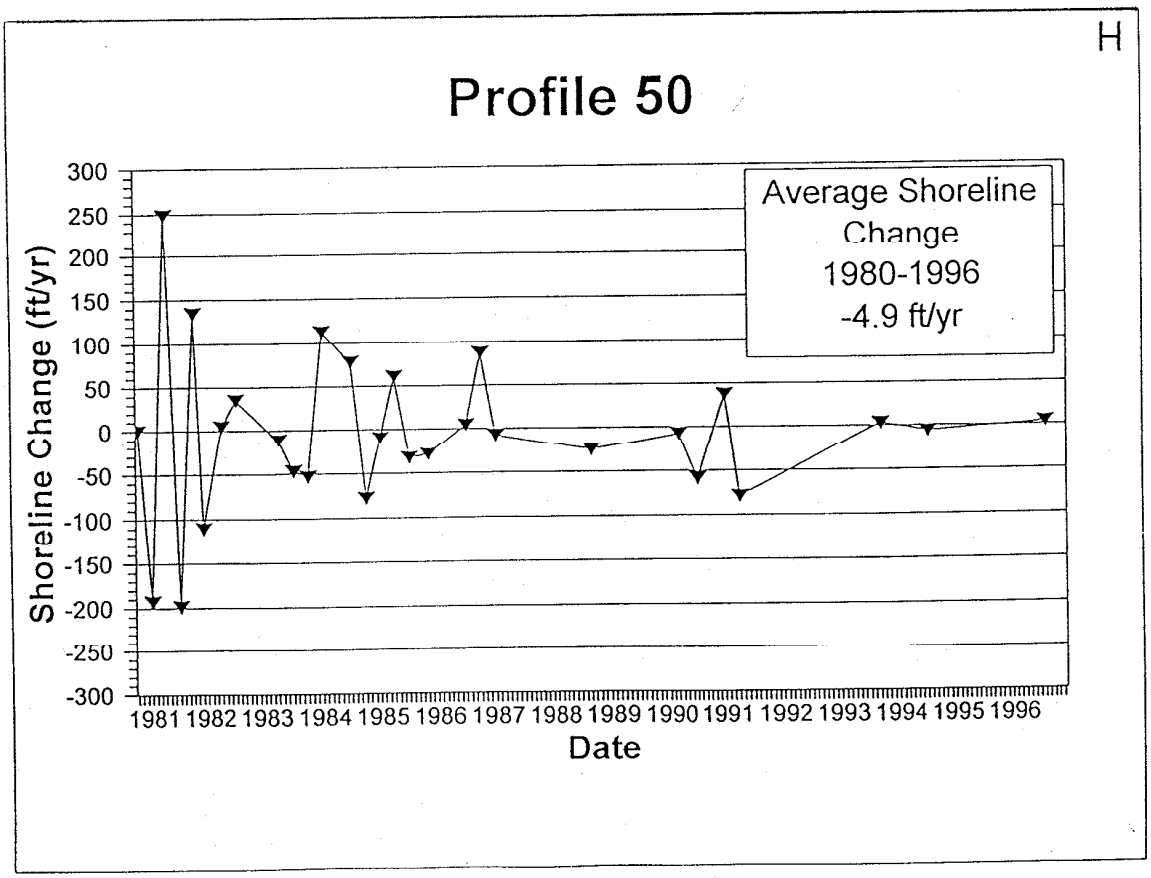

Figure 10. Rate of shoreline change for G) profile 49 and H) profile 50.

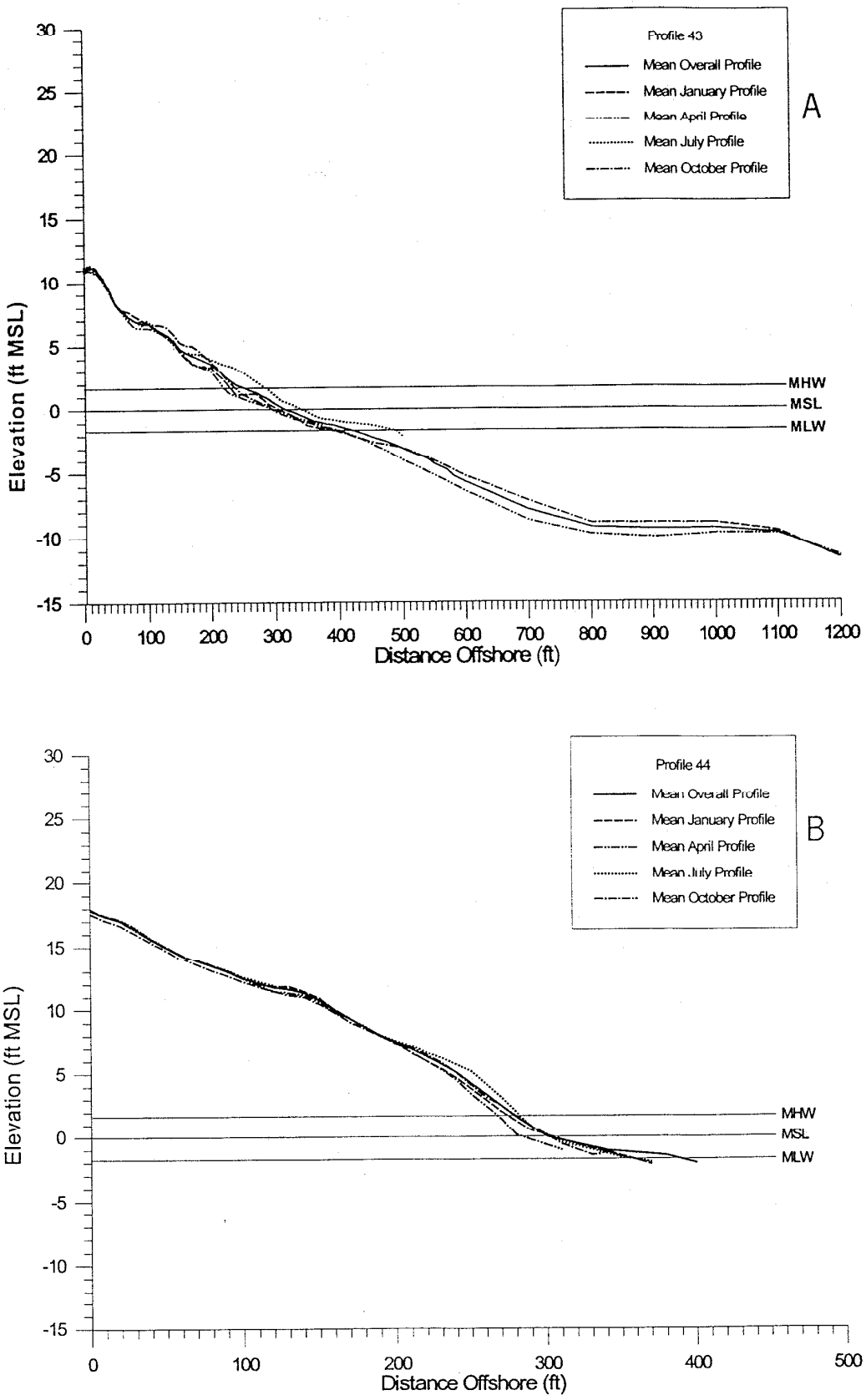

Figure 11 Seasonal changes in A) profile 43 and B) profile 44.

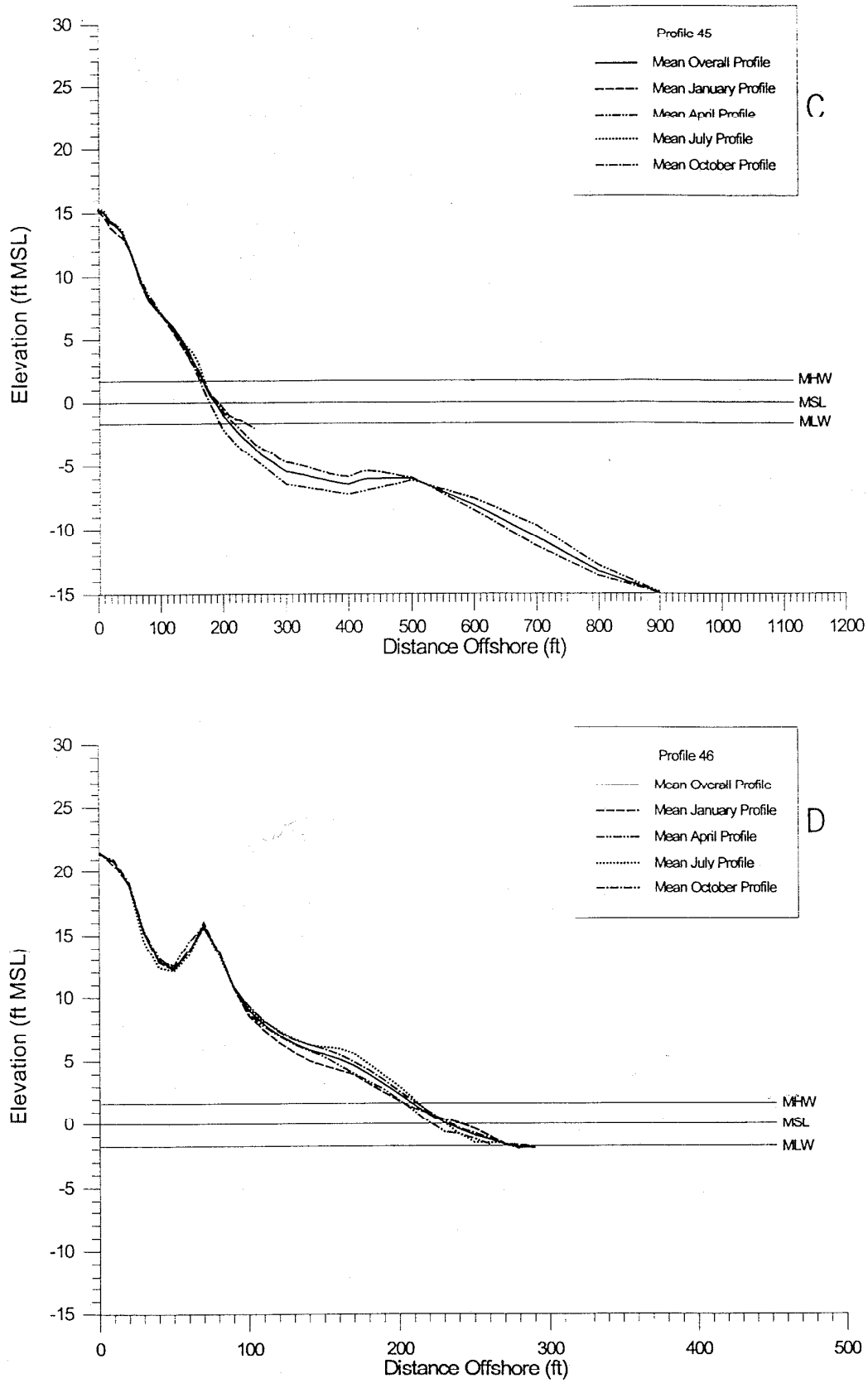

Figure 11 Seasonal changes in C) profile 45 and D) profile 46.

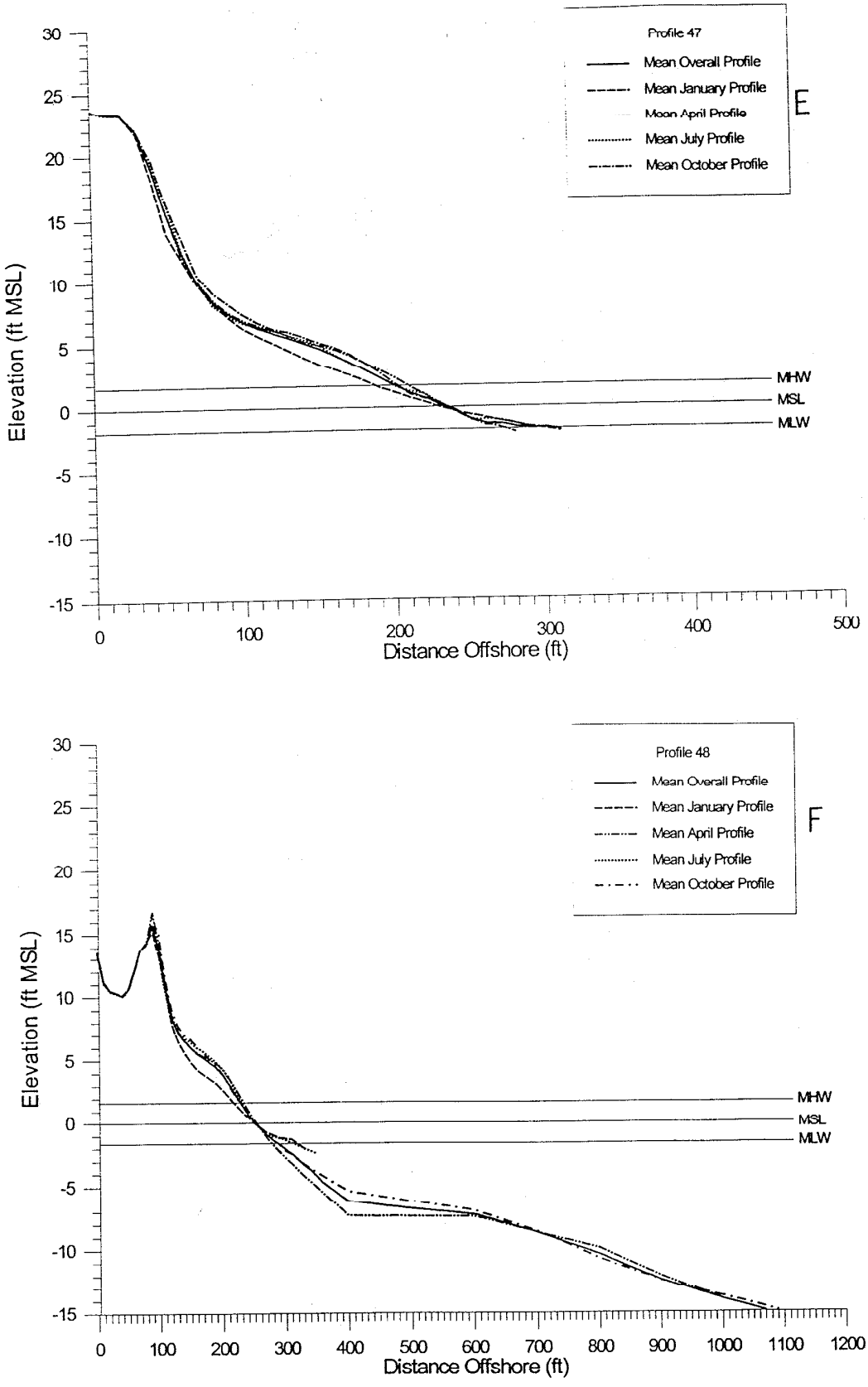

Figure 11. Seasonal changes in E) profile 47 and F) profile 48.

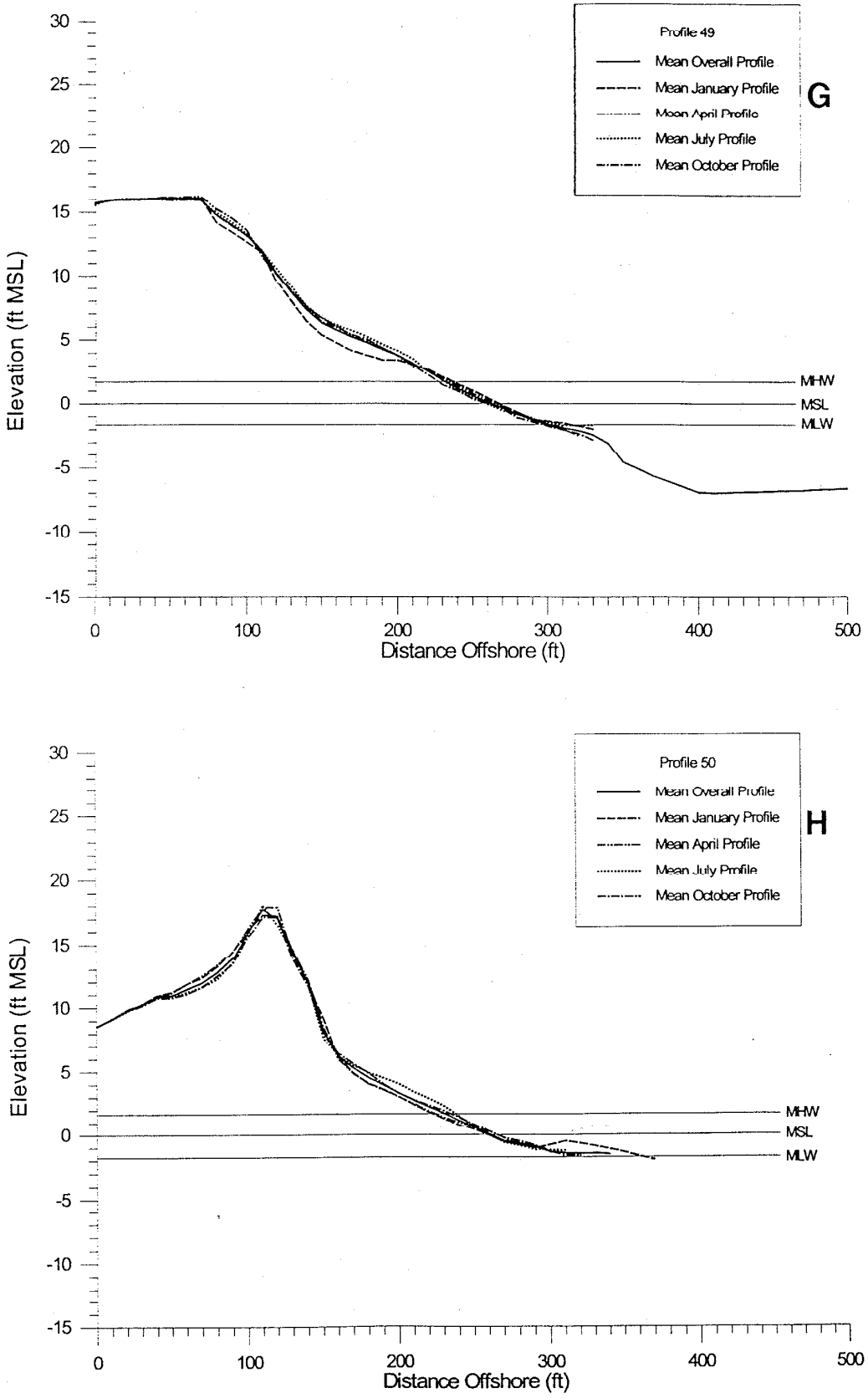

Figure 11. Seasonal changes in G) profile 49 and H) profile 50.

the October profile is higher than the April profile landward of the crossing point. The crossing point occurs at about 10 ft. below MSL at profile 43 (Figure 11A), 6 ft. below MSL at profile 45 (Figure 11C), and at 8.5 ft. below MSL at profile 48 (Figure 11F). The crossing point appears as a berm or bar feature, that is the seaward edge of a lower beach face terrace, and is seaward and deeper than the breaker zone inner bar feature. The sand eroded during the winter appears to be stored further offshore, seaward of the crossing.

Table 3

January	April	July	October
January 19, 1981	April 19, 1981	July 19, 1981	October 19, 1980
January 19, 1982	April 19, 1982	July 19, 1982	October 19, 1981
January 19, 1984	April 19, 1983	July 19, 1983	October 19, 1983
January 19, 1985	April 19, 1985	July 19, 1984	October 19, 1984
January 19, 1987	March 22, 1990	July 19, 1985	November 19, 1985
January 17, 1991	April 10, 1991	July 19, 1996	October 19, 1986
January 14, 1993	April 20, 1993	July 3, 1990	September 28, 1988
February 25, 1994		June 2, 1992	November 21, 1991
		July 9, 1993	September 8, 1993
		July 21, 1994	October 20, 1993
		August 19, 1996	

Survey dates assigned to seasonal groupings.

This feature was recognized by Larson and Kraus (1994) for spring and fall profiles taken at Duck, North Carolina. They called it a pivot point located at about -8.5 ft. water depth. For the southeast ocean coast of Virginia, this may be an outer bar feature since it appears to be persistent through time. The inner bar, usually found toward shore, is difficult to see in the long profiles most likely due to the lack of summer and winter data. Larson and Kraus (1994) found the average depth of the inner bar at Duck, North Carolina to be -5.2 ft. MSL based on 230 bi-monthly profiles. The outer bar crest was less persistent and resided at an average depth of 12.4 ft.. The trend of the inner bar and outer bar is less discernable along this subreach shoreline.

Figures 12A-12H reflect the maximum and minimum profiles for the survey data set as well as the mean profile and standard deviation. The plots for the long profiles (43, 45 and 48) utilize all data until 5 or less points are available offshore. Offshore closure is not reached but can be projected to be between 25 and 30 ft. below MSL. The short profiles generally do not extend below MLW, but most reach a subaerial beach “closure”.

The standard deviation is a measure of variability of the profiles. For all the subaerial beach surveys, the common area of vertical excursion occurs in the active swash zone between the beach berm and about MSL; this zone has an average standard deviation of 1.7 ft. Profiles 46, 48,

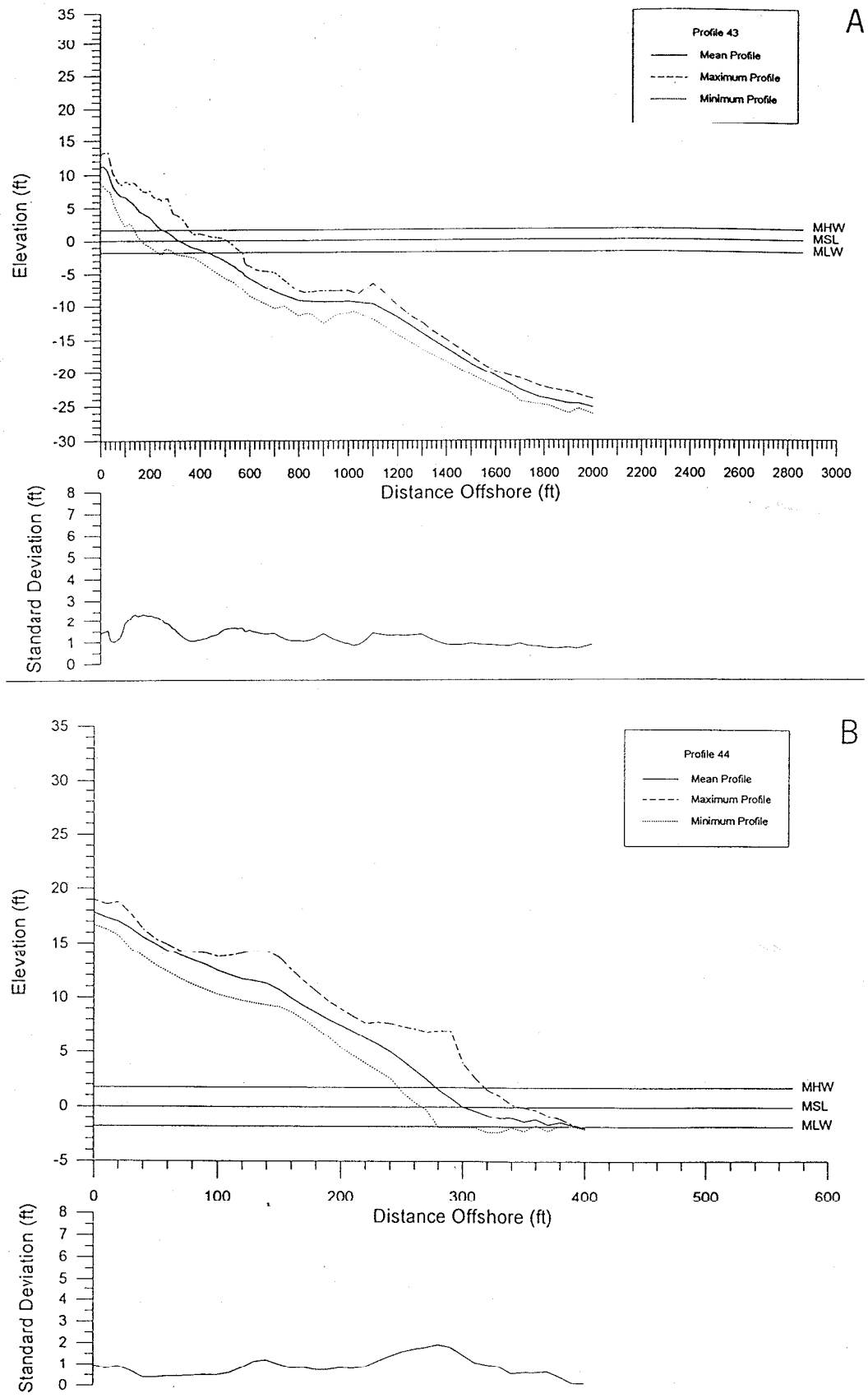

Figure 12. Maximum, minimum, and mean plots, with standard deviation, for A) profile 43 and B) profile 44.

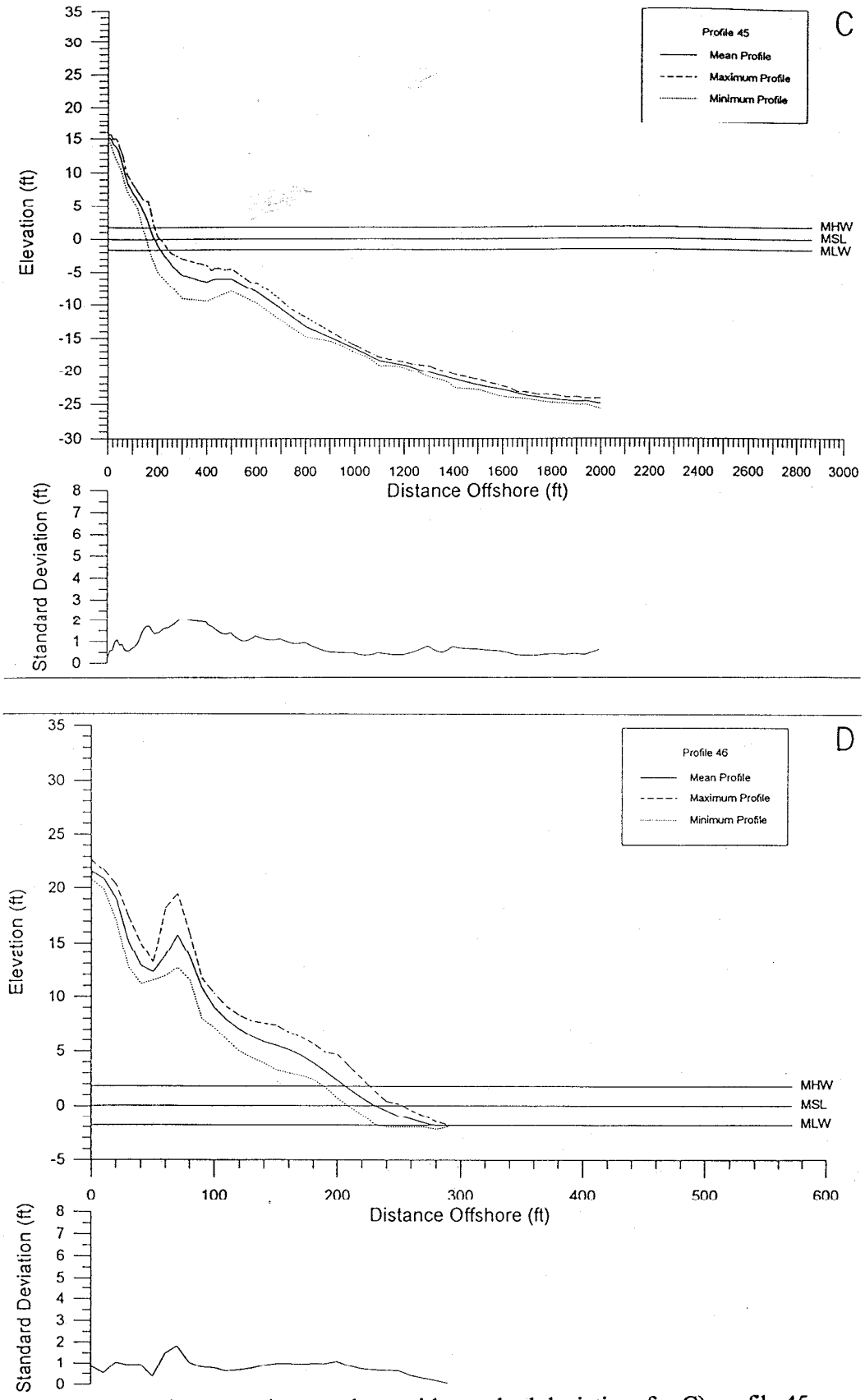

Figure 12. Maximum, minimum, and mean plots, with standard deviation, for C) profile 45 and D) profile 46.

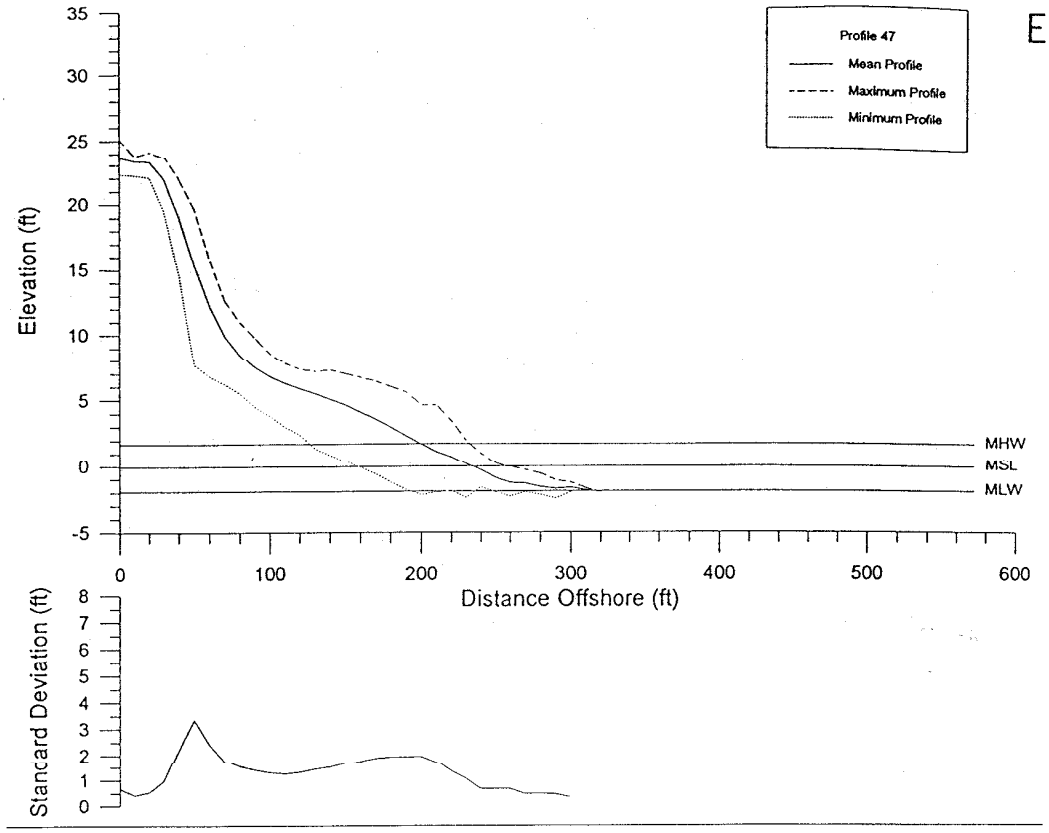

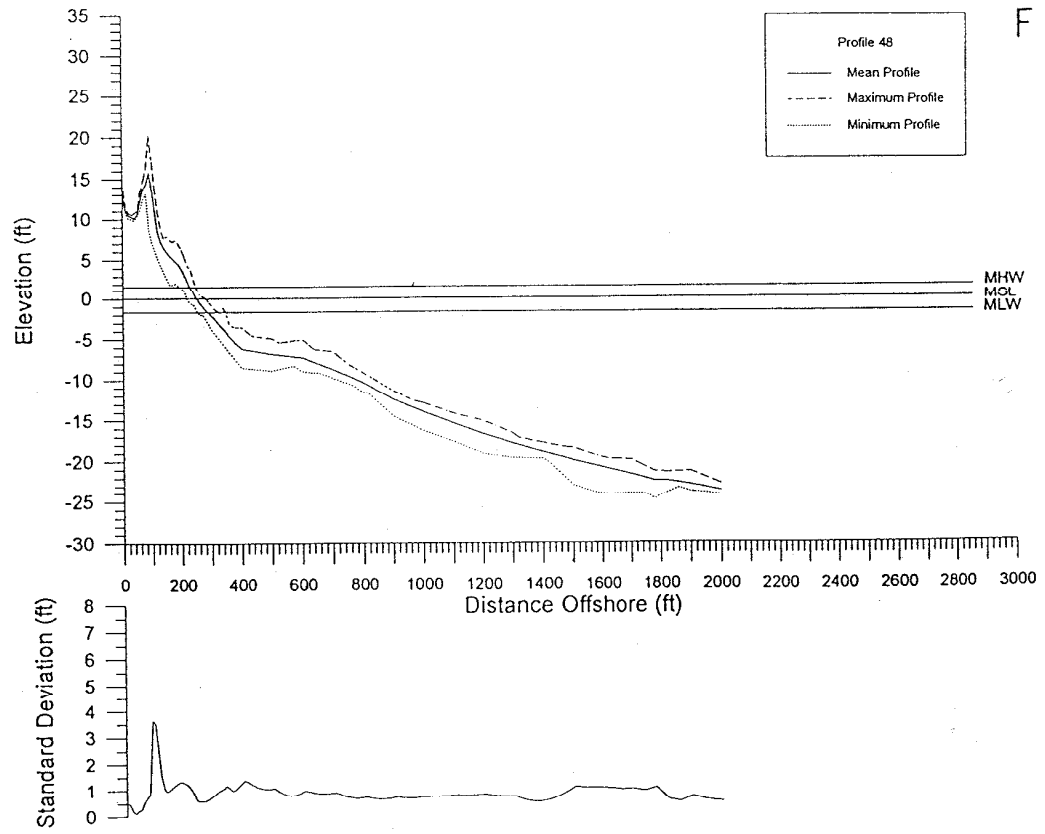

Figure 12. Maximum, minimum, and mean plots, with standard deviation, for E) profile 47 and F) profile 48

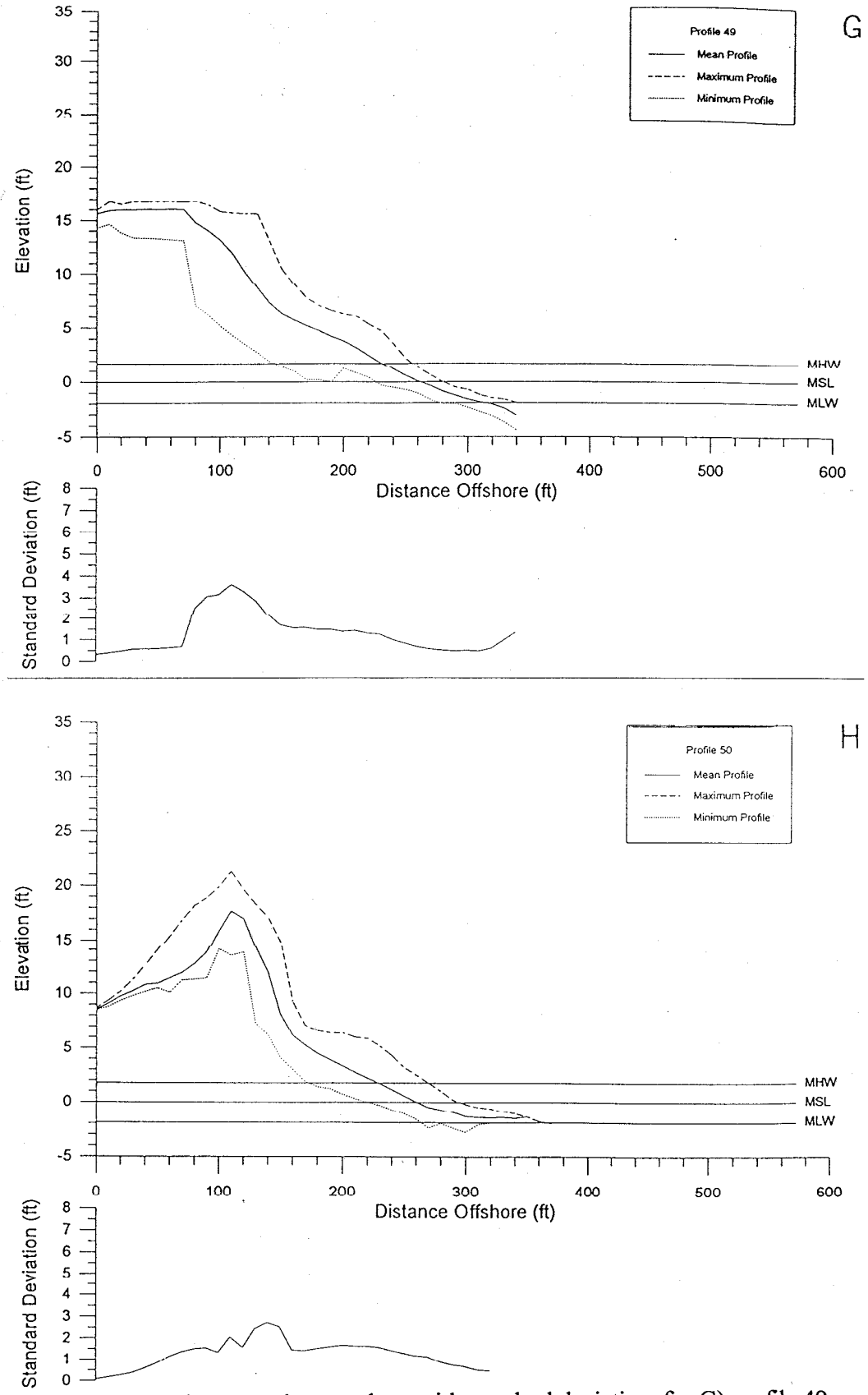

Figure 12. Maximum, minimum, and mean plots, with standard deviation, for G) profile 49 and H) profile 50.

49 and 50 show significant fluctuations in the foredune. Vertical changes in the base of dune have a standard deviation of 3.4 ft. on profile 47. The average standard deviation for the dune face for all profiles is 2.6 ft. (Table 4).

For the maximum, minimum and mean analysis of the long profiles (43, 45 and 48), the offshore bar/terrace feature (pivot point) seen in the seasonal profiles is once again apparent. The area of the largest vertical profile excursion along the offshore segment occurs landward of the pivot point at the base or toe of the beach face. Standard deviations and depths of the toe of the beach face are shown in Table 4.

Table 4

Profile	Beach Berm	Dune Crest/Face/Base	Toe of Beach Face
43	2.4	1.5	1.6 = Standard Deviation Depth = -4.0 ft
44	1.9		
45	1.7	1.2	2.0 = Standard Deviation Depth = -5.5 ft
46	1.2	1.9	
47	2.0	3.4	
48	1.4	3.7	1.4 = Standard Deviation Depth = -6.5 ft
49	1.5	3.6	
50	1.8	2.7	
Average	1.7	2.6	

Standard deviation (ft.) of selected beach features resulting from the maximum, minimum, and mean analysis.

Dam Neck Beach Nourishment Project, 1996-1997

The DNBNP came online after this study was geared toward a profile and sediment analysis of the Sandbridge shore subreach. It was decided to take advantage of this opportunity to track the movement of the beach nourishment for one year. Sampling of the beach and nearshore region was performed to note significant changes in profile trends and sedimentology. The eight aforementioned City profiles were chosen as reference lines for this evaluation. Surveys and samples were performed prior to the DNBNP (August 1996), about 6 months after the project (May 1997) and after about one year (October/November 1997). The one year sampling took two days. The beach and dune were surveyed and sampled in October 1997 while the offshore work was not accomplished until November 1997. Between the two sampling dates, a moderate northeaster occurred (October 15 to 19) and impacted beach morphology and offshore sedimentation processes. Also, City profile data was used for the August 1996 profile plots;

however, no City data was available for profiles 45 and 46 so the mean summer profile was used for the August 1996 date.

The following discussion of analyses resulting from VIMS's one-year monitoring will be separated into 1) the subaerial beach and nearshore surveys, and 2) the sediment sampling and its analysis. Most of the historic shore change data and much of the City's profile data only covers the "subaerial" beach zone, but some City profile data covers the upper shoreface, an area that will be impacted by the DNBNP.

Subaerial Beach and Nearshore Surveys

Profile plots of the three sampling periods include the subaerial beach and nearshore (Figures 13-20). The subaerial beach may be defined as that area of the profile from about MSL to the dune crest. Two plots are posted for each profile to better see the beach. The nearshore portion of the profile is what lies below MSL. Two nearshore profiles include August 1996 and November 1997. When City data was not used (i.e. their short profiles), the bathymetry was determined by the coordinates at the sediment sample location (Appendix A). The beach and nearshore surveys were done on separate days for the data taken one year after the initial fill project. For this nearshore survey, the profile from 6 ft. below MLW seaward was taken in November 1997 but is plotted with the subaerial beach (data taken in October 1997); the following plots show data from both dates, even if October 1997 is the date on the plots.

There is considerable upper profile variability on profile 43 (Figure 13A and 13B) that is most likely attributable to Rudee Inlet, which acts as a littoral barrier, and the associated dredging. Dredging was being done during the May 1997 survey. Vertical changes are most significant between about +5 ft. MSL and -10 ft. MSL. A general loss of material form the beach and very nearshore occurred between August 1996 to October 1997; however, during that time, there also was an increase in beach berm elevation. Below the -7 ft. contour, there was a net increase of sand volume between August 1996 and October 1997.

Heavy equipment was pushing sand around the backshore at profile 44 (Figures 14A and 14B) during the May 1997 survey. This activity modifies the natural patterns of profile change along the subaerial beach zone. The subaerial beach berm grows in elevation and becomes an obvious feature on the profile by October 1997. Profile 44 acquires an inner bar in May 1997 and October 1997 and what may be a "pivot" point occurs about 1,000 ft. on the survey line at about 10 ft. below MSL. Profile 44 was historically a short profile in the City's data set.

Profile 45 (Figures 15A and 15B), a long City profile with a data set that only extends four years, lies about mid-way between profiles 44 and 46. Subaerial beach changes indicate beach berm and beach face growth. Nearshore erosion occurred down to the -4 ft. contour from August 1996 to May97 but then an accretionary trend occurred by October 1997 with bar growth occurring 380 ft. offshore.

Profile 46 (Figures 16A and 16B) is located about 1000 ft. north of the limit of beach fill associated with the DNBNP. The October 1997 survey shows an accretionary trend of the beach berm (Figure 16A) and a general profile decrease across the nearshore segment of the profile

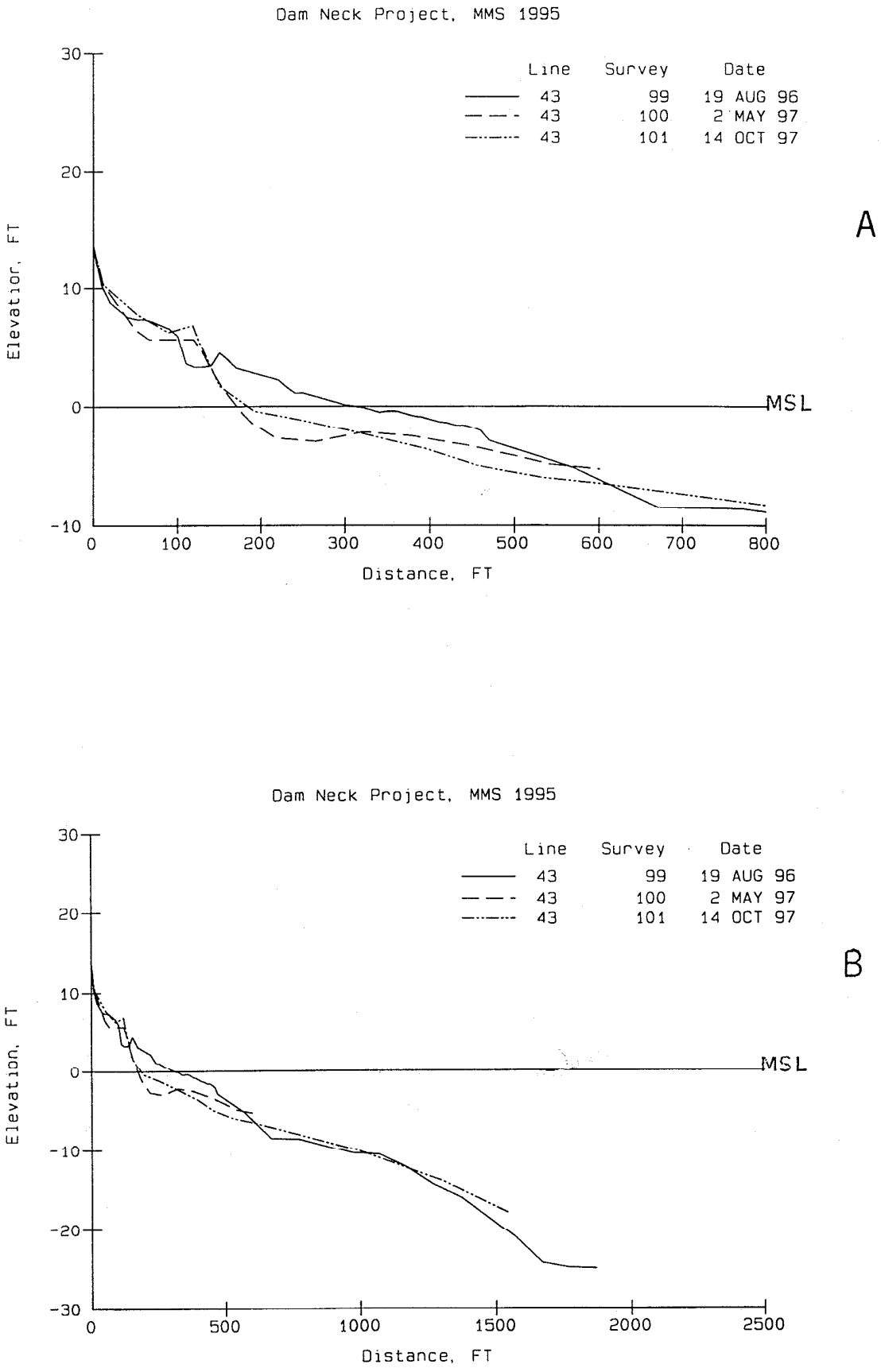

Figure 13. Profile 43 A) subaerial beach plot and B) long profile plot.

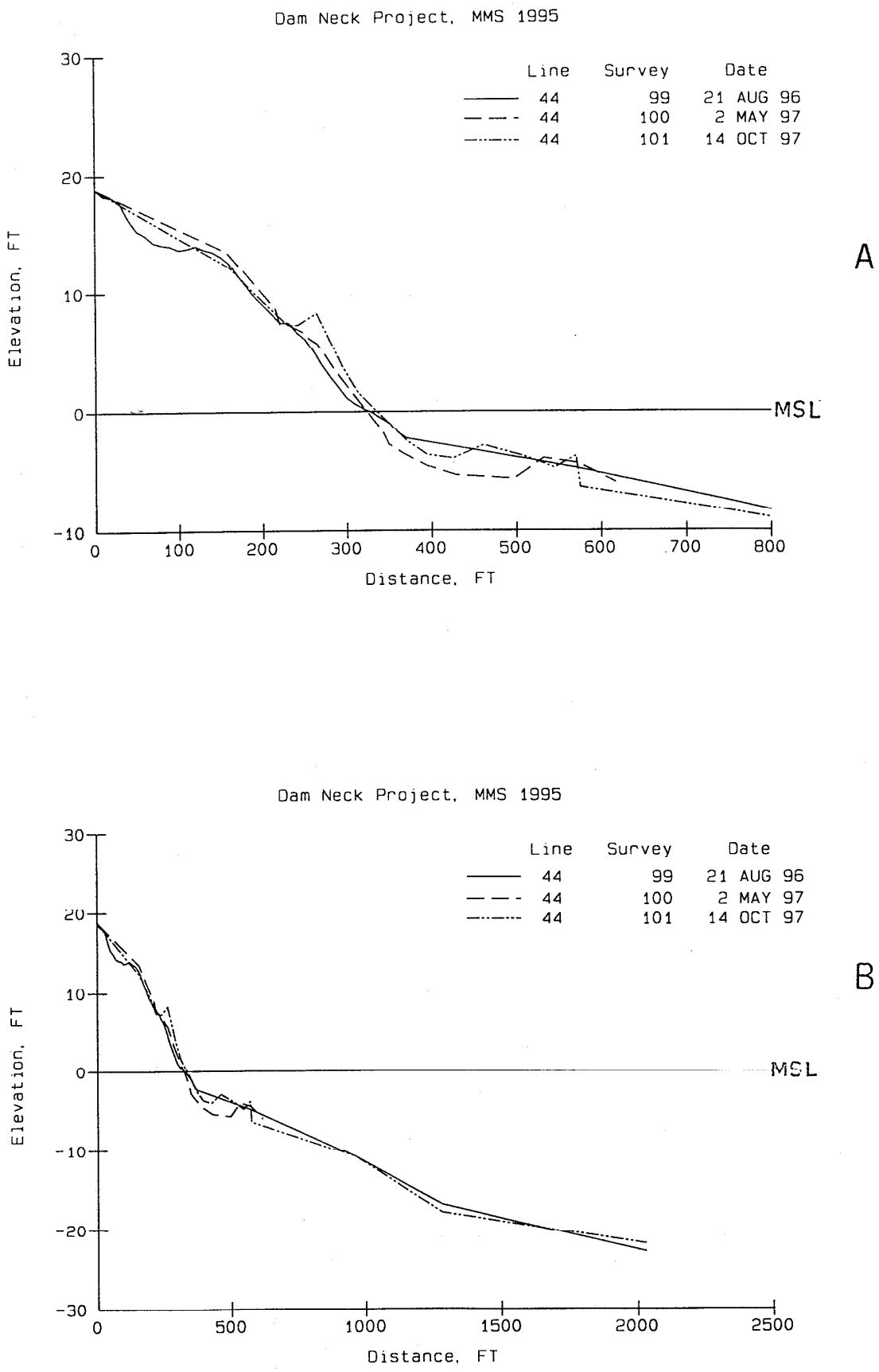

Figure 14. Profile 44 A) subaerial beach plot and B) long profile plot.

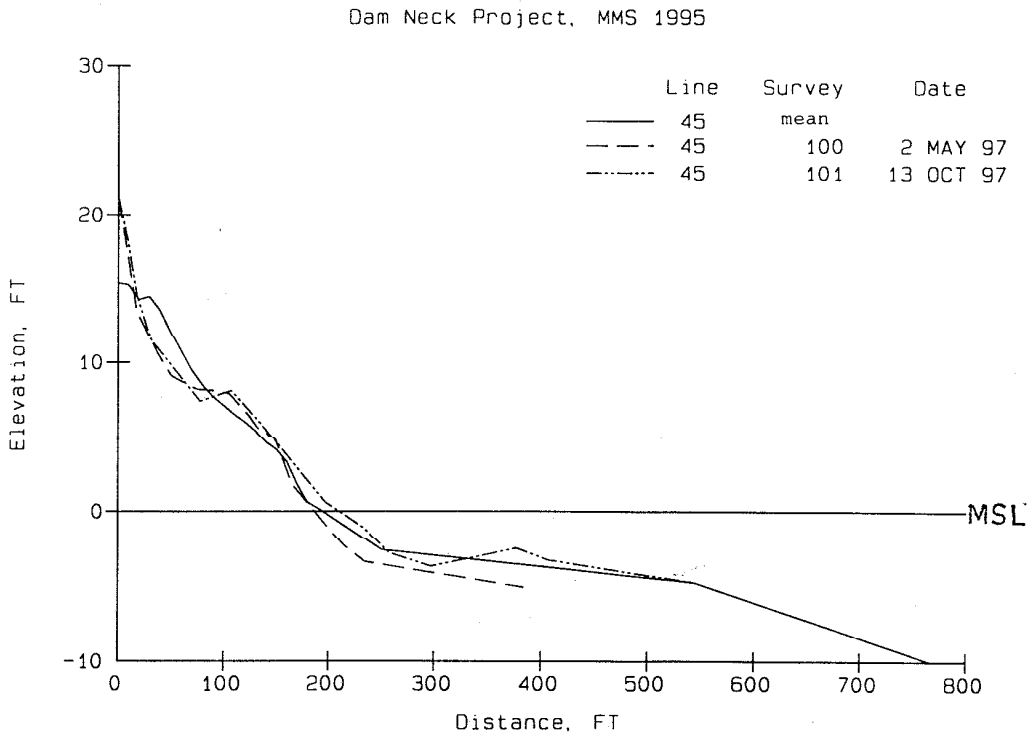

A

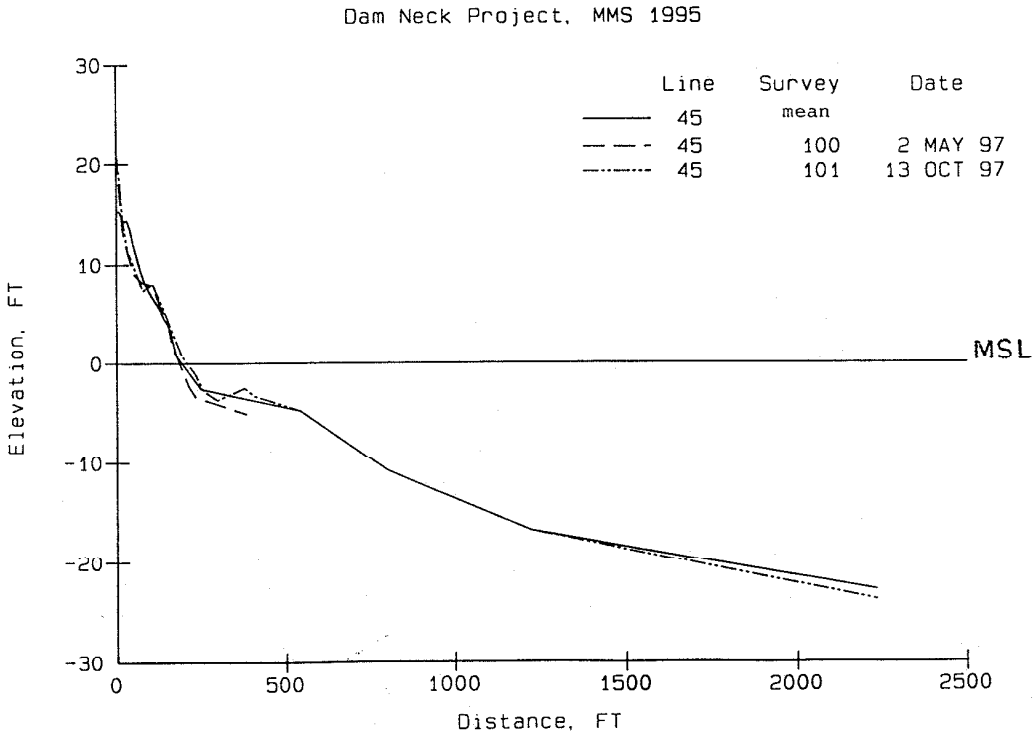

B

Figure 15. Profile 45 A) subaerial beach plot and B) long profile plot.

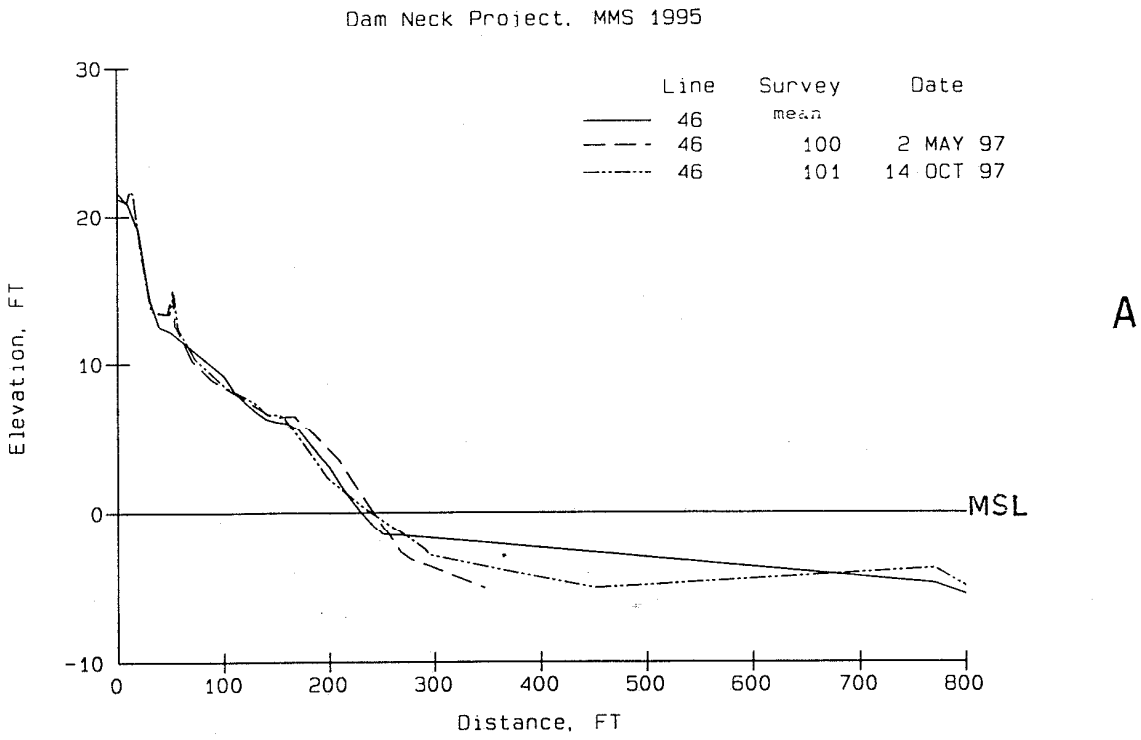

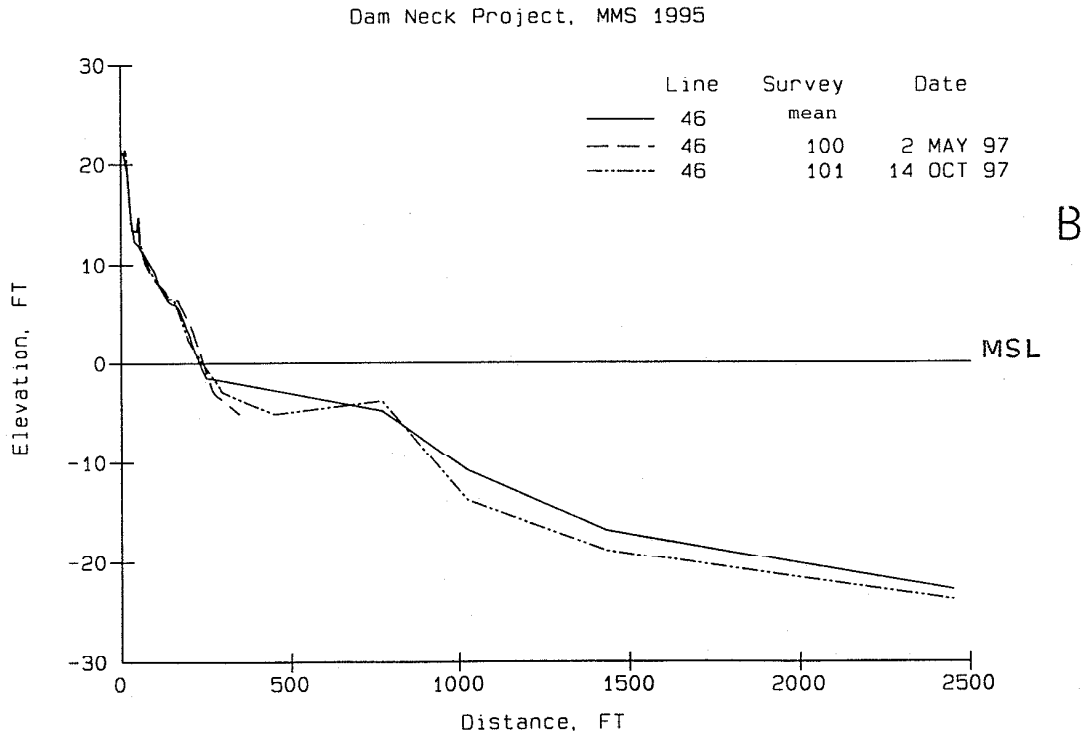

Figure 16. Profile 46 A) subaerial beach plot and B) long profile plot.

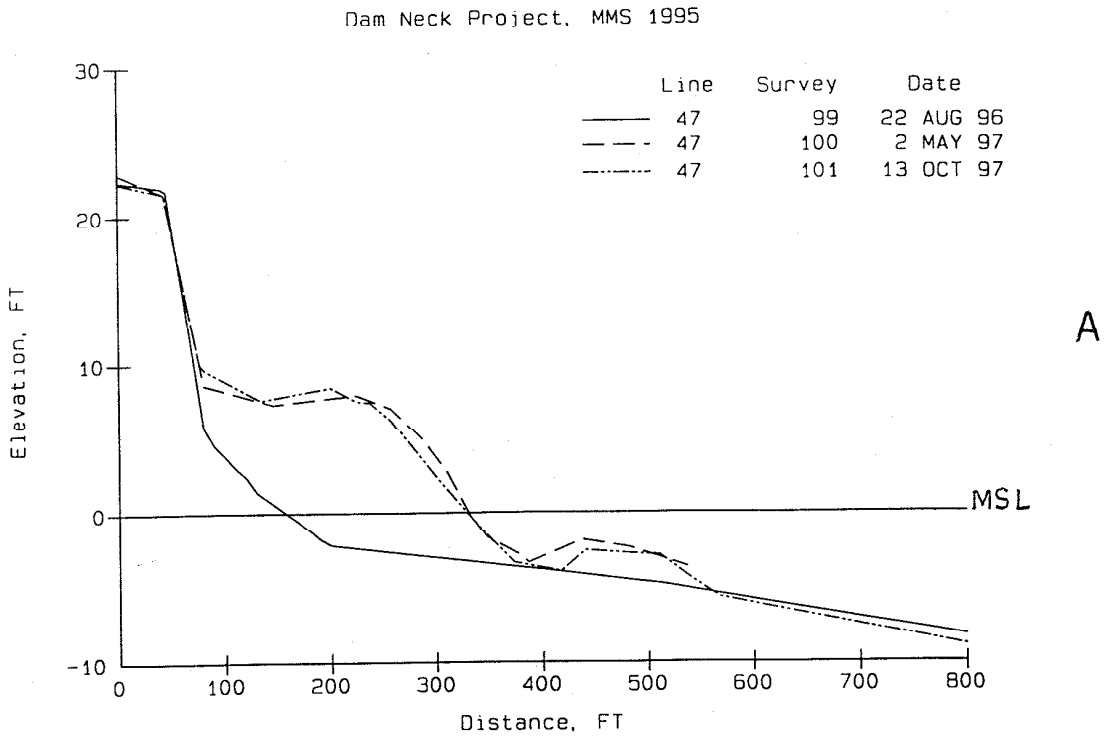

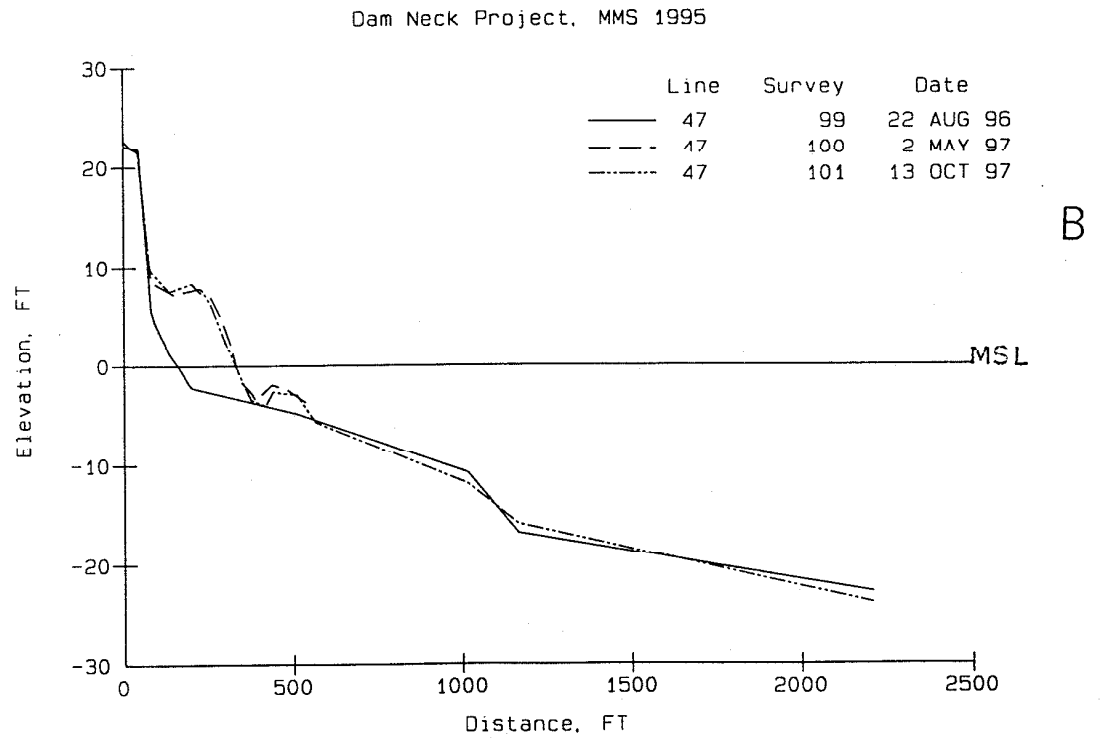

Figure 17. Profile 47 A) subaerial beach plot and B) long profile plot.

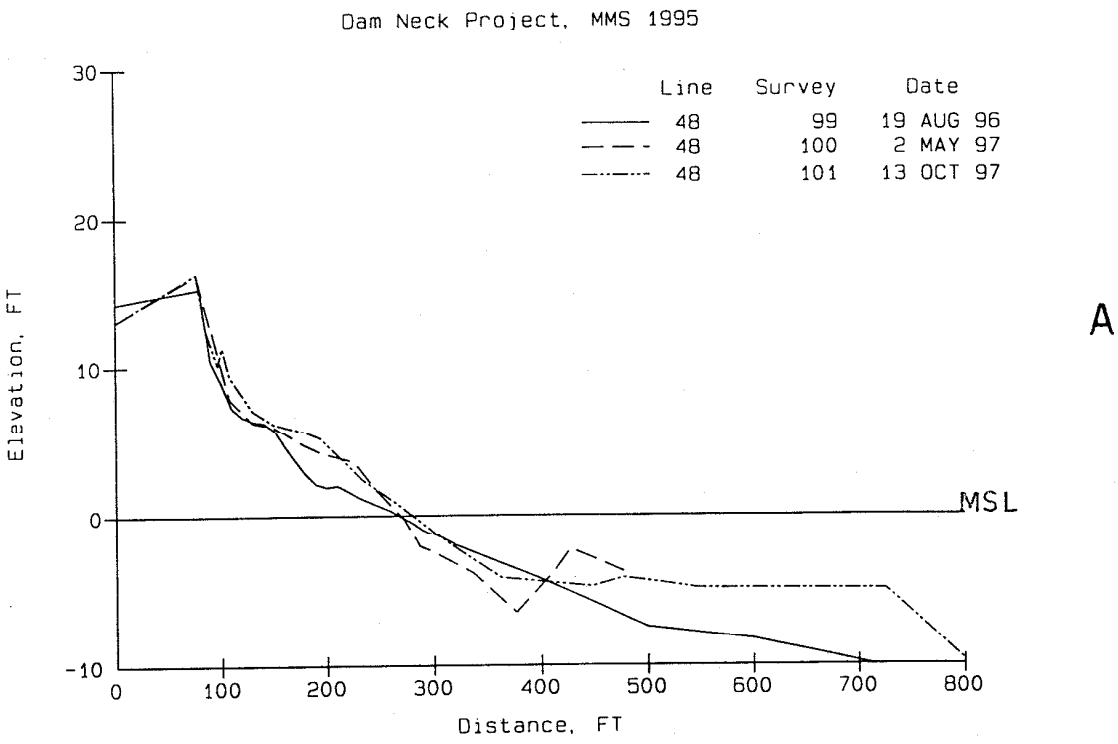

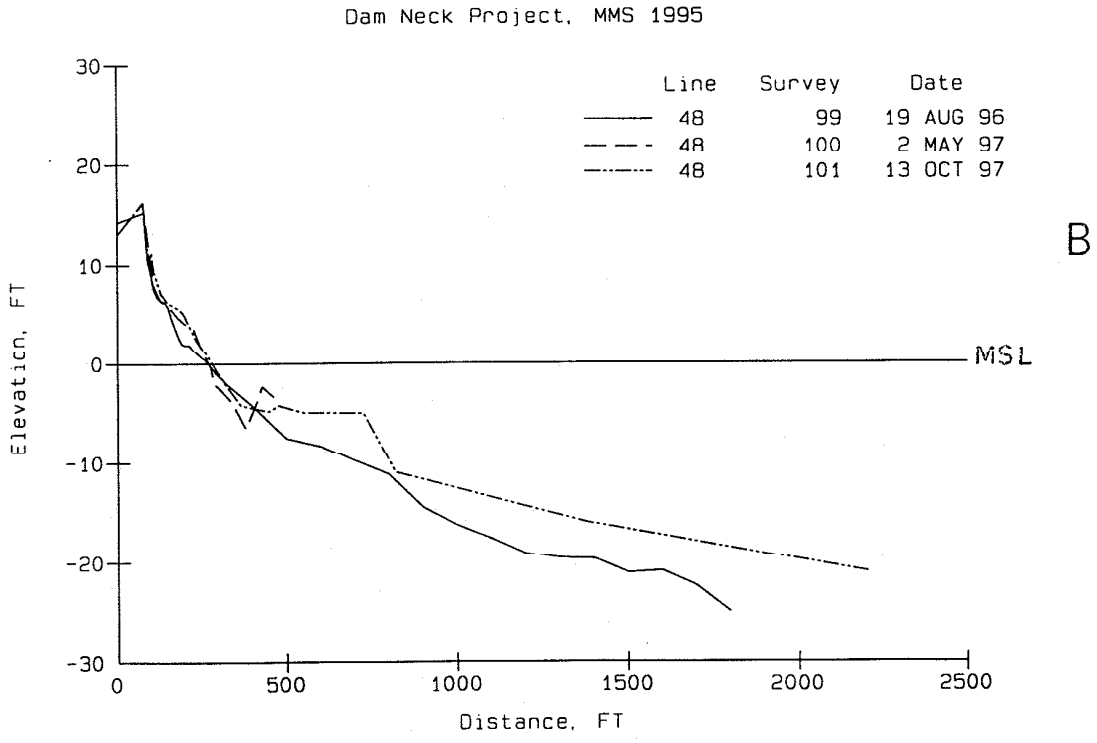

Figure 18. Profile 48 A) subaerial beach plot and B) long profile plot.

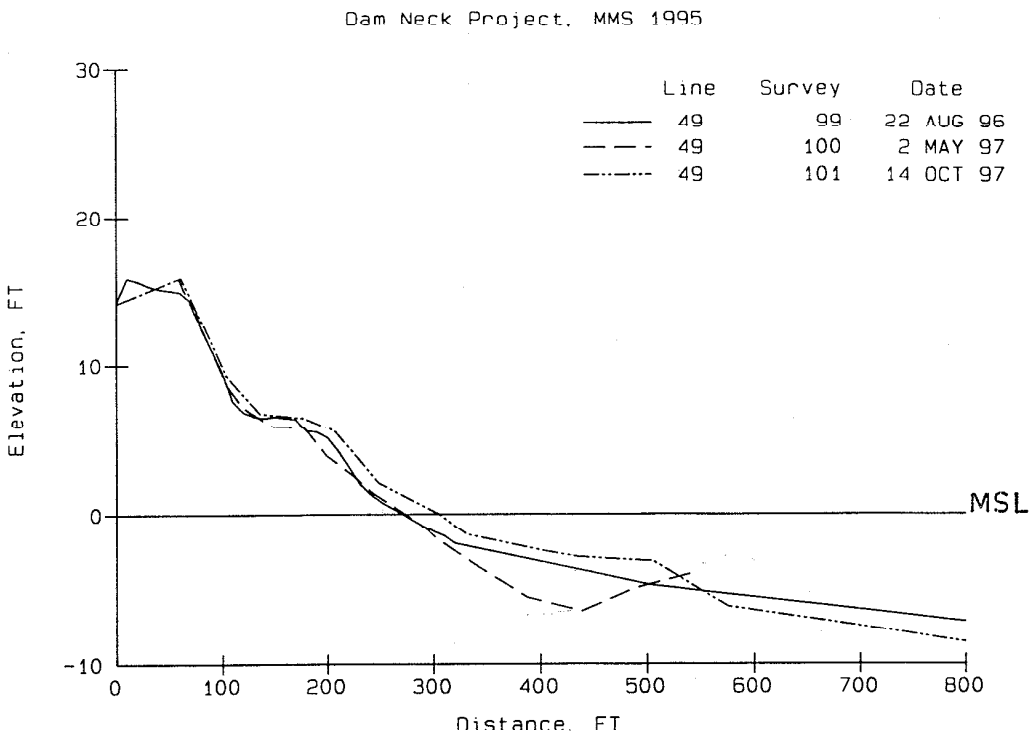

A

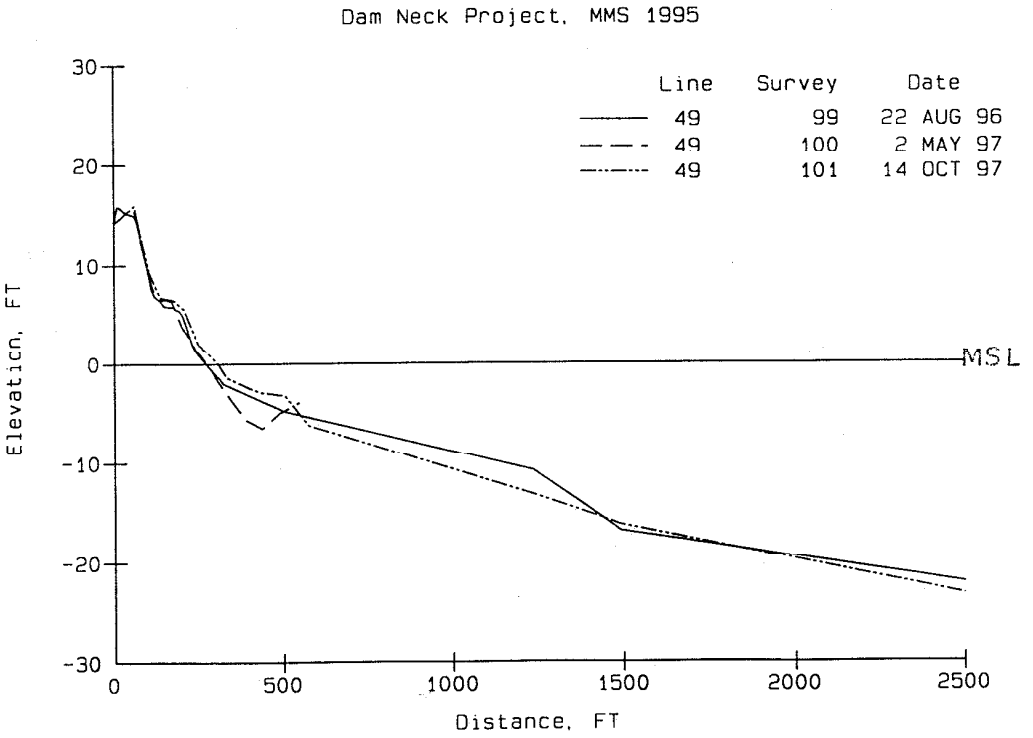

B

Figure 19. Profile 49 A) subaerial beach plot and B) long profile plot.

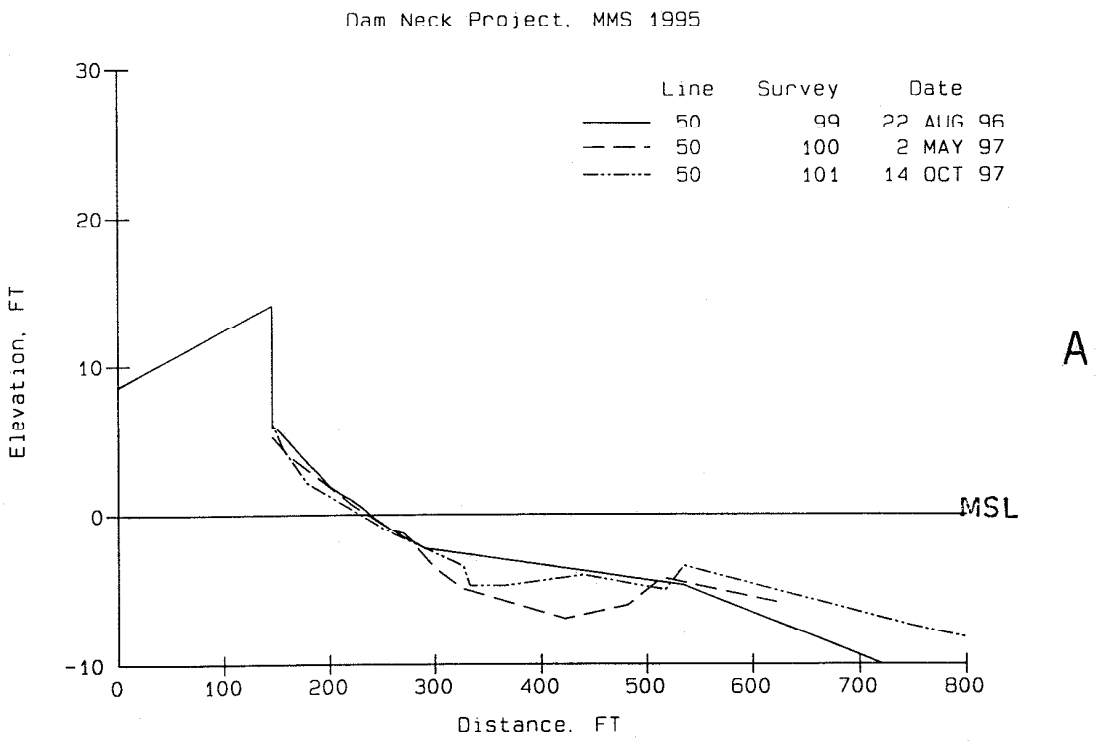

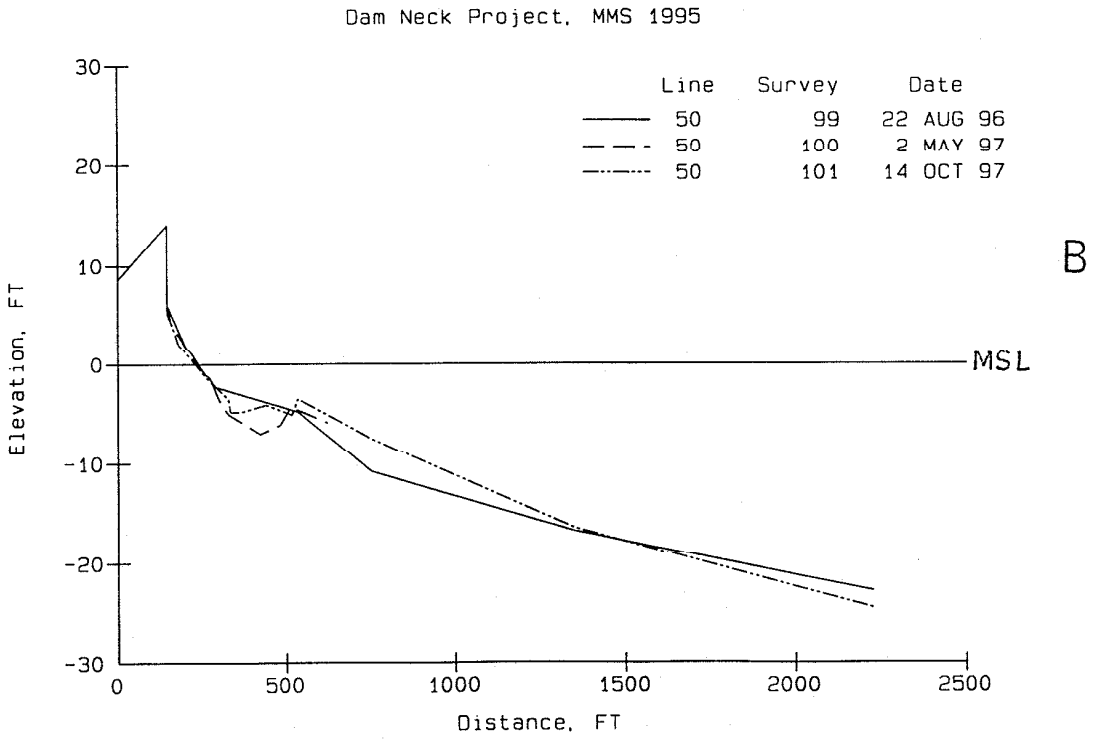

Figure 20. Profile 50 A) subaerial beach plot and B) long profile plot.

(Figure 16B). This offshore change may reflect the storm (October 1997) wave interaction with the beach fill mass to the south where wave refraction might scour the shoreface at that point.

Profile 47 is located at about the middle of the beach nourishment project, and the beach fill berm is quite obvious in Figures 17A and 17B. Initial landward adjustments to the beach face and inner bar is evident between surveys May 1997 and October 1997 as is some washover and base of dune accretion. The inner bars appear to have developed off the face of the adjusting beach fill. Changes further offshore do not appear to be significant, even after several days of northeaster waves. A slight cut and fill relationship occurred at about the -10 ft. MSL contour between August 1996 and October (November) 1997.

Figures 18A and 18B show profile 48 which is located about 2,000 ft. south of the southern limit of the DNBNP. A progressive, accretionary beach berm is shown between May and October 1997 surveys, and sand volume significantly increases below MSL. This may reflect a response of the upper shoreface to the Oct 15-19 northeaster. The data imply that there was a southward flow of material from the beach fill mass along the subaerial and offshore segments of the south bound area.

Continued accretion of the subaerial beach and nearshore from about +5 ft. MSL to -4 ft. MSL is noted in profile 49 (Figures 19A and 19B). A bar is located at the offshore limit of accretion, and net profile erosion occurs out to the -16 ft. MSL contour. Profile 49 appears to have a southward movement of the beach fill along the subaerial and very nearshore profile segments but not further offshore.

This is an erosional trend of the beach face in front of the bulkhead at profile 50 (Figures 20A and 20B). An inner bar and trough develops in the May 1997 and October 1997 surveys. Between August 1996 and October 1997, an accretionary trend tapered seaward from the inner bar feature offshore to about the -16 ft. MSL contour. Beyond that there is a slight erosional trend toward the seaward end of the profile.

The above profile trends are summarized by plotting the rate of change in the lateral position of MHW and the -2 ft. MSL contour for the three study surveys (Figures 21A and 21B). Beach fill trends after six month (August 1996-May 1997) show that seaward movement of MHW at profile 45 is negligible, but during the next six months, the profile accretes seaward. This same pattern and magnitude occurs at profile 49 which is about the same distance south of the southern fill limit that profile 45 is north of the northern fill limit. For the subaerial beach, this indicates relatively equal dispersion of the fill alongshore equidistant from the fill limits.

Profiles 46 and 48 straddle the fill area, 1,000 and 2,000 ft. away, respectively. These profiles have similar patterns of MHW movement initially, advancing during the first six months but then significantly receding on profile 46 and remaining unchanged on profile 48. Profile 47, in the heart of the beach fill, shows the expected high rate of shoreline advance after the first six month, then a slight erosional trend over the second six months.

The -2 ft. MSL contour change is somewhat more variable. A significant seaward advance took place during the second six months for the northern four profiles and profile 49.

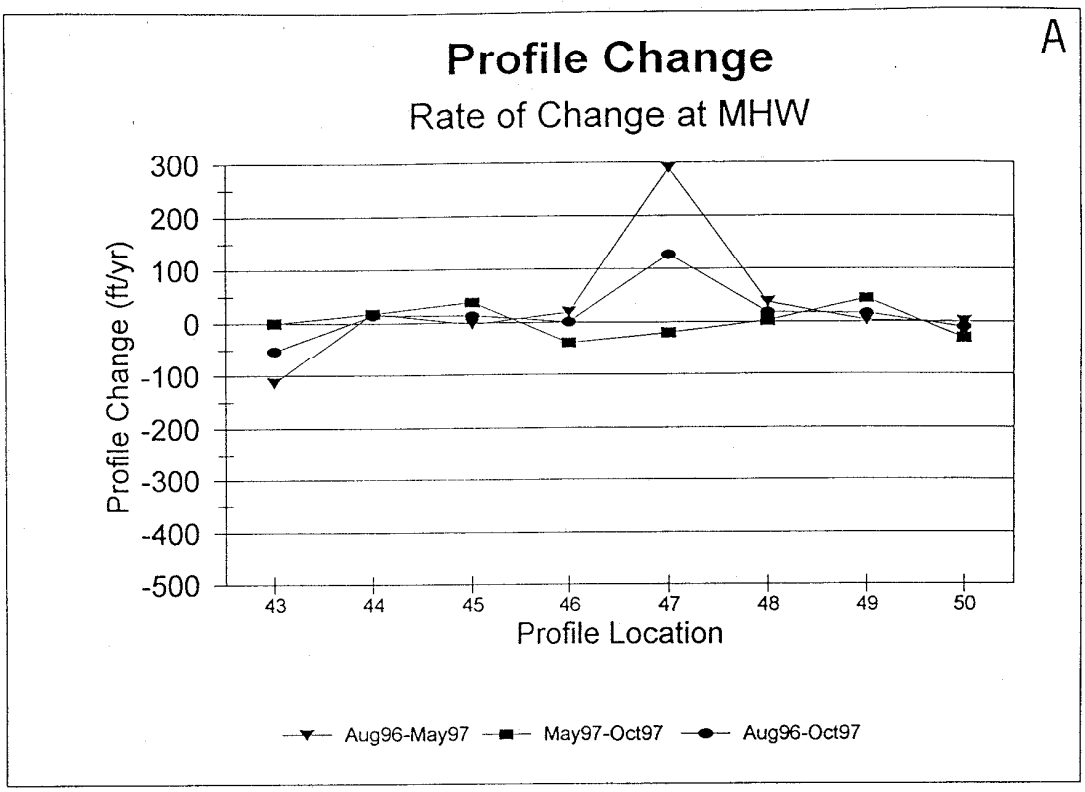

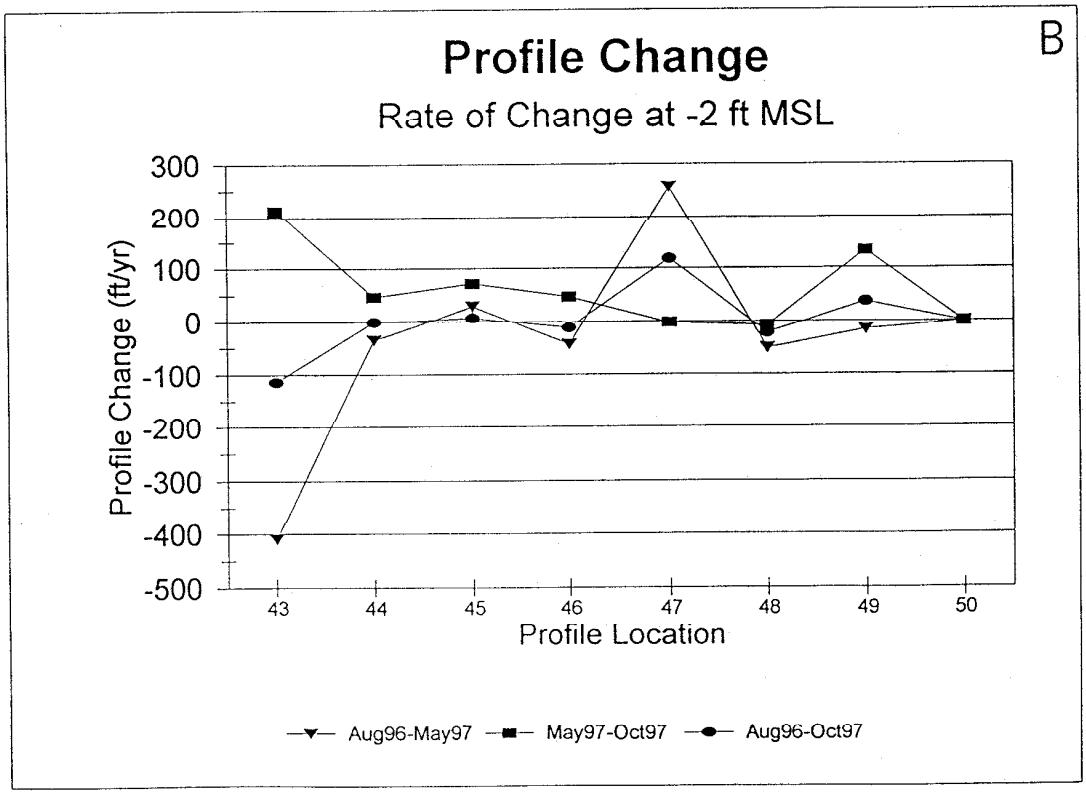

Figure 21. Profile change at A) MHW and B) 2 ft. below MSL.

This may reflect alongshore transport via the nearshore bar and swale zone which does not appear in the pre-fill survey. At about mid-fill, profile 47, a similar trend as MHW is seen but there is little movement of the -2 ft. MSL contour. It must be kept in mind that the land survey for the October 1997 data were performed prior to the October 15 to 19 northeaster.

Volumetric changes were calculated for the area of the profiles above MSL and below MSL. Patterns similar to changes in MHW are evident in volume change (cubic yards/linear ft., cy/ft) above MSL (Figure 22A). The subaerial beach at profile 47 shows the mass of sand placed on the beach during the project. Between August 1996 and May 1997, little volume change occurred above MSL north and south of the fill at profiles 44, 45, 48, 49, and 50. However, between May and October 1997, north and south of the fill was accreting (profiles 43, 44, 45, and 49) and little change occurred at profiles 46, 47, and 50. The large subaerial loss at profile 43 between August 1996 and May 1997 can be attributed to the dredging at Rudee Inlet.

Figure 22B shows the net volume change between pre-fill and one year after the fill below MSL. The same patterns of erosion and accretion are seen below MSL but to a much lesser extent volumetrically than the subaerial beach. Little change occurs at profile 50 over the year of this study.

The spreading of the beach fill also was tracked with aerial imagery where MHW was taken off low-level, non-rectified aerial photos. The MHW plot, Figure 23, shows the northward and southward spreading of the beach mass. Erosional areas are seen along the front cusp of the beach fill feature showing the differential loss of the fill there.

Subaerial Beach and Nearshore Sediments

The subaerial beach and nearshore was sampled for sediment characteristics. Samples were taken at the Dune (crest), Base of Dune (BOD), Midberm, Berm, Midbeach, TOE of beach face and the -2 MSL contour (Figure 7). The offshore was characterized by sediments taken at "-6", "-12", "-18", and "-24" ft.. The beach at profile 47 was not sampled prior to the fill since it would be buried after the project. The complete sediment analyses are presented in Appendix A. For this discussion, the median grain size and sorting are plotted together for each sample location. Figures 24A and 24B depict the sediment parameters for the natural foredune crest. Data are missing because either there was no dune crest feature or the profile line began seaward of the dune crest. On average, the median grain size gets slightly coarser with time (Figure 24A) and stays well sorted (Figure 24B).

The average alongshore grain size of the base of dune (BOD) becomes slightly finer from August 1996 to May 1997 but gets coarser again in October 1997 (Figure 25A). Profile 47, the beach fill, is slightly coarser than adjacent reaches. Sorting goes from well-sorted (August 1996) toward moderately well-sorted by May 1997 and October 1997 (Figure 25B). Both dune crest and BOD were primarily influenced by aeolian processes over the study period. The occurrence of high water and wave runup were negligible.

The midberm region's average alongshore grain size goes from a fine to medium sand to a medium sand (Figure 26A). Post-fill samples coarsen slightly to the north of the fill and fine to

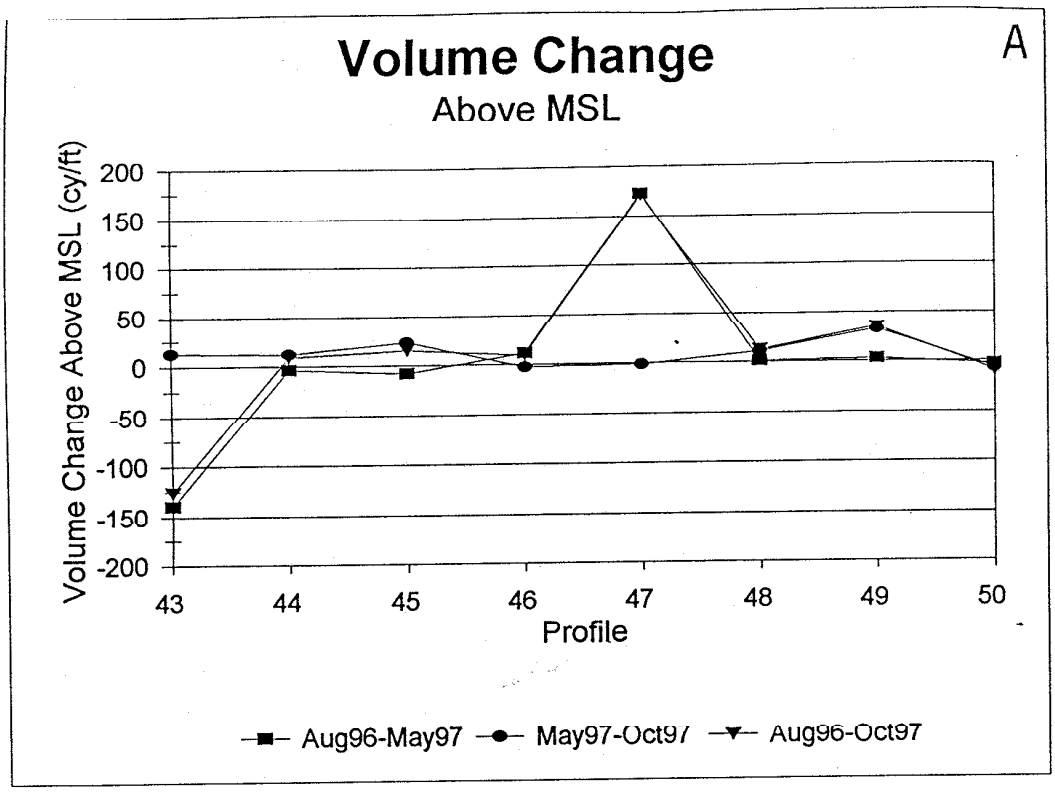

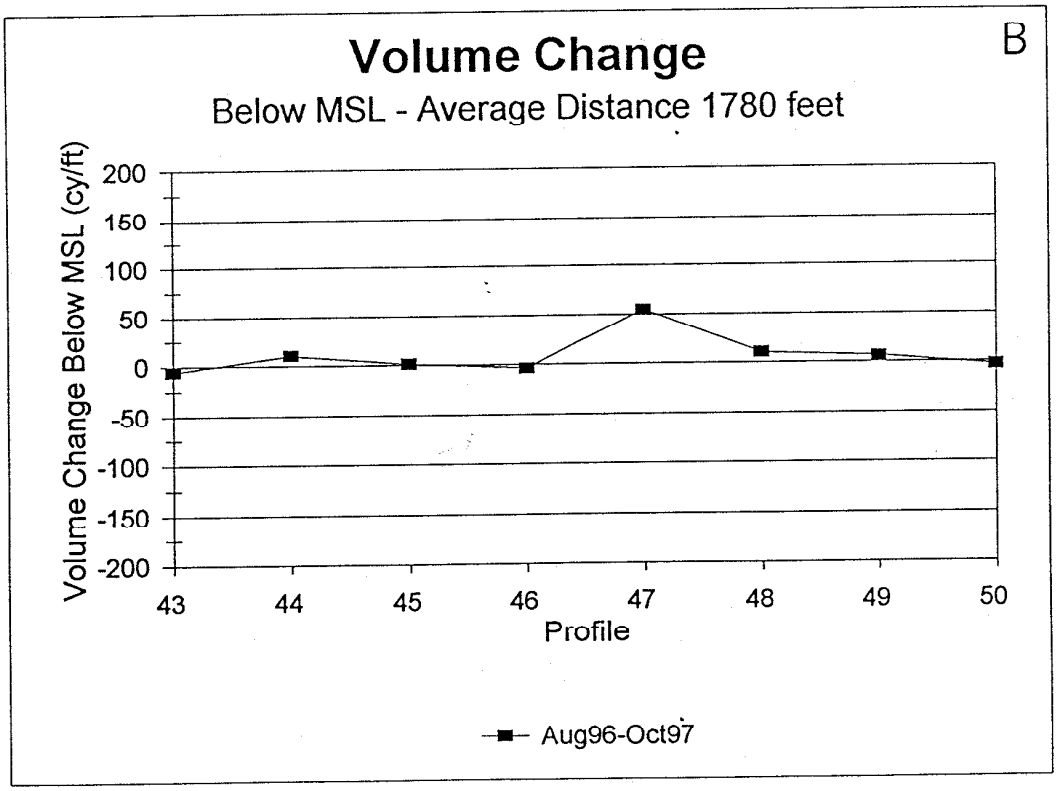

Figure 22. Volume change A) above MSL and B) below MSL to an average distance of 1,780 ft. from the benchmark.

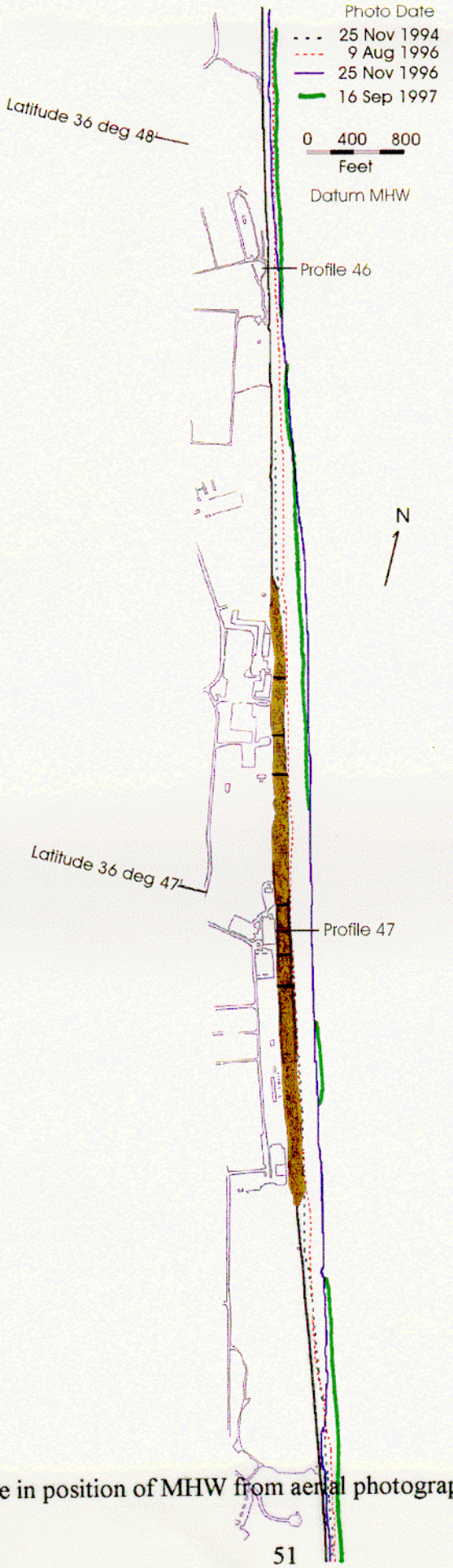

Figure 23. Change in position of MHW from aerial photography.

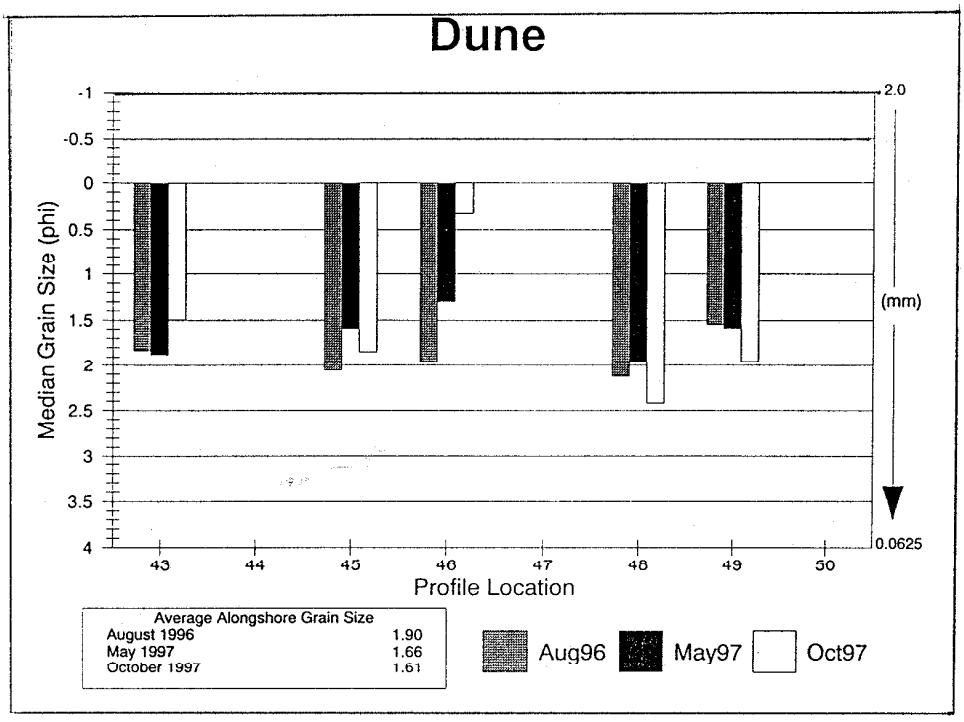

A

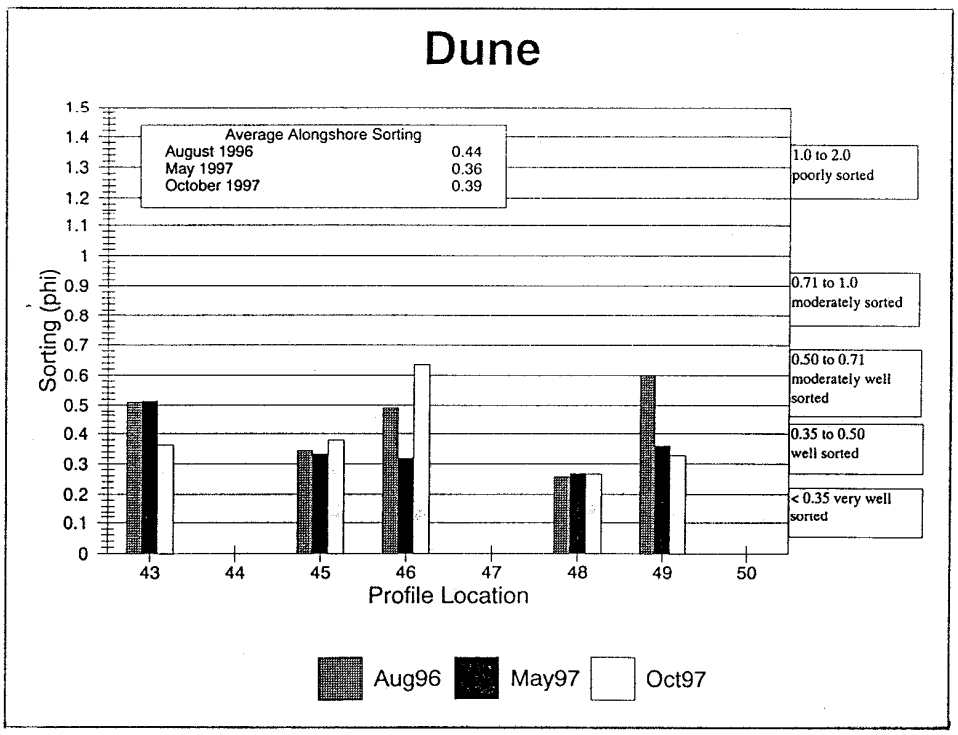

B

Figure 24. Dune A) median grain size and B) sorting.

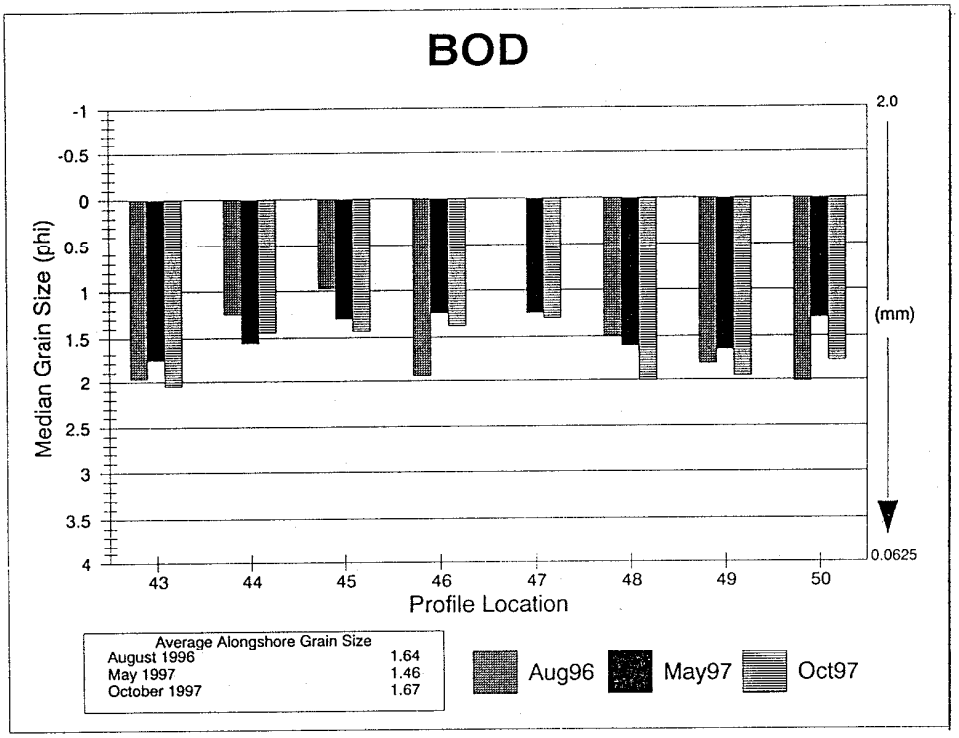

A

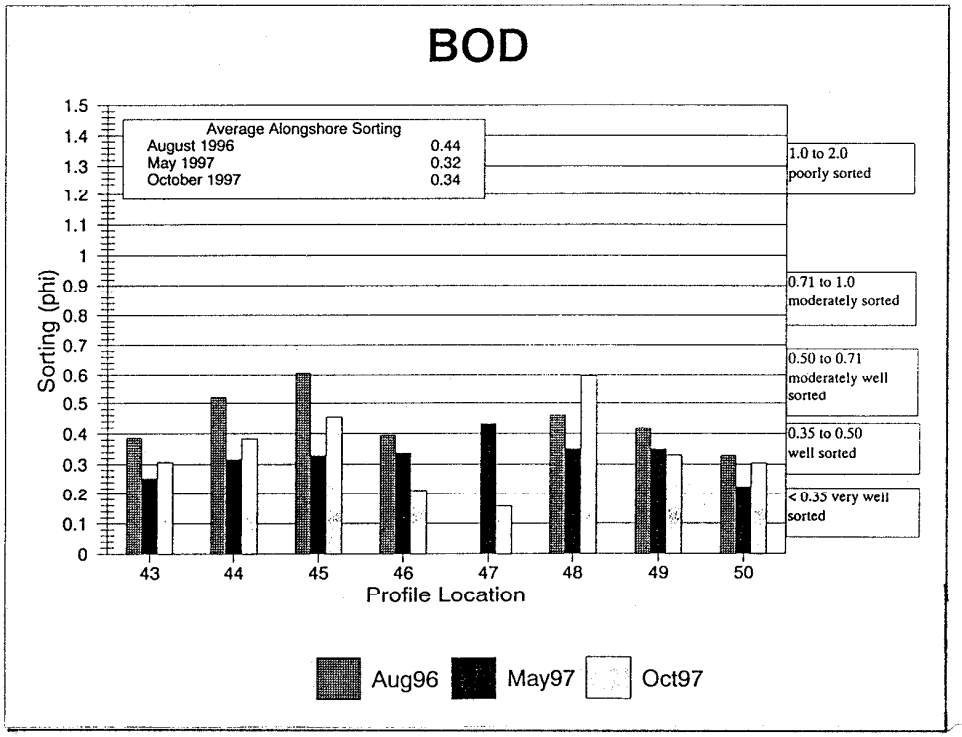

B

Figure 25. Base of dune A) median grain size and B) sorting.

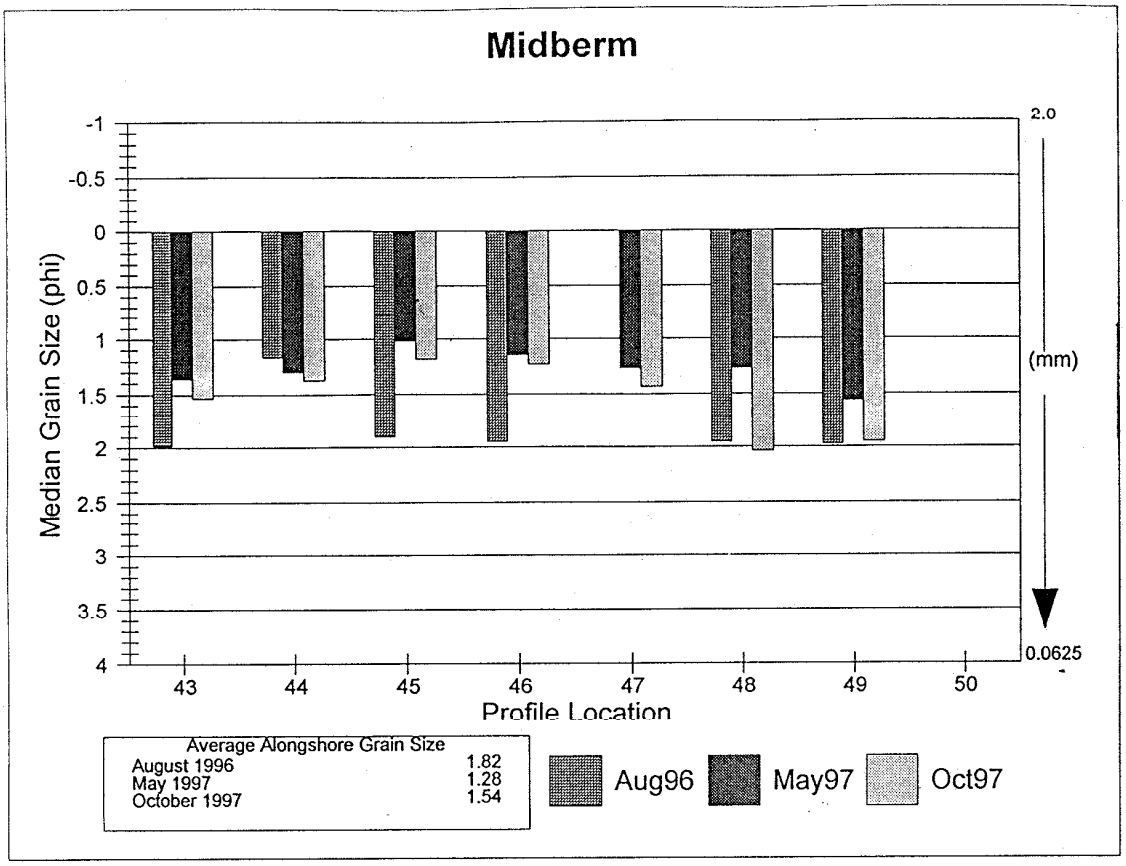

A

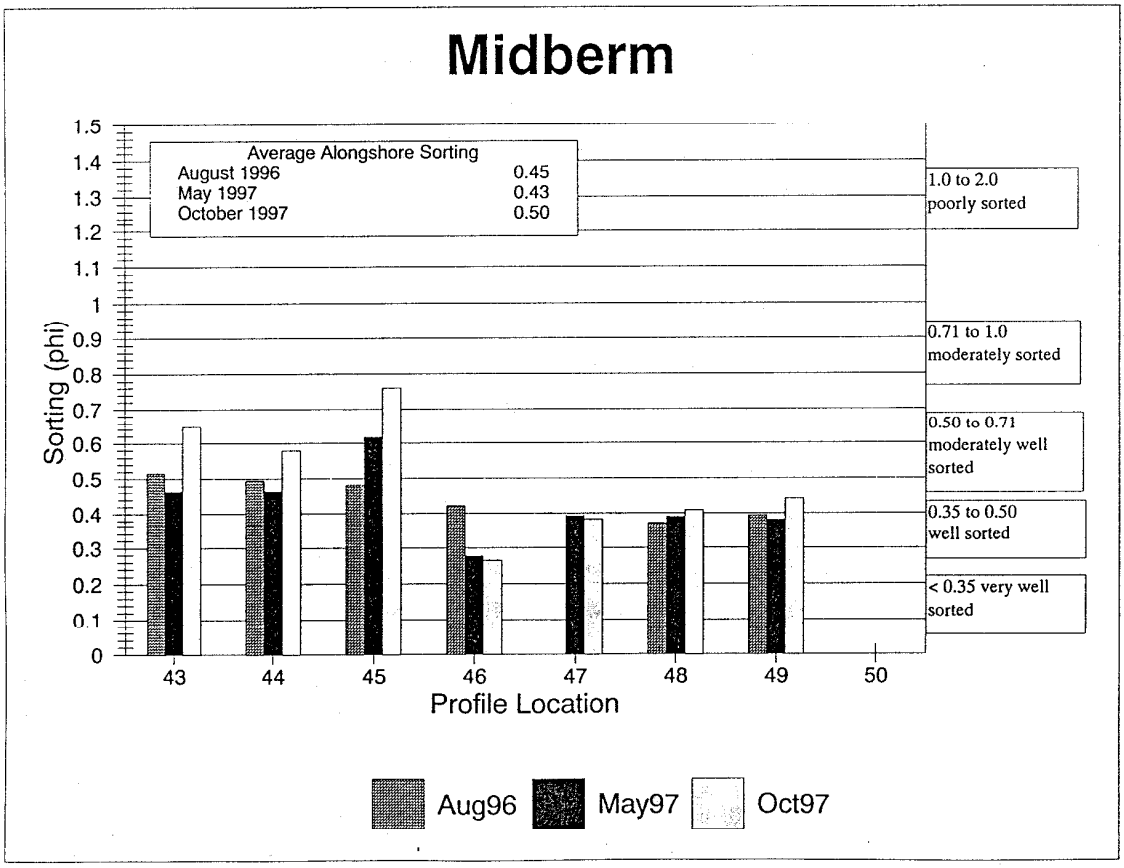

B

Figure 26. Midberm A) median grain size and B) sorting.

the south. Sorting patterns, in general, show better sorting from profile 46 south (Figure 26B). The overall average pushes the study total to a moderately well sorted status over time.

The berm feature shows a significant increase in the average alongshore grain size from August 1996 to May 1997 with a slight decrease by October 1997 (Figure 27A). With the exception of profile 44 and 46, this trend occurs at each profile where there are 3 samples for three dates. Profiles 48 and 49 show a fining median grain size in October 1997 about equal to the August 1996 sample. The average alongshore sorting is generally well-sorted (Figure 27B).

The average alongshore grain size variability for the midbeach zone is significant (Figure 28A). There is an average increase of about one phi size from August 1996 to May 1997 and a one phi size decrease from May 1997 to Oct97. This may be a seasonal trend in the active beach zone. Between August 1996 and May 1997, the midbeach zone becomes coarser north of the fill and at profile 50. All profiles become finer from May 1997 to October 1997. The average sorting is within the moderately well sorted range (Figure 28B). The May 1997 and October 1997 sorting is better or toward the well sorted range for profiles 46 to 50 relative to the northern profiles (i.e. 43,44 and 45).

The beach TOE or step is quite variable for median grain both alongshore and through time (Figures 29A and 29B). The average alongshore grain size increases by one phi size from August 1996 to May 1997 and then becomes finer by an average of one and one-half phi size from May 1997 to October 1997. This variability also may be explained as seasonal trends. The TOE sediments become generally better sorted through time (Figure 29B).

The “-2" average alongshore median grain size is generally finer than the subaerial beach sediments with a coarsening trend from August 1996 to May 1997 and a fining trend from May 1997 to October 1997 (Figure 30A). Once again this appears seasonal. Also, the May 1997 data was obtained near the inner bar crest. The general trend for sorting is to become better sorted with time (Figure 30B).

The “-6" sediments become slightly coarser with time (Figure 31A), and there is little significant change in sediment sorting (Figure 31B). The “-12" sediments trend slightly finer with time and become slightly better sorted (Figures 32A and 32B).

The “-18" sediment samples get slightly coarser between August 1996 and May 1997. Between May and October 1997, however, the average grain size has returned to what it was in August 1996, indicating a seasonal change in sediment size (Figure 33A). At this depth and distance offshore, the sand size fraction is very fine sand. The sorting differs from the median grain size in that it becomes better sorted between August 1996 and May 1997, but between May and October 1997, the sorting value does not change (Figure 33B). The “-24" sediment trends are slightly coarser then finer with time (Figure 34A). The sorting is generally very well-sorted becoming slightly better sorted over the study period (Figure 34B). At individual profiles, the median grain size stays relatively the same, but sorting values vary at profiles 48 and 50.

The overall sample can be characterized by the percentage of gravel, sand, silt, and clay in the sample. Generally, the samples contained mostly sand. Overall, the samples taken in the

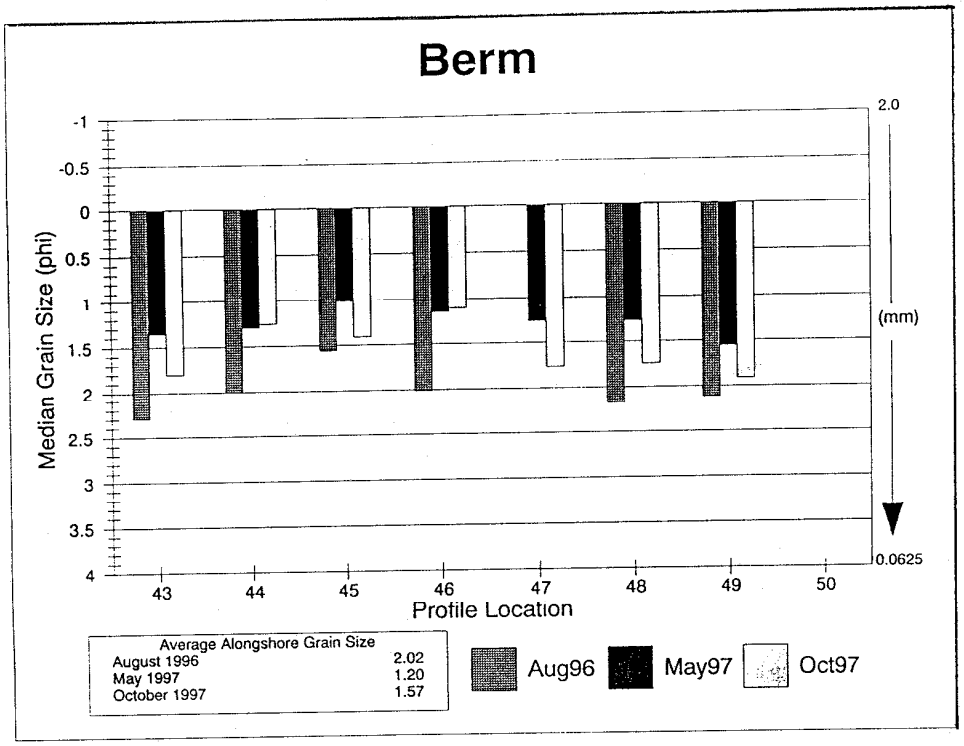

A

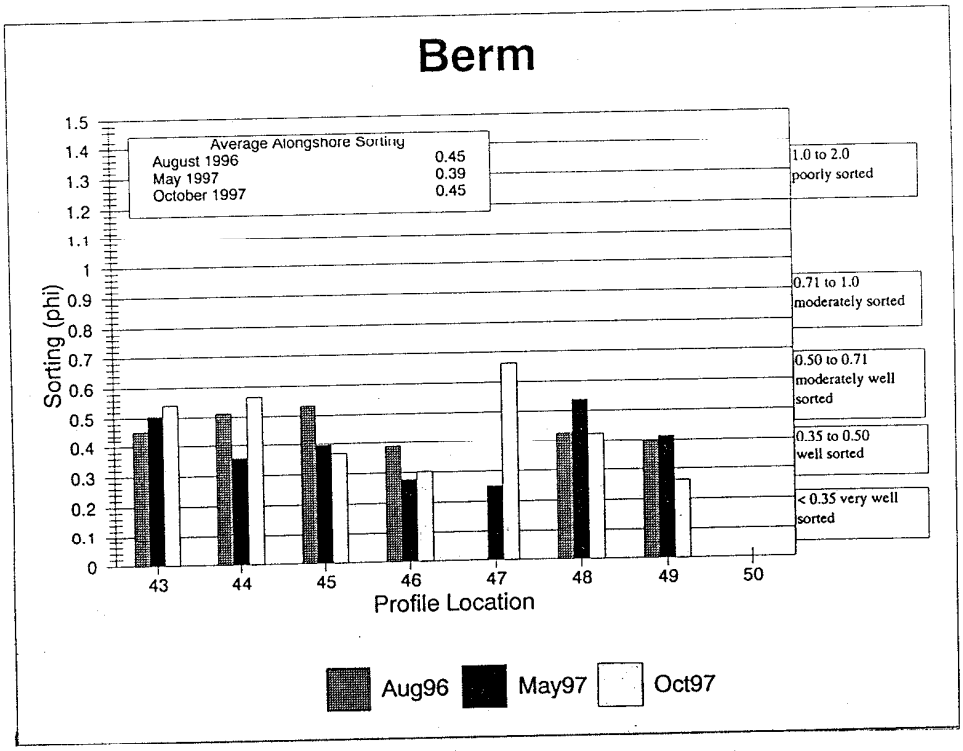

B

Figure 27. Berm A) median grain size and B) sorting.

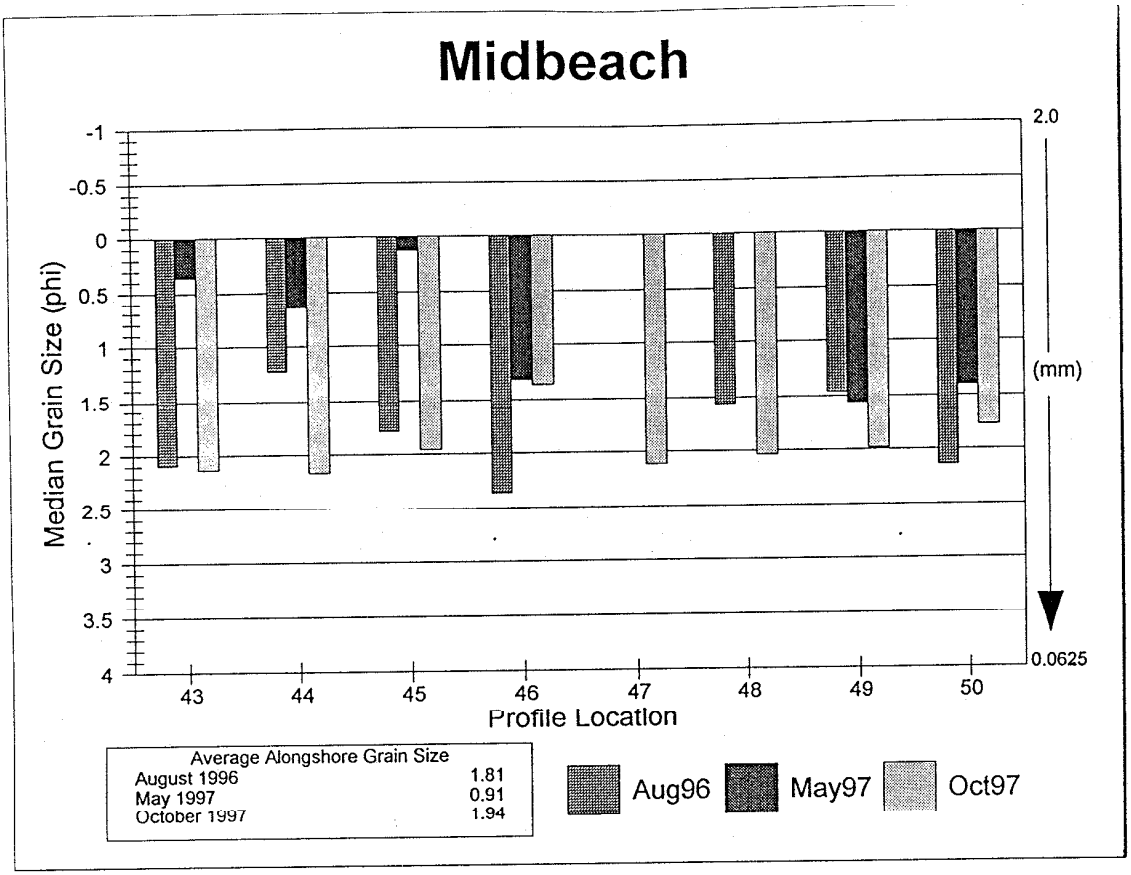

A

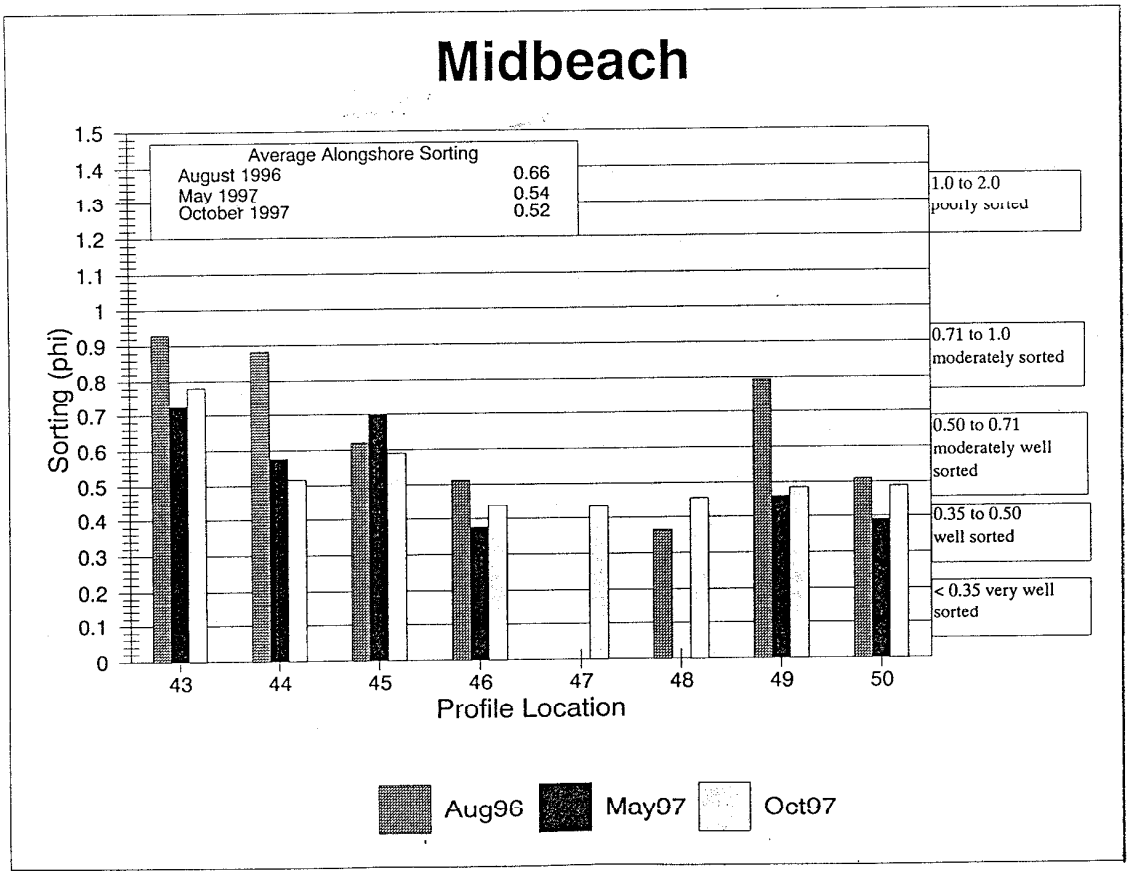

B

Figure 28. Midbeach A) median grain size and B) sorting.

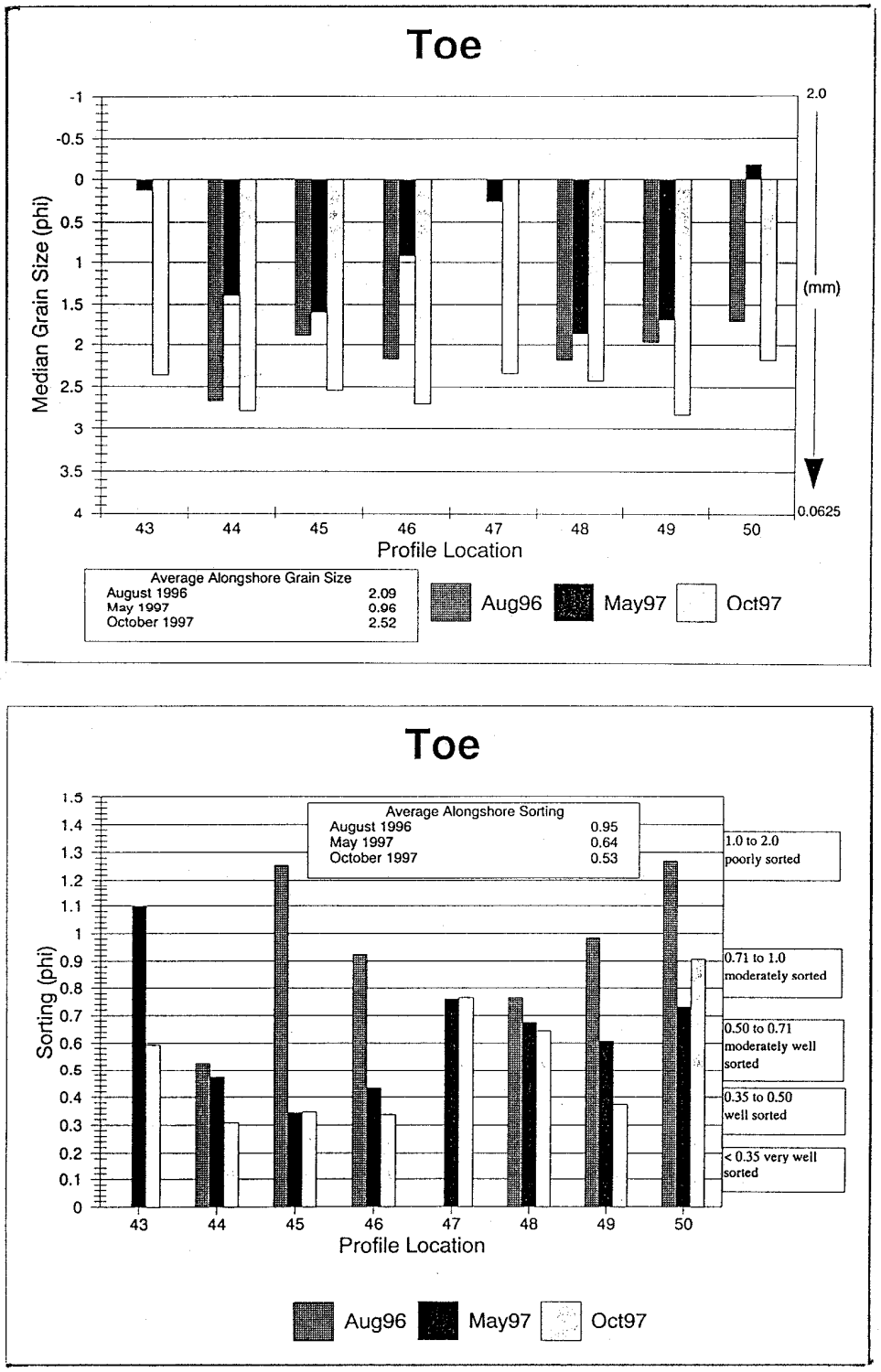

Figure 29. TOE A) median grain size and B) sorting.

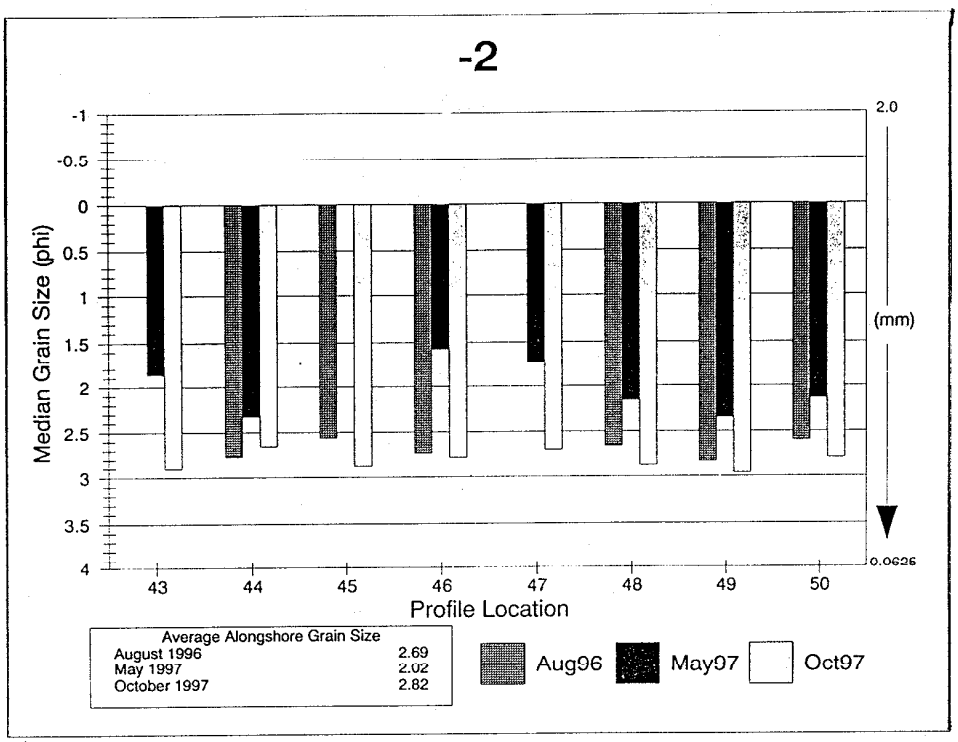

A

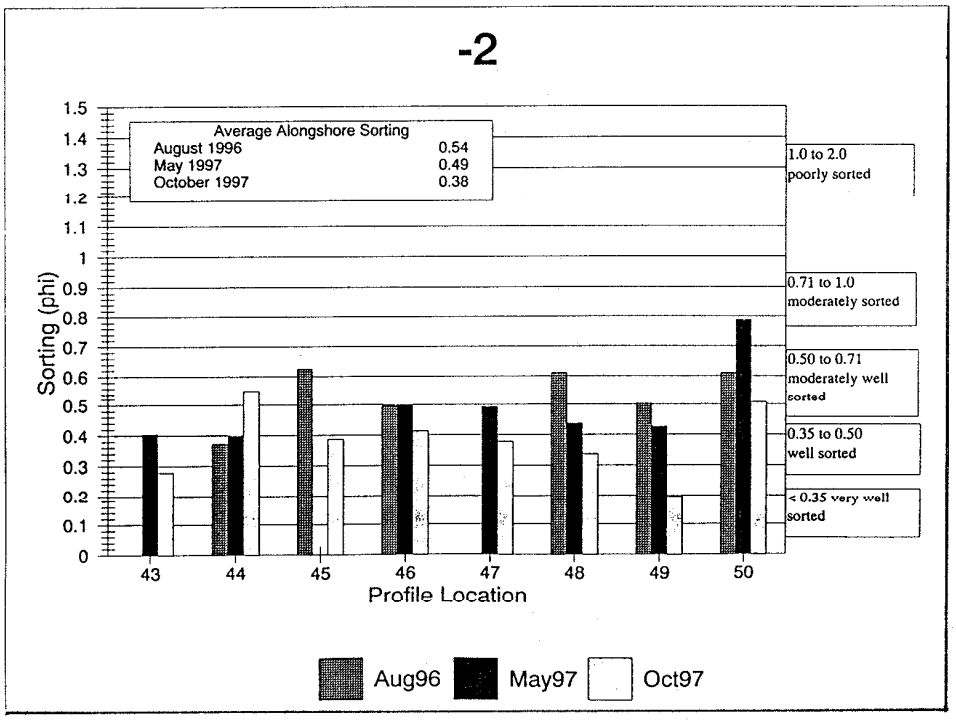

B

Figure 30. "-2" A) median grain size and B) sorting.

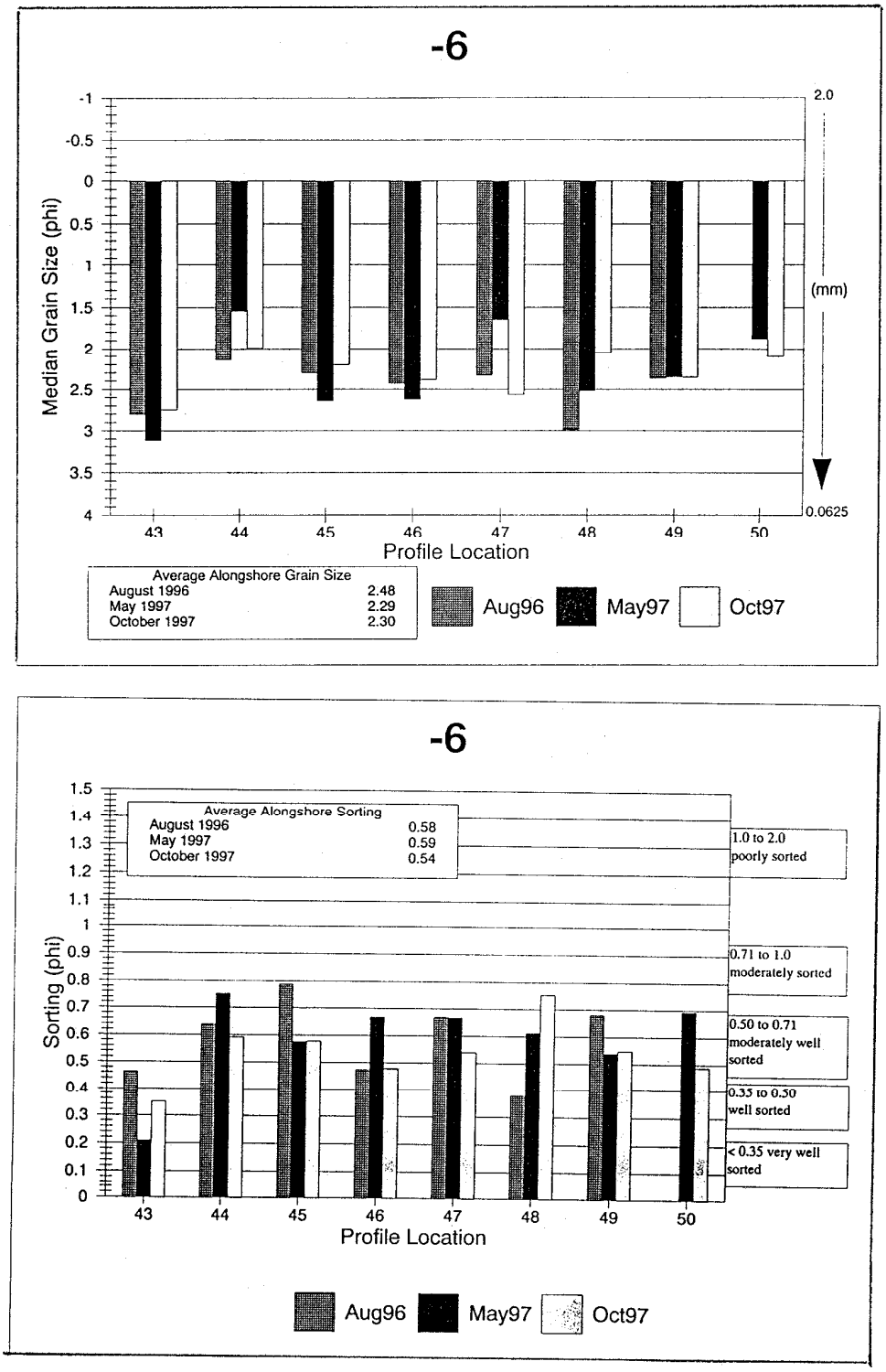

Figure 31. "-6" A) median grain size and B) sorting.

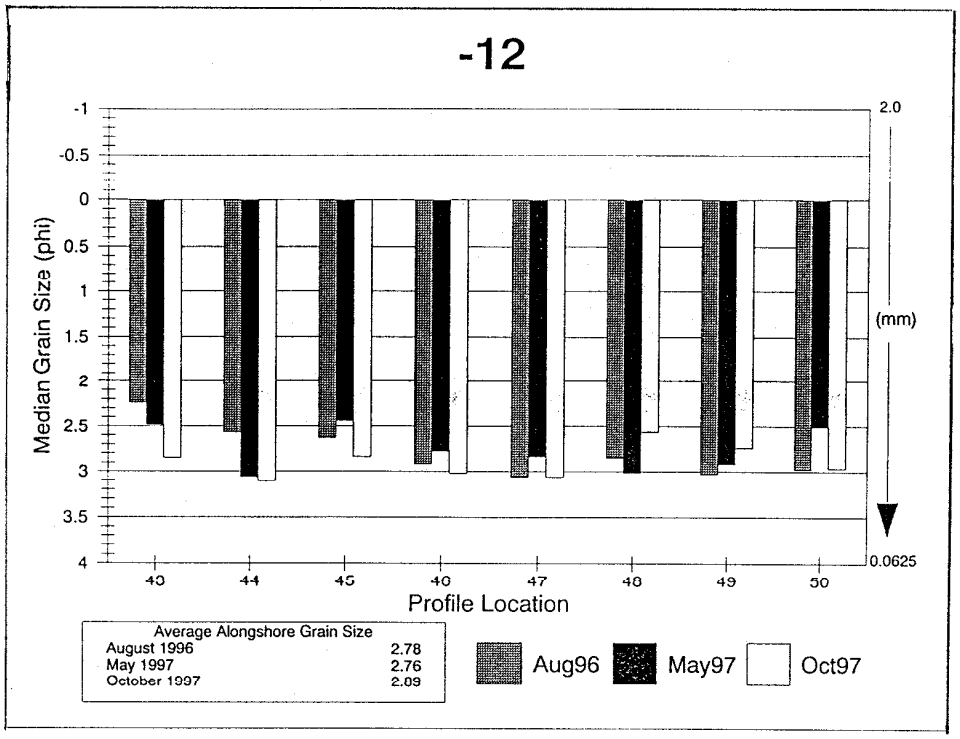

A

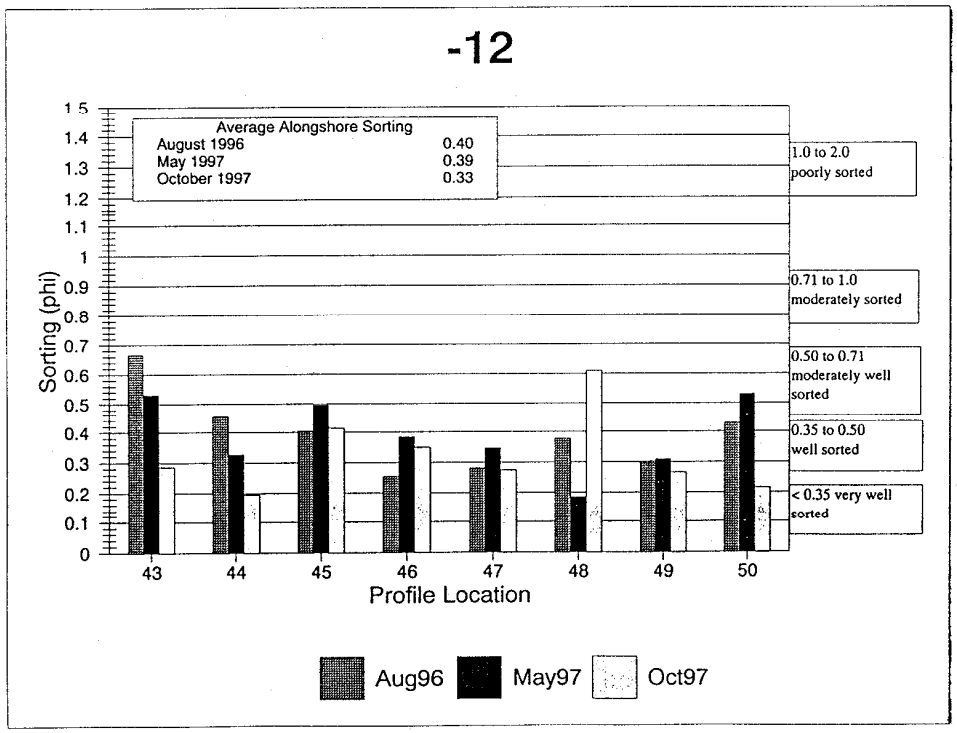

B

Figure 32. "-12" A) median grain size and B) sorting.

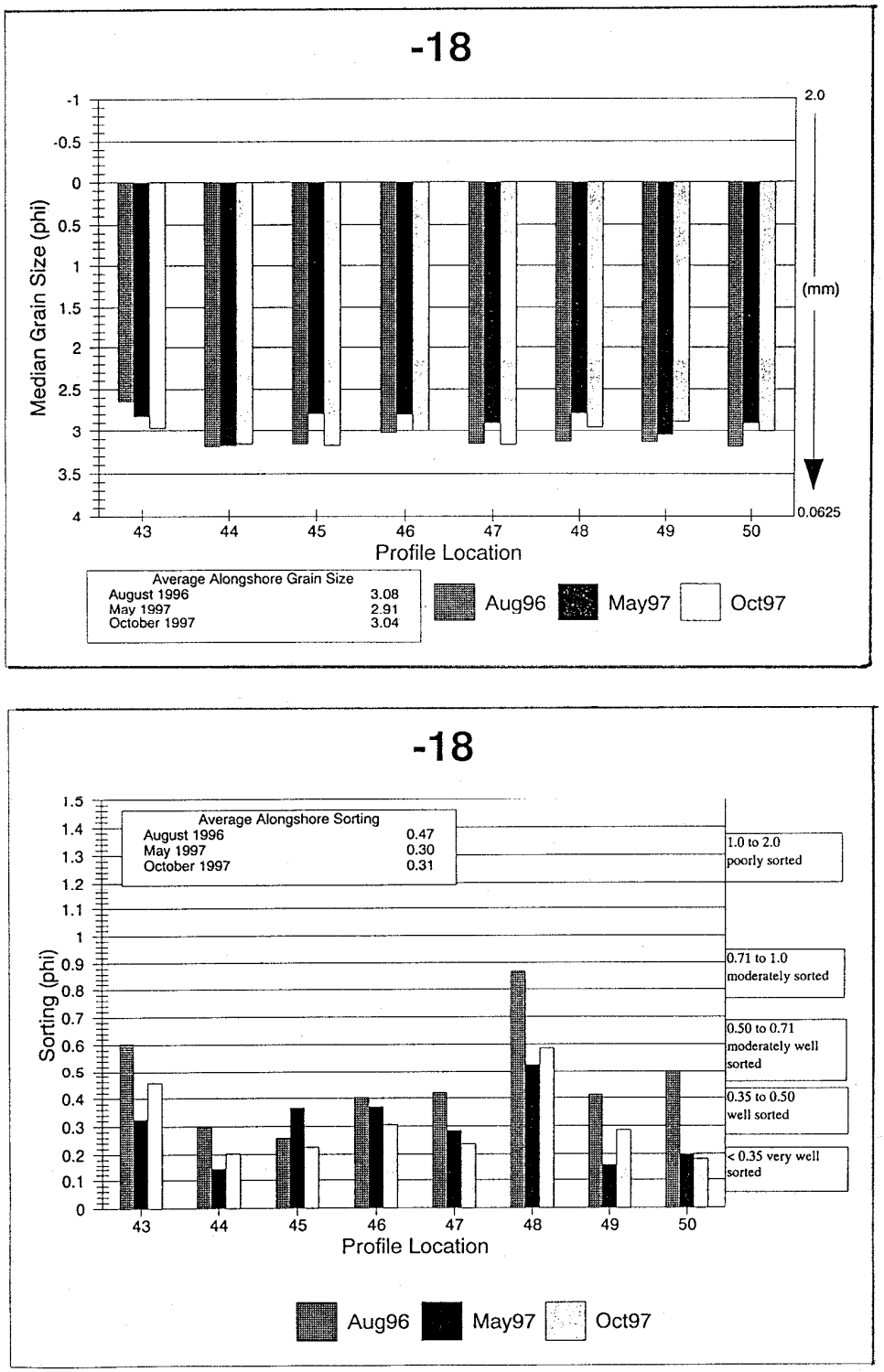

Figure 33. "-18" A) median grain size and B) sorting.

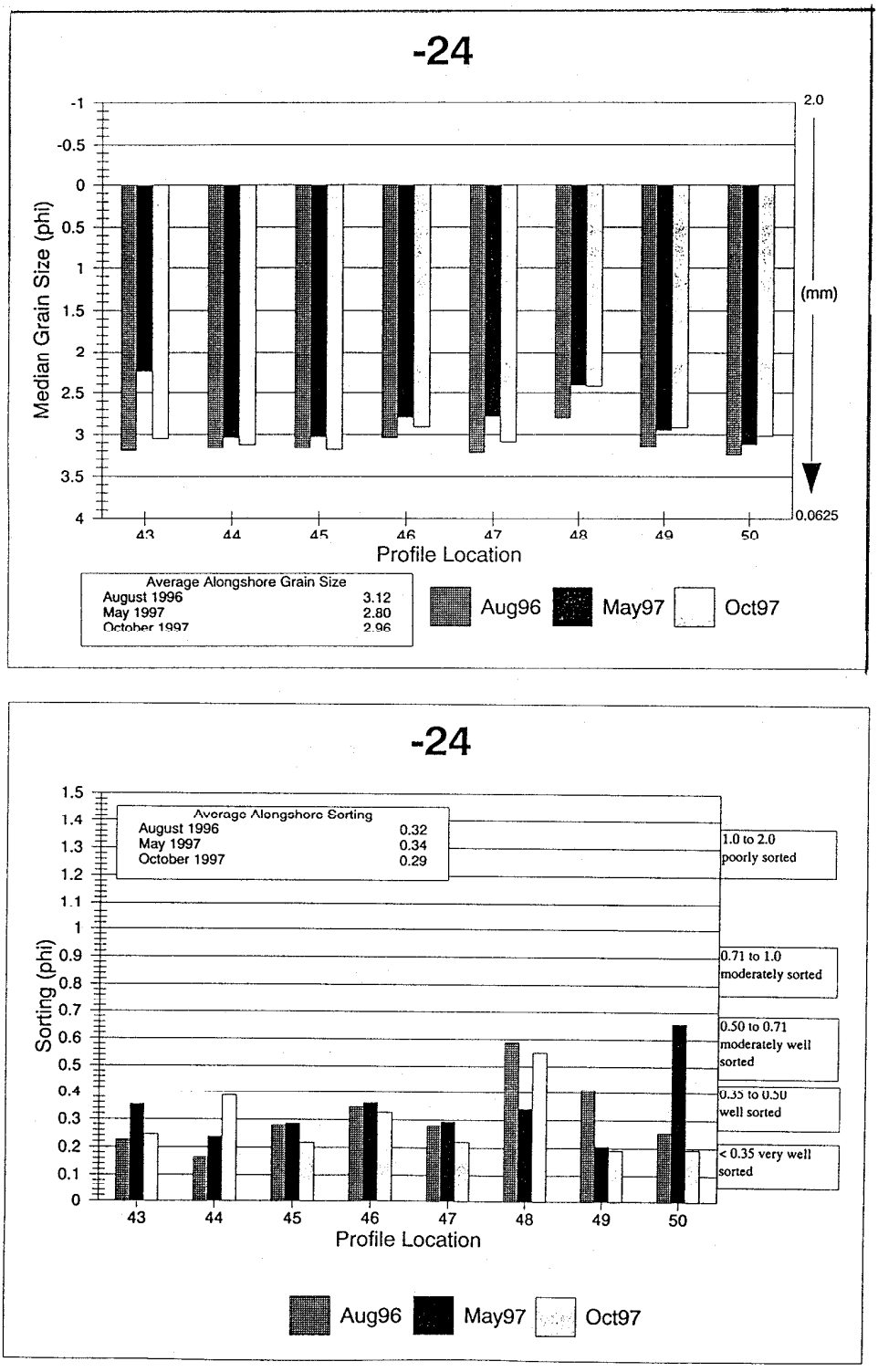

Figure 34. "-24" A) median grain size and B) sorting.

course of this study contained little silt and clay, so they are discussed collectively as mud. The samples taken in August 1996 revealed very little gravel, and most of the mud was located in the offshore samples. The mud content was highest at the “-24" sample; profile 44, sample “-24" contained 51% mud, and profile 50, sample “-24" had 14% mud. In May 1997, the highest mud content generally was in the offshore samples with profile 43, sample “-24" having the highest content at 20%. The samples taken in May 1997 had about the same gravel content as in August 1996. The samples taken in October 1997 contained much less gravel and mud than in May 1997. In October, none of the samples had over 3% mud in the sample. The TOE at profile 47 had 24% gravel, and the TOE at profile 45 had 9% gravel. Other than these samples, no others had more than5% gravel in the sample.

Discussion

Several trends are evident in the results of the one year monitoring study of the DNBNP. The movement of the beach fill material has taken place both alongshore and offshore. The subaerial beach change of the position of MHW and the -2 ft. contour through time (Figures 20A and 20B) are qualified in Table 5. Generally, there is significant accretion associated with the beach fill mass from August 1996 to May 1997. Then erosion of the seaward side of the main fill (profile 47) occurs as the material spreads laterally.

Table 5

	MHW	Change Figure 20A	-2	Change Figure 20B
Profile	Aug96-May97	May97-Oct97	Aug96-May97	May97-Oct97
43	erosion	no change	erosion	accretion
44	small accretion	small accretion	erosion	accretion
45	no change	accretion	accretion	accretion
46	accretion	erosion	erosion	accretion
47	accretion	erosion	accretion	no change
48	accretion	no change	erosion	no change
49	no change	accretion	erosion	accretion
50	no change	erosion	no change	no change

Summary of relative profile change at the position of MHW and the -2 ft. contour as shown in Figures 20A and 20B.

Volume changes (Table 6) above MSL show gains in the subaerial beach either side of the fill. Volumetrically there appears to be a net gain of subaerial beach to the south. This is also evident more dramatically of the offshore gains southward especially profile 48. These trends indicate a net southward movement of the beach fill mass after one year. This trend was

occurring before the October 15 to 19, 1997 northeasters for the subaerial beach. That same storm period is most likely responsible for the offshore trend associated with the southward movement. Wind data obtained at Norfolk International Airport from that event reflects primarily a north and northeast wind field with consequent southward driving wave conditions. This storm had the most impact to the project since placement in the fall of 1996.

Table 6

	Volume Change	Above MSL Figure 21A	Volume Change Below MSL Figure 21B
Profile	Aug96-May97	May97-Oct97	Aug96-Oct97
43	loss	gain	small loss
44	no change	gain	small gain
45	loss	gain	no change
46	gain	no change	small loss
47	gain	no change	gain
48	no change	gain	gain
49	no change	gain	small gain
50	no change	no change	small loss

Summary of relative volume changes above and below MSL as shown in Figures 21A and 21B.

The one year (Aug96-Oct97) rate of change for MHW, obtained during the course of this study, is compared against historic trend and trends in City data (Figure 35). Profile 46 appears as an anomaly considering the large mass of sand placed only 1,000 ft. to the south. The net change over one year is about zero after an initial loss of about 40 ft. from August 1996 to May 1997. This may be attributable to wave refraction across the beach fill mass causing a localized wave energy concentration or a “hot spot” with sediment loss relative to adjacent shorelines. With time and the occurrence of storms, the beach planform will move toward a dynamic equilibrium in the longshore directions.

Equilibrium of the October 1997 steep, nourished beach face profile also will take place. This offshore shifting of fill sand has occurred as evidenced by the large inner bar features on profile 47. From historic City survey data, the natural inner bar is a more subtle feature. With the advent of the DNBNP, more distinct inner bars may develop due to the increased sand volume within the reach. The large bar and nearshore increase in sediment volume on profile 48 are evidence of the net offshore and southward movement of the beach fill beyond its original limits; these features are not seen on adjacent profiles north of the project. The offshore impacts of beach fill movement may extend beyond the depths of “closure” (approximately 30 ft. below MSL), at least initially.

Sediment trends for the subaerial beach (BOD to -2 ft) are seasonal changes with coarser sands occurring after the winter season (May 1997) and a return to finer grained material after the

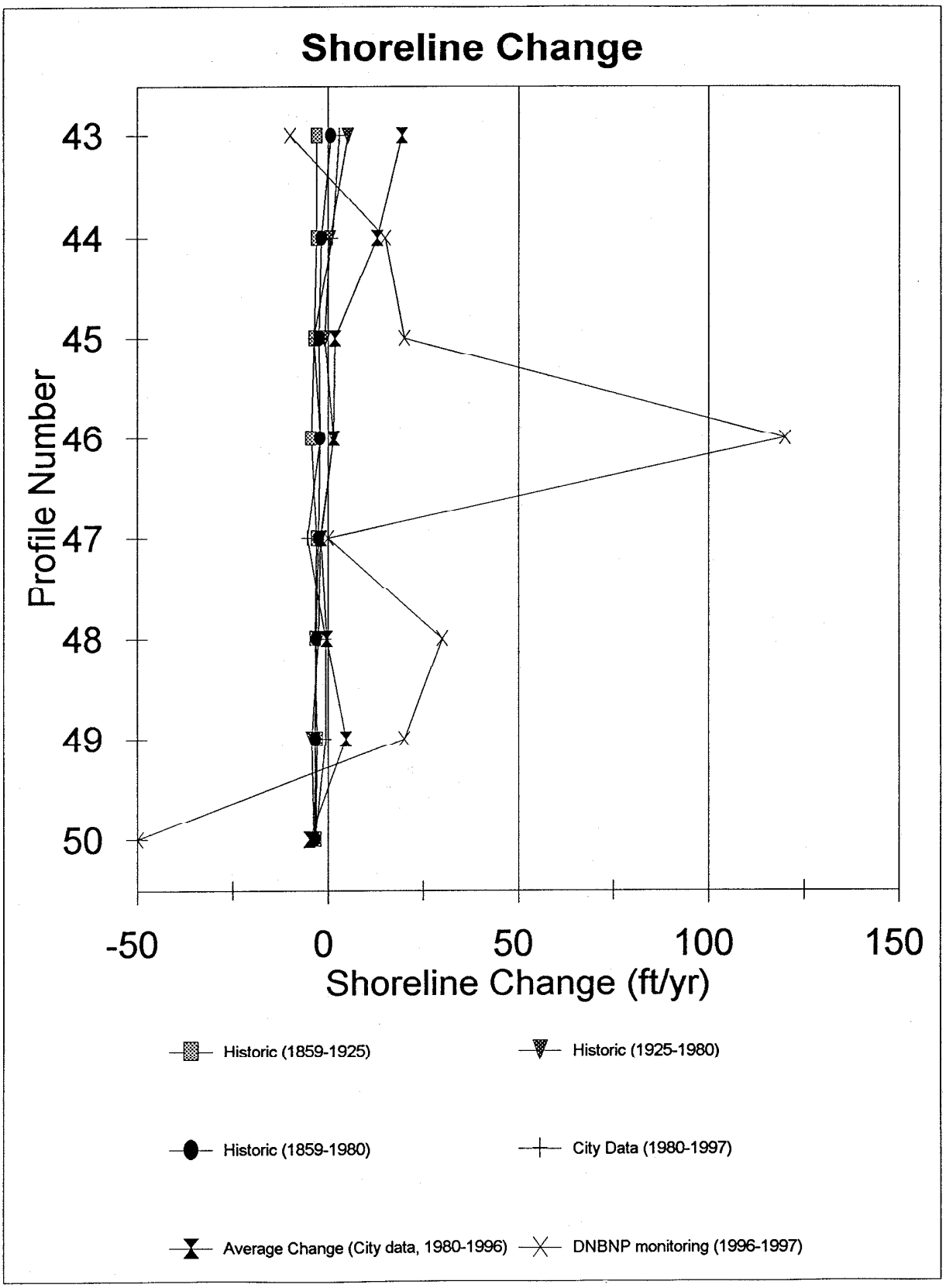

Figure 35. Rate of shoreline change using historical data, City survey data, and data obtained during the one year monitoring of DNBNP.

summer season (October 97). Table 7 qualifies this trend. The only two profile locations to get coarser with time are the Dune crest and the -24 ft.locations, the profile end points that are impacted separately by winds and waves respectively. Sorting generally gets better with time for the whole sediment suite except for the berm and midberm.

Table 7

	Median	Grain Size	Sorting	
Sample	Aug96-May97	May97-Oct97	Aug96-May97	May97-Oct97
Dune	coarser	no change	better sorted	little change
BOD	coarser	finer	better sorted	little change
Midberm	coarser	finer	no change	less sorted
Berm	coarser	finer	better sorted	less sorted
Midbeach	coarser	finer	better sorted	better sorted
TOE	coarser	finer	better sorted	better sorted
“-2"	coarser	finer	better sorted	better sorted
“-6"	coarser	no change	little change	little change
“-12"	little change	finer	better sorted	better sorted
“-18"	coarser	finer	better sorted	no change
“-24"	coarser	finer	little change	better sorted

Summary of the relative average alongshore sediment statistics of the study site as shown in Figures 23-33.

VII. Conclusion

On a regional scale, the DNBNP lies within an area of historic shoreline recession. False Cape and Cape Henry and their associated shoal systems act as headlands that modify the wave energies impacting the shoreline. Between the two headlands a long, curvilinear embayment has formed as the shoreline has adjusted to the waves impacting the shore. The wave energy impacting the shore generally comes from the southeast with northeast storms occurring during the winter. The waves are modified by a complex offshore bathymetry that tends to concentrate wave energy in Sandbridge just south of the study area. This system is difficult to characterize since it is so variable. Data collected indicate large seasonal changes in morphology and sedimentology as well as variable rates of change through time.

In addition to natural trends, man has also impacted this shore reach. The only interruption along the shoreline is Rudee Inlet. The weir and jetty system at Rudee Inlet has influenced the shore morphology through time by acting as a littoral barrier and allowing sediments to accrete southward with only intermittent losses due to annual dredging. Since 1988, bulkheads have been built and the beach bulldozed all along Sandbridge as erosion threatened structures. Although these actions have led to a loss of the subaerial beach, the bulkheads have stabilized the rates of change in the area.

Beach nourishment as a means of shore protection has long been suggested as the best means to abate erosion along this shore reach. The DNBNP has added over 1,000,000 cubic yards of good quality beach sand to the littoral system. Whether the fill will be effective as shore protection at Dam Neck for 12 years, the Navy's projected fill life expectancy before renourishment is required, is yet to be seen. However, the impacts to the beach and nearshore region of adjacent shores will be positive in the sense that increased profile dimensions not only will abate shore recession but the added critical mass should reduce the historic losses for some time. The proposed addition of another 1,000,000 cubic yards to the south along Sandbridge in the spring of 1998 will complement the DNBNP.

In general, the DNBNP has spread both alongshore and cross-shore as material is eroded from the center of the fill. The mechanisms for transport indicate that, in addition to being moved subaerially, as seen with the creation of a high water berm, sediment also may be moving to the north in the nearshore region through the bar and trough system. The direction of sediment movement relates to the predominant wave direction. The net northward transport rate indicates that more sand moves north than south over time, but the initial net subaerial movement of the fill is to the south. Increased dredging may be necessary at Rudee Inlet as the fill moves north since more sand is available for transport at least for a few years.

Acknowledgments

The authors would like to thank those individuals who put forth considerable effort in helping collect data -- in particular, Bob Gammisch, Eric Grant, Andrew Trojan, and Linda Meneghini, who also analyzed the sediment data. In addition, thanks to Andy Porter and Jim Bonavita from the Navy for their help in coordinating our data collection efforts. Also, the

authors would like to thank several individuals for facilitating our access to restricted areas within the study area: MSgt Donald R. Bains, USAR, Virginia Army National Guard, Camp Pendleton; OS1 Samuel Renfroe, USN, Little Creek Port Ops and Training; CWO3 Dayle Wright, USMC, Marine Air Control Squadron 24; GySgt T.L. Walker, USMC, Marine Corps Security Forces Battalion, Range Detachment, Dam Neck; and Mr. James Finley, Range Manager, Naval Special Warfare Development Group, Dam Neck.

References

Basco, D.R., 1991. Boundary conditions and long-term shoreline change rates for the southern Virginia ocean coastline. *Shore and Beach*, 8-13.

Basco, D.R.; Bellomo, D.A.; Hazelton, J.M.; and Jones, B.N., 1997. The influence of seawalls on subaerial beach volumes with receding shorelines. *Coastal Engineering*, 30, 203-233.

Bascom, W.N., 1959. The relationship between sand size and beach face slope. *American Geophysical Union Transactions*, 32(6), 866-874.

Berquist, C.R., and Hobbs, III, C.H., 1989. Heavy mineral potential of offshore Virginia. *Marine Geology*, 90, 83-86.

Boon, J.D., 1997. Environmental Studies relative to Potential Sand Mining in the vicinity of the City of Virginia Beach, Virginia. Part 3: Nearshore Wave and Currents – Observations and Modeling. 21 pp. + app.

Crowell, M.; Leatherman, S.P., and Buckley, M.K., 1991. Historical shoreline change: Error analysis and mapping accuracy. *Journal of Coastal Research*, 7(3), 839-852.

Crowell, M.; Douglas, B.C.; and Leatherman, S.P., 1997. On forecasting U.S. shoreline positions: a test of algorithms. *Journal of Coastal Research*, 13(4), 1245-1255.

Dolan, R., 1985. Sandbridge Beach and Back Bay. Technical Report, Sandbridge Beach Restoration Association.

Dolan, R.; Fenster, M.S. and Holme, S.J., 1991. Temporal analysis of shoreline recession and accretion. *Journal of Coastal Research*, 7(3), 723-744.

Ebersole, B.A.; Cialone, M.A.; and Prater, M.D., 1986. RCPWAVE - A Linear Wave Propagation Model for Engineering Use. CERC-86-4, U.S. Army Corps of Engineers, 260 pp.

Everts, C.H.; Battley Jr., J.P.; and Gibson, P.N., 1983. Shoreline Movements: Report 1; Cape Henry, Virginia, to Cape Hatteras, North Carolina, 1849-1980. Technical Report *CERC-83-*,Report 1, U.S. Army Corps of Engineers, 111 pp.

Fenster, M.S.; Dolan, R.; and Elder, J.F., 1993. A new method for predicting shoreline positions from historical data. *Journal of Coastal Research*, 9(1), 147-171.

Folk, R.L., 1980. Petrology of Sedimentary Rocks. Hemphill Publishing Company, Austin, TX, 184 pp.

Foster, E.R. and Savage, R.J., 1989. Methods of historical shoreline analysis. *In*: Magoon, O.T., Converse, H.; Miner, D.; Tolbin, L.T., and Clark, D. (eds.) *Coastal Zone '89*, 5, 4434-4448.

Friedman, G.M. and Sanders, J.E., 1978. Principles of Sedimentology. John Wiley and Sons, New York, NY, 792 pp.

Goldsmith, V.; Sturm, S.C.; Thomas, G.R., 1977. Beach Erosion and Accretion at Virginia Beach, Virginia, and Vicinity. Miscellaneous Report No. 77-12, U.S. Army Corps of Engineers, Coastal Engineering Research Center, Fort Belvoir, VA, 185 pp.

Hardaway, Jr., C.S. and Thomas, G.R., 1990. Sandbridge Bulkhead Impact Study. SCRAMSOE No. 305, Virginia Institute of Marine Science, College of William and Mary, Gloucester Point, VA.

Hardaway, Jr., C.S.; Thomas, G.R.; and Li, J.H., 1991. Chesapeake Bay Shoreline Studies: Headland Breakwaters and Pocket Beaches for Shoreline Erosion Control. SRAMSOE No. 313, Virginia Institute of Marine Science, College of William and Mary, Gloucester Point, VA, 42 pp. + app.

Hobbs, III, C.H., 1997. Sediments and Shallow Stratigraphy of a Portion of the Continental Shelf of Southeastern Virginia. Contract Report for the Mineral Management Service. Virginia Institute of Marine Science, College of William and Mary, Gloucester Point, VA , 102 pp + app.

Kimball, S.M. and Dame, II, J.K., 1989. Geotechnical Evalution of Sand Resources on the Inner Shelf of Southern Virginia. Final Contract Report, Virginia Institute of Marine Science, College of William and Mary, Gloucester Point, VA, 73 pp + app.

Larson, M. and Kraus, N.C., 1994. Temporal and spatial scales of beach profile change, Duck, North Carolina. *Marine Geology*, 117,75-94.

Ludwick, J.C., 1978. Coastal currents and an associated sand stream off Virginia Beach, Virginia. *Journal of Geophysical Research*, 83(C5), 2365-2372.

Maa, -Y. J.P., 1995. Investigation of Isolated Sand Shoals on the Inner Shelf of Virginia Relative to the Potential for Aggregate Mining. Report on Task 4: Possible physical impact of dredging at Sandbridge Shoal of the 1993-1995 U.S. Minerals Management Service - Commonwealth of Virginia Cooperative Project, Virginia Institute of Marine Science, College of William and Mary, Gloucester Point, VA, 51 pp.

Maa, J. P.-Y. and C. H. Hobbs, III, in press. Physical impact of waves on adjacent coasts resulting from dredging at Sandbridge Shoal, Virginia. *Journal of Coastal Research*.

Morton, R.A., 1991. Accurate shoreline mapping: Past, present, and future. *Coastal Sediments '91*, American Society Civil Engineers, 1, 997-1010

Niedoroda, A.W.; Swift, D.J.P.; Figueiredo, Jr., A.G.; and Freeland, G.L., 1985. Barrier island evolution, middle Atlantic shelf, U.S.A., Part II: Evidence from the shelf floor. *Marine Geology*, 63, 363-396.

Shalowitz, A.L., 1964. Shoreline and Sea Boundaries. V-2, Publication 10-1, U.S. Dept. of Commerce, Coast and Geodetic Survey, U.S. Government Printing Office, Washington, D.C.

Stauble, D.K.; Garcia, A.W.; Kraus, N.C.; Grosskopf, W.G.; and Bass G.P., 1993. Beach Nourishment Project Response and Design Evaluation: Ocean City Maryland, Report 1, 1988-1992. Technical Report CERC-93-13, U.S. Army Corps of Engineers, Coastal Research Program 224 pp. + app.

Swift, D.J.P.; Niedoroda, A.W.;Vincent,C.E., and Hopkins, T.S., 1985. Barrier island evolution, Middle Atlantic Shelf, U.S.A. Part I: Shoreface dynamics. *Marine Geology*, 63, 331-361.

U.S. Army Corps of Engineers, 1994. Interactive Survey Reduction Program (ISRP).

Waterway Surveys & Engineering Ltd., 1986. Engineering Study for Disposal of Dredged Material from Atlantic Ocean Channel on Sandbridge Beach between Back Bay and Dam Neck. Virginia Beach, VA, 79 pp + app.

Williams, S.J., 1987. Geologic Framework and Sand Resources of Quaternary Deposits Offshore Virginia, Cape Henry to Virginia Beach. Open-File Report 87-667. Dept. of the Interior, U.S. Geological Survey, Reston, VA, 60 pp.

Wright, L.D.; Boon, J.D.; Kim, S.C.; and List, J.H., 1991. Modes of cross-shore sediment transport on the shoreface of the Middle Atlantic Bight. *Marine Geology*, 96, 19-51.

Wright, L.D.; Kim, C.S.; Hardaway, S.C.; Kimball, S.M.; and Green, M.O., 1987. Shoreface and beach dynamics of the coastal region from Cape Henry to False Cape, Virginia. Technical Report, Virginia Institute of Marine Science, College of William and Mary, Gloucester Point, VA, 116 pp.

Appendix A

Results of Sediment Analysis

Profile Number
Location of Sample
Distance from Benchmark in ft. for Beach Samples
Latitude of Offshore Samples, Minutes Shown in Column
Longitude of Offshore Samples, Minutes Shown in Column

Entire Sample Analyses
Percent of Gravel in Sample
Percent of Sand in Sample
Percent of Silt in Sample
Percent of Clay in Sample
Percent of Mud (%Silt+%Clay) in Sample

Measures of the Sand Portion of the Sample
Moment Method of Analysis (M1, M2, M3, M4)
Graphic Mean (Mn)
Graphic Median (Md)
Sorting or Inclusive Graphic Standard Deviation
Inclusive Graphic Skewness
Graphic Kurtosis

1 aug 1996																		
Profile	Location	Dist (ft)	Latitude	Longitude	%grvl	%sand	%silt	%clay	%mud	M1	M2	M3	M4	Mn	Md	Sorting	Skewness	Kurtosis
			36 deg	75 deg										(Phi)	(Phi)	(Phi)		
			minutes	minutes														
43	Dune Crest	30			0.0	100.0	0.0	0.0	0.0	1.7659	0.5294	-0.4733	3.5667	1.7771	1.8242	0.5117	-0.1471	0.48
	BOD	43			0.0	100.0	0.0	0.0	0.0	1.946	0.4192	-0.7755	9.2604	1.9442	1.9625	0.3856	-0.0507	0.3533
	MIDBERM	80			0.0	100.0	0.0	0.0	0.0	1.8825	0.5396	-0.7739	3.8431	1.8916	1.9823	0.5167	-0.2626	0.4605
	BERM	157			0.0	100.0	0.0	0.0	0.0	2.2823	0.4978	-0.1013	4.5626	2.291	2.2936	0.4544	-0.0502	0.3801
	MIDBEACH	230			0.0	100.0	0.0	0.0	0.0	1.7815	0.908	-0.7326	2.3642	1.7668	2.0909	0.9296	-0.4669	0.5762
	-6		49.721	58.031	2.7	97.3	0.0	0.0	0.0	2.6954	0.5981	-2.4142	11.9005	2.7641	2.8018	0.4645	-0.2467	0.3297
	-12		49.759	57.931	0.0	100.0	0.0	0.0	0.0	2.0958	0.7705	-1.6705	7.3838	2.1443	2.243	0.6654	-0.2521	0.4965
	-18		49.67	57.88	0.0	100.0	0.0	0.0	0.0	2.5109	0.7253	-2.1701	8.2989	2.6248	2.6415	0.6036	-0.2861	0.5151
	-24		49.81	57.86	4.2	93.0	1.5	1.3	2.8	3.1482	0.3349	-4.3969	40.0882	3.1869	3.1998	0.226	-0.213	0.1716
44	BOD	158			0.0	100.0	0.0	0.0	0.0	1.2831	0.5197	0.459	3.1358	1.2711	1.2498	0.5194	0.099	0.5552
	MIDBERM	220			0.0	100.0	0.0	0.0	0.0	1.2278	0.5486	1.0234	5.9938	1.2022	1.1659	0.4942	0.1652	0.5733
	BERM	254			0.0	100.0	0.0	0.0	0.0	1.9885	0.5126	0.0134	2.9268	1.9917	1.9954	0.5123	-0.0227	0.4148
	MIDBEACH	298			0.0	100.0	0.0	0.0	0.0	1.2379	0.8726	0.1247	1.9842	1.2393	1.2287	0.8819	0.0215	0.5905
	TOE	358			0.0	98.3	1.7	0.0	1.7	2.5311	0.5898	-1.6895	6.1606	2.6007	2.6643	0.526	-0.345	0.4386
	-2	388			0.0	100.0	0.0	0.0	0.0	2.7634	0.5131	-0.4719	9.794	2.765	2.7689	0.3726	-0.0729	0.2889
	-6		49.13	57.94	0.0	100.0	0.0	0.0	0.0	2.0637	0.6375	-0.5431	3.2374	2.0764	2.1472	0.6386	-0.1821	0.522
	-12		49.13	57.86	0.0	100.0	0.0	0.0	0.0	2.5005	0.6065	-2.6174	14.4469	2.5727	2.5677	0.4542	-0.0793	0.3369
	-18		49.13	57.79	0.0	92.1	6.4	1.4	7.9	3.1547	0.1647	-0.4542	3.9933	3.1641	3.1635	0.1636	-0.036	0.1212
	-24		49.19	57.65	0.0	48.8	51.2	0.0	51.2	3.0826	0.4522	-4.5479	34.8329	3.1322	3.1855	0.3008	-0.4073	0.2299
45	DUNE CREST	0			0.0	100.0	0.0	0.0	0.0	2.0556	0.3755	-0.7645	8.3274	2.0572	2.0588	0.3443	-0.0134	0.315
	BOD	32			0.0	100.0	0.0	0.0	0.0	1.0211	0.6028	0.3605	2.8533	1.0057	0.9696	0.6056	0.1133	0.7093
	MIDBERM	73			0.0	100.0	0.0	0.0	0.0	1.8607	0.4745	-0.2469	2.8575	1.8574	1.9036	0.482	-0.1394	0.4181
	BERM	88			0.0	100.0	0.0	0.0	0.0	1.5488	0.5363	0.0061	2.8406	1.549	1.5562	0.5336	-0.0065	0.4963
	MIDBEACH	132			0.0	99.4	0.0	0.6	0.6	1.7748	0.6276	-0.2835	2.9553	1.7999	1.7901	0.6204	-0.0161	0.4791
	TOE	200			4.2	95.8	0.0	0.0	0.0	1.5704	1.2342	-0.447	1.901	1.5822	1.8854	1.2548	-0.3346	0.6211
	-2				0.0	100.0	0.0	0.0	0.0	2.3935	0.7431	-1.9026	8.217	2.4651	2.5626	0.6252	-0.3189	0.4421
	-6		48.457	57.766	0.0	100.0	0.0	0.0	0.0	2.1557	0.7714	-0.7127	2.8634	2.1734	2.3036	0.7887	-0.2717	0.5108
	-12		48.494	57.722	0.0	100.0	0.0	0.0	0.0	2.6159	0.4781	-2.0956	14.3914	2.6472	2.6337	0.4042	-0.0164	0.2767
	-18		48.521	57.641	0.0	98.4	1.4	0.2	1.6	3.1056	0.2652	-1.2504	7.2657	3.1155	3.1579	0.2585	-0.2702	0.1737
	-24		48.582	57.444	0.0	95.6	3.5	0.9	4.4	3.0745	0.4179	-4.2325	32.0613	3.1182	3.1668	0.2797	-0.3407	0.2015
46	DUNE FACE	54			0.0	98.9	0.0	1.1	1.1	1.9572	0.4919	-0.0068	2.7018	1.9577	1.967	0.4923	-0.0272	0.3974
	BOD	69			0.0	100.0	0.0	0.0	0.0	1.9286	0.4033	-0.1059	3.849	1.9281	1.9434	0.3936	-0.0422	0.3633
	MIDBERM	89			0.0	99.5	0.0	0.5	0.5	1.9243	0.4265	-0.043	3.0114	1.9215	1.9467	0.4221	-0.0702	0.3724
	BERM	103			0.0	100.0	0.0	0.0	0.0	2.0078	0.3892	0.1078	3.2517	2.0019	2.0106	0.3879	-0.0271	0.3601
	MIDBEACH	147			0.0	98.2	0.0	1.8	1.8	2.2872	0.5042	-0.3262	2.5687	2.2865	2.3619	0.5128	-0.2001	0.3658
	TOE	219			2.6	96.3	0.0	1.1	1.1	1.9564	0.9466	-0.8922	3.4127	1.9979	2.1667	0.9251	-0.3148	0.616
	-2	266			0.0	100.0	0.0	0.0	0.0	2.6456	0.529	-1.1355	4.7877	2.688	2.7308	0.4957	-0.2261	0.3451
	-6		47.881	57.569	0.0	100.0	0.0	0.0	0.0	2.3792	0.4724	-0.4086	2.8825	2.3862	2.4313	0.4739	-0.1458	0.3462
	-12		47.91	57.526	0.0	99.2	0.8	0.0	0.8	2.8998	0.2802	-2.622	33.9126	2.9089	2.9129	0.2535	-0.0571	0.1704
	-18		47.928	57.444	0.3	93.5	6.2	0.0	6.2	2.9173	0.4536	-1.3319	5.8932	2.9531	3.0252	0.4021	-0.2955	0.2615
	-24		47.908	57.221	0.0	93.0	5.3	1.7	7.0	2.9705	0.366	-0.8422	4.2208	2.9828	3.0404	0.3471	-0.239	0.228

1 aug 1996																		
Profile	Location	Dist (ft)	Latitude	Longitude	%grvl	%sand	%silt	%clay	%mud	M1	M2	M3	M4	Mn	Md	Sorting	Skewness	Kurtosis
			36 deg	75 deg										(Phi)	(Phi)	(Phi)		
			minutes	minutes														
47	-6		46.997	57.348	0.0	99.4	0.0	0.6	0.6	2.2554	0.6649	-0.5514	3.2094	2.2749	2.3321	0.6684	-0.1442	0.4679
	-12		47.009	57.246	1.0	97.7	1.3	0.0	1.3	3.0236	0.2797	-0.5281	2.9449	3.0303	3.064	0.2816	-0.1846	0.188
	-18		47.016	57.217	0.5	95.3	3.7	0.5	4.2	3.0265	0.5102	-2.2635	11.1204	3.0733	3.1526	0.4197	-0.3396	0.2711
	-24		47.074	57.014	0.0	93.9	4.3	1.8	6.1	3.1926	0.3691	-4.3712	38.9583	3.2121	3.2184	0.2778	-0.0768	0.1726
48	DUNE CREST	77			0.0	100.0	0.0	0.0	0.0	2.1453	0.3349	-2.7768	31.2847	2.1402	2.1211	0.258	0.165	0.2544
	BOD	107			0.0	100.0	0.0	0.0	0.0	1.5771	0.4622	0.4043	3.3617	1.5469	1.507	0.4604	0.1392	0.4892
	MIDBERM	130			0.0	100.0	0.0	0.0	0.0	1.9438	0.3875	-0.0909	4.107	1.9442	1.9564	0.3723	-0.0491	0.3527
	BERM	150			0.0	100.0	0.0	0.0	0.0	2.1552	0.5293	-1.9832	14.0231	2.1799	2.1769	0.4251	0.017	0.3693
	MIDBEACH	177			0.0	97.6	1.3	1.1	2.4	1.5743	0.4163	-0.3327	7.7990	1.5827	1.5596	0.3646	0.0915	0.4213
	TOE	300			0.0	100.0	0.0	0.0	0.0	2.2003	0.7293	-0.0755	1.9982	2.2059	2.1829	0.7636	0.0127	0.4353
	-2	412			0.0	99.3	0.0	0.7	0.7	2.5323	0.6467	-1.1616	4.5615	2.5709	2.6619	0.6102	-0.2955	0.396
	-6		46.023	56.986	0.0	99.8	0.2	0.0	0.2	2.9404	0.3813	-0.5532	3.3216	2.9501	2.9829	0.3773	-0.146	0.2509
	-12		46.062	56.979	0.0	99.9	0.1	0.0	0.1	2.7814	0.4642	-1.8528	8.2184	2.8343	2.8478	0.3771	-0.1891	0.2911
	-18		46.08	56.865	0.0	98.1	1.0	0.9	1.9	2.693	0.864	-0.796	2.1171	2.6865	3.1312	0.8689	-0.6527	0.3951
	-24		46.102	56.697	0.4	97.3	2.2	0.1	2.3	2.6921	0.7239	-2.0856	9.3323	2.7693	2.8013	0.5888	-0.2197	0.4163
49	DUNE CREST	70			0.0	100.0	0.0	0.0	0.0	1.4597	0.6158	-0.6402	3.7268	1.4808	1.5488	0.5985	-0.2419	0.6454
	BOD	104			0.0	100.0	0.0	0.0	0.0	1.8138	0.4172	-0.0157	3.1096	1.8106	1.8203	0.4188	-0.0185	0.4108
	MIDBERM	148			0.0	100.0	0.0	0.0	0.0	1.958	0.417	0.3586	4.4445	1.9491	1.9729	0.3945	-0.0476	0.3902
	BERM	178			0.0	100.0	0.0	0.0	0.0	2.104	0.3975	-0.022	3.0157	2.1053	2.1094	0.3977	-0.0257	0.3356
	MIDBEACH	228			0.0	100.0	0.0	0.0	0.0	1.5169	0.7689	0.1925	2.388	1.519	1.4712	0.7944	0.0763	0.6057
	TOE	337			0.0	100.0	0.0	0.0	0.0	1.7583	1.1652	-1.0327	3.588	1.8884	1.965	0.9843	-0.1801	0.5873
	-2	393			0.0	100.0	0.0	0.0	0.0	2.7286	0.5534	-1.7841	10.4823	2.7536	2.8315	0.5018	-0.2699	0.3159
	-6		45.613	56.895	0.0	100.0	0.0	0.0	0.0	2.3362	0.6722	-0.4722	3.0247	2.3641	2.369	0.6803	-0.0694	0.4377
	-12		45.653	56.754	0.0	98.6	1.2	0.2	1.4	2.9948	0.3635	-3.2032	30.1904	3.004	3.0274	0.3008	-0.092	0.1982
	-18		45.663	56.704	0.0	98.5	1.5	0.0	1.5	3.0286	0.5858	-3.5801	21.259	3.1163	3.1362	0.4116	-0.2704	0.3181
	-24		45.658	56.451	0.0	95.3	4.0	0.7	4.7	3.0062	0.5341	-2.7349	14.5795	3.0604	3.1535	0.4135	-0.4313	0.2999
50	BASE OF BULK	146			0.0	100.0	0.0	0.0	0.0	2.0346	0.34	0.1621	3.3627	2.0367	2.0158	0.3288	0.0913	0.3129
	MIDBEACH	186			0.0	100.0	0.0	0.0	0.0	2.1077	0.5262	-0.7471	5.5013	2.131	2.1396	0.5101	-0.0493	0.3737
	TOE	285			0.0	100.0	0.0	0.0	0.0	1.3917	1.2057	-0.6614	2.3602	1.3642	1.6987	1.2698	-0.3621	0.7925
	-2	342			0.0	100.0	0.0	0.0	0.0	2.4753	0.6222	-0.8724	3.4587	2.5082	2.5964	0.6102	-0.2796	0.3874
	-6		45.192	56.698	0.0	100.0	0.0	0.0	0.0									
	-12		45.254	56.686	0.0	100.0	0.0	0.0	0.0	2.8613	0.5148	-2.224	11.2057	2.9248	2.975	0.4289	-0.346	0.3493
	-18		45.261	56.561	7.2	91.7	1.0	0.0	1.0	2.9851	0.7246	-3.0222	13.6225	3.0898	3.1846	0.5026	-0.4837	0.3945
	-24		45.31	56.389	0.0	86.2	11.6	2.2	13.8	3.2197	0.3457	-3.0893	16.9761	3.263	3.2466	0.2542	-0.0536	0.1859

	16 April 1997																	
Profile	Location	Dist (ft)	Latitude	Longitude	%grvl	%sand	%silt	%clay	%mud	M1	M2	M3	M4	Mn	Md	Sorting	Skewness	Kurtosis
			36 deg	75 deg										(Phi)	(Phi)	(Phi)		
			minutes	minutes														
43	DUNE CREST	30			0.00	100.00	0.00	0.00	0.00	1.9080	0.5645	0.5156	4.6773	1.8735	1.9085	0.5152	-0.0311	0.4780
	BOD	42			0.00	100.00	0.00	0.00	0.00	1.7692	0.2988	-0.1808	11.7862	1.7651	1.7676	0.2547	-0.0184	0.2876
	MIDBERM	80			0.00	100.00	0.00	0.00	0.00	1.4160	0.5619	1.2438	7.0392	1.3775	1.3591	0.4647	0.0846	0.5315
	BERM	149			0.00	100.00	0.00	0.00	0.00	0.9941	0.5252	0.8298	5.1075	0.9524	0.9520	0.5051	0.0426	0.6636
	MIDBEACH	184			0.00	100.00	0.00	0.00	0.00	0.5085	0.7909	1.4009	5.7411	0.4291	0.3579	0.7236	0.2543	1.2422
	TOE	219			0.00	100.00	0.00	0.00	0.00	0.3634	1.1115	0.7683	2.6586	0.3752	0.1271	1.0990	0.3529	1.1142
	-2	247			0.00	100.00	0.00	0.00	0.00	1.8135	0.4326	-0.0391	4.5345	1.7949	1.8647	0.4048	-0.2145	0.3990
	-6		49.721	58.031	0.00	97.84	2.16	0.00	2.16	3.1057	0.2093	-0.3136	3.6234	3.1049	3.1198	0.2088	-0.1002	0.1595
	-12		49.759	57.931	0.00	100.00	0.00	0.00	0.00	2.3781	0.6085	-1.4169	7.2670	2.4192	2.4877	0.5317	-0.2763	0.4368
	-18		49.67	57.88	0.00	100.00	0.00	0.00	0.00	2.7343	0.4788	-3.6640	22.8869	2.7889	2.8223	0.3247	-0.2585	0.2515
	-24		49.81	57.86	0.90	79.44	19.66	0.00	19.66	2.2614	0.4111	-1.2832	8.4546	2.2863	2.2497	0.3547	0.0512	0.3409
44	BOD	158			0.00	100.00	0.00	0.00	0.00	1.5574	0.3543	0.7766	6.8652	1.5512	1.5587	0.3164	-0.0372	0.3747
	MIDBERM	220			0.00	100.00	0.00	0.00	0.00	1.2897	0.5185	0.6564	6.4899	1.2636	1.2991	0.4645	-0.0899	0.5451
	BERM	266			0.00	100.00	0.00	0.00	0.00	1.3706	0.3973	0.5654	6.2109	1.3638	1.3568	0.3578	0.0129	0.4382
	MIDBEACH	298			0.00	100.00	0.00	0.00	0.00	0.6972	0.6891	1.5980	7.1887	0.6503	0.6554	0.5771	0.0940	0.8445
	toe	368			0.00	100.00	0.00	0.00	0.00	1.3408	0.5174	-0.4607	4.1608	1.3558	1.3969	0.4720	-0.1728	0.5522
	-2	533			0.00	99.98	0.02	0.00	0.02	2.3652	0.4179	-0.0834	4.1866	2.3767	2.3322	0.3968	0.1352	0.3363
	-6		49.13	57.94	0.35	99.65	0.00	0.00	0.00	1.3717	0.7643	-0.6259	2.9300	1.3615	1.5461	0.7547	-0.3225	0.5794
	-12		49.13	57.86	1.61	95.67	1.72	1.00	2.72	2.9177	0.5015	-3.4854	19.1546	2.9769	3.0609	0.3275	-0.5160	0.2530
	-18		49.13	57.79	0.00	93.13	6.87	0.00	6.87	3.1675	0.1397	-0.3364	3.7311	3.1703	3.1775	0.1415	-0.1220	0.1026
	-24		49.19	57.65	0.00	88.73	11.27	0.00	11.27	2.9789	0.4069	-6.3726	60.8802	3.0110	3.0410	0.2386	-0.2322	0.1782
45	DUNE CREST	0			0.00	100.00	0.00	0.00	0.00	1.5872	0.4381	-1.2709	14.5722	1.5975	1.5960	0.3332	0.0076	0.3823
	BOD	18			0.00	100.00	0.00	0.00	0.00	1.3134	0.4001	0.7259	10.2451	1.2908	1.3031	0.3282	-0.0075	0.3959
	MIDBERM	75			16.11	83.89	0.00	0.00	0.00	0.9821	0.6079	0.0816	3.2591	0.9378	1.0151	0.6170	-0.1378	0.6899
	BERM/CUSP	149			0.00	100.00	0.00	0.00	0.00	1.4212	0.3929	-0.0573	3.1206	1.4096	1.4459	0.3949	-0.1025	0.4369
	MIDBEACH	165			0.00	100.00	0.00	0.00	0.00	0.1976	0.7145	0.6644	4.2864	0.1220	0.1281	0.6975	0.0351	0.9956
	TOE	214			0.00	100.00	0.00	0.00	0.00	1.6019	0.4037	-0.8620	11.5745	1.6093	1.5970	0.3449	0.0432	0.3679
	-6		48.457	57.766	0.00	100.00	0.00	0.00	0.00	2.4629	0.6415	-1.4214	5.0021	2.5232	2.6425	0.5760	-0.4149	0.4146
	-12		48.494	57.722	2.18	96.47	1.35	0.00	1.35	2.3982	0.6717	-2.4620	14.2013	2.4524	2.4464	0.4960	-0.0619	0.3772
	-18		48.521	57.641	0.00	96.55	3.37	0.08	3.45	2.7498	0.4082	-1.2234	5.989	2.777	2.7933	0.3663	-0.1448	0.2501
	-24		48.582	57.444	0.00	90.80	7.32	1.87	9.20	2.9504	0.4286	-4.4883	35.8809	2.9833	3.0281	0.2863	-0.2894	0.2056
46	DUNE FACE	54			0.00	100.00	0.00	0.00	0.00	1.2579	0.3709	-1.0612	10.7880	1.2694	1.2988	0.3197	-0.1579	0.4206
	BOD	70			0.00	100.00	0.00	0.00	0.00	1.2022	0.4044	-0.0142	6.8774	1.2078	1.2428	0.3369	-0.1161	0.4580
	MIDBERM	89			0.00	100.00	0.00	0.00	0.00	1.1944	0.3490	2.4014	15.7701	1.1654	1.1529	0.2773	0.1404	0.4267
	BERM	103			6.24	93.76	0.00	0.00	0.00	1.1768	0.3390	1.6546	14.4142	1.1644	1.1664	0.2769	0.0373	0.4140
	MIDBEACH	246			0.00	100.00	0.00	0.00	0.00	1.3430	0.3937	0.0861	4.1844	1.3378	1.3240	0.3760	0.0636	0.4766
	TOE	267			0.00	100.00	0.00	0.00	0.00	0.9264	0.4876	-0.2446	5.6645	0.9160	0.9212	0.4325	-0.0300	0.6115
	-2				0.00	100.00	0.00	0.00	0.00	1.5533	0.5191	-0.0205	3.7481	1.5546	1.5755	0.4997	-0.0701	0.5201
	-6		47.881	57.569	2.08	97.92	0.00	0.00	0.00	2.3951	0.7673	-1.9063	6.1139	2.5013	2.6229	0.6669	-0.4974	0.5937
	-12		47.91	57.526	0.00	98.82	1.18	0.00	1.18	2.7336	0.5919	-3.7272	24.5379	2.7965	2.7791	0.3842	-0.0456	0.2908
	-18		47.928	57.444	1.65	92.47	4.78	1.10	5.88	2.7456	0.4739	-2.5694	16.7073	2.7893	2.8031	0.3693	-0.1432	0.2640
	-24		47.908	57.221	0.00	96.25	3.75	0.00	3.75	2.7460	0.4440	-2.1278	13.7757	2.7762	2.7953	0.3613	-0.1597	0.2432

	16 April 1997																	
Profile	Location	Dist (ft)	Latitude	Longitude	%grvl	%sand	%silt	%clay	%mud	M1	M2	M3	M4	Mn	Md	Sorting	Skewness	Kurtosis
			36 deg	75 deg										(Phi)	(Phi)	(Phi)		
			minutes	minutes														
47	BOD	80			0.00	100.00	0.00	0.00	0.00	1.1817	0.4904	0.2401	6.3521	1.1922	1.2486	0.4333	-0.2302	0.5875
	MIDBERM	146			0.00	100.00	0.00	0.00	0.00	1.3042	0.5902	-0.3156	8.8395	1.2877	1.2686	0.3931	0.3107	0.3107
	BERM	224			0.00	100.00	0.00	0.00	0.00	1.2821	0.2611	-1.3279	14.3626	1.2849	1.2904	0.2505	-0.0124	0.3330
	TOE	348			0.00	100.00	0.00	0.00	0.00	0.2925	0.7433	0.6223	3.6796	0.3206	0.2589	0.7604	0.0799	1.0924
	-2	480			0.00	100.00	0.00	0.00	0.00	1.7206	0.5313	-0.2883	4.5997	1.7294	1.7283	0.4928	-0.0159	0.4735
	-6		46.997	57.348	0.43	99.57	0.00	0.00	0.00	1.5746	0.6860	-0.3830	3.9634	1.5792	1.6535	0.6672	-0.2081	0.7085
	-12		47.009	57.246	0.00	79.03	20.97	0.00	20.97	2.7506	0.4818	-3.1572	19.2570	2.7955	2.8338	0.3467	-0.2509	0.2509
	-18		47.016	57.217	0.43	96.65	2.17	0.74	2.91	2.8639	0.3768	-2.4763	14.3380	2.9020	2.9007	0.2845	-0.0996	0.2073
	-24		47.074	57.014	0.00	97.27	2.73	0.00	2.73	2.7706	0.3573	-2.0882	18.1177	2.7971	2.7844	0.2943	-0.0090	0.2185
48	DUNE CREST	77			0.00	100.00	0.00	0.00	0.00	1.9626	0.2722	-0.0526	3.4920	1.9605	1.9662	0.2681	-0.0336	0.2664
	BOD	108			0.00	100.00	0.00	0.00	0.00	1.5921	0.3939	-0.3260	10.3059	1.5963	1.6067	0.3510	-0.0522	0.3803
	MIDBERM	130			0.00	100.00	0.00	0.00	0.00	1.2791	0.4137	0.2033	4.7981	1.2724	1.2715	0.3904	0.0401	0.4515
	BERM/CUSP	225			0.00	100.00	0.00	0.00	0.00	1.3000	0.5352	0.4100	3.3961	1.2869	1.2895	0.5393	0.0107	0.5487
	TOE	297			0.00	100.00	0.00	0.00	0.00	1.7175	0.6923	-0.4933	3.1082	1.7055	1.8651	0.6754	-0.3378	0.5485
	-2	412			0.00	100.00	0.00	0.00	0.00	2.0887	0.5529	-2.2729	12.4314	2.1463	2.1576	0.4375	-0.1223	0.4188
	-6		46.023	56.986	0.32	99.07	0.61	0.00	0.61	2.3413	0.6090	-0.8834	3.2132	2.3456	2.5159	0.6131	-0.4023	0.4232
	-12		46.062	56.979	0.00	97.47	1.89	0.64	2.53	2.9917	0.3067	-8.3865	111.0962	3.0101	3.0173	0.1849	-0.1074	0.1329
	-18		46.08	56.865	0.61	96.84	1.90	0.65	2.55	2.5969	0.6389	-2.0262	7.4993	2.6813	2.7855	0.5258	-0.4838	0.4411
	-24		46.102	56.697	0.51	98.82	0.67	0.00	0.67	2.4465	0.3988	-0.8735	7.6859	2.4681	2.4121	0.3412	0.2218	0.2820
49	DUNE CREST	70			0.00	100.00	0.00	0.00	0.00	1.5928	0.4000	-0.5266	6.0195	1.6077	1.5879	0.3601	0.0444	0.4132
	BOD	104			0.00	100.00	0.00	0.00	0.00	1.6810	0.4042	0.5886	7.6079	1.6662	1.6682	0.3507	0.0121	0.3700
	MIDBERM	148			0.00	100.00	0.00	0.00	0.00	1.5460	0.5294	-1.0779	12.3236	1.5605	1.5603	0.3823	0.0013	0.4182
	BERM	178			0.00	100.00	0.00	0.00	0.00	1.1900	0.4814	1.6939	8.3677	1.1499	1.1348	0.4150	0.1596	0.5259
	MIDBEACH	228			0.00	100.00	0.00	0.00	0.00	1.5472	0.4830	0.5255	4.6949	1.5305	1.5608	0.4623	-0.0734	0.4515
	TOE	337			0.00	100.00	0.00	0.00	0.00	1.5438	0.6682	-1.0840	5.0533	1.5685	1.6801	0.6074	-0.3006	0.5773
	-2				0.24	96.58	3.18	0.00	3.18	2.2900	0.4529	-0.9323	5.7570	2.3127	2.3489	0.4262	-0.1600	0.3449
	-6		45.613	56.895	0.00	97.44	2.56	0.00	2.56	2.2334	0.5979	-1.4629	5.9600	2.2819	2.3498	0.5401	-0.3007	0.4678
	-12		45.653	56.754	0.22	97.27	2.51	0.00	2.51	2.8340	0.3726	-1.8896	8.2936	2.8708	2.9120	0.3089	-0.3286	0.2383
	-18		45.663	56.704	0.17	99.13	0.70	0.00	0.70	2.9928	0.4097	-6.1804	47.1480	3.0447	3.0518	0.1605	-0.1906	0.1228
	-24		45.658	56.451	0.00	97.69	2.31	0.00	2.31	2.9247	0.3131	-5.2435	58.7097	2.9563	2.9502	0.2059	-0.0724	0.1580
50	BASE OF BULK	146			0.00	100.00	0.00	0.00	0.00	1.3184	0.2459	1.5241	12.0964	1.3123	1.3029	0.2259	0.0809	0.3187
	MIDBEACH	188			0.00	100.00	0.00	0.00	0.00	1.4157	0.3860	0.0648	2.9550	1.4072	1.4078	0.3901	0.0144	0.4472
	TOE	301			1.81	98.19	0.00	0.00	0.00	0.0648	0.7442	1.1927	3.6442	0.0334	-0.1731	0.7326	0.4893	2.3646
	-2				0.00	93.89	1.83	4.28	6.11	2.0462	0.7856	-1.3801	5.2857	2.1344	2.1332	0.7894	-0.2154	0.6932
	-6		45.192	56.698	0.00	100.00	0.00	0.00	0.00	1.8185	0.3904	-0.2433	2.5077	1.8167	1.8810	0.6937	-0.1303	0.4871
	-12		45.254	56.636	0.76	98.44	0.81	0.00	0.81	2.3932	0.5874	-1.3394	4.9015	2.4652	2.5099	0.5315	-0.3035	0.5056
	-18		45.261	56.581	0.39	96.98	2.63	0.00	2.63	2.8695	0.4072	-6.3759	55.8555	2.9007	2.9028	0.1976	-0.0343	0.1440
	-24		45.31	56.389	0.53	99.47	0.00	0.00	0.00	2.8595	0.3227	-2.9762	11.0385	3.0234	3.1183	0.6581	-0.7039	0.7211

Oct 1997																		
Profile	Location	Dist (ft)	Latitude	Longitude	%grvl	%sand	%silt	%clay	%mud	M1	M2	M3	M4	Mn	Md	Sorting	Skewness	Kurtosis
			36 deg	75 deg										(Phi)	(Phi)	(Phi)		
			minutes	minutes														
43	DUNE CREST	30			0.00	100.00	0.00	0.00	0.00	1.5558	0.3892	0.9839	4.6905	1.5529	1.4975	0.3622	0.2662	0.4566
	BOD	42			0.00	100.00	0.00	0.00	0.00	2.0535	0.3116	0.0045	3.5536	2.0545	2.0519	0.3071	0.0083	0.2908
	MIDBERM	119			0.00	99.75	0.25	0.00	0.25	1.4870	0.6497	-0.1597	2.4333	1.4949	1.5370	0.6466	-0.0975	0.5472
	BERM	148			0.00	100.00	0.00	0.00	0.00	1.7120	0.5585	-0.8021	3.5606	1.7355	1.8010	0.5420	-0.2204	0.4945
	MIDBEACH	180			0.00	100.00	0.00	0.00	0.00	1.8557	0.8014	-1.1036	3.6042	1.9138	2.1320	0.7806	-0.4728	0.5679
	TOE	342			0.00	99.07	0.93	0.00	0.93	2.2312	0.6479	-1.3252	4.7469	2.2743	2.3627	0.5917	-0.3527	0.5425
	-2	560			0.00	99.45	0.55	0.00	0.55	2.8843	0.3793	-3.5095	25.7590	2.9123	2.9104	0.2774	0.0001	0.1928
	-6		49.721	58.031	0.00	100.00	0.00	0.00	0.00	2.7213	0.3446	-0.5207	2.6481	2.7267	2.7446	0.3493	-0.1194	0.2229
	-12		49.759	57.931	0.00	100.00	0.00	0.00	0.00	2.7844	0.4639	-3.4256	19.1380	2.8468	2.8474	0.2861	-0.1377	0.2241
	-18		49.67	57.88	0.00	100.00	0.00	0.00	0.00	2.7679	0.6382	-2.8126	12.0441	2.8819	2.9604	0.4562	-0.5225	0.4060
	-24		49.81	57.86	0.00	100.00	0.00	0.00	0.00	2.9907	0.4283	-5.7527	47.9308	3.0278	3.0481	0.2453	-0.1567	0.1735
44	BOD	158			0.00	100.00	0.00	0.00	0.00	1.4515	0.3802	-0.1619	3.3433	1.4506	1.4485	0.3836	0.0152	0.4123
	MIDBERM	230			0.00	100.00	0.00	0.00	0.00	1.2995	0.6465	-1.2347	6.1244	1.3420	1.3796	0.5792	-0.2059	0.7103
	BERM	264			0.00	100.00	0.00	0.00	0.00	1.2077	0.6025	0.2284	3.8040	1.2279	1.2589	0.5653	-0.0990	0.6105
	MIDBEACH	313			0.00	100.00	0.00	0.00	0.00	2.0647	0.5387	-1.0081	4.0218	2.0952	2.1680	0.5173	-0.2751	0.4169
	TOE	370			0.00	99.76	0.24	0.00	0.24	2.7382	0.3106	-0.7344	3.5345	2.7531	2.7819	0.3079	-0.1922	0.2245
	-2	461			0.00	99.84	0.16	0.00	0.16	2.4995	0.6236	-1.8336	7.0228	2.5678	2.6563	0.5513	-0.3902	0.4137
	offshore	545			0.00	99.75	0.25	0.00	0.25	2.7129	0.4062	-0.7040	2.7116	2.7203	2.7844	0.4132	-0.2738	0.2637
	-6		49.13	57.94	0.00	100.00	0.00	0.00	0.00	1.9801	0.5972	-0.5041	4.1366	1.9954	1.9938	0.5906	-0.0169	0.5324
	-12		49.13	57.86	0.00	100.00	0.00	0.00	0.00	3.1025	0.2080	-0.6949	4.7742	3.1117	3.1117	0.1952	-0.0789	0.1491
	-18		49.13	57.79	0.00	97.02	2.94	0.04	2.98	3.1405	0.2201	-0.9637	5.4741	3.1635	3.1580	0.2013	-0.0734	0.1629
	-24		49.19	57.65	0.00	99.86	0.09	0.05	0.14	3.0223	0.4539	-2.7004	20.1687	3.0377	3.1237	0.3872	-0.3510	0.2895
45	DUNE CREST	0			0.00	100.00	0.00	0.00	0.00	1.7806	0.3829	-0.7381	3.5544	1.7939	1.8457	0.3787	-0.2324	0.3785
	BOD	32			0.00	100.00	0.00	0.00	0.00	1.3951	0.4460	-0.2359	2.6476	1.3910	1.4351	0.4539	-0.1211	0.4636
	MIDBERM	78			4.74	95.26	0.00	0.00	0.00	0.9603	0.7605	-0.8664	2.8235	0.9841	1.1875	0.7597	-0.4242	0.7396
	BERM/CUSP	135			0.00	100.00	0.00	0.00	0.00	1.4426	0.3616	0.1888	2.6170	1.4402	1.4167	0.3680	0.0963	0.4130
	MIDBEACH	171			0.00	100.00	0.00	0.00	0.00	1.9096	0.5914	-0.3230	3.0935	1.9160	1.9592	0.5900	-0.1237	0.4847
	TOE	233			9.04	89.05	1.91	0.00	1.91	2.4862	0.3421	-0.6184	3.0333	2.4981	2.5443	0.3464	-0.2220	0.2646
	-2	407			0.00	99.83	0.17	0.00	0.17	2.7541	0.5499	-3.5882	22.8011	2.8204	2.8842	0.3867	-0.3797	0.2835
	-6		48.457	57.766	0.00	100.00	0.00	0.00	0.00	2.1146	0.5974	-0.8915	4.0626	2.1409	2.2035	0.5782	-0.2055	0.4768
	-12		48.494	57.722	0.00	100.00	0.00	0.00	0.00	2.7500	0.5038	-2.2938	12.5567	2.8016	2.8326	0.4130	-0.2417	0.2890
	-18		48.521	57.641	0.00	99.85	0.15	0.00	0.15	3.1534	0.2223	-0.3194	3.3889	3.1520	3.1745	0.2248	-0.1432	0.1592
	-24		48.582	57.444	0.17	99.58	0.25	0.00	0.25	3.1496	0.2185	-0.7241	3.7339	3.1564	3.1799	0.2170	-0.2122	0.1546
46	DUNE FACE	54			0.00	100.00	0.00	0.00	0.00	0.3247	0.6867	0.8111	5.4721	0.3232	0.3291	0.6359	-0.0126	0.9631
	BOD	73			0.00	100.00	0.00	0.00	0.00	1.3375	0.4131	-3.9969	23.9836	1.3906	1.3745	0.2133	-0.0113	0.3210
	MIDBERM	102			2.39	97.61	0.00	0.00	0.00	1.2034	0.2880	-0.4513	5.4642	1.2157	1.2351	0.2653	-0.1182	0.3863
	BERM	158			0.00	100.00	0.00	0.00	0.00	1.1167	0.3168	-0.0177	3.4259	1.1102	1.1061	0.3021	0.0359	0.4331
	MIDBEACH	198			0.00	100.00	0.00	0.00	0.00	1.3247	0.4998	-1.1754	5.9427	1.3412	1.3665	0.4377	-0.1473	0.5394
	TOE	295			1.85	97.79	0.37	0.00	0.37	2.6529	0.3839	-1.7790	8.9909	2.6887	2.6998	0.3367	-0.1561	0.2717
	-2	451			0.00	99.91	0.09	0.00	0.09	2.6950	0.4937	-2.7840	18.8403	2.7380	2.7841	0.4132	-0.2768	0.3029
	-6		47.881	57.569	0.00	100.00	0.00	0.00	0.00	2.3446	0.4790	-0.4739	3.0755	2.3653	2.3849	0.4791	-0.0910	0.3517
	-12		47.91	57.526	0.00	100.00	0.00	0.00	0.00	2.9026	0.4491	-2.6126	15.7725	2.9447	3.0181	0.3489	-0.3690	0.2370
	-18		47.928	57.444	0.00	99.94	0.06	0.00	0.06	2.9453	0.3009	-0.4049	2.2186	2.9481	3.0000	0.3064	-0.2423	0.1894
	-24		47.908	57.221	0.00	99.61	0.39	0.00	0.39	2.8536	0.3722	-1.3836	7.0493	2.8783	2.9087	0.3266	-0.1717	0.2214

Oct 1997																		
Profile	Location	Dist (ft)	Latitude	Longitude	%grvl	%sand	%silt	%clay	%mud	M1	M2	M3	M4	Mn	Md	Sorting	Skewness	Kurtosis
			36 deg	75 deg										(Phi)	(Phi)	(Phi)		
			minutes	minutes														
47	BOD	76			0.00	100.00	0.00	0.00	0.00	1.3132	0.3314	3.5335	26.0432	1.2689	1.2950	0.1582	-0.1846	0.3186
	MIDBERM	134			3.13	96.88	0.00	0.00	0.00	1.4491	0.4670	0.8252	7.2698	1.4258	1.4343	0.3832	0.0021	0.4764
	BERM/CUSP	257			0.00	100.00	0.00	0.00	0.00	1.8315	0.6761	0.4321	3.3026	1.8111	1.7685	0.6622	0.1591	0.6570
	MIDBEACH	302			0.00	100.00	0.00	0.00	0.00	2.0631	0.4613	-0.6512	4.2386	2.0825	2.1125	0.4331	-0.1450	0.3805
	TOE	351			24.18	75.82	0.00	0.00	0.00	2.0771	0.8071	-1.2798	4.1065	2.1346	2.3419	0.7648	-0.4854	0.5734
	-2	537			0.00	99.84	0.16	0.00	0.16	2.6669	0.3940	-1.0991	6.5967	2.6852	2.6992	0.3789	-0.1227	0.2571
	-6		46.997	57.348	0.00	100.00	0.00	0.00	0.00	2.5509	0.5244	-0.1503	1.9058	2.5569	2.5625	0.5401	-0.0526	0.2974
	-12		47.009	57.246	0.00	100.00	0.00	0.00	0.00	3.0003	0.3334	-2.9112	22.5741	3.0178	3.0637	0.2745	-0.3338	0.2040
	-18		47.016	57.217	0.00	100.00	0.00	0.00	0.00	3.1060	0.3516	-5.6364	57.0287	3.1336	3.1606	0.2361	-0.2200	0.1694
	-24		47.074	57.014	0.00	99.94	0.06	0.00	0.06	3.0927	0.2185	0.3271	3.4362	3.0859	3.0815	0.2195	0.0629	0.1577
48	DUNE CREST	77			0.00	100.00	0.00	0.00	0.00	2.4845	0.3410	1.8388	7.5239	2.4511	2.4191	0.2660	0.2874	0.2601
	BOD	108			0.00	100.00	0.00	0.00	0.00	2.1295	0.6655	1.2037	3.8694	2.0265	2.0029	0.5967	0.2473	0.6184
	MIDBERM	130			0.00	100.00	0.00	0.00	0.00	2.0502	0.4362	-1.1706	11.7417	2.0516	2.0370	0.4084	0.0698	0.3298
	BERM	194			0.00	100.00	0.00	0.00	0.00	1.7491	0.4216	0.1109	2.8522	1.7477	1.7426	0.4235	0.0219	0.3852
	MIDBEACH	233			0.00	99.91	0.09	0.00	0.09	1.9734	0.4657	-0.3984	2.8140	2.0014	2.0363	0.4571	-0.1566	0.3795
	TOE	314			0.00	99.90	0.10	0.00	0.10	2.2298	0.6823	-1.3669	4.5838	2.2625	2.4250	0.6447	-0.4494	0.5113
	-2	547			0.00	99.94	0.06	0.00	0.06	2.7790	0.4082	-2.0000	8.4823	2.8217	2.8780	0.3364	-0.3448	0.2427
	-6		46.023	56.986	0.00	100.00	0.00	0.00	0.00	1.9545	0.7534	-0.4636	3.0964	1.9558	2.0440	0.7549	-0.1463	0.5868
	-12		46.062	56.979	0.00	100.00	0.00	0.00	0.00	2.4040	0.6596	-1.6326	7.3138	2.4336	2.5662	0.6091	-0.3590	0.3707
	-18		46.08	56.865	0.00	99.79	0.21	0.00	0.21	2.7172	0.6667	-1.7185	5.6052	2.7613	2.9526	0.5851	-0.5821	0.4190
	-24		46.102	56.697	0.00	100.00	0.00	0.00	0.00	2.4822	0.5637	-0.7792	6.7315	2.5093	2.4241	0.5513	0.1734	0.3312
49	DUNE CREST	61			0.80	99.20	0.00	0.00	0.00	1.9110	0.3782	-1.5719	10.2662	1.9229	1.9469	0.3275	-0.1338	0.3319
	BOD	104			0.00	100.00	0.00	0.00	0.00	1.9319	0.3488	-0.3605	4.0462	1.9359	1.9559	0.3305	-0.1150	0.3359
	MIDBERM	136			0.00	100.00	0.00	0.00	0.00	1.8693	0.4892	-0.9838	5.4397	1.8859	1.9514	0.4424	-0.2699	0.4430
	BERM	206			0.00	100.00	0.00	0.00	0.00	1.9143	0.2763	0.2586	4.3421	1.9147	1.9149	0.2619	-0.0038	0.2693
	MIDBEACH	247			0.00	100.00	0.00	0.00	0.00	2.0124	0.4670	0.1711	2.5043	2.0134	1.9883	0.4853	0.0817	0.3968
	TOE	435			0.00	100.00	0.00	0.00	0.00	2.6971	0.5572	-3.2302	16.3504	2.7832	2.8209	0.3740	-0.3367	0.3179
	-2	576			0.00	99.96	0.04	0.00	0.04	2.8911	0.5144	-5.2799	33.4376	2.9619	2.9635	0.1964	-0.1172	0.1484
	-6		45.613	56.895	0.00	100.00	0.00	0.00	0.00	2.2706	0.6251	-0.5791	5.2877	2.2927	2.3518	0.5493	-0.2313	0.4468
	-12		45.653	56.754	0.00	100.00	0.00	0.00	0.00	2.7659	0.2517	0.2150	2.5112	2.7770	2.7375	0.2657	0.1569	0.1865
	-18		45.663	56.704	0.19	99.81	0.00	0.00	0.00	2.8202	0.4993	-4.0024	24.6955	2.8907	2.8859	0.2847	-0.1426	0.2278
	-24		45.658	56.451	0.00	99.84	0.16	0.00	0.16	2.9315	0.1987	0.3630	3.2030	2.9278	2.9153	0.1908	0.1076	0.1373
50	BASE OF BULK	146			0.00	100.00	0.00	0.00	0.00	1.7785	0.3269	0.3697	5.1716	1.7774	1.7848	0.3038	-0.0200	0.3262
	MIDBEACH	179			0.00	99.92	0.08	0.00	0.08	2.1902	0.4730	-0.0122	2.3392	2.1919	2.1765	0.4891	0.0207	0.3498
	TOE	262			0.00	100.00	0.00	0.00	0.00	1.7823	0.9047	-0.3201	1.9355	1.8026	1.9095	0.9072	-0.1693	0.4978
	-2	517			2.85	97.15	0.00	0.00	0.00	2.6338	0.6328	-2.3385	9.6422	2.7217	2.7879	0.5078	-0.4091	0.4404
	-6		45.192	56.698	0.00	100.00	0.00	0.00	0.00	2.0112	0.4978	-0.6613	3.5291	2.0263	2.0982	0.4879	-0.2552	0.4202
	-12		45.254	56.686	0.00	100.00	0.00	0.00	0.00	2.9752	0.2164	0.4165	3.2735	2.9716	2.9634	0.2157	0.0929	0.1563
	-18		45.261	56.561	0.00	100.00	0.00	0.00	0.00	2.9678	0.3978	-7.6880	73.5455	2.9998	3.0060	0.1808	-0.0622	0.1253
	-24		45.31	56.389	0.00	99.77	0.17	0.07	0.23	3.0102	0.1884	0.1340	2.9888	3.0077	3.0117	0.1936	-0.0044	0.1348

Final Report

January 1998

Environmental Studies Relative to Potential Sand Mining in the Vicinity of the City of Virginia Beach, Virginia

Part 3: Nearshore Waves and Currents Observations and Modeling

Author:

John D. Boon
Virginia Institute of Marine Science

Project Manager:

Carl H. Hobbs, III
Virginia Institute of Marine Science

Prepared under MMS Cooperative Agreement 14-35-0001-3087 through Virginia Institute of Marine Science of the College of William & Mary

MMS U.S. Department of the Interior
Minerals Management Service

College of William and Mary
Virginia Institute of Marine Science
School of Marine Science

DISCLAIMER

This report has been reviewed by the Minerals Management Service and approved for publication. Approval does not signify that the contents necessarily reflect the views and policies of the Service, nor does mention of trade names or commercial products constitute endorsement or recommendation for use.

The Department of the Interior

As the Nations's principal conservation agency, the Department of the Interior has responsibility for most of our nationally owned public lands and natural resources. This includes fostering sound use of our land and water resources, protecting our fish, wildlife, and biological diversity, preserving the environmental and cultural values of our national parks and historic places; and providing for the enjoyment of life through outdoor recreation. The Department assesses our energy and mineral resources and works to ensure that their development is in the best interests of all our people by encouraging stewardship and citizen participation in their care. The Department also has a major responsibility for American Indian reservation communities and for people who live in island territories under U.S. Administration.

The Minerals Management Service Mission

As a bureau of the Department of the Interior, the Minerals Management Service's (MMS) primary responsibilities are to manage the mineral resources located on the Nations's Outer Continental Shelf (OCS), collect revenue from the Federal OCS and onshore federal and Indian lands, and distribute those revenues.

Moreover, in working to meet its responsibilities, the Offshore Minerals Management Program administers the OCS competitive leasing program and oversees the safe and environmentally sound exploration and production of our Nation's offshore natural gas, oil and other mineral resources. The MMS Royalty Management Program meets its responsibilities by entrusting the efficient, timely and accurate collection and distribution of revenue from mineral leasing and production due to Indian tribes andallottees, States and the U. S. Treasury

the MMS strives to fulfill its responsibilities through the general guiding principles of: (1) being responsive to the public's concerns and interests by maintaining a dialog with all potentially affected parties and (2) carrying out its programs with an emphasis on working to enhance the quality of life for all Americans by lending MMS assistance and expertise to economic development and environmental protection.

Environmental Studies Relative to Potential Sand Mining in the Vicinity of the City of Virginia Beach, Virginia

Nearshore Waves and Currents – Observations and Modeling

Introduction

This report will address nearshore wave modeling results for the City of Virginia Beach and the beach community of Sandbridge, Virginia. Wave and near-bottom current observations made near the Chesapeake Bay entrance will not be presented here in order to focus attention on wave modeling results for a now active sand mining site located approximately 5 km (2.7 nm) due east of Sandbridge. A nested-grid, spectral wave propagation model was applied to investigate the potential change in maximum wave heights expected for the nearshore region between that site and the surf zone at Sandbridge. The purpose of this report is to describe the model and its application to the Virginia Beach – Sandbridge coastal sector, and to provide an analysis of the results obtained.

Sand Mining Borrow Areas

Detailed site information was recently received for two adjacent borrow areas located on a nearshore ridge formation known as Sandbridge Shoal (Fig. 1). One of these areas, designated borrow site "A" by Federal authorities, was dredged in mid-1996 to yield approximately 810,000 cubic yards (619,289 cu. m.) of beach nourishment material for the U.S. Navy's Fleet Combat Training Center at Dam Neck, Virginia. At the time of writing of this report, it was anticipated that an additional 1.3 million cubic yards (994,000 cu. m.) of material would be extracted from borrow area "A" or a closely located second site to the north designated borrow site "B". This material will be used for restoration of Sandbridge Beach to the south of Dam Neck. Approximately 500,000 cubic yards (383,000 cu. m.) of material is to be removed at two year intervals in the future. Borrow area "A" has an irregular plan-view area of approximately 2.4 million square meters and borrow area "B" occupies an area of about 2.1 million square meters.

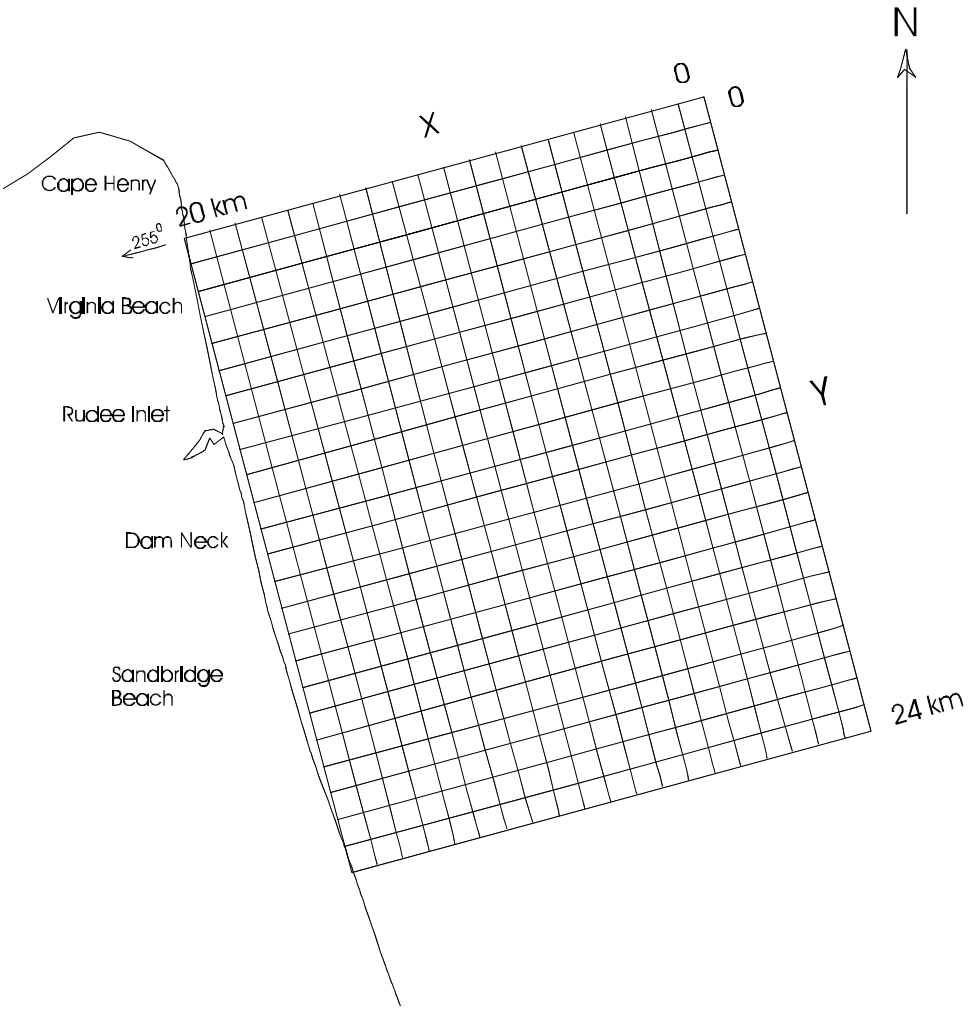

Figure 1. Map showing location of Virginia Beach – Sandbridge reference grid

Wave Model Description

The wave model selected for use in this study is the University of Delaware's combined refraction/diffraction model for spectral wave conditions, REF/DIF S (Kirby and Ozkan, 1992). It differs from its monochromatic wave predecessor, REF/DIF 1 (Dalrymple and Kirby, 1991), in that it simulates the behavior of a random sea through use of a two-dimensional wave spectrum

in which the wave energy density is a function of both frequency and direction. Water surface elevation at any point in the model domain is thus represented by a series of component waves,

$$h = \sum_{f} \sum_{q} A(f,q) e^{iy} \qquad (1)$$

where *A(f,2)* is the complex amplitude for a wave of frequency f and direction *2*, and

$$y = \int \vec{k} \cdot d\vec{x} - wt + f \qquad (2)$$

is its phase given

$$\vec{k} = \vec{i}k_x + \vec{j}k_y = 2p\vec{i} / L_x + 2p\vec{j} / L_y$$

as the wave number vector defined by its components (wavelengths) in the x and y directions, $T = 2\pi f$ as the radian frequency, and ϕ as a random phase component.

For input, REF/DIF S requires a two-dimensional wave spectrum specified by a matrix of discrete, band-centered values of frequency and direction. The separate wave components represented by the elements in this matrix are propagated simultaneously through a model grid, permitting a statistical representation of the local wave height at each intersection in the grid. Although the model does not account for interaction between wave components, it is weakly nonlinear and permits efficient calculation of a wave height parameter employing an adequate sample size. For example, a spectrum represented by 11 directions for each of 11 frequency bands would yield a total of n=121 discrete wave components propagated simultaneously. REF/DIF S calculates the significant wave height as

$$H_s = \left[8 \sum_{p=1}^{n} \left| A_p \right|^2 \right]^{1/2} \qquad (3)$$

where $\boldsymbol{A_p}$ is the complex amplitude of the *p*th component wave at a given grid location. In most applications, the significant wave height, H_s, and the zero-moment wave height, Hm_o, are considered equivalent. H_s ,or $H_{1/3}$, is defined as the average height of the highest one-third of the waves in a sample record. Hm_o is defined on the basis of the total wave energy, m_0, as

$$Hm_0 = 4\sqrt{m_0} \qquad (4)$$

with m_0 computed as the variance of the surface elevation. Wave heights throughout this report will be referred to as the zero-moment wave height, $Hm_o \approx H_s$.

REF/DIF 1 and REF/DIF S are both parabolic wave models based on the mild slope equation

$$\nabla_h \cdot (CC_g \nabla_h h) + k^2 CC_g h \qquad (6)$$

with $C = \sqrt{(g/k)\tanh kh}$ as the wave celerity and $C_g = C(1 + 2kh/\sinh 2kh)/2$ as the wave group velocity, and g = acceleration of gravity. A linear approximation to eq. (6),

$$\frac{\partial A}{\partial x} = \frac{i}{2k}\frac{\partial^2 A}{\partial y^2} - \frac{w}{2C_g}A - \alpha A \qquad (7)$$

is used to simulate waves traveling over irregular bottom topography and includes the effects of shoaling, refraction, energy dissipation (*w* is an energy dissipation factor), wave breaking (α is a breaking coefficient) and diffraction (Kirby, 1986; Kirby and Dalrymple, 1986). A restriction of the present REF/DIF models is that waves must propagate within approximately 50^0 of the principal wave direction that is usually aligned with the downwave or positive x-axis of the model grid. The user must specify a constant complex amplitude, $A(f,\theta)$, for each f,θ pair along the y-axis of the starting row. Dalrymple and Kirby (1991) list the following additional assumptions and features of REF/DIF S:

Mild Bottom Slope. Model equations are based on the assumption that variations in depth occur over distances that are long in comparison to a wavelength. Solutions are considered accurate for bottom slopes up to 1:3 and to show the correct trends in wave height over steeper slopes.

Weak nonlinearity. The model is based on a Stokes perturbation expansion and is therefore restricted to deep-water applications where Stokes waves are valid. Nonlinearity is measured by

the Ursell parameter $U=HL^2/h^3$. When U>40, Stokes waves are considered invalid and a "patch" to a solitary wave is used that is considered valid in shallow water. To achieve this, REF/DIF S uses a hybrid model with a modified dispersion relationship for shallow water incorporating H_s calculated for each grid row proceeding in the landward direction

$$s^2 = gk \tanh(kh(1 + H_s / 2h)) \qquad (8)$$

Turbulent bottom boundary layer. Three options for wave energy dissipation are available in REF/DIF S. The option used in the present study was that of a turbulent bottom boundary layer represented by a constant value of the Darcy-Weisbach friction factor, f_w = 0.01, in the dissipation factor,

$$w = \frac{2s\,kf_w|A|}{3p\,\sinh 2kh \sinh kh} \qquad (9)$$

It should be noted that f_w can be expected to vary as a function of the bed roughness so that it is likely to vary from point to point in the bottom grid.

Wave breaking. The breaking model used in REF/DIF S is that of Thornton and Guza (1983). The decay of the wave height is obtained from the energy dissipation for breaking waves (bore dissipation) given by

$$\frac{\partial EC_g}{\partial x} = -e_b \qquad (10)$$

where $E = \frac{1}{8}\rho g H_{rms}^2$ and $e_b = \frac{3\sqrt{\pi}}{16}\frac{\rho g f_p B^3}{\gamma^4 h^5} H_{rms}^7$

In the above, f_p is the spectral peak frequency, $H_s=1.414H_{rms}$, and B, γ are constants (B=1 and γ=0.6). The breaking coefficient α, as used in eq. (7), is very small for nonbreaking waves but, computed as

$$a = \frac{4e_b}{\rho g H_{rms}^2} \qquad (11)$$

becomes large as breaking conditions are reached and wave height reduces accordingly.

Subgrids. One of the most useful features of REF/DIF S is the subgrid option. After the user has first constructed a coarse-scale, rectangular **reference grid** of position and depth values defining the model domain, a rectangular **subgrid** may be set up defining a fine-scale sub-region of that domain. One can choose a grid cell-size for the subgrid that is many times smaller than that used for the reference grid. This allows local representation of key benthic features (e.g., artificial mounds or depressions) on a spatial scale of tens of meters while the remainder of the domain is represented at scales of hundreds of meters or kilometers.

Reference grid - subgrid combinations are particularly advantageous when used with spectral wave models because spectral wave information (measured or simulated) is usually available (and spatially uniform) only at offshore sites in deep water and not in the shallow nearshore region where the interaction of waves with bottom topography is frequently the study object. Spectral models propagate a combination of waves of different frequency and direction through the transition region from deep to shallow water. Because these component waves respond differently to dynamic processes (shoaling, refraction, diffraction, breaking) along the way, predicting the final sum of their heights at each grid intersection is anything but trivial. Local wave height extremes (high or low) may result from a combination of superposed waves travelling the same or different routes. This depends not only on the topography en route but also

on spectrum widths (broad or narrow) and selective wave breaking. Clearly, these same extremes could not be reproduced using a monochromatic wave model.

Other features and some restrictions. In addition to the features just described, REF/DIF S can model wave-current interaction. To use this option, the user must include horizontal (u,v) current components at reference grid (subgrid) intersections along with depth. The user may also choose an option that computes radiation stress components S_{xx}, S_{xy}, and S_{yy} at each intersection and writes them to an output file. While these features are available within the model domain, there is no interaction between propagating wave components nor is there any provision for momentum

transfer to any of these components from the atmosphere through specification of a surface wind field.

Spectral Input – the TMA Spectrum and Mitsuyasu-type Spreading Function

To provide input to REF/DIF S, a directional wave spectrum is required representing the distribution of wave energy in the frequency domain and in direction (angle θ). The relationship is expressed as

$$S(f,q) = S(f)G(f;q) \tag{12}$$

where $G(f;\theta)$ is the directional spreading function given by Mitsuyasu et al. (1975) as

$$G(f:q) = G_0 \cos^{2s}\left(q/2\right) \tag{13}$$

where θ is the direction angle measured counterclockwise from the principal wave direction or mean direction of wave advance (θ_m) and *s* is a parameter related to the frequency. If $\theta_{min} = -\pi$ and $\theta_{max} = \pi$, the constant G_0 becomes

$$G_0 = \frac{1}{p} 2^{2s-1} \frac{\Gamma^2(s+1)}{\Gamma(2s+1)} \tag{14}$$

where Γ is the Gamma function. The parameter *s* represents the degree of directional energy concentration and reaches a peak value, s_{max}, near the peak frequency, f_p. Goda and Suzuki (*in* Goda, 1985), introduced s_{max} as an engineering parameter in the expression

$$s = s_{max}(f / f_p)^5 \text{ when } f \le f_p; \text{ otherwise, } s = s_{max}(f / f_p)^{-2.5}$$

Goda (1985) considered s_{max} = 10 to be typical of local wind waves with s_{max} = 25 representing swell with a short decay distance and relatively large wave steepness. Figure 2 shows an example of the Mitsuyasu-type spreading function.

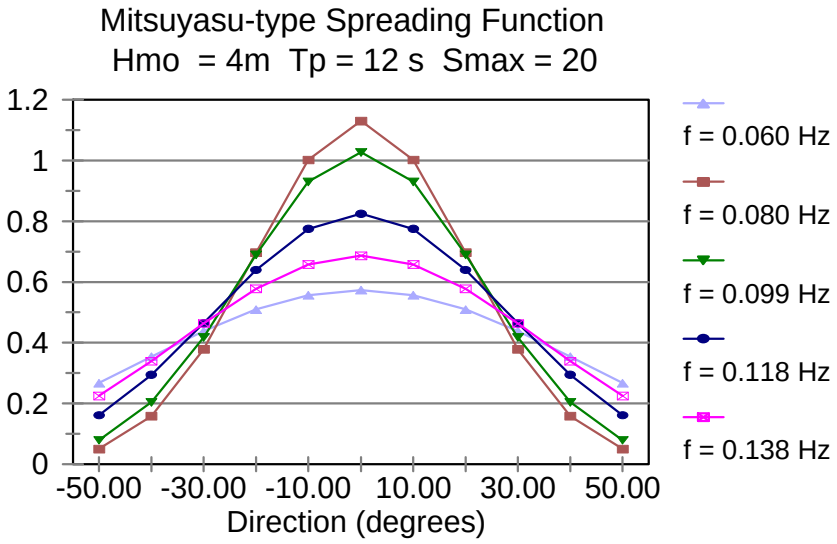

Figure 2. Mitsuyasu-type spreading function varying as a function of frequency.

Considering the frequency distribution in eq. 12, one may use experimentally derived formulations such as the JONSWAP spectrum, $S_J(f)$, (Hasselmann et al., 1973) for deep water or the TMA spectrum, $S_{TMA}(f,h)$, (Bouws et al., 1985) for finite depths. The JONSWAP spectrum and the TMA spectrum differ by $\phi_K(\omega_h)$, a transformation factor (Kitaigorodskii et al.,1975) in

$$S_{TMA}(f,h) = S_J(f) f_K(w_h) \qquad (15)$$

where $\omega_h = 2\pi f(h/g)^{1/2}$ is the dimensionless radian frequency, h = depth, g = acceleration due to gravity. In deep water ($\omega_h > 2$) ϕ_K is equal to unity and the two spectral forms in eq.(15) are equivalent. However, in shallow ($\omega_h < 1$) and intermediate ($1 \le \omega_h \le 2$) depths, they differ by ϕ_K =

$0.5\omega_h^2$ and $\phi_K = 1 - 0.5(2-\omega_h)^2$, respectively [Hughes, 1984]. The JONSWAP spectrum itself may be computed in terms of wave height, frequency, and a spectrum "peakedness" parameter, λ, as

$$S_f(f) = \frac{b\ H_s^2}{f(f/f_p)^4}\exp\left[\frac{-1.25}{(f/f_p)^4}\right]g^{\exp\left[\frac{-(f/f_p-1)^2}{2s^2}\right]} \qquad (16)$$

in which

$$b \cong \frac{0.0624}{0.230 + 0.033g - 0.185(1.9+g)^{-1}}$$

$$g = 3.3, \qquad s = \begin{cases} 0.07: & f \le f_p \\ 0.09: & f \ge f_p \end{cases}$$

A typical TMA spectrum is shown in figure 3. When combined with the spreading function (eq. 13), the directional wave spectrum is the result (eq. 12).

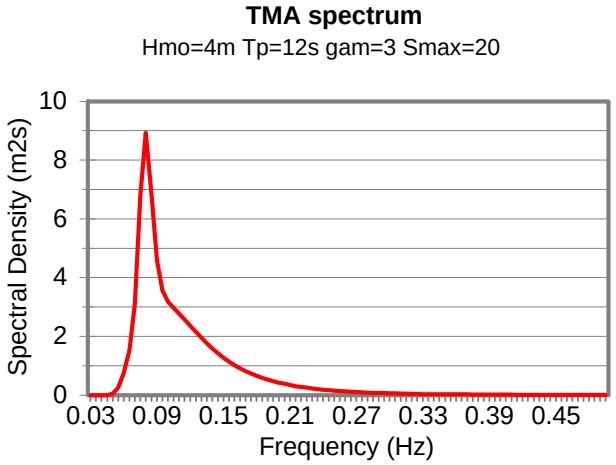

Figure 3. Example of the TMA frequency spectrum for waves in finite depths.

It should be noted that integration of the directional spectrum across all frequencies and directions by definition yields the total wave energy; i.e.,

$$m_0 = \int_0^{\infty} \int_{-p/2}^{p/2} S(f,q)\,dq\,df \qquad (17)$$

Because of the REF/DIF S directional limitation (50 degrees to either side of the x+ grid axis), a portion of the spectral energy calculated by eq. (17) may be lost depending upon the shape of the spreading function for the selected wave frequencies. In this study, eleven band-centered frequencies are selected in the range 0.035 to 0.5 Hz using a fixed bandwidth interval chosen so that the lowest and the highest frequencies span more than 96% of the total energy resulting from the first integration in eq. (17). Eleven directions relative to the grid are used, including one 0.0^0 direction coincident with the x+ grid axis and five directions at 10^0 intervals to either side.

Given the principal wave direction (θ_m) measured counterclockwise from the x+ grid axis, a representative wave amplitude is calculated for each *f,q* pair using eq. (12). These amplitudes are then entered as the first row of the computational grid and propagated forward (downwave) as REF/DIF S computes new solutions row by row. θ_m cannot be made very large or a significant fraction of the total wave energy will not be "gated" into the model domain.

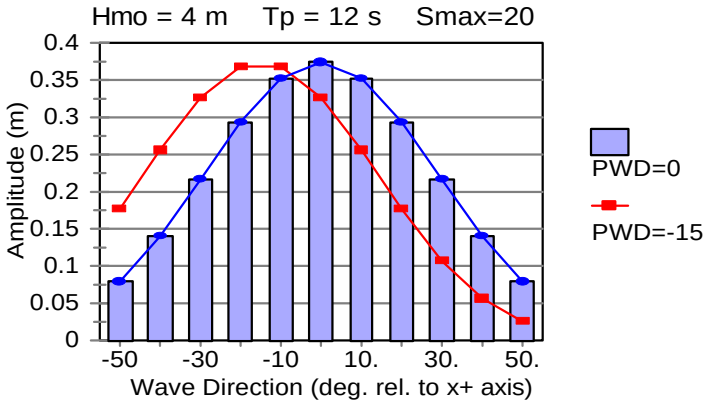

Figure 4. Graph showing wave amplitudes for 11 directions at *fp*=0.08 Hz before and after a change in principal wave direction (PWD).

Figure 4 illustrates this effect. If the principal wave direction, θ_m, is more than 15 degrees relative to the x+ grid axis, the model reference grid should be re-oriented to reduce θ_m accordingly.

Wave Climate Information

Spectral wave models such as REF/DIF S require detailed input information of the type discussed in the previous section. In order for the resulting model predictions to be representative, knowledge of the local wave climate is required. Directional wave observations for the nearshore region of Virginia Beach and Sandbridge do not exist; However, a 20-year simulated (hindcast) data set is available (Hubertz et al., 1993) and has been used as model input for the present study. Hubertz et al. (1993) provide a revision of an earlier data set created for the years 1956-1975, based on hindcast wind fields and using the latest Corps of Engineers wave hindcast model (WISWAVE 2.0). Information is given for 108 nearshore locations along the U.S. Atlantic coastline, stations 58 and 59 being applicable to the present study (Figure 5).

An examination of the WIS data for Atlantic Stations 58 and 59 shows that the largest hindcast Hmo heights are for waves arriving most frequently from 090^0 (east) and 045^0 (northeast). Tables 1 and 2 show the distributions for these directions at station 59. From Table 1 (045^0), the most extreme waves will have Hmo heights between 4 and 5 m with peak spectral

Table 1. WIS Hindcast Data 1956-1975, Atlantic Station 59.
Direction 022.5^0-067.5^0 (045^0), number of waves per category.

									Tp (sec)
Hmo(m)	4	6	8	**10**	**12**	14	16	18	20
0 - 1	1074	295	36	0	0	0	0	0	0
1 - 2	218	1054	92	1	0	0	0	0	0
2 - 3	0	80	236	12	0	0	0	0	0
3 - 4	0	0	27	42	16	0	0	0	0
4-5	0	0	0	**13**	**8**	0	0	0	0
5 - 6	0	0	0	0	0	0	0	0	0
6 - 7	0	0	0	0	0	0	0	0	0
7 - 8	0	0	0	0	0	0	0	0	0
8 - 9	0	0	0	0	0	0	0	0	0

Table 2. WIS Hindcast Data 1956-1975, Atlantic Station 59.
Direction 067.5^0-112.5^0 (090^0), number of waves per category.

					Tp (sec)				
Hmo(m)	4	6	8	10	**12**	**14**	**16**	18	20
0 - 1	908	1194	5060	5222	2267	540	112	23	2
1 - 2	81	1224	1256	1646	1226	418	28	0	0
2 - 3	0	50	386	405	211	115	24	2	0
3 - 4	0	0	29	131	134	50	2	2	0
4 - 5	0	0	0	16	58	21	0	1	0
5-6	0	0	0	0	**7**	**24**	**1**	0	0
6-7	0	0	0	0	0	**8**	0	0	0
7 - 8	0	0	0	0	0	0	0	0	0
8 - 9	0	0	0	0	0	0	0	0	0

periods between 10 and 12 seconds. From Table 2 (090^0) the most extreme waves will have Hmo heights between 5 and 7 m and peak spectral periods between 12 and 16 seconds. Values in this range were selected for REF/DIF S model simulations.

Model Reference Grid

The model reference grid used in this study is shown in figure 1. It extends 20 km in the shoreward (x+) direction and 24 km in the longshore (y+) direction. The origin of the grid (x=0, y=0) lies at the northernmost corner which has UTM coordinates 430988.48064, 4088916.01676 for UTM zone 18. The azimuth for the x+ grid axis is 255 degrees measured clockwise from true north. The reference grid cell size is 250 m x 250 m with interpolated depths provided at each grid intersection point. Depths in meters below mean lower low water (MLLW) were obtained at irregularly-spaced points from the NOAA/NOS bathymetric data base named GEODAS. Files searched in GEODAS were corrected to refer all horizontal reference coordinates to the North American Datum of 1983 (NAD 83). GEODAS-supplied depths were found to be sparse in a few specific locations such as the test firing range seaward of the Dam Neck Naval Facility.

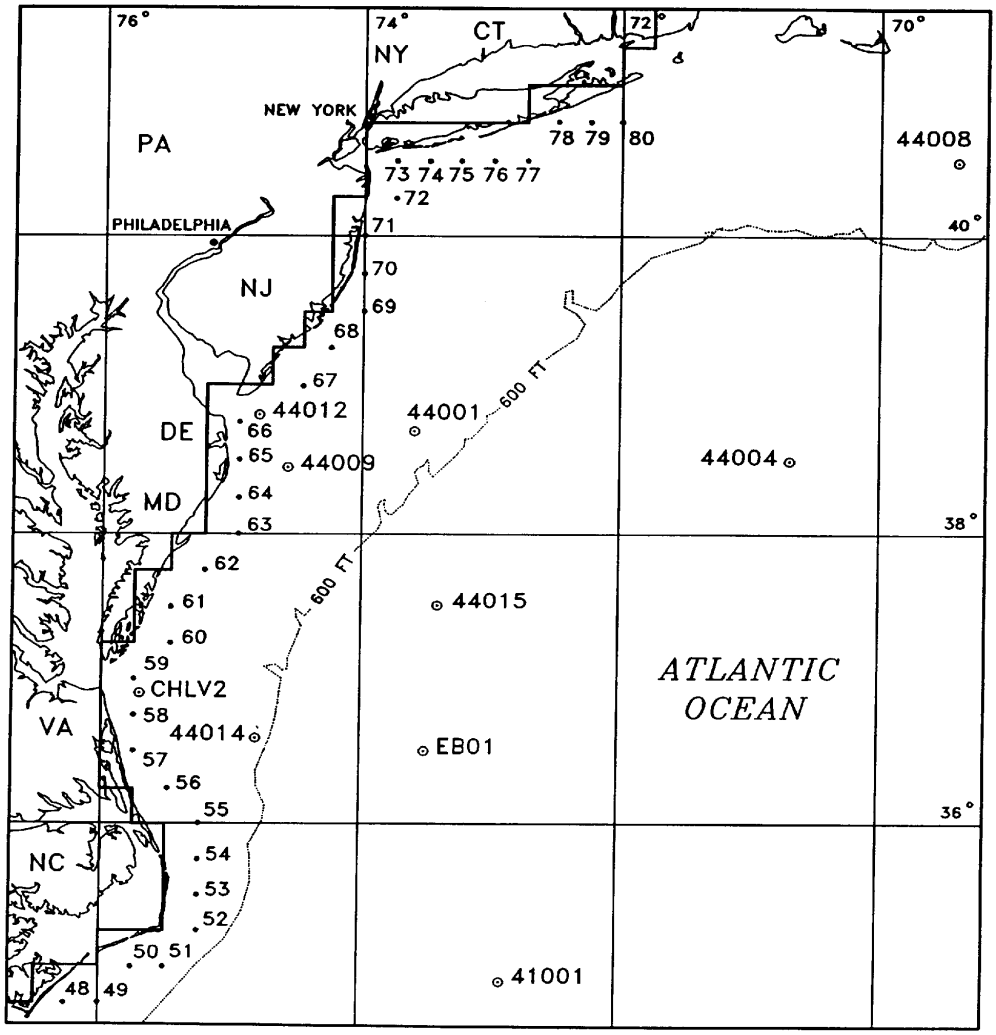

Figure 5. Map showing the location of WIS Atlantic Hindcast Wave Information Stations, U.S. Army Corps of Engineers. Other stations shown include NOAA observation buoys (e.g., 44001) and non-directional wave sensor at the Chesapeake Light Tower (CHLV2).

Supplemental soundings were obtained during a two-day, intensive hydrographic survey conducted by the NOAA ship FERREL in areas designated by the author. The resulting bathymetric grid for the Virginia Beach – Sandbridge coastal sector is shown in Appendix A, Plate 1.

While the reference grid horizontal spacing was fixed at 250 m x 250 m as noted above, the computational grid spacing actually used by REF/DIF S was made smaller through available

user options. Options were selected that subdivided y-axis spacings by four (to 62.5 m) and x-axis spacings by ten (to 25.0 m). The intervening depths were calculated by REF/DIF S at run-time using a linear, twisted surface routine.

Because of the present study focus on sand mining of the nearshore feature known as Sandbridge Shoal, an 8 km by 6 km subgrid was created to develop finer bathymetric detail in this region as shown in Appendix 1, Plate 2. Depths for the Sandbridge Shoal Subgrid were obtained at 25 m intervals in the x direction and at 62.5 m intervals in the y direction, thus matching the spacing of the computation grid discussed above. However, with a subgrid it is possible for the user to enter detailed depth information either to show high-density soundings representing the actual bottom or to develop hypothetical, fine-scale bathymetry (e.g., mounds or dredged areas) for test purposes. In displays such as the 3D mesh plot in Appendix A, Plate 2 (drawn using MATLAB Graphics), only every 4^{th} data point in the x-direction is shown.

Idealized Nearshore Bathymetry Model

Before propagating spectral waves across the actual bathymetry in the Virginia Beach - Sandbridge model domain, a series of test runs was conducted using a idealized approximation to that surface. The resulting model of the shoreface will be described before discussing the outcome of these runs.

A variation of Dean's equilibrium beach profile (Dean, 1977) was applied using the equation

$$h = A \cdot X^{m} \qquad (18)$$

where h = depth, X = distance from the shoreline in the seaward direction, and A, m are profile scale and shape parameters. Strictly speaking, eq. (18) is applicable only to the surf zone or a slight distance beyond in a region where bottom sediment is capable of being mobilized by wave action. In a theoretical derivation, Dean showed that m=2/3 results assuming uniform wave energy dissipation by spilling breakers across the surf zone and this value is the one generally

accepted by those who model natural beaches by this means. A similar assumption, however, yields m=0.4 and this value, along with A=0.39, results in the best fit in the least squares sense to the full profile crossing Sandbridge Shoal and continuing across the model domain to a maximum depth of about 20 m. The inshore part of this profile is shown in figure 6. The three-dimensional surface developed by extending the $h = 0.39 \times ^{0.4}$ profile uniformly in the y-direction is herein called the equilibrium shoreface surface (see Appendix A, Plate 3).

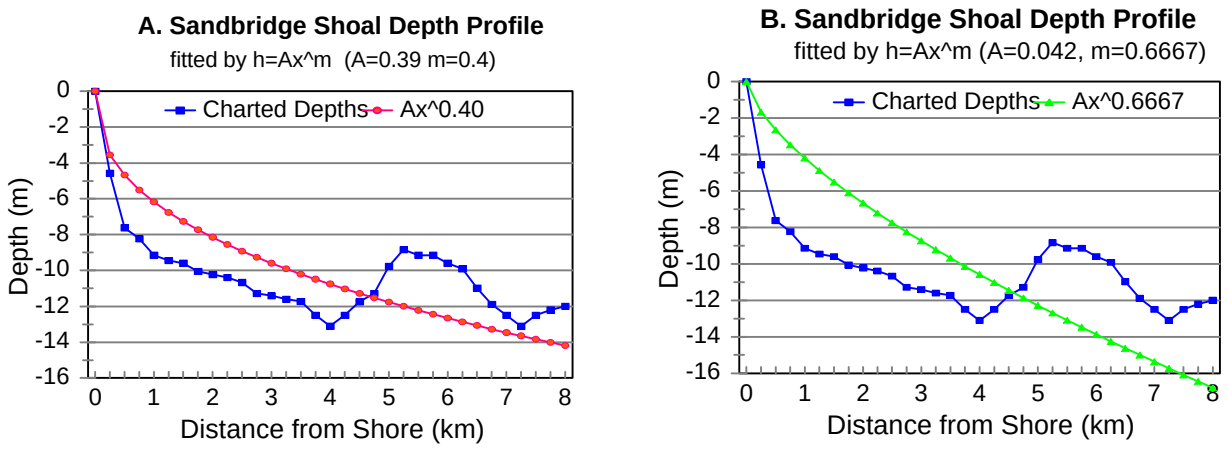

Figure 6. Equilibrium beach profile fitted to nearshore bottom in the Sandbridge subgrid using m=0.4 (A) and m=2/3 (B). m=2/3 (B) fails to match 20 m depth offshore.

From figure 6 (A), one of the simplest approximations to the natural bottom in the region of the Sandbridge Shoal subgrid is a surface developed using $h = 0.39 X^{0.4}$ with a mound rising 3 m above the surface to represent the shoal (Appendix A, Plate 3). The sides of the mound in Plate 3 have an approximately 1:10 slope with rounded corners. Using an idealized model of the upper shoreface at Sandbridge Shoal is by no means intended to replace the study of the actual bathymetry. It simply allows additional testing of a complex wave model to determine its response to changes in the basic elements of the bathymetry; i.e., the presence or absence of the shoal in its simplest configuration. The configuration is also one that can be easily replicated and tested by others who may have made improvements to REF/DIF S and perhaps other models that they wish to advance.

Equilibrium Shoreface Surface – Model Test Runs

1. General - Plate 1, Appendix B, illustrates the primary type of output that the REF/DEF S wave model is capable of producing; i.e., a surface contour plot of the Hmo wave heights distributed within the model domain. A moderate storm wave input was used (Hmo = 3 m, T_p = 11 s) as input for this run. Information on wave direction is more difficult to obtain. Although it combines a relatively large number of component waves of varying frequency and direction at each point on the computational grid, REF/DIF S does not generate directional spectra at these points and thus cannot produce vector plots of the spectral peak or principal wave direction. REF/DIF S does produce estimates of the radiation stress components S_{xx}, S_{xy}. and S_{yy}. These can be used to obtain information on gradients in radiation stress which define the driving force for longshore transport within the surf zone. Radiation stress gradients were not addressed in the present study.

2. Wave breaking – As previously noted, REF/DIF S uses the breaking model by Thorton and Guza (1983). Rather than handling wave breaking through an "on" "off" switch, eq. (11) is used continuously to determine a breaking coefficient that becomes very large at the onset of breaking, thus initiating rapid dissipation of wave energy as indicated in eq. (10). Plate 2A, Appendix B, shows the expected shore-parallel bands of diminishing wave height that begin a very rapid decay (breaking) within the final 300 m or so before reaching the shoreline. Plate 2B, Appendix B, shows a large area of affected wave heights down wave from the +3m mound placed 5m seaward of the shoreline. Wave heights increase by about 0.3 m at the lateral edges of the mound with smaller increases and decreases occurring in conically-spreading bands trailing the two edges. This perturbation on Hmo wave heights persists until within about 900 m of shore as the breaking band begins to develop. Within this band, longshore variations in Hmo effectively cease.

3. Principal Wave Direction - The Principal Wave Direction (PWD) in REF/DIF S is specified relative to the X+ reference grid axis. The latter has a heading of 255^0 measured clockwise from true north (000^0). The reciprocal of this heading is 075^0. Two test runs were made with a more

intense storm wave spectrum (Hmo = 4 m, T_p = 12s), varying the Principal Wave Direction by 15^0 to either side of the X axis. These directions conform to the WIS hindcast sectors (045^0 and 090^0) shown in Tables 1 and 2. Plates 3A and 3B, Appendix B, show the results of these runs using the test mound. A skewed distribution of wave heights appears to the right and left which are mirror images of one another or approximately so. This allows confidence in the assumption that the directional response is uniform; i.e., no lateral boundary effect even though the mound (and Sandbridge Shoal) is far from being centered within the reference grid.

4. Increase in offshore wave height - Increasing the height of the input wave offshore causes more pronounced longshore variations in Hmo wave height in the lee of the test mound, variations that extend closer to shore. This is clearly shown in Plates 2, 3, and 5 of Appendix B. In addition, the maximum offshore wave height tested (Hmo = 7 m, T_p = 15s) produced a strong, trident-shaped refraction-diffraction pattern in the lee of the rectangular mound (Plates 6A and 6B, Appendix B). As explained in the final section of the present report, this pattern was noted in other areas of the main reference grid when the actual bathymetry was used with the model.

5. Change in directional spreading parameter, S_{max} – Variations in S_{max} govern the degree of directional energy concentration as reflected by the narrowness of the directional spreading function about its peak value. The degree of directional spreading is known to affect both wave refraction and diffraction and is related to wave steepness (Goda, 1985). However, test runs using S_{max} = 10 (wind waves) and S_{max} = 20 (swell with short decay distance) for extreme storm waves (Hmo = 7m, Tp = 15s) show relatively small changes in wave height distributions (Plates 6A and 6B, Appendix B).

Model Runs with Existing and Locally Modified Bathymetry

1. **General -** Plate 1, Appendix C, shows what may be regarded as a typical example of moderately extreme storm wave propagation across the Virginia Beach- Sandbridge reference grid. The existing bathymetry (Plate 1, Appendix A) is more complex and reflects the fact that the actual Virginia Beach – Sandbridge shoreline is slightly concave seaward and the innermost depths are greater than zero (about 3m MLLW in the mid-section of the last row). The presence of two, trident-shaped, refraction-diffraction patterns ('crow's feet') can be seen, similar to but larger than, the patterns appearing down wave of the rectangular mound in the test runs. Plate 1 of Appendix C also shows that longshore variation in Hmo wave height is quite pronounced near the shoreline. Areas of lowest Hmo wave height appear to occur between the toes of the 'crow's feet'. The largest of these is situated immediately down wave of borrow area "A" at the crest of Sandbridge Shoals.

2. **Depth of Dredging, Borrow Area "A" –** Dredging has been done in borrow area "A" to depths of approximately -1 to –2 m, with –3 m occurring in some areas. For the purpose of wave model analysis to determine the possible impact of dredging, it was assumed that borrow area "A" was either un-dredged (condition 1) or dredged uniformly to a depth of –3 m (condition 2). It is estimated that the total yield for condition 2 would be 8.2 million cubic yards (6.3 million cubic meters). A comparison of plates 2A and 2B, Appendix C, suggests that the effect of this amount dredging would be to increase Hmo wave heights in limited areas offshore while creating a wider zone of low wave heights approaching the surf zone off Sandbridge Beach.

3. **Extreme Wave Conditions -** Extreme waves (Hmo = 5 to 7 m, T_p = 12 to 15 s) cause much larger waves to reach farther into the nearshore zone, particularly at the south end of the reference grid near Sandbridge Shoals and Sandbridge Beach (Plates 3 and 5, Appendix C). The effect of dredging borrow area "A" still appears to be one of lessening, not increasing, Hmo wave heights in the down wave shadow-zone approaching the surf zone. The decrease, however, is not large; i.e., less than 0.5 m in most places.

4. **Change in directional spreading parameter, S_{max} -** As with the test runs presented in Appendix B, using different values of S_{max} causes only a slight change in the distribution of Hmo wave heights as can be seen in Plates 7A and 7B, Appendix C. The change that results is much less than the change that occurs due to dredging (Plates 6A and 6B, Appendix C).

Summary and Conclusions

This investigation has shown that a spectral wave model, such as REF/DIF S, offers considerably more insight into the behavior of random wave fields in nature than is possible to achieve using a monochromatic wave model. Although intuitive guidance such as the depiction of wave refraction by means of converging or diverging wave rays is not possible with a spectral model, the latter does provide a critically important statistical basis for describing wave heights locally and throughout the model domain. The key parameter in that instance is the zero-moment wave height or its equivalent, the significant wave height.

In addition to its spectral wave features, REF/DIF S has another feature that is extremely useful, namely the subgrid. One can divide the rectangular reference grid into smaller cells within any selected sub-region to define a subgrid. The finer resolution of the subgrid is used only where needed to develop small-scale bottom features in detail while simultaneously allowing wave transformation to be studied over a much broader region. In this study, bottom features with length scales on the order of tens of meters were investigated within a 6 x 8 km subgrid using a 62.5 x 25 m cell size. The subgrid in turn was placed within a 20 x 24 km reference grid with 250 x 250 m cell size. In this way, deep water waves were transmitted from offshore sites, where spectral wave information was available, to the local site of immediate

concern, a region beginning at Sandbridge Shoal and extending landward to the surf zone in front of Sandbridge Beach.

The results of the wave modeling described in this report indicates that full development of a dredging site at Sandbridge Shoal, known as borrow area “A”, will cause slight but clearly perceptible changes in Hmo wave heights on the order of 0.5 m with higher differences in isolated regions near the site. In general, the effect of dredging will be to reduce wave heights slightly in a cone-shaped region between borrow area “A” and the surf zone. Although the model predicts uniform and rapid wave decay (wave breaking) in the surf zone, there are clear indications of significant longshore variations in Hmo wave height of a cyclical nature that will likely contribute to the forcing that enables two-dimensional circulation (rip currents) within the surf zone. More research is needed in this area, particularly with regard to longshore variations in wave height and local gradients in radiation stress.

References

Dalrymple, R.A. and J.T. Kirby, 1991. "*REF/DIF 1 version 2.3, Documentation Manual*", Report No. CACR 91-2, Center for Applied Coastal Research, Dept. of Civil Engineering, Univ. of Delaware, Newark, 19p.

Dean, R.G., 1977. "*Equilibrium beach profiles: U.S. Atlantic and Gulf coasts*", Ocean Eng. Tech. Rep. No. 12, University of Delaware, Newark.

Goda, Y., 1985. *Random seas and design of maritime structures,* University of Tokyo Press, 309 p., Appendix.

Hasselmann, K., T. Barnett, E. Bouws, H. Carlson, D. Cartwright, K. enke, J. Ewing, H. Gienapp, D. Hasselmann, P. Kruseman, A. Meerburgh, P. Muller, D. Olbers, K. Richter, W. Sell and H. Walden, 1973. "*Measurement of wind-wave growth and swell decay during the Joint North Sea Wave Project (JONSWAP*), Deutsches Hydrographisches Zeitschrift Reihe A (8^0), No. 12.

Hubertz, J.M., R.M. Brooks, W.A. Brandon, B.A. Tracy, 1993. "*Wave information studies of U.S. coastlines: Hindcast wave information for the U.S. Atlantic coast*", WIS Report 30, U.S. Army Corps of Engineers, Waterways Experiment Station, Vicksburg, MS., 20p., three appendices.

Hughes, S.A., 1984. "*The TMA shallow-water spectrum, description and applications*", Tech. Rep. CERC-84-7, U.S. Army Waterways Experiment Station, 39 p., appendix.

Kirby, J.T., 1986. "Higher-order approximations in in the parabolic equation method for water waves", *J. Geophys. Res.,* **91**:933-952.

Kirby, J.T. and R.A. Dalrymple, 1986. "An approximation model for nonlinear dispersion in monochromatic wave propagation models", *Coast. Eng*., **9**: 545-561.

Kirby, J.T., and H.T. Ozkan, 1992. "*Combined refraction/diffraction model for spectral wave conditions: documentation and user's manual*", Report No. CACR-92-06, Center for Applied Coastal Research, Dept. of Civil Engineering, Univ. of Delaware, Newark, 102p.

Thorton, E.B. and R.T. Guza, 1983. "Transformation of wave height distribution", *J. Geophys. Res*., **88**:5925-5938.

APPENDIX A

REF/DIF S WAVE MODEL BATHYMETRY

Bathymetry developed for REF/DIF S and the Virginia Beach – Sandbridge reference grid consists of a matrix of water depths corresponding to the array of regularly-spaced grid intersection points covering the model domain.

Actual water depths relative to mean lower low water were obtained from NOAA hydrographic surveys. In addition, a hypothetical Equilibrium Shoreface Surface (ESS) was developed for testing purposes using $h(x,y) = A \times^{m}$ with A=0.39, m=0.4. In some of these tests, an underwater mound was placed on the ESS at a distance of 5km from shore.

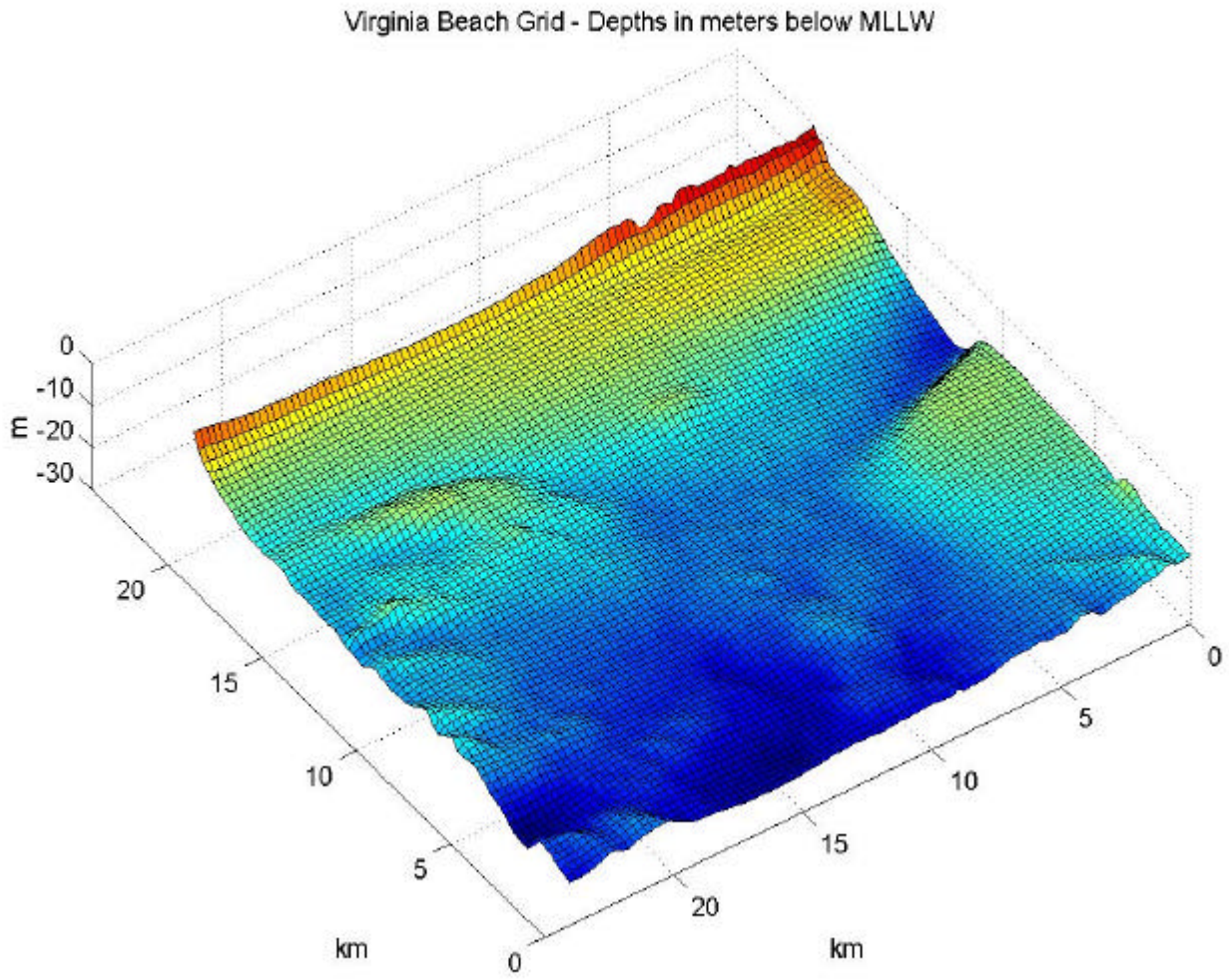

Plate 1. Bathymetry for the Virginia Beach – Sandbridge model reference grid.

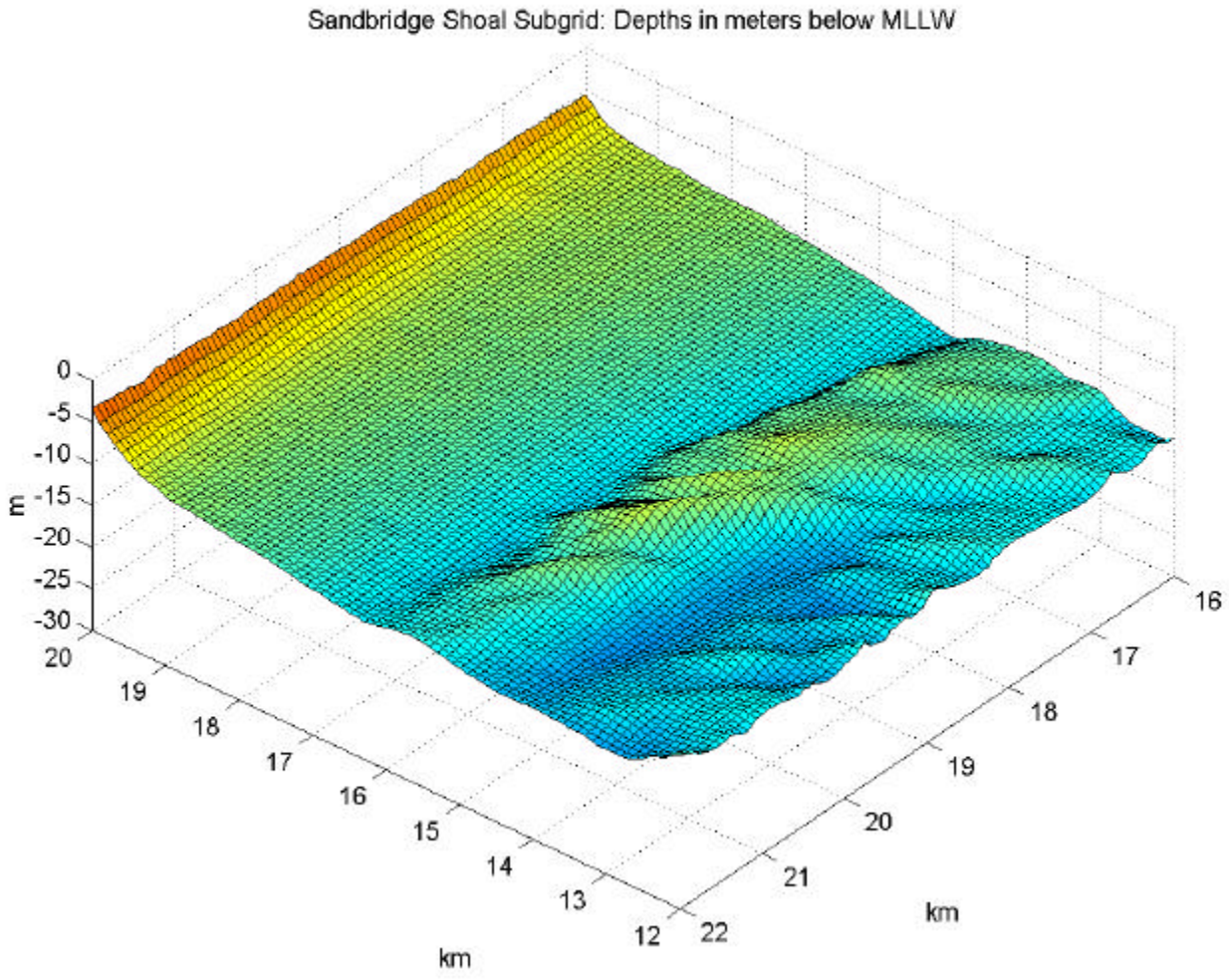

Plate 2. Location and bathymetry of Sandbridge Shoals subgrid

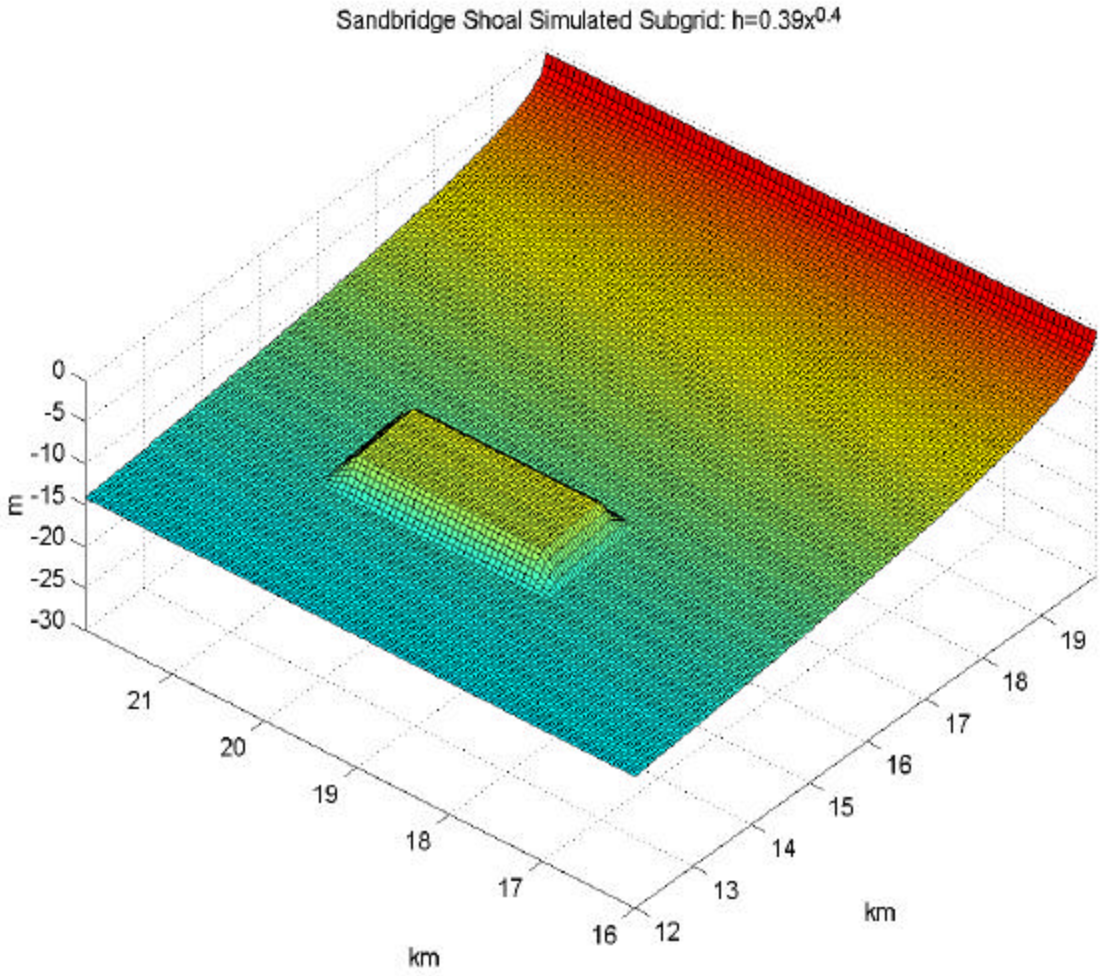

Plate 3. Equilibrium Shoreface Surface, Sandbridge Shoal subgrid.

APPENDIX B

REF/DIF S WAVE MODEL TEST RUNS

Test runs made using a hypothetical Equilibrium Shoreface Surface, $h(x,y) = A x^{m}$ with A=0.39, m=0.4 for the Virginia Beach – Sandbridge reference grid. Tests include selected runs with an underwater mound placed on the ESS at a distance of 5km from shore.

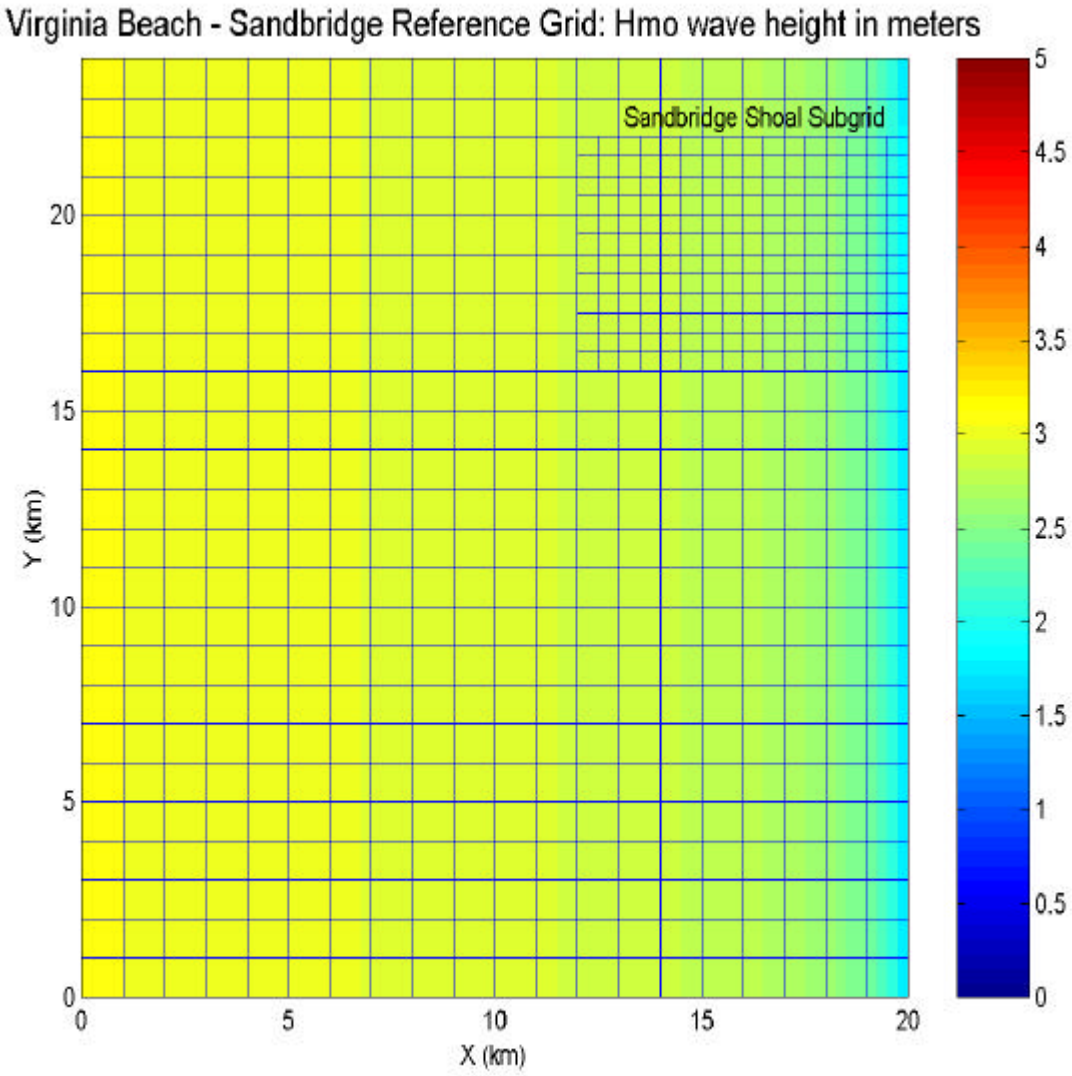

Plate 1. Model reference grid and color display of Hmo wave heights.
Model run 01: Hmo=3m, Tp=11s, Smax=10, PWD=0.

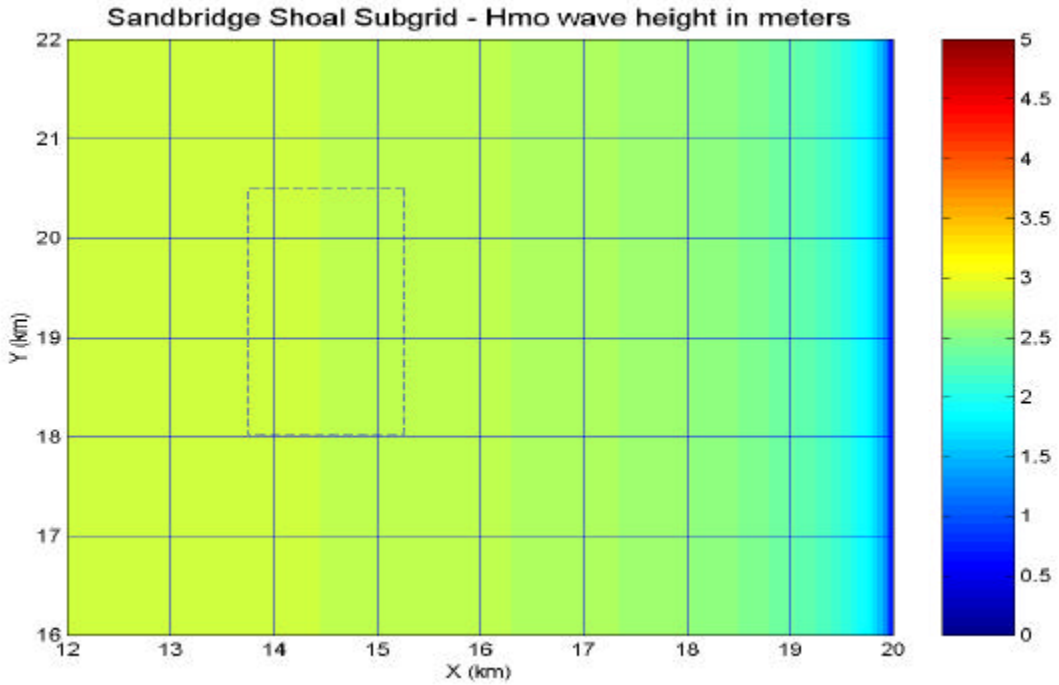

Plate 2A. Model run 01: Hmo=3m, Tp=11s, Smax=10, PWD=0
Condition: Test mound (dashed line) absent

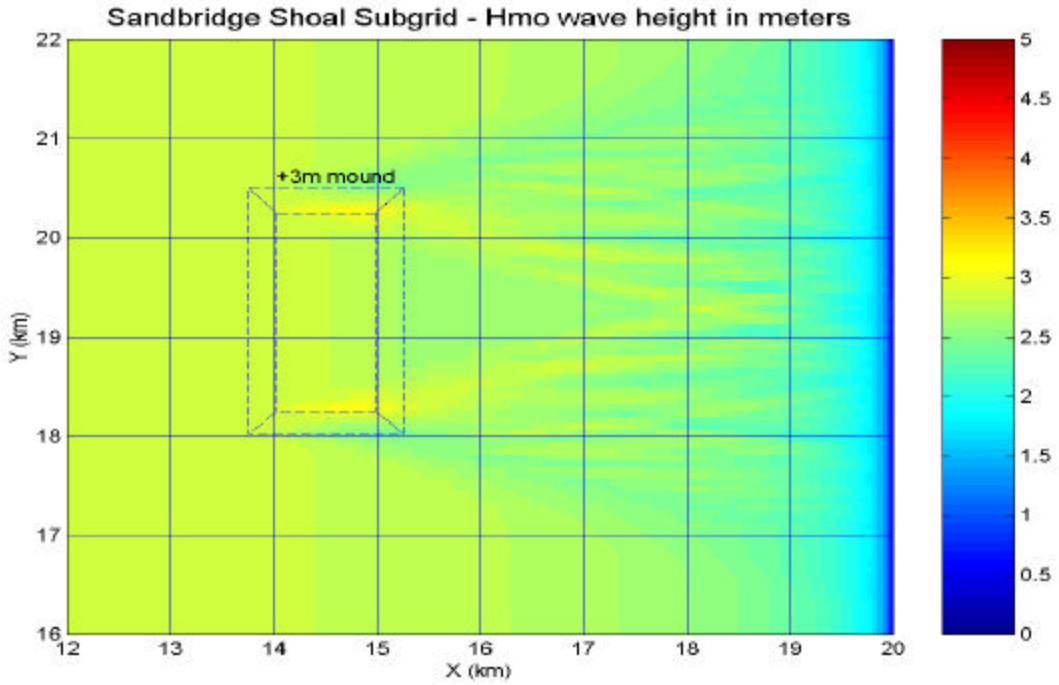

Plate 2B. Model run 02: Hmo=3m, Tp=11s, Smax=10, PWD=0
Condition: +3m test mound (dashed line) present

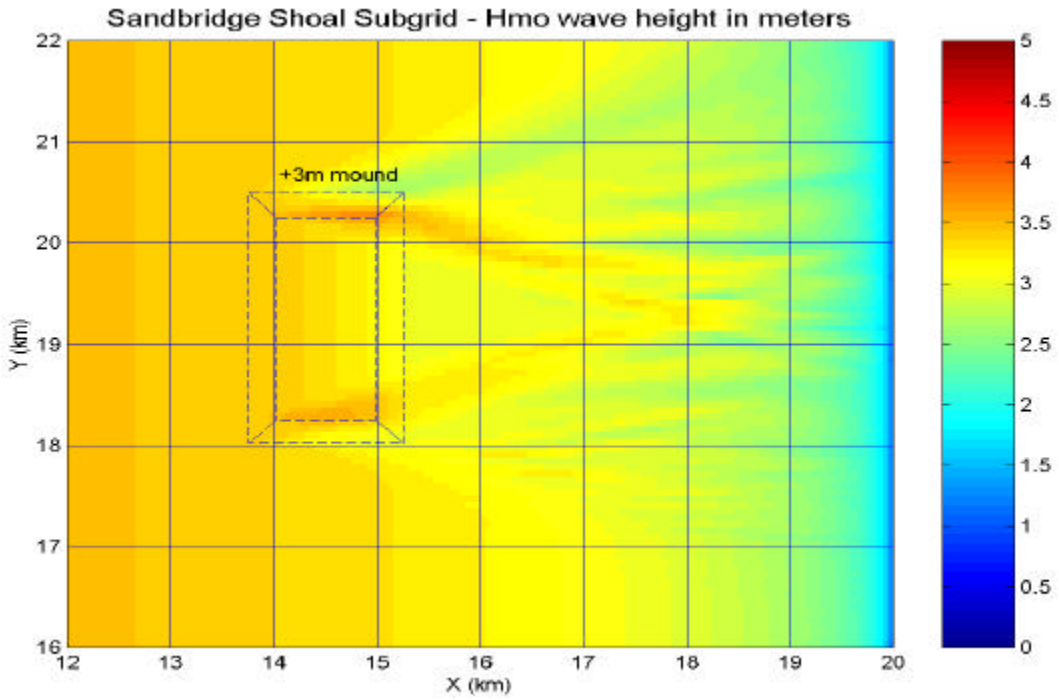

Plate 3A. Model run 03: Hmo=4m, Tp=12s, Smax=20, PWD=15
Condition: +3m test mound (dashed line) present

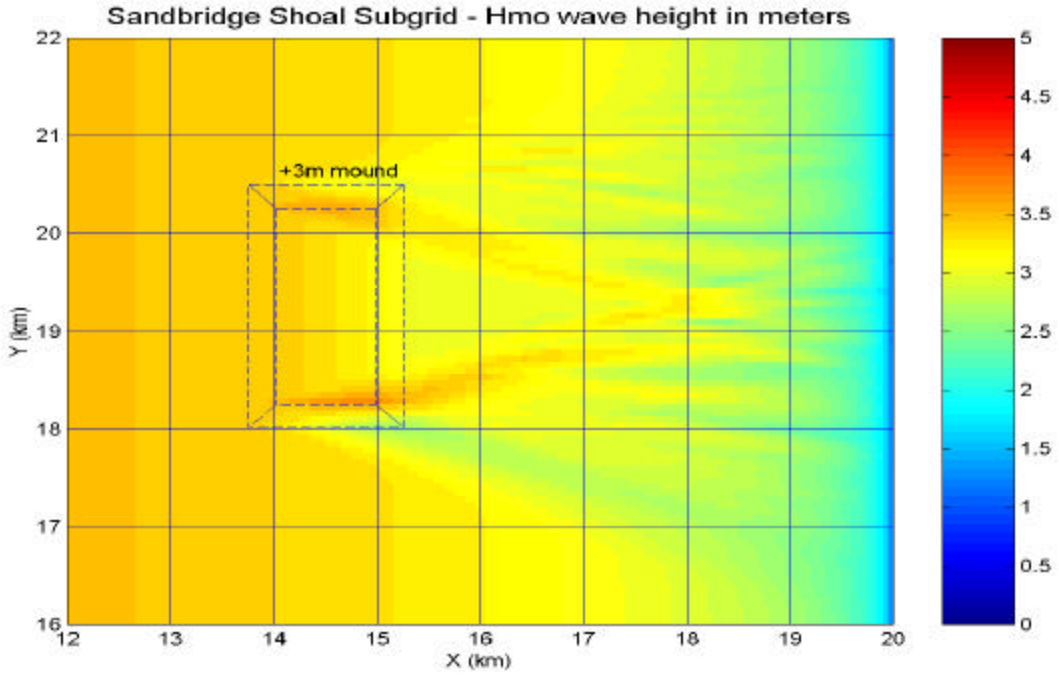

Plate 3B. Model run 04: Hmo=4m, Tp=12s, Smax=20, PWD= -15
Condition: +3m test mound (dashed line) present

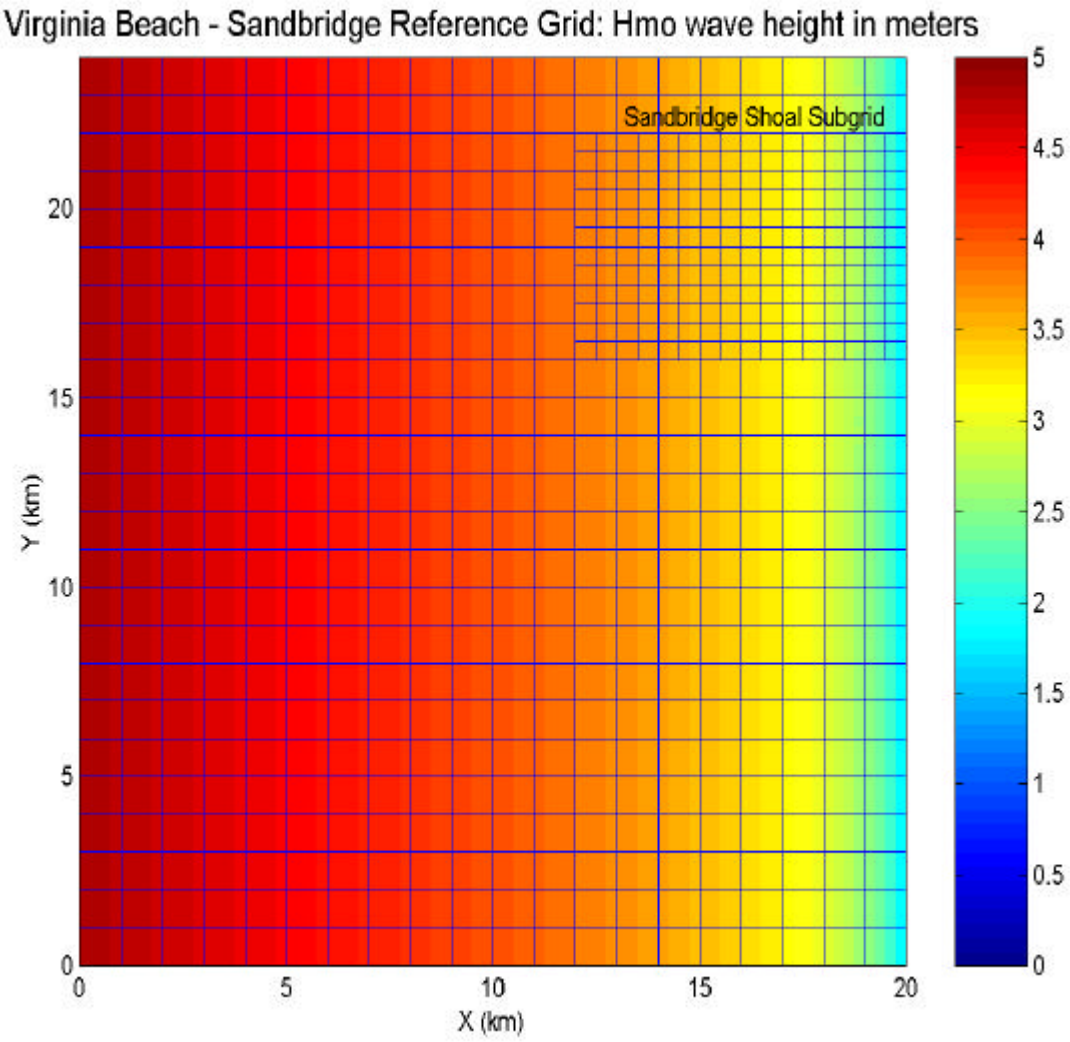

Plate 4. Reference grid and color display of Hmo wave heights.
Model run 05: Hmo=5m, Tp=12s, Smax=10, PWD=0.

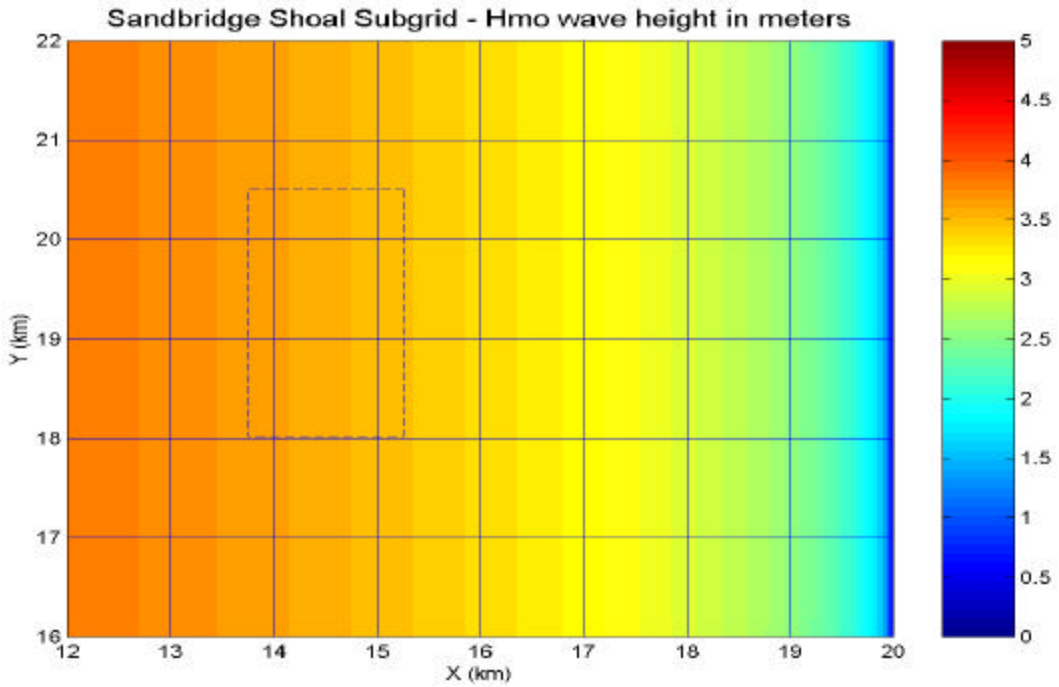

Plate 5A. Model run 05: Hmo=5m, Tp=12s, Smax=10, PWD= 0
Condition: test mound (dashed line) absent

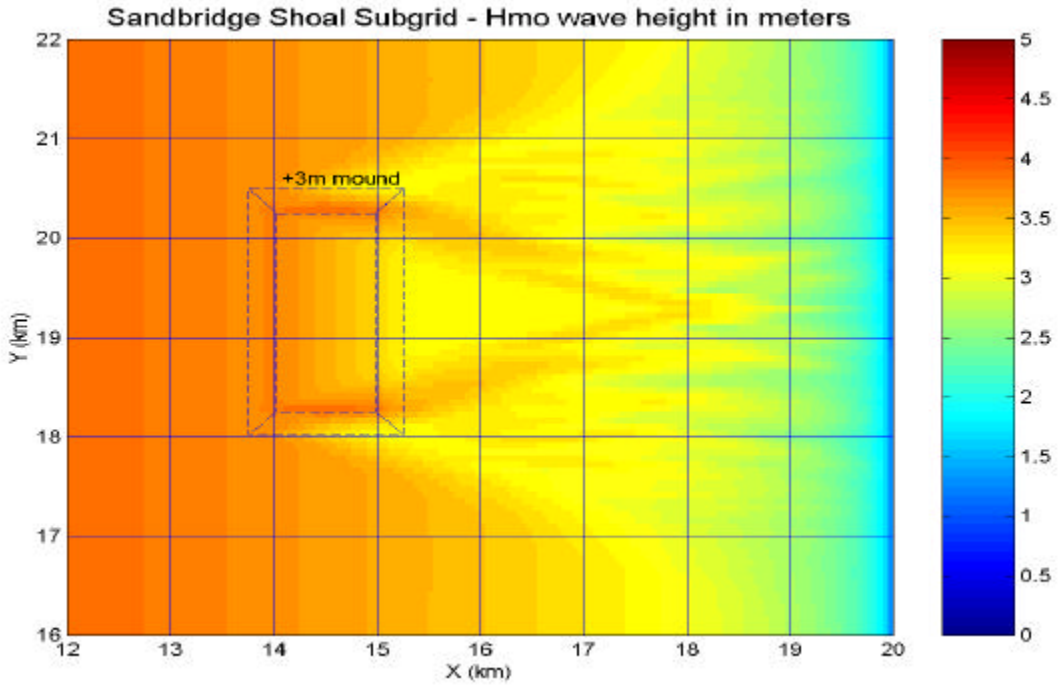

Plate 5B. Model run 06: Hmo=5m, Tp=12s, Smax=10, PWD= 0
Condition: +3m test mound (dashed line) present

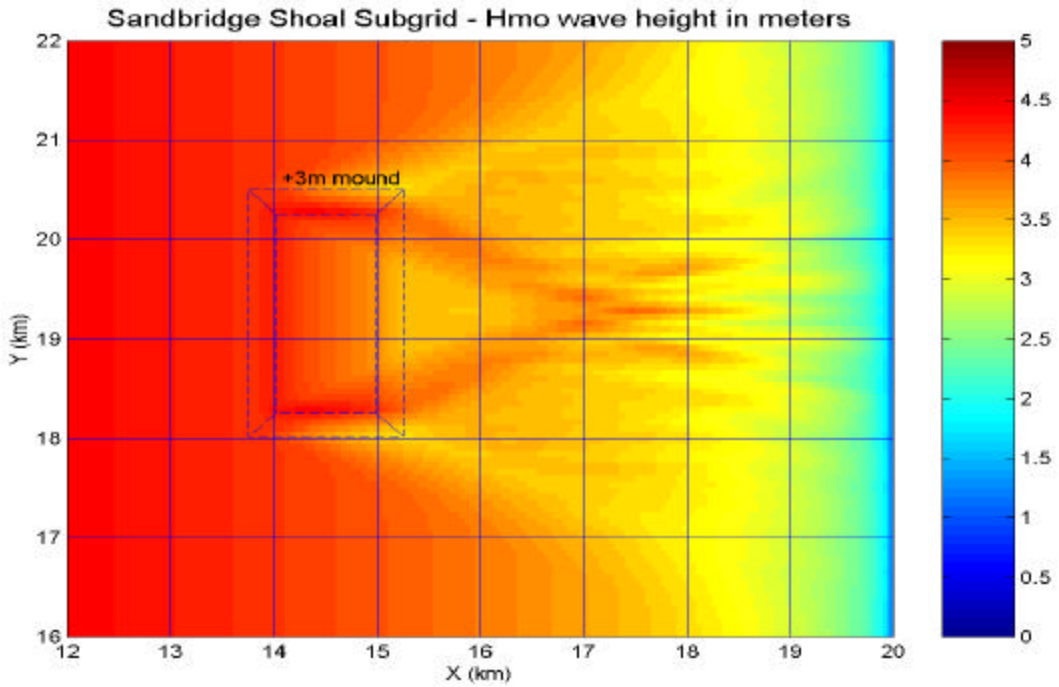

Plate 6A. Model run 07: Hmo=7m, Tp=15s, Smax=10, PWD= 0
Condition: +3m test mound (dashed line) present

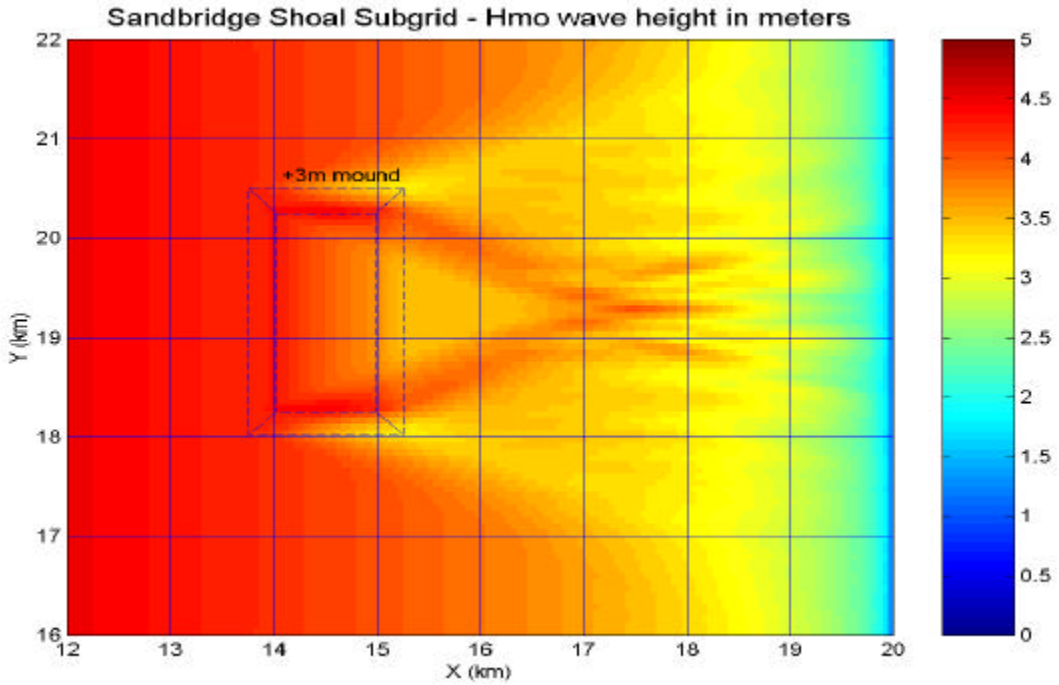

Plate 6B. Model run 08: Hmo=7m, Tp=15s, Smax=20, PWD= 0
Condition: +3m test mound (dashed line) present

APPENDIX C

REF/DIF S WAVE MODEL SITE RUNS

Model runs made using local bathymetry for the Virginia Beach – Sandbridge reference grid. Selected runs made to show effects of dredging borrow area “A” to a depth of –3 m.

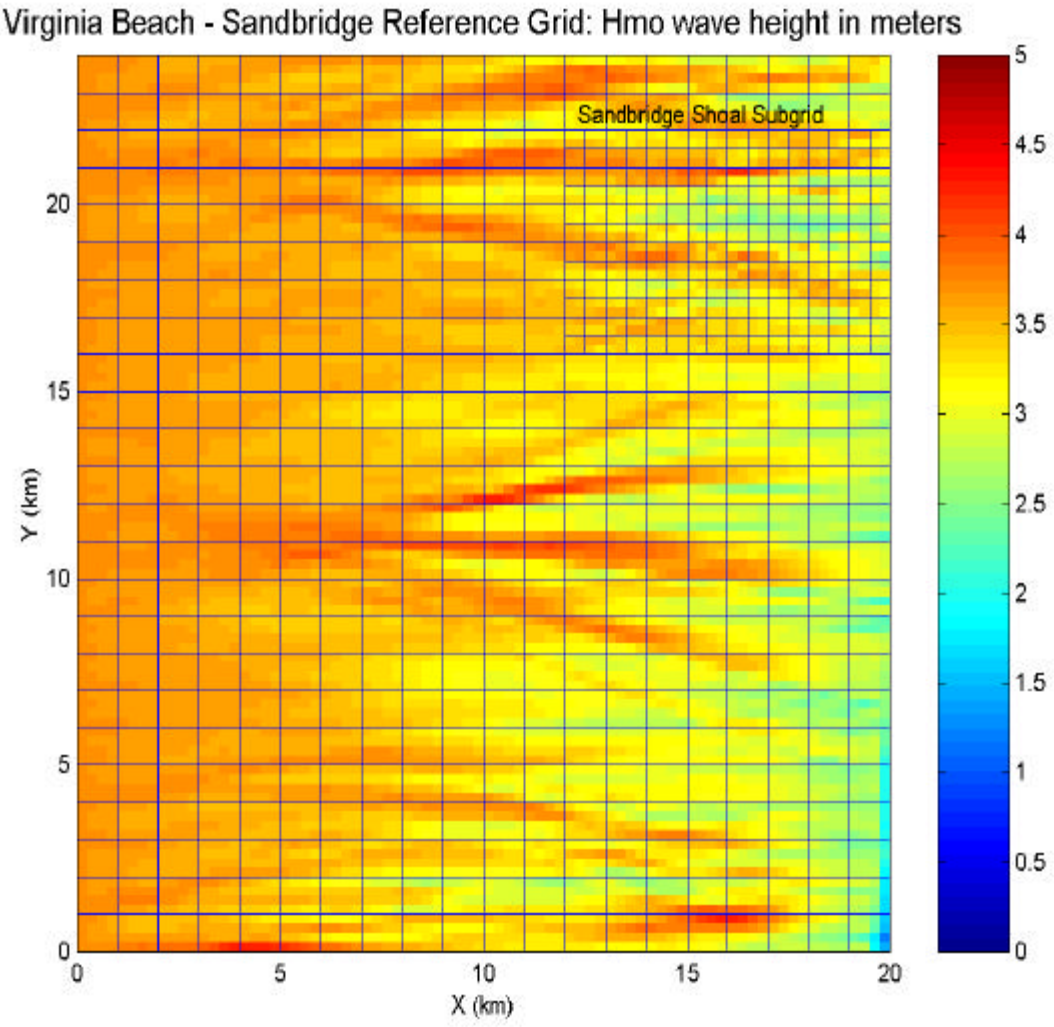

Plate 1. Model reference grid and color display of Hmo wave heights.
Model run 16: Hmo=4m, Tp=12s, Smax=10, PWD=0.

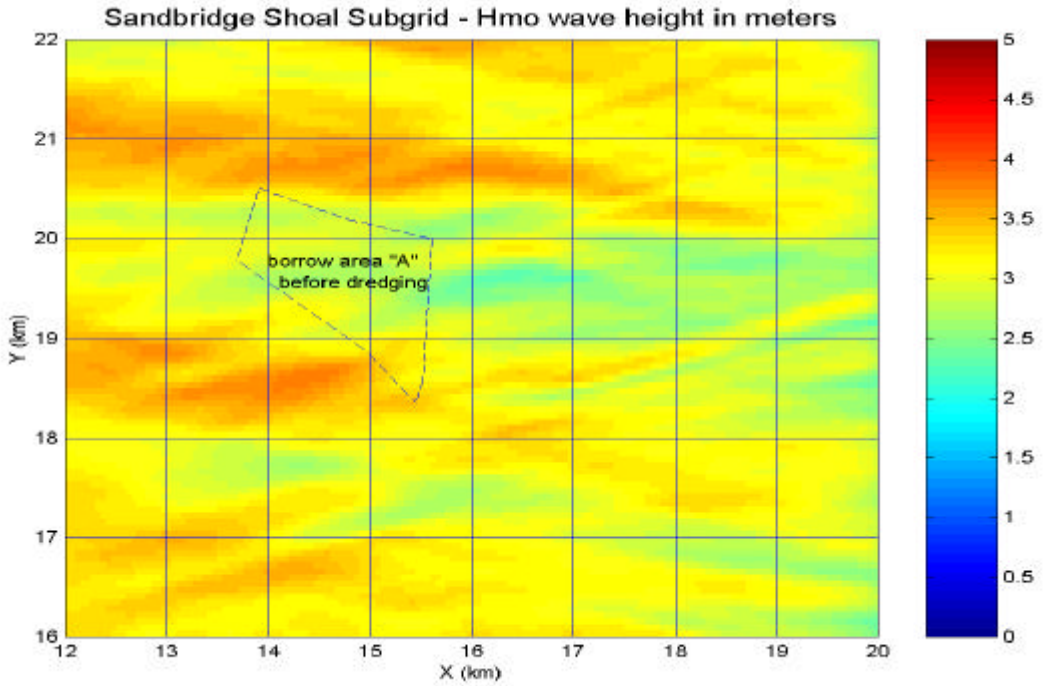

Plate 2A. Model run 17: Hmo=4m, Tp=12s, Smax=10, PWD= 0
Condition: Area “A” (dashed line) before dredging.

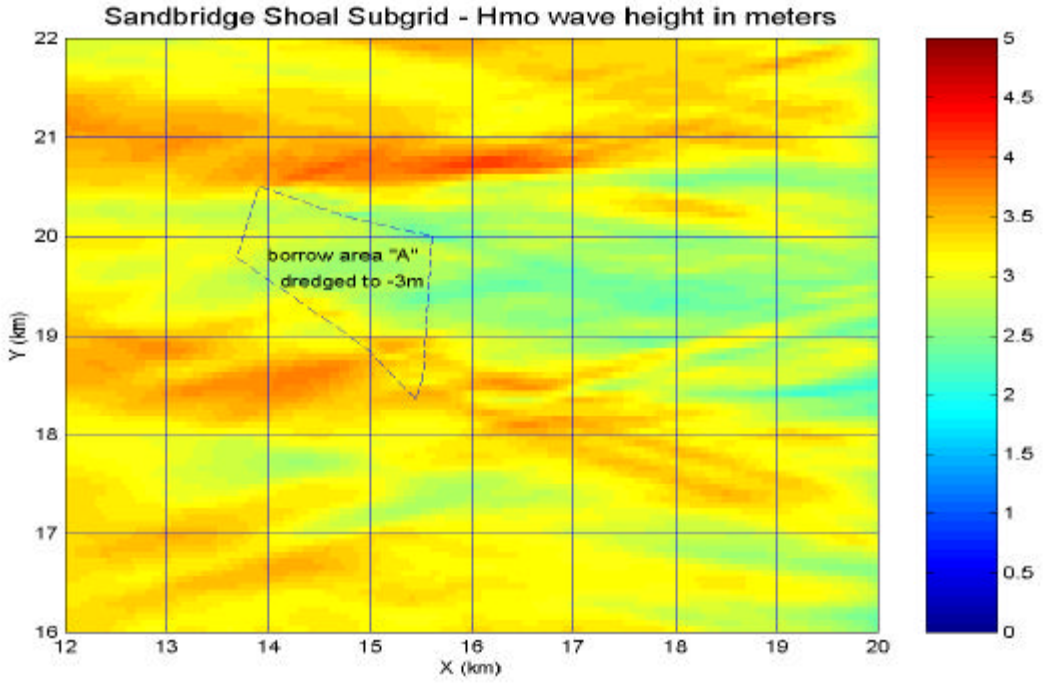

Plate 2B. Model run 16: Hmo=4m, Tp=12s, Smax=10, PWD= 0
Condition: Area “A” (dashed line) dredged to –3m.

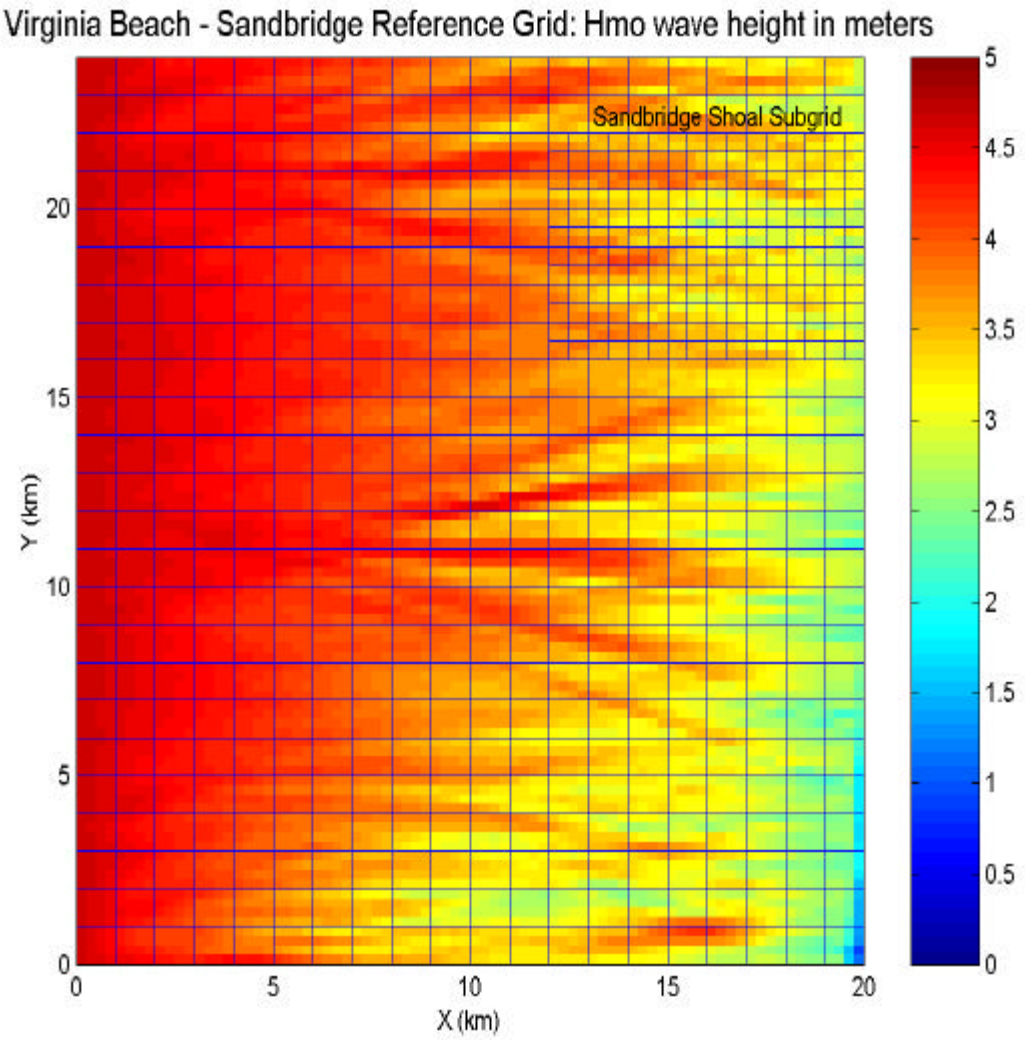

Plate 3. Model reference grid and color display of Hmo wave heights. Model run 18: Hmo=5m, Tp=12s, Smax=20, PWD=0.

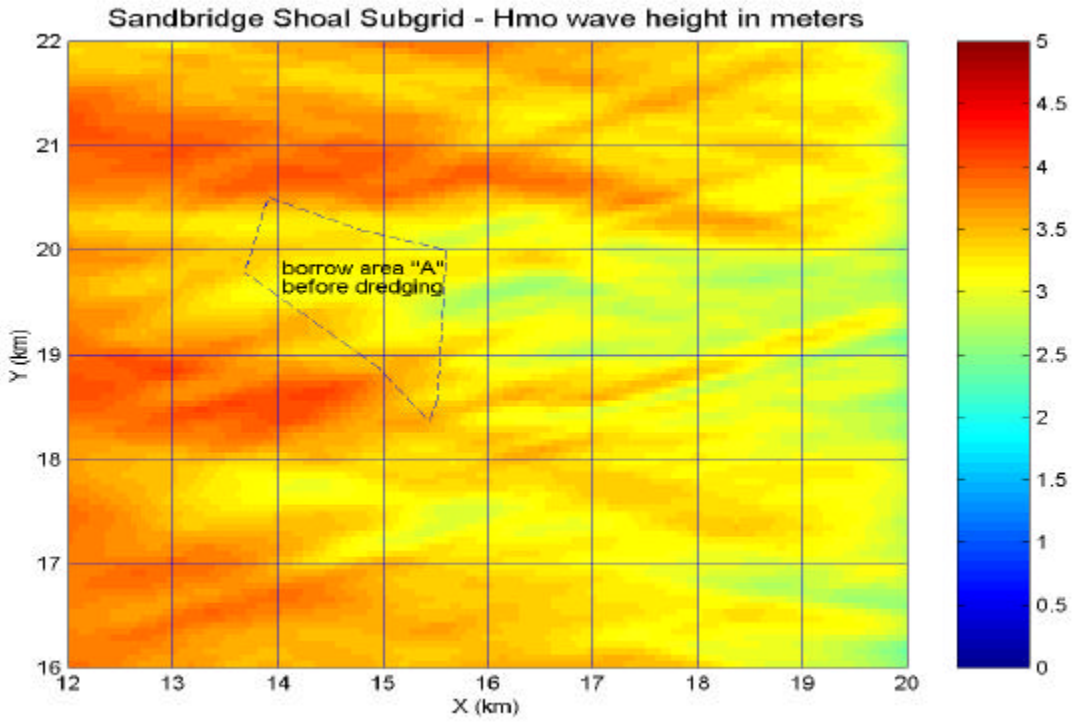

Plate 4A. Model run 18: Hmo=5m, Tp=12s, Smax=20, PWD= 0
Condition: Area "A" (dashed line) before dredging.

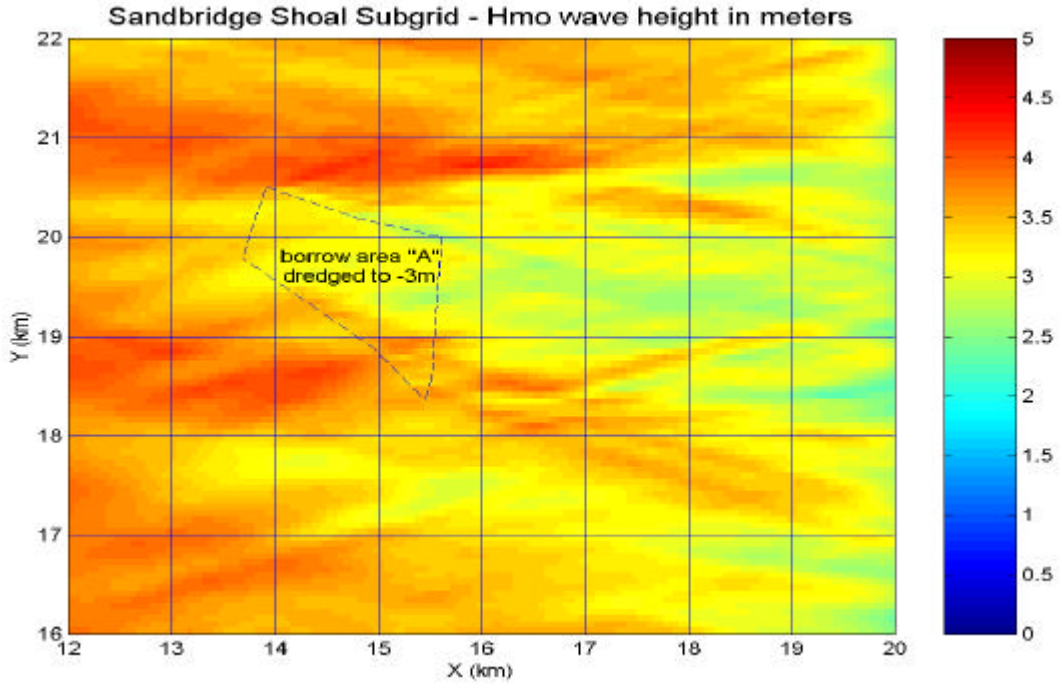

Plate 4B. Model run 19: Hmo=5m, Tp=12s, Smax=20, PWD= 0
Condition: Area "A" (dashed line) dredged to –3m.

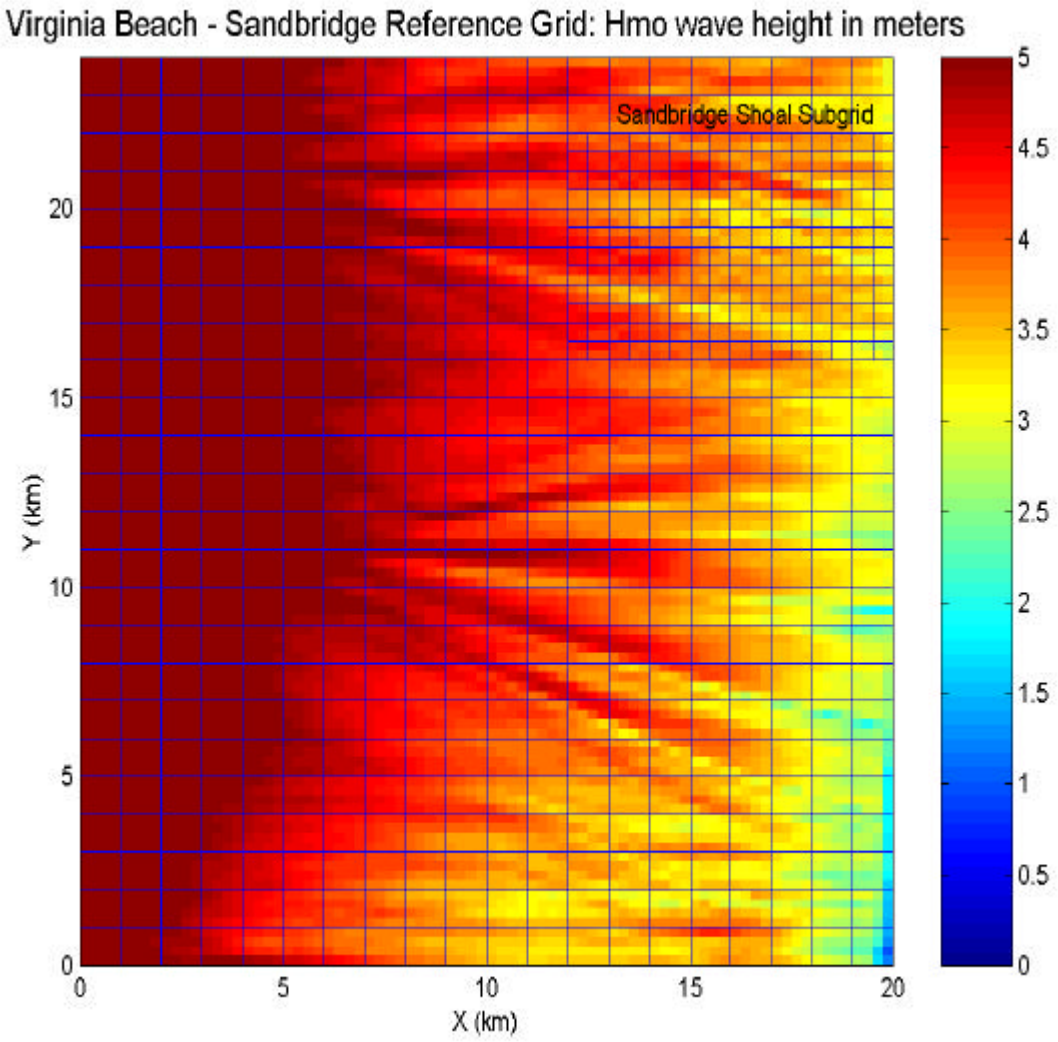

Plate 5. Model reference grid and color display of Hmo wave heights. Model run 20: Hmo=7m, Tp=15s, Smax=20, PWD= -15.

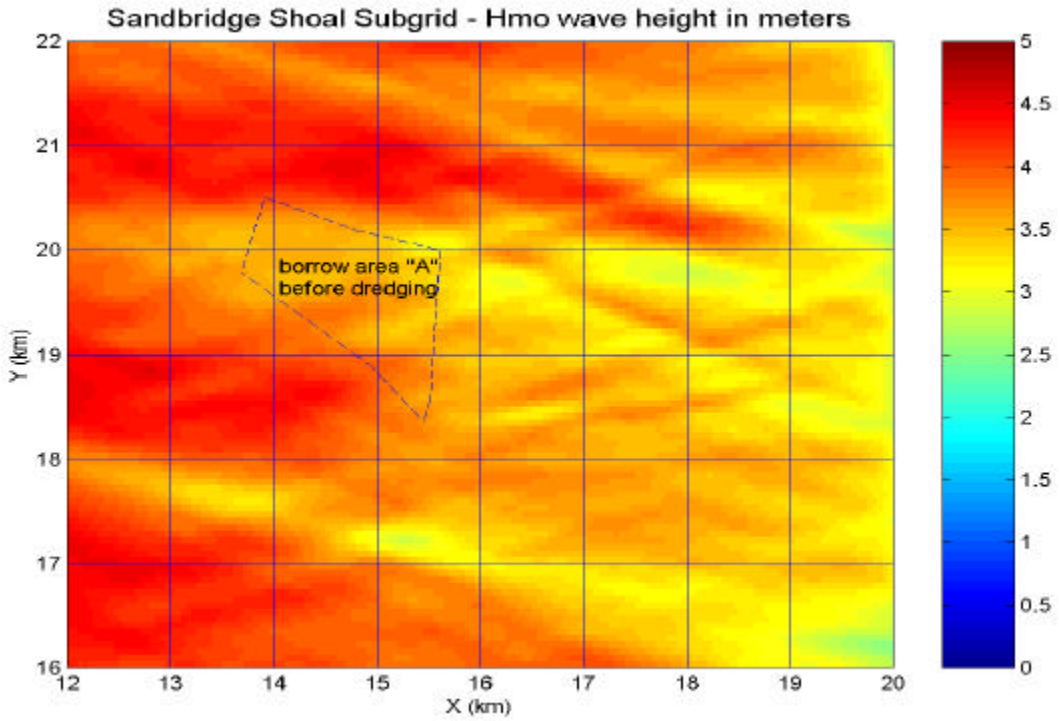

Plate 6A. Model run 20: Hmo=7m, Tp=15s, Smax=20, PWD= -15
Condition: Area “A” (dashed line) before dredging.

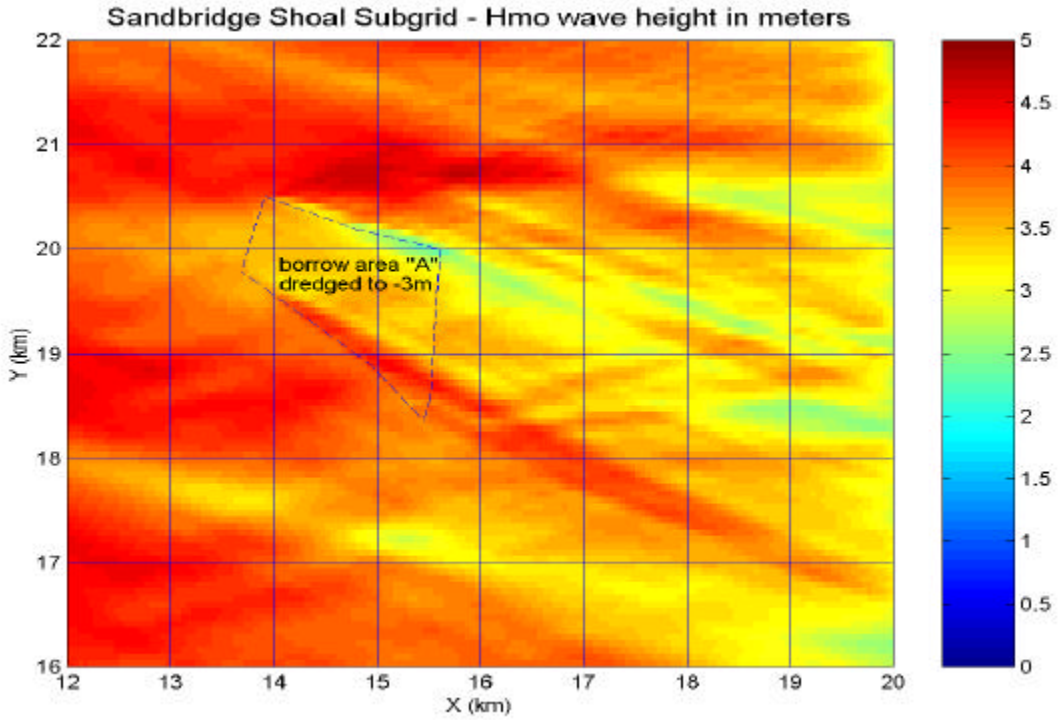

Plate 6B. Model run 21: Hmo=7m, Tp=15s, Smax=20, PWD= -15.
Condition: Area “A” (dashed line) dredged to –3m.

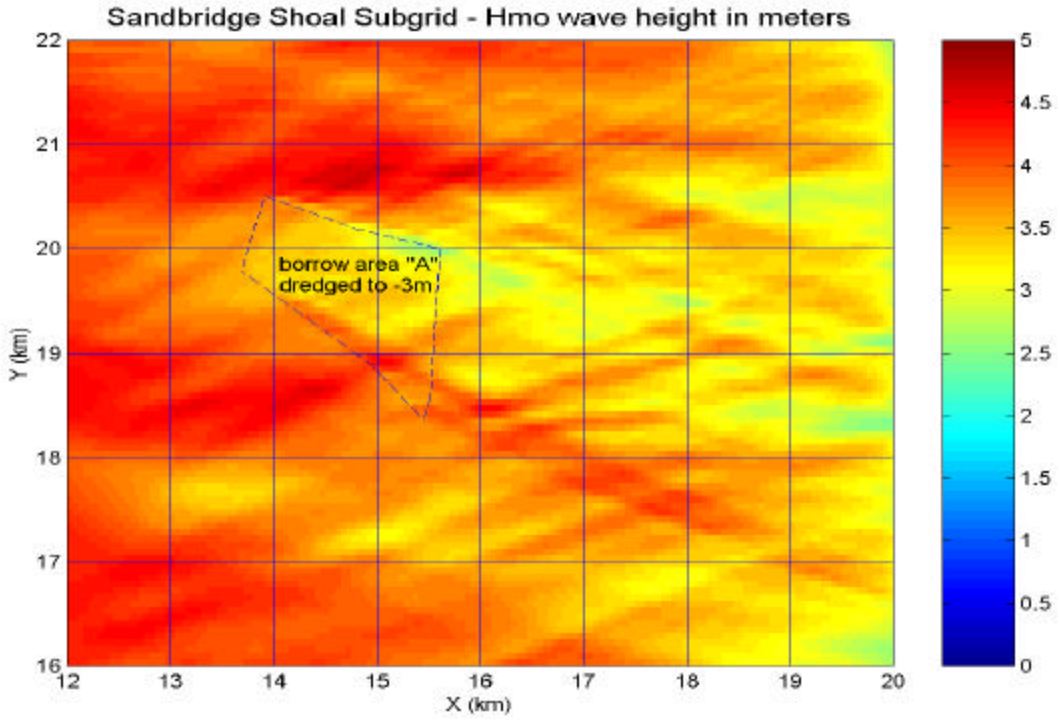

Plate 7A. Model run 22: Hmo=7m, Tp=15s, Smax=10, PWD=0.

Condition: Area “A” (dashed line) dredged to –3m.

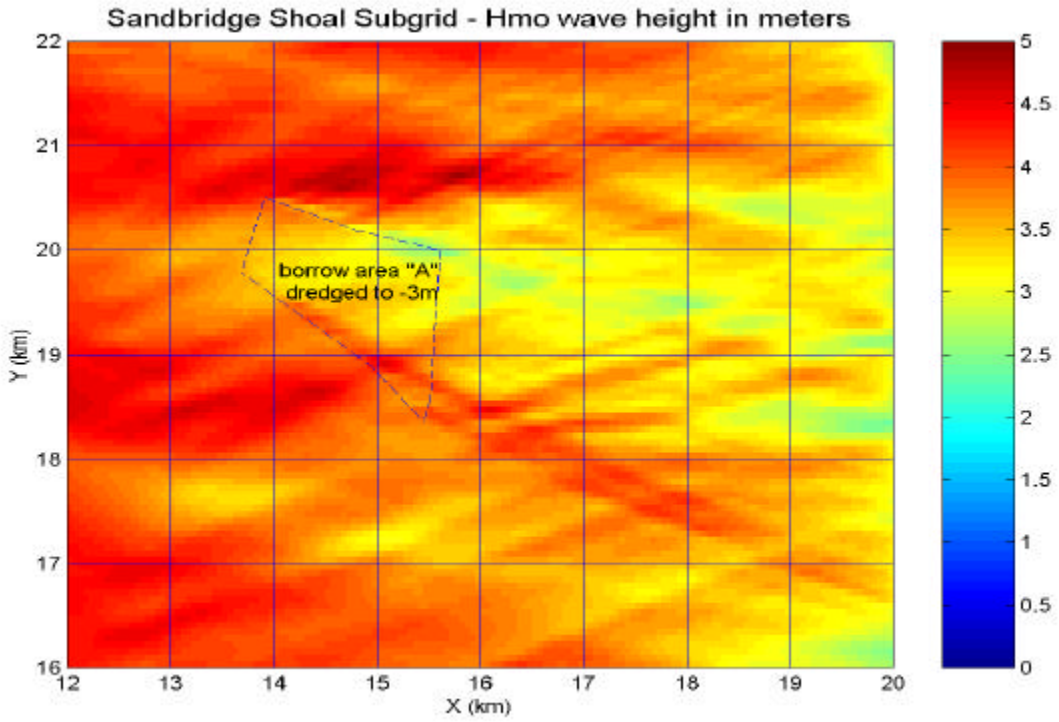

Plate 7B. Model run 23: Hmo=7m, Tp=15s, Smax=20, PWD=0.
Condition: Area “A” (dashed line) dredged to –3m.

Environmental Studies Relative to Potential Sand Mining in the Vicinity of the City of Virginia Beach, Virginia

Part 4: Coastal Currents

Final Report

January 1998

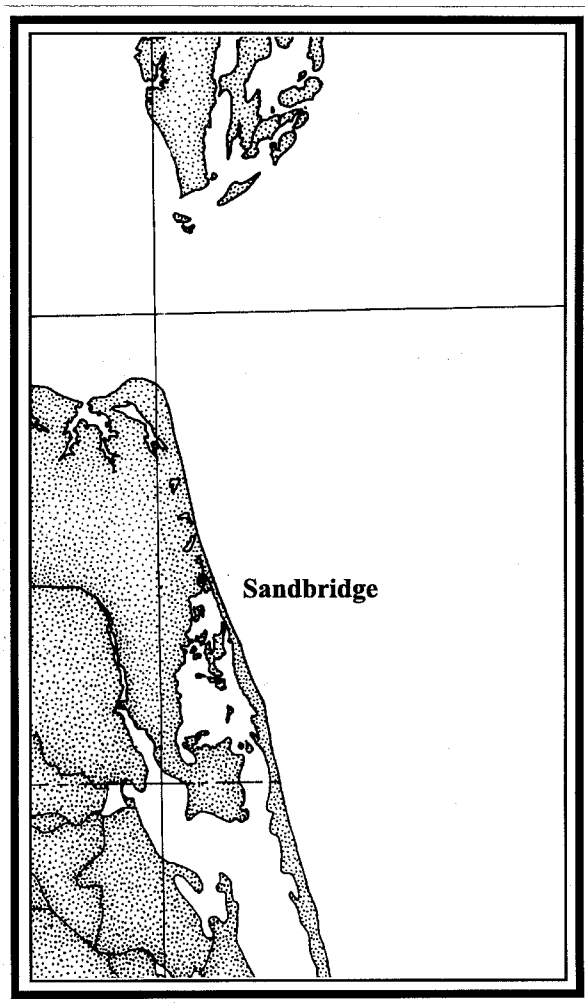

MMS U.S. Department of the Interior
Minerals Management Service

College of William and Mary
VIMS
Virginia Institute of Marine Science
School of Marine Science

Environmental Studies Relative to Potential Sand Mining in the Vicinity of the City of Virginia Beach, Virginia

Part 4: Coastal Currents

Final Report

January 1998

Author:

Arnoldo Valle-Levinson
Old Dominion University

Project Manager:

Carl H. Hobbs, III
Virginia Institute of Marine Science

Prepared under MMS Cooperative
Agreement 14-35-0001-3087 through
Virginia Institute of Marine Science of the
College of William & Mary

MMS U.S. Department of the Interior
Minerals Management Service

College of William and Mary
VIMS
Virginia Institute of Marine Science
School of Marine Science

DISCLAIMER

This report has been reviewed by the Minerals Management Service and approved for publication. Approval does not signify that the contents necessarily reflect the views and policies of the Service, nor does mention of trade names or commercial products constitute endorsement or recommendation for use.

The dynamics and structure of currents in the vicinity of Virginia Beach

This document reports on the activities performed by A. Valle-Levinson and L.P. Atkinson under the project funded by the U.S. Minerals Management Service under Cooperative Agreement No. 14-35-0001-30807 with the Virginia Institute of Marine Science. The activities consisted of a series of seven cruises at and off the Chesapeake Bay entrance. The cruises took place in September 1995, March 1996, June 1996, September 1996, November 1996, February 1997, and May 1997. The main objective of these cruises was to determine the influence of bathymetric variations on the flow field in the area of study. Water density and current velocity data were collected during each of those cruises. Most of the current velocity measurements were collected with an acoustic Doppler current profiler (ADCP), which gave high spatial resolution (approximately 75 m) of the water velocity field under different conditions of river discharge, tidal forcing, and wind forcing. This project has contributed to educational activities within the Oceanography Department, Old Dominion University, as it has supported two graduate students: K. Holderied and E. Haskell. The participation of more than twenty people on all the cruises has allowed them to become familiar with state-of-the-art technology in current velocity measuring techniques. The results of this effort have produced five manuscripts that have been submitted for publication in peer-reviewed literature. Two of these manuscripts have already been accepted for publication. These manuscripts are follow and constitute the bulk of the report for this segment of the MMS funded project.

The main finding of this work is that bathymetry plays a crucial role in influencing the shape and strength of the flows in the study area. The dynamics in the relatively deep channel appears to be fundamentally different from that of the adjacent shoals. The results suggest that the subtidal flows in the channel are mainly produced by density gradients that are modified by friction arising from bottom stresses, vertical mixing, and wind stresses. In contrast, the subtidal flows over the sallow regions may be produced by tidal forcing (tidal residual) modified by wind stresses. The tidal flows are in general stronger along the Chesapeake Channel (the channel entering Chesapeake Bay) and lag behind those over the shoals by up to three hours at the entrance to the bay. These large phase lags in the tidal flows allow the development of flow convergences (flow in opposite directions) that persist between 1 and 2 hours at the transition between channel and shoals. These convergences give rise to frontal features that accumulate material at the surface. The results from these studies suggest that changes in bathymetry of approximately 50% (or more) relative to the ambient depth (e.g. from 10 m to 15 m) produce significant alterations to the tidal and subtidal flows. If the sand borrow area off Sandbridge, Virginia, were to be flattened relative to its surrounding depths, the effects of this change on the flow field in the area would probably be less than the effects caused by a depression in the bathymetry relative to the surroundings.

(Project Manager's Note: The five manuscripts referred to above form the next portion of this report. Only their physical formats, *e.g.* margins, fonts, spacing, *etc*., have been altered.)

Environmental Studies Relative to Potential Sand Mining in the Vicinity of the City of Virginia Beach, Virginia

Part 4: Coastal Currents

Final Report

January 1998

On the Influence of Downwelling Winds on the Chesapeake Bay Outflow, by Arnoldo Valle-Levinson and Kamazima M. M. Lwiza.

Rapid Assessment of Current Velocities in the Coastal Ocean, by Arnoldo Valle-Levinson and Kamazima M. M. Lwiza.

On the Influence of Estuarine Outflow and Bathymetry on Semidiurnal Tidal Currents, by Andrew G. E. Haskell, Arnoldo Valle-Levinson and Kamazima M. M. Lwiza.

Hydrographic and Flow Structure in the Chesapeake Bay Mouth and Plume Region Under High Freshwater Discharge Conditions, by Kristine Holderied and Arnoldo Valle-Levinson.

Flow Patterns at the Chesapeake Bay Entrance, by Arnoldo Valle-Levinson, Chuyan Li, Thomas C. Royer and Larry P. Atkinson.

MMS U.S. Department of the Interior
Minerals Management Service

College of William and Mary
VIMS
Virginia Institute of Marine Science
School of Marine Science

On the influence of downwelling winds on the Chesapeake Bay outflow

Arnoldo Valle-Levinson
Center for Coastal Physical Oceanography, Old Dominion University, Norfolk, Virginia, USA

Kamazima M.M. Lwiza
Marine Sciences Research Center, The University at Stony Brook, NY, USA

ABSTRACT

With the purpose of studying the hydrography and flow structure off the mouth of the Chesapeake Bay, a series of transects were sampled continuously with a 600 kHz acoustic Doppler current profiler (ADCP) and a thermosalinograph during late September 1995. Hydrographic (CTD) stations were combined with underway measurements and occupied every 4 km along the transects to look at the vertical structure of the density field. This is the first time an ADCP has been towed in the waters off the Chesapeake Bay mouth. The study was carried out at the end of a two-day period of northeasterly winds. The surface salinity distribution showed that winds kept a well-defined Chesapeake Bay plume within a few kilometers from the coast. Near-bottom salinity fields displayed weaker horizontal gradients than the near-surface field. The ADCP observations yielded excellent resolution of the flow field from which a subtidal distribution was inferred. The subtidal near-surface flow showed a spatially coherent southward component in the area of observation in response to the downwelling winds. The southward coastal ambient flow advected the turning region of the plume to the south of the mouth of the estuary, which was consistent with numerical model results. The region of influence by the plume could be defined from the subtidal flows by an area where the difference between the near-surface and near-bottom flows was large. This area, off the Chesapeake Bay mouth, overlapped with that of subtidal flow divergence as calculated with the near-surface subtidal flow. Within the region of plume influence, the balance was probably semigeostrophic with modifications by friction in the along-flow direction. Outside that region, the momentum balance was apparently dominated by friction.

1 INTRODUCTION

The study of estuarine discharges onto the continental shelf has received widespread attention as these discharges transport land-derived and estuarine-derived materials to the coastal oceans. The Chesapeake Bay outflow is a typical example of a buoyant discharge from a wide estuary. This discharge is derived from an annual mean river input of 2400 m^3/s (Hargis, 1981). The hydrography of the Chesapeake Bay plume has been described in several studies by Boicourt (1973; 1981), and Boicourt *et al.* (1987). These studies have shown that under the influence of downwelling winds, or northeasterly winds blowing onshore, the buoyant discharge from the estuary is restricted to a narrow band to the south of the estuary's mouth. With upwelling winds, or southwesterly winds blowing offshore, the buoyant water extends off the mouth of the Chesapeake Bay, forming a wide turning region.

Despite of having a relatively good idea of the modifications to the plume's density field by wind forcing, knowledge on the response of the flow field is restricted to records of scattered moored instruments. Comprehensive descriptions of the flow field have only been described with numerical models (e.g. Chao and Boicourt, 1986; Chao, 1988; Zhang *et al.*, 1987; Weaver and Hsieh, 1987; Oey and Mellor, 1993). Prior to the present study, no measurements had been made of the spatial structure of the flow field in the Chesapeake Bay outflow region. The main objective of this study is to describe the flow structure associated with a weak plume under the influence of downwelling winds. This constitutes the first effort that studies the Chesapeake Bay plume using underway current measurements obtained with an acoustic Doppler current profiler (ADCP). These observations help validate models of plume dynamics under downwelling winds.

2 DATA COLLECTION

A series of transects (Fig. 1) was sampled with a 600 kHz broadband acoustic Doppler current profiler (ADCP) during 26 hours from September 25 to 26, 1995. Table 1 summarizes the details of the ADCP data collection. The ADCP was mounted on a catamaran and towed from the National Oceanic Atmospheric Administration (United States) ship R/V Ferrel. This was the first time an ADCP was towed in the waters off the Chesapeake Bay mouth. Simultaneously to the current velocity measurements, near-surface temperature and salinity were recorded every 10 seconds with a Sea Bird thermosalinograph (SBE-1621). Underway measurements were combined with Conductivity-Temperature-Depth (CTD - Sea Bird SBE-25) stations, occupied every 4 km along the transects, to elucidate the vertical structure of the density field. The sampling grid extended for approximately 60 km in the alongshelf direction from Cape Charles, Virginia, to False Cape, at the border between Virginia and North Carolina, and 20 km in the cross-shelf direction.

Acoustic Frequency	600 kHz
Beam Angle	30°
Ping Rate	0.95 Hz-PBT, 2 Hz-PDT & PET
Sampling Interval	30 s
Blanking Interval	1 m
Center of First Bin	2 m
Beam Length	0.5 m
Bottom Track	Yes, during the entire study
Data Acquisition	RDI Transect
Navigation	GPS

Table 1. ADCP Specifications

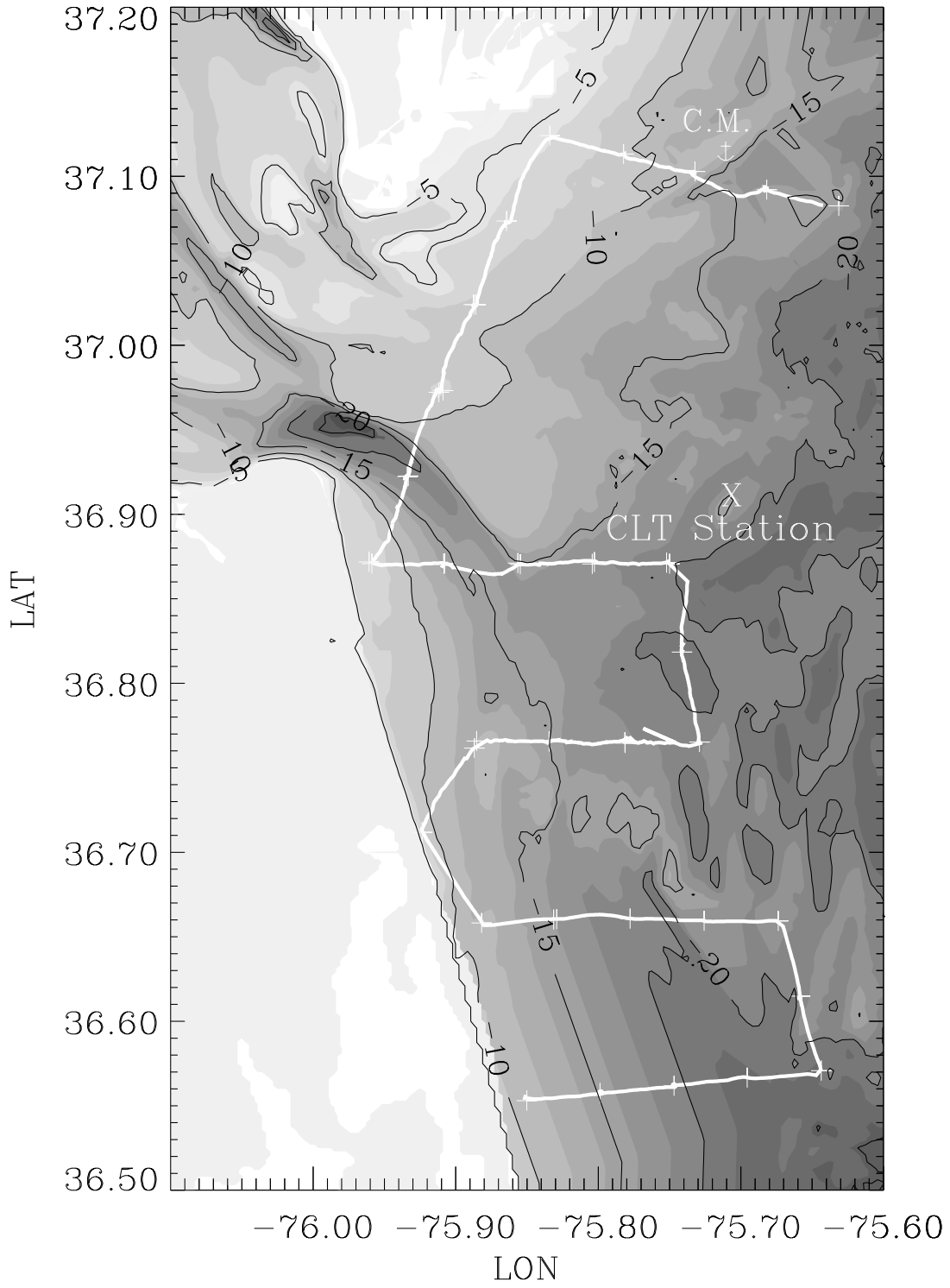

Figure 1. Study area with location of transects (thick white line), of current meter (C.M.) mooring, of wind data (station CLT), and of CTD stations ('+'). Bathymetry is contoured at 2 m intervals.

Prior to the beginning of the underway measurements, a mooring with near-surface and near-bottom current meters was also deployed. The instruments used were SensorData 6000 (see Valle-Levinson, 1995 for an explanation of the instruments). The records from these instruments were used to look at the tidal variations of the flow at one location, which provided a guide in the process of separating the tidal and non-tidal signals from the ADCP data. Wind data from the Chesapeake Light Tower (Fig. 1) were used to relate the observed velocity and density fields to wind forcing conditions.

3 DESCRIPTION OF OBSERVATIONS

The measurements of flow and density fields were carried out in early autumn, when river discharge to the Chesapeake Bay is at its minimum (Valle-Levinson and Lwiza, 1997a). It also coincided that the observations were obtained at the end of a two-day period of northeasterly, or downwelling, winds (Fig. 2a). These winds caused a predominant southward current during our survey (Figs. 2b and 2c). The tidal current barely reversed the wind-induced current during the first tidal cycle of ADCP observations. The current meter records were obtained under vertically homogeneous conditions and were used to validate the procedure of separating tidal and non-tidal contributions to the ADCP data in the vicinity of the mooring.

The low freshwater discharge and the wind forcing previous to and during the study reflected the low buoyancy-high mixing hydrographic regime in the lower Chesapeake Bay as proposed by Valle-Levinson and Lwiza (1997a). The surface salinity showed relatively high values (greater than 28) and a Chesapeake Bay plume confined to within a few kilometers (approximately 5-10 km) from the coast (Fig. 3a). Near-bottom salinity fields displayed weaker horizontal gradients than the near-surface field (Fig. 3b) and the difference between surface and bottom salinities was typically 2 in the region closest to the coast. This salinity field suggested the decoupling of near-surface fluid from near-bottom dynamics, at least near the mouth of the bay. The near-surface and near-bottom subtidal flows derived from the ADCP measurements provided further evidence of this decoupling as discussed later.

The current velocity profiles obtained with the ADCP yielded excellent resolution of the flow field along the sampling track. The raw near-surface flow (Fig. 3a) exhibited the characteristic pattern of the mean flow of a wide estuary plume: turning region of the outflow due to Coriolis acceleration, transition to a coastal current with noticeable flow convergence, and formation of a coastal current downstream of the region of convergence. The unprocessed measurements displayed large differences between the near-surface and near-bottom tidal flows at the southernmost transects. These current velocity profiles are, however, tidally aliased. Therefore, the signal related to the tidal currents had to be isolated from the observations in order to examine the ambient field. The technique of detiding is described next.

3.1 Detiding of ADCP and Surface Salinity Data

The ADCP data bins closest to the surface (at approximately 2 m depth) and bottom (at 85% of the total depth), along with the near-surface continuous salinity data from the thermosalinograph, were subjected to a least squares fit of a semidiurnal tidal wave with the help of predefined base functions. Near-bottom salinity was not detided because the CTD casts did

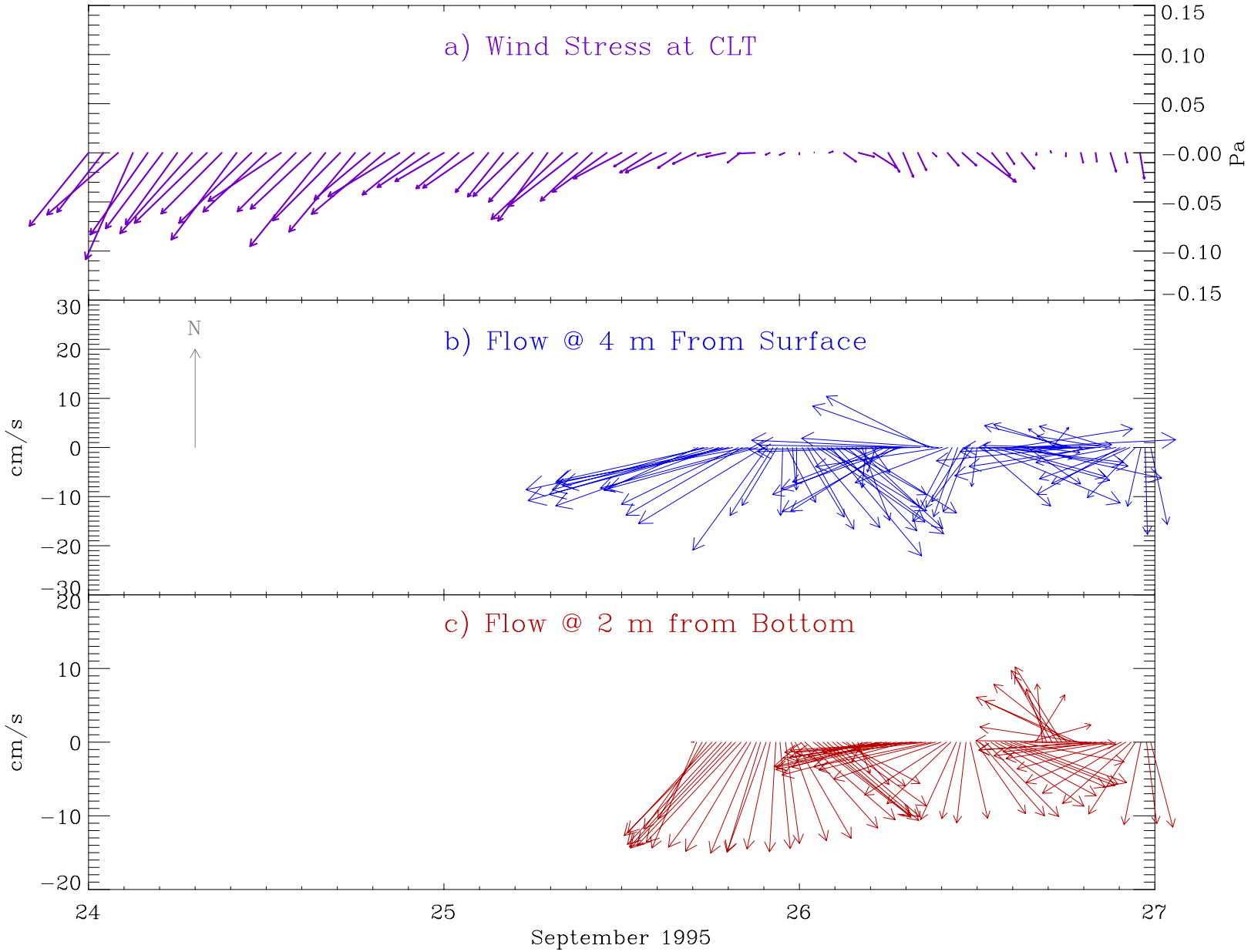

Figure 2. (a) Wind stresses (Pa) at CLT using the oceanographic convention (vectors point in the direction toward which the wind blows). (b) and (c) Current velocities during the period of ADCP measurements.

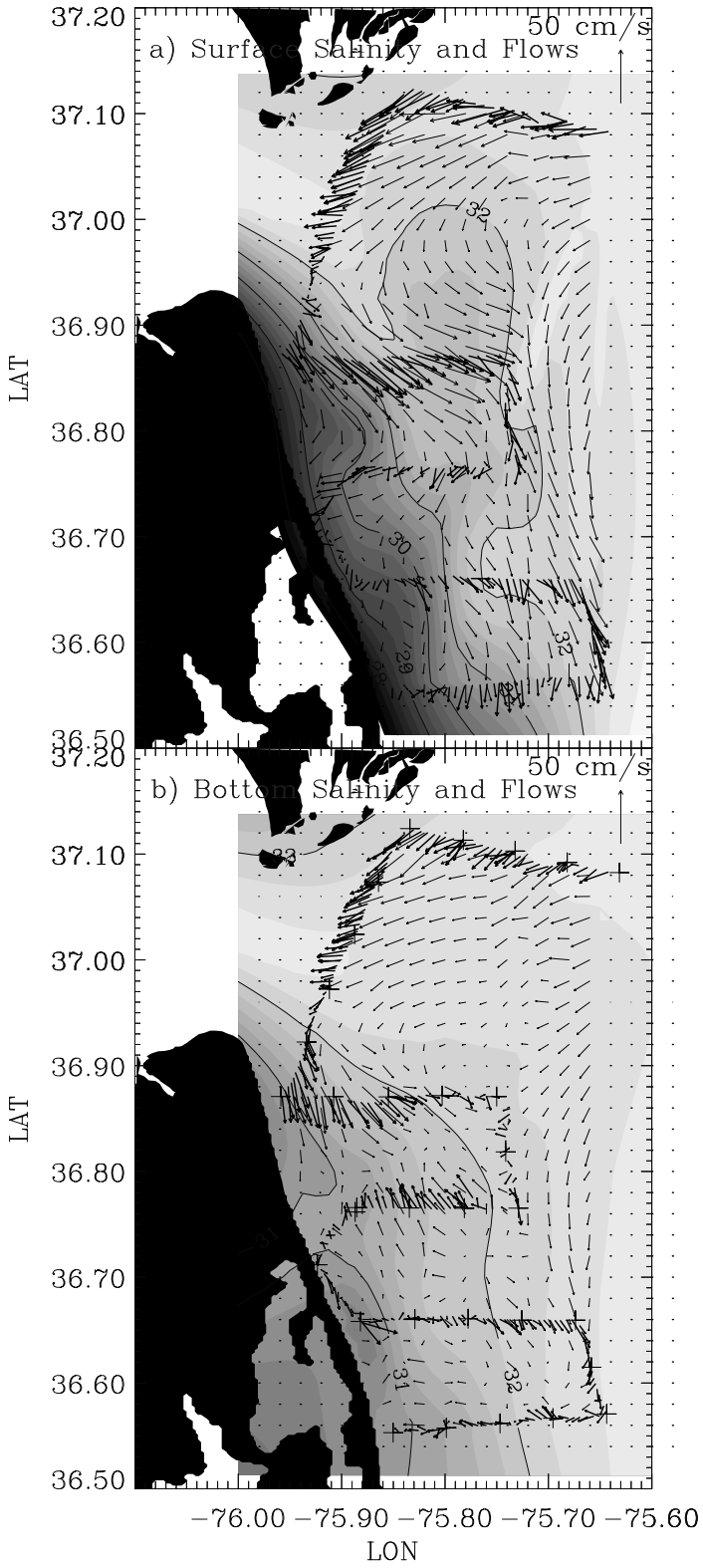

Figure 3. Instantaneous salinity (shaded contours) and flow (vectors) fields as measured with CTD and ADCP. The flow fields are plotted along the ship track and at regular grid points, where they were interpolated from the observations along the track. Salinity values are contoured at increments of 1. (a) Near-surface, and (b) near-bottom fields.

not yield enough spatial resolution to produce reliable results as the number of degrees of freedom is small. The detiding method and the errors associated with it have been outlined by Candela *et al.* (1992), and Wong and Münchow (1995). The method is presented more explicitly here. To obtain the fit, it was assumed that each observed velocity component, $u_{io}(x,y,t)$, and the near surface salinity signals varied in horizontal space (x,y) and were formed of a subtidal component u_{im} plus a semidiurnal (period = 12.42 hrs) tidal component plus noise, *i.e.*,

$$u_{io}(x,y,t) = u_{im}(x,y) + a_i(x,y)\cos(\omega_{M2}\, t) + b_i(x,y)\sin(\omega_{M2}\, t) + \text{noise}\,(x,y,t), \quad (1)$$

where ω_{M2} is the frequency of the lunar semidiurnal tidal component ($2\pi/12.42$ h). The subtidal flow component (or salinity), and the functions $a_i(x,y)$ and $b_i(x,y)$, are given by:

$$u_{im}(x,y) = \sum_l \alpha_l(x,y)\, \phi_l(x,y),$$
$$a_i(x,y) = \sum_l \beta_l(x,y)\, \phi_l(x,y),$$
$$b_i(x,y) = \sum_l \gamma_l(x,y)\, \phi_l(x,y).$$

The parameters α_l, β_l, γ_l, are to be found by minimizing the least square error between observations and fit at each of the "l" nodes located at (x_l, y_l). $\phi_l(x,y)$ are base functions that, for this application, have been chosen as biharmonic splines (Wong and Münchow, 1995), *i.e.*,

$$\phi_l(x,y) = \{(x - x_l)^2 + (y - y_l)^2\}\, \{\ln([(x - x_l)^2 + (y - y_l)^2]^{1/2}) - 1\}.$$

Differentiating the squared error $(u_{io} - u_{i\,fit})^2$ with respect to each unknown parameter α_l, β_l, γ_l, and equating to zero, yields a set of 3L equations, where L is the total number of nodes. The set of 3L equations can be arranged in the following matrix form to solve for α_l, β_l, γ_l (contained in X):

$$F\,X = O \quad (2).$$

Matrix F is symmetric and has the following general form:

$$\begin{bmatrix}
\sum_N \phi_1\phi_1 \ldots \sum_N \phi_L\phi_1 & \sum_N \phi_1\phi_1 \sin\omega t \ldots \sum_N \phi_L\phi_1 \sin\omega t & \sum_N \phi_1\phi_1 \cos\omega t \ldots \sum_N \phi_L\phi_1 \cos\omega t \\
\ddots & & \\
\sum_N \phi_L\phi_L & & \\
 & \sum_N \phi_1\phi_1 \sin^2\omega t & \sum_N \phi_1\phi_1 \cos\omega t \sin\omega t \quad \ldots \\
 & \ddots & \ddots \\
 & \sum_N \phi_L\phi_L \sin^2\omega t & \\
 & \sum_N \phi_1\phi_1 \sin\omega t \cos\omega t \quad \ldots & \sum_N \phi_1\phi_1 \cos^2\omega t \\
 & \ddots & \ddots \\
 & & \sum_N \phi_L\phi_L \cos^2\omega t
\end{bmatrix}.$$

The vector X is $[\alpha_1, \ldots, \alpha_L, \beta_1, \ldots, \beta_L, \gamma_1, \ldots, \gamma_L]$; and the vector O has the elements $[\sum_N u_{io}\phi_1, \ldots, \sum_N u_{io}\phi_L, \sum_N u_{io}\phi_1\sin\omega t, \ldots, \sum_N u_{io}\phi_L\sin\omega t, \sum_N u_{io}\phi_1\cos\omega t, \ldots, \sum_N u_{io}\phi_L\cos\omega t]$. The solution X is obtained by inverting the matrix F.

3.2 Fitted Data

The least squares fit obtained with equations 1-2 and 5 nodes, reproduced the most prominent variations of both components of the observed flow (Fig. 4a, b) and of the surface salinity. The fit depends on the position of the nodes, *i.e.*, variations to the node location yield different subtidal and tidal flow fields. The node locations chosen here were optimized in such a way that the noise had zero mean and variance that was a small fraction (less than 10%) of the variance of the observations (Wong and Münchow, 1995). In addition, the optimal node locations were chosen for those that reproduced the tidal currents from moored instruments.

The subtidal component u_{im} of the fit contains the currents produced by winds, density gradients, and oscillations longer than 12.42 hrs. Therefore, the subtidal flow field thus obtained, reflected the wind and buoyancy forcing during the period of study. The subtidal near-surface flow and salinity calculated along the ship track (Fig. 1), were interpolated to a grid with 1.77 km spacing in the east-west direction (0.02° lon), and 2.22 km in the north-south direction (0.02° lat). This grid spacing was chosen arbitrarily. The interpolation was carried out through the construction of a Delaunay triangulation that produces interpolated values computed from nearby points only. This is an intrinsic function in the data processing package Interactive Data Language (IDL).

The gridded subtidal salinity field at the surface (Fig. 5) showed a relatively thin (< 10 km from the coast) band of buoyant water along the coast to the south of the Chesapeake Bay mouth. This band is constrained by the internal radius of deformation (-6 km) and by the downwelling winds. Comparing the mouth of the bay (width of outflow) to the radius of deformation yields a Kelvin number greater than 1, which indicates that rotation effects play a major role in the dynamics of the plume (Wiseman and Garvine, 1995; Garvine, 1995). On the same figure 5, the smooth character of the subtidal flow is due to the biharmonic splines and does not necessarily reflect actual conditions. This near-surface subtidal flow showed a southward component (V) that was coherent throughout the region of study. This was consistent with the moored velocity observations and was most probably related to the downwelling wind forcing. In fact, a complex regression between the wind velocity (W_x, W_y in m/s) and the near-surface subtidal flow (U, V in m/s) during the study period yielded the following fit

$$U = 0.04\, W_x$$
$$V = -0.04 + 0.04 W_y,$$

where the x and y subscripts denote east-west and north-south components, respectively. The flow pattern produced by this fit was very similar to that shown in Figure 5 and explained 90% of the spatial variability of the subtidal flow (Valle-Levinson and Lwiza, 1997b). The large

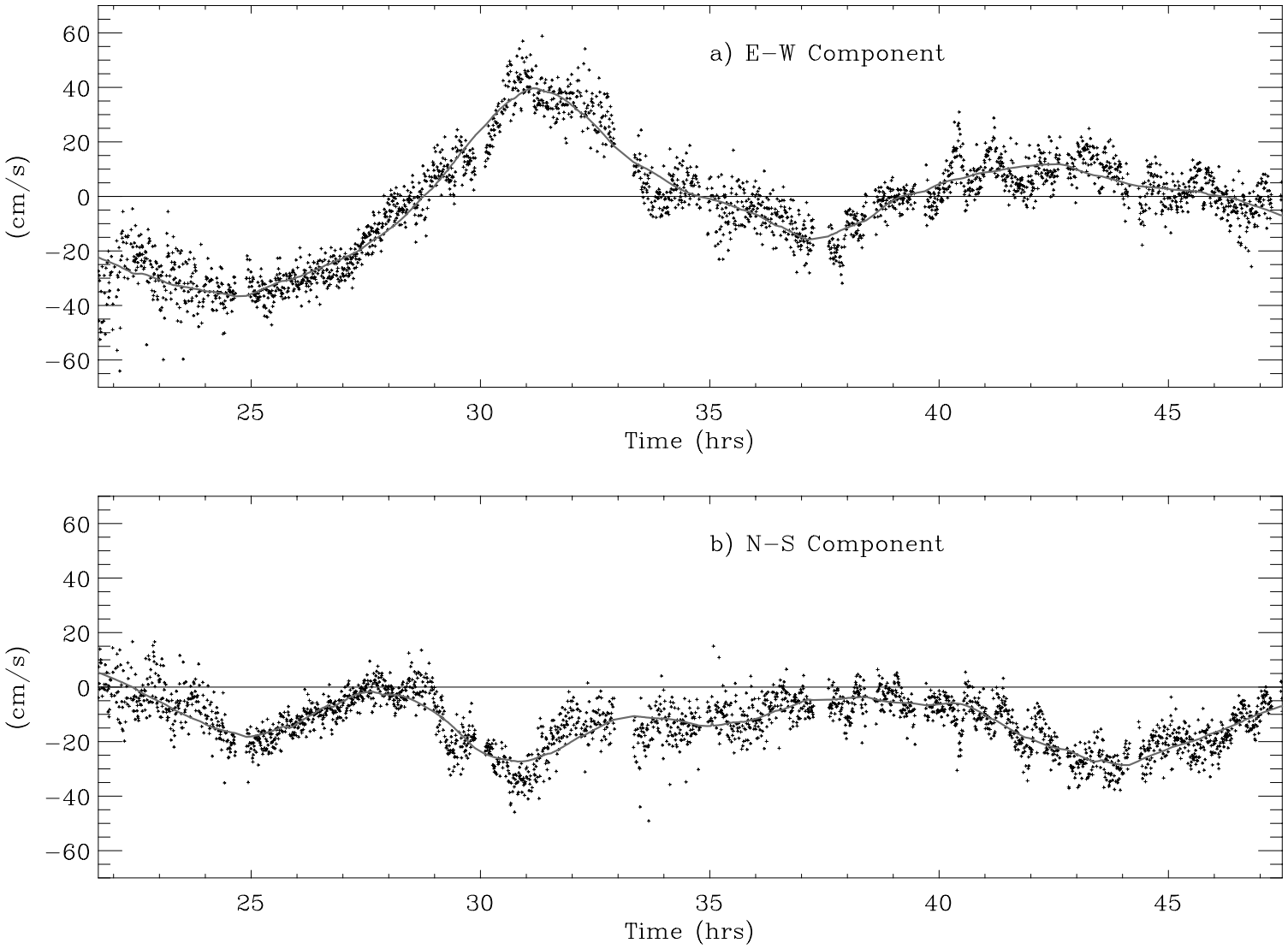

Figure 4. Comparison between observed components of the flow (dots) and fitted values (smooth, continuous line). (a) East-west component, and (b) north-south component.

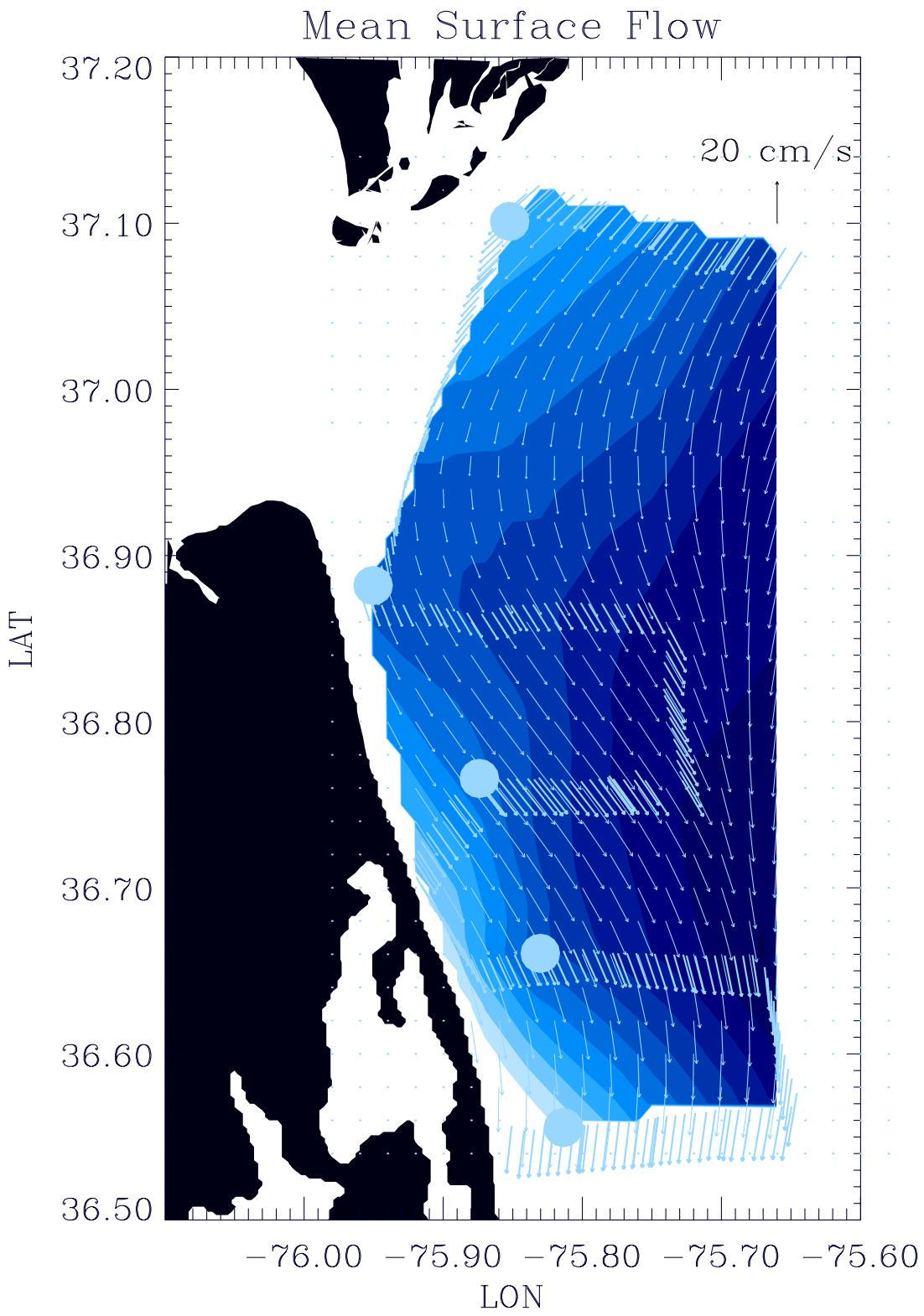

Figure 5. Subtidal near-surface (2 m deep) salinity (shaded contours) and flow (vectors). The nodes that anchored the fit are shown as filled circles.

variability explained by the fit indicates that wind forcing was mostly responsible for the subtidal flow observed under these weak plume conditions. The –0.04 offset of the fit to the *V* component is related to the southward ambient flow.

Another important and innovative result of this study is that the turning region of the outflow plume is advected southward of the mouth by the along-shelf southward flow. This behavior is consistent with numerical results (Valle-Levinson *et al.*, 1996) of a plume discharging to a shelf where a coastal flow is active (Fig. 6a). The ambient flow plunges underneath the plume at the zone where they encounter and the plume thickness increases as a consequence of mixing (O'Donnell, 1990). The ambient flow is quite influential to the dynamics of the plume because the suppression of the coastal flow allows the offshore spreading of the plume (Fig. 6b).

The subtidal near-bottom flow showed regions where it opposed the near-surface flow and regions where it flowed in approximately the same direction (Fig. 7a). Near the mouth of the Chesapeake Bay the subtidal near-bottom flow was directed into the estuary suggesting decoupled dynamics from the near-surface fields. This is the area of possible influence of the density pressure gradients on the subtidal flow thus generating estuarine-like circulation. Southward of this zone apparently dominated by baroclinic forcing, the near bottom flow diverged and became aligned to the direction of the wind forcing, which suggested barotropic flow. The subtidal near-bottom flow also showed the formation of anticyclonic circulation associated with a bathymetric shoaling of 2 m with respect to the surrounding depth. The region of inflow near the mouth, the divergence south of this region, and the anticyclonic circulation are features that are consistent with the results obtained by Norcross and Stanley (1967) with bottom drifters (Fig. 7b). This adds validity to the detided results, in addition to the fact that the noise had an average of almost zero and a small variance relative to the variance of the observed near-bottom flow.

The baroclinic character of the subtidal flows was determined by subtracting the near-bottom from the near-surface N-S component of the subtidal flows. This estimate gave an idea of the possible regions of decoupled dynamics from surface to bottom. The areas of greatest vertical difference in the subtidal flows (Fig. 8a) appeared right off the mouth of the Chesapeake Bay, within what should be the plume region, *i.e.*, the zone of strongest baroclinicity. This region was probably where the plume was detached from the bottom. The detachment was confirmed by the salinity measurements obtained off the mouth of the bay (not shown). Another region with large vertical differences in subtidal flow developed above the shoaling that generated the near-bottom anticyclonic circulation. The former zone must have been a result of the density field, and the latter reflected bathymetric effects. These zones of greatest shear coincided with the regions where the N-S subtidal component pointed in opposite directions, as shown on Figure 8a. The regions of large vertical differences in subtidal flow could have produced instabilities in the density field (Wiseman and Garvine, 1995). The hydrographic observations did not have the sufficient spatial resolution to verify this.

The separation in distinct regions by the subtidal shears suggests different dynamical implications for each. Within the plume region, near the mouth of the estuary, the circulation must be estuarine-like, *i.e.*, the momentum balance must be semigeostrophic with modifications

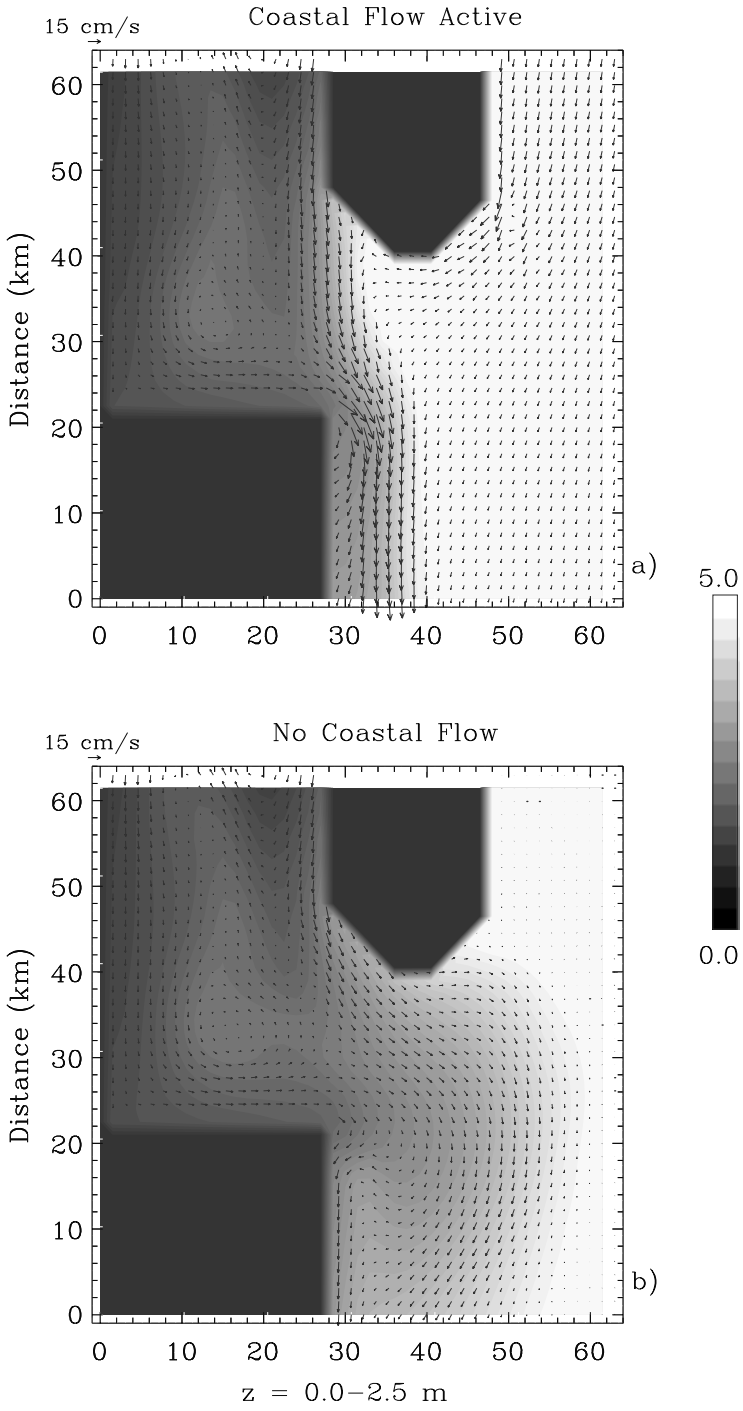

Figure 6. Surface fields of salinity (shaded) and flows (vectors) obtained numerically by Valle-Levinson *et al.* (1996) for (a) southward coastal flow active, and (b) no coastal flow. The color bar indicates the salinity contrast.

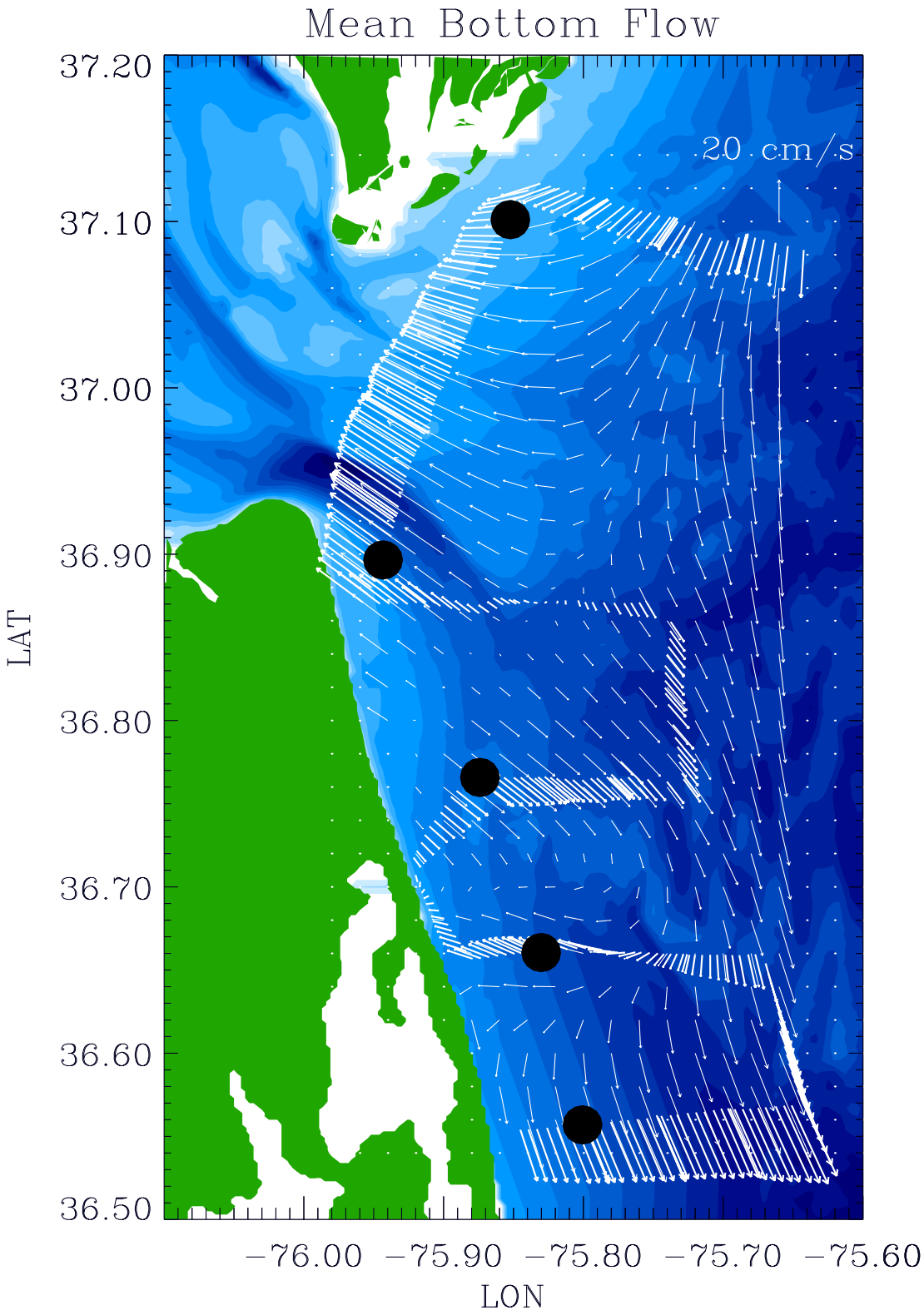

Figure 7(a) Subtidal near-bottom (last usable ADCP bin) flow (vectors) plotted over the bathy metry of the study region. The nodes that an cho red the fit are shown as filled circles.

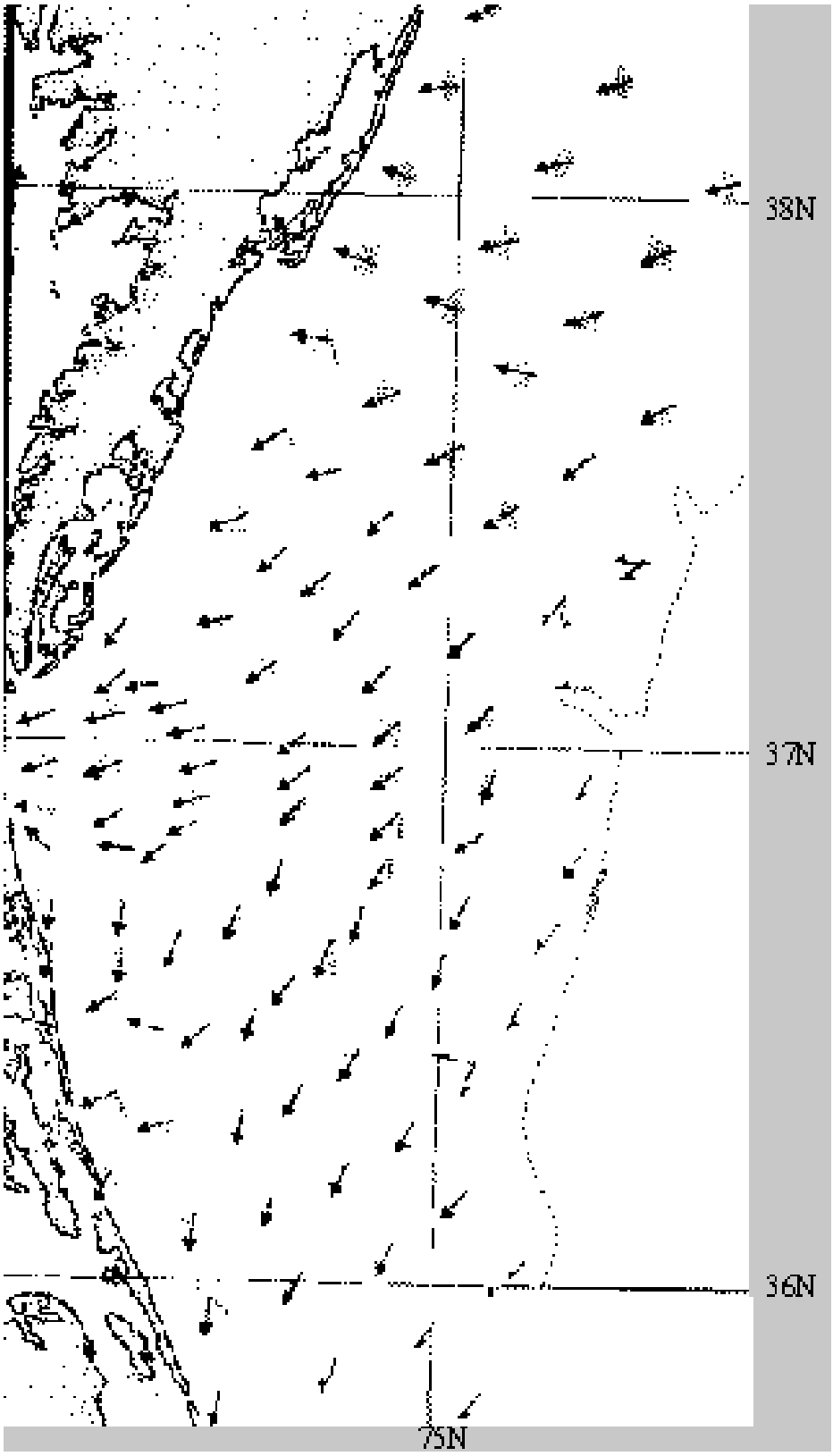

Figure 7(b) Bottom drift derived from seabed drifter recoveries (from Norcross and Stanley, 1969).

from frictional influences (wind stress, vertical mixing, and bottom stress) in the alongflow direction. This is in agreement with the 'slender' plume discussed by Garvine (1995). Outside of the region where subtidal surface flow opposes bottom flow, the momentum balance is probably frictional with the wind stress being balanced by the bottom stress. The suggested dynamics within the distinct regions is consistent with the numerical experiments of Valle-Levinson *et al.* (1996).

In addition to the estimate of vertical difference in the subtidal flows, the horizontal divergence of the near-surface flow was calculated to characterize the regions of plume influence. The divergence field (Fig. 8b) showed a zone of positive values (divergent flow) off the mouth of the Chesapeake Bay. Most of this region overlaps with that of large vertical difference in the subtidal flows. Also, the transition from convergence to divergence to the north of the bay mouth is suggestive of the plunging of the ambient flow underneath the plume as proposed above.

4 SUMMARY

This was the first study that involved underway ADCP measurements of the Chesapeake Bay plume. The ADCP data was separated into subtidal and semidiurnal components with the statistical method previously used by Wong and Münchow (1995) for the Delaware coastal current. Further efforts on separating tidal from subtidal flows should involve dynamically consistent methods such as that outlined by Dowd and Thompson (1996) and compare the results to the statistical method. The present study was carried out under downwelling winds that produced the response diagnosed by modeling results, *i.e.*, buoyant fluid constrained to a narrow band and subtidal flow in the direction of the wind. A main finding of this study is the advection of the turning region of the plume downwind of the estuary mouth by the downwind ambient flow. Also, the observations of this study support the idea of separation of regions with different dynamics based on the surface to bottom difference in subtidal currents. This idea is summarized in Figure 9.

Acknowledgments

This work was supported by the U.S. Minerals Management Service under Cooperative Agreement No. 14-35-0001-30807. Thanks to the personnel onboard NOAA's ship Ferrel under the able command of LCDR Susan McKay for their help during the cruise. Tom Wilson and R.C. Kidd were responsible for the technical aspects of the data collection. Andreas Münchow helped us understand the detiding technique. Animations of the near-surface and near-bottom flow, as well as color versions of some of the figures shown here, can be seen at the URL http://www.ccpo.odu.edu/~arnoldo/tfocbm/tfocbm.html

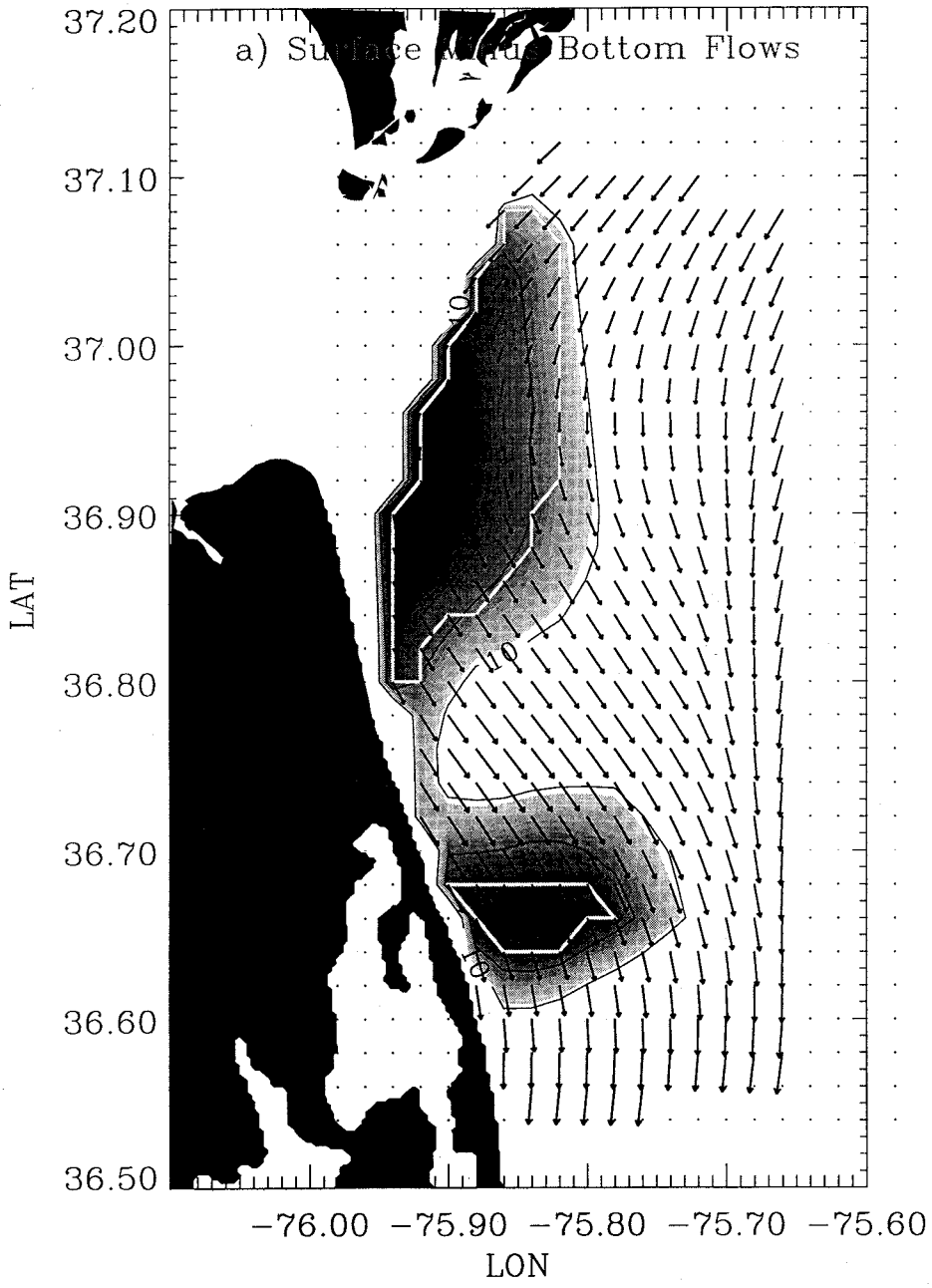

Figure 8(a). Difference between near-surface and near-bottom subtidal flows (dark shades), compared to the near-surface subtidal flow (vectors). The regions with opposing N-S flows at the surface and bottom are within the white-contoured area.

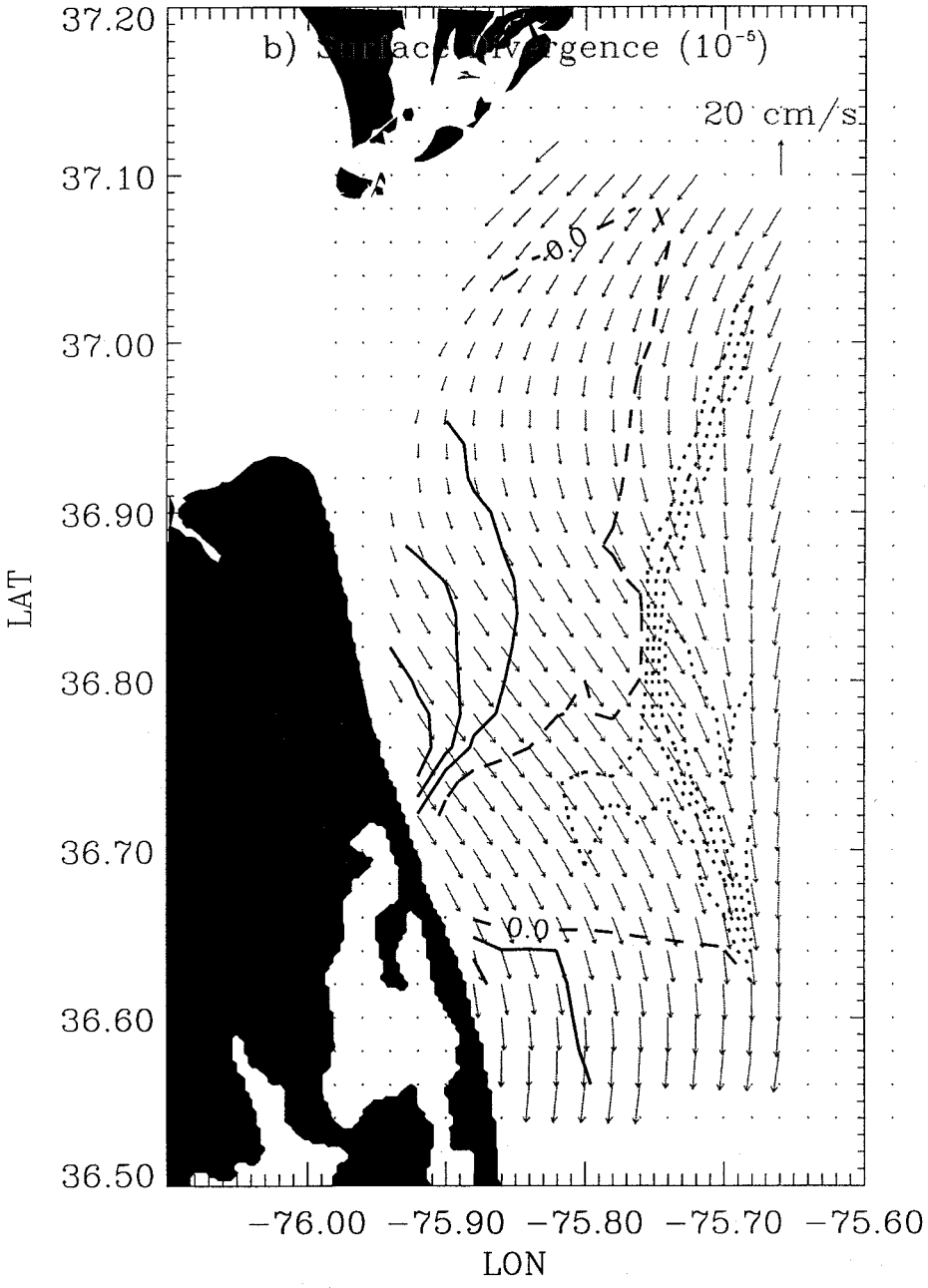

Figure 8 (b). Contours of surface divergence at intervals of 0 .5**H**10^{-5} s^{-1}, compared to the near-surface subtidal flow (vectors).

SUMMARY

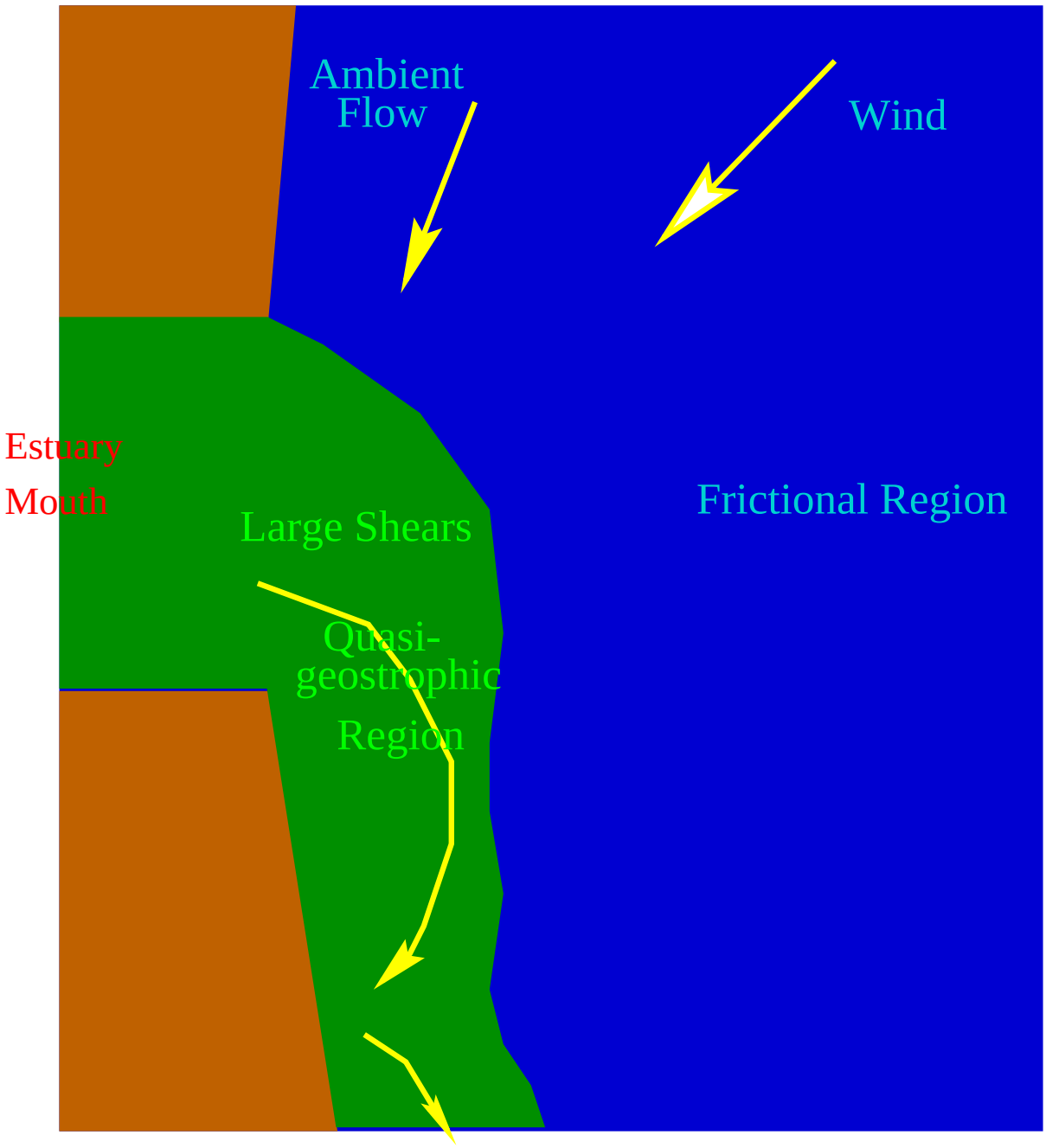

Figure 9. Schematics of the influence on down welling winds on the dynamics of a plume dis charging onto the coastal ocean based on the observations.

REFERENCES

Boicourt, W.C. 1973. The circulation of water on the continental shelf from Chesapeake Bay to Cape Hatteras. Johns Hopkins Univ. Ph.D. Dissertation. 183 pp.

Boicourt, W.C. 1981. Circulation in the Chesapeake Bay entrance region: estuary-shelf interaction. In J. Campbell and J. Thomas (eds), Chesapeake Bay Plume Study: Superflux 1980. NASA Conference Publication 2188: 61-78.

Boicourt, W.C., S.Y. Chao, H.W. Ducklow, P.M. Gilbert, T.C. Malone, M.R. Roman, L.P. Sanford, J.A. Fuhrman, C. Garside, and R.W. Garvine 1987. Physics and microbial ecology of a buoyant estuarine plume on the continental shelf. *Trans. Amer. Geophys. Union.* 68(31): 666-668.

Candela, J. M., R.C. Beardsley, and R. Limeburner 1992. Separation of tidal and subtidal currents in ship-mounted acoustic Doppler current profiler (ADCP) observations. *J. Geophys. Res.* 97: 769-788.

Chao, S.-Y. 1988. River-forced estuarine plumes. *J. Phys. Oceanogr.* 18: 72-88.

Chao, S.-Y. and W.C. Boicourt 1986. Onset of estuarine plumes. *J. Phys. Oceanogr.* 16: 2137-2149.

Dowd, M. and K.R. Thompson 1996. Extraction of tidal streams from a ship-borne acoustic Doppler current profiler using a statistical-dynamical model. *J. Geophys. Res.* 101(C4): 8943-8956.

Garvine, R.W. 1995. A dynamical system for classifying buoyant coastal discharges. *Cont. Shelf Res.* 15(13):1585-1596.

Hargis, W.J. 1981. A benchmark multi-disciplinary study of the interaction between the Chesapeake Bay and adjacent waters of the Virginian sea. In J. Campbell and J. Thomas (eds). Chesapeake Bay Plume Study: Superflux 1980. NASA Conference Publication 2188: 1-14.

Norcross, J.J. and E.M. Stanley 1969. Inferred surface and bottom drift. In: Circulation of shelf waters off the Chesapeake Bight, W. Harrison, J.J. Norcross, N.A. Pore, and E.M. Stanley (eds). U.S. Dept. of Comm., Environ. Sci. Serv. Admin. Prof. Paper 3: 11-42.

O'Donnell, J. 1990. The formation and fate of a river plume: A numerical model. *J. Phys. Oceanogr.* 20: 551-569.

Oey, L.Y., and G.L. Mellor 1993. Subtidal variability of estuarine outflow plume, and coastal current: a model study. *J. Phys. Oceanogr.* 23: 164-171.

Valle -Levinson, A., 1995 Barotropic and baroclinic exchanges in the lower Chesapeake Bay. *Cont. Shelf Res.* 15: 1631-1647.

Valle -Levinson, A., J.M. Klinck, and G.H. Wheless 1996. Inflows/outflows at the transition between a coastal plain estuary and the coastal ocean. *Cont. Shelf Res.* 16: 1819-1847.

Valle-Levinson, A. and K.M.M. Lwiza 1997a. Bathymetric influences on the lower Chesapeake Bay hydrography. *J. Mar. Syst.* 12: 221-236.

Valle-Levinson, A. and K.M.M. Lwiza 1997b. Rapid assessment of current velocities in the coastal ocean. *Proc. SACLANT Rapid Env. Asst. Conf.* Lerici, Italy.

Weaver, A.T. and W.W. Hsieh 1987. The influence of buoyancy flux from estuaries on continental shelf circulation. *J. Phys. Oceanogr.* 17: 2127-2140.

Wiseman, W.J. Jr. and R. W. Garvine 1995. Plumes and coastal currents near large river mouths. *Estuaries.* 18(3): 509-517.

Wong, K.-C. and A. Mhnchow 1995. Buoyancy forced interaction between estuary and inner shelf: observation. *Cont. Shelf Res.* 15(1): 59-88.

Zhang, Q.H., G.S. Janowitz, and L.J. Pietrafesa 1987. The interaction of estuarine and shelf waters: A model and applications. *J. Phys. Oceanogr.* 17: 455-469.

Rapid Assessment of Current Velocities in the Coastal Ocean

Arnoldo Valle-Levinson
Center for Coastal Physical Oceanography
Old Dominion University
Norfolk, Virginia, USA 23529
Email: arnoldo@ccpo.odu.edu

Kamazima M.M. Lwiza
Marine Sciences Research Center
State University of New York
Stony Brook, New York, USA, 11794-5000
E-mail: kamazima@kafula.msrc.sunysb.edu

Abstract

The circulation off the mouth of a coastal plain estuary, the Chesapeake Bay, was assessed under conditions of weak freshwater discharge. Current velocity observations obtained with an acoustic Doppler current profiler during 25 hours in September 1995 were separated into tidal and subtidal contributions. The subtidal flow was dominated by wind forcing. The tidal flow was presented as ellipses that illustrated the preferred orientation of this flow, which was influenced by the coastal morphology.

1. Introduction

The rapid assessment of coastal current velocities in a given area has important implications for environmental and military applications. The present study illustrates one example of describing the coastal circulation in a region influenced by buoyant discharges. The region of the Chesapeake Bay outflow is used as a test case. The Chesapeake Bay is located on the eastern coast of the United States and is the largest estuary of the country. Its plume is derived from a mean annual discharge of approximately 2000 m^3/s. The hydrography of the plume has been described in several studies [1], [2], [3] that show the importance of wind forcing on the fate of the buoyant discharges. The plume spreads offshore with southwesterly winds and remains close to the mouth of the estuary and to the coastline with northeasterly winds. The circulation associated with this plume, however, has not yet been described in detail. This paper begins to address this issue.

The overall objective of this study is to rapidly assess the coastal circulation off the mouth of an estuary under weak river discharge conditions, and in particular, to determine the influence of wind forcing on that coastal circulation. In order to accomplish this objective, an acoustic Doppler current profiler (ADCP) was towed for 25 hours between September 25 and 26, 1995 off the mouth of the Chesapeake Bay along the track shown in Figure 1. This rapid sampling of the area allowed the assessment of the coastal circulation within a period of 30 hours after the experiment started.

2. Data Collection

The survey was carried out during the time of the year of weakest discharge and in the driest year of the decade. The mean river discharge into Chesapeake Bay in September 1995 was less than 500 m^3/s, considerably less than the climatological mean of 1000 m^3/s for that month. The survey also took place under the influence of northerly winds, and after a period of relatively strong (~0.1 Pa) northeasterly winds as recorded at the Chesapeake Light Tower and at the Chesapeake Bay Bridge Tunnel by the U.S. National Oceanic and Atmospheric Administration (NOAA).

The current velocity data were obtained with a 600 kHz broadband ADCP manufactured by RD Instruments. The instrument was mounted on a catamaran and towed from the NOAA *R/V Ferrel*. The vertical resolution (or bin size) of the velocity measurements was 0.5 m so that the first usable bin was centered at approximately 2.25 m. The velocity data were collected in ensembles of 30 s, which gave a horizontal resolution of 75 m towing at a speed of ~2.5 m/s . The collection of ADCP data was combined with conductivity-temperature-depth (CTD) profiles obtained every 2 nautical miles along the ship track to characterize the potential influence of freshwater in the area. Navigation was performed with the aid of differential Global positioning system (DGPS). The grid over which the survey took place was approximately 60 km in the along-shelf direction from Cape Charles, Virginia, to False Cape, at the border between Virginia and North Carolina, and 20 km in the cross-shelf direction.

3. Data Description

3.1. Instantaneous Data

Given the river discharge and wind forcing conditions prevailing at the time of this survey, a very weak plume was observed off the mouth of the Chesapeake Bay. The salinity difference between plume and ambient waters was around 2 as indicated by instantaneous measurements (Fig. 1a). This weak salinity difference is quite contrasting to the salinity difference of September of 1996 when it was more than 10. Therefore, the buoyancy forcing was very weak and probably had a minor influence on the coastal circulation in the area at the time of the study. This idea is explored later by assessing the importance of wind forcing on the coastal circulation.

The instantaneous measurements of near-surface flow and salinity (Fig. 1a) showed spatial distributions that are typical of a plume influenced by downwelling winds as characterized in the modeling studies of [4] and [5]. These typical characteristics are: a region where the plume turns anticyclonically, the turning region; a transition region where the flow converges between the turning region and the coastal current as seen by the speed decrease in the alongshore flow south of the mouth of the bay; and the formation of a coastal current. Also, the freshest water remains constrained to a very narrow band, narrower than the internal radius of deformation of around 7 km, along the coast. These instantaneous measurements are, however, tidally aliased, *i.e.*, they are biased by the different stages of the tidal cycle over which the observations were made. Then, in order to obtain a synoptic picture of the flow field, the influence of the tides on the instantaneous flow must be distinguished from the subtidal (or mean) current.

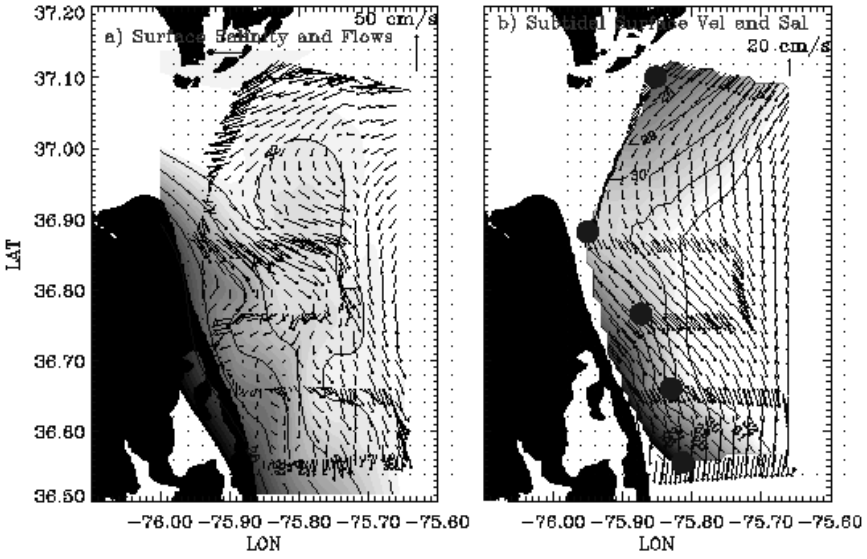

Figure 1. Study area off the mouth of the Chesapeake Bay. (a) Instantaneous observations of near-surface flow (vectors) and salinity (shaded contours). (b) Subtidal near-surface flow and salinity. The ship track is denoted by the closely spaced vectors. The gridded vectors are generated from interpolation. The location of the l nodes at which the least squares fit is performed is denoted by the filled circles in (b).

3.2. Fitting Technique

In order to separate the tidal signal from the instantaneous measurements, a least-squares technique was used. This technique has been used by [6] and assumes that each component of the current velocity observed $u_{io}(x,y,t)$, where the subscript i denotes one component, has a contribution from a subtidal current u_{im} plus one from a lunar semidiurnal (period of 12.42 h) tidal current, *i.e.*,

$$u_{io}(x,y,t) = u_{im}(x,y) + a_i(x,y)\cos(\omega_{M2}\,t) + b_i(x,y)\sin(\omega_{M2}\,t), \qquad (1)$$

where ω_{M2} is the frequency of the lunar semidiurnal tidal component ($2\pi/12.42$ h). The subtidal flow component (or could also salinity), and the functions $a_i(x,y)$ and $b_i(x,y)$, are given by:

$$u_{im}(x,y) = \sum_l \alpha_l(x,y)\,\phi_l(x,y),$$
$$a_i(x,y) = \sum_l \beta_l(x,y)\,\phi_l(x,y),$$
$$b_i(x,y) = \sum_l \gamma_l(x,y)\,\phi_l(x,y).$$

The parameters α_l, β_l, γ_l, are to be found by minimizing the least square error between observations and fit at each of the "l" nodes located at (x_l, y_l). The functions $\phi_l(x,y)$ are base

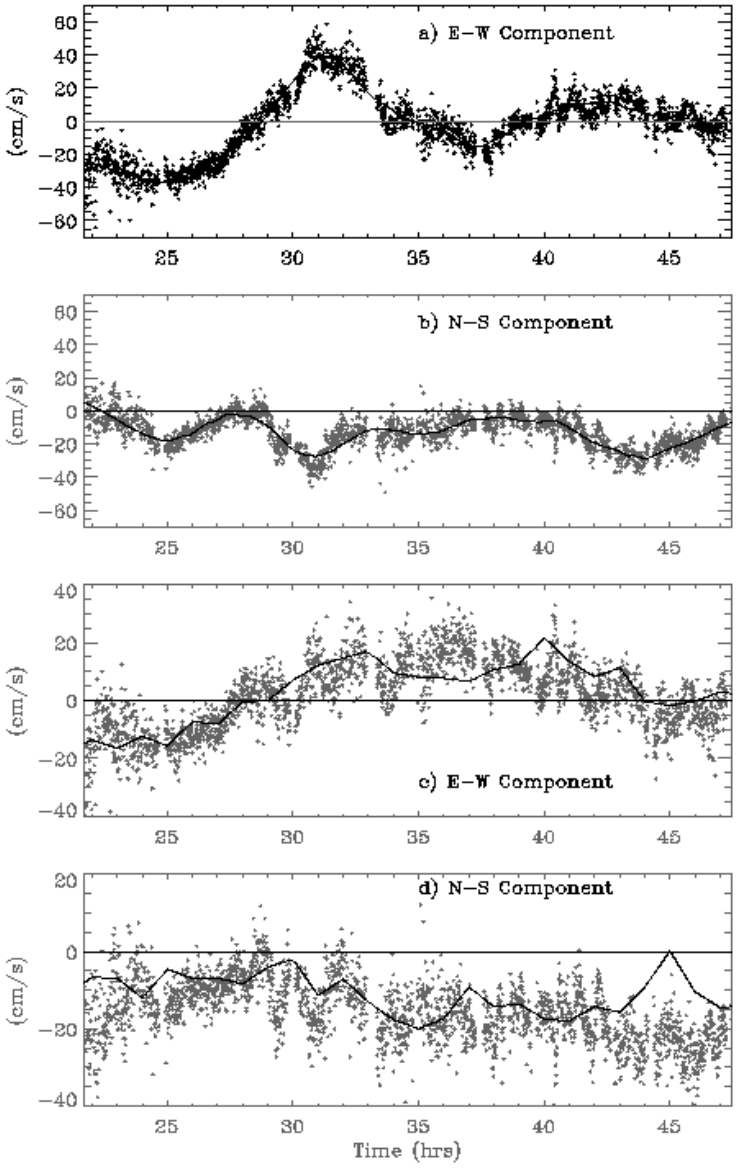

Figure 2. Instantaneous observations, represented by dots, compared to the least squares fit, denoted by continuous lines in (a) and (b). (c) and (d) present the subtidal flow components, as dots, compared to the wind-induced flow (continuous lines) as explained by (3).

functions that have been chosen as biharmonic splines [6], *i.e.*

$$\phi_l(x,y) = \{(x - x_l)^2 + (y - y_l)^2\} \{\ln([(x - x_l)^2 + (y - y_l)^2]^{1/2}) - 1\}. \quad (2)$$

The least squares fit obtained with equations 1-2 and 5 nodes (Fig. 1b), reproduced the most prominent variations of both components of the observed flow (Fig. 2a, b). The goodness of fitdepends on the position of the nodes, *i.e.*, variations to the node location yield different subtidal

and tidal flow fields. The node locations chosen here were optimized in such a way that the noise (difference between observations and fitted values) had zero mean and variance that was a small fraction (less than 10%) of the variance of the observations. In addition, the optimal node locations were chosen for those that reproduced the tidal currents from moored current meters (data not presented here).

3.3. Subtidal Data

The subtidal flow obtained with the technique mentioned above reflects the contribution from wind forcing, from density gradients, and from forcing with periods greater than one tidal cycle (*e.g.* coastal waves). The resulting subtidal flow (Fig. 1b) showed a general tendency for southward flow throughout the domain. As seen later, this was due mostly to the forcing from the predominantly northerly winds. Another feature of the subtidal flow was the southward translation of the turning region of the Chesapeake Bay outflow. This turning region appeared to the south of the Chesapeake Bay mouth due to the interaction between the southward ambient flow and the estuarine outflow as suggested by the numerical results of [7]. The band of low salinity (Fig. 1b) remains very thin and close to the coast as a consequence of the weak buoyancy forcing from the estuary. An interesting question to answer is how much of the subtidal flow obtained from the least squares fit and shown in Figure 1b is due to wind forcing?

In order to assess the influence of wind forcing on the subtidal flow, a complex regression between the wind velocity and the detided velocity was performed. Hourly wind observations were interpolated to 30 s to match the sampling interval of the current velocities. This allowed the complex regression estimate to relate wind forcing to subtidal flow. The relationship between the wind and the subtidal flow was evident (Fig. 2c and 2d). In fact, the wind-induced flow produced a flow pattern that was very similar to the subtidal flow of Figure 1b according to the complex regression that yielded the following equations:

$$\begin{aligned} u &= 0.04\ W_x \\ v &= -0.04 + 0.04\ W_y\ . \end{aligned} \qquad (3)$$

These relationships explained 90% of the spatial variability of the subtidal flow. In (3), u and v were the east-west and north-south components of the current velocity, respectively, and W_x, W_y were the corresponding components of the wind velocity. This fit indicated that the north-south and the east-west components of the flow were approximately 4% of the north-south and the east-west components of the wind velocity, respectively. The -0.04 on the v component of the flow denoted a residual flow of 0.04 m/s directed to the south when the wind velocity is zero. This was consistent with the typical ambient coastal flow in this area of the Mid-Atlantic Bight [2]. The very high percentage of the subtidal flow variability explained by wind forcing was a consequence of the weak freshwater discharge onto the coastal ocean at the time of the study. This simple relationship between wind velocity and surface velocity allows the rapid assessment of the subtidal near-surface coastal circulation off the Chesapeake Bay only with wind velocity measurements. This assessment will, of course, be restricted to periods of weak freshwater discharge to the coastal ocean.

3.4. Tidal Data

The semidiurnal tidal contribution to the observations was obtained with the second and third terms on the right hand side of (1). The coefficients $a_i(x,y)$ and $b_i(x,y)$ were used to calculate the semidiurnal tidal ellipses following [8]. These ellipses are drawn in Figure 3 over the bathymetry of the study region. The orientation and ellipticity (ratio of the semi-minor axis of the ellipse to the semi-major axis) of the near-surface tidal currents appeared influenced by the coastline morphology. The ellipticity was lowest at the entrance to the Chesapeake Bay as the tidal currents were funneled into and out of the estuary. The ellipticity was greatest to the North and East as reflection of the rotary character of the tidal currents. The orientation of the ellipses suggested, once more, the funneling effect that the bay mouth has on the tidal currents entering and leaving the estuary. This orientation also suggested the influence of coastline morphology on the distribution of tidal currents. This representation of tidal properties was the first high-spatial resolution (less than 5 km) effort to characterize the distribution of the semidiurnal tidal ellipses off the Chesapeake Bay mouth. This is not the definitive distribution of tidal properties in the study area but offers an idea (and rapid assessment) of the spatial patterns that should prevail.

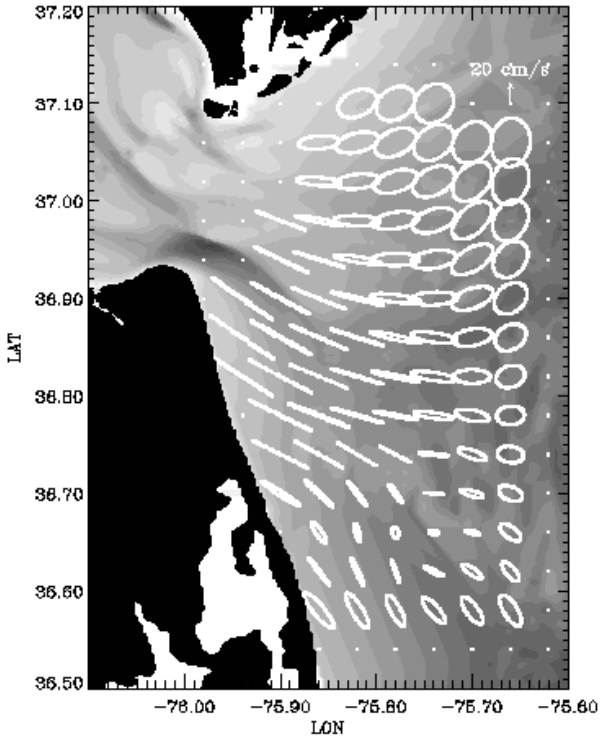

Figure 3. Near-surface semidiurnal tidal ellipses plotted over a regular grid of interpolates from the ship track shown in Figure 1. The bathymetry of the area is shown, for comparison with the orientation and ellipticity of the ellipses, as shaded contours. Deep areas are represented by darker shades.

4. Summary

Current velocity measurements with high spatial resolution were made off the mouth of the Chesapeake Bay in order to rapidly assess the coastal circulation off the mouth of an estuary under weak river discharge conditions. In particular, the influence of wind forcing on the coastal circulation was elucidated. The current velocity measurements were obtained with a towed acoustic Doppler current profiler during 25 hours between September 25 and 26, 1995. Ancillary measurements consisted of water temperature and salinity, and wind velocity. The current velocity measurements contained tidal and subtidal signals that were separated with a least squares technique as in [6]. The least squares fit was very good as it reproduced the salient temporal variations of the instantaneous measurements. The fit yielded a subtidal flow that featured a predominantly southward component and a turning region of the estuarine outflow that was advected southward by the coastal ambient flow. The latter feature agreed with numerical results dealing with a similar problem of an estuarine outflow interacting with an ambient flow [7]. The subtidal flow field was mostly caused by wind forcing as buoyancy forcing was very weak. This subtidal velocity flowed at 4% of the wind velocity. In addition to the wind-induced component, the subtidal flow was influenced by a southward ambient flow of 0.04 m/s.

The least squares fit also identified a semidiurnal tidal flow contribution that showed influence of the coastal morphology on the orientation and ellipticity of the tidal ellipses. These tidal ellipses were more elliptic away from the mouth and became more rectilinear at the constriction of the estuary. The orientation of the ellipses roughly followed the morphology of the coastline. The spatial distribution of these tidal ellipse properties confirmed the expected funneling effect of the Chesapeake Bay entrance on the tidal flows entering and leaving the estuary.

The analysis technique used in this study allows the assessment of the coastal circulation of a region influenced by tidal and other forcings (*e.g.* wind and buoyancy) in approximately 30 hours: 25 hours of measurements and a few hours of data processing and analysis. The advantage of this technique is that it is relatively simple to apply to a data set and produces rapid results. The disadvantage is that it produces results that are statistically reliable but not dynamically reliable because the technique disregards any hydrodynamic aspect of the study area.

5. Acknowledgments

This study was funded by the U.S. Minerals Management Service under contract 14-35-0001-30807. The able command of Cdrs. Tim Tisch and Susan Mc. Kay, as well as the rest of the crew of the NOAA ship *Ferrel* allowed the success of the measurements presented here. Ship time was provided by Sea Grant. A. Münchow kindly provided information for the application of the least squares technique used. Thanks to R.C. Kidd, T.M. Wilson, K. Bock, D. Ruble, J. Miller, and N. Metzger for their help in collecting the data. J. Dixon from the NOAA office in Chesapeake, VA., kindly provided the wind data from the Chesapeake Bay Bridge Tunnel.

6. References

[1] Boicourt, W.C. 1973. The circulation of water on the continental shelf from Chesapeake Bay to Cape Hatteras. Johns Hopkins Univ. Ph.D. Dissertation. 183 pp.
[2] Boicourt, W.C. 1981. Circulation in the Chesapeake Bay entrance region: estuary-shelf interaction. In J. Campbell and J. Thomas (eds), Chesapeake Bay Plume Study: Superflux 1980. NASA Conference Publication 2188: 61-78.
[3] Boicourt, W.C., S.Y. Chao, H.W. Ducklow, P.M. Gilbert, T.C. Malone, M.R. Roman, L.P. Sanford, J.A. Fuhrman, C. Garside, and R.W. Garvine 1987. Physics and microbial ecology of a buoyant estuarine plume on the continental shelf. *Trans. Amer. Geophys. Union.* 68(31): 666-668.
[4] Chao, S.-Y. 1988. River-forced estuarine plumes. *J. Phys. Oceanogr.* 18: 72-88.
[5] Chao, S.-Y. and W.C. Boicourt 1986. Onset of estuarine plumes. *J. Phys. Oceanogr.* 16: 2137-2149.
[6] Wong, K.-C. and A. Münchow 1995. Buoyancy forced interaction between estuary and inner shelf: observation. *Cont. Shelf Res.* 15(1): 59-88.
[7] Valle -Levinson, A., J.M. Klinck, and G.H. Wheless 1996. Inflows/outflows at the transition between a coastal plain estuary and the coastal ocean. *Cont. Shelf Res.* 16, 1819-1847.
[8] Souza A. J. and J. H. Simpson 1996. The modification of tidal ellipses by stratification in the Rhine ROFI. *Cont. Shelf Res.*, 16, 997-1007.

On the Influence of Estuarine Outflow and Bathymetry on Semidiurnal Tidal Currents

Andrew G.E. Haskell[*]
Arnoldo Valle-Levinson[*]
Kamazima M.M. Lwiza[†]

[*] Center for Coastal Physical Oceanography
Old Dominion University
Norfolk, VA 23529

[†] Marine Sciences Research Center
State University of New York
Stony Brook, NY 11794-5000

Submitted to Continental Shelf Research

ABSTRACT

Current velocity profiles from an Acoustic Doppler Current Profiler (ADCP) were used to investigate the influence of estuarine outflows and bathymetry on the semidiurnal tidal flow along a cross-shore transect outside of the Chesapeake Bay. The shelf transect was repeated eight times during one neap tidal cycle on March 26-27, 1996 under the effects of a well-defined Chesapeake Bay plume. The bathymetry of the transect featured an 18 m deep channel flanked by 10 m shoals to the sides. The observations showed that the maximum subtidal velocity perpendicular to the transect was associated with the plume outflow, reaching values of nearly 0.6 m s^{-1}. The mean flow parallel to the transect had typical values of 0.1 m s^{-1}, which could have been related to a quasi-geostrophic flow within the turning region of the plume. The amplitude and phase of the tidal flow inside the bay plume were significantly different from those of the underlying shelf water. The plume outflow caused the surface tidal flow to lag behind the near-bottom frictionally influenced flow by 40 degrees (~80 minutes). The tidal amplitude exhibited a subsurface maximum that was centered over the channel. The channel location of the maximum amplitude reflected frictional influences and the subsurface location was explained with the output of a one-dimensional mixed-layer model. The mixed-layer model showed that the subsurface maximum in tidal amplitude developed under the combined influence of various factors: large horizontal salinity gradients (4 units in 10 km), relatively weak tidal (0.5 m s^{-1}) and wind forcing (< 0.1 Pa), and over relatively deep (> 15 m) regions as was observed in the field. The subsurface maximum appeared at the base of the pycnocline where turbulence was suppressed, which was indicated by zero vertical eddy viscosities. Any modification to those factors caused the maximum to appear at the surface.

INTRODUCTION

The outflow of low-salinity estuarine water into the ocean forms a plume that tends to deflect anticyclonically in the Northern Hemisphere and form a boundary current with the coastline on its right-hand side (*e.g.* Münchow *et al.*, 1992). The current scope of information on the interaction between these estuarine outflows and the tidal currents on the shelf is restricted to idealized numerical experiments performed over narrow (width smaller than one internal radius of deformation) inlets (Kapolnai *et al.*, 1996; Wheless and Valle-Levinson, 1996). This interaction, jointly with wind influences, ultimately determines the fate of suspended and dissolved matter and biota that can be found near the estuary mouth.

Estuarine plumes derived from wide systems have been studied by numerical methods that ignore tidal influences or that use distantly spaced data, for example, moored instruments or density profiles (*e.g.* Münchow *et al.*, 1992; Weaver and Hsieh, 1987; Chao, 1988; Chao and Boicourt, 1986). More recently, with the Acoustic Doppler Current Profiler (ADCP), current data can be measured on relatively fine spatial scales. A horizontal resolution of approximately 60-75 m is attained with 30 second ensembles (or averages) and cruising speeds of 4-5 knots. This resolution is sufficient to study general features of estuarine plumes like those from the Chesapeake Bay, which is a typical example of wide (width greater than one internal radius of deformation) estuarine plumes.

The Chesapeake Bay is located in the mid-Atlantic region of the United States and is the largest estuary in the country. The temporal variability of the flow through the mouth of the Chesapeake Bay is dominated by tidal forcing (*e.g.* Browne and Fisher, 1988), but wind forcing and freshwater discharge also may produce important variations (*e.g.* Valle-Levinson, 1995; Valle-Levinson and Lwiza, 1997). The spatial variability of the flow in the lower Chesapeake Bay is greatly influenced by the bathymetry (Valle-Levinson and Lwiza, 1995).

The bathymetry of the inner continental shelf, near the entrance to the Chesapeake Bay, is characterized by a channel (Fig. 1) that is expected to cause spatial variability in the flow. It is also expected to influence the formation of frontal features along the region of the channel with the greatest bathymetry curvature, as in the Delaware Bay coastal current (Sanders and Garvine, 1996). Currently, little is known about how the Chesapeake Bay plume structure varies with the tidal cycle because it is difficult to avoid tidal aliasing inherent to surveys of high spatial resolution and several kilometers extent. Also, little is known about the influences of plume outflow and of the bathymetry on the tidal flows. Several studies have shown that a rapid change in water depth is a controlling factor in determining the position of tidally induced fronts (*e.g.* Largier, 1992; Huzzey, 1982; and Largier and Taljaard, 1991). These fronts may form at the mouths of estuaries when inner shelf flood waters meet buoyant estuarine waters.

The purpose of this study was to describe the effects that a plume of buoyant water flowing from an estuary to an inner shelf with abrupt bathymetry had on the tidal currents. These effects were assessed in terms of the spatial distribution of tidal amplitude and phase along a section influenced by the Chesapeake Bay outflow. The present study differed from previous ones in that it was the first to report on a complete cross-section of a freshwater plume using the high resolution capabilities of the ADCP. Other studies have used ADCPs to measure different

characteristics of the tidal currents (*e.g.*, Simpson and Souza, 1995; Souza and Simpson, 1996; Sanders and Garvine, 1996) however none of these examined the features addressed in this study.

Both Souza and Simpson (1996) and Simpson and Souza (1995) used a combination of seabed mounted ADCPs and moored current meters to gather current data at distinct points. Sanders and Garvine (1996) did perform a repeated transect using an ADCP but only reported results at several locations instead of a continuous cross section as presented here. In addition to advancing the general knowledge of the effects of buoyancy outflow and bathymetry on tidal currents, this study described the influence of the vertical eddy viscosity, as influenced by tidal currents and wind forcing, on the vertical profile of the tidal current amplitude.

STUDY AREA

The study area was located to the south of the Chesapeake Bay mouth, approximately 8 km south of Cape Henry (Fig. 1). The bathymetry is characterized by a complex system of shoals and navigational channels. The mean depth of the region is approximately 10 m with depths reaching 30 m over Chesapeake Channel off Cape Henry. This channel follows the coastal morphology at the inner shelf and shoals rapidly to the south. The influence of this bathymetry on tidal amplitude and phase outside of the bay mouth is essentially unknown. Also, little is known about the direction and magnitude of the tidal currents off the Virginia Beach coast. It is recognized that the principal constituent of the tidal energy of the area is the lunar semidiurnal

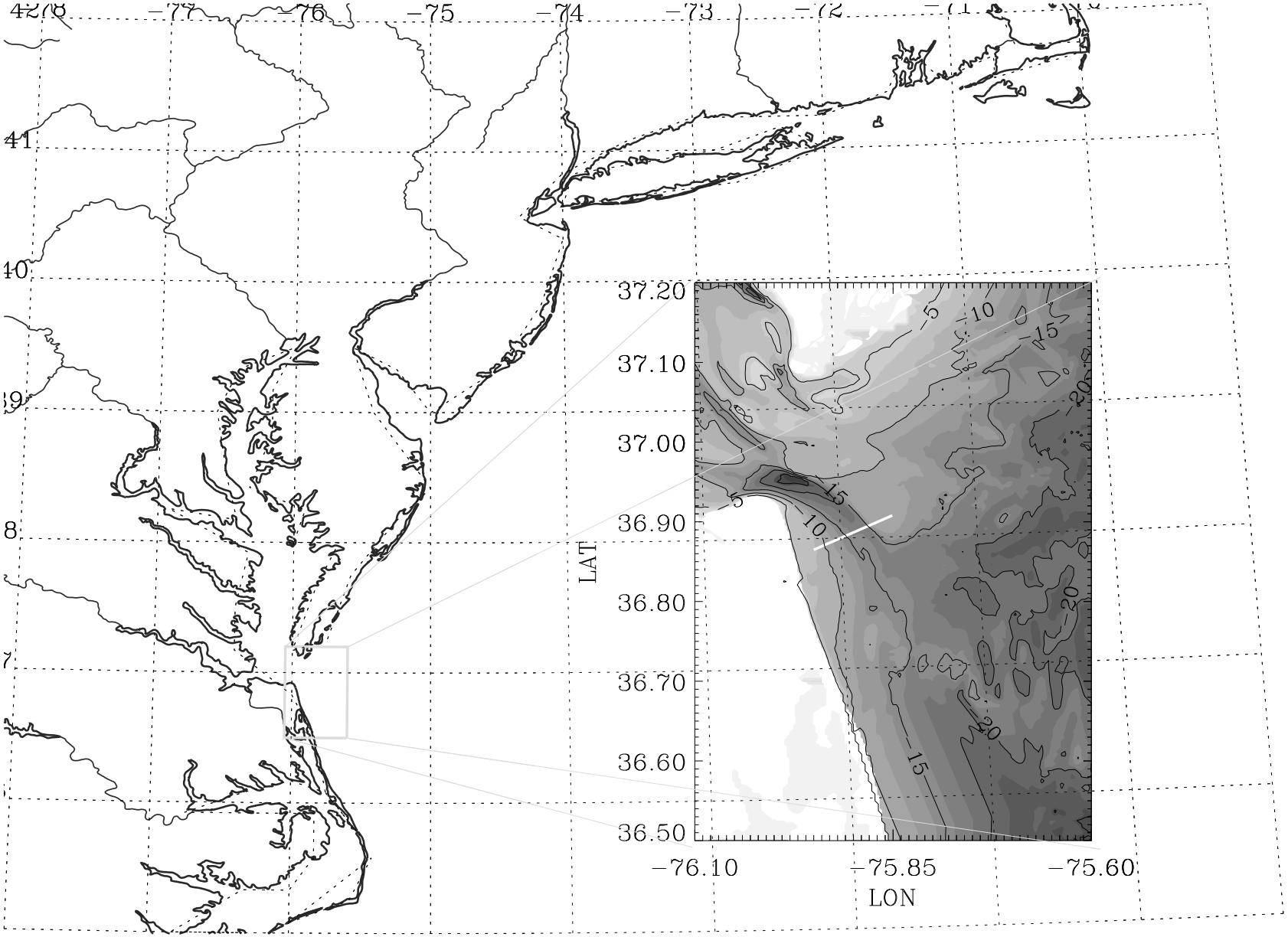

Figure 1. Lower Chesapeake Bay and inner continental shelf. Inset shows the location of the transect studied (white line) and the bathymetry of the area including the Chesapeake Channel. The bathymetry is contoured at 10m intervals. The transect ran nearly perpendicular to the coastline and started 3 km off the Virginia Beach coast and extended approximately 10 km seaward.

(M_2) (Fisher, 1986; Browne and Fisher, 1988) and that the tidal phase in the Mid-Atlantic Bight propagates northward from Cape Hatteras (Redfield, 1958). Further details are explored in this work.

The influence of the plume generated by the Chesapeake Bay outflow on the shelf produces, in general, southward subtidal surface currents off Virginia Beach (Boicourt, 1973; 1981). The shape and extension of the plume and its outflow are affected by wind forcing. Northeasterly winds cause the plume to accelerate, lengthen and narrow while winds from the southwest decelerate and widen the plume (Boicourt, 1981). The near-bottom subtidal flow is likely to be affected by wind direction but a clear pattern of response has not yet been identified. This near-bottom flow may move in the same direction of the wind or in opposite direction depending on water column stratification (Johnson, 1985). Wind forcing in the vicinity of the Chesapeake Bay entrance typically tends to be strongest and northeasterly in the fall and winter, and weakest and southwesterly in the summer (Paraso and Valle-Levinson, 1996).

DATA ACQUISITION

Current velocity profiles and near-surface temperature and salinity were obtained along one transect that started 3 km off the Virginia Beach coast and extended approximately 10 km seaward. Current velocity measurements consisted of towing a broadband 600 kHz RD Instruments ADCP. The ADCP was towed looking downward from the NOAA ship *R/V Ferrel* at a speed of approximately 2 m s^{-1} (4 kn). Navigation was carried out with a differential Global Positioning System (DGPS). The length of the transect was chosen to accommodate the greatest extension possibly covered in 1.5 hrs while sampling continuously at 2 m s^{-1}. The transect ran perpendicular to the coastline that parallels the Chesapeake Channel (Fig. 1). The objective of the sampling scheme was to complete as many repetitions as possible within one tidal cycle to effectively distinguish the tidal signal from the records. Eight repetitions of the transect were completed on 26-27 March 1996 within 12.5 hours. Sampling occurred with NNE winds of 5-7 m s^{-1}, following a 36 hour period of SSE winds of ~5 m s^{-1}. Sampling also coincided with a period of large freshwater discharge. For one month prior to the survey, freshwater discharge was more than 3 times (~7600 m^3 s^{-1}) the 46-year average for the Chesapeake Bay (~2200 m^3 s^{-1}) (United States Geological Survey -USGS- press releases on the World Wide Web).

Each ADCP profile represented a 30 second average of approximately 120 pings. The ADCP velocities were separated vertically into 0.5 m bins with an approximate horizontal spacing of 200 m. Data with error velocities (the difference between the redundant vertical velocities) greater than 0.08 m s^{-1} were discarded. The bin closest to the surface was centered at a depth of 2.75 meters. The sampling period at each gridded location varied from ~80 minutes over the mid-channel to a range of 10 to 160 min over the shoals near the ends of the transect. Data from the ends of each repetition were discarded to ensure a ten-minute minimum interval between the locations defined as the ends of the transect. Also, data collected while moving to avoid traffic were discarded. The ADCP velocities were calibrated as in Joyce (1989), which yielded a misalignment angle of -1.023° and a scaling factor of 1.0603. The data were then rotated from the earth's coordinate frame to a frame representing along and across channel (along and across shore) directions (12° west of north). Finally the data were interpolated to a uniform grid of 48 points in the horizontal and 33 in the vertical.

The time series of eight values at each grid-point was fitted, using least squares, to a sinusoid with an M_2 period (12.42 hours) as in Lwiza *et al.* (1991). This procedure produced the subtidal flow (periods greater than semidiurnal) along with the semidiurnal tidal amplitude and phase at each grid point. Along-channel and across-channel components were treated separately. The fifth repetition of the transect showed noisy values and was discarded from the least squares analysis. This elimination reduced the overall root mean square error values by 0.07 m s^{-1} in the along-shore direction and by 0.20 m s^{-1} in the across-shore direction.

Simultaneously to current profiling, near-surface temperature and salinity were measured by continuously pumping water from a depth of ~1 m through a Sea Bird 1621 thermosalinograph with a sampling interval of 10 s. The near surface temperature and salinity were also fitted to a semidiurnal sinusoid to obtain the subtidal structure along the transect. Vertical profiles of salinity and temperature were not collected in order to optimize the ADCP data quality and their time of acquisition.

DESCRIPTION OF OBSERVATIONS

First, the structure of the estuarine outflow was described in terms of the subtidal flow and salinity fields. The bathymetric influence on the estuarine outflow was also explored through examination of subtidal fields. Second, the effects of bathymetry and of estuarine outflow on the semidiurnal tidal currents were described in terms of the tidal fields. The interpretation of the effects of estuarine outflow on tidal currents was supported by the output of a mixed layer model.

Subtidal Fields

The along-channel subtidal flow (Fig. 2) showed southward flow throughout the section studied. Maximum values reached 0.55 m s^{-1} in the region that was most likely related to the core of the Chesapeake Bay outflow. These magnitudes seemed consistent with a surface to bottom density difference of O(10 kg m^3) (Turner, 1973), which agreed with the strongest stratification observed in the lower Chesapeake Bay during spring tides in March 1996 (unpublished data). This large subtidal flow could have been a result of the barotropic forcing, from high river discharge and southwestward winds, combined with the baroclinic forcing, from the large density gradients. However, there was no evidence of the influence of baroclinic forcing as the subtidal along-shore current flowed only in one direction. As shown by Noble *et al.* (1996) large river discharges drove near-bottom currents in the direction of the discharge. This suggested that the subtidal flow observed, which consisted of a relatively sluggish southward ambient flow (0.10 - 0.15 m s^{-1}) underlying a relatively swift surface plume, was primarily driven by river discharge and wind forcing. The integrated transport through the observed section was 14,485 m^3 s^{-1}. The monthly averaged freshwater discharge into the bay during February and March of 1996 was approximately 4000 m^3 s^{-1} which corresponded to the area of the plume extending approximately 5.5 m deep and 5.5 km from the start of the transect. The remaining 10,000 m^3 s^{-1} could possibly be supplied by the ambient coastal current flowing southward at the observed rate of 10 cm s^{-1}.

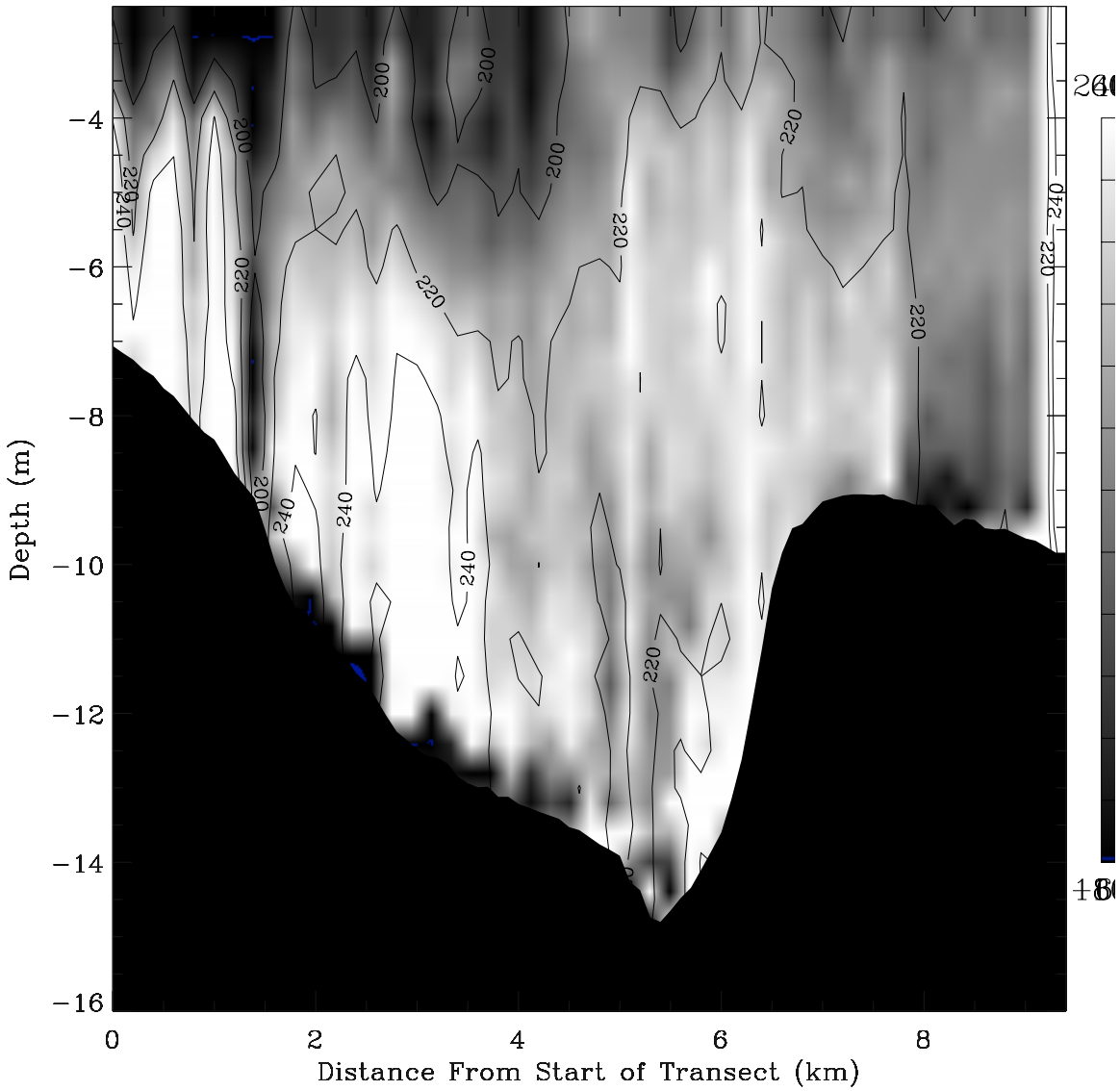

Figure 2. Lower Chesapeake Bay and inner continental shelf. Inset shows the location of the transect studied (white line) and the bathymetry of the area including the Chesapeake Channel. The bathymetry is contoured at 10m intervals. The transect ran nearly perpendicular to the coastline and started 3 km off the Virginia Beach coast and extended approximately 10 km seaward

The across-channel subtidal flow was comparatively weaker than the along-channel flow (Fig. 3). It was negative (shoreward) practically everywhere along the section and the highest values appeared near the surface. The negative character of both subtidal flow components indicated a southwestward flow that probably resulted from the Coriolis accelerations acting on the flow produced by river and wind forcing. It is likely that the sampling transect was located within the quasi-geostrophic anticyclonic or turning region of the outflow plume, as suggested by the numerical results of Chao (1988) and Valle-Levinson *et al.* (1996).

The surface salinity and temperature values (Fig. 4) showed the plume offshore front existing at the same location over the channel as suggested by the along-shore subtidal flow. Although only one distinct along channel front was evident in the present study, a near shore front was also noted visually during the cruise but was shoreward of our sampling limit. The existence of two fronts over the maximum concave curvature of a channel connecting to an estuary mouth was also noted by Sanders and Garvine (1996) for the Delaware Bay coastal current. The bathymetry and the inertia of the plume leaving the bay mouth caused the bulk of the plume to separate from the coast, producing both offshore and onshore fronts, before Coriolis acceleration organized the flow in a southward coastal current as suggested by the numerical models of Chao and Boicourt(1986), Chao(1988), and Valle-Levinson *et al.* (1996). The amplitude of the surface salinity variation was related to the amplitude of the along-channel semidiurnal flow (as presented later). This was a reflection of the elastic straining of the salinity field by the tidal currents.

Tidal Fields

The first effect of the estuarine outflow on the tidal fields was noticed in the phase of the M_2 along-shore tidal current. The phase showed near surface lags of 80 min (40 degrees) in an area that was presumably associated with the southward flowing Chesapeake Bay plume (Fig. 5). This indicated that the tidal currents near the surface lagged behind the underlying shelf water. The phase lag within the plume was consistent with the upward propagation of the tidal phase and with the decoupled dynamics between the baroclinically driven buoyant outflow and the barotropically driven interior flow. The phase lag was due to the combined effects of friction and inertia that allowed a faster response of near-bottom flows to tidal forcing (Valle-Levinson and Lwiza, 1995). The greatest phase lag was laterally delimited by sharp bathymetric changes, which also suggested a bathymetric delimitation of the outflow plume as in the Delaware Bay (Sanders and Garvine, 1996). In general, the water inside the channel responded more slowly to tidal forcing than the surrounding water, which was probably related to the distinct hydrographic characteristics in the channel as observed in the lower Chesapeake Bay (Valle-Levinson and Lwiza, 1997), where the channel flow tends to favor the flood direction due to baroclinic inflow.

Additional effects of bathymetry and buoyant outflow on the tidal currents were evident in the distribution of the amplitude of the along-shore component. The maximum amplitude of the along-channel M_2 flow was found over the channel at approximately 6 km from the coast (Fig. 6) similarly to Münchow *et al.* (1992) and Valle-Levinson and Lwiza (1995). This was a consequence of reduced frictional effects over the deeper areas. An interesting finding was that the maximum appeared at a depth of 5.5 m and not near the surface, where the largest amplitude is usually expected because of the greatest distance from bottom frictional effects. The subsurface location of the strongest semidiurnal tidal currents could have coincided with the pycnocline that delimited the plume outflow, which effectively decreased frictional effects through a reduction of

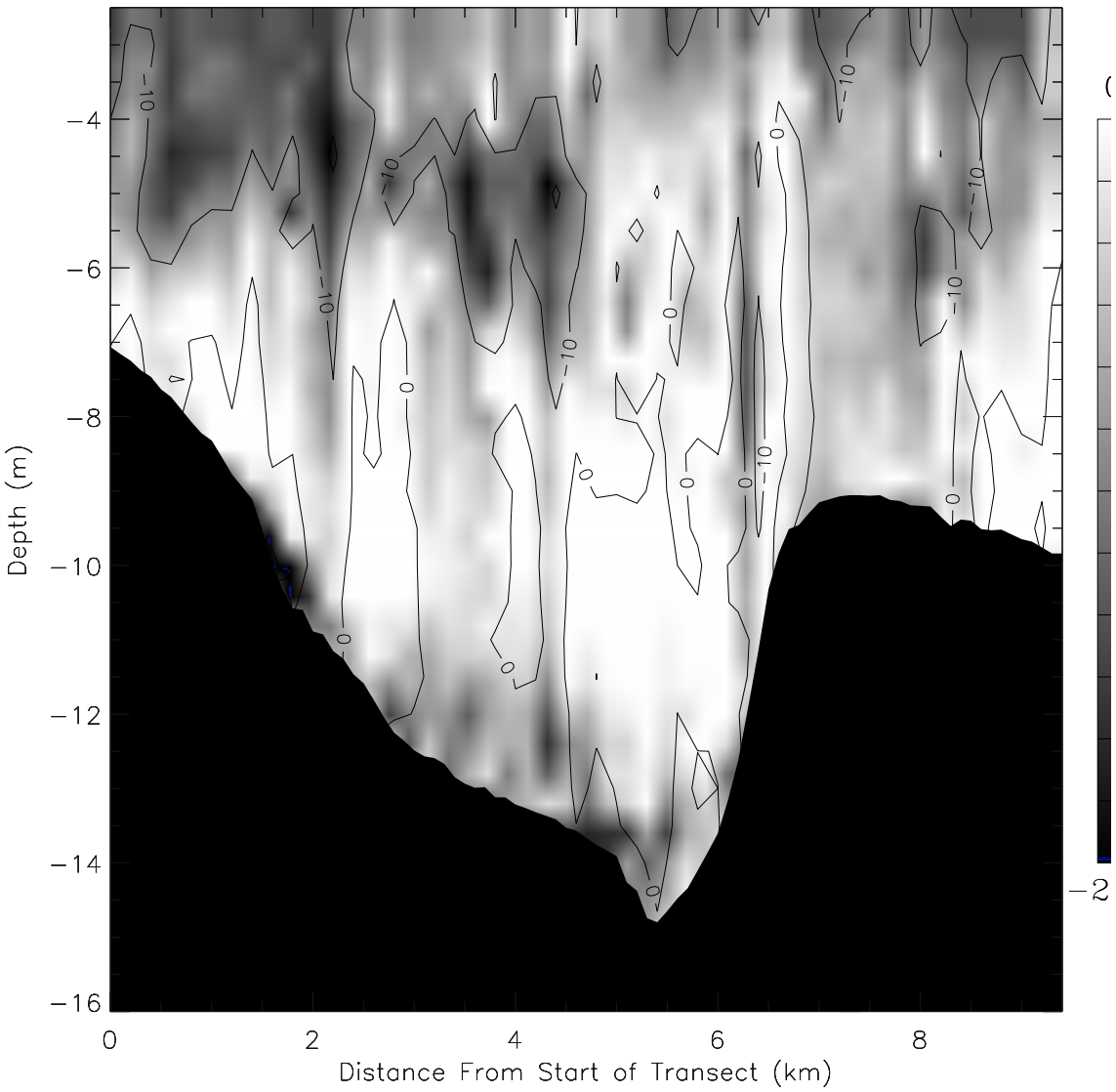

Figure 3. Across-channel subtidal flow (centimeters per second) along the cross section studied. Contour interval is 10 cm s^{-1}, negative values represent westward or shoreward flows. Dark regions represent high values.

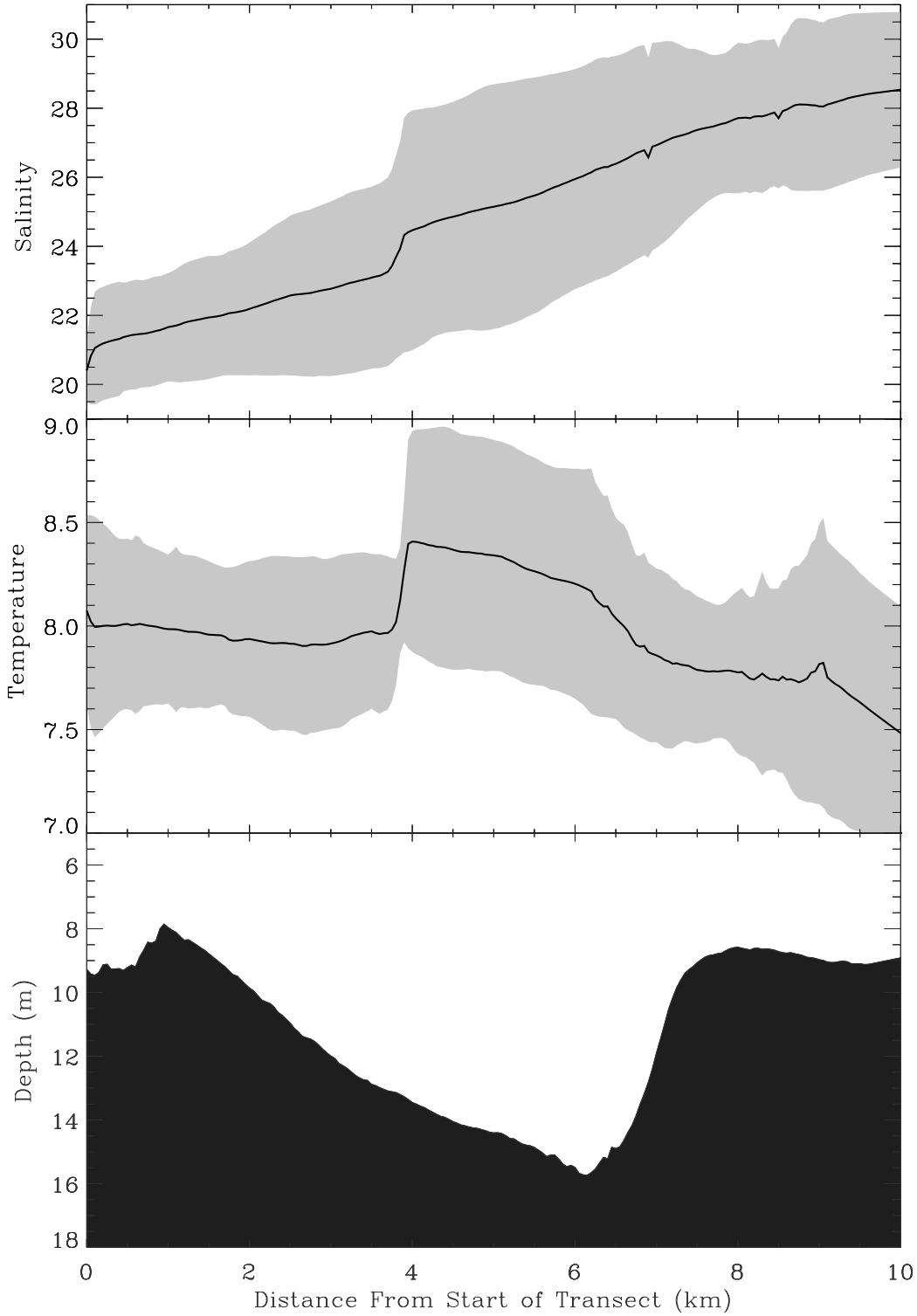

Figure 4. Surface salinity (top) and temperature (middle, °C) values shown over the bathymetry (bottom) of the transect studied. The dark line in the top two panels denotes the mean value of all 8 repetitions while the shaded area shows the rmse range.

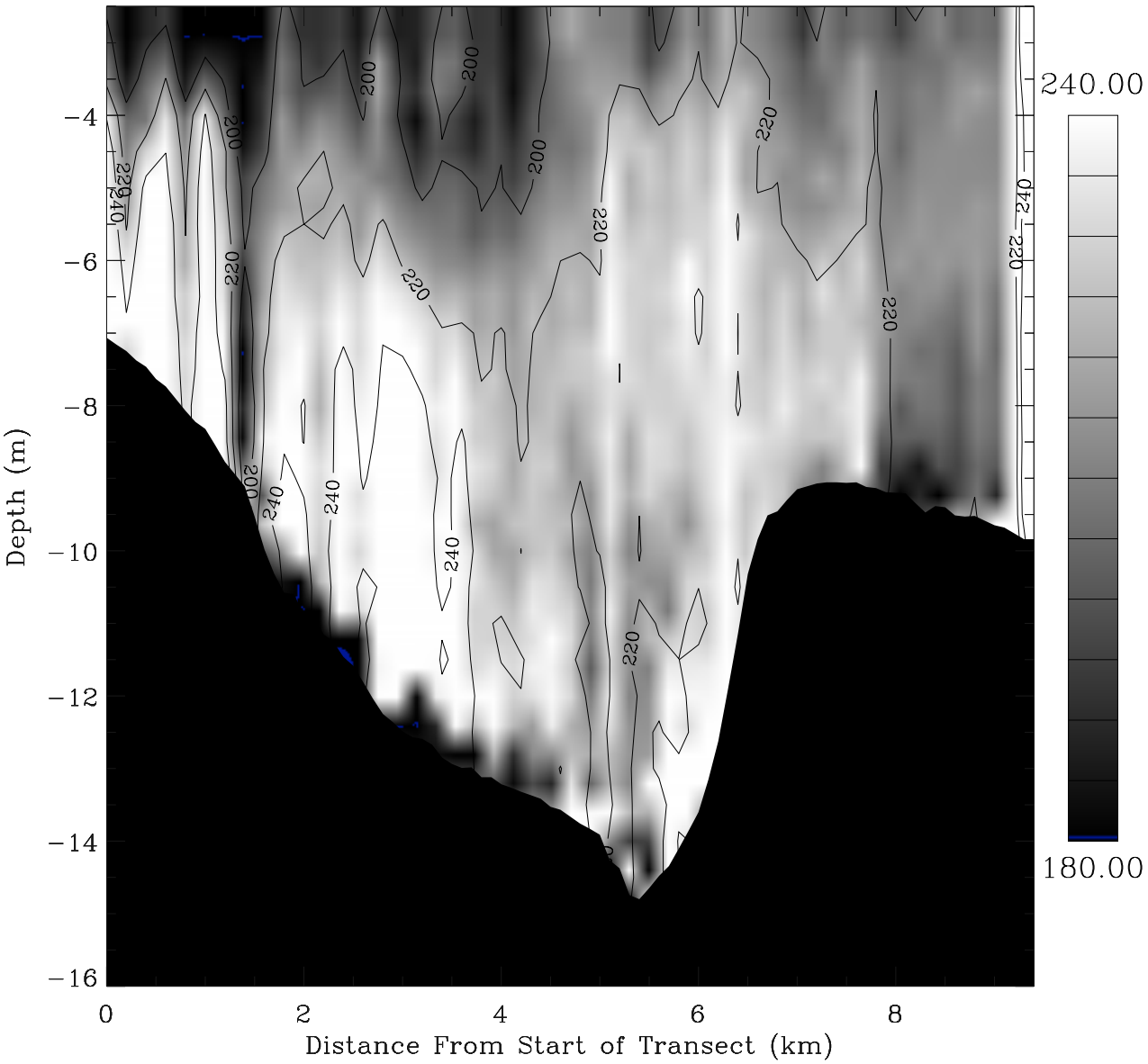
240.00
180.00
Depth (m)
−4
−6
−8
−10
−12
−14
−16
0
2
4
6
8
Distance From Start of Transect (km)
200
220
240

the eddy viscosity and of turbulence. The influence of the density field (plume outflow) on the eddy viscosity and in turn on the tidal current amplitude was addressed with a simplified one-dimensional mixed layer model presented next.

MIXED LAYER MODEL

A total of eight process-oriented experiments with a mixed layer model helped to elucidate the effects of buoyant outflow on the tidal current amplitude as observed outside the Chesapeake Bay mouth. The eight experiments performed are summarized in Table 1. Experiment 1 looked at the effect of the plume on weak tidal currents and constituted the base case. Experiment 2 investigated the same influence under strong tidal currents. Experiment 3 extended the effects of Experiment 1 to include the effects of a wind stress acting in the same direction of the density gradient, *i.e.*, same direction as the plume outflow. The observations were obtained during a period of wind blowing in the same direction as the along-shore pressure gradient. Experiment 4 also examined wind effects but in the opposite direction to the outflow. Experiments 5 and 6 examined the sensitivity of the results of the base case to the prescription of the longitudinal density gradient and to the depth of the water column, respectively. Experiments 7 and 8 investigated the sensitivity of the base case and of experiment 5 to the prescription of an initially homogeneous water column.

The one-dimensional (vertical) mixed layer numerical model solved the momentum equation and the salinity and temperature balances in the direction of the density gradient (along shore in this case). The values of the horizontal velocity component u (m s^{-1}), salinity S, temperature T (°C), and density ρ (kg m^{-3}) were estimated as a function of depth z (positive upwards) and time t at one vertical station with depth H equals 15 m, subdivided into 30 equally spaced levels. The dynamic balances were evaluated with time- and depth-varying turbulent (eddy) coefficients [A_v, A_{vS}, A_{vT} (m^2 s^{-1})] obtained from closure (Mellor and Durbin, 1975). The horizontal density gradient was prescribed as 3 kg m^{-3} in 10 km (or 4 salinity units), based on hydrographic observations collected in March 1996 and every month in the lower Chesapeake Bay (Valle-Levinson, unpublished data).

Governing Equations

The momentum balance included a barotropic and a baroclinic pressure gradient in the along-channel direction x and vertical mixing (vertical transfer of horizontal momentum):

$$\frac{\partial u}{\partial t} + g\frac{\partial \eta}{\partial x} + \frac{g}{\rho_0}\int_H^z \frac{\partial \rho}{\partial x} dz = \frac{\partial}{\partial z}[A_v \frac{\partial u}{\partial z}],$$

η was the surface elevation; g was the acceleration due to earth's gravity (9.8 m s^{-2}), ρ_0 was an average value of the density ρ; and A_v was the eddy diffusivity of momentum and was estimated according to the turbulence closure formulation of Mellor and Durbin (1975). This model, that also included an equation for the balance of dissolved oxygen, has been used by Valle-Levinson *et al.* (1995) to study hypoxia in western Long Island Sound.

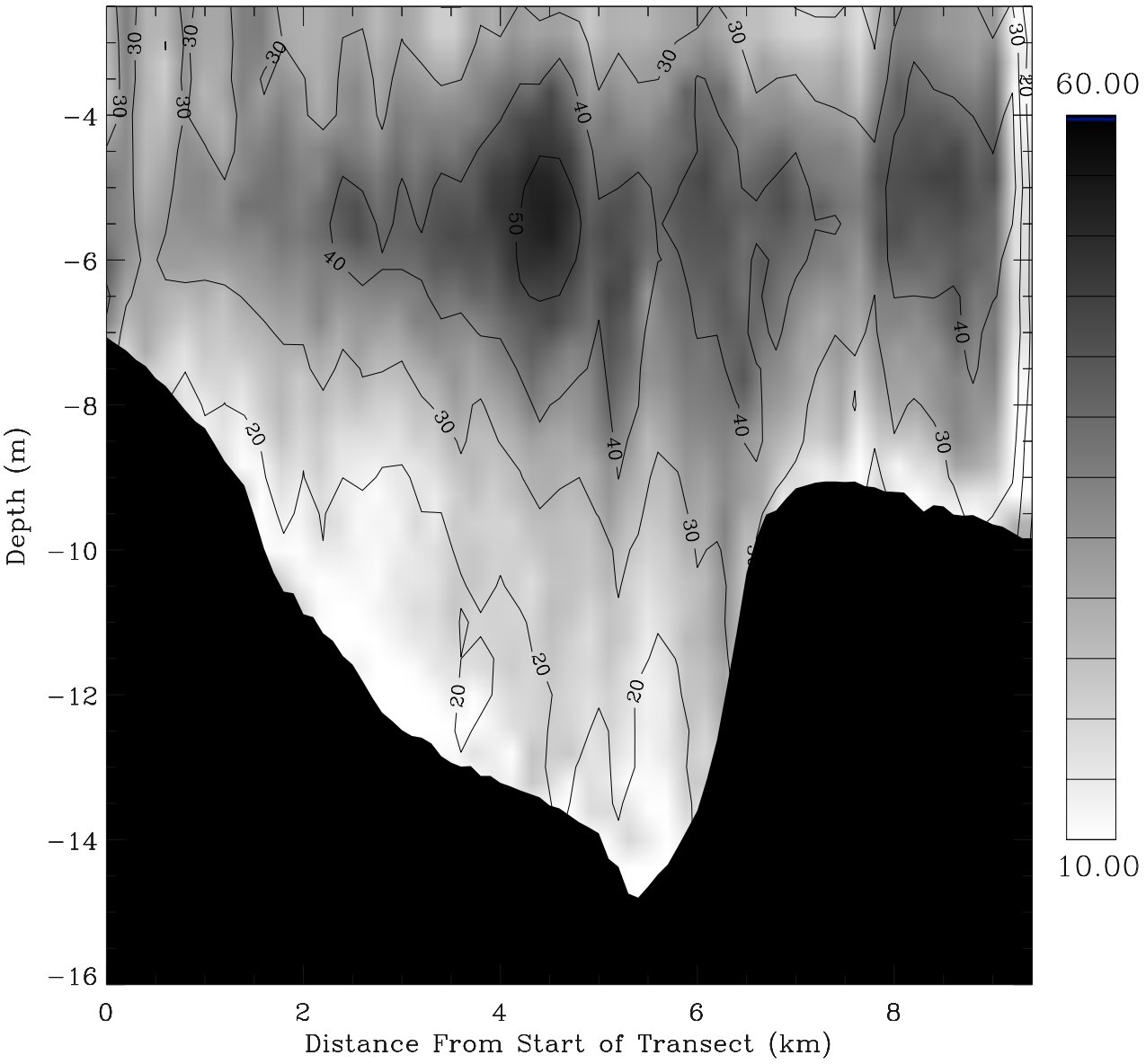
60.00
10.00
Depth (m)
−4
−6
−8
−10
−12
−14
−16
0
2
4
6
8
Distance From Start of Transect (km)

Experiment	Uo (m/s)	t_x (Pa)	DS/10 km	Depth (m)	DS (bot-top)
1	0.5	0	4	15	10
2	0.7	0	4	15	10
3	0.5	1	4	15	10
4	0.5	-1	4	15	10
5	0.5	0	1	15	10
6	0.5	0	4	12	10
7	0.5	0	4	15	0
8	0.5	0	1	15	0

Table 1. Summary of experiments carried out with the mixed layer model.

Intratidal variations of *T* and *S* were determined by a balance between vertical mixing and horizontal advection with horizontal gradients specified to be constant with depth and time:

$$\frac{\partial C}{\partial t} + u\frac{\partial C}{\partial x} = \frac{\partial}{\partial z}[A_{vC}\frac{\partial C}{\partial z}]$$

where *C* indicated the property of interest, *i.e.*, *T* or *S*, and A_{vC} represented the vertical eddy diffusivity coefficient. In this particular application, the vertical eddy diffusivity of heat, A_{vT}, was assumed equal to the vertical eddy diffusivity of salt, A_{vS}. Local density values were obtained from *T* and *S* using the equation of state of sea water (*e.g.* Gill, 1982, p. 599).

Boundary and Initial Conditions

For the momentum equation, quadratic surface and bottom shears were specified in the form: $A_v\, \partial u/\partial z = (\rho_a/\rho)\, C_D\, w\, |w|$, at the surface; and $A_v\, \partial u/\partial z = C_B\, w\, |w|$ at the bottom. The coefficient C_D represented nondimensional surface drag (0.0015); ρ_a was the air density (1.2 kg m^{-3}); *w* was the wind velocity, positive in the direction of the density gradient; and C_B was a nondimensional bottom drag coefficient (0.002). For temperature, a vertical heat flux *Q* could be specified at the surface, prescribed as zero here, and was negligible at the bottom. For salinity, it was assumed that there were no vertical fluxes of salt at either the air-water interface or the water-sediment interface. Experiments 1 through 6 began with vertically homogeneous *T* (17°C)

and a step in *S* between 5 and 6 m. The upper 5 m had homogeneous *S* of 20, and between 6 and 15 m the initial *S* was homogeneous at 30. Experiments 7 and 8 began with vertically homogeneous *S* of 30. As will be seen, the shape of the initial salinity profile played a minor role in determining the shape of the profile of the tidal current amplitude. A forcing velocity with *u* amplitude of 0.50 m s^{-1} (0.70 m s^{-1} for Experiment 2), oscillating at a frequency of $2\pi/12$ h was specified. Results represented the fifth tidal period after four tidal cycles of "spin-up" time as in Valle-Levinson and Wilson (1994).

Results of Simulations

The output of simulations was presented in Figure 7 that showed the time-depth variations of *u* and *S* within the tidal cycle, the amplitude of the tidal flow (determined with a least squares fit on the hourly flow values), and the corresponding tidal average of the vertical eddy viscosity. In the base case, the strongest ebb tidal currents (positive values) appeared at the surface as the barotropic pressure gradient from tidal forcing acted in concert with the baroclinic pressure gradient. This baroclinic pressure gradient was most positive at the surface because of its cumulative nature from bottom to surface. In contrast, the barotropic pressure gradient opposed the baroclinic pressure gradient during flood tidal currents and the strongest flood currents appeared under the surface, at the base of the pycnocline. This effect of the flood stages translated into tidal current amplitudes that increased with depth and reached a maximum at the pycnocline, as the measurements indicated (Fig. 6). The location of the core of maximum amplitude was related to the distribution of eddy viscosity (A_v) with depth, which was essentially zero between the surface and the base of the pycnocline. Vertical mixing was suppressed throughout that top 'slippery' layer and the energy of the flood currents was concentrated at approximately 5.5 m depth during most of the flood period. This base case could be considered as applicable to neap tides as was the case of the observations described before (Fig. 6).

The second experiment considered stronger tidal forcing than the base case to determine whether the core of maximum current amplitude changed depth. In this case, maximum ebb and maximum flood occurred at the surface (Fig. 7). Flood tidal currents were able to overcome the opposing baroclinic pressure gradient. As expected, stratification was weaker than in the base case and was even broken down by the end of flood. The coefficient A_v was non-zero everywhere in the water column and the tidal current amplitude was maximum at the surface and decreased with depth. The vertical migration of the core of maximum amplitude of semidiurnal tidal currents from the interior of the water column during neap tides to the surface during spring tides, has been observed in the James River (Valle-Levinson, Wong and Lwiza, in preparation). It is worth mentioning a cautionary note here because during spring tides, the semidiurnal tidal constituents (M_2, S_2, N_2) are in phase and the estimate of the semidiurnal (*e.g.* M_2) tidal current amplitude over one tidal cycle will reflect greater amplitudes than those during neap, when the constituents are in quadrature (90 degrees out of phase). Therefore, these results should be interpreted cautiously as they did not reflect time variations of one single tidal constituent but the interaction of several constituents of similar period, in this case, those near 12 hrs.

The next experiment (3) considered the effects of wind forcing in the same direction of the density gradient, *i.e.*, in the direction of ebb tidal currents and of the plume outflow. The

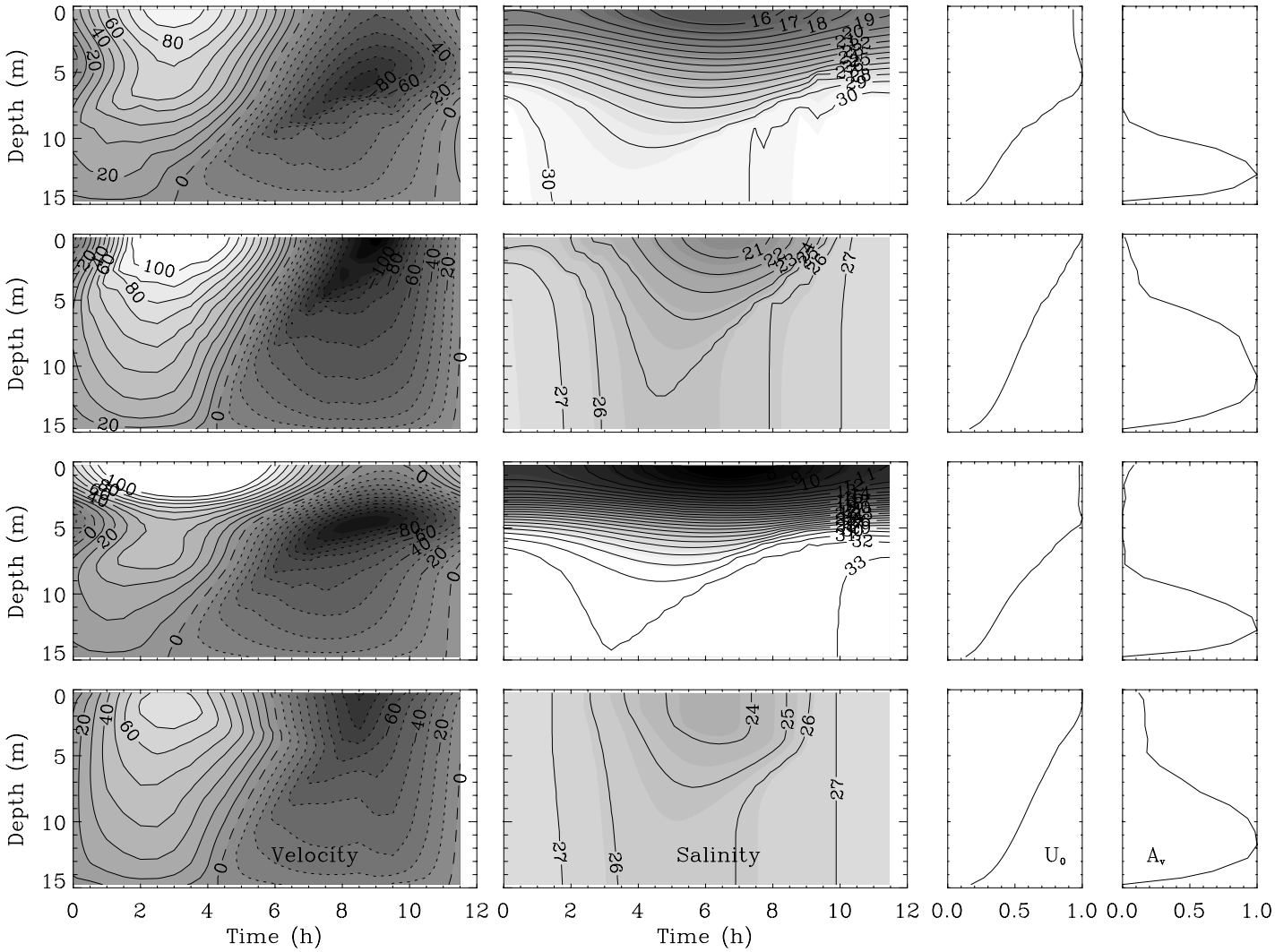

Figure 7. Results of experiments 1-4 of the one-dimensional mixed layer model. Panels in column one show variations of the tidal flow (centimeters per second) within the tidal cycle. Contour interval is 10 cm s^{-1}. Positive values (light areas) denote ebb flow. Panels in column two show variations in salinity within the tidal cycle. Contour interval is 1. Dark regions denote high salinity. Column three shows tidal amplitude (cm s^{-1}) scaled such that a value of 1.0 denotes maximum amplitude for the experiment. Column four shows tidal average of the vertical eddy viscosity (cm^2 s^{-1}) also scaled such that a value of 1.0 denotes maximum viscosity for the experiment. Values of maximum amplitude and viscosity for the four experiments are as follows: Exp 1: U0 78, Av 68; Exp 2: U0 118, Av 200; Exp 3: U0 82, Av 80; Exp 4: U0 76, Av 109.

behavior of the tidal currents and their amplitude was somewhat similar to that of the base case (Fig. 7). Obviously, ebb tidal currents were stronger in this experiment and flood tidal currents at the surface competed against the combined forcing from wind stress and baroclinic pressure gradient. Wind effects appeared only within the upper 8 m of the water column. In consequence, stratification was greatly enhanced as the wind mostly contributed to buoyancy advection because vertical mixing was restricted to a thin surface layer approximately 4 m thick, where the mean eddy viscosity was non-zero. The maximum amplitude of the tidal currents again appeared at the pycnocline region, where A_v was effectively suppressed. Under the wind-influenced layer, the profile of the mean eddy viscosity was essentially the same as the base case and reflected the exclusive effects of tidal forcing. This wind forcing enhanced the stratifying effects of tidal straining during ebb.

The effects of a wind blowing in the opposite direction to the density gradient (Experiment 4), *i.e.*, in the direction of flood tidal currents were analogous to the effects of strong tidal forcing (Fig. 7). In this case, ebb tidal currents were weaker than in the base case, which reduced the straining of the density field that favors stratification. After maximum ebb, the strongest ebb tidal currents appeared underneath the surface as wind forcing opposed the baroclinic pressure gradient and tidal forcing. On the other hand, the destratifying effects of tidal straining during flood were greatly enhanced by wind forcing. Stratification was much weaker than in previous cases and A_v was greater in general throughout the water column. This allowed the development of greatest tidal current amplitudes at the surface, where A_v was minimum, and decreasing with depth.

The effect of decreasing the longitudinal salinity gradient (Experiment 5) was to produce weak stratification (Fig. 8), non-zero eddy viscosities and tidal current amplitudes that decreased with depth. Decreased depth (Experiment 6) hindered the development of a sub-surface jet at the pycnocline because the baroclinic density gradient was not large enough (remember that this is an integration of the density gradient from bottom to surface, thus, the deeper the water column, the larger the baroclinic pressure gradient for a given longitudinal density gradient) to weaken barotropic flow (from flood tidal flows) at surface. Initial vertical homogeneity (Experiment 7) did not preclude the appearance of a subsurface maximum amplitude as stratification developed from the adjustment of the longitudinal density gradient. Initial vertical homogeneity and weak horizontal density gradient (Experiment 8) did preclude the appearance of a subsurface jet as mixing was non-zero throughout water column. Therefore, the conditions that combined to allow the development of a subsurface maximum in tidal current amplitude were weak tidal currents and winds blowing in the same direction as the surface density gradient, strong longitudinal density gradients, and moderate depths. All these conditions prevailed during the survey carried out in March of 1996 on the inner shelf to the south of the Chesapeake Bay mouth.

SUMMARY

The influence of buoyant discharges and bathymetry on semidiurnal tidal currents was investigated along an inner-shelf cross-shore transect outside of the Chesapeake Bay. Underway measurements of current velocity obtained with an ADCP and of near-surface temperature and salinity were carried out during one semidiurnal tidal cycle (12 hours) on March 26-27, 1996. These observations reflected the forcing of winds from the NNE and high discharge conditions.

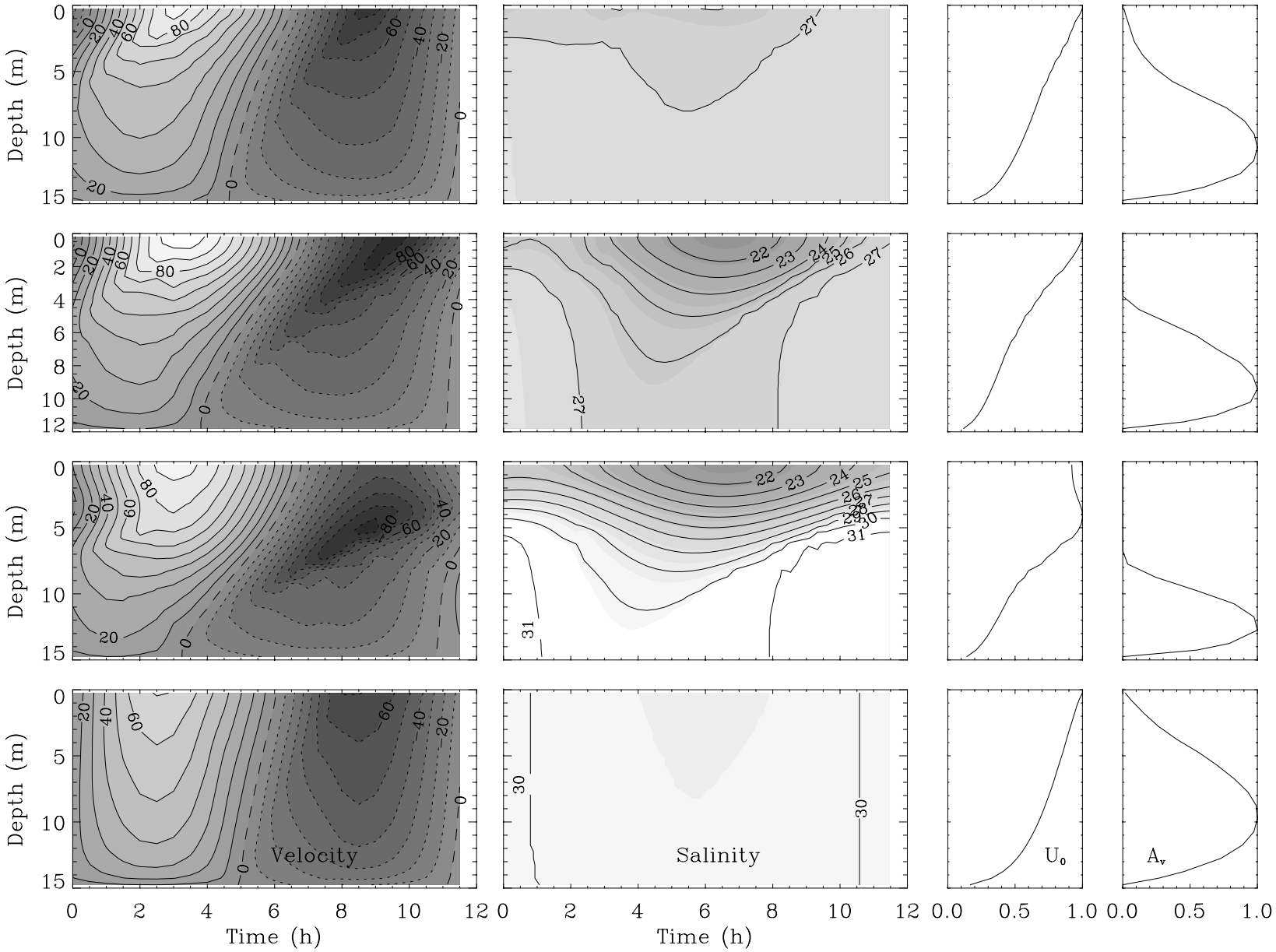

Figure 8. Results of experiments 5-8 of the one-dimensional mixed layer model. Description follows that of Figure 7. Values of maximum amplitude and viscosity for the four experiments are as follows: Exp 5: U0 78, Av 140; Exp 6: U0 96, Av 97; Exp 7: U0 81, Av 83; Exp 8: U0 69, Av 102.

The year of 1996 began with the wettest January and became the wettest year on record according to the USGS. The subtidal and semidiurnal tidal contributions to the data collected were separated using a least squares technique.

The subtidal flow along the shelf showed values that reached 0.55 m s^{-1} within the southward flowing plume of the Chesapeake Bay. The outflow developed over an ambient subtidal current that also flowed to the south throughout the section measured. The cross-shore component of the subtidal flow was in general directed onshore thus suggesting that the transect was located within the quasi-geostrophic turning region of the Chesapeake Bay plume. The surface salinity and temperature values displayed an along-shore front that delimited the offshore extent of the plume. The location of the plume front over the channel coincided with the offshore limit of the core of subtidal flow attributed to the plume.

The buoyant discharge related to the plume and the channel-shoals bathymetry noticeably modified the phase and amplitude of the semidiurnal tidal currents. The phase of the tidal currents inside the plume lagged behind the currents over the adjacent waters by approximately 80 minutes. Also, the phase inside the channel lagged behind the surrounding water due to the combined effects of bottom friction (less in the channel) and inertia (more in the channel). The amplitude of the tidal currents exhibited a maximum centered over the channel due to reduced friction there. The maximum amplitude was located at a depth of approximately 5 m in response to the decreased turbulent vertical eddy viscosity near the pycnocline, as shown by a one-dimensional mixed layer model.

A total of eight experiments with the mixed-layer model were carried out to investigate the effects of tidal forcing, wind stress, water column depth, and vertical and horizontal density gradients on the profile of the tidal current amplitude and the development of a subsurface maximum. This subsurface maximum formed under the combined influence of strong horizontal salinity gradients (4 units in 10 km), relatively weak tidal (0.5 m s^{-1}) and wind (< 0.1 Pa) forcing, and relatively deep (> 15 m) regions. It appeared in the zone of the pycnocline where turbulence was suppressed, as indicated by zero vertical eddy viscosities, thus eliminating any vertical transfer of horizontal momentum. The initial salinity (or density) profile prescribed in the model did not have a significant influence in altering the profile of the tidal current amplitude. The subsurface maximum in tidal current amplitude migrated to the surface with weaker salinity gradients, stronger tidal currents, stronger wind velocities (or winds blowing in the direction opposite to the baroclinic flow at the surface), or shallower water column depths than those mentioned above.

The results of this study suggested that the tidal currents on an inner shelf can be affected by both the plume of buoyant water flowing from an estuary and by any possible abrupt bathymetric changes of the area.

REFERENCES

Boicourt W. C. (1973) The circulation of water on the continental shelf from Chesapeake Bay to Cape Hatteras, Ph.D. Thesis, John Hopkins University, Baltimore, MD, 183 pp.

Boicourt W. C. (1981) Circulation in the Chesapeake Bay entrance region: estuary-shelf interaction. In: *Chesapeake Bay Plume Study: Superflux 1980*, NASA Conference Publication 2188, J. Campbell and J. Thomas, editor, Hampton, VA, pp. 61-78.

Browne D. R. and C. W. Fisher (1988) Tide and tidal currents in the Chesapeake Bay. NOAA Technical Report NOS OMA 3, U.S. Department of Commerce, Washington, DC, 84 pp.

Chao S.-Y. (1988) River-forced estuarine plumes. *Journal of Physical Oceanography*, **18**, 72-88.

Chao S.-Y. and W. C. Boicourt (1986) Onset of estuarine plumes. *Journal of Physical Oceanography*, **16**, 2137-2149.

Fisher C. W. (1986) Tidal circulation in Chesapeake Bay. Ph.D. Dissertation, Old Dominion University, Norfolk, VA, 255 pp.

Gill, A. E. (1982) *Atmosphere-Ocean Dynamics*, Academic Press, San Diego, CA. 662 pp.

Huzzey L. M. (1982) The dynamics of a bathymetrically arrested estuarine front. *Estuarine, Coastal & Shelf Science*, **15**, 527-552.

Johnson, D. R. (1985) Wind-forced dispersion of blue crab larvae in the Middle Atlantic Bight. *Continental Shelf Research*, **4**, 733-745.

Joyce T. M. (1989) On in situ "Calibration" of Shipboard ADCPs. *J. Atmos. Oceanic Technol.*, **6**, 169-172.

Kapolnai A., F. E. Werner and J. O. Blanton (1996) Circulation, mixing and exchange processes in the vicinity of tidal inlets: A numerical study. *Journal of Geophysical Research*, **101**, 14,253-14,268.

Largier J. L. and S. Taljaard (1991) The dynamics of tidal intrusion retention and removal of seawater in a bar-built estuary. *Estuarine, Coastal & Shelf Science*, **33,** 325-338.

Largier J. L. (1992) Tidal intrusion fronts. *Estuaries*, **15,** 26- 39.

Lwiza K. M. M., D. G. Bowers and J. H. Simpson (1991) Residual and tidal flow at a tidal mixing front in the North Sea. *Continental Shelf Research*, **11**, 1379-1395.

Mellor G. L. and P. A. Durbin (1975) The structure and dynamics of the ocean surface mixed layer. *Journal of Physical Oceanography*, **5**, 718-728.

Münchow A., A. K. Masse and R. W. Garvine (1992) Astronomical and nonlinear tidal currents in a coupled estuary shelf system. *Continental Shelf Research*, **12**, 471-498.

Noble, M. A., W. W. Schroeder, W. J. Wiseman Jr., H. F. Ryan, and G. Gelfenbaum (1996) Subtidal circulation patterns in a shallow, highly stratified estuary: Mobile Bay, Alabama. J. Geophys. Res. **101(C11)**. 25,689-25,703.

Paraso M. C. and A. Valle-Levinson (1996). Atmospheric forcing effects on sea level and water temperature in the lower Chesapeake Bay: 1992. *Estuaries*, **19(3)**, 548-561.

Redfield A. C. (1958) The influence of the continental shelf on the tides of the Atlantic coast of the United States. *Journal of Marine Research*, **16**, 432-448.

Sanders T. M. and R. W. Garvine (1996) Frontal observations of the Delaware Coastal Current source region. *Continental Shelf Research*, **16**, 1009-1021.

Simpson J. H. and A. J. Souza (1995) Semidiurnal switching of stratification in the region of freshwater influence of the Rhine. *Journal of Geophysical Research*, **100**, 7037-7044.

Souza A. J. and J. H. Simpson (1996) The modification of tidal ellipses by stratification in the Rhine ROFI. *Continental Shelf Research*, **16**, 997-1007.

Turner, J.S. (1973) *Buoyancy effects in fluids*. 367 pp. Cambridge University Press, New York.

Valle-Levinson A. (1995) Observations of barotropic and baroclinic exchanges in the lower Chesapeake Bay. *Continental Shelf Research*, **15**, 1631-1647.

Valle-Levinson A. and K. M. M. Lwiza (1997) Bathymetric influences on the lower Chesapeake Bay Hydrography. *Journal of Marine Systems*, in press.

Valle-Levinson A., J. M. Klinck and G. H. Wheless (1996) Inflows/outflows at the transition between a coastal plain estuary and the coastal ocean. *Continental Shelf Research*, **16**, 1819-1847.

Valle-Levinson A. and K. M. M. Lwiza (1995) The effects of channels and shoals on exchange between the Chesapeake Bay and the adjacent ocean. *Journal of Geophysical Research*, **100,** 18551-18563.

Valle-Levinson, A. and R. E. Wilson (1994) Effects of sill bathymetry, oscillating barotropic forcing, and vertical mixing on estuary/ocean exchange. *Journal of Geophysical Research*, **99,** 5149-5169.

Weaver A. T. and W. W. Hsieh (1987) The influence of buoyancy flux from estuaries on continental shelf circulation. *Journal of Physical Oceanography*, **17**, 2127-2140.

Wheless G. H. and A. Valle-Levinson (1996) A modeling study of tidally driven estuarine exchange through a narrow inlet onto a sloping shelf. *Journal of Geophysical Research*, **101(C11)**, 25,675-25,687.

HYDROGRAPHIC AND FLOW STRUCTURE IN THE CHESAPEAKE BAY MOUTH AND PLUME REGION UNDER HIGH FRESHWATER DISCHARGE CONDITIONS

Kristine Holderied*

Arnoldo Valle-Levinson

Center for Coastal Physical Oceanography
Old Dominion University
Norfolk, Virginia, USA, 23529

*Corresponding Author: kris@ccpo.odu.edu

Prepared for Continental Shelf Research

November 1997

ABSTRACT

Hydrographic and horizontal velocity measurements were obtained along three transects in the Chesapeake Bay mouth and plume region in order to characterize the spatial and temporal variability of salinity and flow in this area during a period of high river discharge and moderate wind forcing (3-7 June 1996). All three transects were characterized by a bathymetry consisting of a channel flanked by shoals. Tidal variability of the salinity and flow was dominated by the semidiurnal constituents, but contributions from the diurnal constituents were significant. Intratidal features included sharpening of the pycnocline in the channel after maximum ebb currents, due to tidal straining, and development of surface fronts over the channel shoulders, due to horizontal velocity convergence. Away from the bay mouth, intratidal observations indicated that the cross-shore movement of the low-salinity plume was controlled by direct wind forcing. However, both at the mouth and offshore, the subtidal, low-salinity core of the outflow plume was consistently located over the deep channel, reflecting the influence of bathymetry and inertial forces on subtidal circulation, and the dominance of gravitational forcing over the channel. Subtidal velocity data suggested the presence of a surface anticyclonic gyre at the northern portion of the bay entrance and a second anticylonic gyre south of the bay mouth, formed as the plume separated from the coast before turning southward. Subtidal horizontal velocity convergence of order 10^{-4} s^{-1} was consistently observed over the shoulders of the channel, produced by differences in the vertical structure of the flow over the shoals and in the channel. For the first time, subtidal salinity and flow fields were measured at sufficient spatial resolution to estimate the net, normalized salinity transport across the Chesapeake Bay mouth, which was calculated to be 1.36×10^4 m^3/s into the estuary.

INTRODUCTION

The study of interactions between estuarine and continental shelf circulations is crucial to understanding the fate of nutrients, pollutants and larvae transported between the estuary and the shelf. The exchange of water between the estuary and the ocean is complicated by the presence of multiple forcing mechanisms, including tides, freshwater runoff, winds, and barometric pressure. Bathymetry interacts with these mechanisms to modify the flow patterns. The typically shallow areas of the lower part of a coastal plain estuary and of the near coastal region allow for relatively rapid responses of circulation to changes in the local wind forcing. This rapid response, along with a typically large influence from the tides, results in circulation patterns that shift rapidly on time scales of a few hours.

The Chesapeake Bay is one example of a relatively wide coastal plain estuary with freshwater input from extensive river runoff over a large watershed. Circulation in the bay mouth and outflow region is significantly influenced by both buoyancy and tidal forcing, and depths in this region are shallow enough that local wind forcing is important. Several studies have shown the response of the density (Boicourt, 1981; Boicourt, *et al.*, 1987; Paraso and Valle-Levinson, 1996) and flow (Valle-Levinson and Lwiza, submitted) fields in the Chesapeake Bay plume to changes in the wind field. Northeasterly (onshore) winds have been shown to increase subtidal water elevations at the bay mouth and confine the plume tightly to the southern part of the estuary and along the coast to the south of the bay mouth. Conversely, southwesterly (offshore) winds reduce subtidal water elevations at the bay mouth and allow the plume to move further offshore before turning south along the coast. The semidiurnal tidal constituent dominates tidal forcing in the lower Chesapeake Bay, with interaction between the M_2, N_2, and S_2 constituents causing fortnightly and monthly tidal variability (Browne and Fisher, 1988). A distinct difference emerges between successive spring (or neap) tides, creating primary and secondary spring (and neap) tides within one month.

Our understanding of the effects of these forcing mechanisms on the Chesapeake Bay estuarine-coastal circulation has come primarily from information collected with moored instruments, with only limited spatial resolution. Recent measurements with a towed acoustic Doppler current profiler (ADCP) have provided much better spatial resolution of the flow field (Valle-Levinson and Lwiza, submitted), but only limited temporal resolution. Even with these limitations, such studies have illustrated the strong spatial and temporal variability, at relatively small scales, in this region. In order to describe and understand this variability, there is a need for basic hydrographic and current data, at the spatial scales of local bathymetric features and the temporal scales of tidal variability.

The objective of this study is to describe the hydrographic structure and flow field in the Chesapeake Bay outflow region during a period of moderate winds and high freshwater discharge. The detailed observations of the salinity and current fields in this study will facilitate interpretation of future ADCP current measurements obtained in the same region by different research programs. The observations will also help validate models of the Chesapeake Bay mouth and outflow region. It is intended that these observations will be compared to data from future studies in the region, under different wind and density forcing conditions.

DATA COLLECTION AND PROCESSING

Three transects (Figure 1) were surveyed from June 3 to 7, 1996, onboard the United States National Oceanic and Atmospheric Administration (NOAA) ship *Ferrel*. Ten repetitions were made of each transect over three successive, 25-hour periods. Using an Applied Microsystems EMP-2000 Conductivity-Temperature-Depth (CTD) recorder and current meter, vertical stations were occupied at approximately 1.8 km intervals along each transect. The CTD/current meter assembly was held for five seconds at approximately 0.5 meter depth intervals to accomodate the response time of the current meter, which had an accuracy of 0.015 m/s. The 25-hour sampling period facilitated separation of tidal and subtidal contributions from the observations. On June 3 and 4, ten stations were occupied along Transect 3, extending offshore 16.8 km to the east-northeast from Virginia Beach. On June 4 and 5, eleven stations were occupied along Transect 2, extending offshore 18.3 km to the northeast from Virginia Beach. Ten stations along Transect 1, extending 15.9 km across the Chesapeake Bay mouth from Cape Henry to Fishermans Island, were occupied on June 5 and 6. All three transects were approximately perpendicular to Chesapeake Channel and were characterized by a channel/shoals bathymetry. The northern portion of Transect 1 also crossed the shallower North Channel, just south of Fishermans Island.

The current velocity data were rotated to create along-channel (perpendicular to the transect) and across-channel (parallel to the transect) velocity components. The salinity, temperature, density and current velocity data were then interpolated to a grid with 300 m spacing in the horizontal, across-channel (along-transect) direction and 0.5 m in the vertical direction. Contoured hydrographic and flow fields on an across-channel versus depth grid were produced for each repetition of each transect, with data from the end stations used twice on successive repetitions. The buoyant surface water leaving the bay was warmer than the more saline shelf water, so the salinity, temperature and density fields had the same spatial and temporal structure. Only the salinity data are shown and discussed in detail here, with the understanding that they also represent patterns in the temperature and density data.

Wind and atmospheric pressure data were recorded by the ship's anemometer and barometer and also obtained from the southernmost island of the Chesapeake Bay Bridge-Tunnel (CBBT) and from the Chesapeake Light Tower (CLT) (see Figure 1 for locations). Wind observations on the ship and at CLT did not differ significantly from the observations on the CBBT, so only plots of CBBT winds are provided in this paper. Water elevation data were obtained from the CBBT tide gauge. Monthly freshwater discharges to the Chesapeake Bay before and during the study period were obtained from the United States Geological Survey (USGS). These values are calculated as the sum of net discharges measured from each of the major rivers in the bay.

Following the technique of Lwiza *et al.* (1991), a least squares fit, with periods of 12.42 hours (M_2 tidal component) and 23.93 hours (K_1 tidal component), was applied to the time series of salinity, density, and velocity components at each gridpoint for which there was data from every transect repetition. The fit produced the amplitude and phase for each of the chosen periods and the subtidal signal. The combined diurnal and semidiurnal tidal signal was then reconstructed from these parameters. Although the fit used the periods of the M_2 and K_1

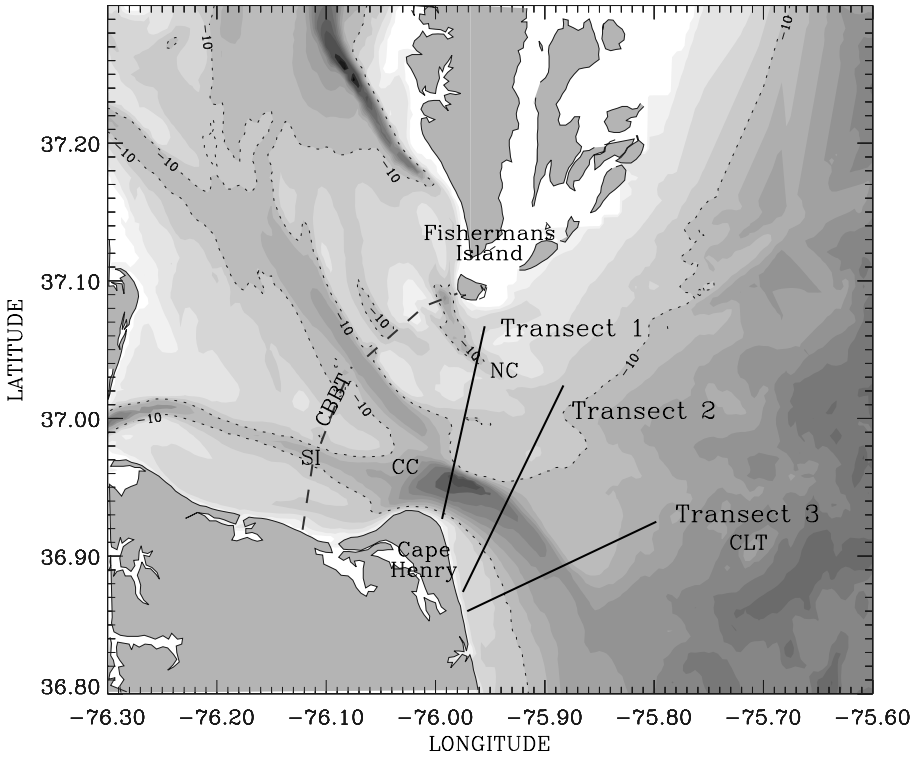

Figure 1. Lower Chesapeake Bay on the eastern coast of the United States. The map shows the locations of the three transects sampled during the cruise, with shaded bathymetry (dark tones are deep areas) and dotted lines marking the 10 m isobath. The Chesapeake Channel is marked as CC and the North Channel is marked as NC. The Chesapeake Bay Bridge-Tunnel (CBBT) is presented as a dashed line (marked as CBBT). The NOAA sea level and meterological station on the south island of the CBBT (marked as SI), and the NOAA meteorological station at the Chesapeake Light Tower (marked as CLT) provided wind and sea level information.

constituents, the 25-hr record from each transect was not sufficiently long to isolate these constituents from other semidiurnal (N_2 and S_2) and diurnal (0_1) constituents, so the fit actually reflected the combined effects of the semidiurnal constituents and the combined effects of the diurnal constituents. The least squares fit was effective in reproducing the observations along each of the transects, explaining a significant portion of the variability and yielding relatively low rms errors between fit and observed values (Figures 2, 3 and 4). The two component fit was better at Transect 1 than the other two transects, due to the reduced influence of tidal variability

at Transects 2 and 3. The fit for along-channel velocity was also generally better than that to across-channel velocity along each transect. An initial fit of the data to just the semidiurnal tidal component (not shown) generally explained 20-40% less of the variability and produced larger rms errors than did the fit with the two constituents. Similarly, adding an M_4 tidal constituent to the fit (not shown), did not produce noticeable improvement in either the amount of variability explained or in the rms error.

DESCRIPTION OF OBSERVATIONS

River discharge, water elevation and wind

The effects of river discharge at the bay mouth lag river discharge into the Chesapeake Bay by approximately one month, so the monthly averaged river discharge data from May were taken to be representative of the discharge conditions at the bay mouth in June. The monthly freshwater discharge data (Figure 5) indicated that high discharge conditions prevailed during the first six months of 1996 (which was a record year for freshwater discharge into the Chesapeake Bay), with values near 7,000 m^3/s in January decreasing to near 4,000 m^3/s from February through May, and continuing to decrease during the summer. May discharge amounts were relatively high, compared to the average monthly discharge of approximately 2,500 m^3/s (Goodrich, 1988).

The beginning of the study period coincided with predicted spring tides for the month and the subsequent neap tide occurred on June 8, after the end of the study period. Comparison of the CBBT water elevation observations with predicted tidal elevations for the same station indicated that a sea-surface set-up of up to 0.35 m occurred at the bay entrance immediately before sampling on Transect 3 (Figure 6). This set-up was caused by a brief period of relatively strong (up to 10 m/s) onshore (easterly and northeasterly) winds on June 3. After that, the water elevation dropped abruptly on June 4 with the onset of moderate to strong northwesterly and then southwesterly winds. For the rest of the study period, the water elevations remained just slightly above predicted values (by 0.1 m), under weaker winds that shifted to a mostly easterly direction later in the day on June 5.

Hydrography and Currents

Descriptions of the salinity and velocity data include intratidal features from the quasi-synoptic fields, and tidal properties and subtidal features from the fields reconstructed with the least squares fit.

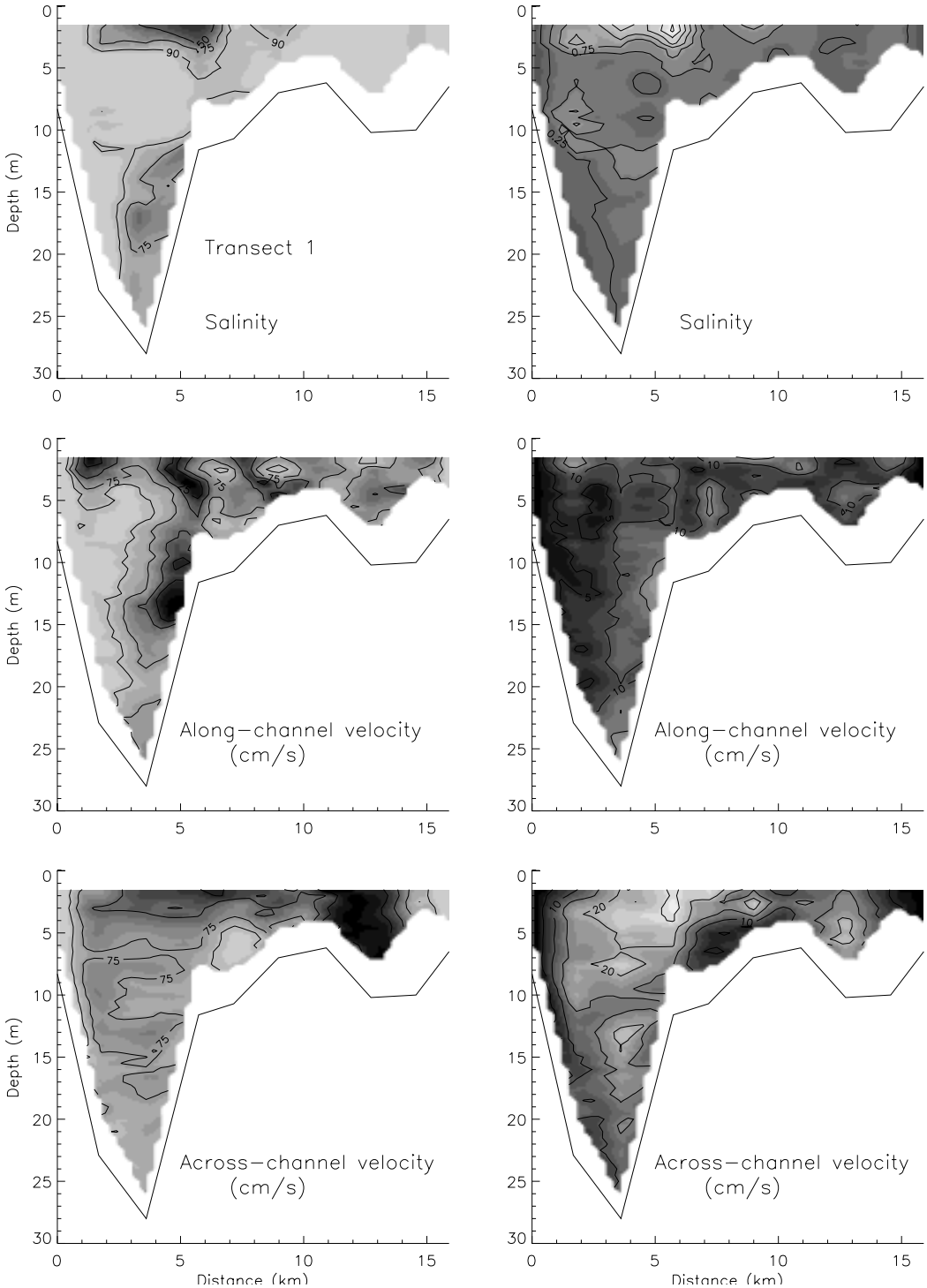

Figure 2. Percent variance explained by the least-squares fit to the semidiurnal and diurnal tidal frequencies (left column) and root-mean-square (rms) error between the fit and observed values (right column) for the salinity, along-channel velocity, and across-channel velocity fields of Transect 1. Percent variance is contoured at the 90, 75, 50 and 25 percent levels. Rms error contours are drawn at 0.25 psu intervals for salinity and 5 cm/s intervals for velocity. Lighter shading indicates higher values in each case and plots are drawn looking into the estuary.

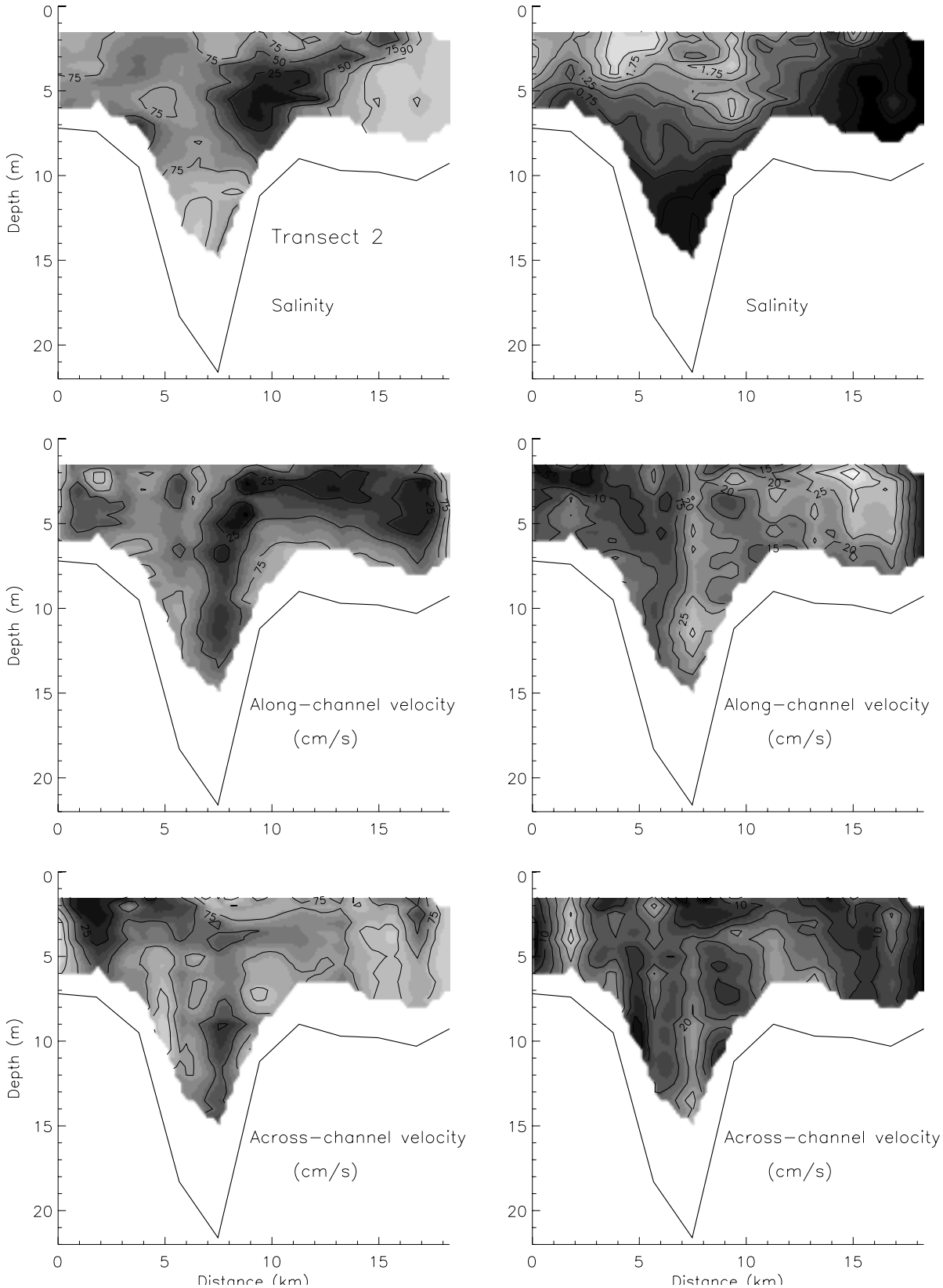

Figure 3. Same as Figure 2 for Transect 2.

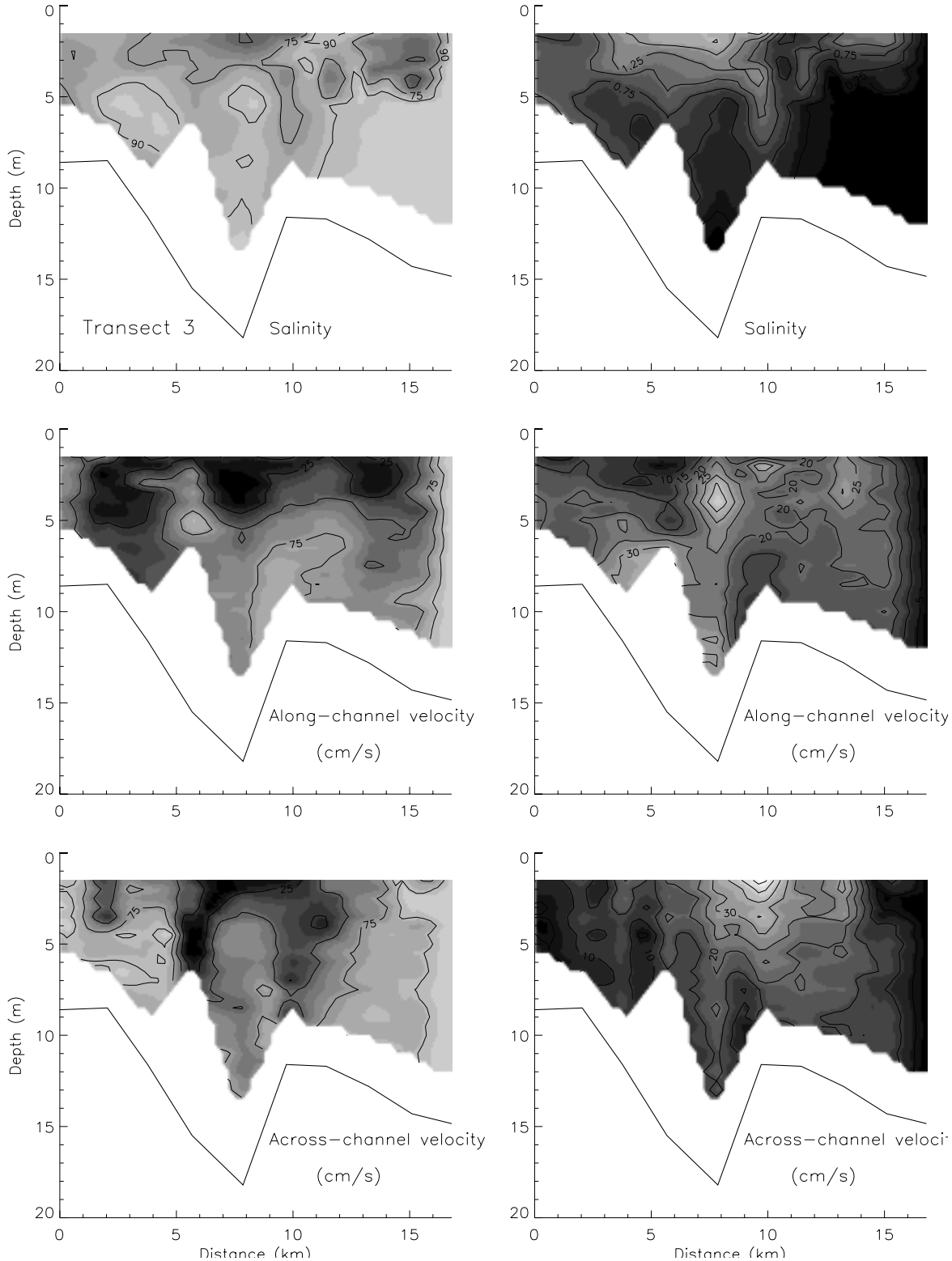

Figure 4. Same as Figure 2 for Transect 3.

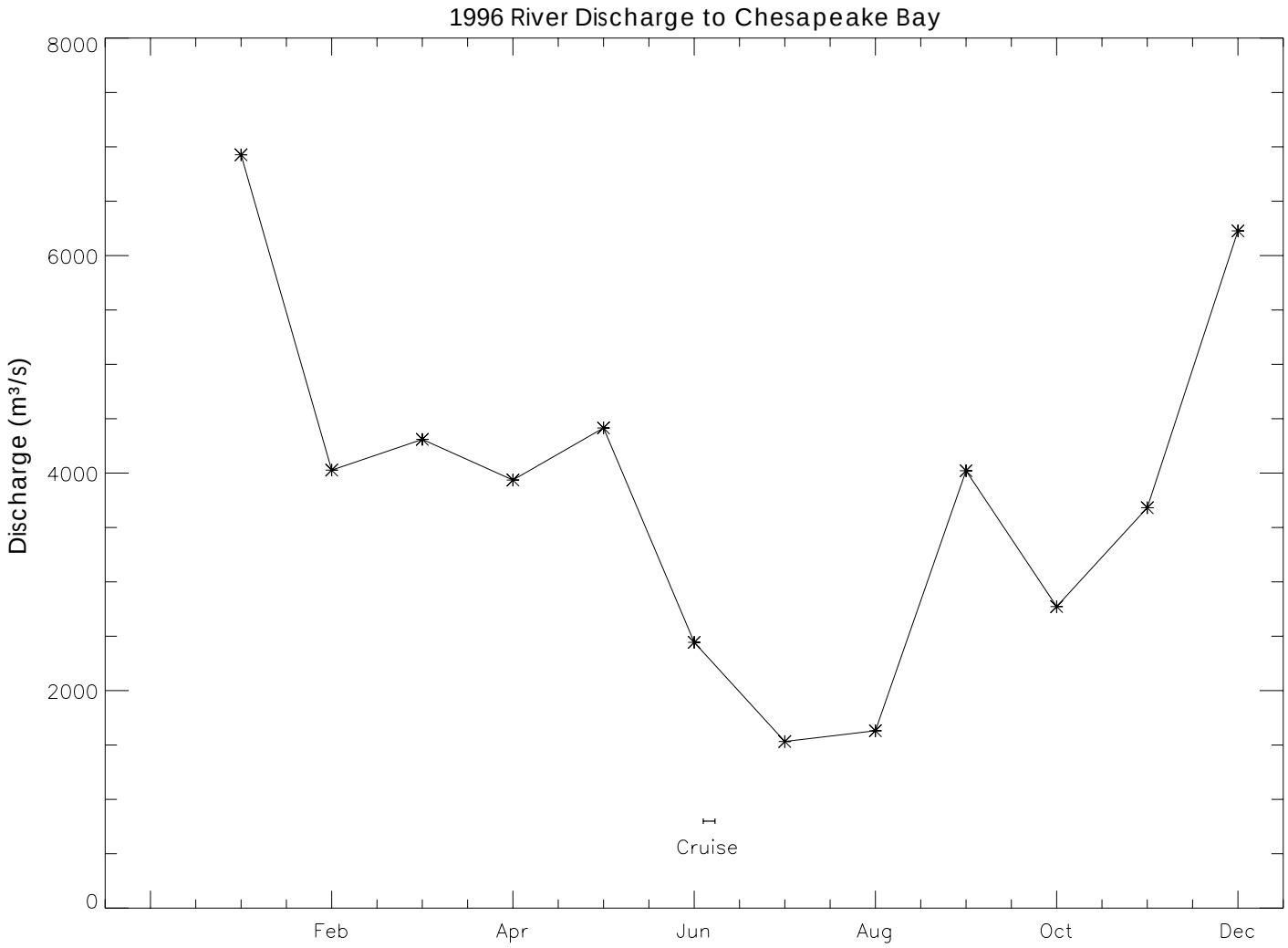

Figure 5. Monthly freshwater discharge (m^3/s) to the Chesapeake Bay for 1996, with the sampling period of this study marked on the plot. Note that freshwater forcing at the bay mouth lags river discharge by approximately one month.

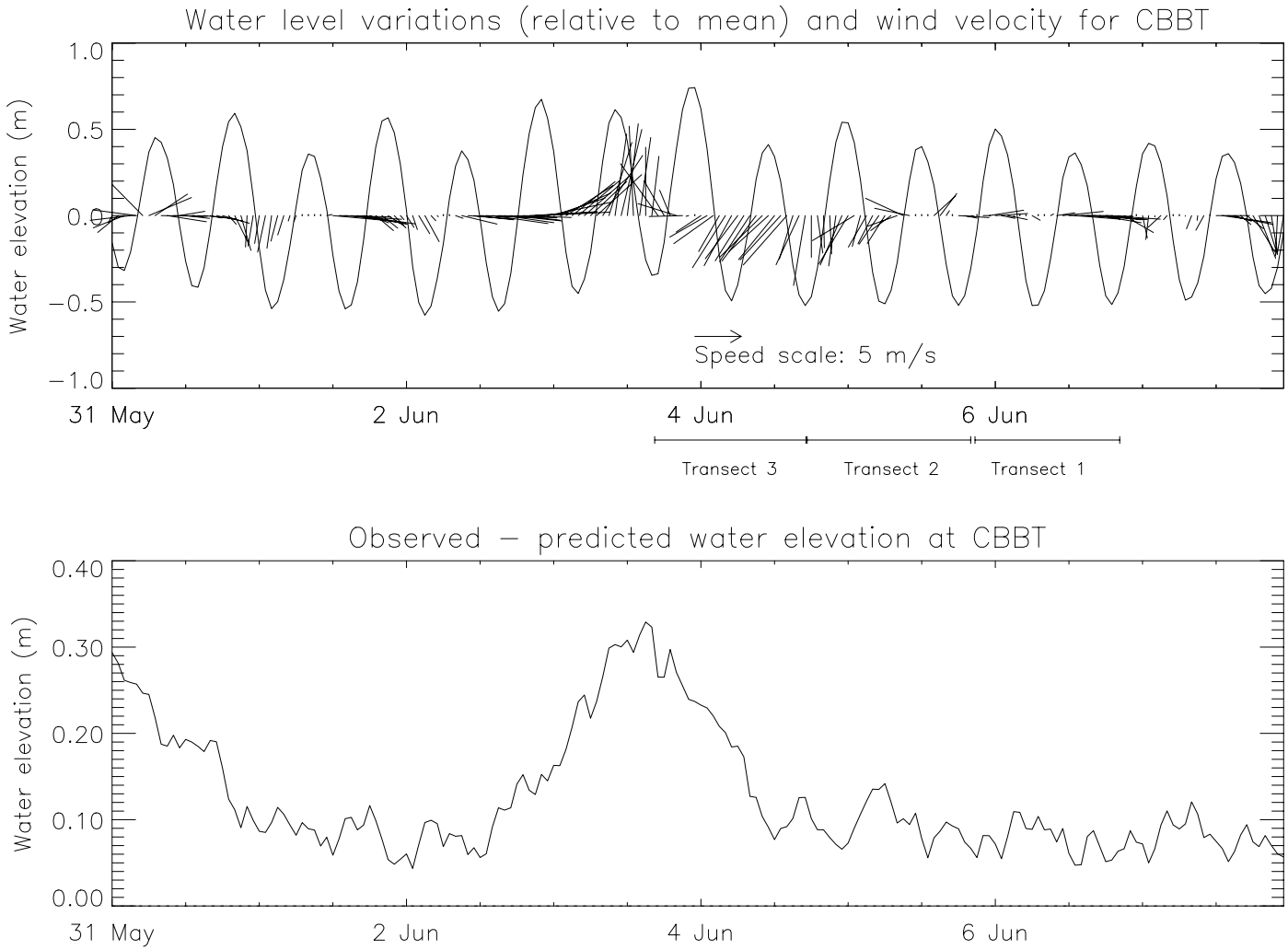

Figure 6. Water level variations, relative to sample mean, and wind velocity data from the NOAA tide gauge and meteorological station at the South Island of the CBBT (upper plot). Difference between observed and predicted water elevations at the CBBT tide gauge (lower plot). Wind direction is in the meteorological sense, indicating the direction that the wind is coming from. The duration of sampling along each transect is marked between the two plots.

Intratidal Patterns

Quasi-synoptic snapshots of salinity and velocity along each transect (Figures 7, 8 and 9) illustrate the intratidal salinity and flow variations during the study period. The substantial changes observed in the fields between successive transect repetitions illustrate the dynamic nature of the circulation in the plume region and the difficulty of capturing a truly synoptic picture. Features from the quasi-synoptic data fields are discussed below for each transect.

Transect 1: Along Transect 1 (Figure 7), stratification persisted throughout the tidal cycle in the channel, with fresher surface outflow over the more saline, subsurface inflow. The sharpest pycnocline developed just after maximum ebb tidal currents in the channel, with vertical density gradients as high as 4 σ_t /m. Surface fronts developed over the northern shoulder of the channel near the time of maximum flood currents in the channel and were associated with horizontal surface convergence in the across-channel velocities (repetition 8). Near the end of flood currents, a narrow band of higher salinity water intruded along the southern coast, creating a second surface front between these shelf waters and the buoyant surface outflow that was pushed slightly offshore. Over the shoals in the northern portion of the transect, the water column was vertically mixed for most of the sampling period, with salinity increasing to the north.

The strongest instantaneous along-channel currents (0.8 m/s) of Transect 1 occurred as inflow over the channel, within a subsurface core centered at approximately 15 m depth (repetition 8). Outflow velocities reached 0.7 m/s at maximum ebb, generally with maximum currents at the surface, although subsurface maxima were also found over the shoals. Vertical shears in the along-channel flow were as high as 0.2 s^{-1} over the channel when ebbing surface currents opposed flooding currents at depth (repetition 1). The instantaneous across-channel velocities were generally smaller than the along-channel velocities, but did reach up to 0.7 m/s (repetition 5). Examination of vector plots (not shown) indicated that these high across-channel velocity values occurred as tidal currents rotated from outflow to inflow after the end of ebb currents.

Transect 2: The channel of Transect 2 was located further offshore than it was on Transect 1, but the most stratified conditions (up to 4 σ_t /m) still occurred over the channel just after maximum ebb currents (Figure 8). Surface fronts developed over the north shoulder of the channel (repetitions 6 and 8), and at times over the south shoulder as well (repetition 6), as was observed by Sanders and Garvine (1996) for the Delaware Coastal Current. The sharpest front occurred towards the end of flood currents over the northern shoulder of the channel (repetition 6), however, a front also occurred over the same shoulder shortly after maximum surface ebb currents in the channel (repetition 8). The buoyant plume moved laterally to a much greater extent than it did in Transect 1, with the core of lower salinity surface water moving completely across the transect during the tidal cycle.

Instantaneous velocity fields over Transect 2 had highest values (1.3 m/s) in a northwestward (inflow) subsurface jet in the channel associated with the flood tide. The strongest southeastward flow (outflow) reached 0.9 m/s, with surface maxima found both over the channel and over the shoals. Relatively strong subsurface outflow was also found over the shoals and southwest channel shoulder, similar to the Transect 1 data. Vertical shears in the along-channel local instability in the density fields evident at the location of the highest velocity shears

(repetition 1). In contrast to Transect 1, high vertical shear in the along-channel velocity was also found over the northeastern shoal, rather than being confined to the channel. This high shear accompanied the lateral movement of the plume over the shoal. The instantaneous across-channel flow of up to 0.6 s^{-1} and development of a sharp pycnocline occurred after maximum ebb currents, with low was also significant, reaching up to 0.7 m/s when tidal currents rotated between ebb and flood stages. Surface front formation was again associated with horizontal convergence in the across-channel flow (repetition 3).

Transect 3: Enhanced stratification over the channel, with more homogeneous conditions over the shoals was also found along Transect 3 (Figure 9). As in the previous transects, the pycnocline sharpened (vertical density gradients up to 2 σ_t /m) over the channel as saline inflow at depth opposed the ebbing surface flow (repetition 1). A surface front (6 σ_t in 1300 m horizontal distance) appeared over the right (looking into the bay) shoulder of the channel at the end of flood currents in the channel (repetition 4). The low salinity plume extended across most of the transect at times, with surface flood currents over the channel occasionally separating two surface salinity minima over the shoals on either side (repetitions 6 and 7).

The instantaneous velocity fields of Transect 3 exhibited a subsurface inflow jet (1.3 m/s) during flood, and a slightly weaker (0.7 m/s) surface outflow maximum during ebb. Over the channel and eastern shoal, vertical shears in the along-channel flow of up to 0.2 s^{-1} were again found when surface ebb flow opposed flood currents at depth (repetition 1). In the channel, flow was persistently northwestward (toward the bay mouth), and even the surface currents did not always reverse direction toward the southeast during ebb, but simply decreased in magnitude. The across-channel flow had maximum values reaching 1.1 m/s. Strong horizontal convergence of the across-channel flow was again associated with the formation of surface fronts (repetitions 1 and 4).

Tidal Patterns

Along Transect 1, a maximum in the semidiurnal tidal amplitude of the salinity field, extended north from the southern side of the transect, centered at 4 to 6 meters depth (Figure 10). This maximum was due to the relatively large salinity variations associated with the lateral movement of the surface plume and intrusion of more saline shelf water along the southern coast. Both the semidiurnal and diurnal amplitudes in salinity were reduced at depth in the deep channel, as bottom friction reduced the tidal excursions. The semidiurnal tidal amplitude of the along-channel velocity had a subsurface maximum centered over the deep channel, decreased over the shoals, and then increased slightly over the North Channel. The semidiurnal phase of the along-channel velocity also varied laterally, with the shoals and the southern side of the channel leading the center portion of the deep channel. The diurnal along-channel velocity amplitudes had a subsurface maximum over the south side of the channel, a minimum near the surface over the northern shoulder of the channel, and a secondary surface maximum over the shoal area. The across-channel velocity had semidiurnal and diurnal tidal amplitude maxima over the channel.

Similar features were found in the tidal properties along Transect 2 (Figure 11) and Transect 3 (Figure 12), with highest amplitudes tending to occur in the channel and phase leading near the bottom relative to the surface and over the shoals relative to the channel. In some cases, amplitude maxima occurred below the surface, near the pycnocline. The amount of spatial

variability in the amplitude and phase contours probably reflected difficulty in resolving the intratidal flow reversals with the given station spacing in distance and time between stations.

Subtidal Patterns

Transect 1: The subtidal salinity and velocity fields for Transect 1 are shown in Figure 13a. Lowest salinity water was confined to a core, approximately 3 km wide, at the surface over the southern side of the Chesapeake Channel, separated from Cape Henry. Highest salinity water along the transect was found in the deepest part of the Chesapeake Channel. At the surface there was along-channel outflow over the north shoulder of the deep channel associated with the plume (0.3 m/s maximum), a narrow inflow along the coast off Cape Henry and an inflow maximum (0.25 m/s) over the shoal. A weak outflow (northeastward) was present at all depths in the North Channel. Along the southern coast, the plume narrowed with increasing depth, reaching a depth of 10 m. In the deep channel, the outflowing surface vectors rotated anticyclonically with depth to an inflow (northwestward) direction. The transition to inflow occured at shallower depths over the channel axis and at greater depths over the shoals. The deeper flow was into the bay, aligned with the Chesapeake Channel and reaching a subsurface maximum of 0.4 m/s. The across-channel subtidal velocities were smaller than the along-channel velocities, with maximum values of 0.2 m/s and most values less than 0.1 m/s. Subtidal surface convergences of order 10^{-4} s^{-1} were found over each side of the Chesapeake Channel, with surface divergences of similar magnitude over the center of the deep channel and over the shoal.

Transect 2: The subtidal, low salinity surface plume was also centered over the channel along Transect 2 (Figure 13b), with higher values than those observed on Transect 1, as expected, since Transect 2 was further from the bay mouth. Surface salinities increased over the shoal areas on each side, with higher surface values on the seaward side and highest overall salinity found in the bottom of the channel. The along-channel velocity had a surface outflow (southeastward) maximum over the seaward shoulder of the channel (0.25 m/s) with outflow continuing over the seaward shoal, but surface inflow present along the coast. At greater depths, the flow near the coast continued to flow toward the bay mouth, while flow along the rest of the transect rotated anticylonically with depth from outflow to inflow. Below approximately 8 m depth, all flow was towards the bay mouth and aligned with the bathymetry, with a subsurface maximum (0.6 m/s) in the center of the channel. The across-channel subtidal flow was again weaker than the along-channel flow (maximum near 0.25 m/s) and had horizontal convergences of up to 10^{-4} s^{-1} over both shoulders of the channel.

Transect 3: The subtidal, low salinity plume was quite broad along Transect 3, but was still centered over the channel (Figure 13c). Highest salinities were now found at depth at the offshore end of the transect, rather than in the channel, because the channel was not much deeper than the offshore station. The subtidal outflow (southeastward) was weak (< 0.1 m/s) and was only found above 2 meters depth, seaward of the center of the channel, with weak inflow at the surface on the landward half of the transect. The subtidal flow reflected the influence of offshore plume movement as winds shifted to a southerly direction during sampling on this transect. The surface outflow rotated quickly to inflow (northwestward) with increasing depth, and only inflow was found below 4 m depth. The vertical rotation was again anticyclonic, and occurred at shallower depths in the channel and deeper depths over the shoals. With increasing depth, the

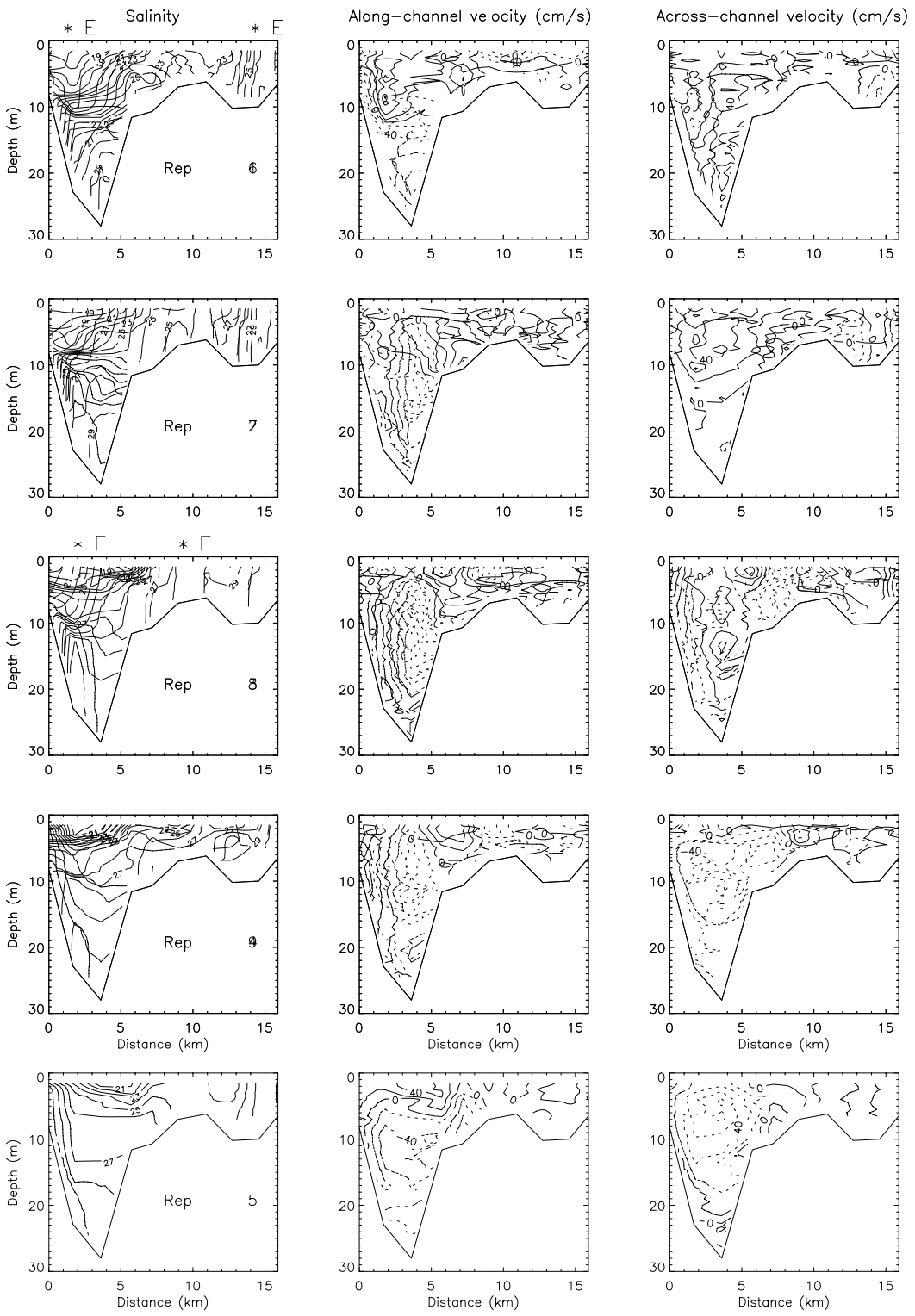

Figure 7. Contoured salinity, along-channel velocity and across-channel velocity data for successive repetitions of Transect 1. Contours are drawn at intervals of 1 salinity unit and 5 cm/s for velocity. Positive values of along-channel velocity indicate flow out of the bay, and positive values of across-channel velocity indicate northward flow. Times of maximum flood and ebb currents at depth in the channel are marked with asterisks above the salinity plot. Plots are drawn looking into the estuary.

TRANSECT 1

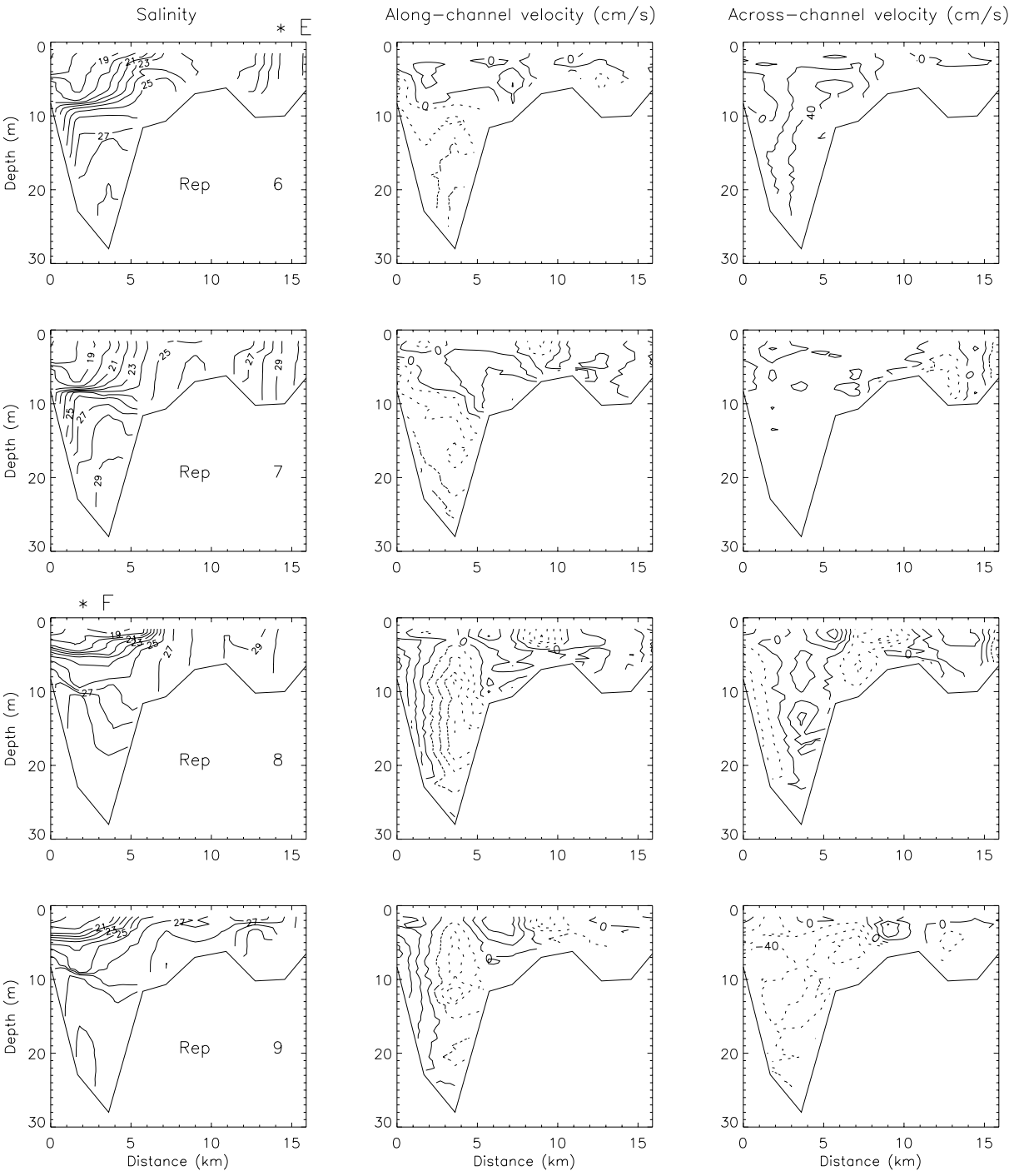
Salinity
Along−channel velocity (cm/s)
Across−channel velocity (cm/s)
* E
* F
Depth (m)
Rep 6
Rep 7
Rep 8
Rep 9
Distance (km)

TRANSECT 2

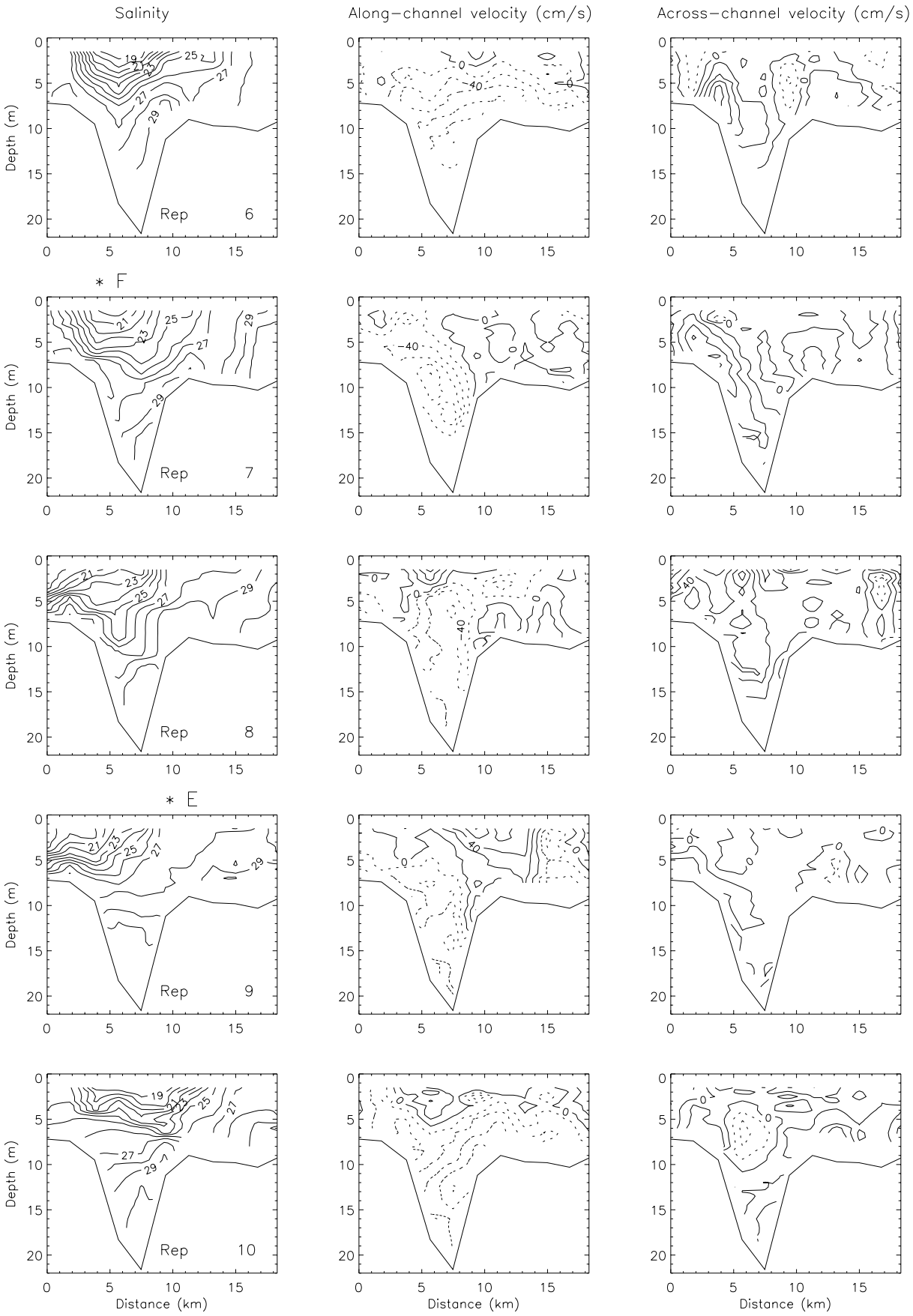
Salinity
Along−channel velocity (cm/s)
Across−channel velocity (cm/s)
Depth (m)
Rep 6
* F
Rep 7
Rep 8
* E
Rep 9
Rep 10
Distance (km)

TRANSECT 2

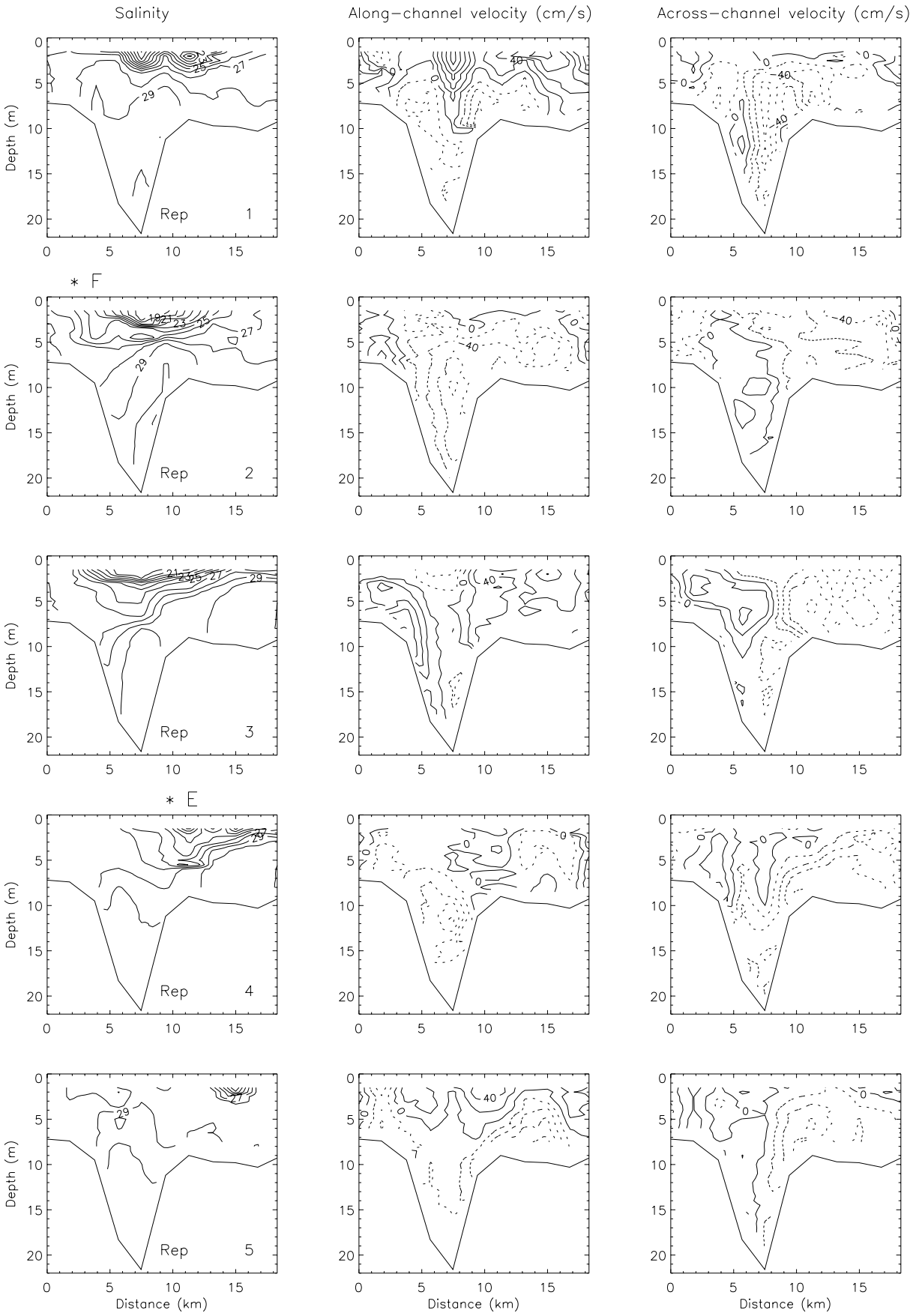
Salinity
Along−channel velocity (cm/s)
Across−channel velocity (cm/s)
Depth (m)
Rep 1
* F
Rep 2
Rep 3
* E
Rep 4
Rep 5
Distance (km)

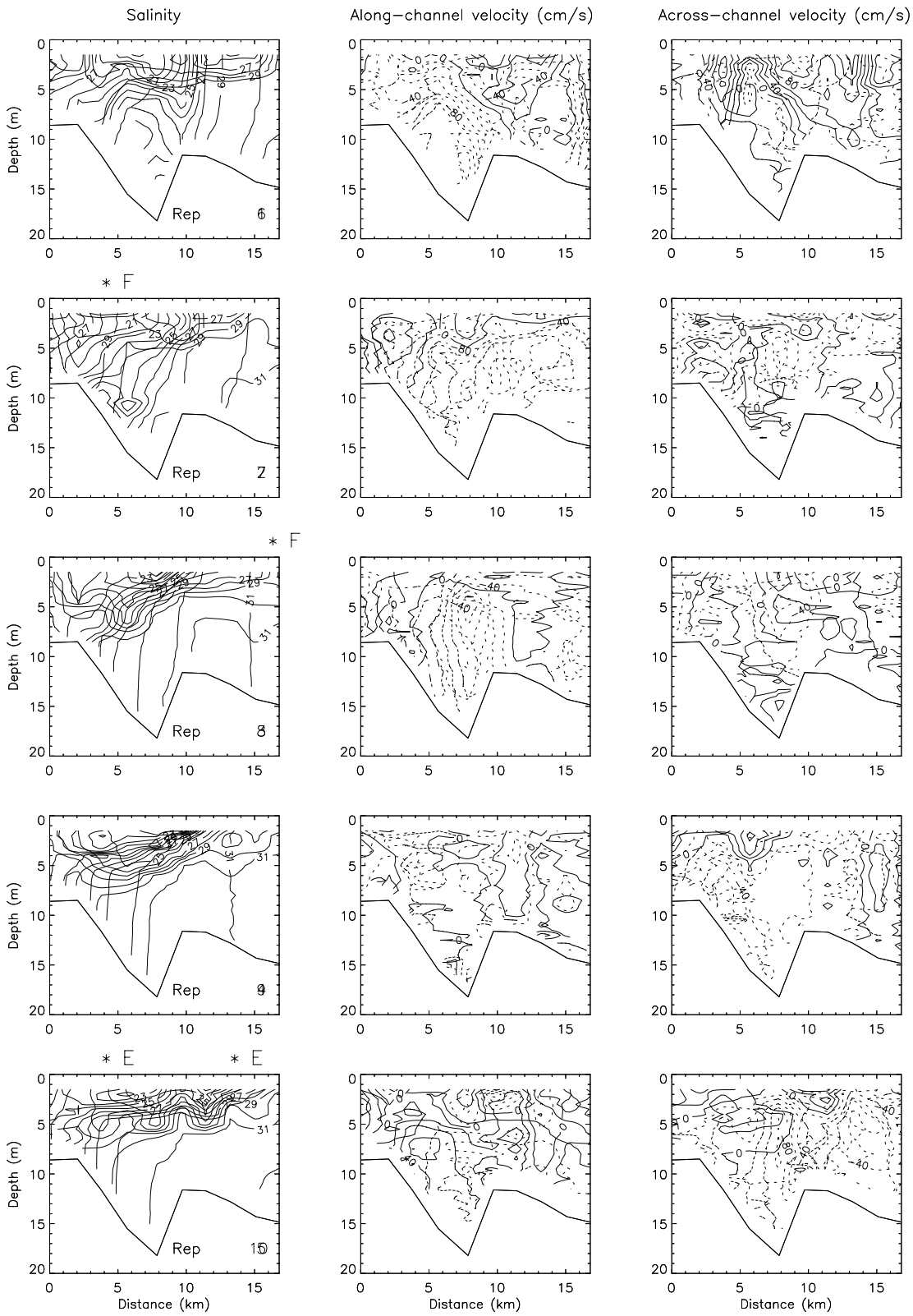

Figure 9. Same as Figure 7 for Transect 3. Positive values of along-channel velocity indicate northwestward flow toward the bay mouth. Positive values of across-channel velocity indicate east-northeastward or seaward flow.

TRANSECT 3

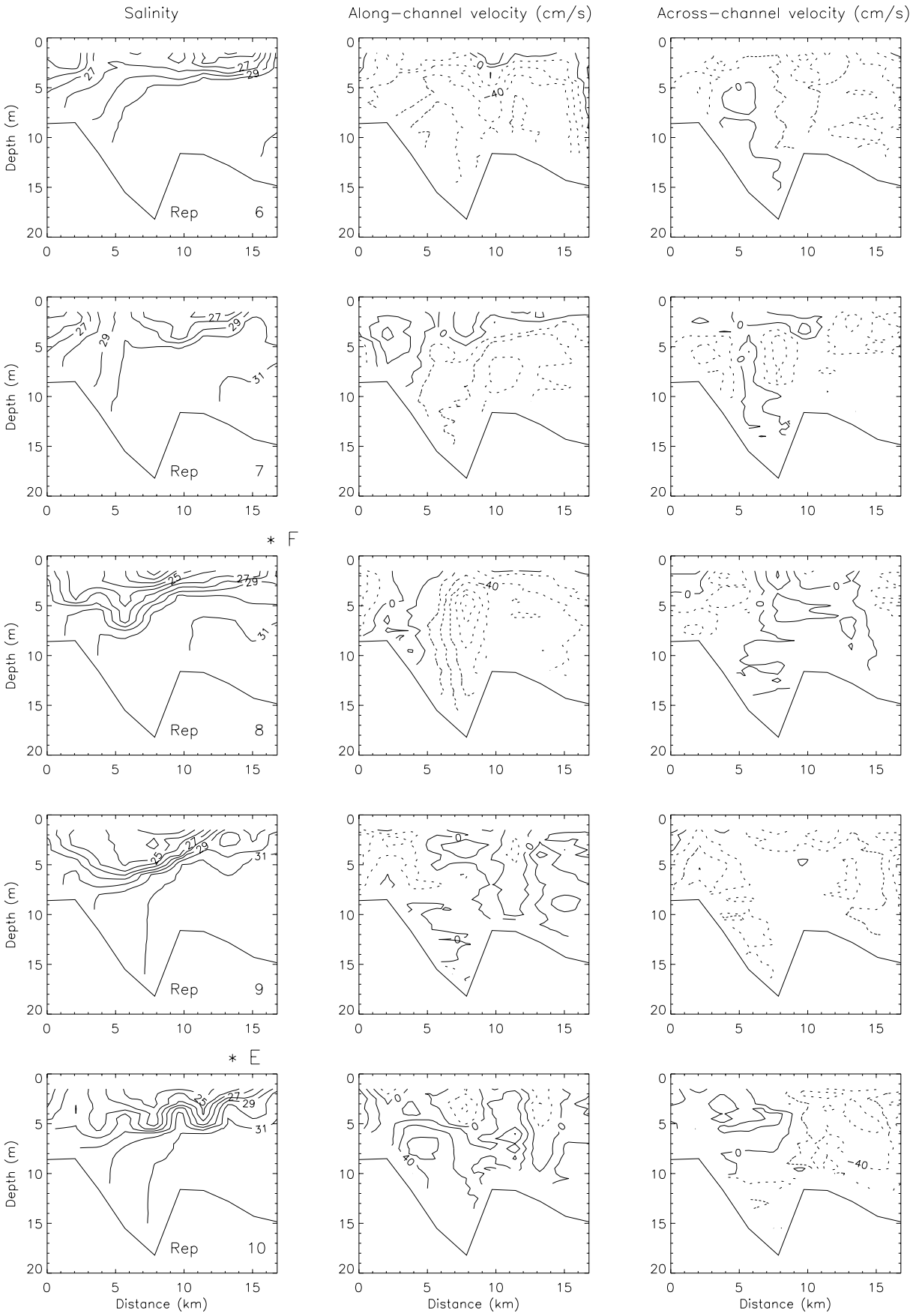
Salinity
Along−channel velocity (cm/s)
Across−channel velocity (cm/s)
Depth (m)
Rep 6
Rep 7
* F
Rep 8
Rep 9
* E
Rep 10
Distance (km)

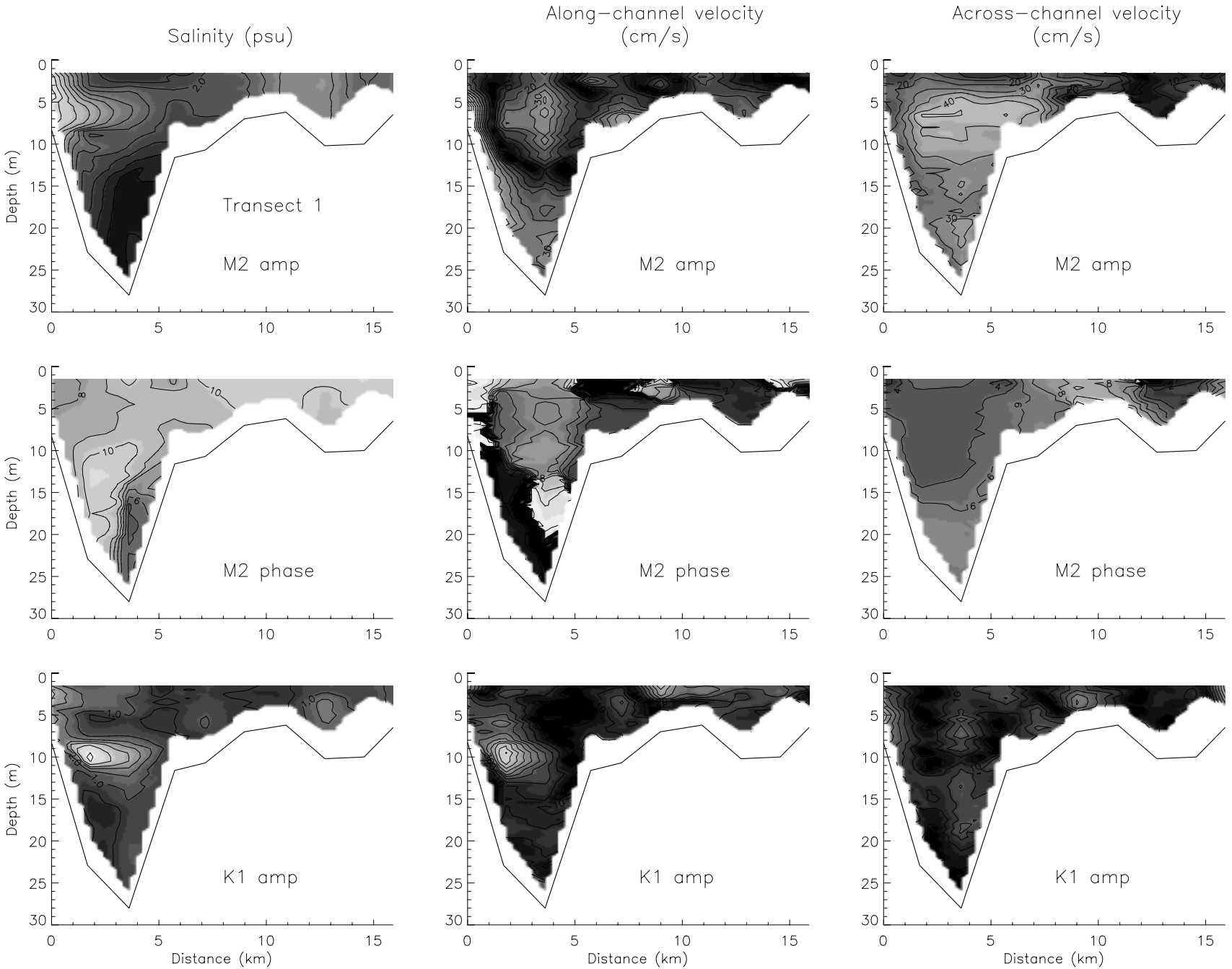

Figure 10. Contoured semidiurnal amplitudes and phases and diurnal amplitudes for salinity, along-channel velocity and across-channel velocity for Transect 1. Tidal amplitudes are contoured at intervals of 0.5 salinity units and 5 cm/s for velocity. Tidal phases are contoured at 1 hour intervals. Lighter shading indicates higher values in all cases and plots are drawn looking into the estuary.

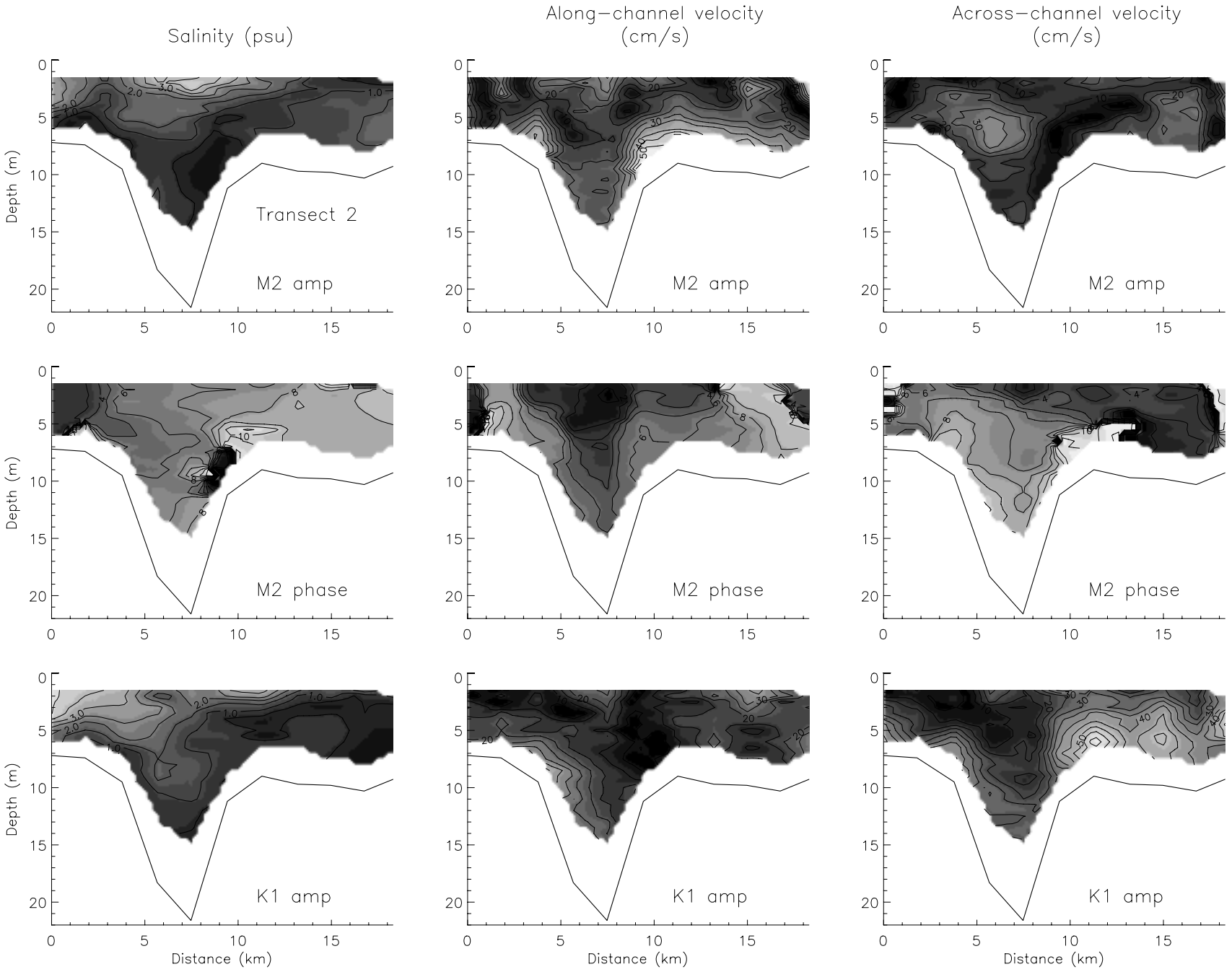

Figure 11. Same as Figure 10 for Transect 2.

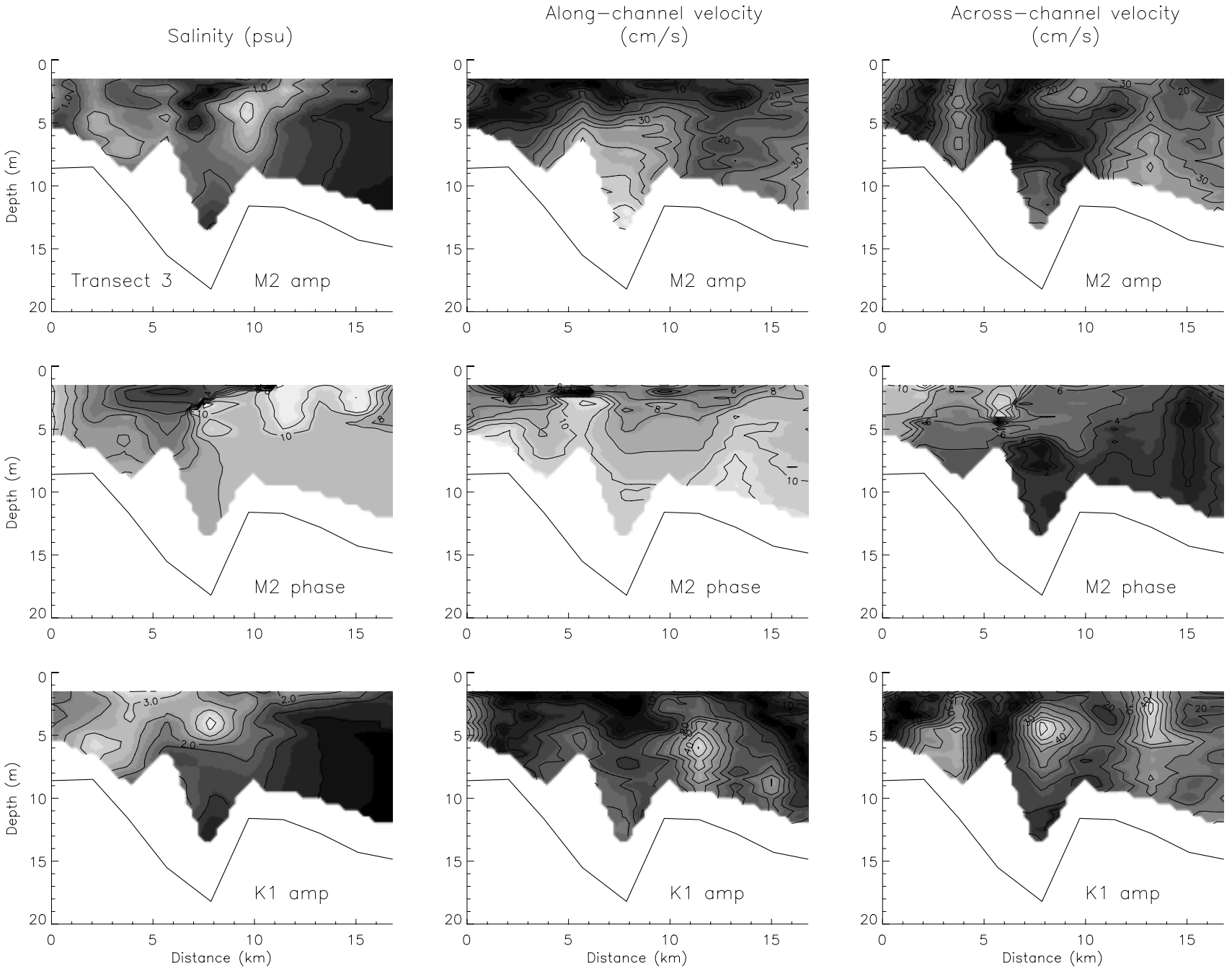

Figure 12. Same as Figure 10 for Transect 3.

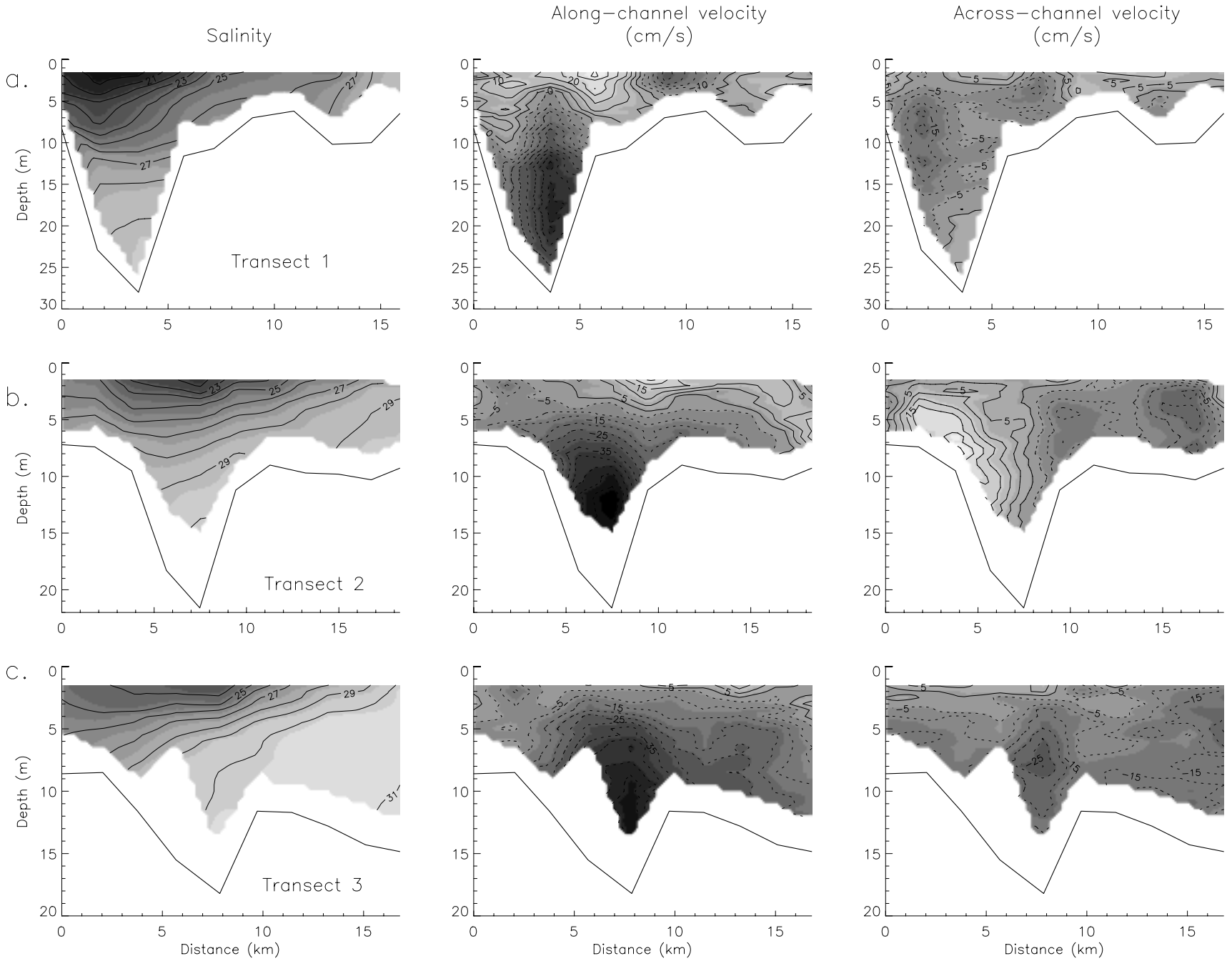

Figure 13. Contoured subtidal salinity, along-channel velocity and across-channel velocity data for: a. Transect 1, b. Transect 2, and c. Transect 3. Salinity data are contoured at intervals of 1 salinity unit and velocity data are contoured at 5 cm/s intervals. Plots are drawn looking into the estuary.

inflow aligned with the channel bathymetry, reaching a subsurface maximum of 0.5 m/s in the channel. The across-channel velocity was mostly landward, with a subsurface maximum (0.3 m/s) in the channel. Seaward across-channel velocities were found near the surface on the southern side of the transect, producing horizontal surface convergences of order 10^{-4} s^{-1} over the seaward shoulder of the channel.

DISCUSSION

Earlier studies in the region of the Chesapeake Bay entrance (Boicourt, 1981; Goodrich, 1987; Valle-Levinson and Lwiza, 1995; Valle-Levinson and Lwiza, submitted) have described mean flow patterns and looked at features such as the influence of the channel/shoal bathymetry on lateral locations of the flow. Numerical simulations of estuary-shelf circulation patterns induced by wind, tidal and gravitational forcing have shown that these mean flows may affect larval recruitment through the transport and dispersal of planktonic larvae to and from the Chesapeake Bay (Johnson and Hess, 1990). Smaller-scale circulation features will also impact processes such as larval recruitment if their time and space scales match the scales associated with the biological processes, such as spawning location and duration of the larval stage. Therefore, characterizing and understanding the smaller-scale patterns in the hydrographic and flow fields at the bay mouth, under various forcing conditions, is a necessary part of understanding the variability in processes such as larval recruitment. In this study, we used hydrographic and velocity observations, collected at a 2 km spatial resolution, to examine such smaller-scale features in the intratidal, tidal and subtidal fields at the bay mouth and in the offshore plume region. Our study period was characterized by high freshwater discharge and moderate wind forcing conditions. Tidal forcing was also relatively strong, with spring tides occurring at the beginning of the cruise.

Intratidal patterns: High spatial and temporal variability in the intratidal salinity and flow fields were observed in this study along all three transects (Figures 7, 8 and 9). Stratified conditions and two-way flow persisted over the Chesapeake Channel on all three transects (also occurring to a lesser extent in the North Channel along Transect 1), while vertically homogeneous conditions and unidirectional currents predominated over the shoals for most of the tidal cycle. Depth-independent tidal flow over the shoals was associated with increased vertical mixing (either tidally-induced or wind-driven) in shallow waters, while higher stratification and two-way circulation in the channel indicated the greater influence of gravitational forcing. In the channels, maximum vertical stratification occurred towards the end of ebb currents due to tidal straining (Simpson, *et al*, 1990), as has also been observed by Valle-Levinson and Lwiza (1995) along a transect upstream of the CBBT. Strong vertical shears of up to 0.4 s^{-1} in the along-channel velocity and sharp pycnoclines (with vertical density gradients of up to 4 σ_t /m) developed in the channel along each transect when surface outflow opposed subsurface inflow. Bulk Richardson numbers were calculated for local areas of high velocity shear in the water column and ranged from 0.03 to 1.0, with values less than 0.25 indicating that shear instability may sometimes dominate the density distribution at vertical scales of ~l m. Vertical spreading of the isopycnals was observed in some cases in these regions, and the observation of stronger velocity shears (0.6 s^{-1}) along Transect 2 was accompanied by indications of instability in the density data over ~1 m depth. However, the density contrast between the fresher surface outflow and more saline inflow maintained stratification over the entire water column in each case.

Surface fronts developed over the right shoulder of the channel (looking into the estuary) along all three transects, and were associated with horizontal convergence in the across-channel velocity. These fronts developed at different stages of the tidal flow in the channel, including after maximum ebb currents (Transect 2, repetition 6), near maximum flood currents (Transect 1, repetition 8), and near the end of flood currents (Transect 2, repetition 8; Transect 3, repetition 4). The front that formed in the latter stages of ebb flow along Transect 2 was accompanied by a second front over the left shoulder of the channel, suggesting formation of a plume front along the edge of the advancing plume, which was centered over the channel at that time. Frontal formation at the other stages of the tide appeared to be associated with large phase shifts (up to 3 hrs) between tidal flow over the shoals and in the channel, which produced horizontal velocity convergence over the right shoulder of the channel. Along Transect 1, formation of a front offshore from Cape Henry was associated with the inflow of shelf water and surfacing of isohalines along the coast near the end of flood currents.

Increased lateral movement of the low-salinity core of the plume towards and away from the coast in the offshore region south of Cape Henry (Figures 8 and 9), relative to the bay mouth (Figure 7), was associated with the increased influence of inertial effects as the plume exited the bay and with temporal changes in wind forcing. Away from the mouth, inertial effects were expected to be most influential at maximum ebb currents, when the surface velocities were strong enough to overcome the tendency of the Coriolis force to constrain the plume to the coast. There was some evidence of this behavior along Transect 2 (repetition 4), but, overall, wind forcing appeared to have more of an effect than inertial forcing on lateral plume location along both Transects 2 and 3. At the beginning of sampling on Transect 3, relatively strong (near 10 m/s) northerly and northwesterly winds prevailed, then shifted to southwesterly (Figure 6). The salinity minimum and strongest southward surface flow were located close to the coast at the beginning of the sampling period (Figure 9, repetitions 1-3) and then migrated offshore after the onset of southwesterly winds (Figure 9, repetition 4). So offshore movement of the plume along Transect 3 was associated with direct frictional coupling of the southwesterly winds with the ocean surface and subsequent offshore transport. Along Transect 2, the salinity minimum associated with the plume remained offshore (Figure 8) until after the winds shifted from a southerly (with speeds of 5-10 m/s) to more northerly direction (5 m/s). As the southwesterly winds relaxed and then shifted to a northerly direction, the plume moved toward the coast and remained there through the remainder of sampling along Transect 2, suggesting that northerly winds (or the absence of southwesterly winds) allowed the plume to return to the coast. Thus, the instantaneous lateral location of the offshore surface plume did appear to be strongly influenced by wind forcing. At Transect 1, the low-salinity plume remained relatively close to the coast during the entire period (Figure 7), under light, easterly wind conditions.

Tidal patterns: The semidiurnal tidal constituent was consistently more important than the diurnal constituent for salinity and along-channel velocity, but the diurnal constituent was still significant and necessary to produce a fit that reproduced the observations reasonably well. The two-constituent fits to the salinity and along-channel velocity data were better along Transect 1 than either of the other two transects, with smaller rms differences between the observed and fit values and a greater amount of variance explained. The better performance of the fit along Transect 1 indicated that tidal forcing was relatively more important at the bay mouth than in the region immediately offshore from the mouth (or conversely, that the offshore region was affected

more by nontidal processes), which is consistent with the previously discussed links between wind forcing and the observed intratidal patterns. Some tidal amplitude maxima were located near the surface over the channel, as had been found by Valle-Levinson and Lwiza (1995) further inside the bay. However, in some cases the tidal amplitude maxima in the channel also occurred below the surface, near the mean pycnocline. As discussed by Jay and Smith (1990) for data from the Columbia River, stratification can inhibit vertical turbulent momentum transfer and enhance shear in the water column. Numerical simulations by Haskell *et al.* (submitted) indicate that this inhibition of vertical momentum transfer in the pycnocline may dampen upward transmission of the tidal phase, resulting in a subsurface maximum tidal amplitude under high stratification. Tidal amplitude maxima were also found over the channel shoulders or shoals, but some of this structure may simply have reflected the difficulty of capturing a highly variable flow field with data from stations at intervals of approximately 2 km in distance and up to three hours in time. Tidal phase shifts of up to 3 hours were observed between the channel and shoals and from surface to bottom in the channel. These phase shifts appeared to be important in producing horizontal velocity convergence over the right (looking into the bay) shoulder of the channel.

Subtidal patterns: The greatest subtidal flow of shelf water directed towards the bay was found in the channel on all three transects, despite differences in the lateral location of the channel along the transect. So, the effects of bathymetry appeared to outweigh the effects of Coriolis, which would tend to confine the inflow to the right side of the transect (looking into the bay). These findings are consistent with the results from Boicourt (1981) and Goodrich (1987) for moored current meters in the region, from the ADCP measurements by Valle-Levinson and Lwiza (1995), and with the numerical results of Valle-Levinson and O'Donnell (1996). Similarly, the location of the subtidal outflow plume was not constrained to the left side of each transect, but was separated from the coast, with the salinity minimum located over the channel axis and higher surface salinity found to the left of the channel. This persistent, two-way subtidal exchange in the channel, with outflow at the surface and inflow at depth, reflected the influence of gravitational forcing on flow in the channel.

The influence of wind-forcing was also evident in the subtidal velocity fields along Transect 3, as the predominantly northward flow across the transect reflected the prevailing southerly winds (Figure 13c). The light to moderate (5 m/s) east-southeasterly and easterly winds that prevailed during the transits of Transect 1 may have driven the subtidal inflow observed over the shoal (Figure 13a), since the winds would have the most impact on circulation in that shallow (approximately 6 meter depth) area. The tidal fits for both salinity and along-channel velocity explained relatively less of the data variability over this shoal, another indication that subtidal forces were important. However, subtidal surface inflow over this shoal has been frequently observed, under all but southwesterly wind conditions, as part of an anticyclonic gyre formed between this inflow and outflow over North Channel (Valle-Levinson, *et al*, submitted). The inflow over the shoal has been attributed to the effects of tidal rectification over a channel-shoal bathymetry, as discussed by Li and O'Donnell (1997). Since stratification was reduced or absent over this shoal area, wind-forcing and tidal rectification would be expected to dominate over gravitational forcing, thus producing the observed inflow.

The separation of the subtidal plume from the coast along all three transects and persistent near-surface inflow along Cape Henry were consistent with development of an anticylonic gyre in

the subtidal velocity field as the plume left the bay mouth. Such gyres have been observed by Geyer and Signell (1990) around a headland in Vineyard Sound, Massachusetts, modeled by Klinger (1994) around a rounded cape, and generated in numerical simulations of circulation at the Chesapeake Bay mouth (Valle-Levinson *et al.*, 1996). Our observations are consistent with Klinger's (1994) hypothesis that upwelling of the pycnocline can control separation of a density current from a rounded cape, when the coastline's radius of curvature is small enough that centrifugal forces become significant. The Rossby number ($R_o = u/fL$) is close to unity for the observed subtidal plume width and velocity along Transect 1 (R_o=1.1 for u=0.3 m/s and L=3 km). Therefore, the formation of this gyre may be sensitive to changes in forcing, such as river discharge, that affect the width and strength of the subtidal surface outflow.

For every transect, subtidal horizontal convergence was observed in the across-channel velocities, especially over the right (looking towards the bay) side of the channel. Subtidal velocity vectors in Figure 14 provide one example of this convergence and its location over both sides of the channel, especially along Transect 2. From subtidal velocity vector plots at successive depths (not shown), it was evident that much of the strong, subsurface horizontal convergence was caused by differences in how the surface outflow rotated with depth to subsurface inflow over the channel relative to the adjacent shoals. Locally, outflow rotated to inflow at a shallower depth over the channel than over the shoals, producing horizontal convergence near the shoulders of the channel, most frequently over the right shoulder (looking into the bay). Over the left shoulder of the channel, horizontal convergence was also affected by the subtidal surface inflow along the coast, which acted either to increase or decrease convergence at different depths, depending on the direction of flow over the channel. Another interesting local feature of the subtidal velocity was that surface outflow consistently rotated anticyclonically with depth to subsurface inflow, thereby producing a vertical structure in the velocity field that emulated an Ekman spiral.

Mean salinity was calculated from the subtidal salinity data and ranged from 25.7 at Transect 1 to 28.5 at Transect 3. Subtidal volume and normalized salinity transports were calculated across each transect, using the subtidal along-channel velocity and salinity fields (Table 1). Net volume transport was consistently into the bay (or toward the bay mouth for Transects 2 and 3). The net northwestward volume and salinity transports across Transects 2 and 3 were consistent with northward flow of shelf water driven by direct frictional coupling of the southerly winds along the shelf. Across the bay mouth (Transect 1), most transport in and out of the bay occurred over Chesapeake Channel (92% of inflow and 57% of outflow), with weaker inflow and outflow (and a small net outflow) over the shoal, and a net outflow over North Channel (Figure 15). Inflows and outflows were separated vertically over the deep channel, but horizontally over the shoal. Net salinity transport (normalized by the sectionally averaged salinity) into the bay was calculated to be 1.36×10^4 m^3/s, which is the first available estimate of this transport for the Chesapeake Bay mouth.

Table 1

Salinity transports:
($m^3/s \times 10^3$)

	In	Out	Net	Mean Salinity
Transect 1	18.6	-5.6	13.6	25.7
Transect 2	20.5	-2.9	17.6	27.2
Transect 3	28.4	-0.3	28.1	28.5

Volume transports:
($m^3/s \times 10^3$)

Transect 1	17.3	-5.5	11.8
Transect 2	19.7	-3.0	16.7
Transect 3	27.6	-0.3	27.3

Salinity and volume transports. Salinity transports have been normalized by the mean salinity for each transect cross-section, which are also given in the upper table. Positive values indicate transport into (or toward) the bay, while negative values indicate transport out of (or away from) the bay.

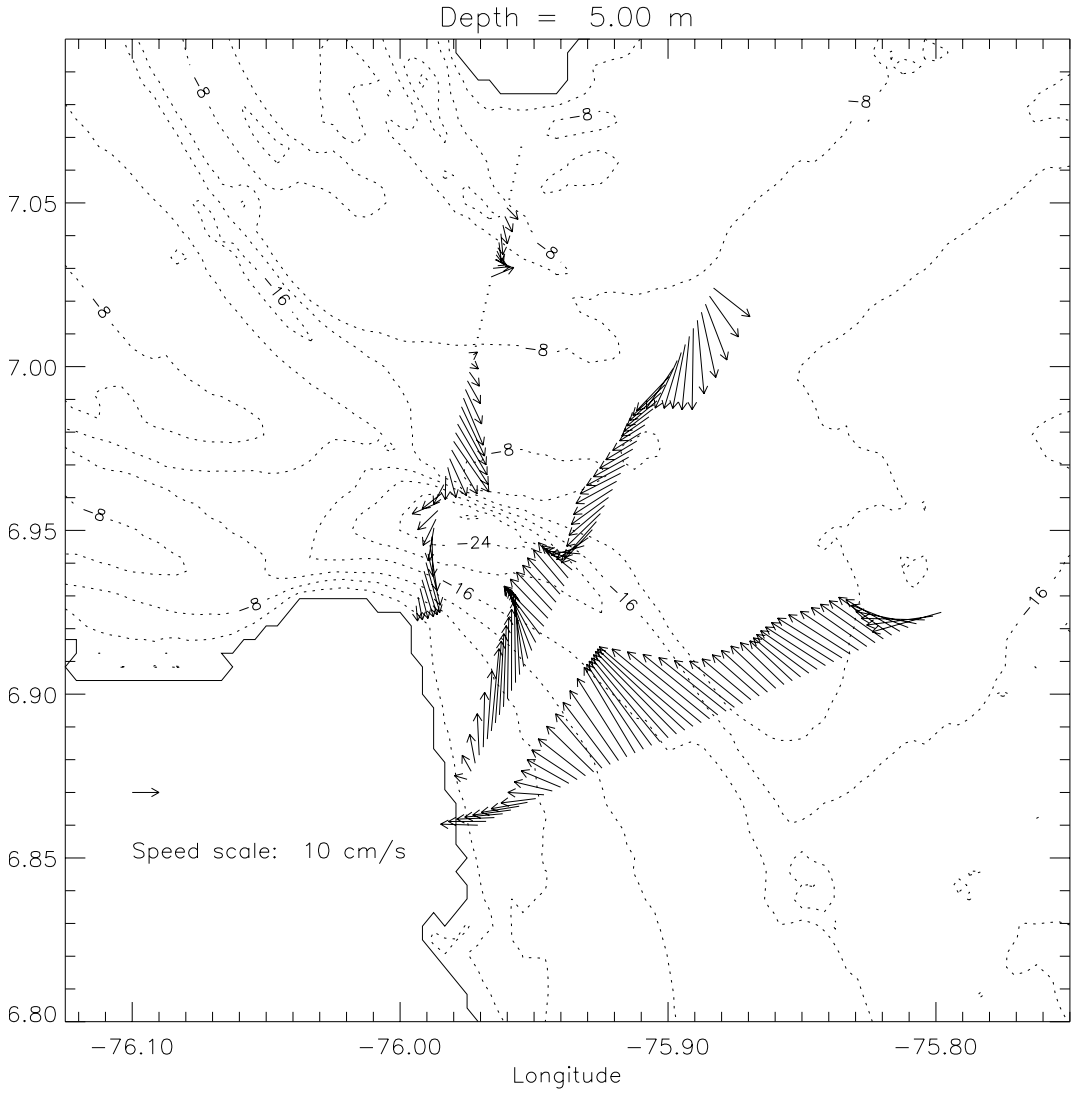

Figure 14. Subtidal velocity vectors at 5 m depth along Transects 1-3. Note that the data used to calculate the subtidal velocities along each transect came from successive 25-hour periods and were therefore not synoptic.

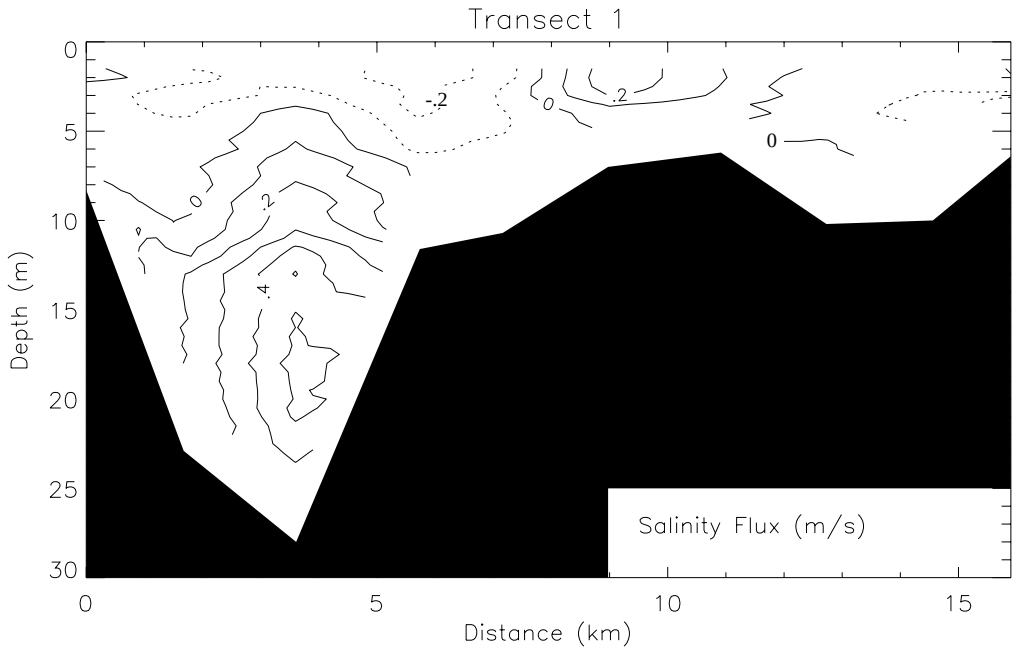

Figure 15. Salinity flux along Transect 1 (Chesapeake Bay mouth), normalized by the mean salinity for the cross-section (<u><s_n>). Plot is drawn looking into the bay and contour intervals are 0.1 m/s. Positive (negative) values are plotted as solid (dashed) lines and indicate flux into (out of) the bay.

SUMMARY

This study described the spatial (horizontal and vertical) and temporal variability of salinity and velocity fields in the Chesapeake Bay plume region under high freshwater discharge and moderate wind forcing conditions. The observed complex vertical and lateral patterns in the fields were explained by interaction between the multiple forces (tidal, gravitational, wind and inertial) affecting circulation in the area, as modified by the channel/shoal bathymetry and coastline morphology. Interesting features in the subtidal circulation that merit further investigation include a surface anticylonic gyre in the northern portion of the bay entrance, a surface anticyclonic gyre to the south of the mouth, and persistent horizontal velocity convergence over the channel shoulders. The smaller-scale transient and subtidal hydrographic and circulation features described in this study may help explain variability in processes, such as larval recruitment, that are sensitive to the structure of the density, salinity and flow fields at the bay mouth. The location, timing and persistence of these features may therefore have a significant impact on processes such as larval recruitment and pollutant dispersal. Future high-resolution sampling of the Chesapeake Bay mouth and plume region, under different wind and freshwater discharge conditions from those of this study, will help to refine our understanding of the effects of these forces on estuary-shelf exchange in this dynamic area.

ACKNOWLEDGMENTS

This work was mainly funded by the U.S. Mineral Management Service under Cooperative Agreement No. 14-35-001-30807. It was also sponsored in part by the NOAA Office of Sea Grant, under Grant No. NA56RG0489 to the Virginia Graduate Marine Science Consortium and Virginia Sea Grant College Program. Ship time on the NOAA ship *Ferrel* was provided by the National Sea Grant College Program. We greatly appreciate the professional support and cooperation from the crew of the *Ferrel* under the able command of LCDR S.D. McKay. K. Bosley from the NOAA National Ocean Service (NOS) provided the sea level and meteorological data. We also appreciate the technical support of R.C. Kidd and the participation of S. Paraso, E. Haskell, J. Koziana, M. Moore, S. Wathanaprida, and B. Wheless on the cruise.

REFERENCES

Boicourt, W. C. (1981) Circulation in the Chesapeake Bay entrance region: estuary-shelf interaction. In: *Chesapeake Bay Plume Study: Superflux 1980, NASA Conference Publication 2188*, J.Campbell and J.Thomas, editors, Hampton, VA, pp.61-78.

Boicourt, W. C., S. Y. Chao, H. W. Ducklow, P. M. Gilbert, T. C. Malone, M. R. Roman, L. P. Sanford, J. A. Fuhrman, C. Garside and R. W. Garvine (1987) Physics and microbial ecology of a byoyant estuarine plume on the continental shelf. *Transactions of the American Geophysical Union*, 68, 666-668.

Browne, D. R. and C. W. Fisher (1988) Tide and tidal currents in the Chesapeake Bay. *NOAA Technical Report NOS OMA 3*, Rockville, MD, 84 pp.

Geyer, W. R. and R. Signell (1990) Measurements of tidal flow around a headland with a shipboard acoustic doppler current profiler. *Journal of Geophysical Research*, 95, 3189-3197.

Goodrich, D. M. (1987) Nontidal exchange processes at the Chesapeake Bay entrance. In: *Hydraulic Engineering 1987*, R. Ragan, editor, American Society of Civil Engineers, New York, pp. 493-498.

Goodrich, D. M. (1988) On meteorologically induced flushing in three U. S. East Coast estuaries. *Estuarine, Coastal & Shelf Science*, 26, 111-121.

Haskell, A., A. Valle-Levinson and K. M. M. Lwiza. On the influence of estuarine outflow and bathymetry on semidiurnal tidal currents. Submitted to *Continental Shelf Research*.

Jay, D. A. and J. D. Smith (1990) Circulation, density distribution and neap-spring transitions in the Columbia River Estuary. *Progress in Oceanography*, 25, 81-112.

Johnson, D. F. and K. W. Hess (1990) Numerical simulations of blue crab larval dispersal and recruitment. *Bulletin of Marine Science*, 46, 195-213.

Klinger, B. A. (1994) Inviscid current separation from rounded capes. *Journal of Physical Oceanography*, 24, 1805-1811.

Li, C. and J. O'Donnell (1997) Tidally driven residual circulation in shallow estuaries with lateral depth variation. *Journal of Geophysical Research*, in press.

Lwiza, K. M. M., D. G. Bowers, and J. H. Simpson (1991) Residual and tidal flow at a tidal mixing front in the North Sea. *Continental Shelf Research*, 11, 1379-1395.

Paraso, M. C. and A. Valle-Levinson (1996). Atmospheric forcing effects on sea level and water temperature in the lower Chesapeake Bay: 1992. *Estuaries*, 19, 548-561.

Sanders, T. M. and R. W. Garvine (1996). Frontal observations of the Delaware Coastal Current source region. *Continental Shelf Research*, 16, 1009-1021.

Simpson, J. H., J. Brown, J. P. Matthews, and G. Allen (1990). Tidal straining, density currents and stirring in the control of estuarine circulation. *Estuaries*, 12, 125-132.

Valle-Levinson, A. and J. O'Donnell (1996). Tidal interaction with buoyancy-driven flow in a coastal plain estuary. In: *Coastal and Estuarine Studies, Vol. 53*, American Geophysical Union, pp. 265-281.

Valle-Levinson, A. and K. M. M. Lwiza (1995). The effects of channels and shoals on exchange between the Chesapeake Bay and the adjacent ocean. *Journal of Geophysical Research*, 100, 18551-18563.

Valle-Levinson, A. and K. M. M. Lwiza. Observations on the influence of downwelling winds on the Chesapeake Bay outflow. Submitted to *Proceedings of the 8th International Biennial Conference on Physics of Estuaries and Coastal Seas*.

Valle-Levinson, A., C. Li, T.C. Royer, and L.P. Atkinson. Flow patterns at the Chesapeake Bay entrance. Submitted to *Continental Shelf Research*.

Valle-Levinson, A., J. M. Klinck and G. H. Wheless (1996). Inflows/outflows at the transition between a coastal plain estuary and the coastal ocean. *Continental Shelf Research*, 16, 1819-1847.

Wheless, G. H. and A. Valle-Levinson (1996). A modeling study of tidally driven estuarine exchange through a narrow inlet onto a sloping shelf. *Journal of Geophysical Research*, 101, 25675-25687.

FLOW PATTERNS AT THE CHESAPEAKE BAY ENTRANCE

Arnoldo Valle Levinson*
Chunyan Li
Thomas C. Royer
Larry P. Atkinson
Center for Coastal Physical Oceanography
Old Dominion University
Norfolk, Virginia, USA, 23529

*Corresponding Author: arnoldo@ccpo.odu.edu

Prepared for Continental Shelf Research

September 1997

ABSTRACT

The spatial and temporal variability of water entering and leaving the Chesapeake Bay estuary was determined with a spatial resolution of 75 m. The four cruises during which the observations were made took place under different conditions of freshwater discharge, tidal phase, and wind forcing. The tidal variability of the flows was dominated by the semidiurnal constituents that displayed greatest amplitudes and phase lags near the surface and in the channels that lie at the north and south sides of the entrance. The subtidal variability of the flows was classified into two general scenarios. The first scenario occurred during variable or persistently non-southwesterly winds. Under these conditions there was surface outflow and bottom inflow in the two channels, inflow over the shoal between the two channels, and possible anticyclonic gyre formation over the shoal. The flow pattern in the channels was produced by gravitational circulation and wind forcing. Over the shoal it was caused by tidal rectification and wind forcing. The second scenario occurred during persistently southwesterly winds. The anticyclonic gyre over the shoal vanished suggesting that wind forcing dominated the tidal rectification mechanism over the shoal, while gravitational circulation and wind forcing continued to cause the flows in the channels. In both scenarios, most of the volume exchange took place in the channels.

INTRODUCTION

The study of flows that enter and leave an estuary is essential to assess the fluxes of materials transported into and out of the estuary. Because these transports affect estuarine living resources and water quality we must understand the processes that determine the water exchange between estuaries and their adjacent ocean. The Chesapeake Bay entrance is and has been the focus of several studies because the bay is a habitat for species of commercial and ecological importance that depend on the oceanographic processes at the entrance of the estuary for their

recruitment and development. Research activities also are focused in this area because of the interaction of strong density gradients, tidal currents and variable winds that affects the large buoyant plume and generates complicated frontal features and flow patterns. Until very recently, the flows that enter/leave the Chesapeake Bay at its entrance had only been studied with scattered moored instruments (Boicourt, 1981; Goodrich, 1987), but did not have the spatial resolution required to elucidate relevant processes with scales on the order of 100 meters as presented here.

This study is part of an on-going effort that has the goal of understanding exchange processes between estuaries and the adjacent coastal ocean. The objective of this study is to describe the spatial structure of the subtidal and tidal flows at the entrance of the Chesapeake Bay under different conditions of wind velocity, tidal phase, and river discharge. This is the first effort in this region that describes the spatial distribution of inflows/outflows at resolutions consistent with the coherence length scales. This was accomplished by measurements of current velocities using a towed acoustic Doppler current profiler (ADCP).

STUDY AREA

The Chesapeake Bay entrance is representative of many wide, partially mixed coastal plain estuaries with a characteristic channel and shoals cross-sectional bathymetry (Fig. 1). The relatively wide (~4 km) and deep (28 m) Chesapeake Channel is located off Cape Henry near the southern entrance to the bay. In the central part of the entrance lies the eastward extension of Middle Ground, which is about 10 m deep. To the north-northeast of Middle Ground, depths are about 6 m and we will call this area the Six-Meters Shoal. Between Six-Meters Shoal and Fishermans Island lies the North Channel. North Channel is 13 m deep: roughly one half the depth of Chesapeake Channel and twice the depth of Six-Meters Shoal.

Chesapeake Bay is influenced by seasonal wind forcing that is predominantly from the northeast and the southwest (Paraso and Valle-Levinson, 1996). Northeasterly winds prevail from late summer to early spring, while southwesterly winds dominate during the summer. However, during any season, strong winds can occur from either direction. The most energetic wind events are usually from the northeast or northwest during late fall and winter, although southwesterly winds can occasionally be very energetic. Wind speeds tend to be between 4 and 6 m/s throughout the year, except during the summer months, when they are weaker. Due to the orientation of the bay entrance, northeasterly and southwesterly winds cause the greatest effects on the subtidal sea level and current variability in the area (Valle-Levinson, 1995; Paraso and Valle-Levinson, 1996). The response time of the flow to wind forcing from those two directions in the lower bay is less than 10 hours. A northeasterly wind tends to cause net barotropic inflow and an increase in subtidal sea surface elevation at the entrance. Conversely, a southwesterly wind causes net barotropic outflow through the entrance and sea level drop at the lower bay.

River discharge variability can cause significant variability in exchange processes in the Chesapeake Bay entrance. The Chesapeake Bay receives a mean annual freshwater discharge of approximately 2,500 m^3/s from a large number of rivers (Goodrich, 1988). Of these rivers, the Susquehanna contributes 50% of the discharge, followed by the Potomac (18%) and the James (14%) (Hargis, 1981). The discharge of the rivers peaks during the months of March and April and is least during August and September. As a result, the mean surface salinity is lowest

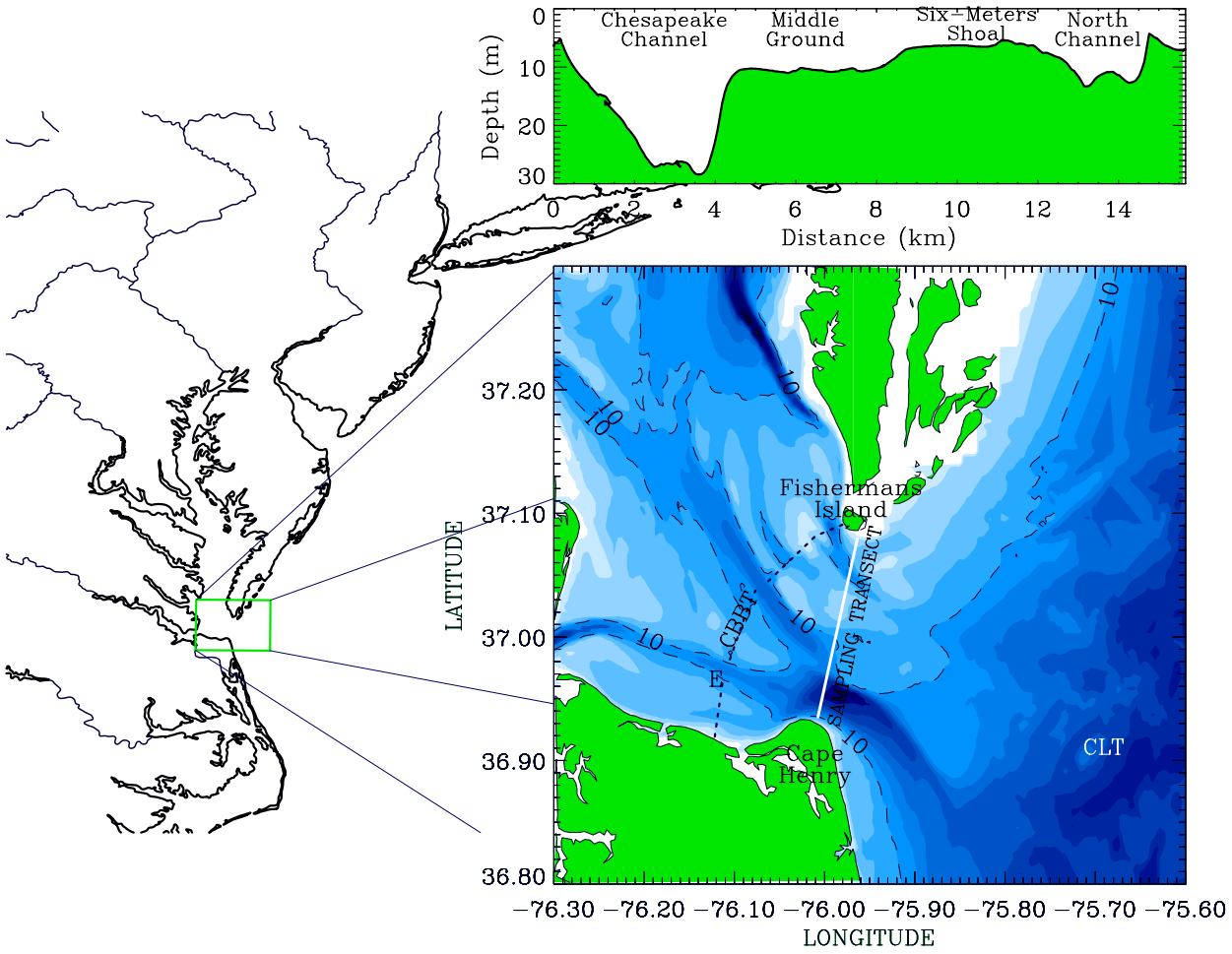

Figure 1. Mid-Atlantic Bight on the eastern coast of the United States showing the area of the lower Chesapeake Bay (lower panel), and a bathymetric profile at the entrance, looking into the estuary (upper panel). The lower panel shows the location of the transect sampled during the four cruises and the outline of the 10-m isobath (dashed contours). Dark tones represent deep areas. The Chesapeake Bay Bridge-Tunnel (CBBT) is presented as a dotted line for reference. The meteorological station at the Chesapeake Light Tower (CLT) and the sea level station at CBBT (E) provided the ancillary data. The upper panel shows Chesapeake Channel to the left and North Channel to the right. Middle Ground and the Six-Meters Shoal are located 4.5 to 8.5 km and 8.5 to 12 km. from Cape Henry. Middle Ground has an averaged depth of about 10 m while Six-Meters Shoal has a depth of about 6 m.

throughout the bay in the April-May period and highest in September-November (roughly one month after the river discharge extremes). The low-discharge period is coincident with increased wind-induced vertical mixing associated with cold air outbreaks and extra-tropical storms. However tropical and extra-tropical storms may produce anomalously high runoff during seasons of normally low runoff and cause extremely reduced salinities throughout the bay. The combination of wind forcing and river discharge results in strongly stratified (top to bottom differences in salinity of order 10) conditions in April-May, and nearly homogeneous (maximum top to bottom salinity difference of less than 2) conditions in October-November (Valle-Levinson and Lwiza, 1997).

The tidal forcing affecting the lower Chesapeake Bay is predominantly semidiurnal (Browne and Fisher, 1988). The interaction among the three semidiurnal tidal constituents (M_2, N_2 and S_2) generates fortnightly and monthly variability in the tidal currents. Owing to the fact that the N_2 constituent dominates over the S_2 in the lower bay, there is a marked asymmetry between consecutive spring (or neap) tides thus causing a primary and a secondary spring (or neap) tide during one month. During spring tides, the currents in the lower bay may exceed 1 m/s, resulting in reduced stratification and weaker subtidal flows than during neap tides (Valle-Levinson, 1995). Thus, bathymetric variations, wind velocity, freshwater discharge, and tidal forcing are expected to influence the volume exchange between the Chesapeake Bay and its adjacent coastal ocean.

Our understanding of the mean flow in this area comes from studies using sparsely moored current meters during the summer (Boicourt, 1981; Goodrich, 1987). The mean flow showed marked bathymetric influences with mean inflow restricted to Chesapeake Channel and mean outflow elsewhere. The tendency for net inflow in channels and outflow over shoals has also been observed a few kilometers upstream of the bay entrance during early October 1993 (Valle-Levinson and Lwiza, 1995). This pattern is different from the classical view of estuarine circulation modified by the earth's rotation, which consists of net inflow appearing to the right and net outflow to the left (looking into the estuary in the northern hemisphere). The present study investigates whether the bathymetric partition of inflows/outflows as found by Boicourt (1981), Goodrich (1987), and Valle-Levinson and Lwiza (1995) is persistent under different forcing conditions.

DATA COLLECTION AND PROCESSING

Current velocity data were collected from the NOAA ship *Ferrel* with an RD Instruments broadband 600 kHz ADCP along the transect between Cape Henry and Fishermans Island, at the entrance to the Chesapeake Bay (Fig. 1). The ADCP was mounted looking downward on a small catamaran (1.2 m long). The catamaran was towed mid-ship with a three-point bridle so the catamaran traveled off the starboard side in water undisturbed by the ship's wake. The instrument was towed at a speed of approximately 2.5 m/s and recorded velocity profiles averaged over 30 seconds. This gave a horizontal spatial resolution of about 75 m. The bin size for vertical resolution was 0.5 m. The ADCP specifications are shown in Table 1. Compass calibration and data correction were performed following Joyce (1989).

The Cape Henry-Fishermans Island transect was sampled repeatedly throughout two tidal cycles on four different cruises: September 24-25, 1996, November 14-15, 1996, February 20-21, 1997 and May 12-13, 1997 (hereafter Sep96, Nov 96, Feb97, and May97, respectively). This data set represents the most comprehensive high-spatial resolution current velocity measurements yet at the entrance to Chesapeake Bay. The transect sampling coincided with expected seasonally variable conditions of weak river discharge in September, strong wind forcing in November and February, and strong freshwater input in May. However, 1996 was the wettest year on record for the Chesapeake Bay and Sep96 and Nov96 actually took place during anomalously high river discharges for those months (more than 3000 m^3/s). The observations in Feb97 and May97 were during river discharges close to the annual mean of 2500 m^3/s. In addition, the Sep96 cruise took place one day before spring tides with offshore winds (southwesterly to northwesterly). The Nov 96 cruise was carried out 3 days after spring tides with onshore winds (northeasterly). The Feb97 cruise also had northeasterly winds and took place two days before secondary spring tides (the weaker spring tides of the month). Finally, the May97 transect was sampled two days before neap tides under southwesterly winds (directed offshore).

The length of the transect was roughly 16 km so that it took slightly less than two hours to sample along the complete transect. A total of 14, 11, 13, and 12 transects were made during the two semidiurnal tidal cycles sampled in Sep96, Nov96, Feb97, and May97, respectively. The current velocity values obtained from each transect were interpolated to a uniform grid with a horizontal spacing of 200 m (78 grid points) and a vertical spacing of 0.5 m (60 grid points). This grid had roughly 1500 active (useful) grid points as most of the grid points were at the bottom or within side lobe effects of the ADCP signal. The velocity values were rotated 11° clockwise from true north to obtain transverse (along the estuary entrance) and longitudinal (into and out of the estuary) components.

The time series of current velocity components for each separate cruise was fitted, using a least-squares technique, to a periodic function with semidiurnal (period of 12.42 hrs) and diurnal (period of 23.93 hrs) constituents (Lwiza *et al.*, 1991). This procedure yielded five parameters related to the flow at the entrance to Chesapeake Bay: the subtidal flow during the period of observation, the amplitude and phase of the semidiurnal constituent, and the amplitude and phase of the diurnal constituent. The least-squares fit with only the semidiurnal constituent consistently explained more than 70% (mean of 85%) of the variability observed in the longitudinal component of the flow at every grid point. The addition of the diurnal constituent to the fit improved the longitudinal flow variability explained to an average of 92%. The improved fit yielded root-mean-squared errors between the fit and the observations that in general remained below 0.05 m/s. The percent of variability explained by the fits for the transverse flow component were slightly less (average of 82%), which indicated reduced tidal influences on this component.

Table 1

Acoustic Frequency	600 kHz
Beam Angle	20°
Pings per Ensemble	8
Profiling Mode	4
Sampling Interval	30 s
Blanking Interval	0.5 m
Center of First Bin	1.5 m
Beam Length	0.5 m
Bottom Track	Yes, all the time
Data Acquisition	RD Instruments Software = Transect
Navigation	Differential Global Positioning System (DGPS)

ADCP Specifications

TIDAL PROPERTIES OF FLOW IN THE BAY ENTRANCE

In this section the semi-diurnal and diurnal properties of flow in the bay entrance are described.

a) Semidiurnal

The amplitude of the semidiurnal tidal flow (Fig. 2) showed similarities and differences from cruise to cruise. The consistent features were the persistent location of the greatest near-surface amplitudes in North Channel and to the south of Six-Meters Shoal. North of Chesapeake Channel, over Middle Ground and Six-Meters Shoal, isopleths paralleled the bathymetry indicating frictional effects on the tidal flows. These frictional effects became less evident in the Chesapeake Channel, where differences appeared from cruise to cruise. The amplitude of the semidiurnal tidal flow in Chesapeake Channel increased with depth in Sep96 and May97, and showed a mid-water minimum in Nov96 and Feb97. The increase of amplitude with depth was probably due to the strong pycnocline associated with the low salinity plume that hindered the upward transmission of the tidal phase as a consequence of low eddy viscosities at the pycnocline. This effect of plume outflow on tidal currents has been shown with a mixed layer model by Haskell *et al*. (1997). The semidiurnal amplitude over the transect also varied from cruise to cruise depending on the tidal phase within the month. Greater amplitudes were near spring tides (Sep96 and Feb97) as the dominant semidiurnal constituents (M_2, N_2, and S_2) were close to being

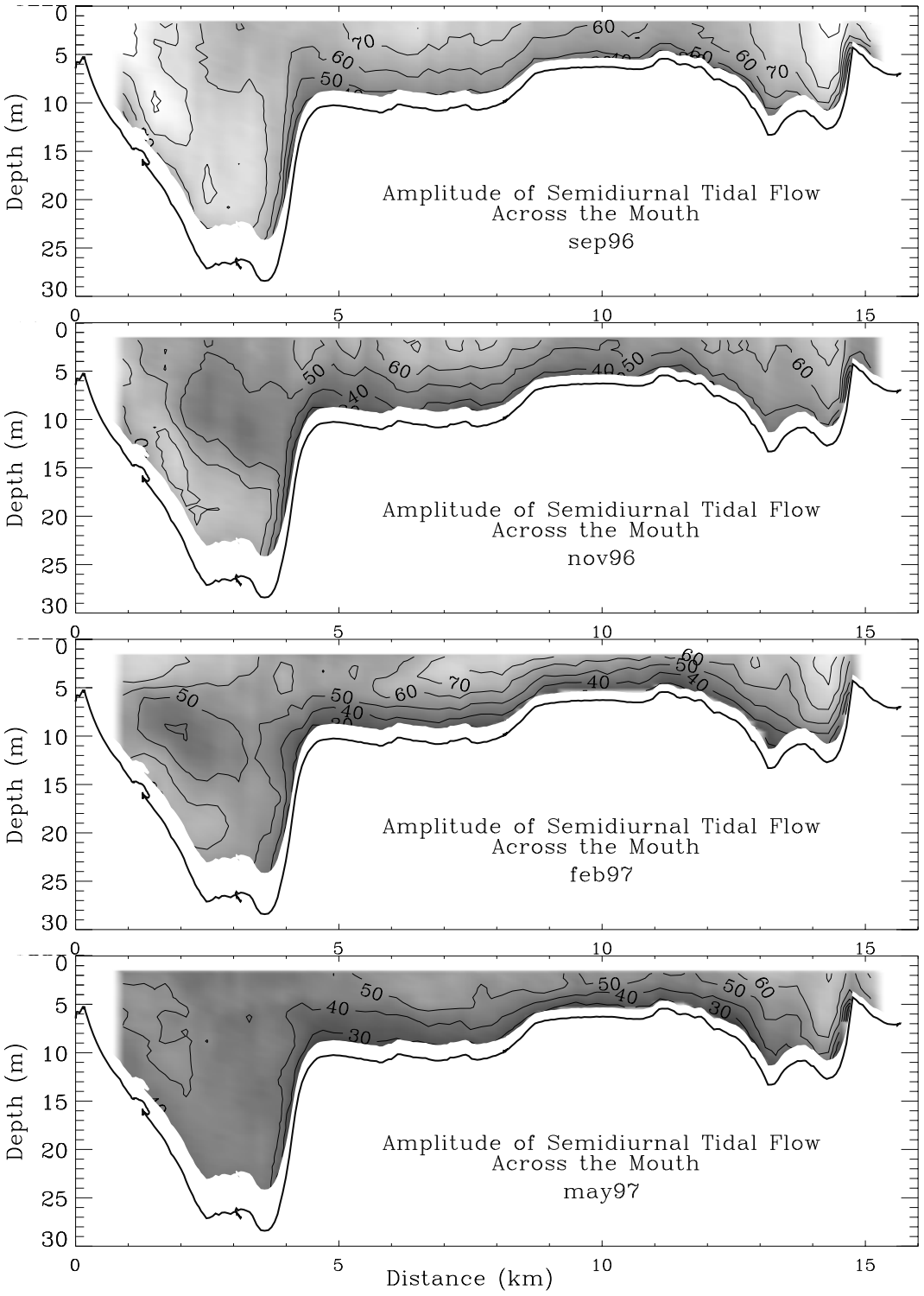

Figure 2. Amplitude of semidiurnal tidal flow (cm/s) perpendicular to the sampling transect during the four cruises. Contour interval is 10 cm/s. Lighter tones represent larger amplitudes.

in phase. Similarly, the amplitudes were lowest in May97, two days before neap tides as the constituents were out of phase. Although the fit was made to the period of the M_2 constituent, the 25-hr long record of each cruise was not long enough to isolate the contributions of the N_2 and the S_2 from the M_2. That is why Figure 2 reflected the combined effect of all semidiurnal constituents and not the individual effect of M_2.

The phase of the semidiurnal tidal currents also showed similarities and discrepancies from cruise to cruise (Fig. 3). Low phase values (in degrees) indicated that the tidal currents turned first. During every cruise, lower phases appeared near the bottom compared to the surface, which indicated the expected upward transmission of the tidal phase. Also during every cruise, the tidal currents over Six-Meters Shoal, the shallowest portion of the section, lead those from the rest of the section. This region of phase lead coincided with the area of lowest tidal current amplitudes, which indicated that the weak currents responded more quickly to tidal forcing due to their low inertia. The near-surface portion in Chesapeake Channel showed the greatest lags, up to 100° behind (~3.3 hrs later than) Six-Meters Shoal. The area of large lags appeared at the expected region of the outflowing plume from the Chesapeake Bay. This area of large lags was of different size from cruise to cruise, probably related to the strength of the plume. The area in North Channel also showed phase lags up to 30° (or one hour) relative to Six-Meters Shoal. This again was caused by the stronger tidal currents in the channel than those over the nearby shoals, as they responded more slowly to changes in tidal forcing. Beneath the near-surface area of large lags off Cape Henry, the phases occurred approximately 30° before in Sep96 and Nov96, but were farther ahead by 60 to 70° (up to 2 hrs) in Feb97 and May97. The cause of this increased near-surface lag relative to the bottom in 1997 is unknown but will be explored in conjunction with the subtidal flow description. The features of the amplitude and phase of the semidiurnal tidal currents, both in the transverse and vertical directions, were similar to those described by Valle-Levinson and Lwiza (1995) except in Chesapeake Channel. These features should be expected to be general characteristics of the tidal flows in the area.

b) Diurnal

The amplitude of the diurnal tidal flow was in general lower than 0.10 m/s (Fig. 4). Although it was smaller than the subtidal flow, inclusion of this constituent in the analysis improved the fit, by explaining an additional 7% of the variability observed. The improvement to the fit, however, was restricted mainly to the Chesapeake Channel, where the diurnal amplitudes were greatest. These greatest amplitudes (higher than 0.10) were related to the position of the plume. In Nov96 the diurnal amplitudes were particularly large and also could have been the result of the atmospheric forcing with diurnal periodicity.

SUBTIDAL FLOWS

The calculated subtidal flows contained all those motions with periods greater than the diurnal including the different effects of gravitational circulation (or density gradients), wind forcing, and tidal rectification. The 25-hour time series observed during this study covered two semidiurnal tidal cycles and thus was not long enough to reliably separate the contribution of each subtidal flow component. Nevertheless, analysis of even this short records yields information on the general features of the subtidal flow. The following subsections discuss the net volumes

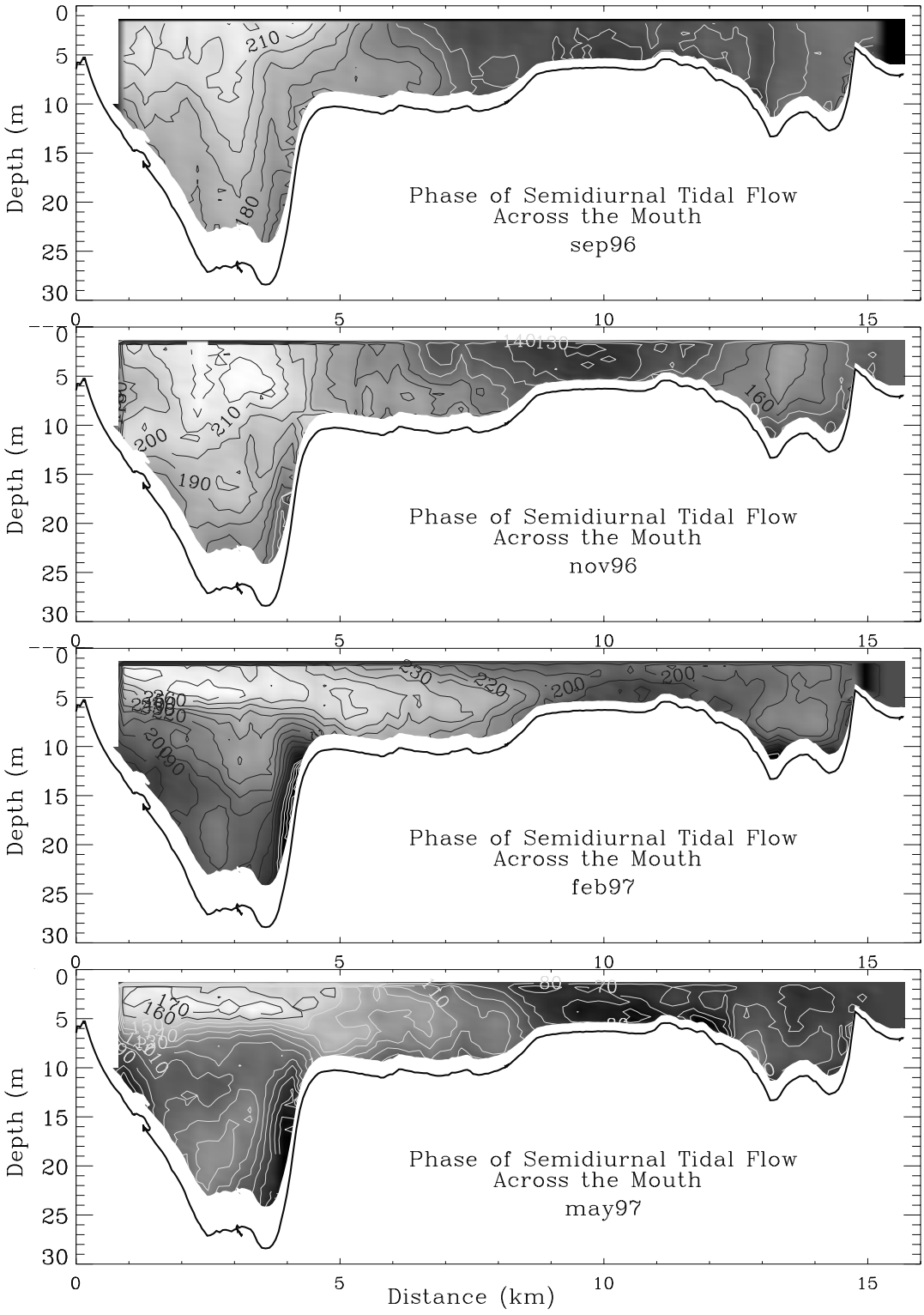

Figure 3. Phase of semidiurnal tidal flow (in degrees) perpendicular to the sampling transect during the four cruises. Contour interval is 10 degrees. Lighter tones represent larger phase lags, *i.e.* tidal changes occur first at the areas denoted by dark tones.

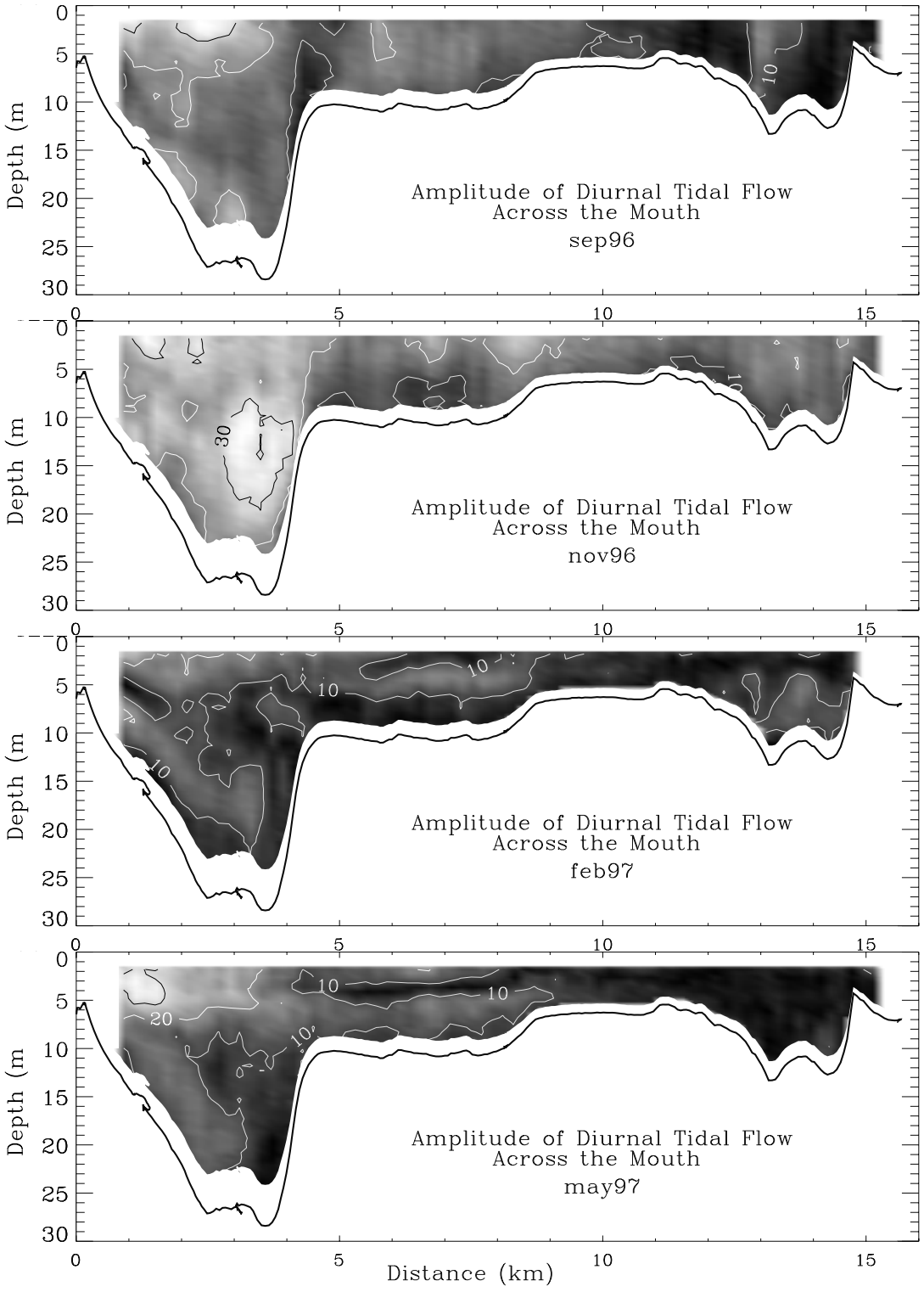

Figure 4. Amplitude of diurnal tidal flow (cm/s) perpendicular to the sampling transect during the four cruises. Contour interval is 10 cm/s. Lighter tones represent larger amplitudes.

transported into and out of the bay, followed by discussions of the variability in the along-estuary and transverse flows.

a) Volume Transport

Appreciable differences occurred in the volumes of water that entered and left the estuary during the four cruises (Table 2). The cruises in Sep96 and Nov96 were associated with high river discharge of about 3000 to 4000 m^3/s. In contrast, the river discharge for Feb97 and May97 was about 2000 m^3/s. Furthermore, the cruises in Sep96 (one day prior to spring tides) and May97 (two days before neap tides) were influenced predominantly by offshore winds (southwesterly) that in general caused the subtidal sea level to drop (Fig. 5). The sea level drop produced greater volume outflows (net outflow integrated over the section) than inflows (net inflow integrated over the section) during both cruises (Table 2). In May97 there was a net volume export of approximately 8×10^3 m^3/s which was accounted for by the river discharge and the barotropic transport induced by the sea level set-down as follows. On the basis of mass conservation, the barotropic transport can be estimated from the flow induced by the subtidal change in sea level ($\partial\eta/\partial t$), according to the relationship 0.75 (A/W) $\partial\eta/\partial t$ (*e.g.* Wong, 1994), where A is the surface area being influenced by the set-up/set-down, *i.e.*, the area of the main stem of the Chesapeake Bay (8×10^9 m^2), and W is the cross-sectional area at the entrance to the estuary (2×10^5 m^2). Thus, in May97 the sea level set-down (0.08 m in 24 hrs) accounted for 6×10^3 m^3/s (or 75%) of the volume exported by the estuary and the river discharge accounted for the other 2×10^3 m^3/s. Similarly, in Sep96 the net volume exported by the estuary was 1.2×10^4 m^3/s, of which, 7×10^3 m^3/s were accounted for by the set-down (0.08 m in 20 hrs) and close to 4×10^3 m^3/s were attributed to the river discharge. Approximately 1×10^3 m^3/s remained unaccounted for, which was within the accuracy of the estimates.

On the other hand, the cruises in Nov96 (3 days after spring tides) and Feb97 (2 days before secondary spring tides) reflected onshore winds (northeasterly and southeasterly) (Fig. 6) that caused greater volume inflows than outflows (Table 2). In Feb97 the net volume inflow of 1.1×10^4 m^3/s gained by the estuary was accounted for by the sea level set-up during the observation period (0.16 m in 25 hrs). In Nov96 the wind velocities were relatively low compared to the other cruises and there was no apparent sea level set-up. Consequently, the net volume inflow of 1×10^3 m^3/s was relatively small and within the error of the estimates. Still, the subtidal volume inflows and outflows were large, which indicates that even if there is no sea level set-up/set-down, the volume exchanged through the entrance of an estuary may be quite large. The results above agreed qualitatively with the findings of Paraso and Valle-Levinson (1996) and Valle-Levinson (1995) that winds with westerly component cause volume loss in the lower bay and easterly winds produce volume gain, *i.e.*, the volume exchange in the lower bay is sensitive to the easterly component of the wind. The results were also consistent with the modeling results of Valle-Levinson *et al*. (1996) that showed that increased wind-induced coastal flow towards the south favored net inflow into the bay.

b) Along-estuary Flow

The common features of the longitudinal (or along-estuary) subtidal flow component were that in general, two-way exchange with flow reversal with depth was observed in the channels and

Table 2

	Sept 96	Nov 96	Feb 97	May 97
Transport In ($\times 10^4$ m^3/s)	0.3	0.8	1.4	0.4
Transport Out ($\times 10^4$ m^3/s)	1.5	0.7	0.3	1.2
Net Transport ($\times 10^4$ m^3/s)	1.2 Out	0.1 In	1.1 In	0.8 Out
River Flow	Hi	Hi	Low	Low
Tide (days	1 - spring	3 + spring	2 - sec. spring	2 - Neap
Winds	SW	NE weak	NE & SE	SW
Sea Level	Dropping	Neutral	Rising	Dropping

Subtidal volume transports into and out of Chesapeake Bay after each 25-hr period of observations, typical forcing agents, and resulting subtidal sea level.

circulation modified by rotation with near-surface outflow shifted to the left and the near-bottom inflow shifted to the right (looking into the estuary).

Appreciable distinctions from cruise to cruise were also noted in the spatial structure of the subtidal flow (Fig. 6). Throughout the cruises, the subtidal outflows were concentrated near the surface in both Chesapeake and North channels with maximum speeds of between 0.3 and 0.5 m/s in the Chesapeake Channel. In fact, most of the volume exchanged through the entrance of the Chesapeake Bay occurred in the two channels (Fig. 7). Except for Sep96, when 60% of the volume inflow developed between Chesapeake and North channels, more than 72% of the volume outflow or inflow to the estuary developed in the channels, and most of that volume exchanged in channels occurred over Chesapeake Channel. The proportion of volume inflow through the channels increased from Sep96 to May97, *i.e.*, volume inflows became more concentrated in the channels. For instance, 99% of the volume inflow in May97 was found in the channels, as compared to only 40% in Sep96. Inversely, the proportion of volume outflow through the channels decreased from Sep96 to May97 so that net outflow also appeared over Middle Ground and Six-Meters Shoal. In Sep96, 93% of the subtidal outflow appeared in the channels and by May97 this proportion was reduced to 73%. This shift in location of the subtidal flows throughout the entrance of the estuary was reflected in the tilt of the interface between outflows and inflows in the Chesapeake channel. The tilt was similar between both 1996 and between the 1997 cruises, but was different from 1996 to 1997. The common forcing in 1996, as well as in 1997, was the river discharge. It seems that increased river discharge caused the outflow to be concentrated near the surface in the channels and the inflow to appear near the bottom throughout the section. The reason for this shift of outflow in channels/inflow over shoal to inflow in channel/outflow over shoals is not obvious but could be attributed to a shift from a baroclinic-dominated exchange, related to high river discharge, to a barotropic-dominated exchange, with

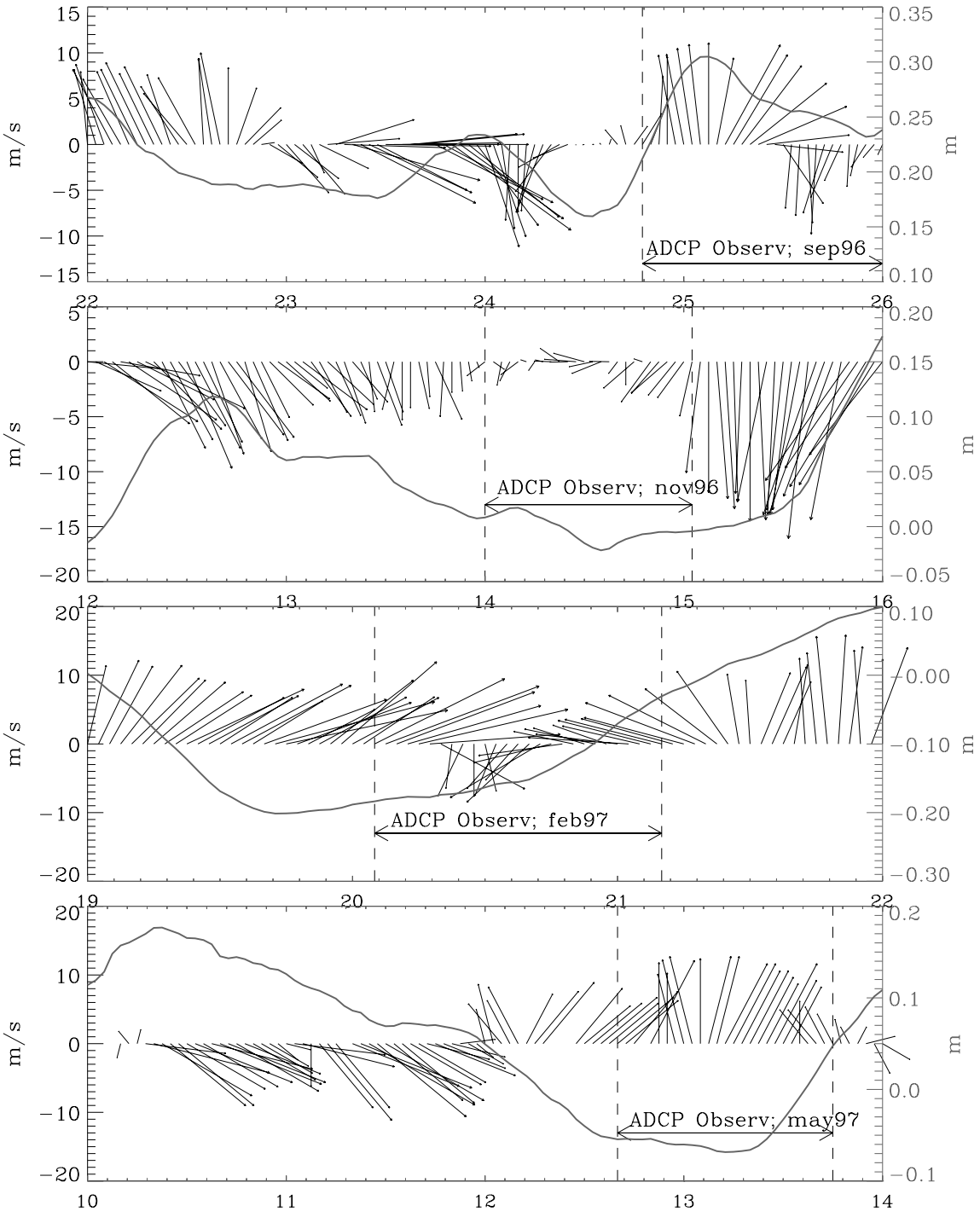

Figure 5. Wind velocity (vectors in oceanographic convention) from the Chesapeake Light Tower (CLT on Fig. 1) and subtidal sea level variations (solid line) from the Chesapeake Bay Bridge-Tunnel (E on Fig. 1) recorded around the period studied (delimited by dashed lines) during each one of the four cruises. The scale for the wind vectors appears on the left and the scale for sea level appears on the right. The abscissa indicates the day of the month when the cruise took place.

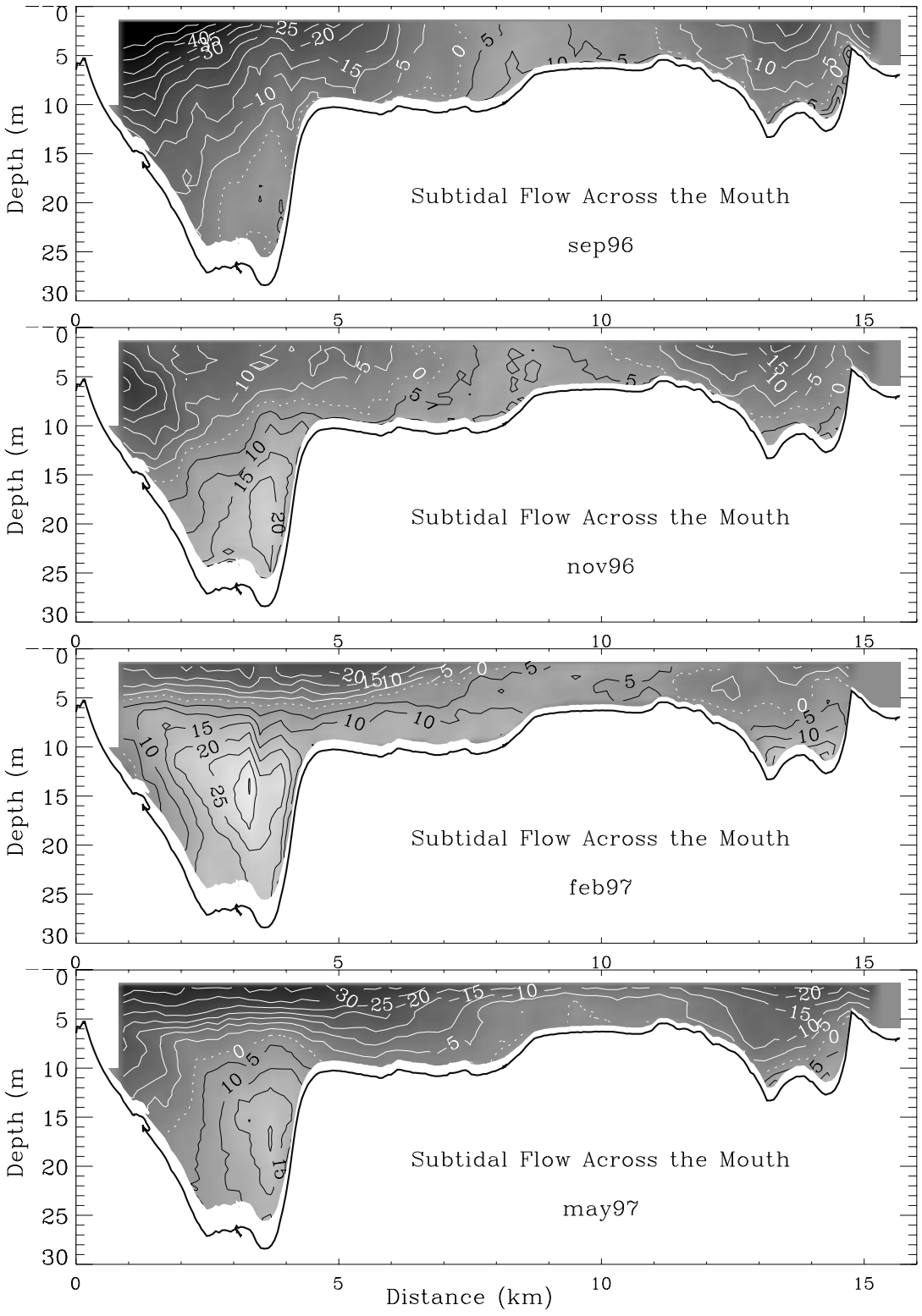

Figure 6. Subtidal flow (cm/s) perpendicular to the sampling transect during the four cruises. Contour interval is 5 cm/s. Light tones and dark (positive) contours represent net inflows.

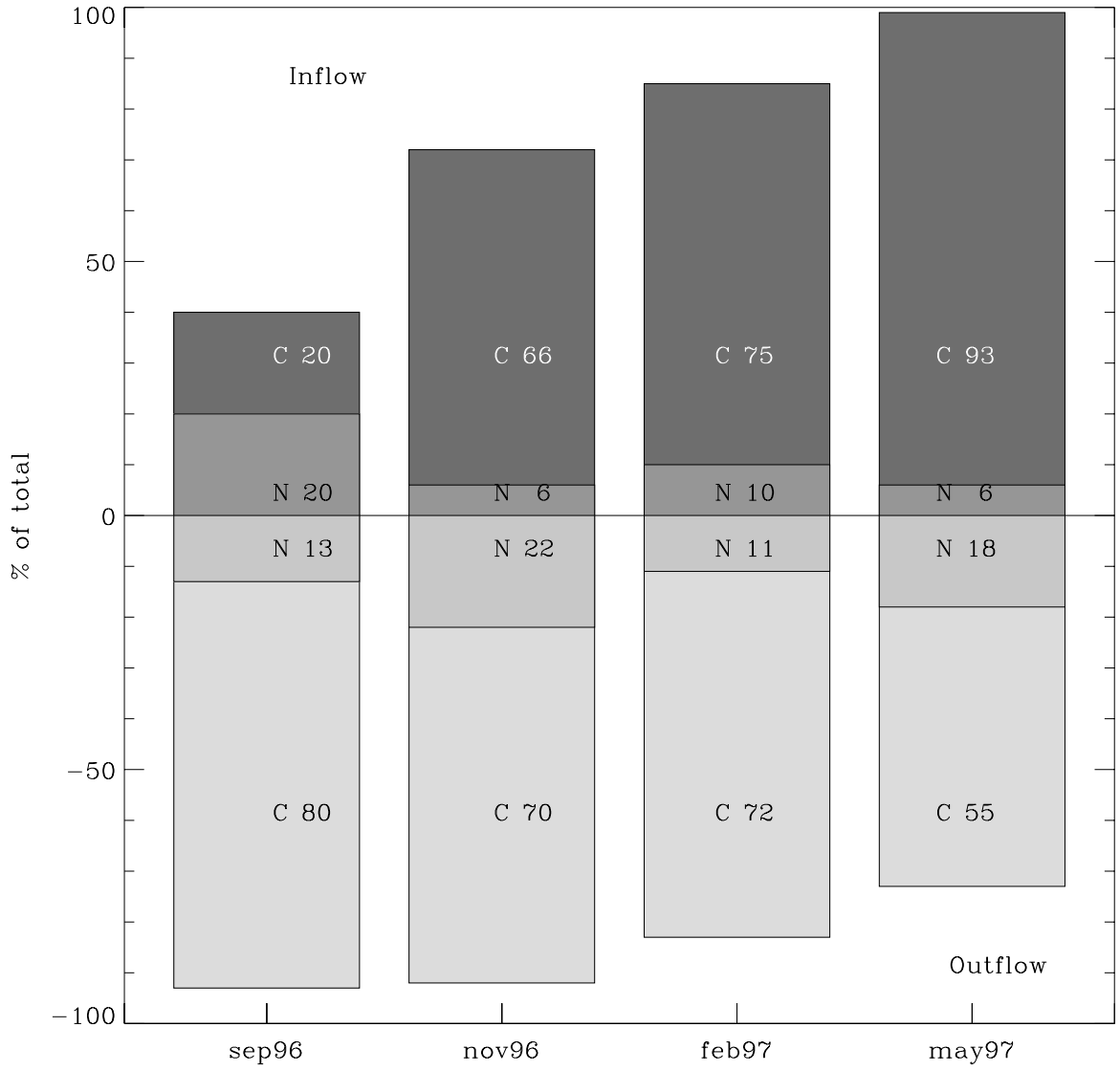

Figure 7. Percent of subtidal volume exchanged in the channels during each one of the four cruises. The percent of the total appearing in each of the two channels (Chesapeake channel- C, and North channel - N) is denoted by the numbers. For instance, in Sep96 40% of all the inflow through the entrance of the bay occurred in the channels, 20% over Chesapeake channel and 20% over North channel; 93% of all the outflow appeared in the channels, 80% in Chesapeake and 13% in North.

unidirectional flow was observed over the shoal (Fig. 6). This suggested that density-induced (gravitational) circulation was prevalent in the channels at the entrance to the bay. It appeared that both channels acted as separate, independent estuaries subject to the classical gravitational weaker river discharge, as suggested by Li *et al*. (submitted). Nonetheless, the proportion of the volume exchanged in the channels indicated their importance as conduits of material from and into the estuary.

c) Transverse Flow

The subtidal transverse flow was consistent with rotational effects acting on the longitudinal flow. During the cruises when net volume outflow developed (Sep96 and May96) the transverse component was predominantly to the south, *i.e.*, from Fishermans Island to Cape Henry (Fig. 8). Similarly, the cruises with net volume inflow reflected transverse flow to the north, more markedly in Feb97 than in Nov96 due to the much greater inflow during the former. A common feature to all cruises was the convergence associated with the southern flank of the North Channel. The southern flank of Chesapeake Channel was not resolved by these cruises, but also is expected to be a zone of convergence in the subtidal transverse flow. The zones of convergence were also appreciable in the near-surface velocity vectors (Fig. 9). During all four cruises convergence zones developed over the same general location that corresponds to observations of foam lines where floating material accumulates.

d) Gyre Formation

An additional interesting feature in the subtidal velocity field was the apparent formation of an anticyclonic gyre around Six-Meters Shoal during three of the four cruises. This is consistent with tidal rectification tendencies over a bump or shoal (*e.g.* Zimmerman, 1978; 1981; Robinson, 1981; and Park, 1990, Li, 1996). Also, in a channel-shoal bathymetry, inflow is expected to develop over the shoals as a consequence of tidal rectification (Li and O'Donnell, 1997). The development of the anticyclonic gyre suggests that tidal rectification dominated over gravitational circulation at the shallow portions of the Chesapeake Bay entrance. This observation was expected as stratification over the shoals tends to be much weaker than in the channels (*e.g* Valle-Levinson and Lwiza, 1997). The absence of the anticyclonic gyre in the May97 cruise was attributed to the persistent southwesterly wind forcing (Fig. 5) that reversed the inflow over the shoals. Thus, wind forcing had a preponderant influence on the subtidal flows throughout the entrance to the bay. The strength of the pattern of near-surface outflow in channels and inflow over shoals was modulated by the wind speed, direction, and persistence. The strong near-surface outflow and weak inflow of Sep96 was explained by the period of southwesterly winds coincident with the observations. The shift of the wind direction to north-northeasterly favored the inflow over the shoal, in contrast to its suppression in May97. The relatively strong near-surface inflow over shoal and weak near-surface outflow in channels of Nov96 and Feb97 was explained by the onshore winds that prevailed during both cruises.

SUMMARY

A series of four cruises were carried out at the Chesapeake Bay entrance in order to characterize the spatial and temporal variability of the flows in this region. These were the first

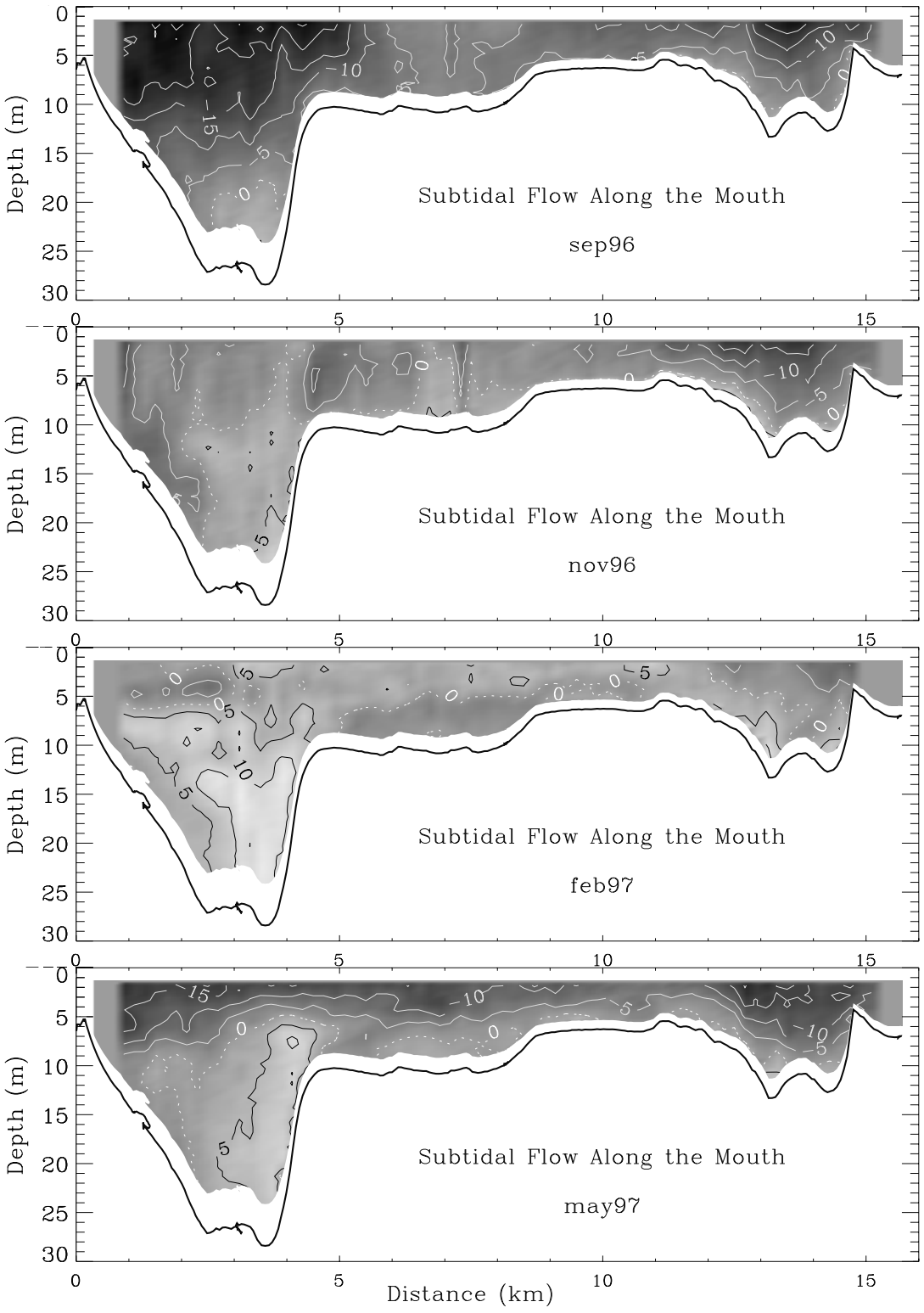

Figure 8. Transverse subtidal flow (cm/s) during the four cruises. Contour interval is 5 cm/s. Light tones and dark (positive) contours represent flows to the north (to the right on the figure).

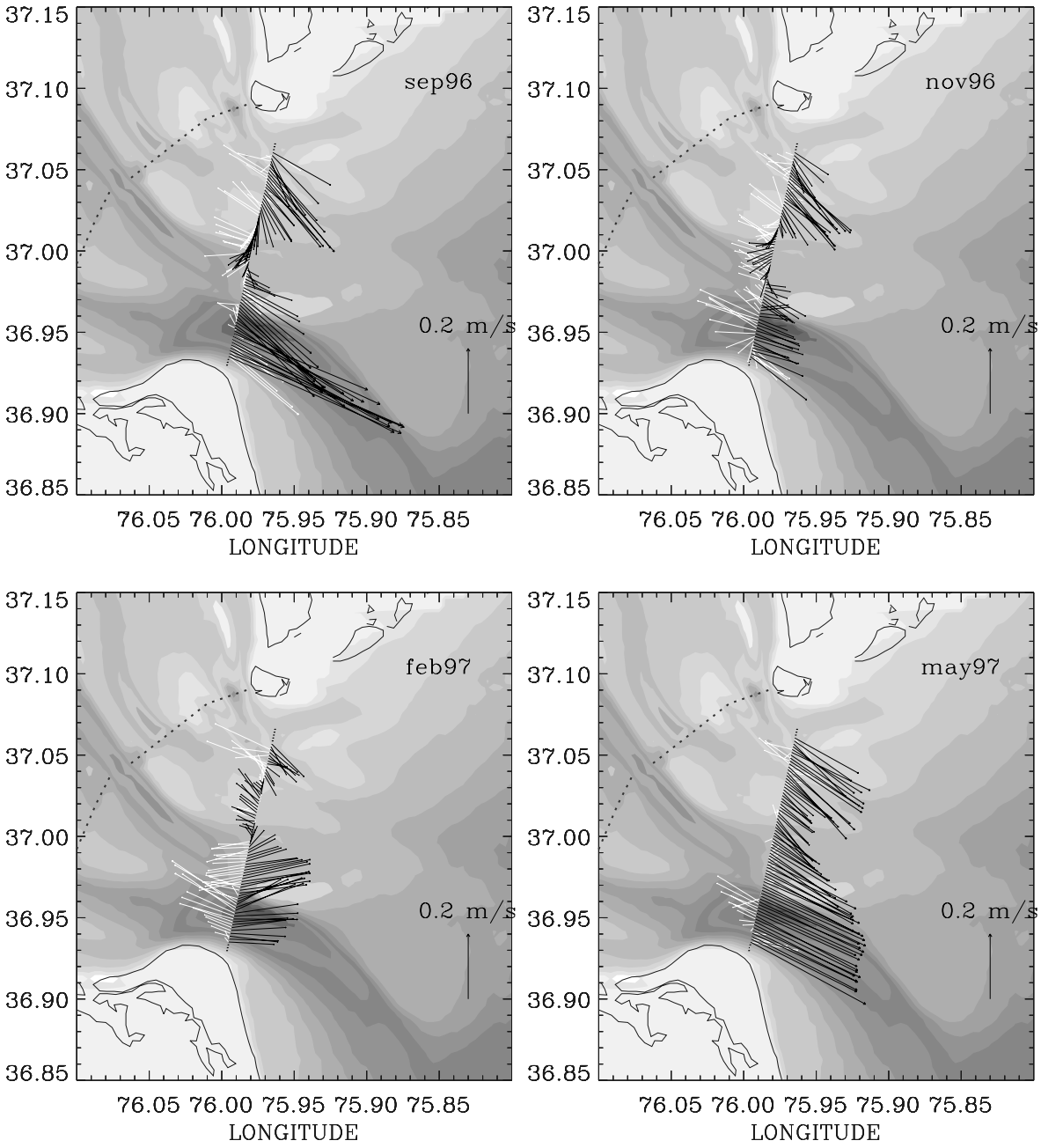

Figure 9. Near-surface (dark vectors) and near-bottom (white vectors) velocity vectors plotted every 200 m over the bathymetry at the entrance to Chesapeake Bay.

high spatial resolution observations of the flow field in this area. An acoustic Doppler current profiler was towed by the NOAA ship *Ferrel* during periods of at least 25 hours on 24-25 September 1996, 14-15 November 1996, 20-21 February 1997, and 12-13 May 1997. The measurements took place along an approximately 16 km-long transect between Cape Henry and Fishermans Island. The transect featured bathymetry consisting of two channels near its ends (Chesapeake to the south and North to the north) separated by a relatively shallower portion, that occupies almost one half of the transect with shoals up to 6 m. The cruises occurred during different conditions related to river discharge, tidal phase, and wind forcing and allowed the description of the variability of tidal and subtidal properties.

The amplitude of the semidiurnal tidal currents was, in general, greatest near the surface and away from the shoals and decreased with depth. The contours of co-amplitude followed the bathymetry thus suggesting frictional effects on the tidal flows. These frictional effects, combined with the inertia of the tidal currents, caused the phases of the semidiurnal tidal flows to occur first over Six-Meters Shoal relative to the rest of the section. The near-surface tidal phases in Chesapeake Channel occurred at least 3 hours later than those over Six-Meters Shoal. The tidal phase propagated in general from bottom to surface.

The subtidal results showed the important role played by wind forcing on the volume exchange between the Chesapeake Bay and the adjacent ocean. This was the first time that the responses to different wind forcing were quantified in terms of volume exchanged at the Chesapeake Bay entrance. The net volume gained and lost by the bay during various forcing events was accounted for by mass conservation through sea level variations and river discharges. Associated with the net volume gained and lost by the bay, there were larger volumes entering and leaving the bay simultaneously, as was the case in Nov96, when 8×10^3 m^3/s entered and 7×10^3 m^3/s left resulting in a net gain of 1×10^3 m^3/s. Therefore, it is important to look at the two-way exchange instead of the unidirectional transport produced only by sea level variations. This two-way exchange at the Chesapeake Bay entrance took place primarily in the two channels in terms of the volume transported. The exchange in the channels appeared to be influenced by the competition between gravitational (or density-induced) circulation and wind-induced flow, and over Six-Meters Shoal it was produced by tidal rectification and wind forcing. The subtidal flows observed in the four cruises drew two main scenarios for the volume exchange at the Chesapeake Bay entrance, which are summarized schematically on Figure 10. The first scenario depicts variable and/or non-southwesterly winds. In this, near-surface outflow is found in the channels and near-surface inflow over the shoals associated with an anticyclonic gyre. Near-bottom inflows develop practically everywhere across the entrance, but are strongest in the channels. The second scenario depicts persistent southwesterly winds. In this scenario, the near-surface anticyclonic gyre is not present due to wind forcing and the near-surface flow is directed seaward everywhere, weakest over Six-Meters Shoal. Near-bottom flow is directed into the estuary only in the channels.

ACKNOWLEDGMENTS

This work was mainly funded by the U.S. Minerals Management Service under Cooperative Agreement No. 14-35-0001-30807. It was also sponsored in part by the NOAA Office of Sea Grant, under Grant No. NA56RG0489 to the Virginia Graduate Marine Science

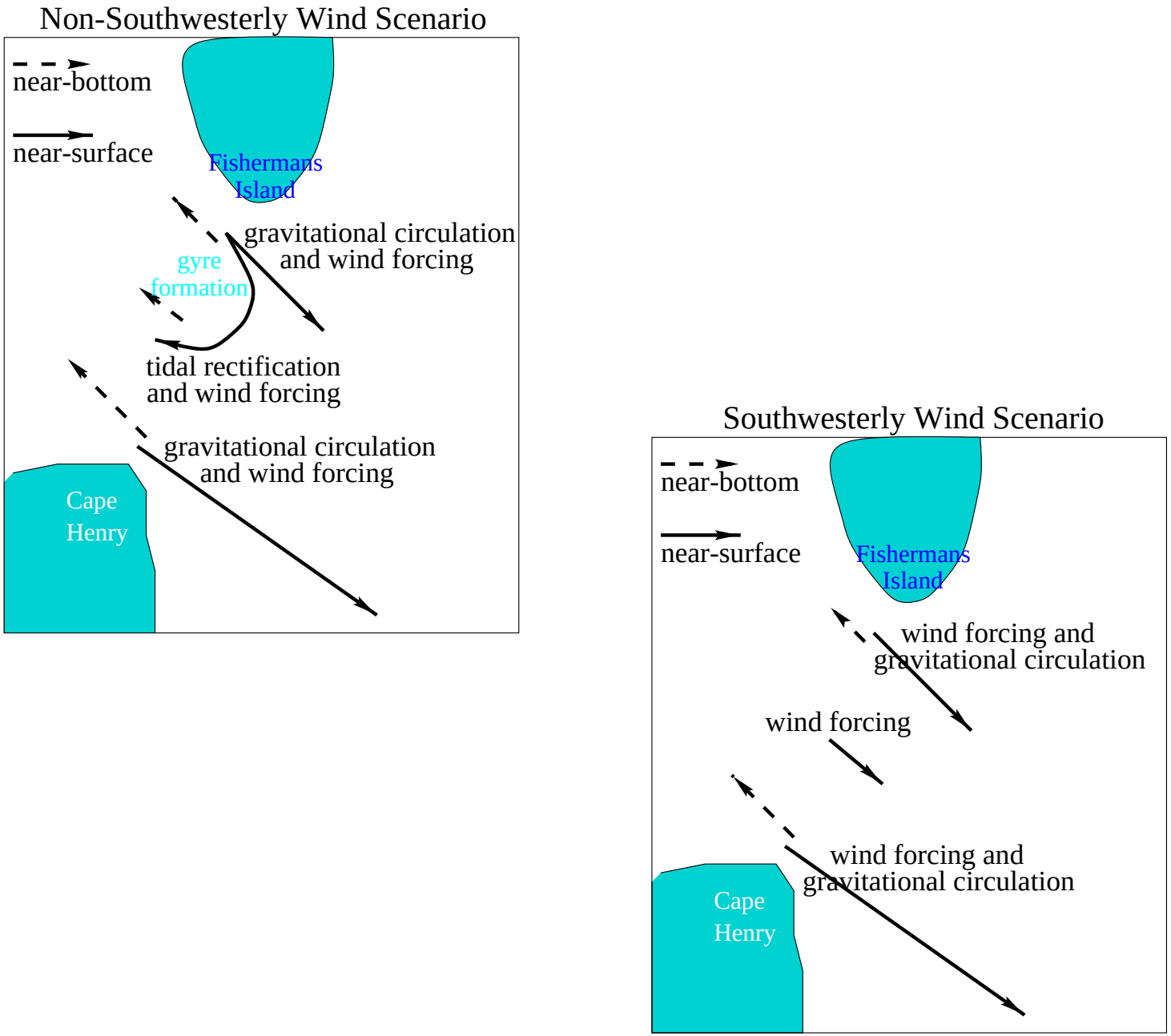

Figure 10. Scenarios derived from the observed subtidal flows. Continuous vectors represent near-surface velocities and dashed vectors represent near-bottom velocities.

Consortium and Virginia Sea Grant College Program and the NOAA National Ocean Service (NOS) under funding to establish the Ocean Systems Test and Evaluation Facility. Ship time on the NOAA ship *Ferrel* was provided by the National Sea Grant College Program. We appreciate the cooperation from the crew of the *Ferrel* under the able command of LCDRs S. D. McKay and I. Byron. K. Bosley and J. Dixon from the NOAA NOS office in Chesapeake VA kindly provided the sea level and meteorological data. We also appreciate the technical support of R.C. Kidd in every cruise and the participation and help of L. Heilman, K. Holderied, C. Reyes, R. Ellison, B. Fach, M. Gruber, G. Jiang, S. Kibler, J. Klinck, R. Locarnini, T. McCarthy, M. Moore, S. Ouelette, M. Paraso, B. Parsons, C. Reiss, D. Ruble, J. She, and K. Wong on different cruises.

REFERENCES

Boicourt, W.C. Circulation in the Chesapeake Bay entrance region: estuary-shelf interaction. In J. Campbell and J. Thomas, eds., Chesapeake Bay Plume Study: Superflux 1980. NASA Conference Publication 2188. pp. 61-78, 1981.

Browne, D.R. and C.W. Fisher. Tide and tidal currents in the Chesapeake Bay. NOAA Technical Report NOS OMA 3. Rockville, MD. 84 pp. plus appendices., 1988.

Goodrich, D.M., On meteorologically induced flushing in three U.S. east coast estuaries, *Est. Coast. Shelf Sci., 26,* 11-121, 1988.

Goodrich, D.M. Nontidal exchange processes at the Chesapeake Bay entrance. In Hydraulic Engineering 1987, Ragan R., Ed., American Society of Civil Engineers, New York, 493-498, 1987.

Hargis, W.J. A benchmark multi-disciplinary study of the interaction between the Chesapeake Bay and adjacent waters of the Virginian sea. In J. Campbell and J. Thomas, eds., Chesapeake Bay Plume Study: Superflux 1980. NASA Conference Publication 2188. pp. 1-14, 1981.

Haskell, A., A. Valle-Levinson, and K.M.M. Lwiza, On the influence of estuarine outflow and bathymetry on semidiurnal tidal currents, submitted to *Cont. Shelf Res.*

Heilman, L., A. Valle-Levinson, and L. P. Atkinson, Spatial gradients produced by an estuarine channel, submitted to *Estuaries*.

Joyce, T. M., On in situ calibration of shipboard ADCPs, *J. Atmos. Oceanic Technol., 6(1),* 169-172, 1989.

Li, C., Tidally induced residual circulation in estuaries with cross channel bathymetry, Ph.D. Dissertation, University of Connecticut, 242 pp., 1996.

Li, C. and J. O'Donnell, Tidally driven residual circulation in shallow estuaries with lateral depth variation. *J. Geophys. Res.*, in press, 1997.

Li, C., A. Valle-Levinson, K.-C. Wong, and K. Lwiza, Separating baroclinic flow from tidally induced flow in coastal plain estuaries, submitted to *J. Geophys. Res.*

Lwiza, K. M. M., D. G. Bowers, and J. H. Simpson, Residual and tidal flow at a tidal mixing front in the North Sea, *Cont. Shelf Res., 11(11),* 1379-1395, 1991.

Paraso, M. C., and A. Valle-Levinson, Meteorological influences on sea level and water temperature in the lower Chesapeake Bay: 1992, *Estuaries, 19,* 548-561, 1996.

Park, M.J. Transient tidal vorticity in coastal seas. Ph.D. dissertation. State University of New York. Stony Brook. 105 pp. 1990.

Robinson, I.S. Tidal vorticity and residual circulation. *Deep Sea Res., 28,* 195-212, 1981.

Valle-Levinson, A., Observations of barotropic and baroclinic exchanges in the lower Chesapeake bay, *Cont. Shelf Res., 15,* 1631-1647, 1995.

Valle-Levinson, A., J.M. Klinck, and G.H. Wheless. Inflows/outflows at the transition between a coastal plain estuary and the coastal ocean. *Cont. Shelf Res.* 16, 1819-1847. 1996.

Valle-Levinson A. and K. M. M. Lwiza. The effects of channels and shoals on exchange between the Chesapeake Bay and the adjacent ocean. *J. Geophys. Res., 100,* 18551-18563, 1995.

Valle-Levinson, A. and K.M.M. Lwiza. Bathymetric influences on the hydrography of the lower Chesapeake Bay. *J. Mar. Syst.*, in press. 1997.

Wong, K.-C., On the nature of transverse variability in a coastal plain estuary, *J. Geophys. Res., 99*, 14,209-14,222, 1994.

Zimmerman, J.T.F. Topographic generation of residual circulation by oscillatory (tidal) currents. *Geophys. Astrophys. Fluid Dyn., 11*, 35-47, 1978.

Zimmerman, J.T.F. Dynamics, diffusion and geomorphological significance of tidal residual eddies. *Nature, 290*, 549-555, 1981.

Environmental Studies Relative to Potential Sand Mining in the Vicinity of the City of Virginia Beach, Virginia

Part 5: Benthic Foraminifera and Ostracoda from Virginia Continental Shelf

Final Report

January 1998

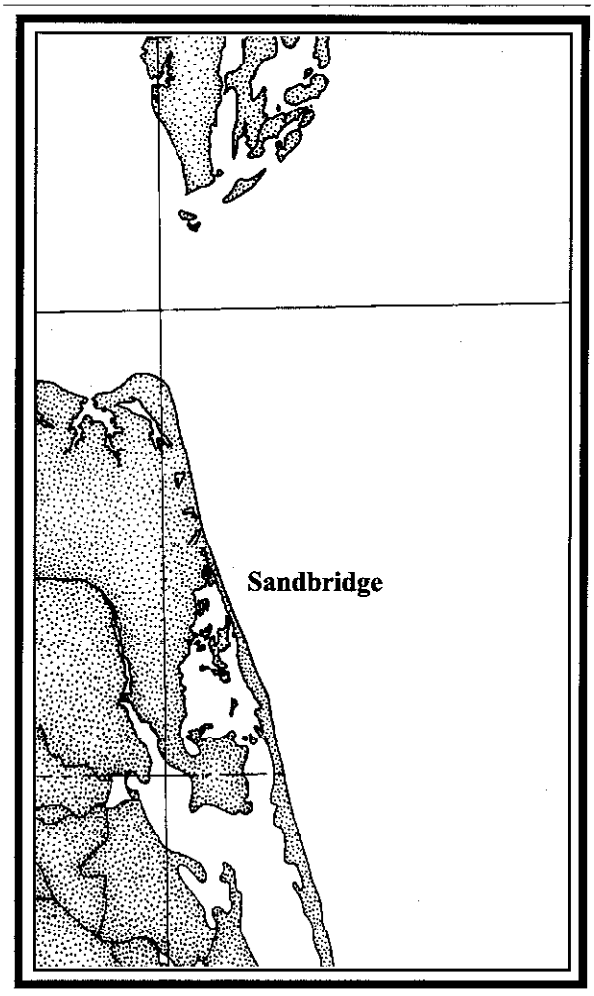

MMS U.S. Department of the Interior
Minerals Management Service

College of William and Mary
VIMS
Virginia Institute of Marine Science
School of Marine Science

Environmental Studies Relative to Potential Sand Mining in the Vicinity of the City of Virginia Beach, Virginia

Part 5: Bentic Foramininifera and Ostracoda from Virginia Continental Shelf

Final Report

January 1998

Authors:

Thomas M. Cronin
Scott Ishman,
Robert Wagner
U. S. Geological survey
G. R. Cutter, Jr.
Virginia Institute of Marine Science

Project Manager:

Carl H. Hobbs, III
Virginia Institute of Marine Science

Prepared under MMS Cooperative Agreement 14-35-0001-3087 through Virginia Institute of Marine Science of the College of William & Mary

MMS U.S. Department of the Interior
Minerals Management Service

College of William and Mary
VIMS
Virginia Institute of Marine Science
School of Marine Science

DISCLAIMER

This report has been reviewed by the Minerals Management Service and approved for publication. Approval does not signify that the contents necessarily reflect the views and policies of the Service, nor does mention of trade names or commercial products constitute endorsement or recommendation for use.

This report is preliminary and has not been reviewed for conformity with the U.S. Geological Survey editorial standards nor with the North American Stratigraphic Code. Any use of trade, product, or firm names is for descriptive purposed only and does not imply endorsement by the U.S. Government

Benthic Foraminifera and Ostracoda from Virginia Continental Shelf

Introduction

Benthic meiofaunas living on continental shelves comprise a significant proportion of the total biomass and species diversity in shallow marine environments and play important roles in shallow marine ecosystem functioning. Two important meiofaunal groups, benthic foraminifers (protists) and ostracodes (bivalved Crustacea), have been especially important in studies of benthic communities living along the U.S. Atlantic continental shelf. Buzas and Culver (1980) estimated that the number of benthic foraminifers in marine environments exceeds 10^6 per square meter and wet-weight biomass ranges from 0.02 to more than 10 g/m^2. Numerous other studies have documented the zoogeographic and bathymetric distribution of more than 800 species of benthic foraminifera (*e.g.*, Culver and Buzas 1980; Buzas and Culver 1980) and several hundred species of marine ostracodes (Valentine 1971; Hazel 1970, 1975; Cronin 1983) along the U.S. Atlantic coast.

Most previous studies of Atlantic continental shelf foraminifers and ostracodes, however, were conducted at very large spatial and temporal scales. For example, the large USGS/Woods Hole Continental Margin Program which took thousands of Atlantic shelf and slope sediment samples during the 1960's (Emery 1968) provided extensive ostracode zoogeographic data spanning several marine zoogeographic provinces and climatic zones (*e.g.* Hazel 1970). Likewise, Culver and Buzas (1980) compiled foraminiferal species' distribution data from hundreds of published sources to produce distribution maps of the 150 most common species for the western North Atlantic Ocean. Prior studies of fossil benthic foraminifers and ostracodes of the Atlantic margin have also focused on long-term changes in microfaunal assemblages resulting from glacial-interglacial climatic cycles

(Hazel 1968; Cronin 1988) and from community evolution over millions of years (Buzas and Culver 1984, 1989).

While these studies of living and fossil foraminifers and ostracodes provide excellent baseline information, they are insufficient to understand the small scale distribution of species within a limited region of the continental shelf, nor to understand short-term variability in meiobenthic populations. Such information is essential in the evaluation of potential impacts of short-term environmental disturbances from sand mining, pollution and nutrient influx or high-frequency climatic variability on continental shelf ecosystems.

Our main goal in the present study is to provide baseline information on the abundance and species diversity of foraminifers and ostracodes living in three potential sand mining areas off Virginia Beach. This study was carried out in collaboration with the Virginia Institute of Marine Science, College of William and Mary, in support of the Minerals Management Service program to understand environmental aspects of potential sand mining off the city of Virginia Beach, Virginia.

Study Area

The study region is located in the warm temperate marine climatic zone of the western North Atlantic Ocean between about 36.7 to 37.91 ° N and 75.85 to 75.92 ° W. (Figure 1). The oceanography of the region is dominated by the cool, southward flowing Virginia Coastal Current and the warmer, northward-flowing Gulf Stream/Florida Current. These currents converge near Cape Hatteras where strong isothermal convergence creates thermal barriers to the poleward and equatorward distribution of thermophilic (warm water) and cryophilic (cool water) species respectively. Off southeastern Virginia, the coldest bottom waters usually occur during February and range from about 5 to 10 °C, with generally cooler temperatures closer to shore. The warmest temperatures occur in August-

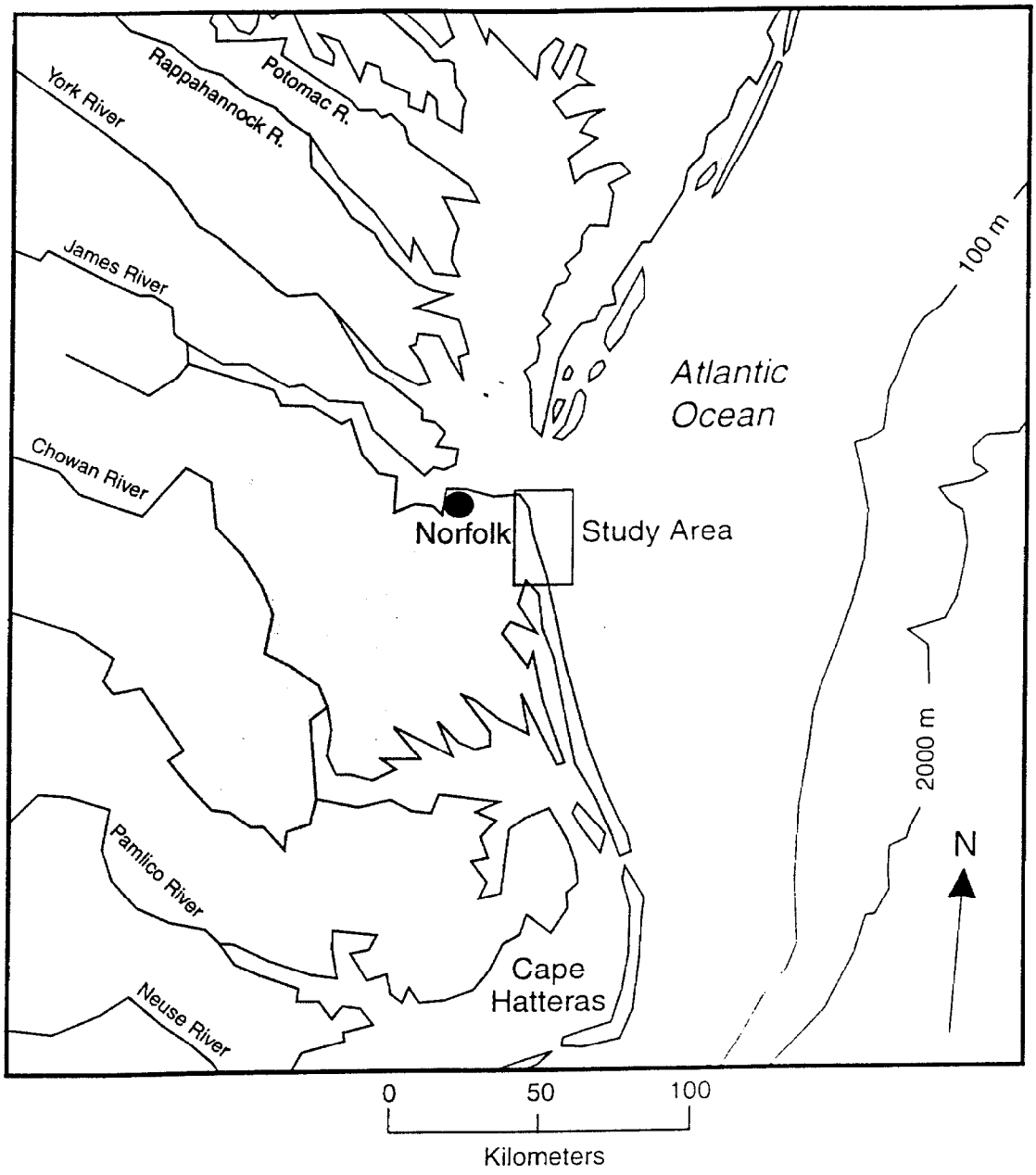

Figure 1: Map showing general location of the Virginia shelf study area.

September when they reach > 25 °C, decreasing offshore to 17-20 °C in the middle shelf region (Walford and Wicklund 1968).

On the geographic scale of faunal provinces, winter and/or summer bottom water temperatures are dominant factors influencing the large-scale latitudinal distribution of ostracode and foraminiferal species on continental shelves (Hazel 1970). The Virginia shelf is located just north of the major zoogeographic boundary near the Cape Hatteras region. The benthic fauna off southeastern Virginia is composed mainly of temperate species common in regions north of Cape Hatteras. Many species living on the Virginia shelf are near the southernmost limit of their latitudinal distribution because either they cannot tolerate warmer water temperatures to the south or they require cooler winter temperatures for survival and/or reproduction (Hazel 1970).

As one moves from nearshore to offshore regions of the Atlantic margin (from the continental shelf to the slope), factors such as dissolved oxygen, light penetration, sediment texture and composition, and decreasing temperatures of the thermocline affect the distribution of species. For example, environmental gradients at the shelf/slope transition result in a major bathymetric turnover of benthic ostracode (Cronin 1983) and foraminiferal species (Culver and Buzas 1983) between 150-500 m water depth. All the samples in the present study came from the mid- to inner continental shelf and the studied fauna is not affected by the thermocline or by hypoxia.

Substrate is another important factor in the small-scale distribution of benthic foraminifers and ostracodes. Buzas *et al.* (1989), for example, conducted experiments with benthic foraminifers and showed a small amount of mud in a sandy benthic habitat can have important affects on benthic foraminiferal densities. Many ostracode species are also substrate-specific in nearshore and estuarine habitats (Cronin 1979). The shelf off southeastern Virginia is mainly composed of sands (Hollister 1973) and provides an ideal substrate for sand-dwelling taxa.

Methods

Surface sediment samples were collected on May 15 and June 5-6, 1996 (Spring samples) and October 21 and November 6, 1996 (Fall samples) from the VIMS R/V *Bay Eagle.* Collections were made from three regions which are referred to here as the northern, central and southern regions. There are no obvious barriers between or environmental differences among the three regions. All three are characterized by sandy substrates and generally similar temperature and salinity regimes. Figures 2-11 show sample stations; Appendices 1-3 give the latitude and longitude for each station. Additional information about the cruises can be found in the companion report by Cutter *and Diaz (1998)*

Samples were obtained using a Smith/McIntyre grab sampler. Surface sediment from the uppermost 1-2 cm was scraped from a 10 by 10 cm area within the grab sample and placed in plastic sample bags. The sediment samples were immediately stained shipboard with Rose Bengal to help distinguish between living and dead ostracodes and foraminifera (see Walton 1952).

Surface sediment samples were processed for foraminifera and ostracodes using standard procedures. The sediments were washed through a 63 μm sieve and dried at 50 °C at VIMS laboratories. A total of 300 benthic foraminifers were picked from the residues when available. Samples yielding fewer than 300 specimens were picked of all the foraminifera present. All the samples in Appendices 1 and 2 contained stained representatives and we assume the populations represented at each site were living close to the time of collection. A total of 20 foraminiferal species were found.

Ostracodes were picked at the same time as foraminifers from the same quantity of sediment needed to obtain 300 foraminifers (time constraints did not allow us to pick the entire sample). Ostracodes occurred in most samples; they are typically less abundant than foraminifers in sandy substrates such as those of the Virginia shelf (the number of

ostracodes specimens ranged from 0 to 36 per sample) compared to finer grained substrates of Atlantic estuaries and offshore continental slope regions.

A total of 31 ostracode species were found in the Virginia sandy shelf habitats. Many individual ostracodes (especially *P. edwardsi, P. bradyi, C. seminuda,* and *Bensonocythere*) were preserved as whole carapaces containing chitinous appendages and other "softparts". These specimens stained vivid pink and clearly were living at the time of collection. Other specimens, notably juvenile valves, stained faint pink in color and very likely represent the molt stages of living populations.

Foraminifera and ostracodes were examined under light and electron microscopes at the U.S. Geological Survey in Reston Virginia. Specimens were identified to species level using USGS reference collections, following the taxonomy of Culver and Buzas (1980) and Loeblich and Tappan (1988) for foraminifers and Valentine (1971), Hazel (1975, 1983), and Cronin (1990) for ostracodes. The faunal slides containing foraminiferal and ostracodes are housed in the USGS microfaunal reference collections, Reston, Virginia 20191.

Results

The foraminiferal and ostracode species census data are given in Appendices 1-3 and are available electronically from the authors (tcronin@usgs.gov). Figures 2-11 plot the distribution of more common species of foraminifera and ostracodes; Plates 1-5 illustrate most of the identified species with scanning electron photomicrographs.

Ostracodes

A total of 31 species of ostracode was found in the study area. The ostracode assemblage is dominated by *Peratocytheridea bradyi, Hulingsina* spp., *Cushmanidea seminuda,* and *Protocytheretta edwardsi.* These species are typical inhabitants of sandy

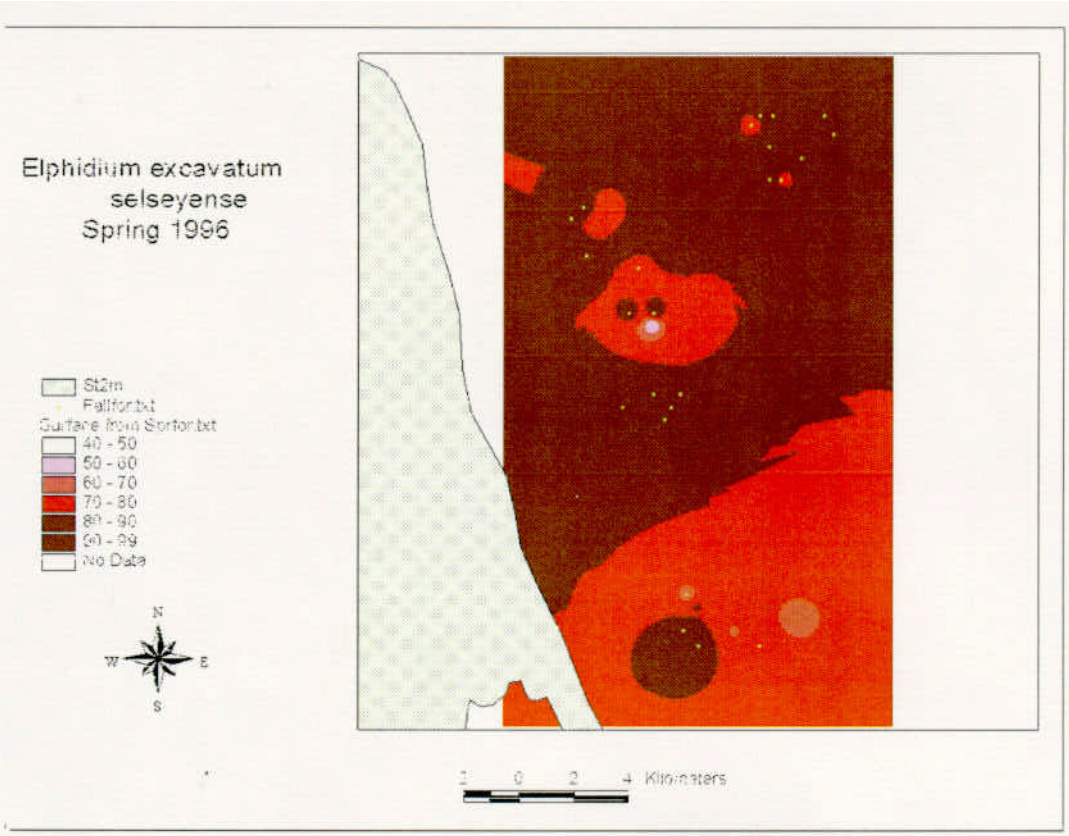

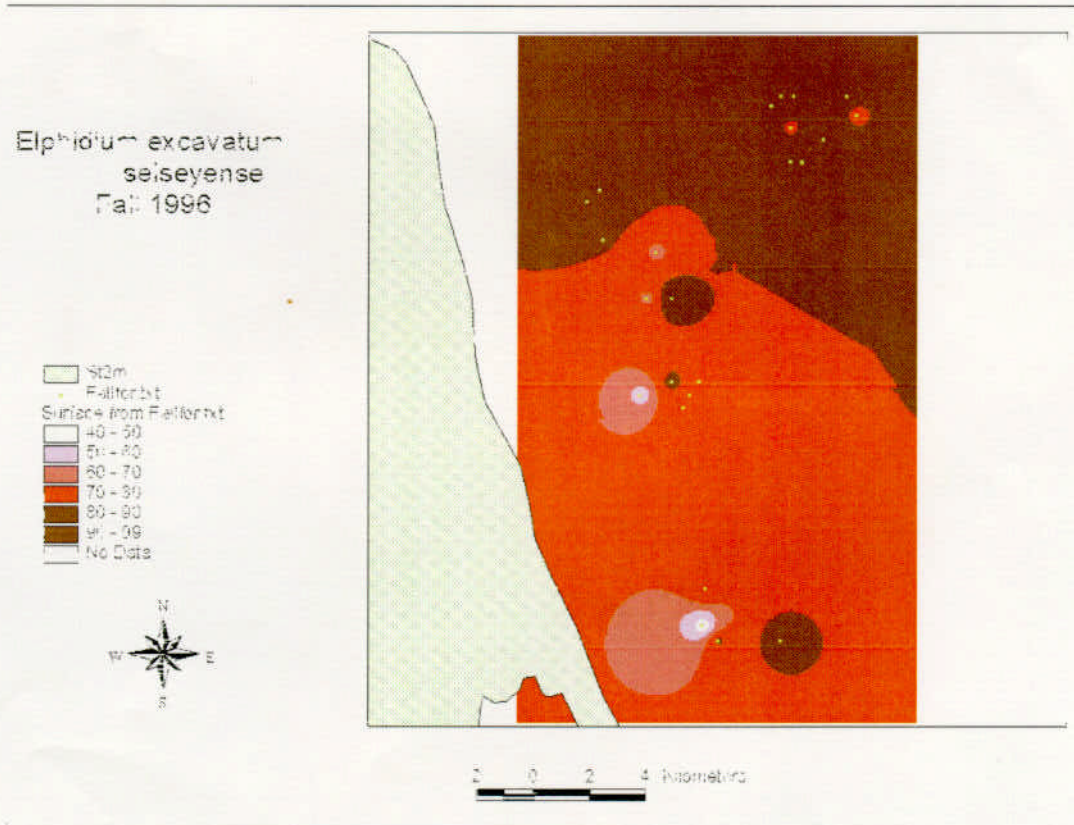

Figure 2: Distribution map showing the proportions of *Elphidium excavatum selseyense* in total formaminiferal population on the continental shelf off Virginia Beach during Spring (upper map) and Fall (lower map) 1996. Small dots indicate station locations.

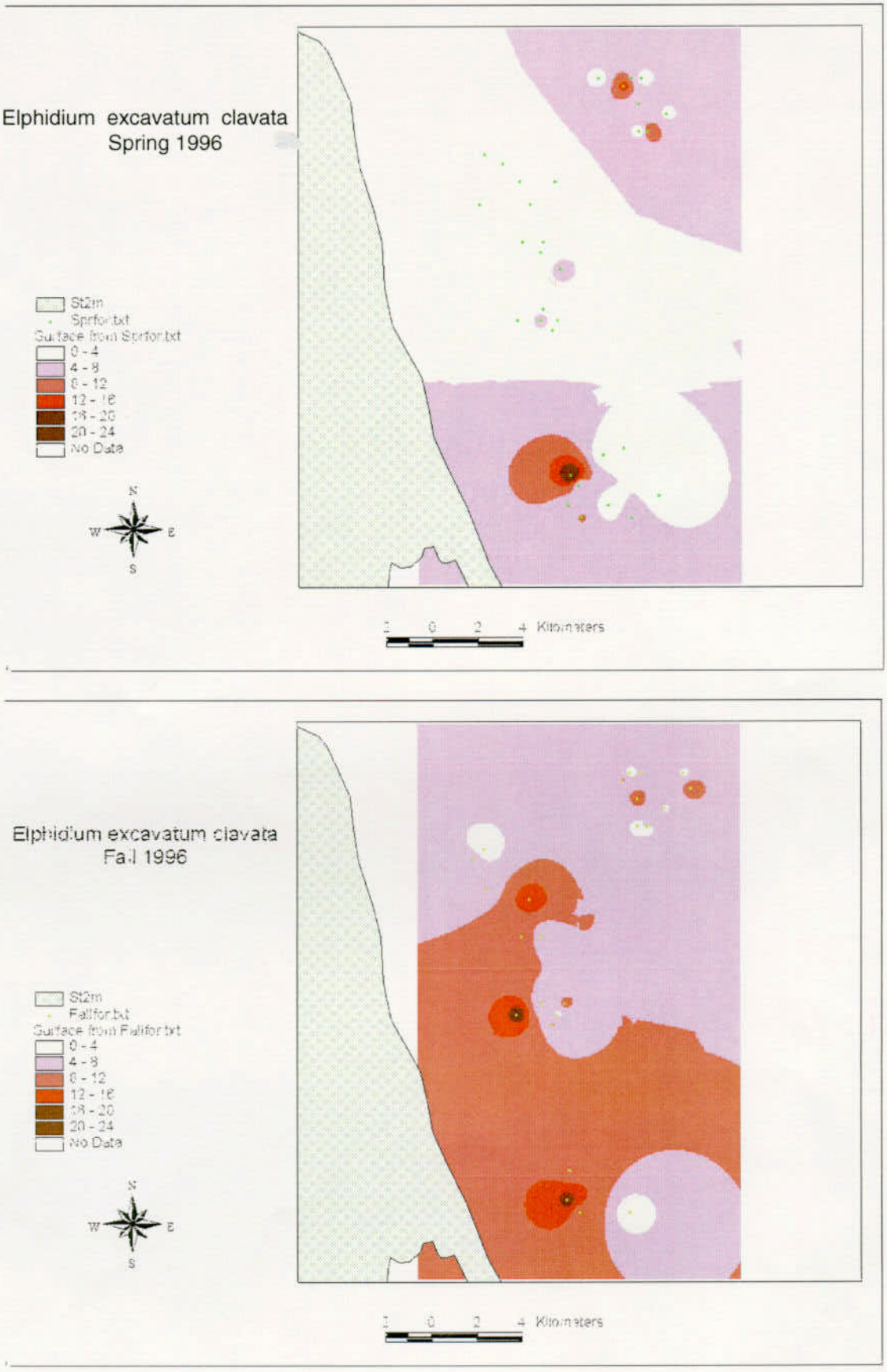

Figure 3: Distribution map showing the proportions of *Elphidium excavatum clavata* in total formaminiferal population on the continental shelf off Virginia Beach during Spring (upper map) and Fall (lower map) 1996. Small dots indicate station locations.

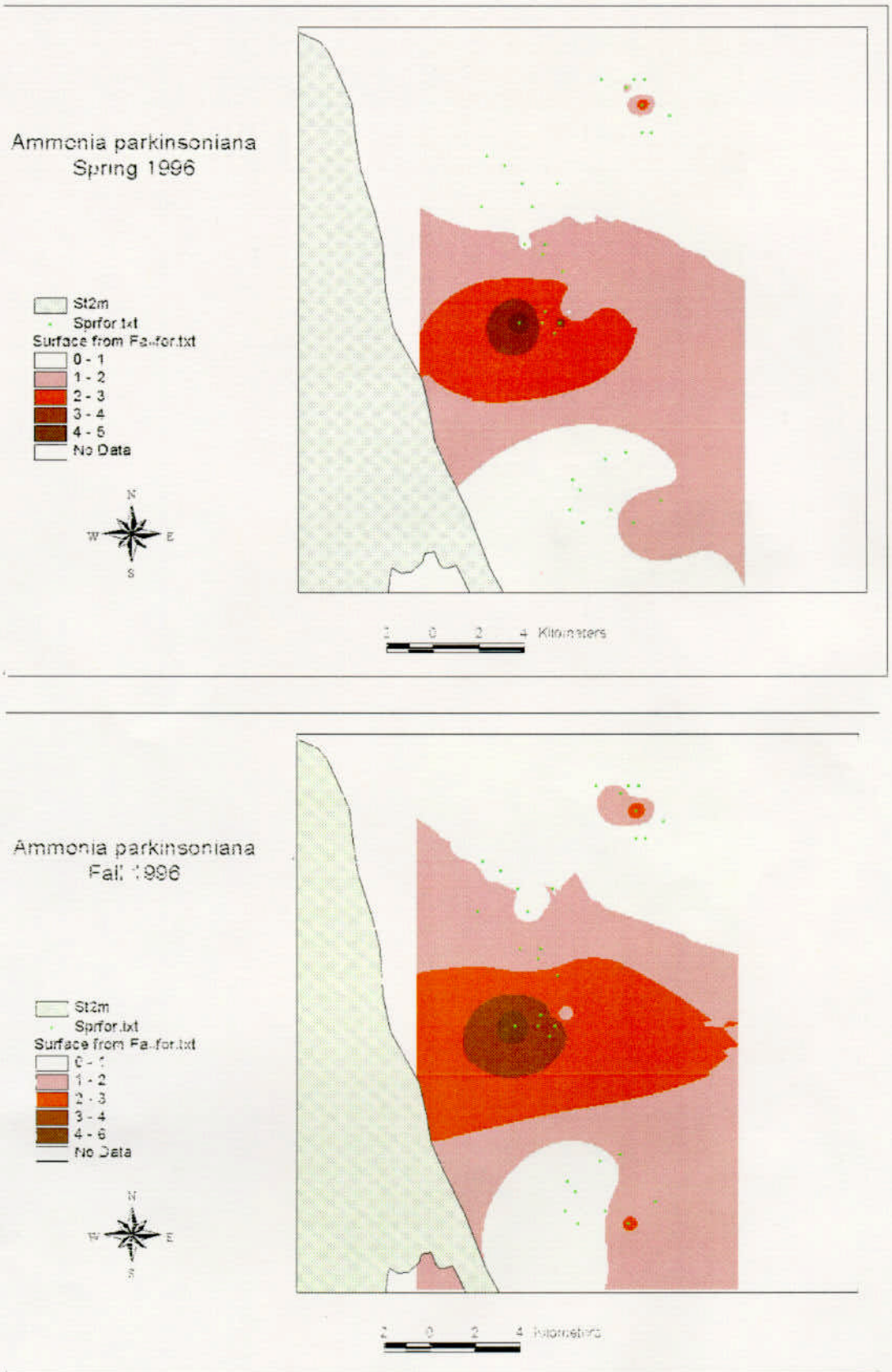

Figure 4: Distribution map showing the proportions of *Ammonia parkinsoniana* in total foraminiferal population on the continental shelf off Virginia Beach during Spring (upper map) and Fall (lower map) 1996. Small dots indicate station locations.

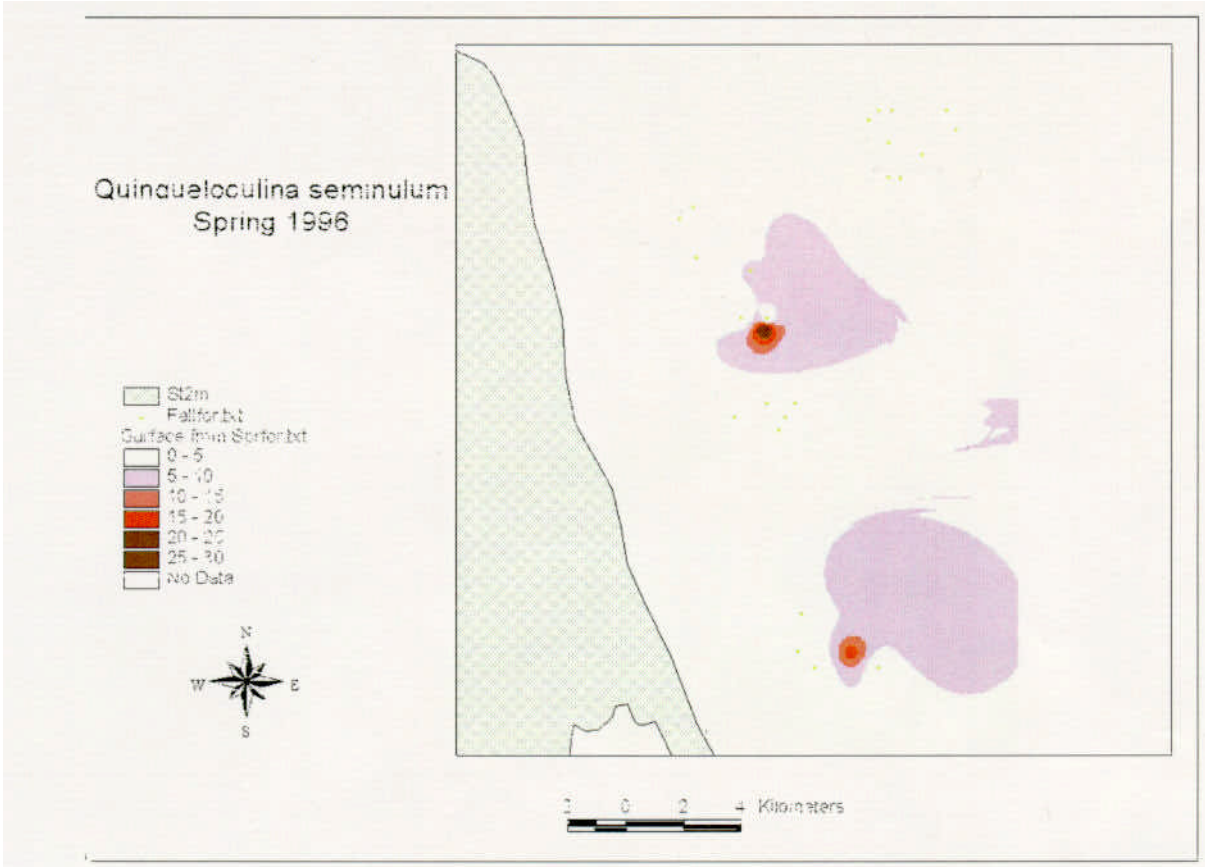

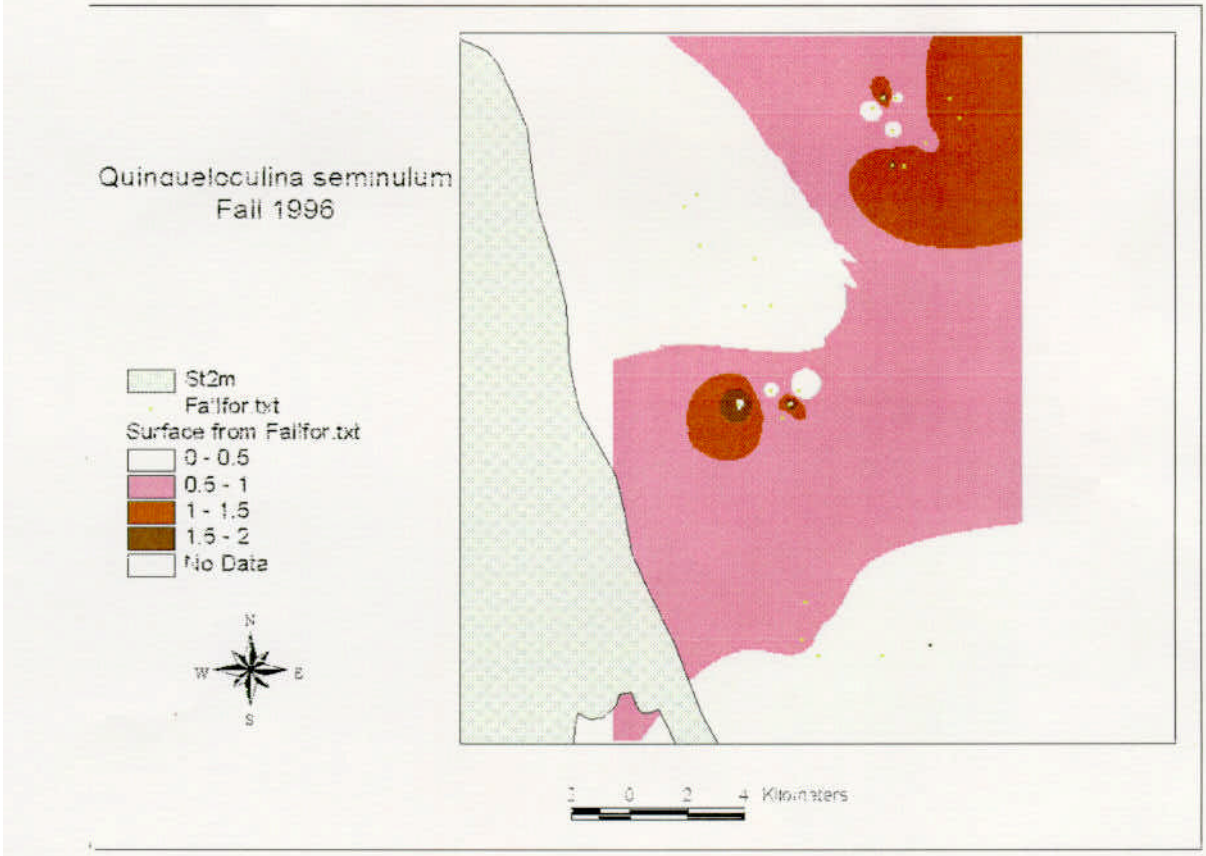

Figure 5: Distribution map showing proportions of *Quinqueloculina seminulum* in total formaminiferal population on the continental shelf off Virginia Beach during Spring (upper map) and Fall (lower map) 1996. Small dots indicate station locations.

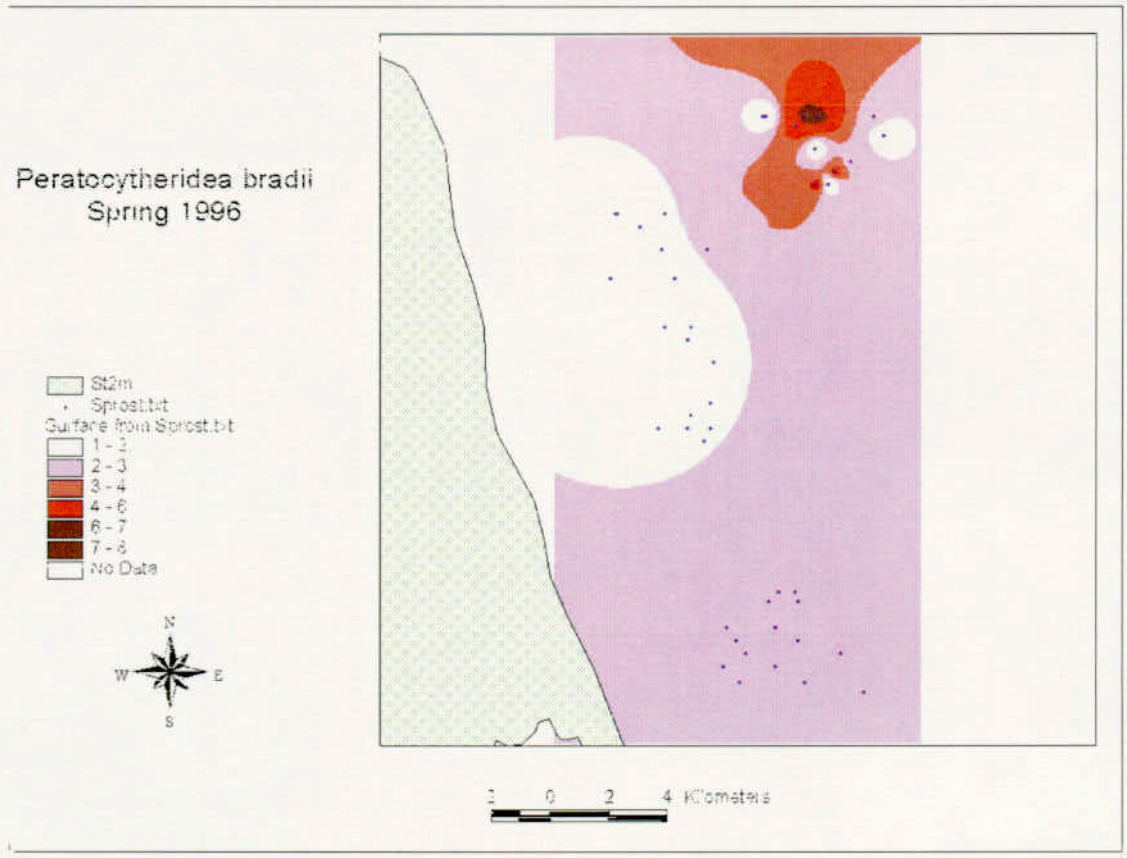

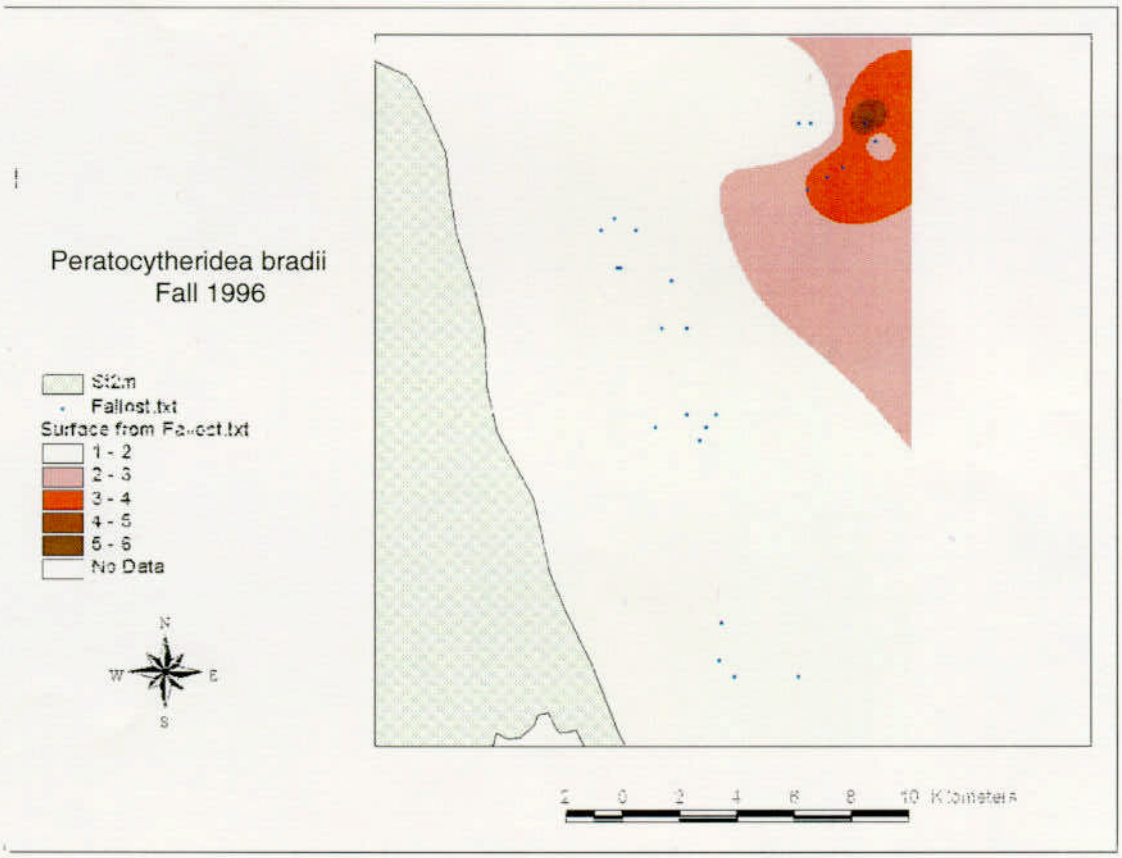

Figure 6: Distribution map showing number of *Peratocytheridea bradyi* specimens on the continental shelf off Virginia Beach during Spring (upper map) and Fall (lower map) 1996. Small dots indicate station locations.

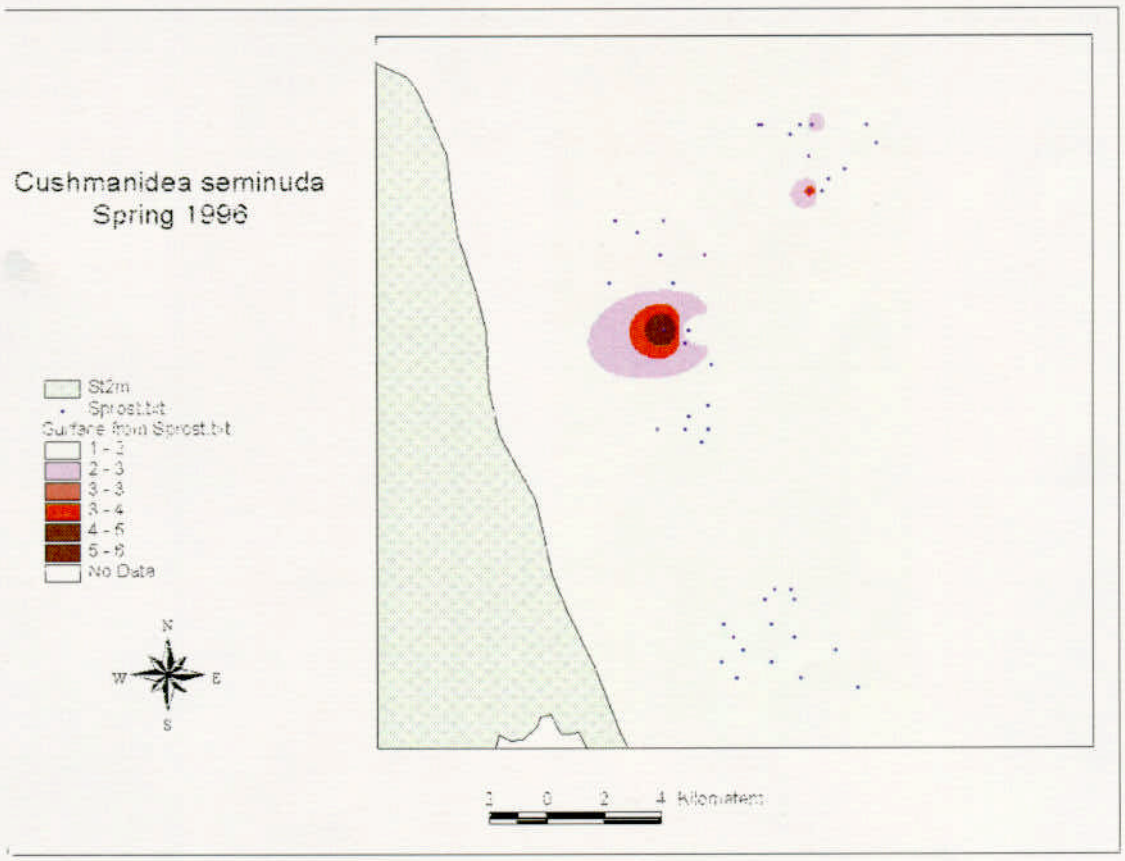

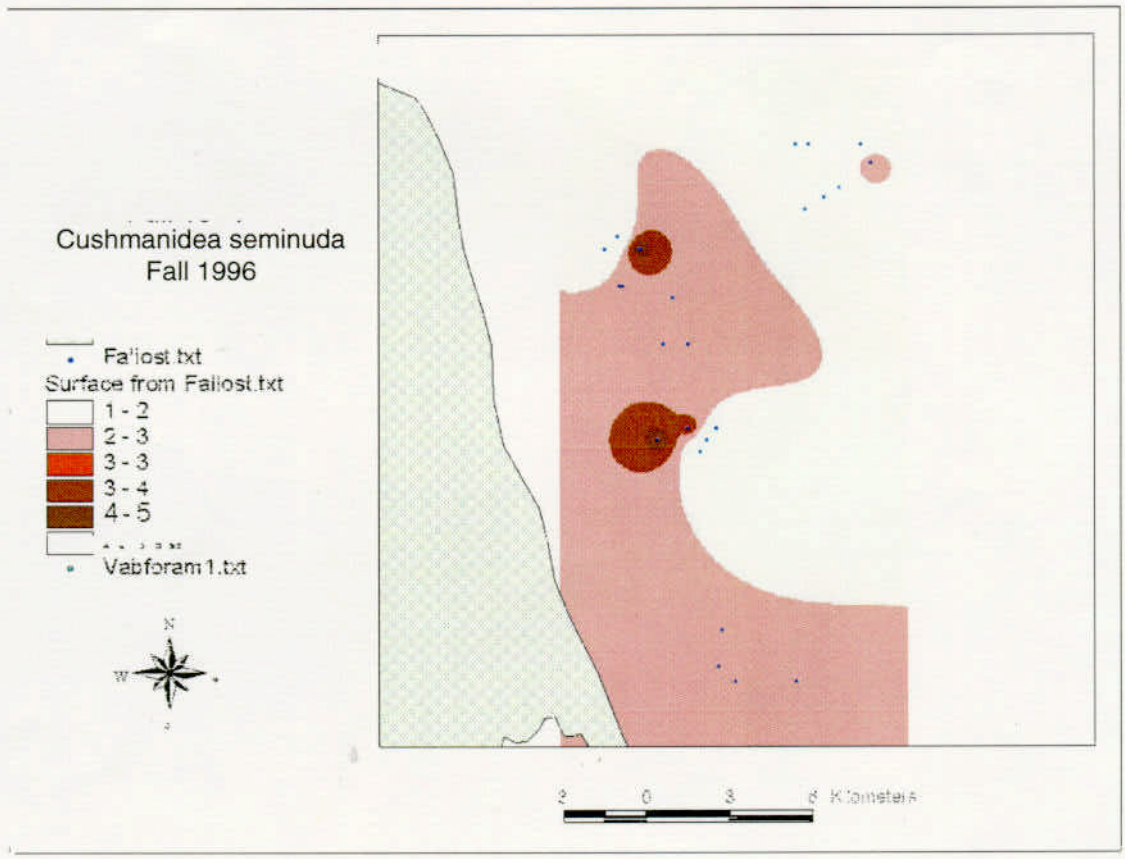

Figure 7: Distribution map showing number of *Cushmanidea seminuda* specimens on the continental shelf off Virginia Beach during Spring (upper map) and Fall (lower map) 1996. Small dots indicate station locations.

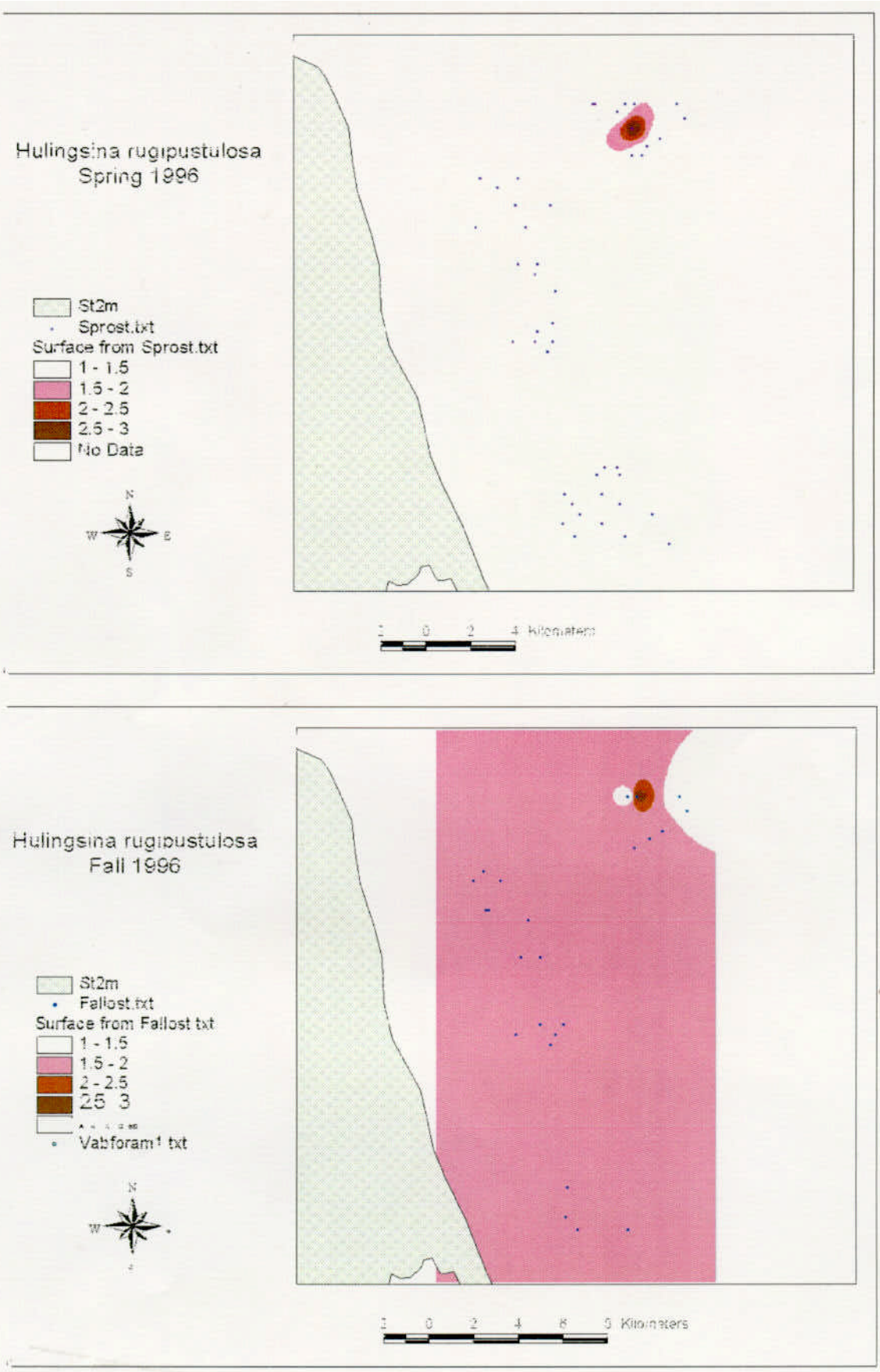

Figure 8: Distribution map showing number of *Hulingsina rugipustulosa* specimens on the continental shelf off Virginia Beach during Spring (upper map) and Fall (lower map) 1996. Small dots indicate station locations.

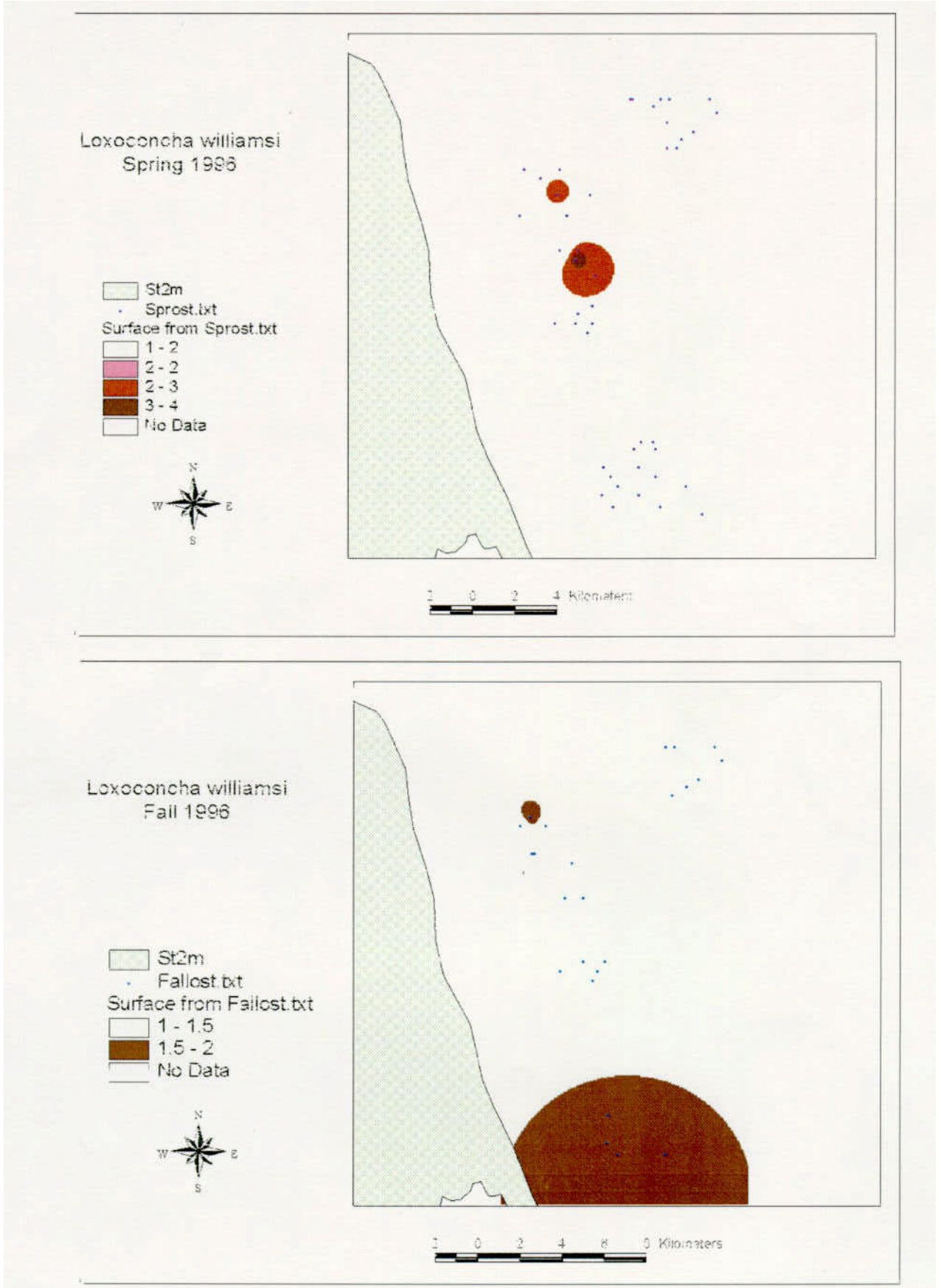

Figure 9: Distribution map showing number of *Loxoconcha williamsi* specimens on the continental shelf off Virginia Beach during Spring (upper map) and Fall (lower map) 1996. Small dots indicate station locations.

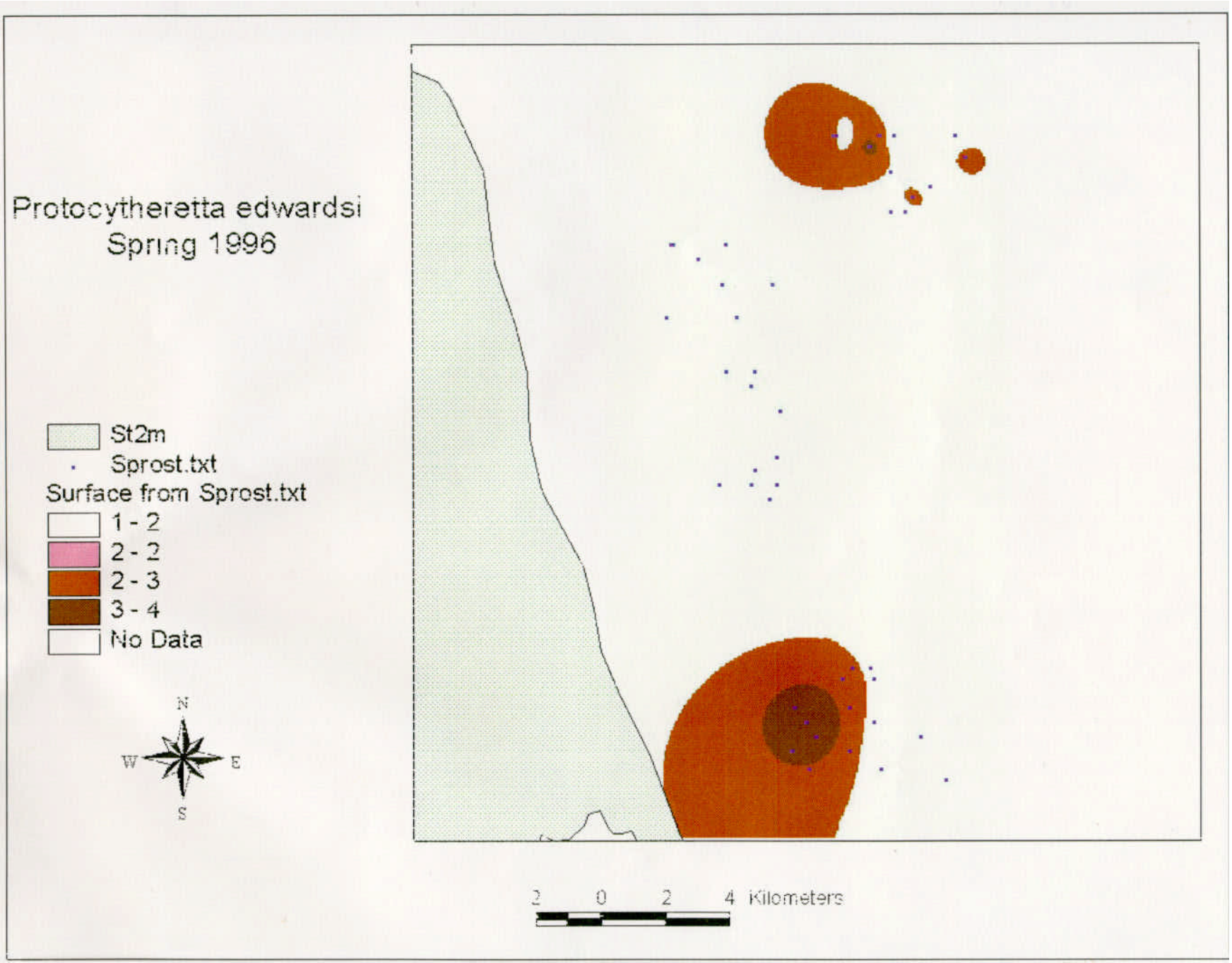

Figure 10: Distribution map showing number of *Protocytheretta edwardsi* specimens on the continental shelf off Virginia Beach during Spring. Small dots indicate station locations.

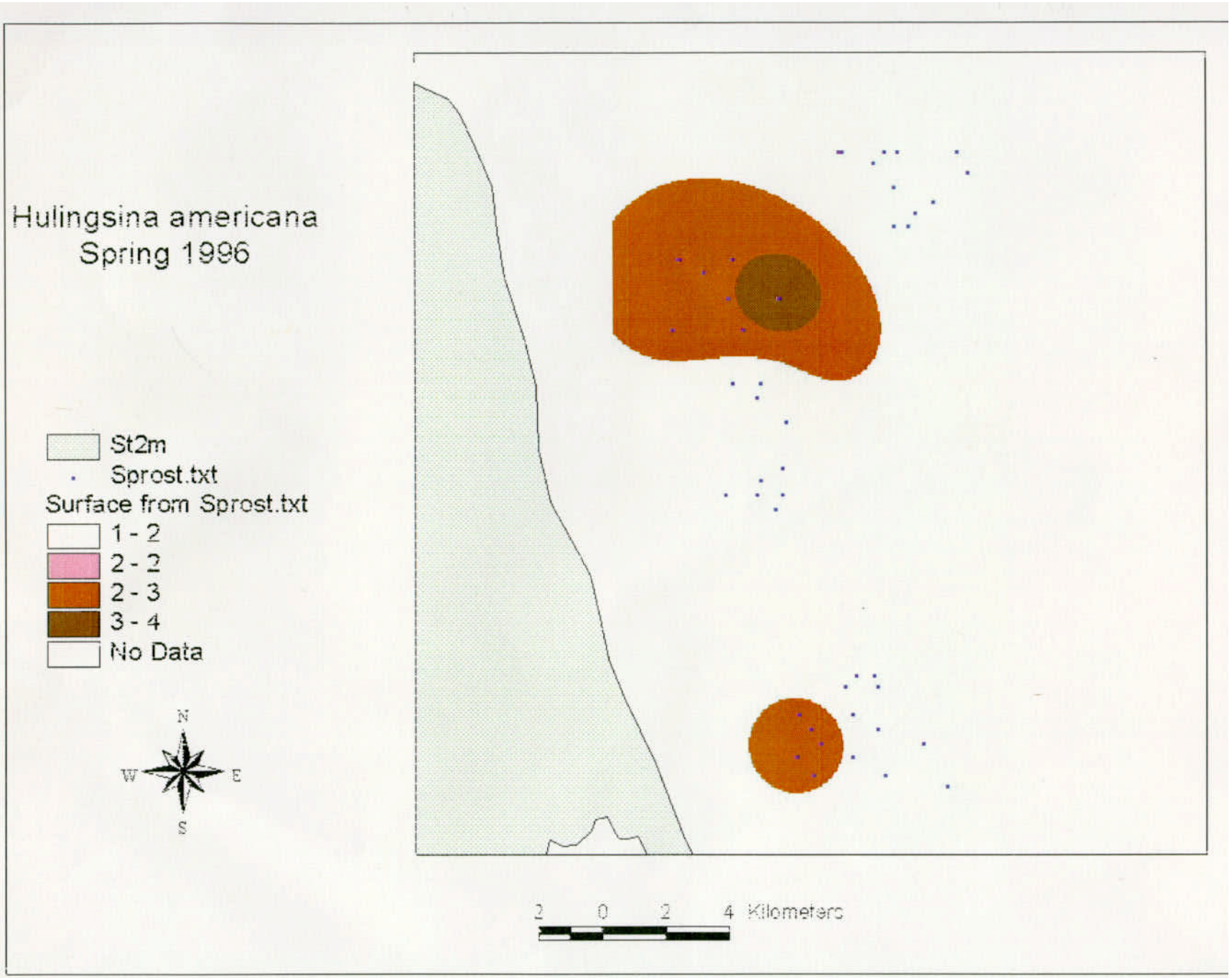

Figure 11: Distribution map showing number of *Hulingsina americana* specimens on the continental shelf off Virginia Beach during Spring. Small dots indicate station locations.

inner continental shelf environments of the temperate marine climatic zone of the Atlantic margin off the eastern United States.

The total species number and the composition of the ostracode assemblage is remarkably similar to that collected 30-35 years ago during the USGS-Woods Hole Oceanographic Institution (WHOI) Continental Margin Program (Emery 1966). A comparison between the assemblage found at station 43 of Valentine (1971) located near the current study area with our total 1996 assemblage indicates that Valentine found the same 31 species at this site in the 1960's sample found in the current study. These results leads to a fundamental conclusion from the current study that there has not been a long-term change in the overall ostracode assemblage at this site.

Although the overall ostracode faunal assemblage has not seen any net change over the past 30 years, we discovered important heretofore undiscovered seasonal and onshore-offshore variability in ostracode distributions revealed from the 1996 sampling program (Figures 6-11). Among the highlights:

- Several key ostracode species (*L. williamsi, H. rugipustulosa, C. seminuda*) have a more limited distribution in the Spring than in the Fall, suggesting there is a seasonal migration into new habitats during the Summer and early Fall months.
- The pattern of Summer/Fall range expansion may be related to the predominant southward direction to bottom drift of this region which may also be related to the prominent sand-swell crests in many regions of the mid-Atlantic shelf (Uchupi 1968; Hollister 1973).
- Several other species contract their range between the Spring and the Fall seasons. *Peratocytheridea bradyi* contracts its range from the northern and southern regions to only the southern region in the Fall. *Hulingsina americana* and *Protocytheretta edwardsi* are present in northern/central and northern/southern regions in the Spring, respectively, but they are almost totally absent from all samples taken in the Fall.

- The Virginia continental shelf contains several species encountered in sediments deposited over the past 1000 years in Chesapeake Bay. The shelf seems to serve as a source area for ostracodes species which periodically inhabit the more saline southern part and the deeper channel of Chesapeake Bay especially during periods when river discharge is reduced (Cronin unpublished data).

These results provide strong evidence that ostracode species have distinct population ecology linked to seasonal variability of the continental shelf. Major seasonal changes in ostracode populations have also been documented in estuarine ostracodes in the Patuxent River (Tressler and Smith 1948) and in Sippewisset Marsh, Cape Cod (Schweitzer and Lohman 1990) but until this time, were unknown for shelf species. We believe the southeastern Virginia 1996 data is the first to document such seasonality in Atlantic shelf marine ostracode distributions. Although additional analyses are merited to further document seasonal trends, we suspect that seasonal variability is related to bottom water currents. Southward flowing currents are considered especially important in affecting the distribution of *L. williamsi*, *H. rugipustulosa*, *C. seminuda.*

Benthic Foraminifera

A total of 20 species were identified from the surficial sediment samples. The dominant genus is *Elphidium*, a genus that includes several species common in nearshore environments of the North Atlantic Ocean. *Elphidium* is represented by three subspecies of *E. excavatum* (these are sometimes referred to separate species or distinct morphotypes of the same species): *Elphidium excavatum clavata*, *E. excavatum selseyensis*, and *E. excavatum excavata.* Figures 2 and 3 show the distributions of *E. excavatum selseyense*, the most abundant species found in our study, and *E. excavatum clavata* during Spring and Fall 1996.

Elphidium excavatum selseyensis is the dominant benthic foraminifer on the Virginia Beach continental shelf comprising up to 93% of the assemblage. The Spring distribution of *E. selseyensis* shows it comprises greater than 80% of the assemblage in northern and central areas, and 70% to 80% of the assemblage in the southern region. The distribution of *E. selseyensis* in the fall is reduced with a greater than 80% occurrence in the northern and central areas, and 60% to 80% in the southern area and the southern part of the central area.

Elphidium excavatum clavata is the dominant benthic foraminifer in the northern and southern areas. It makes up a much smaller percentage (< 8%) of the assemblage in the central area. This species expands to significant proportions in the fall where it composes greater than 8% (sometimes exceeding 16%) in much of the central and southern regions.

The occurrence off southeastern Virginia of these forms of the genus *Elphidium* is consistent with benthic foraminifer distributions reported from the mid-Atlantic continental shelf of North America. Murray (1991) and Culver and Buzas (1980), for example, mapped the *Elphidium* predominance from Cape Cod to Cape Hatteras and off the North American Atlantic coast, respectively. Schnitker (1971) also abundant *Elphidium clavatum* north of Cape Hatteras on the inner shelf.

Other species occurring on the Virginia shelf, in order of abundance, include *Quinqueloculina seminula, Ammonia parkinsoniana, Buccella frigida, Hanzawaia atlanticus, Hanzawaia concentrica* and *Eggerella advena.* Figures 4 and 5 show the distribution of *A. parkinsoniana* and *Q. seminulum* during Spring and Fall, 1996; plates 4 and 5 illustrate most of these species.

Although the relative abundances of *Ammonia parkinsoniana* in the Virginia Beach shelf samples are low, 5% or less, the distribution of this species seems to reflect distinct environmental conditions in the central study area. *A. parkinsoniana* is common throughout the world in estuarine environments due to its tolerance of highly fluctuating

salinities ranging from brackish (oligohaline, 0.5-5 ppt) to hypersaline (>40 ppt). It lives on the surface of fine-grained sediments down to a depth of 10 cm into the substrate and has a complex life history involving bacterial and algal endosymbionts (Goldstein and Moodley 1993). Chandler *et al.* (1996) found that *Ammonia* would only reproduce in culture under specific conditions that included the addition of silty-clay obtained from the Gulf of Mexico and a regular diet of phytoplankton.

The Spring distribution of *A. parkinsoniana* shows its greatest abundance in the southern part of the central area with only sparse occurrences in northern and southern regions. The fall distribution of *A. parkinsoniana* shows a slight expansion into the northern and western sections of the central area 2 but it is still rare to absent in northern and southern regions. It is unlikely that salinity variations restricted *A. parkinsoniana* from inhabiting northern and southern regions. Rather, we suspect that its limited range has more to do with resource limitations such as the availability of food, nutrients and/or finer grained sediments which may be available in the central region.

Quinqueloculina seminula is the dominant miliolid foraminifer that occurs in our surficial samples. It is present in percentages ranging from 5 10% to 20 25% in the central and southern regions in the Spring. However, its distribution changes in Fall when it expands into the northern region but disappears in parts of the central region. In the Fall its abundance is greatly reduced to < 2 %.

Conclusions

The modern benthic foraminiferal and ostracode faunas from three areas on the Virginia Beach continental shelf allow several important new conclusions about the meiobenthic fauna of sandy substrate environments of the continental shelf off Virginia Beach, Virginia.

- The 1996 faunal assemblages are extremely similar in species composition to those obtained in previous sampling program of the North American Atlantic continental shelf conducted during the 1960's. There has been no major long-term changes in the faunas from these regions.
- Seasonal benthic foraminiferal and ostracode distribution data show that significant changes in the relative abundance of the dominant species characterize the Spring and Fall assemblages. Several ostracode species expand their range southward from Spring to Fall suggesting bottom drift currents may play a role in seasonal dispersal of populations. Other ostracode species are common in the Spring but are almost totally absent in the Fall reflecting a complex, still poorly known population ecology.
- Foraminiferal species richness and geographic distributions are slightly greater in the fall with the expansion of the species *E. clavata*, *A. parkinsoniana*, and *Q. seminula*, and reduction in spatial distribution of *E. selseyensis*.
- *Ammonia parkinsoniana* has a distinct range limited to the central study region, possibly due to food and/or substrate limitations.
- The Virginia shelf is an important source habitat for species migrating into Chesapeake Bay. Two examples are the ostracode species, *Loxoconcha williamsi* and *Protocytheretta edwardsi*, which occur commonly on the Virginia shelf and have also been discovered in sediments in Chesapeake deposited prior to large-scale land clearing of the early 19th century.

Overall, our preliminary results indicate that a complex meiobenthic community inhabits the southeastern Virginia shelf. It is very likely that the entire community is potentially sensitive to environmental disruption to surficial sediments. However, due to the variable ecological requirements of each foraminiferal and ostracode species, the impact of habitat disturbance will vary widely among the 50 or so species recovered.

Furthermore, whereas the Virginia shelf is itself important habitat for meiobenthic species, this region must also be considered an important source area region for species able to migrate into coastal estuaries and bays like Chesapeake Bay. Consequently, species' population dynamics in the shelf region must be examined in the context of seasonal monitoring of conspecific populations living in adjacent areas.

Additional benthic sampling of the Virginia shelf through a second seasonal cycle, new sampling of the Virginia shelf/Chesapeake Bay mouth transition, supplemented by physical and chemical oceanographic data, would provide an ideal platform from which to fully understand shallow marine foraminiferal and ostracode species ecology and determine the least disruptive way to mine sand from shelf regions.

Acknowledgments

This study was conducted by the U.S. Geological Survey and Virginia Institute of Marine Science for Minerals Management Service, Cooperative Agreement No. 14-35-001-30807. We appreciate the encouragement of Barry Drucker of MMS during the course of this program, especially his support of multidisciplinary environmental studies of the continental shelf ecosystems. This study would not have been possible without the support and insights of C. H. (Woody) Hobbs, III and Robert Diaz of VIMS. We are grateful to the captain and crew of the *Bay Eagle* for their assistance in obtaining the samples for this study. Special thanks go to Colleen Cunningham for her diligence and patience in processing and picking foraminifera and ostracodes. Debra Willard kindly provided a useful review of this report.

References

Buzas, M. A. and S. J. Culver. 1980. Foraminifera: distribution of provinces in the western North Atlantic. Science, 209: 687-689.

Buzas, M. A. and S. J. Culver. 1984. Species duration and evolution: benthic foraminifera on the Atlantic continental margin of North America. Science, 225: 829-830.

Buzas, M. A. and S. J. Culver. 1989. Biogeographic and evolutionary patterns of continental margin benthic foraminifera. Paleobiology, 15: 11-19.

Buzas, M. A., L. S. Collins, S. L. Richardson, K. P. Severin. 1989. Experiments on predation, substrate preference, and colonization of benthic foraminifera at the shelfbreak off the Ft. Pierce Inlet, Florida. Journal of Foraminiferal Research, 19: 146-152.

Chandler, G. T., D. F. Williams, H. J. Spero, G. Xiaodong. 1996. Sediment microhabitat effects on carbon stable isotopic signatures of microcosm-cultured benthic foraminifera. Limnology and Oceanography, 41: 680-688.

Cronin, T. M. 1979. Late Pleistocene marginal marine ostracodes from the southeastern Atlantic Coastal Plain and their paleoenvironmental interpretations. Geographie Physique et Quaternaire, 33: 121-173.

Cronin, T. M. 1983. Bathyal ostracodes from the Florida-Hatteras slope, the straits of Florida and the Blake Plateau. Marine Micropaleontology, 8: 89-119.

Cronin, T.M. 1988. Evolution of marine climates of the U.S. Atlantic Coast during the last four million years: Philosophical transactions of the Royal Society (London) Series B, 318, no. 1191: 661-678.

Cronin, T. M. 1990. Evolution of Neogene and Quaternary marine Ostracoda: United States Atlantic coastal Plain: Evolution and speciation in Ostracoda IV. U.S. Geological Survey Professional Paper 1367-C.

Culver, S.J. and M. A. Buzas. 1980. Distribution of recent benthic foraminifera off the North American Atlantic coast. Smithsonian Contributions to the Marine Sciences, 6: 512 p.

Culver, S. J. and M. A. Buzas. 1983. Benthic foraminifera at the shelfbreak: North American Atlantic and Gulf margins. Society of Economic Paleontologist and Mineralogists Special Publication No. 33, pp. 359-371.

Cutter, G. R., Jr. and R. J. Diaz, 1998. Benthic Habitats and biological resources off the Virginia Coast 1996 and 1997. Contract Report to the Minerals Management Service. Virginia Institute of Marine Science, Gloucester Point, VA.

Emery, K. O. 1966. Atlantic continental shelf and slope of the United States--Geologic background. U.S. Geological Survey Professional Paper 529-A.

Goldstein, S. T. and L. Moodley. 1993. Gametogenesis and the life cycle of the foraminifer *Ammonia beccari* (Linne) forma *tepida* (Cushman). Journal of Foraminiferal Research, 23: 213-220.

Hazel, J. E. 1968. Pleistocene ostracodes zoogeography in Atlantic coast submarine canyons. Journal of Palcontology, 42: 1264-1271.

Hazel, J. E. 1970. Atlantic continental shelf and slope of the United States--ostracode zoogeography in the southern Nova Scotian and northern Virginian faunal provinces. U.S. Geological Survey Professional Paper 529 E.

Hazel, J. E. 1975. Patterns of marine ostracode diversity in the Cape Hatteras, North Carolina area. Journal of Paleontology, 49: 731-734.

Hazel, J. E. 1983. Age and correlation of the Yorktown (Pliocene) and Croatan (Pliocene and Pleistocene) formations at the Lee Creek Mine. In, C. E. Ray ed., Geology and Paleontology of the Lee Creek Mine, North Carolina, I. Smithsonian Contributions to Paleobiology, 53: 81-199.

Hollister, C. D. 1973. Atlantic continental shelf and slope - Texture of surface sediments from New Jersey to southern Florida. U.S. Geological Survey Professional Paper 529-M.

Loeblich, A.R. and Tappan, H., 1988. Foraminiferal Genera and their Classification. Vols. 1 and 2: Van Nostrand Reinhold, New York.

Murray, J.W., 1991. Ecology and Paleoecology of Benthic Foraminifera, John Wiley and Sons, New York: 397 p.

Schnitker, D., 1971. Distribution of foraminifera on the North Carolina continental shelf. Tulane Studies in Geology and Paleontology, 8: 169-215.

Schweitzer, P. N. and G. P. Lohman. 1990. Life-history and the evolution of ontogeny in the ostracode genus *Cyprideis*. Paleobiology, 16: 107-125.

Tressler, W. L. and E. M. Smith. 1948. An ecological study of seasonal distribution of Ostracoda, Solomons Island, Maryland region. Chesapeake Biological Laboratory Publication No. 71.

Uchupi, E. 1968. Atlantic continental shelf and slope - Physiography. U.S. Geological Survey Professional Paper 529-C.

Valentine, P. C. 1971. Climatic implication of a late Pleistocene ostracode assemblage from southeastern Virginia. U.S. Geological Survey Professional Paper 683-D.

Walford, L. A. and Wicklund, R. I. 1968. Monthly sea surface temperature structure from the Florida Keys to Cape Cod. American Geographical Society Serial Atlas of the Marine Environment. Folio 15.

Walton, W.R., 1952. Techniques for recognition of living foraminifera. Contribution from the Cushman Foundation for Foraminiferal Research, 3: 56-60.

Scanning Electron Microscope Plates of Virginia Shelf Ostracodes and Foraminifera

Plate 1

Figure 1: *Bensonocythere sapeloensis* Hall 1965. x 134, Sta. 64, Cell 308, female, left valve.

Figure 2: *Bensonocythere sapeloensis* Hall 1965. x 133, Sta. 62, Cell 316, female, right valve, internal view.

Figure 3: *Bensonocythere sapeloensis* Hall 1965. x 141, Sta. 1, Cell 209, male, left valve.

Figure 4: *Puriana rugipunctata* (Ulrich and Bassler 1904) , x 143, Sta. 55, Cell 264, female, right valve.

Figure 5: *Muellerina ohmerti* Hazel 1983, x 178, Sta. 52, Cell 52, female, left valve.

Figure 6: *Protocytheretta edwardsi* (Cushman 1906)., x 83,4, Sta. 64, Cell 64, female, right valve.

Figure 7: *Cytherettid*, x 71,3, Sta. 62, Cell 316, female, left valve, internal view.

Figure 8: *Protocytheretta edwardsi* (Cushman 1906, x 91,7, Sta. 204, Cell 204, female, left valve, internal view.

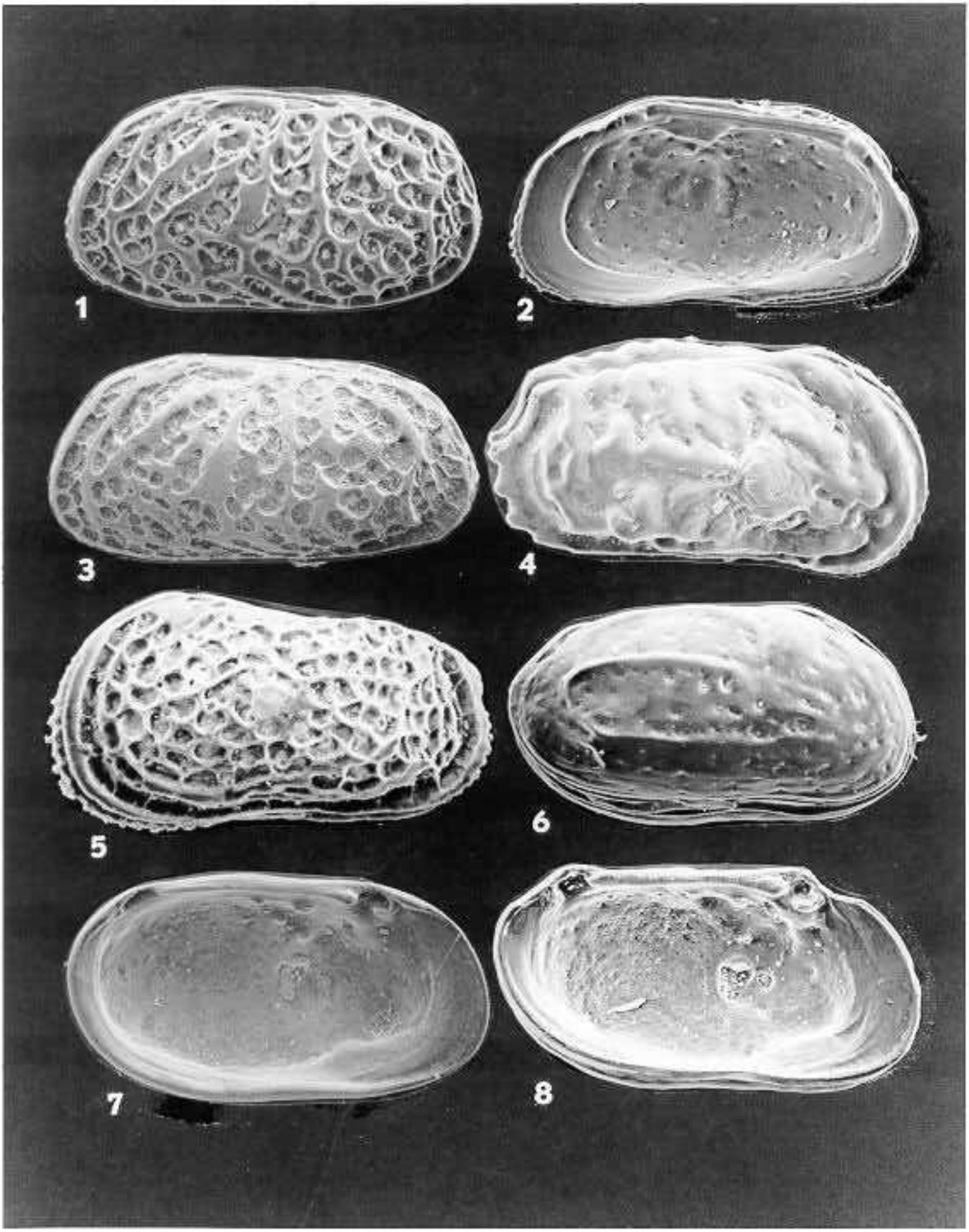
1
2
3
4
5
6
7
8

Plate 2

Figure 1: *Hulingsina americana* (Cushman 1906). x 88,1 , Sta. 64, Cell 308, female?, left valve.

Figure 2: *Cushmanidea seminuda* (Cushman 1906). x 94,2 , Sta. R2, Cell 185, female, right valve.

Figure 3: *Sahnia sp.*, x 141, Sta. 24, Cell 234, male, left valve.

Figure 4: *Hulingsina rugipustulosa* (Edwards 1944) x 147, Sta. 46, Cell 46, female, right valve.

Figure 5: *Peratocytheridea bradyi* (Stephenson 1938). x 139, Sta. 52, Cell 213, female, left valve, internal view.

Figure 6*: Peratocytheridea bradyi* (Stephenson 1938). x 124, Sta. 209, Cell 209, female, left valve.

Figure 7: *Peratocytheridea bradyi* (Stephenson 1938). x 134, Sta. 51, Cell 204, female, left valve, Note hole in middle where predator bored through carapace.

Figure 8: *Eucythere declivis* (Norman 1865). x 151, Sta. R11, Cell 49, female?, left valve, soft parts.

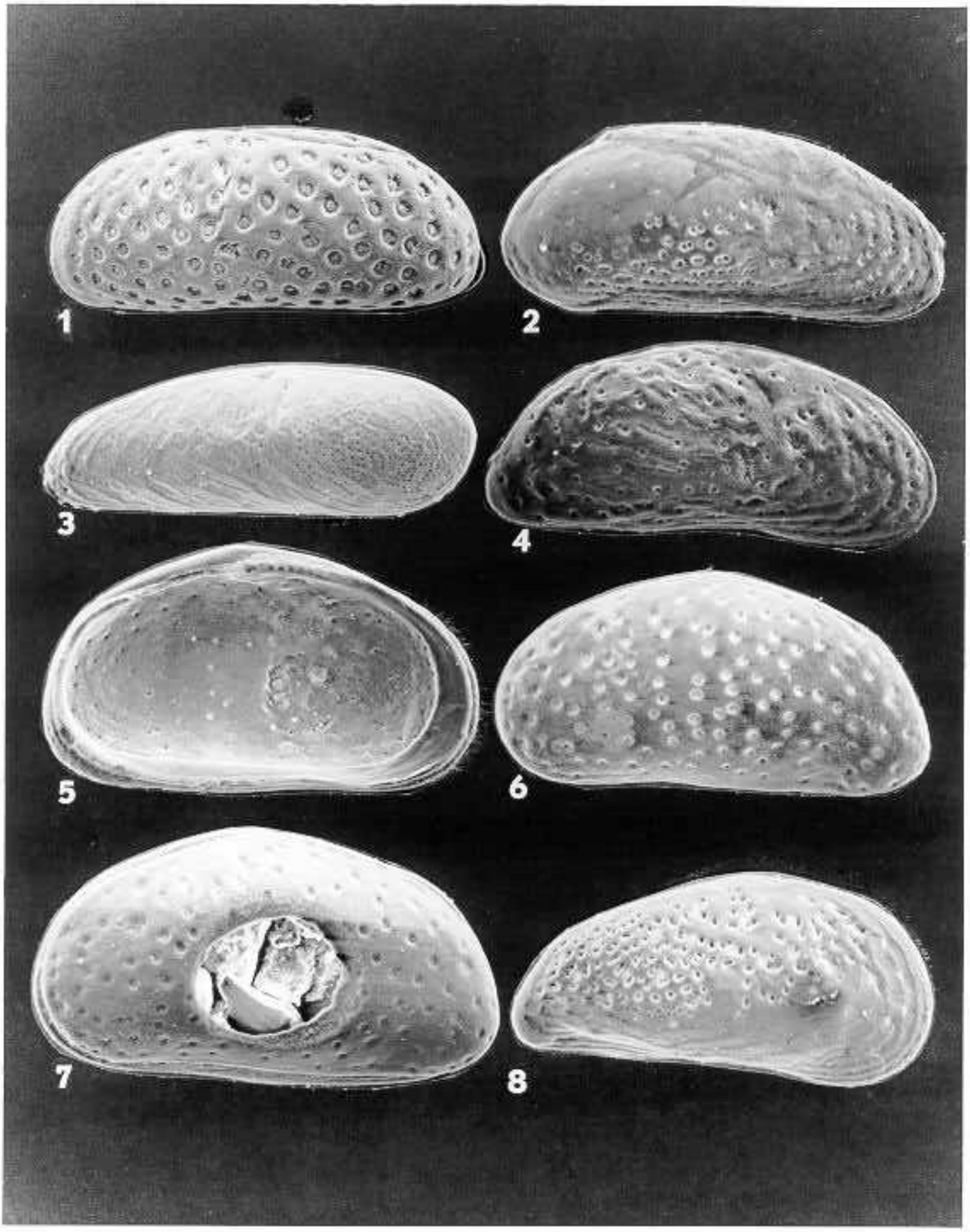
1
2
3
4
5
6
7
8

Plate 3

Figure 1: *Tetracytherura* sp. A of Valentine 1971, x 166, Sta. R11, Cell 49, male, left valve.

Figure 2: *Tetracytherura* sp. A of Valentine 1971, x 166, Sta. 64, Cell 308, left valve, internal view.

Figure 3: *Cytherura* sp., x 167, Sta. 64, Cell 64, female, left valve.

Figure 4: *Cytherura* sp. x 307, Sta. 53, Cell 365, left valve.

Figure 5: *Proteoconcha tuberculata* (Puri 1960). x 104, Sta. 54, Cell 263, male, right valve.

Figure 6: *Proteoconcha tuberculata* (Puri 1960). x 121, Sta. 53, Cell 246, female?, left valve, internal view.

Figure 7: *Loxoconcha williamsi (=* aff *granulata* Sars 1865*).* x 151, Sta. R10, Cell 66, female, left valve.

Figure 8: *Cytherura wardensis* Howe and Brown 1935. x 176, Sta. 229, Cell 229, female, left valve.

Figure 9: *Microcythere* sp., x 280, Sta. 53, Cell 365, lateral view.

Figure 10: *Microcythere* sp. x 307, Sta. 53, Cell 365, dorsal view.

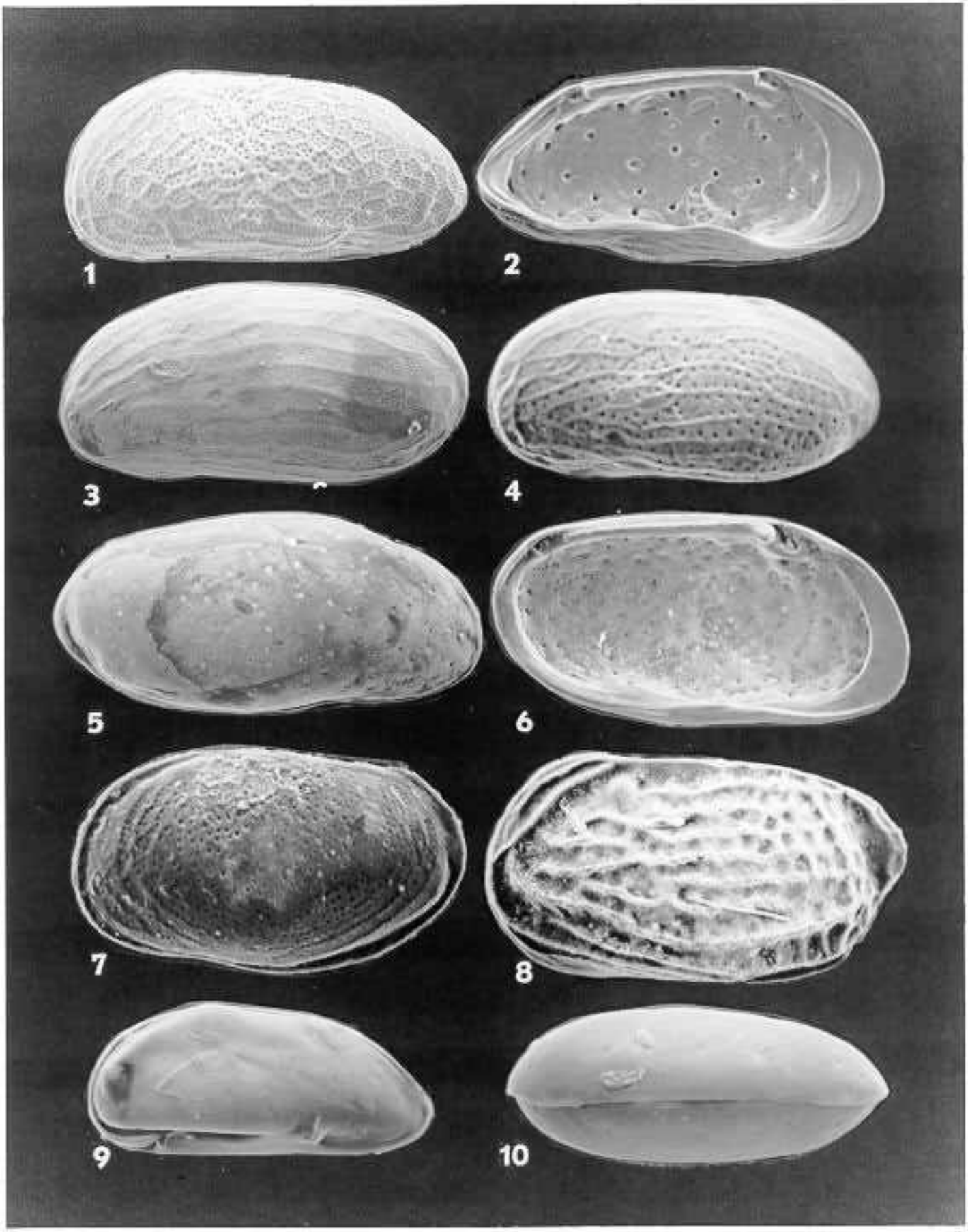
1
2
3
4
5
6
7
8
9
10

Plate 4

Figure 1: *Elphidium clavata,* x 191, Sta. 52, Cell 213.

Figure 2: *E. selseyensis,* x 164, Sta. 57, Cell 372.

Figure 3: *Quinqueloculina seminulum,* x 122, Sta. 54, Cell 332.

Figure 4: *E. clavata,* x 176, Sta. 57, Cell 372.

Figure 5: *E. selseyensis,* x 178, Sta. R11, Cell 49, aperture L.

Figure 6: *Hanzawaia concentrica,* x 147, Sta. R9, Cell 104.

Figure 7: *Ammonia parkinsoniana,* x 176, Sta. R2, Cell 185, spiral side.

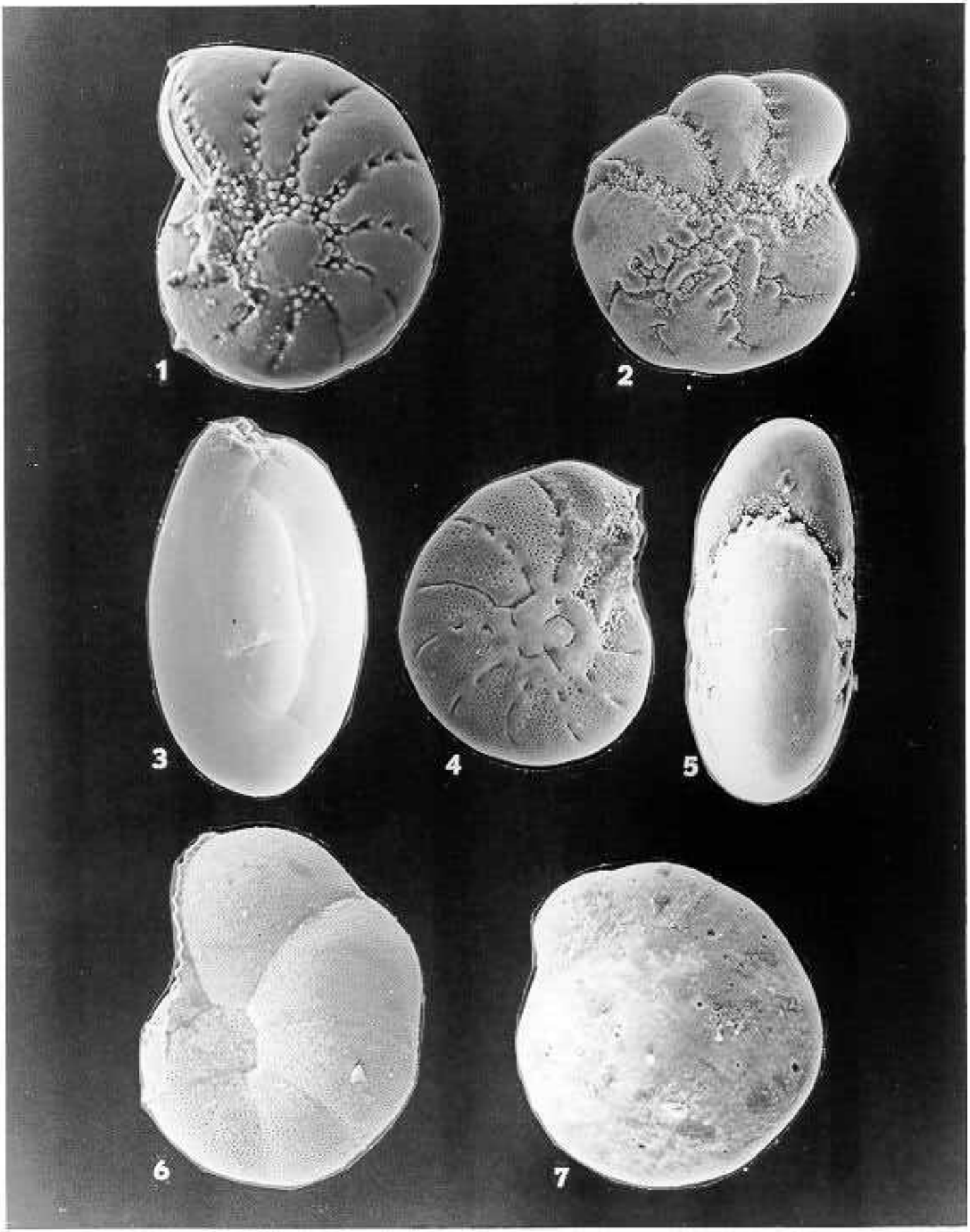
1
2
3
4
5
6
7

Plate 5

Figure 1: *Buccella frigida,* x 217, Sta. 57, Cell 372, umbilical view.

Figure 2: *Ammonia parkinsoniana,* x 181, Sta. R14, Cell 24, umbilical view.

Figure 3: *Planulina mera,* x 141, Sta. 52, Cell 213.

Figure 4: *Hanzawaia atlanticus,* x 122, Sat. R4, Cell 183.

Figure 5: *Guttulina lactea,* x 176, Sta. 59, Cell 360.

Figure 6: *Buccella frigida,* x 217, Sta. R2, Cell 185.

Figure 7: *Hanzawaia concentrica,* x 151, Sta. 51, Cell 204, flat side view.

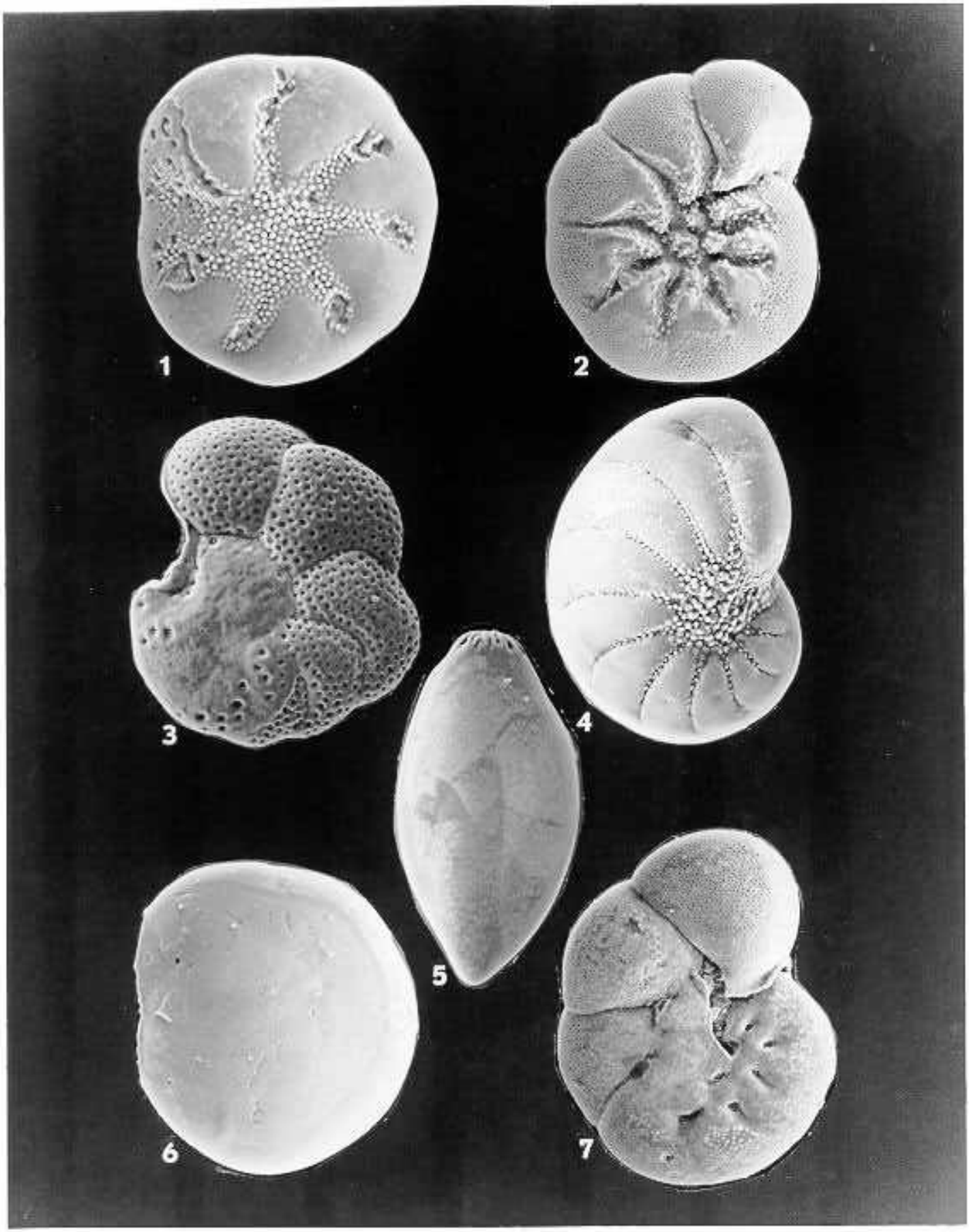
1
2
3
4
5
6
7

Appendix 1: Species Census data of Foraminifera on the Virginia Continental Shelf, Spring 1996

Date	Cell	Longitude	Latitude	*Elphidum excavatum clavata*	*Elphidum excavatum selseyensis*	*Elphidum excavatum excavata*	*Ammonia parkinsoniana*	*Bucella cf hamai*	*Hanzawaia concentrica*	*Quinqueloculina seminula*	*Florilus atlanticus*	*Cibicides bradyi*	*Guttulina lactea*	*Bulimina*	*Quinqueloculina jugosa*	*Bucella frigida*	*Planulina mera*	*Discorbis mira*	*Eggrella advena*	*Trochammina sp.*	Total
6/5/96	174	75.907	36.816	6	206	3	6	2	1	10											234
6/5/96	185	75.901	36.812		188	4	6	2	2	5	2										209
6/5/96	194	75.903	36.808	10	221	9	4	6	2	2	2		2	1							259
6/5/96	183	75.908	36.812	15	234	13	3	4	1		4	1									275
6/5/96	181	75.917	36.812	6	249		3					1	1								260
6/6/96	137	75.9	36.832	1	14			1		1			1								18
6/6/96	115	75.908	36.839	3	140	15	8	2	1	80	2		22		5						278
6/6/96	106	75.907	36.843		209	24				2											235
6/6/96	104	75.915	36.843	4	183	28	2	1	1						1						220
6/6/96	66	75.912	36.858	5	101	13	1			8											128
6/6/96	49	75.902	36.867		227	8		1		22	1		2		3						264
6/6/96	50	75.916	36.867	4	222	32		4	2	2			1								267
6/6/96	61	75.932	36.858	4	228	40				1			1			1					275
6/6/96	24	75.923	36.874	2	223	51	6			3											285
6/6/96	13	75.93	36.878	3	225	44	4			1											277
5/15/96	229	75.869	36.887	6	267	5				3											281
5/15/96	205	75.868	36.908	4	255	15		1		6	1										282
5/15/96	201	75.885	36.908	8	247	20		1		4											280
5/15/96	234	75.869	36.898	12	243	6			1	2	2						2				268
5/15/96	263	75.869	36.887	8	253	16	2	1	2	2	2				1						287
5/15/96	204	75.872	36.908	22	234	16	1		1	3	1						1	1			280
5/15/96	213	75.875	36.905	43	223	20			6	5	1					1	1				300
5/15/96	246	75.858	36.894	10	251	12	1	1	3	8	1						3				290
5/15/96	264	75.865	36.887	38	240	17			5	5	4					3	2				314
5/15/96	264	75.865	36.887	30	207	20	1	1	1	9	2				1		1				273
6/5/96	377	75.872	36.733	23	232	28				1						5			1		290
6/5/96	365	75.881	36.738		16					4			1		1	1					23
6/5/96	342	75.893	36.746	13	241	10	6		2	12	3		2			8					297
6/5/96	332	75.898	36.75	69	192	26															287
6/5/96	372	75.892	36.733	24	253	10	1									3					291
6/5/96	361	75.897	36.738	17	250	6	1		3	2						5					284
6/5/96	360	75.861	36.742	1	77	2			1	9	2		7				1		15	1	116
6/5/96	316	75.883	36.758	1	99	1	3			9	2		10		4				2	1	132
6/5/96	308	75.875	36.761	1	81	1	1	2	1	9	2		3		3						104

Appendix 2: Species Census data of Foraminifera on the Virginia Continental Shelf, Fall 1996

Date	Cell	Longitude	Latitude	*Elphidium excavatum clavata*	*Elphidium excavatum selseyensis*	*Elphidium excavatum excavata*	*Ammonia parkinsoniana*	*Buccella cf hamai*	*Hanzawaia concentrica*	*Quinqueloculina seminula*	*Florilus atlanticus*	*Cibicides bradyi*	*Guttulina lactea*	*Bulimina*	*Quinqueloculina jugosa*	*Buccella frigida*	*Planulina mera*	*Eggrella advena*	*Trochamnina sp.*	*Eponides sp.*	*Rosalina floridana*	*Textularia sp.*	*E. discodale*	Total
10/21/96	13	75.93	36.878	5	272	8	1	1			4					1		1						293
10/21/96	234	75.869	36.898	31	225	14	9			1	3					1		3						287
10/21/96	46	75.913	36.867	13	275	5	2			3						1								299
10/21/96	264	75.865	36.887	22	238	12	2		5	4	6						1							290
10/21/96	64	75.917	36.857	5	273	3	1		2	3	1				1	1	4							294
10/21/96	209	75.851	36.908	11	237			2	3	4	6						6							269
10/21/96	229	75.848	36.902	32	229	23	1		2	4	1	1					1							294
10/21/96	263	75.869	36.887	11	259	5	1	2	3	5	5			1	1		2							295
10/22/96	31	75.934	36.874	17	248	10	4	4		1	2								1					287
10/22/96	213	75.875	36.905	25	239	18	5				2													289
10/22/96	60	75.929	36.862	20	219	23	3	2									3		1					271
10/22/96	66	75.912	36.858	41	182	29	2	5													3	1		263
10/22/96	104	75.915	36.843	33	189	43	4		1		1					2								273
10/22/96	106	75.907	36.843	16	265	3	5	2					2											293
10/22/96	204	75.872	36.908	10	261	6			5	6	2						2			1				293
10/22/96	205	75.868	36.908	13	247	13		1	3	1	1					1	1							281
11/6/96	377	75.872	36.733	1	40		1	2			2		1											47
11/6/96	332	75.896	36.75	28	210	14		1	4	2	2					4								265
11/6/96	372	75.892	36.733	24	199	9			1		1		1	1		9								245
11/6/96	361	75.897	36.738	46	120	77	1		1	2	1					6		1						255
11/6/96	181	75.917	36.812	54	167	38	15	3	6	6	1	1	1											292
11/6/96	194	75.903	36.808	25	231	9	9	4	3	2	5		1			3								292
11/6/96	185	75.901	36.812	11	217	27	11		7	6		1	3		1	2							3	289
11/6/96	174	75.907	36.816	15	223	13	9	2	2	1	1		1			2								269
11/6/96	176	75.898	36.816	26	225	12	4	2	5		1	1				5								281

Appendix 3: Species Census data of Ostracoda on the Virginia Continental Shelf, Spring and Fall 1996

Date	cell	Latitude	Longitude	*Actinc. captionis*	*Benson. sp. A*	*Benson. sapeloensis*	*Benson.whitei*	*Bensonocythere*	*Campylocythere laeva*	*Cytherura howei*	*Cytheromorpha warneri*	*Cytherura sp.*	*Cytherura sp.*	*Cytherides*	*Cushmanidea seminuda*	*Eucythere declivis*	*Hemicytherura*	*Hulings.americana*	*Hulings.rugipustulosa*	*Hulingsina sp.*	*Loxo. sperata*	*Loxo. sp. A*	*Microcythere*	*Microcytherura sp. A*	*Microcytherura sp. B*	*Muellerina ohmerti*	*Paradox. delicata*	*Peratocytherides bradyi*	*Proteo.gigantica*	*Prot.edwardsi*	*Puriana rugipunctata*	*Sahnia*	*Indeterminate*	*Other*	Total
May-96	229	36.902	75.848												1			1										1		3					6
May-96	205	36.908	75.868												3					1								7		1					12
May-96	201	36.908	75.885												1				1											4					6
May-96	234	36.898	75.869																3									1	2			2			8
May-96	229	36.902	75.848												1				1	1								6		1					10
May-96	204	36.908	75.872												2													8	2	3					15
May-96	213	36.905	75.875																1									5	1	4					11
May-96	246	36.894	75.858																1									3	2	1					7
May-96	263	36.887	75.869												4									1				5	2	2					14
May-96	264	36.887	75.865												1				1									1		2	1	2			8
Jun-96	390	36.73	75.854																																0
Jun-96	377	36.733	75.872																																0
Jun-96	365	36.738	75.881									2								1			28		1										32
Jun-96	353	36.742	75.89																																0
Jun-96	342	36.746	75.893		2		1								1			3		1		1		2		1				4					16
Jun-96	332	36.75	75.896	1											1							1							1						4
Jun-96	372	36.733	75.892																																0
Jun-96	361	36.738	75.897					1							2							1				1										5
Jun-96	360	36.742	75.861		2		1			1			1			2							2	6	3					1			2		21
Jun-96	347	36.746	75.874																																0
Jun-96	336	36.75	75.881																																0
Jun-96	316	36.758	75.883		3								6					2		1			6	5	1								1		25
Jun-96	318	36.758	75.874																																0
Jun-96	308	36.761	75.875		1	1							2		1	1		1		1			4	2	2										16
Jun-96	307	36.761	75.88																																0
Jun-96	174	36.816	75.907												2				1							1										4
Jun-96	185	36.812	75.901												2					1															3
Jun-96	194	36.808	75.903																	3										1					4
Jun-96	183	36.812	75.908																																0
Jun-96	181	36.812	75.917												1															1					2
Jun-96	137	36.832	75.9																																0
Jun-96	115	36.839	75.908		5											2		2				4	1	12	10										36

Appendix 3: Species Census data of Ostracoda on the Virginia Continental Shelf, Spring and Fall 1996

Jun-96	104	36.843	75.915												6												1	1							8
Jun-96	66	36.858	75.912																			1		1												2
Jun-96	49	36.867	75.902												2	1		4	1			2		2	1				1							14
Jun-96	50	36.867	75.916						1						1							3														5
Jun-96	61	36.858	75.932		1																	1														2
Jun-96	24	36.874	75.923																1																	1
Jun-96	13	36.878	75.93			1									1					1																3
Jun-97		36.878	75.93												1					1						1							1	1	5
Jun-96		36.8195	75.901												2															2						4
Jun-97	169	36.878	75.9304												1				1								1	1		1					5
Jun-97	13	36.878	75.915																														1	1		1
Jun-97	104	36.843	75.915																	1		1														2
Jun-97		36.908	75.884							2														1					1							4
Jun-97	201	36.908	75.885																	1							1								2
Jun-97	205	36.908	75.868		1										1			1		1							5		3				1	13
Jun-97	209	36.908	75.851		1										1					4							3		1					10	
Jun-97	234	36.898	75.869										1		1					1					1		2						1	7	
Jun-97	246	36.894	75.858								1		1		1				1	1	1						6	1	4				1	18	
Jun-97	255	36.891	75.863										2		2												5		3	1			1	14	
Oct-96	13	36.878	75.93												1							2												3	
Oct-96	24	36.874	75.923												5							1												6	
Oct-96	31	36.874	75.934			1									2							1												4	
Oct-96	46	36.867	75.913							1									2			1					4		1					9	
Oct-96	52	36.862	75.928																							1	1							2	
Oct-96	55	36.863	75.917				1								2				2								4							9	
Oct-96	60	36.862	75.929																			1												1	
Oct-96	64	36.857	75.917								1	1			2												1	2	1	2				10	
Oct-96	66	36.858	75.912													1						1												2	
Oct-96	104	36.843	75.915																			1		1					1					3	
Oct-96	106	36.843	75.907												3					1		1												5	
Oct-96	204	36.908	75.872												2				1								1		1					5	
Oct-96	205	36.908	75.868																3								1							4	
Oct-96	209	36.908	75.851								1				1				1								6							9	
Oct-96	229	36.902	75.848								1				3				1								3						1	9	
Oct-96	263	36.887	75.869									1						1										2						4	
Nov-96	377	36.733	75.872						1																				1					2	
Nov-96	332	36.75	75.896			1														3												2		6	
Nov-96	372	36.733	75.892			1																2												3	
Nov-96	361	36.738	75.897			1										1				2					1									5	
Nov-96	181	36.812	75.917												5											1								6	
Nov-96	194	36.808	75.903			1									1					2							1					1	1	7	
Nov-96	185	36.812	75.901												1										1									2	
Nov-96	174	36.816	75.907												4									1	1									6	
Nov-96	176	36.816	75.898										1																					1	

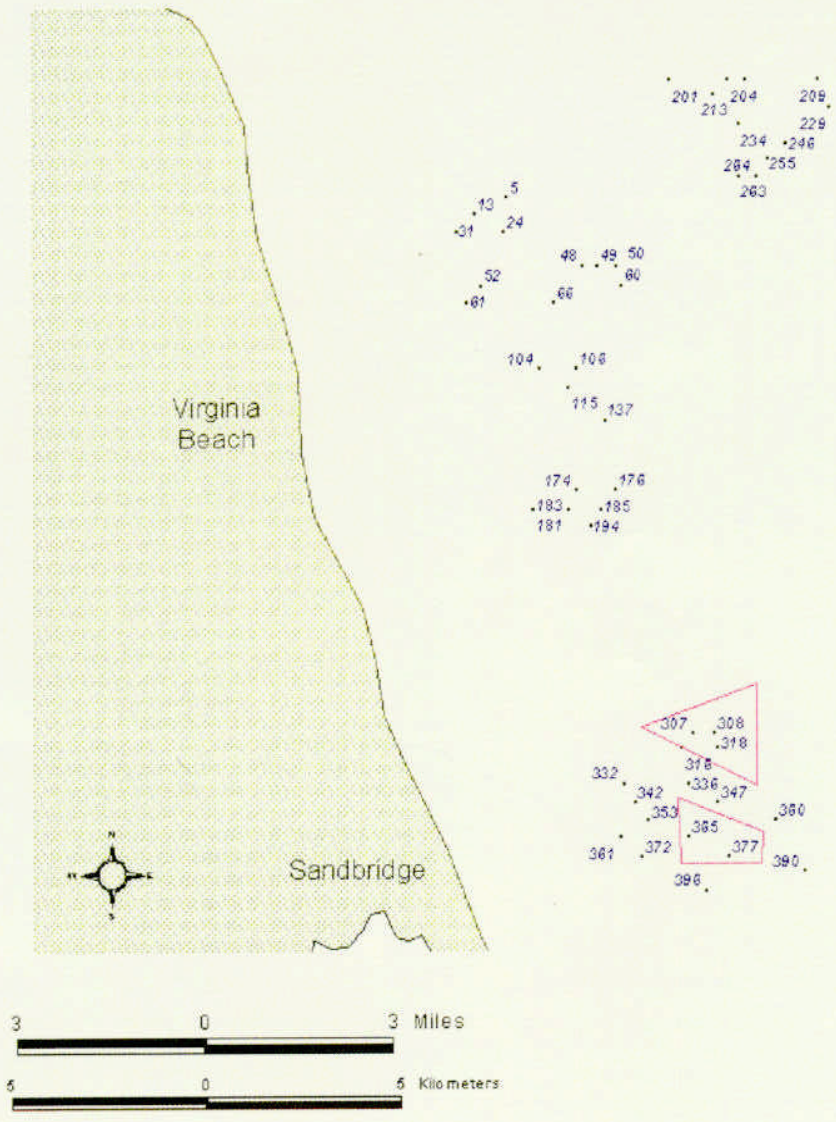

Figure . 1996 Smith-MacIntyre grab sample locations, and proposed borrow areas (delineated by red lines).

The Department of the Interior

As the Nations's principal conservation agency, the Department of the Interior has responsibility for most of our nationally owned public lands and natural resources. This includes fostering sound use of our land and water resources, protecting our fish, wildlife, and biological diversity. preserving the environmental and cultural values of our national parks and historic places; and providing for the enjoyment of life through outdoor recreation. The Department assesses our energy and mineral resources and works to ensure that their development is in the best interests of all our people by encouraging stewardship and citizen participation in their care. The Department also has a major responsibility for American Indian reservation communities and for people who live in island territories under U.S. Administration.

The Minerals Management Service Mission

As a bureau of the Department of the Interior, the Minerals Management Service's (MMS) primary responsibilities are to manage the mineral resources located on the Nations's Outer Continental Shelf (OCS), collect revenue from the Federal OCS and onshore federal and Indian lands, and distribute those revenues.

Moreover, in working to meet its responsibilities, the Offshore Minerals Management Program administers the OCS competitive leasing program and oversees the safe and environmentally sound exploration and production of our Nation's offshore natural gas, oil and other mineral resources. The MMS Royalty Management Program meets its responsibilities by entrusting the efficient, timely and accurate collection and distribution of revenue from mineral leasing and production due to Indian tribes andallottees, States and the U. S. Treasury

the MMS strives to fulfill its responsibilities through the general guiding principles of: (1) being responsive to the public's concerns and interests by maintaining a dialog with all potentially affected parties and (2) carrying out its programs with an emphasis on working to enhance the quality of life for all Americans by lending MMS assistance and expertise to economic development and environmental protection.